PHYSICAL

A Journal of experimental and theoretical physics

Published by the American Institute of Physics
for the
AMERICAN PHYSICAL SOCIETY

Officers

President

G. E. Uhlenbeck
University of California
Berkeley, California

Vice-President

E. P. Wigner
Princeton University
Princeton, New Jersey

Secretary

E. U. Condon
Bell Telephone Laboratories
Office:
Columbia University
New York 27, New York

Treasurer

G. B. Pegram
Columbia University
New York 27, New York

Local Secretary
for the Pacific Coast

Herbert A. Neumann
University of California
Berkeley, California

Managing Editor

S. A. Goudsmit
Brookhaven National Laboratory
Upton, Long Island
New York

Board

S. A. Goudsmit ... S. [illegible]

1950–1951

W. A. Fowler ... G. [illegible]
Kenneth Greisen ... R. [illegible]
Charles Kittel ... R. [illegible]
R. E. Marshak ... J. R. [illegible]
W. K. H. Panofsky ... Lewis [illegible]
V. F. Weisskopf ... Gregory [illegible]

Manuscripts for publication should be addressed to S. A. [illegible], Brookhaven National Laboratory, Upton, Long Island, New [illegible]. authors' institutions are requested to pay a publication charge of [illegible] page which, if honored, entitles them to 100 reprints. Instructions [illegible] be sent with galley proofs.

Proof and all correspondence concerning papers in the process of publi[illegible] should be addressed to the Managing Editor, American Institute of Physics, 57 East 55 Street, New York 22, New York.

Subscription

United States and Canada ... $[illegible]
Elsewhere ... $[illegible]

Back Numbers

Forty-back number and index complete available

Prior to 1940, $[illegible]
Thereafter, $[illegible]

Single copies: $[illegible] each, prior to [illegible]
$[illegible] each, July, 1[illegible] 1947;
$[illegible] each, January, [illegible], 1948;
$[illegible] each, current issue.

General Index, [illegible] 1949 ... $[illegible]

Subscriptions, renewals, and [illegible] should be addressed to the American Institute of Physics, [illegible] New York 22, N. Y.

Changes of address [illegible] should be addressed to the American Physical Society [illegible] other subscription matters to the American Institute of Physics.

The Physical Review is published semi-monthly at [illegible]

Entered as second-class matter March 6, 1918, at the Post Office at [illegible] under the act of March 3, 1879. Acceptance for mailing at special rate of postage provided for in paragraph [illegible] Act of February 28, 1925, embodied in paragraph [illegible]

THE
PHYSICAL REVIEW

A journal of experimental and theoretical physics established by E. L. Nichols in 1893

SECOND SERIES, VOL. 100, No. 3 NOVEMBER 1, 1955

Neutron-Induced Fission Cross Sections of U^{234} and U^{236}

R. W. LAMPHERE, *Oak Ridge National Laboratory, Oak Ridge, Tennessee*

AND

R. E. GREENE, *K-25 Plant, Union Carbide Nuclear Company, Oak Ridge, Tennessee*

(Received June 8, 1955)

The fission cross sections of the uranium isotopes, 234 and 236, have been measured from their thresholds to 4.0-Mev neutron energy by use of neutrons from the $T(p,n)He^3$ reaction. Neutron energy spread varied from 60 to 100 kev for most points.

U^{234} has a threshold at about 300 kev, rises to 1.24 barns at 850 kev, dips to 1.08 barns at 1.06 Mev, rises to 1.47 barns at 1.9 Mev, dips to 1.40 barns at 2.4 Mev, and then rises to 1.55 barns at 4.0 Mev. Variations in between these points appear smooth with the energy spread present in the neutron beam.

Similarly, U^{236} has a threshold at about 670 kev, rises to 0.36 barn at 970 kev and remains nearly constant to 1.04 Mev when it again rises, reaching 0.75 barn at 1.4 Mev, falling to 0.66 barn at 1.56 Mev, rising to 0.89 barn at 2.5 Mev, falling to 0.87 barn at 2.7 Mev, and then rising to 0.99 barn at 4.0 Mev.

The thresholds referred to are the energies at which the cross sections are only about 1% of their values on the relatively flat portion of the curve between 2 and 3 Mev.

Results are believed to be accurate to 6.0%.

INTRODUCTION

THE U^{234} cross section has been measured earlier at this laboratory,[1] but with foils having a large uncertainty in the amount of uranium deposited. Through the efforts of one of us foils were prepared which had an estimated error of less then 1% in the amount of deposited uranium. Foils were plated with the isotopes 234, 236, and also 235 which was used as the flux monitor. Although U^{236} had been measured previously at Los Alamos and at this laboratory it was felt advisable to run over it again since there was some question of foil accuracy in the earlier work.

The fission cross section of U^{234}, or U^{236}, was compared to that of U^{235} by mounting two foils back-to-back in the double ionization chamber shown in Fig. 2, and placing the chamber in a beam of neutrons of known energy. The ratio of cross sections obtained from the raw data is subjected to various corrections to be described, and then multiplied by the U^{235} cross section to yield the fission cross section of the isotopes, 234 and 236, as plotted in Fig. 1.

A correction was determined for the effect of neutrons scattered from the fission chamber material. This amounted to 0.6% for U^{234} and 1.9% for U^{236}. Accordingly all measured values were increased by these amounts. The U^{236} results are in good agreement with the latest Los Alamos work.[2] The U^{234} results show that the cross section reported in reference 1 should be increased by 16%.

Other fast neutron fission cross sections which have been published in the unclassified literature include Np^{237},[3] Th^{232},[4] and natural uranium.[4]

RESULTS

Figure 1 shows the fission cross sections of U^{234} and U^{236}, and Tables I and II list the points upon which the curves are based. The number of counts varies widely from point to point. The statistics listed apply to the count ratio of unknown to monitor foil, and so reflect the statistical counting accuracy of the cross section. Background was zero in all cases. Those points on the curve which have very good statistics are circled. The way in which the neutron energy spread varied

[1] R. W. Lamphere, Phys. Rev. 91, 655 (1953).

[3] R. L. Henkel (private communication).

[3] E. D. Klema, Phys. Rev. 72, 88 (1947).

[4] *Neutron Cross Sections*, U. S. Atomic Energy Commission Report AECU-2040 (Technical Information Division, Department of Commerce, Washington, D. C., 1952).

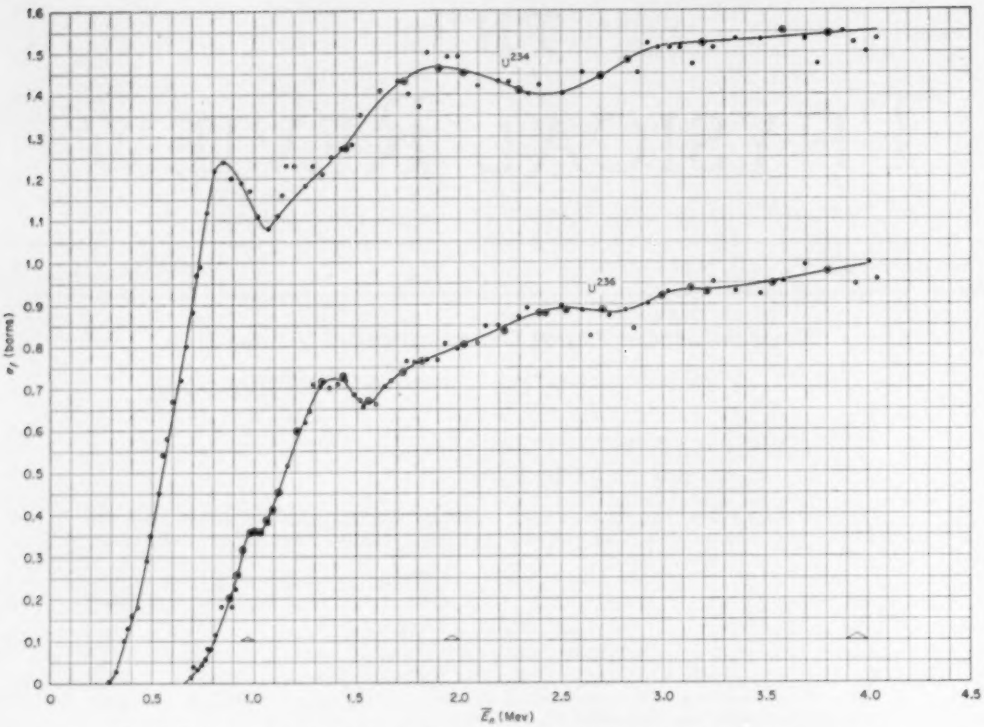

FIG. 1. Fission cross sections of the uranium isotope, 234 and 236, as a function of neutron energy.

with energy is shown by the little triangles below the curves, although in the region of the first irregularity in the U^{238} cross section, resolution was improved somewhat by thinning the gas target. This irregularity was first observed by Henkel *et al.*[2] at Los Alamos. Our findings in this region are in excellent agreement with theirs.

The curves show the cross sections intersecting the zero axis, which of course is not strictly true. The fission reaction, being exothermic, does not show a true threshold, and what one considers as the threshold will depend on the application. For example, these isotopes can still be used as good reliable threshold detectors since the cross sections change so rapidly with energy.

The reason for the dips in the curves is not known. Possibly it is due to resonance effects in certain fission modes with neutron energy. Analysis of fission products obtained with neutrons of energy corresponding to a minimum in cross section, compared to a similar analysis for neutrons corresponding to some other part, say a maximum, of the curve might yield pertinent information on this point.

PROCEDURE

The main features of the procedure were the same as in reference 1. Some changes and additions were made to improve accuracy, and these will be described.

As before, the thick foil technique was used; the thick foils contained 4.0 milligrams of uranium plated over a one inch diameter circle. These were placed back to back in the double fission chamber shown in Fig. 2, one foil containing U^{235} and the other either U^{234} or U^{236}. The Oak Ridge 5-Mev Van de Graaff was used, together with a tritium gas target, to produce the neutrons. The fission chamber was placed in front of the gas cell at 0° relative to the proton beam so that the foils subtended a 15° half-angle as seen from the cell. The chamber was surrounded with a 0.020-inch thick cadmium shield.

The thin foils used for reference contained only 0.200 milligram of uranium. This reduced self-absorption of fission fragments to a very low value so that differences in self-absorption between the U^{235} foils and the U^{234} or U^{236} foils could be neglected. Self-absorption could only be serious if plating was very nonuniform. To check this point several of the thin foils were divided into 4 approximately equal concentric areas by using masks, and the alpha activity from each area measured. The activity per unit area for the thin foils was found to be constant to within 25% in all cases. Examination under a microscope showed the surfaces of the foils to be coated all over, with very little clustering. The backing material was in all cases 0.002-in. thick nickel shim

TABLE I. Points taken to determine curve of $\sigma_f(U^{234})$ *versus neutron energy.*

E_n(Mev)	σ_f(barns)	% statistics	E_n(Mev)	σ_f(barns)	% statistics
0.29	0.003	50.0	1.71	1.43	2.8
0.32	0.025	25.0	1.74	1.43	0.3
0.36	0.098	12.0			
0.38	0.14	6.2	1.76	1.40	2.7
0.40	0.16	13.5	1.81	1.37	2.8
			1.85	1.50	2.8
0.43	0.18	10.0	1.91	1.46	0.8
0.47	0.29	3.6	1.95	1.49	2.7
0.49	0.35	4.5			
0.53	0.45	3.7	2.00	1.49	2.7
0.55	0.54	3.2	2.03	1.45	0.3
			2.10	1.42	2.8
0.57	0.58	3.4	2.20	1.43	2.7
0.60	0.67	3.3	2.25	1.43	2.8
0.64	0.72	1.8			
0.67	0.80	3.0	2.30	1.41	0.8
0.70	0.88	3.0	2.35	1.40	2.7
			2.40	1.42	2.8
0.72	0.97	2.6	2.51	1.40	2.1
0.74	0.99	2.9	2.61	1.45	2.7
0.77	1.12	2.8			
0.81	1.22	1.7	2.70	1.44	0.7
0.85	1.24	1.6	2.83	1.48	0.3
			2.88	1.45	2.7
0.89	1.20	1.9	2.93	1.52	2.1
0.94	1.19	2.8	2.98	1.51	2.7
0.98	1.17	2.2			
1.02	1.11	2.7	3.04	1.51	2.1
1.07	1.08	2.1	3.09	1.51	2.7
			3.15	1.47	2.1
1.12	1.11	2.1	3.20	1.52	0.2
1.14	1.16	2.8	3.25	1.51	2.0
1.16	1.23	2.1			
1.20	1.23	2.8	3.36	1.53	2.7
1.25	1.18	2.2	3.48	1.53	2.7
			3.59	1.55	0.8
1.29	1.23	2.8	3.70	1.53	2.7
1.34	1.21	2.2	3.76	1.47	2.5
1.38	1.25	2.8			
1.43	1.27	2.1	3.81	1.54	0.3
1.45	1.27	0.3	3.88	1.55	2.7
			3.94	1.52	2.1
1.48	1.28	2.8	4.00	1.50	2.8
1.52	1.35	2.0	4.05	1.53	2.8
1.62	1.41	2.6			

stock from the same roll. The same plating setup was used throughout, although different cells were used for the various isotopes to avoid cross-contamination.

Six foils of thin U^{235}, and ten each of U^{234} and U^{236} were prepared. The thermal column of the Oak Ridge graphite reactor was used to compare the fissionability of foils within each group. Since in each case they were made from the same source material, these results should give a constant figure for the fission rate per milligram for the same neutron flux. To obviate the need for flux measurements the comparisons were done as follows:

One of the thin foils, say number 1, was placed in the comparison chamber shown in Fig. 2, facing towards the front of the chamber. Another foil, say number 2, was then inserted facing towards the rear. The chamber was then put into the thermal flux and a fixed number of counts taken on the front foil. The number 2 foil was then replaced with number three and the same number of counts taken on the front foil, and so on for each of the thin foils. In this way the fissionability of all except number 1 could be compared directly without the need for making any flux measurements or corrections for absorption of the thermal neutrons by the foil backing.

The floor of the thermal column is the bottom of a tank of water about 5 feet square. The flux is fairly constant at around 7×10^7 neutrons/cm^2 sec over a square foot at the center but falls off rapidly outside of this area. To find out whether nonuniformities in flux could affect the comparisons, data was taken with the counter face down in the center of the floor of the tank, and also at 4 positions spaced around a 16-in. diameter circle surrounding the center point. At these points the rate of change of flux with radius was quite large, but no effect was apparent in the foil comparisons. Since counting was very fast, very good statistics were taken, about 0.2% being average for the standard deviation of any given ratio.

The foils were also alpha counted and a specific

TABLE II. Points taken to determine curve of $\sigma_f(U^{235})$ *versus neutron energy.*

E_n(Mev)	σ_f(barns)	% statistics	E_n(Mev)	σ_f(barns)	% statistics
0.69	0.014	29.0	1.67	0.717	2.7
0.70	0.038	10.3	1.73	0.737	0.35
0.72	0.034	21.0	1.75	0.766	1.9
0.74	0.044	18.0	1.79	0.763	2.2
0.76	0.056	13.8	1.82	0.763	0.9
0.77	0.081	4.2	1.85	0.766	2.0
0.79	0.080	13.4	1.90	0.768	2.6
0.81	0.115	4.7	1.94	0.807	2.8
0.84	0.182	5.7	2.00	0.794	1.8
0.88	0.203	1.0	2.03	0.803	0.35
0.89	0.182	4.0	2.10	0.807	2.5
0.91	0.224	5.6	2.14	0.847	2.7
0.92	0.259	1.1	2.20	0.849	2.5
0.94	0.316	0.9	2.23	0.835	0.9
0.98	0.358	0.9	2.30	0.871	1.7
1.00	0.361	0.9	2.34	0.891	2.7
1.03	0.358	1.0	2.40	0.879	0.8
1.06	0.387	1.0	2.43	0.876	0.35
1.07	0.380	3.4	2.51	0.895	1.4
1.09	0.413	1.0	2.53	0.884	0.7
1.12	0.452	0.9	2.61	0.885	1.5
1.16	0.516	2.2	2.65	0.823	1.9
1.21	0.598	0.9	2.71	0.886	0.34
1.25	0.618	2.9	2.74	0.872	2.7
1.27	0.645	2.9	2.82	0.885	1.8
1.29	0.710	2.9	2.86	0.840	2.7
1.32	0.701	2.8	2.93	0.900	1.2
1.33	0.717	0.7	3.00	0.918	0.7
1.34	0.718	2.8	3.03	0.928	2.5
1.37	0.700	2.9	3.14	0.937	1.0
1.41	0.710	2.9	3.22	0.926	0.31
1.43	0.723	2.8	3.25	0.951	2.3
1.44	0.728	0.7	3.36	0.928	1.9
1.45	0.719	2.8	3.48	0.922	2.5
1.49	0.684	2.2	3.54	0.947	1.0
1.52	0.671	2.8	3.59	0.951	1.8
1.54	0.656	3.0	3.70	0.991	2.2
1.56	0.670	0.6	3.81	0.976	0.35
1.60	0.662	2.9	3.94	0.944	2.5
1.64	0.702	1.8	4.01	0.996	1.1
			4.05	0.957	5.0

activity obtained on the basis of the weights gotten from the quantitative plating procedure. The results from the alpha and neutron comparisons were used to estimate a probable error in the actual mass of the material on the thin foils. The thick foils were then neutron weighed in the thermal column, using the same thin foil in the front compartment as before for each isotope, and an equivalent weight, W', determined from the thick foil counts compared to the average of all the other thin foils under the same conditions. Thus the use of many thin foils serves not only to estimate our probable foil error, but also to reduce it by the square root of the number of thin foils. This is not a check against any systematic error which might be present in the foil preparation, but since this is a comparison experiment such an error would have to differ between the U^{235} and the U^{234} or U^{236} foils in order to cause errors in the cross sections.

As a check on the possibility of loss of material from the thick foils during the course of the work they were alpha counted immediately after being plated, and once again after all experimental work had been completed with them. In each case counts were to 0.15% statistics, and no loss of material was found.

Having in this manner obtained foils of accurately known equivalent weight, W', the measurements of cross sections of U^{234} and U^{236} proceeded much as in reference 1. Thin (0.05 or 0.10 mil) nickel foil was used to admit the protons into the tritium gas cell. Practically no straggling was observed in proton energy, so that neutron energy spread was taken as the square root of the sum of the squares of energy spread with angle (over a 15° angle) and target thickness.

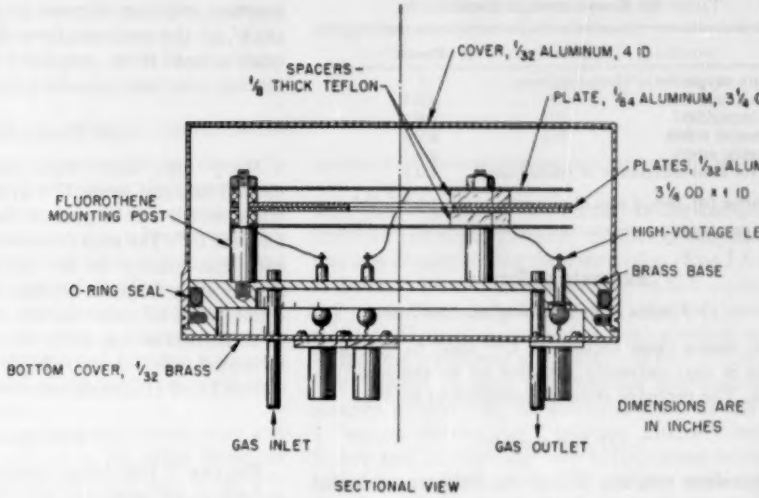

FIG. 2. Fission chamber for counting fission events from two different foils.

PREPARATION OF URANIUM FOILS

The foils were prepared by electrodepositing uranium onto two-thousandths inch nickel shim stock using the method similar to that of Cohen and Hull.[5] Two weights of foils were prepared for each isotope, 0.200 mg and 4.00 mg deposited on an area of one inch diameter centered on a 2¼-inch disk. Quantities of urano-uranic oxide equivalent to forty milligrams of each isotope were accurately weighed in platinum dishes. The platinum dishes were placed in small covered beakers and the uranium oxide was carefully dissolved in nitric acid. The resultant uranyl nitrate solution was quantitively transferred to a fifty-ml volumetric flask and brought to volume with rinsings. From this flask of 0.8 mg uranium per ml a second flask was prepared from a volumetric aliquot to have a concentration of 0.04 mg of uranium per ml.

The four-milligram foils were prepared by pipetting three ml of solution from the parent flask and five ml of 0.4 Molar ammonium oxalate solution (electrolyte) into the plating cell. The plating cell was a short glass cylinder held firmly to the nickel foil by stout rubber bands. A soft rubber gasket between the glass cell and the foil defined the area of the deposit and made a water tight seal between the two. The foil was supported by a stainless steel base plate which held the hooks for the rubber bands. A split watch glass covered the cell. The solution was stirred by a platinum anode, rotating at 450 rpm and the nickel foil served as the cathode. The cell assembly was immersed in a water bath at 90°C during the plating operation. The current was one ampere with an initial voltage of eight volts that increased to fifteen volts as the ammonium oxalate was consumed. After twenty minutes an additional two ml aliquot of the uranium solution was transferred to the cell and, after a total deposition time of thirty minutes, a second five-ml portion of ammonium oxalate solution was added. The 0.200-milligram foils were prepared by adding five ml aliquot of the more dilute uranium solution and five ml of the electrolyte solution to the cell with no further additions of either solution to the cell. The total deposition time for both weights of foils was one hour. The completed foils were ignited for one minute at 400°C to convert the electrodeposited hydrated uranium oxide, of uncertain composition, to urano-uranic oxide.

Since the electrodeposition of the uranium onto the foil was not completely quantitative, averaging about 99.5%, the residual uranium in the deposition solution was determined by counting. The deposition solution of each foil was evaporated to dryness and the ammonium oxalate electrolyte destroyed with nitric acid. This residue was converted to the chloride with hydrochloric acid and transferred quantitatively to a silver residue counting disk, evaporated to dryness, and alpha counted. The count was divided by the specific alpha count of the isotope to determine the amount of uranium, and the foil weight was corrected by this amount.

The standard deviation of each foil computed from known sources of variances has been calculated to be approximately 0.5%. This was determined from the errors attributable to oxide impurities, oxide composition,[6] gravimetric and volumetric uncertainties, and alpha countings of the residues, as shown in Table III.

[5] B. Cohen and D. E. Hull, Report A-1235, August, 1944, Part II.

[6] F. S. Voss and R. E. Greene, (unpublished).

TABLE III. Known errors in uranium foils.

	Percent
Uranium oxygen ratio (deviation from theoretical)	±0.1
Oxide impurities	±0.1
Gravimetric errors	±0.3
Volumetric errors	±0.3
Foil error from uncertainty of residue count	±0.1
Total error (sq. root of sum of squares)	±0.5% Std. dev.

Estimate of Errors

(1) *Fission cross section of monitor foil*

The fission cross section of U^{235} used to get these results is that currently assumed to be the most accurate. The probable error is estimated to be 5%.

(2) *Foil weights*

Equivalent weights, W', of the foils are evaluated together with their probable errors in Appendix B. For the U^{234} cross section the foil uncertainty will be the square root of the sum of the squares of the uncertainties in the U^{234} and the U^{235} foil, and similarly for the U^{236} cross section.

(3) *Statistics*

Due to the slowly varying nature of the curve and the large number of points taken, many to below 1% statistics, the over-all statistical uncertainty is estimated to be ½%.

(4) *Inelastic scattering*

The corrections made for this effect are felt to be good to 0.3 and 0.4% for U^{234} and U^{236}. These are described in detail in Appendix A.

(5) *Nonuniformity of plating*

Alpha counting studies of 4 concentric areas of equal size on the thick foils showed not over ±10% variation (instead of ±25% as was found for the thin ones) in radial distribution of uranium from foil to foil. This, together with the decrease in neutron intensity with angle[7] of the neutrons from the Van de Graaff can cause a small error, calculated to be within 0.2%. oN attempt was made to correct for this.

TABLE IV. Estimate of errors.

Source	U^{236}	U^{234}
W'	0.95	0.70
Statistics	0.50	0.50
Inel. scattering	0.30	0.40
Foil nonuniformity	0.20	0.20
Room scattering	0.00	0.10
Foil separation	0.10	0.10
Beam momentum	0.10	0.10
Gain changes	0.10	0.10
Systematic	1.10	1.10
Std. dev. of ratio	1.59	1.49
Monitor foil error	5.00	5.00
Total	5.25	5.22

(6) *Room scattering*

Many tests have been made, particularly with natural uranium *versus* U^{235} to establish the size of this effect, which will be greatest for natural uranium and least for U^{234}. The tests consisted of taking many counts with the counter in one position, then backing it further away from the neutron source and taking many counts with all other factors the same. The average of these results was 0.3% for natural uranium, so is estimated to be 0.1 and 0.2% for U^{234} and U^{236}. Data in Tables I and II include these corrections.

(7) *Foil separation*

The two U foils being compared are mounted back-to-back so are separated by 0.004 in. of nickel. As the rear foil is farther from the neutron source than the first one the neutron flux density will be reduced (about 0.4% to 0.5% in all these tests). There will also be some attenuation due to the nickel, but this is very slight. The correction from these effects was taken as 0.5%. Data in Tables I and II include this correction.

(8) *Beam momentum*

This correction is estimated to be accurate to 0.1% and is made as described in reference 1.

(9) *Gain changes*

Relative changes in gain between the two electronics channels used to record fission counts can cause error, as described in reference 1. Experience has shown this effect to be very small, not over 0.1%.

(10) *Systematic errors*

Allowance is made here for errors from unknown sources. It is assumed that such errors may be equal to the rms value of errors from all known sources excluding only the uncertainty existing in the monitor foil cross section.

Table IV lists these errors with the final sum, compounding the uncertainties in the usual manner. This shows that the cross-section ratios were obtained to an over-all standard error of 1.6% for U^{234} and 1.5% for U^{236}, and that the over-all standard error for the cross section curves of the U^{234} and U^{236} is 5.3%.

ACKNOWLEDGMENTS

It is a pleasure to acknowledge the help of many other members of the laboratory. In particular we wish to thank B. Harmatz for supplying the uranium, C. R. Baldock and J. R. Sites for the mass analyses, Mrs.

[7] Willard, Bair, and Kington, Phys. Rev. **90**, 865 (1953).

R. D. Ackley for carrying out the plating operations, and members of the 5-Mev Van de Graaff group, J. K. Bair, H. O. Cohn, J. D. Kington, P. H. Stelson, and H. B. Willard for operating the machine.

APPENDIX A. COUNTER SCATTERING CORRECTION

Some of the incident neutrons will be elastically scattered by the material composing the fission comparison chamber and some will be inelastically scattered. Elastically scattered neutrons will need to suffer several collisions to be degraded much in energy so that elastic scattering is not expected to affect the counting ratio noticeably except possibly in the energy region where one of the cross sections is changing rapidly relative to the other. Preferential forward scattering will reduce the percentage of elastically scattered neutrons which enter the foils.

Inelastically scattered neutrons, however, may lose enough energy in one collision to fall below threshold for U^{234} or U^{236}, thus causing the count rate in the U^{235} to be out of proportion to that in the isotope being measured. The effect will be greater the higher the threshold, hence greater for U^{235} than for U^{234}. A rough calculation of this effect for the case of incident neutrons of 2.8 Mev on foils of U^{235} and natural uranium gave 2.9%. A later experimental evaluation of the effect under these conditions gave 2.8 plus or minus 0.3%. Since the calculations were based on simple approximations, such good agreement is fortuitous.

One estimates from geometrical considerations the flux of neutrons inelastically scattered into the uranium foils from the counter components, and then calculates how large this is in relation to the primary neutron flux incident on the foils. Next, it is necessary to make some assumption as to the energy spectrum of the inelastically scattered neutrons. Having done this, it is easy to calculate the effect of these neutrons on the measured fission ratio. This last step requires a numerical integration over the scattered neutron energy spectrum and fission cross section for each foil:

$$\text{Count rate} = N\int_0^\infty \sigma_f(E)\varphi_i(E)dE,$$

where N = number of uranium atoms on a foil, σ_f = fission cross section, φ_i = inelastically scattered neutron flux density, and E = scattered neutron energy. Since this effect is only a small correction, a first-order calculation is sufficient.

Individual level inelastic scattering cross sections are not known in much detail, so one has to work with the total inelastic cross section for each element involved in the construction of the chamber. $\varphi_i(E)$ was obtained as follows for the three metals, Al, brass, and Cd, which accounted for most of the scattering[8]:

$$\varphi_i(E)dE = (CE)\exp[-0.5E(a/E_0)^{\frac{1}{2}}]dE.$$

[8] E. R. Graves and L. Rosen, Phys. Rev. **89**, 343 (1953).

TABLE V. σ_i for various elements.

Element	a(Mev$^{-\frac{1}{2}}$)	σ_i(barns)
Al	56	0.65
Cu	95	1.0
Zn	105	1.3
Cd	129	2.2

This gives the energy distribution of the inelastically scattered neutrons. The total number in this distribution was obtained using the values of σ_i (E_0 = 2.8 Mev) in Table V. Brass was considered to be half copper and half zinc. These calculations say that the measured ratio of the cross sections of natural uranium to U^{235} with primary neutrons of 2.8 Mev will be 3.0% too low.

If, instead of using the foregoing distribution, one assumes instead that the scattered neutrons will have a "square distribution"; constant intensity between 10 kev and 2.5 Mev and zero outside these limits, the calculations are much simpler and one obtains 2.8% instead of 3.0%, thus showing that the result is insensitive to the assumed distribution within wide limits.

Since these calculations are only approximate it was felt advisable to check them experimentally. For this purpose the chamber was fitted with 0.036-in. thick Al plates in place of the 0.016-in. ones. Then sufficient brass was added in the form of a can around the counter to simulate one which would have 2.25 times as much inelastic scattering, the proportions being such that this factor applied separately to the Al plates, the front, side, and rear of the counter, and extra brass added as required to compensate for the difference in its geometrical location from that of the counter parts.

With this arrangement six points were taken to very good statistics with and also without the extra material, along the relatively flat portion of the curve in order to get a correction factor for the chamber at each energy. This was also done for U^{234} and U^{236}. Within statistics these correction factors were independent of primary neutron energy. The results are shown in Table

TABLE VI. Experimental evaluation of counter scattering correction.

	Correction factor in percent		
E_0(Mev)	U^{235}	U^{238}	Natural
1.46	0.53	...	...
1.74	0.47	3.85	...
2.03	−0.17	2.22	...
2.05	...	...	2.56
2.34	...	...	2.64
2.43	...	1.03	...
2.71	...	1.93	2.20
2.83	1.07	...	...
3.00	...	...	2.80
3.22	1.44	1.18	...
3.29	...	...	3.72
3.54	...	...	2.88
3.81	0.39	0.99	...
Average	0.62	1.9	2.8

TABLE VII. Isotopic composition of foils.

	U^{234}	U^{235}	U^{236}
U^{234}	96.16±0.02	0.07±0.01	0.03±0.01
U^{235}	2.82±0.02	99.90±0.01	4.45±0.04
U^{236}	...	...	95.15±0.05
U^{238}	1.02±0.01	0.03±0.003	0.40±0.01

VI. All correction factors have a statistical uncertainty of 0.70%. E_0 is primary neutron energy. The corrections used for U^{234} and U^{236}, respectively, were 0.62 plus or minus 0.3% and 1.9 plus or minus 0.3%. They were assumed constant and applied to all the data to get the final cross sections.

TABLE VIII. Thin foil comparisons.

Foil	Mass	Δf %	$\Delta\sigma$ %
24K1	199.8	monitor	+0.52
24K2	195.1	−2.51	−2.15
24K3	199.4	−2.51	−1.73
24K4	199.9	1.38	1.36
24K5	199.9	1.38	1.08
24K6	199.9	0.36	0.66
24K7	199.8	0.36	0.38
24K8	198.2	−3.74	−3.13
24K9	200.0	2.62	1.22
24K10	199.9	2.62	1.79
Std. error		0.74	0.51
25K5	198.4	0.48	0.46
25K6	194.8	0.07	0.18
25K7	198.3	−0.74	−0.65
25K8	198.2	−0.54	−0.65
25K9	199.0	0.07	0.18
25K10	198.5	0.68	0.46
Std. error		0.21	0.19
26K1	199.7	0.68	1.59
26K2	199.8	−0.94	−1.24
26K3	197.4	monitor	1.05
26K4	199.8	−3.16	−3.16
26K5	199.2	−0.54	−1.14
26K6	199.8	0.47	0.50
26K7	199.5	0.07	−0.33
26K8	199.5	0.88	1.14
26K9	199.6	0.68	0.41
26K10	198.4	1.89	1.14
Std. error		0.45	0.44

APPENDIX B. FOIL COMPARISONS

The isotopic composition of the uranium used in foil preparation was determined by Dr. Baldock and Dr. Sites of this laboratory, by mass spectrographic methods. The results are given in Table VII.

In each case the uranium underwent a chemical purification process and then was plated as previously described; all foils of a given isotope being plated from a single batch to insure the same composition for all. The fission and alpha activities were measured with the results shown in Table VIII for the thin foils. In this table the first two digits of the number indicate the principal isotopic content (24 for U^{234}, etc.). The mass is in micrograms as obtained by direct measurements during foil preparation. The next two columns list the deviations from the average fission and alpha activity per microgram on the basis of the masses listed in the preceding column. The standard errors listed for each group apply to the average for the whole group, as this was what was used to get the W's. The deviation to be expected for a single thin foil will be greater by the square root of the number of foils involved. The standard deviation for the U^{235} thin foils singly would be 0.5%. It is of interest to note that foils of U^{233} and also of natural uranium were prepared in the same way, and these together with the U^{235} foils showed about 0.5% average deviation, which is in good agreement with the expected spread (see paragraph on foil preparation). It is not known what caused the increased spread in the U^{234} and U^{236} foils.

TABLE IX. Equivalent weights of foils used to determine cross sections.

Foil	W'(mg)	% Est. error
24K11	3.405	0.8
25K14	3.571	0.5
26K11	3.583	0.5

The average of the thin foils was used in each case to determine the thick foil equivalent weights as has been described.[1] Counting statistics were 0.2% for thin foil ratios and better than 0.1% for thick foil determinations. The results are given in Table IX.

Gamma Rays from the Reactions $Be^9(\alpha,n\gamma)C^{12}$, $C^{13}(d,p\gamma)C^{14}$, $N^{14}(d,p\gamma)N^{15}$, and $N^{14}(d,n\gamma)O^{15}$†

R. D. Bent,* T. W. Bonner, J. H. McCrary, and W. A. Ranken
The Rice Institute, Houston, Texas

(Received June 15, 1955)

A magnetic-lens pair spectrometer has been used to study the radiations produced by the bombardment of certain light nuclei with α particles and deuterons from The Rice Institute Van de Graaff accelerator. From the bombardment of Be^9 with 4.3-Mev α particles a single γ ray was observed at 4.48±0.06 Mev, doppler corrected. No 7.6-Mev nuclear pair line was observed with an intensity as great as 5% that of the 4.48-Mev internal pair line. No 3.2-Mev γ radiation was observed with an intensity as great as 8% that of the 4.48-Mev γ ray. A comparison of the internal and external pair spectra from the $C^{13}(d,p\gamma)C^{14}$ reaction has been made to obtain information on the multipolarities of the 6.1- and 6.7-Mev γ rays from C^{14}. If the 6.1-Mev γ ray is assumed to be $E1$, the relative intensities of the 6.1- and 6.7-Mev lines suggest that the 6.7-Mev γ ray is $E2$; however, other multipoles such as $E1$, $M1$, and $E3$ cannot be excluded. A study of the γ rays from the reactions $N^{14}(d,p\gamma)N^{15}$ and $N^{14}(d,n\gamma)O^{15}$ shows that the (d,p) cross section is 2.6 times larger than the (d,n) cross section at 2.4-Mev bombarding energy, whereas the two cross sections are about equal at 5.3-Mev bombarding energy.

I. INTRODUCTION

THE magnetic lens pair spectrometer used to make the measurements reported in this paper has been described in an earlier paper.[1] Surveys at 2.5 percent resolution of the γ rays from the deuteron bombardment of C^{13} and N^{14} have been reported earlier.[1,2] More detailed studies of certain aspects of these two reactions are reported here. The recent installation of an α-particle source on The Rice Institute 6-Mev Van de Graaff accelerator has made possible a study of the radiations from the $Be^9(\alpha,n\gamma)C^{12}$ reaction.

II. $Be^9(\alpha,n\gamma)C^{12}$

The absence of ground-state γ-ray transitions from the 7.6-Mev state of C^{12} suggests that the angular momentum of this state is zero. The decay of this state to the 0^+ ground state by the emission of nuclear pairs has been reported by Harries.[3] Several attempts have been made with the pair spectrometer in this laboratory to observe 7.6-Mev nuclear pairs from the reactions $B^{11}(p,\gamma)^*C^{12}$, $B^{11}(d,n)^*C^{12}$, and $N^{14}(d,\alpha)^*C^{12}$. These experiments all yielded negative results.[1,2] The $Be^9(\alpha,n)^*C^{12}$ reaction is particularly well suited for this purpose since the background due to competing reactions is low.

In order to have high intensity, the intermediate image spectrometer arrangement giving 5.5% resolution was used. The internal pair spectrum obtained from the bombardment of a 25 mg/cm² metallic beryllium target with 4.3-Mev α particles is shown in Fig. 1, uncorrected for background effects. The spectrum shows a single peak at 4.51±0.05 Mev, uncorrected for a doppler shift. No line was observed at 7.6 Mev with an intensity as great as 5% that of the 4.4-Mev line. A search was also made for a 3.2-Mev internal pair line which would result from the decay of the 7.6-Mev state to the 4.43-Mev state; however, no 3.2-Mev line was observed with an intensity as great as 5 percent of that of the 4.4-Mev line. The results are summarized in Table I.

A third possible mode of decay for the 7.6-Mev state of C^{12} is into $Be^8+\alpha$. The probability for this can be estimated in the following way. The single particle model suggests that the lifetime for the 3.2 Mev $E2$ transition should be about 7×10^{-13} sec.[4] If the lifetime for the emission of nuclear pairs is assumed to be about equal to that for the similar transition in O^{16}, (5×10^{-11} sec),[5] it follows that the γ-ray cascade transition from the 7.6-Mev state to the 4.4-Mev state is about 70

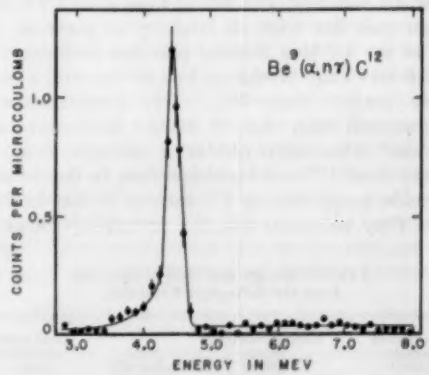

FIG. 1. Internal pair spectrum from the bombardment of a 25 mg/cm² metallic beryllium target with 4.3-Mev α-particles. Spectrometer resolution = 5.5%.

† Supported in part by the U. S. Atomic Energy Commission.
* Now at Columbia University, New York, New York.
[1] Bent, Bonner, and Sippel, Phys. Rev. **98**, 1237 (1955).
[2] Bent, Bonner, McCrary, Ranken, and Sippel, Phys. Rev. **99**, 710 (1955).
[3] G. Harries and W. T. Davies, Proc. Phys. Soc. (London) **A65**, 564 (1952); G. Harries, Proc. Phys. Soc. (London) **A67**, 153 (1954).
[4] J. M. Blatt and V. F. Weisskopf, *Theoretical Nuclear Physics* (John Wiley and Sons, Inc., New York, 1952).
[5] Devons, Goldring, and Lindsay, Proc. Phys. Soc. (London) **A67**, 134 (1954).

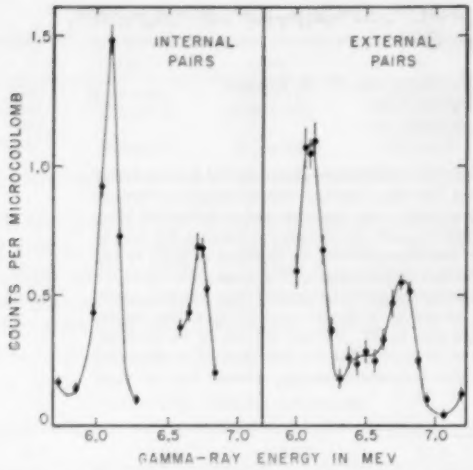

FIG. 2. Internal and external pair spectra of the 6.1- and 6.7-Mev γ rays from the reaction $C^{13}(d,p\gamma)C^{14}$. For the external pair measurement the 3 mg/cm² 48% C^{13} target was separated from a thorium converter 2 mils thick by 2 mm of aluminum. $E_d=4.1$ Mev. Spectrometer resolution = 2.5%.

times more probable than the emission of 7.6-Mev nuclear pairs. The pair spectrometer, however, is about 1000 times more efficient for detecting nuclear pairs than for detecting 3.2-Mev γ rays, since the internal pair formation coefficient for a 3.2-Mev γ ray is about 1.3×10^{-3}.[6] According to the data of Guier, Bertini, and Roberts,[7] the ratio of the intensities of the neutron groups to the 4.4- and 7.6-Mev states is about 8:1. Therefore, if the 7.6-Mev state does not break up into $Be^8+\alpha$ at all, the intensity of the 7.6-Mev nuclear pair line should be 1.3 times greater than that of the 4.4-Mev line. The failure to observe a 7.6-Mev nuclear pair line with an intensity as great as 5% that of the 4.4-Mev internal pair line indicates that the 7.6-Mev state breaks up into $Be^8+\alpha$ with a probability greater than 96%. This interpretation is in agreement with that of Miller, Rasmussen, and Sampson[8] who, with 22-Mev α particles, failed to observe recoil C^{12} nuclei corresponding to the inelastic α-particle group leaving C^{12} excited in the 7.6-Mev state. They estimated that the probability for decay of the 7.6-Mev state into $Be^8+\alpha$ is greater than 80 percent.

TABLE I. Energy and yield of the γ ray from the $Be^9(\alpha,n\gamma)C^{12}$ reaction.

Uncorrected energy (Mev)	Doppler corrected energy (Mev)	Yield ($\gamma/\alpha\times10^6$)	Total cross section[a] (mb)
4.51±0.05	4.48±0.06	0.8	3

[a] Average value $E_\alpha=0$ to 4.3 Mev.

III. $C^{13}(d,p\gamma)C^{14}$

The efficiency of the pair spectrometer for detecting internal pairs is a function of the energy and multipolarity of the transitions, whereas the efficiency for detecting external pairs is a function of the energy only (for a given radiator). It should be possible, therefore, to obtain information on the multipolarities of γ ray transitions by comparing the yields of internal and external pairs.

In order to test this technique, and also to obtain information on the spins and parities of the first two excited states of C^{14}, both the internal and external pair peaks of the 6.1- and 6.7-Mev γ rays from the $C^{13}(d,p\gamma)C^{14}$ reaction were observed. The results obtained at 4.1-Mev bombarding energy are shown in Fig. 2. A 3 mg/cm² 48% C^{13} target was used for both measurements. For the external measurement the target was separated from a 2-mil thorium converter by 2 mm of aluminum absorber. The aluminum absorber was necessary in order to prevent the internal pairs formed in the target from contributing to the external pair spectrum formed in the converter. Enough silver was placed behind the target to prevent the beam from striking the aluminum absorber.

The number of internal pairs transmitted by the spectrometer per quantum has been calculated[9] as a function of the γ-ray energy and multipolarity for the spectrometer arrangement used in the present experiment. The dependence of the cross section for the production of external pairs on γ-ray energy is given by Heitler.[9] The ratio of the intensities of the two external pair peaks, when corrected for the energy dependence of the external pair cross section, gives the ratio of the intensities of the 6.1- and 6.7-Mev γ rays (assuming that the angular distributions of the two γ rays with respect to the beam are not appreciably different). If the multipolarities of the 6.1- and 6.7-Mev γ rays are the same, then the ratio of the intensities of the internal pair peaks, corrected for the energy dependence of the internal pair formation coefficients, should be the same as the ratio obtained from the external pair measurement. A difference in the ratios can be explained by assuming that the multipolarities of the two transitions are different. If the multipolarity of one of the γ rays is known, then information as to the multipolarity of the other can be obtained in this manner. Measurements of the angular distributions of the proton groups from the $C^{13}(d,p)^*C^{14}$ reaction[10] together with measurements of the energy distribution of the internally formed positrons[11] indicate that the spin and parity of the 6.1-Mev state of C^{14} are 1^-. In the present experiment the intensities of the γ rays

[6] M. E. Rose, Phys. Rev. **76**, 678 (1949).
[7] Guier, Bertini, and Roberts, Phys. Rev. **85**, 426 (1952).
[8] Miller, Rasmussen, and Sampson, Phys. Rev. **95**, 649(A) (1954).
[9] W. Heitler, *The Quantum Theory of Radiation* (Oxford University Press, Oxford, 1954).
[10] R. E. Benenson, Phys. Rev. **90**, 420 (1953).
[11] R. G. Thomas and T. Lauritsen, Phys. Rev. **88**, 969 (1952).

were obtained from the heights of the peaks. For the external pairs the ratio of the 6.7-Mev peak height to the 6.1-Mev peak height is 0.51±0.04, whereas for the internal pairs this ratio is 0.47±0.03. If the 6.1-Mev transition is assumed to be $E1$, the ratios can best be explained by assuming that the 6.7-Mev transition is $E2$; however, $E1$, $M1$, and $E3$ are also possible assignments within the experimental errors. $M2$ and $E4$ are slightly outside of the experimental errors, and higher multipole orders seem unlikely. Table II gives possible assignments for the 6.7-Mev transition which are consistent with other assumptions as to the multipolarity of the 6.1-Mev transition. The possibilities are listed in the order of best agreement.

The spectra in Fig. 2 show the advantage of using internal pairs instead of external pairs for studying γ rays at good resolution. The yield of the internal pair lines is greater than that of the external pair lines, and the resolution of the internal and external lines are 2.3 and 3.5%, respectively. The resolution of the external lines is worse than the resolution of the internal lines, partly because of the energy spread in the converter and partly because a converter 7 mm in diameter was used for the external pair measurements, whereas the beam diameter for the internal pair measurements was 3 mm.

TABLE II. Possible multipolarities for the 6.7-Mev transition which are consistent with different assumptions as to the multipolarity of the 6.1-Mev transition.

Assumed multipolarity of 6.1-Mev γ ray	Possible multipolarities for 6.7-Mev γ ray[a]
$E1$	$E2$, $E1$, $M1$, $E3$
$E2$	$M1$, $E3$, $M2$, $E4$, $E2$
$M1$	$E4$, $M2$, $M3$, $E3$, $M1$, $M4$

[a] Listed in order of best agreement.

IV. $N^{14}(d,p\gamma)N^{15}$ AND $N^{14}(d,n\gamma)O^{15}$

When N^{14} is bombarded with deuterons both the (d,p) and (d,n) reactions occur. The residual nuclei are the mirror pair, N^{15} and O^{15}. Since the decay schemes of mirror nuclei should be the same, the relative intensities of corresponding transitions in N^{15} and O^{15} are a measure of the relative (d,p) and (d,n) cross sections. Previous measurements of the γ rays from this reaction[5] showed that the 7.31-Mev γ ray from N^{15} and the 6.81-Mev γ ray from the mirror level in O^{15} are clearly resolved at 2.5% resolution. It was found, at 4.0-Mev bombarding energy, that the (d,p) cross section (average value, E_d=1.6 to 4.0 Mev) to the 7.31-Mev state of N^{15} is 1.5 times larger than the (d,n) cross section to the 6.81-Mev state of O^{15}. The purpose of the present experiment was to investigate the relative (d,p) and (d,n) cross sections at two other bombarding energies.

Figure 3 shows the internal pair spectra obtained from the bombardment of a 17 mg/cm² ZrN target with 2.4-, 4.0-, and 5.3-Mev deuterons. A comparison of the intensities of lines at one bombarding energy with those at another bombarding energy can only be made with an accuracy of about 50% because of possible differences in the setting of the discriminator, which accepts the pulses from the coincidence circuit. The purpose of the experiment is to show how the relative intensities of the 7.31- and 6.81-Mev lines vary with bombarding energy. At 2.4-Mev bombarding energy, the line resulting from the (d,p) reaction is about 3 times more intense than the line resulting from the (d,n) reaction, whereas, at 5.3-Mev bombarding

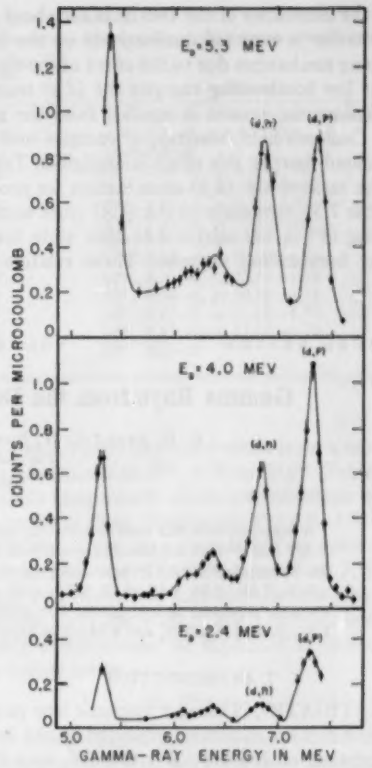

FIG. 3. Internal pair spectra from the bombardment of a 17 mg/cm² ZrN target with 2.4-, 4.0-, and 5.3-Mev deuterons. Spectrometer resolution = 2.5%.

TABLE III. Relative cross-sections for the reactions $N^{14}(d,p)^*N^{15}(7.31)$ and $N^{14}(d,n)^*O^{15}(6.81)$.

Bombarding energy (Mev)	$\frac{\sigma d,p}{\sigma d,n}$
2.4	2.6±0.5[a]
4.0	1.5±0.2[b]
5.3	0.9±0.1[c]

[a] Average cross sections for E_d=0 to 2.4 Mev.
[b] Average cross sections for E_d=1.6 to 4.0 Mev.
[c] Average cross sections for E_d=4.1 to 5.3 Mev.

energy the intensities of the two lines are about equal. This behavior is expected qualitatively on the basis of a stripping mechanism due to the effect of the Coulomb field. At low bombarding energies the (d,p) reaction is favored since the proton is repelled from the nucleus by the Coulomb field, whereas, at energies well above the Coulomb barrier this effect is negligible. Table III gives the ratio of the (d,p) cross section for producing N^{15} in the 7.31-Mev state to the (d,n) cross section for producing O^{15} in the mirror 6.81-Mev state for three different bombarding energies. These relative cross-sections were obtained from the peak heights of Fig. 3 by making corrections for the energy dependence of the efficiency of the spectrometer.

Because of the poor statistics and uncertainties in background corrections, a comparison of the relative intensities of the 6.33- and 6.12-Mev mirror lines cannot be made with significant accuracy.

The increase in intensity of the 5.3-Mev line at high-bombarding energies may be due to an increase in the population of high-excited states in N^{15} which cascade to the 5.3-Mev level.

PHYSICAL REVIEW VOLUME 100, NUMBER 3 NOVEMBER 1, 1955

Gamma Rays from the Deuteron Bombardment of Al^{27} and P^{31}†

R. D. BENT,* T. W. BONNER, J. H. McCRARY, AND W. A. RANKEN
The Rice Institute, Houston, Texas

(Received June 15, 1955)

A magnetic-lens pair spectrometer has been used to study the radiations produced by the bombardment of Al^{27} and P^{31} with 4.6-Mev deuterons from The Rice Institute Van de Graaff accelerator. Gamma rays from the bombardment of Al^{27} were observed at 6.9±0.1, 7.38±0.06, 7.55±0.06, 7.91±0.04, 8.28±0.04, 8.75 ±0.04, 9.08±0.04, 9.45±0.08, 9.87±0.08, and 10.7±0.2 Mev. Gamma rays from the bombardment of P^{31} were observed at 4.41±0.04, 4.71±0.04, 4.94±0.04, 5.29±0.04, 5.79±0.04, 6.11±0.04, 6.84±0.04, 7.46±0.08, 8.16±0.04, and 8.53±0.04 Mev. All energies are doppler-corrected.

I. INTRODUCTION

INVESTIGATIONS using a magnetic lens pair spectrometer of the radiations produced by the deuteron bombardment of Li^7, Be^9, B^{10}, C^{12}, C^{13}, and F^{19}, the proton bombardment of B^{11}, F^{19}, and Ca^{40}, and the α-particle bombardment of Be^9 have been reported in earlier papers.[1-4] The results obtained from investigations of the γ rays produced by the deuteron bombardment of Al^{27} and P^{31} are presented in the present paper. The apparatus and experimental techniques used to make these measurements have been previously described.[1]

II. $Al^{27}+d$

The γ rays produced by the deuteron bombardment of Al^{27} were first investigated with 3.6% resolution using a ring focus spectrometer arrangement. The internal pair spectrum obtained from the bombardment of a 13.5 mg/cm² aluminum foil with 4.6-Mev deuterons is shown in Fig. 1, corrected for a zero magnetic field background equal to about 2% of the 7.5-Mev peak and an accidental rate equal to about 12% of this peak. Data were not taken below 7 Mev because of the large accidental rate caused by the beta rays from Al^{28}.

The region between 7 and 9.4 Mev was investigated further with 2.5% resolution using an intermediate image spectrometer arrangement. The results shown in Fig. 2 have been corrected for an accidental rate equal to about 10% of the 7.5-Mev peak. The zero magnetic field background was small. Data were not taken above 9.4 Mev because of power limitations.

In order to look for γ rays below 7 Mev, a 2.8-mm aluminum absorber was placed behind the target to reduce the energy of the beta rays from Al^{28}, and the

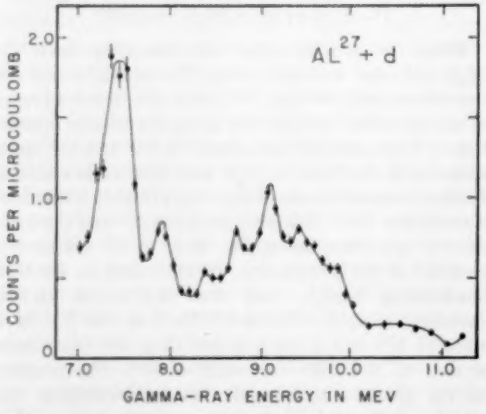

FIG. 1. Internal pair spectrum from the bombardment of a 13.5 mg/cm² aluminum foil with 4.6-Mev deuterons. Spectrometer resolution =3.6%.

† Supported in part by the U. S. Atomic Energy Commission.
* Now at Columbia University, New York, New York.
[1] Bent, Bonner, and Sippel, Phys. Rev. **98**, 1237 (1955).
[2] Bent, Bonner, and McCrary, Phys. Rev. **98**, 1325 (1955).
[3] Bent, Bonner, McCrary, Ranken, and Sippel, Phys. Rev. **99**, 710 (1955).
[4] Bent, Bonner, McCrary, and Ranken, preceding paper [Phys. Rev. **100**, 771 (1955)].

TABLE I. Gamma rays from the deuteron bombardment of Al^{27}.

Uncorrected energy (Mev)	Doppler corrected energy (Mev)	Yield (γ/deut ×10⁶)	Total cross section[a] (mb)	Assignment
6.9 ±0.1	6.9 ±0.1	0.85	2.8	Si^{28} 6.9→0, 8.7→1.78, or 11.4→4.47 Al^{28} 6.9→0, or 6.9→0.03 Mg^{25} 6.9→0
7.41±0.05	7.38±0.06	0.71	2.4	Si^{28} 7.38→0, or 9.16→1.78 Al^{28} 7.38→0, or 7.41→0.03
7.58±0.05	7.55±0.06	0.68	2.3	Si^{28} 7.55→0, or 9.33→1.78 Al^{28} 7.55→0, or 7.58→0.03
7.94±0.03	7.91±0.04	0.57	1.9	Si^{28} 7.91→0, or 9.69→1.78
8.31±0.03	8.28±0.04	0.25	0.8	Si^{28} 8.28→0, or 10.06→1.78
8.78±0.03	8.75±0.04	0.17	0.6	Si^{28} 8.75→0, or 10.53→1.78
9.11±0.03	9.08±0.04	0.31	1.0	Si^{28} 9.08→0, or 10.86→1.78
9.49±0.07	9.45±0.08	0.22	0.7	Si^{28} 9.45→0, or 11.23→1.78
9.91±0.07	9.87±0.08	0.13	0.4	Si^{28} 9.87→0, or 11.65→1.78
10.8 ±0.2	10.7 ±0.2	0.04	0.1	Si^{28} 10.7→0

[a] Average value, E_d=2.7 to 4.6 Mev.

external pairs formed in a thorium converter 2 mils thick were observed. The results obtained are shown in Fig. 3, corrected for an accidental rate equal to about 17% of the 7.5-Mev peak. Additional data were taken down to a γ-ray energy of 4.5 Mev; however, below 6.5 Mev the spectrum was flat and no resolved peaks were observed. In order to keep the accidental rate small, the external pair data had to be taken with about 0.1 microampere of beam current, whereas for the internal pair measurements a beam current of about 2 microamperes was used. The energies and yields of the γ rays obtained from Figs. 1–3 are given in Table I. The 7.41- and 7.58-Mev energies were obtained by assuming that the broad peak at 7.5 Mev is the result of two unresolved γ rays of equal intensities.

DISCUSSION

When Al^{27} is bombarded with deuterons, the following reactions occur:

$$Al^{27}(d,n)Si^{28} \quad Q=9.36 \text{ Mev},$$
$$Al^{27}(d,p)Al^{28} \quad Q=5.50 \text{ Mev},$$
and
$$Al^{27}(d,\alpha)Mg^{25} \quad Q=6.69 \text{ Mev}.$$

States above 7.72 Mev in Al^{28} can break up into $Al^{27}+n$ and hence would not be expected to give rise to strong γ rays. Similarly, states above 7.32 in Mg^{25} can break up into $Mg^{24}+n$. The 7.91-Mev and higher energy γ rays must therefore be assigned to Si^{28}. Except for the 10.8-Mev line (or lines), they may be due either to direct transitions to the ground state or to cascades to the first excited state at 1.78 Mev. Cascades from higher levels to the second excited state at 4.47 Mev would be too weak to observe since the upper level involved can also break up into $Al^{27}+p$. States with angular momenta of 0 or ≥ 2 would be expected to decay predominantly to the 2^+ 1.78-Mev state, whereas states with angular momenta of 1 should decay predominantly to the 0^+ ground state.

The 7.55- and 7.38-Mev γ rays may be due to transitions to the ground or first excited states in either Si^{28} or Al^{28}. The 6.9-Mev line could result from a number of possible transitions in Si^{28}, Al^{28}, or Mg^{25}. Table I lists the possible assignments which are consistent with the known levels[b] of these three nuclei. The 6.9-, 7.55-, 8.28-, and 9.08-Mev lines may correspond to ground-state transitions from states in Si^{28} reported at 7.10, 7.55, 8.18, and 9.16 Mev. The 7.38-Mev line may be due to a transition from the 9.16- to the 1.78-Mev level. The remaining γ rays cannot be explained in terms of the known energy levels.

III. $P^{31}+d$

The γ rays produced by the deuteron bombardment of P^{31} were investigated with the intermediate image spectrometer at 2.5% resolution. The internal pair spectrum obtained from the bombardment of an 11 mg/cm² pressed red phosphorus target with 4.6-Mev

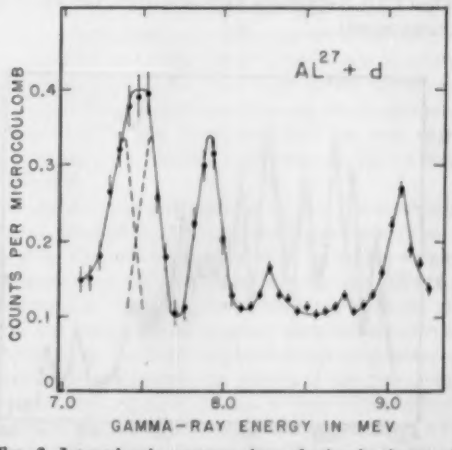

FIG. 2. Internal pair spectrum from the bombardment of a 13.5 mg/cm² aluminum foil with 4.6-Mev deuterons. Spectrometer resolution = 2.5%.

[b] P. M. Endt and J. C. Kluyver, Revs. Modern Phys. 26, 95 (1954).

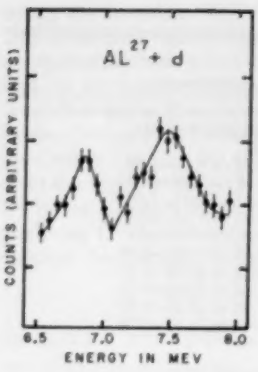

FIG. 3. External pair spectrum from the bombardment of a thick aluminum target with 4.6-Mev deuterons. A thorium converter 2 mils thick and 8 mm in diameter was separated from the target by 2.8 mm of aluminum absorber. Spectrometer resolution = 2.5%.

deuterons is shown in Fig. 4, corrected for a zero magnetic field background equal to about 20% of the 5.8-Mev peak and an accidental rate equal to about 7% of this peak. Data were not taken below 4.4 Mev because of the beta rays from P^{32}. Although the half-life for the decay of P^{32} is about 15 days, the accidental rate, after bombardment for a few hours with 2 microamperes of beam current, was about equal to the true coincidence rate due to pairs at 4.4 Mev and increased rapidly at lower energies. Smaller beam currents improve the true to accidental ratio, but increase the time necessary for the collection of data. The energies and yields of the γ rays are given in Table II. The yields were obtained from the peak heights by making corrections for the dependence of the spectrometer efficiency on γ-ray energy.

DISCUSSION

When P^{31} is bombarded with deuterons, the following reactions occur:

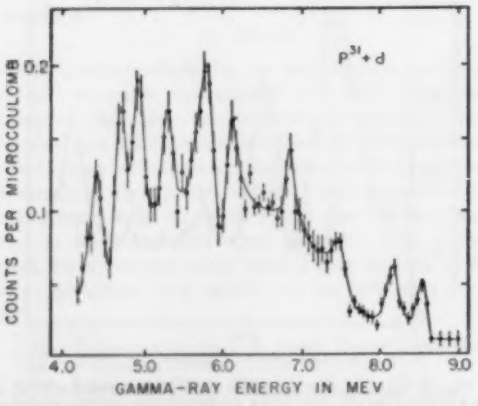

FIG. 4. Internal pair spectrum from the bombardment of an 11 mg/cm^2 red phosphorous target with 4.6-Mev deuterons. Spectrometer resolution = 2.5%.

$P^{31}(d,n)S^{32}$ $Q = 6.63$ Mev,

$P^{31}(d,p)P^{32}$ $Q = 5.70$ Mev,

and $P^{31}(d,\alpha)Si^{29}$ $Q = 8.16$ Mev.

States in P^{32} above 7.93 Mev can break up into $P^{31}+n$ and hence would not be expected to give rise to strong γ rays. Similarly, states in Si^{29} above 8.47 Mev can break up into $Si^{28}+n$, and states in S^{32} above 6.94 Mev can break up into $Si^{28}+\alpha$. The 8.53-Mev γ ray therefore is probably due to a ground-state transition in S^{32}. It is possible, however, that this γ ray is the result of a ground state transition in Si^{29}, since the γ-ray energy value is only slightly higher than that required for neutron emission. A strong γ-emitting state at 8.53 Mev in S^{32} probably would have even parity and odd angular momentum, or *vice versa*, or isotopic spin $T = 1$, since otherwise γ emission would not compete favorably with the break up into $Si^{28}+\alpha$. The decay of the state predominately to the 0^+ ground state rather than to the 2^+ first excited state indicates that the angular momentum is probably 1. Similarly, the 8.16-Mev γ ray may be caused by a ground-state transition from a spin-1 state at 8.16 Mev in S^{32}, or to a ground-state transition in Si^{29}. The lower energy γ rays may be the result of a number of possible transitions in S^{32}, P^{32}, or Si^{29}. Definite assignments cannot be made without further information of the energies and intensities of the particle groups.

TABLE II. Gamma rays from the deuteron bombardment of P^{31}.

Uncorrected energy (Mev)	Doppler corrected energy (Mev)	Yield (γ/deut $\times 10^6$)	Total cross section[a] (mb)	Assignment
4.43±0.03	4.41±0.04	0.90	4.1	S^{32}, P^{32}, or Si^{29}
4.73±0.03	4.71±0.04	1.1	5.0	S^{32}, P^{32}, or Si^{29}
4.95±0.03	4.94±0.04	1.1	5.0	S^{32}, P^{32}, or Si^{29}
5.31±0.03	5.29±0.04	0.82	3.7	S^{32}, P^{32}, or Si^{29}
5.81±0.03	5.79±0.04	0.78	3.5	S^{32}, P^{32}, or Si^{29}
6.13±0.03	6.11±0.04	0.54	2.5	S^{32}, P^{32}, or Si^{29}
6.86±0.03	6.84±0.04	0.35	1.6	S^{32}, P^{32}, or Si^{29}
7.49±0.07	7.46±0.08	0.16	0.7	S^{32}, P^{32}, or Si^{29}
8.19±0.03	8.16±0.04	0.10	0.4	S^{32}, 8.16→0 Si^{29}, 8.16→0
8.56±0.03	8.53±0.04	0.07	0.3	S^{32}, 8.53→0

[a] Average value, $E_d = 2.6$ to 4.6 Mev.

The 8.16- and 8.53-Mev lines can result from the (d,n) reaction but not from the (d,p) reaction, whereas lower energy γ rays may result from both reactions. The rise in the intensity of the spectrum below 7.9 Mev suggests, therefore, that the (d,p) cross section is larger than the (d,n) cross section. This interpretation is in agreement with the results of a study of the γ rays from the deuteron bombardment of N^{14} which showed that, at 4.0 Mev bombarding energy, the (d,p) cross section was 1.5 times larger than the (d,n) cross section.[3] At higher bombarding energies the two cross sections were about equal.[4]

Phase-Shift Analysis of Single-Channel Reactions*†

HARRY LUSTIG,‡ *Department of Physics, University of Illinois, Urbana, Illinois*

AND

J. M. BLATT, *School of Physics, University of Sydney, Sydney, Australia*

(Received February 7, 1955)

The calculation of phase shifts from experimental data has usually involved "matching" of differential cross-section data at a number of angles equal to the number of assumed nonzero phase shifts, followed by minimization of the errors at other angles. It is possible to derive n simultaneous equations for n assumed phase shifts by calculating n "moments" of a suitable expression for the differential cross section. We have derived such a theoretical expression for the problem of single-channel elastic scattering of charged particles with channel spin $\frac{1}{2}$, and performed the integrations. For each particular experimental problem, the cross-section data are to be integrated numerically. Then n simultaneous equations are obtained which may be solved for n phase shifts. As an example of this method, we have analyzed proton-alpha scattering data at an incident energy of 5.78 Mev and obtained values for five assumed phase shifts.

I. INTRODUCTION

IN the long-standing and recently intensified endeavors to discover the laws of nuclear forces from experimental scattering data, the determination of the phase-shifts has proved to be an indispensable step. This phase-shift analysis of the differential scattering cross section has traditionally been beset with such calculational complexities, as to make the treatment of each new problem a tedious and separate mathematical task.

This is particularly true for problems which involve Coulomb forces (in addition to the nuclear forces), and spin-orbit effects. For then, in the traditional formulation of the problem, the spin function and azimuthal projections of the spin must be explicitly introduced. In fact, the complexities are such that no general expression which uses this approach seems to exist in the literature. As an example of the formulation of a *specific* problem, we refer to the work of Critchfield and Dodder on the phase-shift analysis of the scattering of protons by alpha particles.[1] This method involves the "matching" of the expression for the differential cross section at special angles and the step by step improvement of the preliminary values by a fitting process at the other angles. If the nonvanishing of higher phase shifts than those for $l=1$ is suspected, and their values are to be calculated, recourse to a digital computer seems to be called for in the traditional formalism.[2]

It is the purpose of this work to systematize the phase-shift analysis for one large group of problems, that of single-channel elastic scattering of charged particles, and to provide experimenters with a ready made algorithm for the calculation of the phase shifts.

In any effort to systematize the phase-shift analysis procedure and to simplify the approach so as to obviate the necessity for matching at selected angles and for arithmetic fitting at the other angles, three improvements seem desirable:

(1) To get rid of quadratic forms of the Legendre polynomials in the expression for the differential cross section.

(2) To get rid of the dependence on the spin projections in a general way, once and for all.

(3) To get rid of the dependence on θ; i.e. to work with expressions akin to the total cross section, rather than with the differential cross section. This will allow us to make full use of the experimental data at all angles, rather than only at selected angles.

The first two objectives have been realized by Blatt and Biedenharn.[3] Their work is based, in large measure, on two ideas: (1) the fact that the product of two spherical harmonics may (like any other function of θ and ϕ) be written as the linear superposition of spherical harmonics, and (2) the fact that all the summations over magnetic quantum numbers are purely geometric, independent of the particular problem, and can be carried out in a general way with the use of Racah coefficients.

It is the aim of this work to achieve the third objective of eliminating the angular dependence from the analysis. This will be accomplished by taking weighted moments of a suitable expression for the differential cross section, integrated over θ from 0 to π. At the same time the experimental angular distribution curve is multiplied by the same weighted integrating factor and numerically integrated; the results of the two integrations are then equated. If this is done with n different moments, n simultaneous equations are obtained which may be solved for n phase shifts. This may be done, in each particular case, by an iteration process which

* Based, in part, on the Ph.D. dissertation of Harry Lustig at the University of Illinois.

† This work was supported jointly by the U. S. Atomic Energy Commission and the Office of Naval Research.

‡ Present address: Department of Physics, City College of New York, New York 31, New York.

[1] C. L. Critchfield and D. C. Dodder, Phys. Rev. **76**, 602 (1949).

[2] D. C. Dodder and J. L. Gammel, Phys. Rev. **88**, 520 (1952).

[3] J. M. Blatt and L. C. Biedenharn, Revs. Modern Phys. **24**, 258 (1952).

requires only modest effort and the aid of no more than a desk calculator.

After this work had reached completion, a method of analysis by Fluegge[4] which also relies upon the taking of moments was pointed out to us. Fluegge's method makes no claim to applicability in cases in which there are spin-orbit effects. However, several important considerations which make the method inapplicable in *any* problem involving charged particles seem to have been overlooked by him. These will be pointed out at appropriate places in this paper.

II. DIFFERENTIAL CROSS SECTION

We begin with an expression for the differential cross section of a general nuclear reaction, obtained by Blatt and Biedenharn[5] and specialize immediately to a reaction with only one possible channel, in particular the elastic scattering of charged particles with total channel spin $\frac{1}{2}$ (e.g., the scattering of protons by alpha particles).[6] The expression for the differential cross section becomes

$$d\sigma/d\Omega=\tfrac{1}{4}\lambda^2\sum_{L=0}^{\infty}B_L P_L(\cos\theta), \tag{1}$$

where λ is the de Broglie wavelength (divided by 2π), $P(\cos\theta)$ is a Legendre polynomial,[7] and

$$B_L=\tfrac{1}{4}\sum_{j_1}\sum_{j_2}\sum_{l_1}\sum_{l_2}Z^2(l_1j_1l_2j_2;\tfrac{1}{2},L)\times\text{R.P.}\{(1-\exp[2i(\sigma_{l1}+\delta_{l1,j1})]^*)\times(1-\exp[2i(\sigma_{l2}+\delta_{l2,j2})])\}. \tag{2}$$

Here Z is a Racah coefficient and arises from having performed explicitly all sums over magnetic quantum numbers; σ_l is the Coulomb phase shift associated with the lth partial wave and is defined by

$$\exp(2i\sigma_l)=(l+i\eta)!/(l-i\eta)!, \tag{3}$$

where the Coulomb factor η is given by

$$\eta=ZZ'e^2/\hbar v \tag{4}$$

(v being the relative velocity between the two particles); $\delta_{L,j}$ is the unknown nuclear phase shift associated with the lth partial wave and the total angular momentum j. The dummy subscripts 1 and 2 arise from the multiplication of scattering amplitudes in the derivation of this formula. R.P. stands for the real part of the expression in brackets. θ is in the center-of-mass system.

It is known that the expression for the Coulomb amplitude converges extremely slowly in l.[8] Thus, in order to be able to make a calculation which has not only a finite but a small number of terms in the sums over j and l we must somehow isolate and sum explicitly the Coulomb cross section and the Coulomb amplitude wherever they occur. This is accomplished by factorization of the bracket in (2):

$$\begin{aligned}(1-\exp 2i\sigma_{l1}\cdot\exp 2i\delta_{l1,j1})^*(1-\exp 2i\sigma_{l2}\cdot\exp 2i\delta_{l2,j2})&=(1-\exp 2i\sigma_{l1})^*(1-\exp 2i\sigma_{l2})\\&+(\exp 2i\sigma_{l1})^*(1-\exp 2i\sigma_{l2})(1-\exp 2i\delta_{l1,j1})^*\\&+\exp 2i\sigma_{l2}(1-\exp 2i\sigma_{l1})^*(1-\exp 2i\delta_{l2,j2})\\&+(\exp 2i\sigma_{l1})^*(\exp 2i\sigma_{l2})(1-\exp 2i\delta_{l1,j1})^*\\&\times(1-\exp 2i\delta_{l2,j2}).\end{aligned} \tag{5}$$

We may now write

$$d\sigma/d\Omega\equiv(d\sigma/d\Omega)_{\rm I}+(d\sigma/d\Omega)_{\rm II}+(d\sigma/d\Omega)_{\rm III}+(d\sigma/d\Omega)_{\rm IV} \tag{6}$$

where

$$(d\sigma/d\Omega)_{\rm I}=\tfrac{1}{4}\lambda^2\sum_{L}\sum_{l_1}\sum_{l_2}\sum_{j_1}\sum_{j_2}Z^2(l_1j_1l_2j_2;\tfrac{1}{2},L)\times\text{R.P.}[(1-\exp 2i\sigma_{l1})^*\times(1-\exp 2i\sigma_{l2})]P_L(\cos\theta), \tag{7}$$

$$(d\sigma/d\Omega)_{\rm II}=\tfrac{1}{4}\lambda^2\sum_{L}\sum_{l_1}\sum_{l_2}\sum_{j_1}\sum_{j_2}Z^2(l_1j_1l_2j_2;\tfrac{1}{2},L)\times\text{R.P.}[(\exp 2i\sigma_{l1})^*(1-\exp 2i\sigma_{l2})\times(1-\exp 2i\delta_{l1,j1})^*]P_L(\cos\theta), \tag{8}$$

$$(d\sigma/d\Omega)_{\rm III}=\tfrac{1}{4}\lambda^2\sum_{L}\sum_{l_1}\sum_{l_2}\sum_{j_1}\sum_{j_2}Z^2(l_1j_1l_2j_2;\tfrac{1}{2},L)\times\text{R.P.}[\exp 2i\sigma_{l2}(1-\exp 2i\sigma_{l1})^*\times(1-\exp 2i\delta_{l2,j2})]P_L(\cos\theta), \tag{9}$$

and

$$(d\sigma/d\Omega)_{\rm IV}=\tfrac{1}{4}\lambda^2\sum_{L}\sum_{l_1}\sum_{l_2}\sum_{j_1}\sum_{j_2}Z^2(l_1j_1l_2j_2;\tfrac{1}{2},L)\times\text{R.P.}[(\exp 2i\sigma_{l1})^*(\exp 2i\sigma_{l2})\times(1-\exp 2i\delta_{l1,j1})^*\times(1-\exp 2i\delta_{l2,j2})]P_L(\cos\theta). \tag{10}$$

We now proceed to simplify the expressions for these four contributions to the differential cross section. We note that (7) is independent of the nuclear phase shifts and, except for the Racah coefficient, is independent of j. We first perform the sum over j_1:

$$\sum_{j_1}Z^2(l_1j_1l_2j_2;\tfrac{1}{2},L)=(2l_1+1)(2l_2+1)\times(l_1l_200|l_1l_2L0)^2, \tag{11}$$

[4] S. Fluegge, *Theorie der elastischen Streuung von Korpuskeln an zusammengesetzten Atomkernen, Ergebnisse der exakten Naturwissenschaften* (Springer Verlag, Berlin-Goettingen-Heidelberg, 1951).

[5] Reference 3, formulas (4.5) and (4.6).

[6] We put $\alpha=\alpha'$, $s=s'$ and $l=l'$ in the Blatt-Biedenharn formula. The selection $s=\frac{1}{2}$ is made only for the sake of providing a definite example of the use of this method; all of what follows goes through in the same way for any other value of s.

[7] E. U. Condon and G. H. Shortley, *Theory of Atomic Spectra* (Cambridge University Press, Cambridge, 1935).

[8] Fluegge has overlooked this fact in his approach.

where $(l_1 l_2 00|l_1 l_2 L0)$ is a Clebsch-Gordan coefficient as defined in Condon and Shortley.[7] This result follows from the sum rule for Racah coefficients.[9]

The sum over j_2 is exceedingly simple. It contains only the terms $j_2=l_2-\frac{1}{2}$ and $j_2=l_2+\frac{1}{2}$ whence $\sum_{j_2}(2j_2+1)=2(2l_2+1)$ and (7) becomes

$$(d\sigma/d\Omega)_{\mathrm{I}}=\tfrac{1}{4}\lambda^2\sum_L\sum_{l_1}\sum_{l_2}(2l_1+1)(2l_2+1)\times(l_1 l_2 00|l_1 l_2 L0)^2\,\mathrm{R.P.}[(1-\exp 2i\sigma_{l1})^*\times(1-\exp 2i\sigma_{l2})]P_L(\cos\theta). \quad (12)$$

We note that in this expression and in all similar expressions involving sums over L, l_1, and l_2, the sum over L, although it formally extends from 0 to ∞ is in actuality restricted by the condition $L_{\min}=|l_1-l_2|$, $L_{\max}=|l_1+l_2|$. The physical reason for this arises from the rules for vector addition of angular momenta and is reflected in the automatic zero value of the Clebsch-Gordan and Racah coefficients containing arguments which do not satisfy the above restriction.

We may now carry out the sum over L by using the superposition law of spherical harmonics

$$\sum_{L=|l_1-l_2|}^{|l_1+l_2|}(l_1 l_2 00|l_1 l_2 L0)^2 P_L(\cos\theta)=P_{l1}(\cos\theta)P_{l2}(\cos\theta) \quad (13)$$

to give

$$(d\sigma/d\Omega)_{\mathrm{I}}=\tfrac{1}{4}\lambda^2\,\mathrm{R.P.}[\sum_{l_1=0}^{\infty}(2l_1+1)(1-\exp 2i\sigma_{l1})^*\times P_{l1}(\cos\theta)\sum_{l_2=0}(2l_2+1)\times(1-\exp 2i\sigma_{l2})P_{l2}(\cos\theta)]. \quad (14)$$

In this expression, we are able to identify each sum over l_1 and l_2 with a partial wave decomposition of the Coulomb amplitude, as follows:

$$\sum_{l=0}^{\infty}(2l+1)(1-\exp 2i\sigma_l)P_l(\cos\theta)=(-2i/\lambda)f_{\mathrm{Coul}}(\theta)=(2i/\lambda)(ZZ'e^2/2mv^2)\times\csc^2(\theta/2)\exp[-2i\eta\ln\sin(\theta/2)+2i\sigma_0]. \quad (15)$$

Thus we obtain

$$(d\sigma/d\Omega)_{\mathrm{I}}=(\lambda^2/4)(2i/\lambda)(-2i/\lambda)f_{\mathrm{Coul}}f_{\mathrm{Coul}}^*, \quad (16)$$

whence

$$(d\sigma/d\Omega)_{\mathrm{I}}\equiv(d\sigma/d\Omega)_{\mathrm{Coul}}=(ZZ'e^2/2mv^2)^2\csc^4\theta/2. \quad (17)$$

Thus, we have performed the sums over l_1 and l_2 in the first term.

Working next on (8) we again use the sum rule for Racah coefficients to carry out the summation over j_2. We obtain

$$(d\sigma/d\Omega)_{\mathrm{II}}=\tfrac{1}{8}\lambda^2\sum_L\sum_{l_1}\sum_{l_2}\sum_{j_1}(2l_2+1)(2j_1+1)\times(l_2 j_1 00|l_2 j_1 L0)^2\times\mathrm{R.P.}[(\exp 2i\sigma_{l1})^*(1-\exp 2i\sigma_{l2})\times(1-\exp 2i\delta_{l1,j1})^*P_L(\cos\theta). \quad (18)$$

Using again the superposition theorem of spherical harmonics, we arrive at the expression

$$(d\sigma/d\Omega)_{\mathrm{II}}=\tfrac{1}{8}\lambda^2\sum_{l_1}\sum_{j_1}(2j_1+1)P_{l1}(\cos\theta)\times\mathrm{R.P.}[(\exp 2i\sigma_{l1})^*(1-\exp 2i\delta_{l1,j1})^*\times\sum_{l_2=0}^{\infty}(2l_2+1)(1-\exp 2i\sigma_{l2})P_{l2}(\cos\theta). \quad (19)$$

Identifying the sum over l_2 with the Coulomb amplitude as before, we may write

$$(d\sigma/d\Omega)_{\mathrm{II}}=(\lambda/4)(ZZ'e^2/2mv^2)\csc^2\theta/2\times\mathrm{R.P.}[i\exp(-2i\eta\ln\sin\theta/2+2i\sigma_0)\times\sum_{l_1}\sum_{j_1}(\exp 2i\sigma_{l1})^*(1-\exp 2i\delta_{l1,j1})^*\times(2j_1+1)P_{l1}(\cos\theta)]. \quad (20)$$

We note that in deriving this expression we have achieved one of our desired aims; if we assume that the nuclear phase shifts $\delta_{l1,j1}$ approach 0 after a finite and small number of l_1's (a condition which is certainly satisfied for reactions at reasonably low energies), this contribution to the cross section converges rapidly in l_1 and j_1.

The work for (9) is only formally and trivially different from that for (8) and gives us

$$(d\sigma/d\Omega)_{\mathrm{III}}=(\lambda/4)(ZZ'e^2/2mv^2)\csc^2\theta/2\times\mathrm{R.P.}[-i\exp(2i\eta\ln\sin\theta/2-2i\sigma_0)\times\sum_{l_2}\sum_{j_2}\exp 2i\sigma_{l2}(1-\exp 2i\delta_{l2,j2})^*\times(2j_2+1)P_{l2}(\cos\theta)]. \quad (21)$$

Expressions (20) and (21) may now be readily combined by dropping the now superfluous subscripts on l and j and performing the addition of the real parts of the two expressions which are complex conjugates of one another. Since R.P. z+R.P. z^*=2 R.P. z the addition gives

$$(d\sigma/d\Omega)_{\mathrm{II}}+(d\sigma/d\Omega)_{\mathrm{III}}=(\lambda/2)(ZZ'e^2/2mv^2)\csc^2\theta/2\times\mathrm{R.P.}[i\exp(-2i\eta\ln\sin\theta/2+2i\sigma_0)\sum_l\sum_j(2j+1)\times P_l(\cos\theta)(\exp 2i\sigma_l)^*(1-\exp 2i\delta_{lj})^*]. \quad (22)$$

It is evident that this term is the result of interference between the Coulomb and the nuclear scattering.

[9] Biedenharn, Blatt, and Rose, Revs. Modern Phys. **24**, 249 (1952), formula (26).

Taking the real part of the bracket and making use of (4), we may write

$$(d\sigma/d\Omega)_{II}+(d\sigma/d\Omega)_{III}\equiv(d\sigma/d\Omega)_{\text{int}}$$
$$=-(\lambda^2\eta/2)\csc^2\theta/2\sum_l\sum_j(2j+1)P_l(\cos\theta)$$
$$\times\sin\delta_{l,j}\cos(2\eta\ln\sin\theta/2+2\sigma_l-2\sigma_0+\delta_{l,j}). \quad (23)$$

In expression (10), which we recognize to be a nuclear contribution, no real simplification is possible. We note that this sum already converges rapidly in the l's and j's. Taking the real part, we obtain

$$(d\sigma/d\Omega)_{IV}\equiv(d\sigma/d\Omega)_{\text{nucl}}$$
$$=(\lambda^2/2)\sum_L\sum_{l_1}\sum_{l_2}\sum_{j_1}\sum_{j_2}Z^2(l_1j_1l_2j_2;\tfrac{1}{2},L)P_L(\cos\theta)$$
$$\times\sin\delta_{l_1,j_1}\sin\delta_{l_2,j_2}\cos[(2\sigma_{l_1}-2\sigma_0+\delta_{l_1,j_1})$$
$$-(2\sigma_{l_2}-2\sigma_0+\delta_{l_2,j_2})]. \quad (24)$$

Adding (17), (23), and (24), and introducing $\psi_l\equiv\sigma_l-\sigma_0$ the differential cross section becomes

$$d\sigma/d\Omega=(d\sigma/d\Omega)_{\text{Coul}}+(d\sigma/d\Omega)_{\text{int}}+(d\sigma/d\Omega)_{\text{nucl}}$$
$$=(ZZ'e^2/2mv^2)^2\csc^4\theta/2-(\lambda^2\eta/2)\csc^2(\theta/2)$$
$$\times\sum_{l=0}^{\infty}\sum_{j=|l-\frac{1}{2}|}^{|l+\frac{1}{2}|}(2j+1)P_l(\cos\theta)\sin\delta_{l,j}$$
$$\times\cos(2\eta\ln\sin\theta/2+2\psi_l+\delta_{l,j})$$
$$+(\lambda^2/2)\sum_{L=|l_1-l_2|}^{|l_1+l_2|}\sum_{l_1=0}^{\infty}\sum_{l_2=0}^{\infty}\sum_{j_1=|l_1-\frac{1}{2}|}^{|l_1+\frac{1}{2}|}\sum_{j_2=|l_2-\frac{1}{2}|}^{|l_2+\frac{1}{2}|}$$
$$\times Z^2(l_1j_1l_2j_2;\tfrac{1}{2},L)P_L(\cos\theta)\sin\delta_{l_1,j_1}\sin\delta_{l_2,j_2}$$
$$\times\cos[(2\psi_{l_1}+\delta_{l_1,j_1})-(2\psi_{l_2}+\delta_{l_2,j_2})]. \quad (25)$$

III. WEIGHT FUNCTION

Before we can take moments of the differential cross section which involve integrating over θ from 0 to π, we must ascertain whether our expression [formula (25)] lends itself to such treatment. Clearly it does not, as it now stands, for the Coulomb contribution $d\sigma/d\Omega_{\text{Coul}}=(ZZ'e^2/2mv^2)^2\csc^4\theta/2$ diverges and is not applicable at small angles $\theta\to0$. This failing may, however, be corrected without any difficulty, for it is a simple matter to subtract the Coulomb cross section from both sides of Eq. (25).

In the theoretical expression (on the right side of the equation), this subtraction is possible because the cross-section is explicitly given as the sum of Coulomb, interference, and nuclear terms, in contrast to the traditional formulation in which one is usually faced with the ratio of the Coulomb contribution to the whole. In the experimental expression (on the left side of the equation), the subtraction may simply be performed at each net point of the angular distribution curve, since $(d\sigma/d\Omega)_{\text{Coul}}$ is known everywhere. Thus, we obtain a new curve and a modified differential cross section

$$d\sigma'/d\Omega=d\sigma/d\Omega_{\text{int}}+d\sigma/d\Omega_{\text{nucl}}$$
$$=-\lambda^2\eta/2\csc^2\theta/2\cdot\sum_{l=0}^{\infty}\sum_{j=|l-\frac{1}{2}|}^{|l+\frac{1}{2}|}(2j+1)P_l(\cos\theta)$$
$$\times\sin\delta_{lj}\cos(2\eta\ln\sin\theta/2+2\psi_l+\delta_{lj})$$
$$+\lambda^2/2\sum_{L=|l_1-l_2|}^{|l_1+l_2|}\sum_{l_1=0}^{\infty}\sum_{l_2=0}^{\infty}\sum_{j_1=|l_1-\frac{1}{2}|}^{|l_1+\frac{1}{2}|}\sum_{j_2=|l_2-\frac{1}{2}|}^{|l_2+\frac{1}{2}|}$$
$$\times Z^2(l_1j_1l_2j_2;\tfrac{1}{2},L)P_L(\cos\theta)\sin\delta_{l_1,j_1}\sin\delta_{l_2,j_2}$$
$$\times\cos[(2\psi_{l_1}+\delta_{l_1,j_1})-(2\psi_{l_2}+\delta_{l_2,j_2})]. \quad (26)$$

Our difficulties, are, however, not yet all removed. Equation (26) still contains a Coulomb amplitude in the interference term. This Coulomb amplitude makes the modified differential cross section diverge at small angles θ, or, putting it another way, the theoretical expression is incorrect for these small angles near the forward direction, for which shielding needs to be taken into account. The critical angle below which shielding becomes important and (26) is no longer valid is given by[10] $\theta_{\text{crit}}=\lambda/r$ where r is the screening radius. For proton-alpha scattering at moderate energies, this angle is of order 10^{-4} radian.

There is, however, another effect which completely overshadows the theoretical difficulties encountered below the critical angle. This is the fact that for angles near the forward direction (which may be considerably

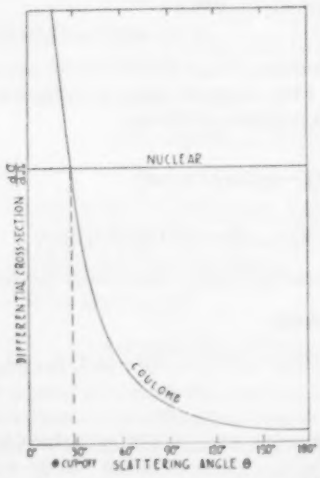

FIG. 1. Theoretical estimate for the cut-off angle θ. The criterion is that the "pure" Coulomb cross section overtake the "pure" nuclear cross section. (The ordinate is not drawn to linear scale, i.e., the Coulomb cross section rises faster than shown.)

[10] W. T. Mott and H. S. W. Massey, *Theory of Atomic Collisions* (Oxford University Press, New York, 1933).

larger than the critical angle) it is experimentally impossible to obtain cross-section data.[11] The cut-off angle, below which no data are available, varies with the parameters of the experiment and with the skill of the experimenter. A theoretical estimate of the cut-off angle, which is in the nature of an upper limit, may be obtained by defining θ_{cutoff} as the angle at which, moving towards $\theta=0$, the Coulomb cross section overtakes the "pure" nuclear cross section in magnitude (see Fig. 1). Setting $d\sigma/d\Omega_{Coul}=d\sigma/d\Omega_{nucl}$ and assuming for this estimate the presence of only an S wave ($l=0$) nuclear phase shift, we have from (25)[12]:

$$(ZZ'e^2/2mv^2)^2 \csc^4\theta/2=\lambda^2 \sin^2\delta_0.$$

Taking for our estimate $\delta_0=90°$ and using (4), we obtain $\theta_{cutoff}\cong(2\eta)^{\frac{1}{2}}$. To cite an illustration, for alpha-proton scattering at an incident energy of 5.78 Mev in the laboratory system, this calculation yields $\theta_{cutoff}\cong 29°$. In their recent work at this energy, Kreger, Jentschke, and Kruger[13] have been able to take measurements for angles as low as 16.13°.

To overcome the difficulty of the absence of data at small angles, two possibilities seem to present themselves. One is to select as the lower limit of integration in both the numerical work and the theoretical expression not 0°, but a larger angle, say θ_{cutoff}. This method has the disadvantage of discontinuity in that all data above θ_{cutoff} would be counted fully and all data below θ_{cutoff} would be discounted completely, and of small usefulness, in that the variation of θ_{cutoff} from problem to problem would necessitate the substitution of a new limit of integration for each case.

The other device is the introduction into every integrand of a weight function which has the property of discounting the contributions to the cross section from the region below θ_{cutoff} in a continuous manner until only a negligible contribution is derived from the region for which no data exist, and which is of such a form as to remove the $\theta=0$ divergence in the theoretical expression.

A little reflection shows that an ideal weight function should satisfy the following four criteria:

(1) As θ goes to 0, the weight function should go to 0 at least as fast as $\sin^2\theta/2$, for $\theta<\theta_{cutoff}$. This will not only allow us to disregard, in the numerical integration, contributions from the nonmeasured region, but will also make the integrand in the interference term of the theoretical expression finite everywhere. (Actually, inasmuch as the integrating factors which will be introduced in the taking of the moments will all contain the factor $\sin\theta$, a fall-off at least as fast as $\sin\theta/2$ would suffice.)

[11] This is another point which Fluegge seems to have overlooked.
[12] The value for the Z coefficient and the values for all other Racah coefficients in this paper are taken from L. C. Biedenharn, *Tables of the Racah Coefficients* (Oak Ridge National Laboratory, Oak Ridge, 1952).
[13] Kreger, Jentschke, and Kruger, Phys. Rev. **93**, 837 (1954).

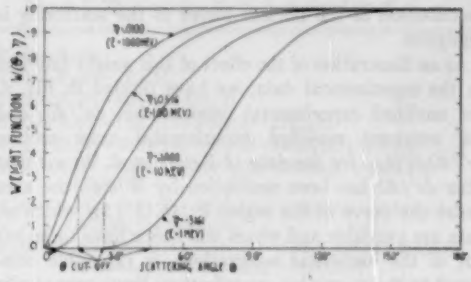

FIG. 2. The weight function

$$W(\theta,\eta)=\exp\left[-\left(2\ln\sin\frac{\theta}{2}\Big/\ln\eta\right)^2\right]$$

versus the scattering angle θ, for several values of E. E is the incident energy, in the laboratory system for $p-\alpha$ scattering, η the corresponding Coulomb factor. The theoretical cut-off angle is shown for each case.

(2) The weight function should go to 1 for $\theta>\theta_{cutoff}$. The reason for this requirement is that we desire to avoid selective distortion of the cross-section data in the measured region.

(3) The weight function should go to 1 as η goes to 0 for all values of θ. η going to 0 results from either high energy, or small charge, or both, and is physically equivalent to a diminished Coulomb effect, and hence improved measurement possibilities in the forward direction.

(4) The weight function should be of such a nature that the moment integrations involving it, the integrating factors, and the modified differential cross section can be carried out in terms of known, tabulated functions.

Criterion (3) necessitates that the weight function depend on η as well as on θ. Criterion (1) can be satisfied by a weight function which has an appropriate exponential dependence on θ. Criterion (4) indicates that the variable in the exponent should be raised to a power no higher than the second. We examined several possible weight functions and selected as the best suited

$$W(\theta,\eta)=\exp\left[-\left(2\ln\sin\frac{\theta}{2}\Big/\ln\eta\right)^2\right]. \qquad (27)$$

In Fig. 2 we have plotted $W(\theta,\eta)$ against θ for several representative values of η. Inspection of this figure and of the form of (27) offers proof that our weight function satisfies the first three criteria. The proof of the satisfaction of the criterion of integrability must be sought and is found in the actual integrations. (See Sec. IV.)

Examination of (27) reveals that as η approaches 1 from below, $W(\theta,\eta)$ approaches 0 for all values of θ. This means that our method is useless for any problem in which $\eta\geq 1$. This discovery is neither surprising, nor disturbing. For in an experiment for which $\eta\geq 1$ (for proton-alpha scattering this corresponds to an incident energy $E\leq 0.1$ Mev) the Coulomb cross section predominates practically everywhere (see Fig. 3) and the

contribution of the nuclear forces to the scattering is negligible.

As an illustration of the effect of this weight function on the experimental data, we have plotted in Fig. 4, the modified experimental cross section $d\sigma'/d\Omega$, and the weighted modified experimental cross section $d\sigma'/d\Omega\, W(\theta,\eta)$ for the data of Kreger *et al.* We see that after $d\sigma'/d\Omega$ has been multiplied by $W(\theta,\eta)$, the area under the curve in the region $\theta < 16.13°$, for which no data are available and which will hence have to be left out of the numerical integrations, is negligible compared to the remaining contribution. Furthermore, the uncertainties in $d\sigma'/d\Omega$ increase as θ decreases, whereas the (weighted) uncertainties in $d\sigma'/d\Omega\, W(\theta,\eta)$ are much more nearly independent of θ.

The point may be made that there is an absence of experimental data not only for θ near 0° but also near 180°. This, however, causes no trouble since the experimental curve may easily be extrapolated in the region near 180°. If the accuracy of this extrapolation is questioned, it may always be improved by an iteration process; i.e., the phase shifts obtained in the manner to be discussed may be substituted back into (26) to give a more accurate extrapolated curve near 180°; improved phase shifts may then be computed, and the iteration repeated until there is no significant change.

We have now reached the point where we must select the set of integrating factors with which the different moments of the modified differential cross section will be obtained. The presence already of Legendre polynomials in (26) suggests the choice of the set of Legendre polynomials in the taking of the moments. Accordingly, we shall take as our integrating factors the set $P_\Lambda(\cos\theta)\times\sin\theta$. Thus, we obtain the moment equations

$$\begin{aligned}
&\int_0^\pi d\sigma'/d\Omega\, W(\theta,\eta) P_\Lambda(\cos\theta)\sin\theta d\theta \\
&= -(\lambda^2\eta/2)\Big\{\int_0^\pi \csc^2(\theta/2) \\
&\quad\times\exp\Big[-\Big(2\ln\sin\frac{\theta}{2}\Big/\ln\eta\Big)^2\Big] P_\Lambda(\cos\theta)\sin\theta d\theta \\
&\quad\times\sum_{l=0}^{\infty}\sum_{j=|l-\frac12|}^{l+\frac12}(2j+1)P_l(\cos\theta)\sin\delta_{l,j} \\
&\quad\times\cos(2\eta\ln\sin\theta/2+2\psi_l+\delta_{l,j})\Big\} \\
&\quad+(\lambda^2/2)\Big\{\int_0^\pi \exp\Big[-\Big(2\ln\sin\frac{\theta}{2}\Big/\ln\eta\Big)^2\Big] \\
&\quad\times P_\Lambda(\cos\theta)\sin\theta d\theta \sum_{L=|l_1-l_2|}^{l_1+l_2}\sum_{l_1=0}^{\infty}\sum_{l_2=0}^{\infty}\sum_{j_1=|l_1-\frac12|}^{l_1+\frac12}\sum_{j_2=|l_2-\frac12|}^{l_2+\frac12} \\
&\quad\times Z^2(l_1j_1l_2j_2;\tfrac12,L)^2 P_L(\cos\theta)\sin\delta_{l_1,j_1}\sin\delta_{l_2,j_2} \\
&\quad\times\cos[(2\psi_{l_1}+\delta_{l_1,j_1})-(2\psi_{l_2}+\delta_{l_2,j_2})]\Big\}. \qquad (28)
\end{aligned}$$

If we assume n nonzero nuclear phase shifts $\delta_{0,\frac12}$, $\delta_{1,\frac12}$, $\delta_{1,\frac32}\cdots\delta_{L,j}\cdots\delta_{(n-1)/2,\,n/2}$, we shall let Λ range from 0 to $n-1$, thus giving us n moment equations. As already pointed out, the integrations of the experimental data on the left side of the equations are to be carried out numerically; we shall denote the resulting numbers by Γ_Λ. The results of the theoretical integrations on the right side will be the functions F_Λ, which will depend on the nuclear phase-shifts δ_{lj} and on the parameter η. We thus arrive at the n simultaneous equations

$$\Gamma_\Lambda = F_\Lambda(\delta_{0,\frac12},\delta_{1,\frac12},\delta_{1,\frac32},\cdots\delta_{L,j},\cdots\delta_{(n-1)/2,\,n/2};\eta), \qquad (29)$$

where $\Lambda=0,\ 1,\ \cdots n-1$.

IV. THEORETICAL INTEGRATIONS

We shall indicate the general method for carrying out the theoretical integrations of (29) and we shall tabulate the functions F_Λ for one, three, and five assumed nonzero phase shifts. These functions F_Λ will then be completely specified save for the substitution into any given problem, of the numerical values for the parameters η and λ.

Let us first work on the "nuclear" contribution to the F_Λ in (29):

$$\begin{aligned}
F_\Lambda(\text{nucl}) &= (\lambda^2/2)\Big\{\int_0^\pi \exp\Big[-\Big(2\ln\sin\frac{\theta}{2}\Big/\ln\eta\Big)^2\Big] \\
&\quad\times P_\Lambda(\cos\theta)\sin\theta d\theta \sum_L\sum_{l_1}\sum_{l_2}\sum_{j_1}\sum_{j_2} Z^2(l_1j_1l_2j_2;\tfrac12,L) \\
&\quad\times P_L(\cos\theta)\sin\delta_{l_1,j_1}\sin\delta_{l_2,j_2} \\
&\quad\times\cos[(2\psi_{l_1}+\delta_{l_1,j_1})-(2\psi_{l_2}+\delta_{l_2,j_2})]\Big\}. \qquad (30)
\end{aligned}$$

We change the variable of integration by putting $x=-\ln\sin(\theta/2)$, we let $\omega=\frac12\ln\eta$, and we use the superposition principle of spherical harmonics

$$P_\Lambda(\cos\theta)\cdot P_L(\cos\theta)=\sum_{N=|\Lambda-L|}^{|\Lambda+L|}(\Lambda L00|\Lambda LN0)^2 P_N(\cos\theta).$$

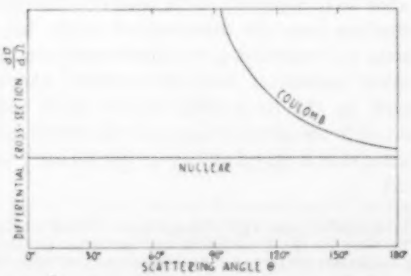

FIG. 3. Relative nuclear and Coulomb contributions to the differential scattering cross section at very low energies ($\eta>1$).

This yields

$$F_A(\text{nucl})=2\lambda^2\sum_{N=|\Delta-L|}^{|\Delta+L|}\sum_L\sum_{l_1}\sum_{l_2}\sum_{j_1}\sum_{j_2}\times(\Delta L00|\Delta LN0)^2Z^2(l_1j_1l_2j_2;\tfrac{1}{2},L)^2\sin\delta_{l_1,j_1}\times\sin\delta_{l_2,j_2}\cos[(2\psi_{l_1}+\delta_{l_1,j_1})-(2\psi_{l_2}+\delta_{l_2,j_2})]\times\int_0^\infty\exp[-(x/\omega)^2-2x]\times P_N[1-2\exp(-2x)]dx. \quad (31)$$

We may conveniently write this as the sum of products of two factors, one of which contains the remaining summations and the other the integration over x:

$$F_A(\text{nucl})=\sum_{N=|\Delta-L|}^{|\Delta+L|}\mu_N H_N(\omega), \quad (32)$$

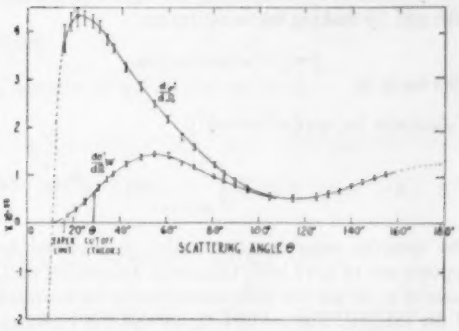

FIG. 4. The nonweighted and the weighted modified differential scattering cross sections for the data of Kreger.[13] $d\sigma'/d\Omega$ is the modified differential cross section, i.e., the differential cross section minus the "pure" Coulomb contribution, W is the weight function

$$W(\theta,\eta)=\exp\left[-\left(2\ln\sin\frac{\theta}{2}\Big/\ln\eta\right)^2\right].$$

The solid curves were obtained from the experimental data, the broken curves are extrapolations.

where

$$\mu_N=2\lambda^2\sum_L\sum_{l_1}\sum_{l_2}\sum_{j_1}\sum_{j_2}(\Delta L00|\Delta LN0)^2\times Z^2(l_1j_1l_2j_2;\tfrac{1}{2},L)^2\sin\delta_{l_1,j_1}\sin\delta_{l_2,j_2}\times\cos[(2\psi_{l_1}+\delta_{l_1,j_1})-(2\psi_{l_2}+\delta_{l_2,j_2})] \quad (33)$$

and

$$H_N(\omega)=\int_0^\infty P_N[1-2\exp(-2x)]\times\exp[-(x/\omega)^2-2x]dx. \quad (34)$$

The factors μ_N may be computed with a knowledge of the Clebsch-Gordan coefficients $(\Delta L00|\Delta LN0)$ and the Racah coefficients $Z(l_1j_1l_2j_2;\frac{1}{2},L)$. Some of the necessary Clebsch-Gordan coefficients we obtained from the tables in Condon and Shortley,[7] and the others we calculated with the use of the formula given by the same source; the Racah coefficients were taken from Biedenharn's tables.[12] The determination of the $H_N(\omega)$ seemingly involves separate integrations for each value of N. We can, however, find a useful recursion formula, by introducing the more general expression

$$H_N(\omega,t)=\int_0^\infty P_N[1-2\exp(-2x)]\times\exp[-(x/\omega)^2-2(1+t)x]dx. \quad (35)$$

Since the Legendre polynomials obey the recursion relation

$$(N+1)P_{N+1}[1-2\exp(-2x)]-(2N+1)\times[1-2\exp(-2x)]P_N[1-2\exp(-2x)]+NP_{N-1}[1-2\exp(-2x)]=0, \quad (36)$$

it is easily proved that

$$H_N(\omega,t)=[(2N-1)/N]H_{N-1}(\omega,t)-2[(2N-1)/N]H_{N-1}(\omega,t+1)-[(N-1)/N]H_{N-2}(\omega,t). \quad (37)$$

We observe that $H_1(\omega,t)$ depends only on $H_0(\omega,t)$ and on $H_0(\omega,t+1)$. It is therefore sufficient to obtain the values of $H_0(\omega,t)$ for $t=0, 1, 2, 3, \cdots N$ in order to find any desired $H_N(\omega,0)$. We list, for convenient reference, in Table I, the expressions for the first nine $H_N(\omega,0)$, obtained by repeated application of Eq. (37). In this tabulation, and in all tables to follow, we suppress the dependence of the H's on ω.

The evaluation of the one necessary integral

$$H_0(\omega,t)=\int_0^\infty P_0[1-2\exp(-2x)]\times\exp[-(x/\omega)^2-2(1+t)x]dx=\int_0^\infty\exp[-(x/\omega)^2-2(1+t)x]dx \quad (38)$$

is accomplished by completing the square in the exponent and by making the substitution

$$y=[x+\omega^2(1+t)]/\omega.$$

TABLE I. The first nine $H_N(0)$ in terms of the $H_0(t)$.

$H_0(0)=H_0(0)$
$H_1(0)=H_0(0)-2H_0(1)$
$H_2(0)=H_0(0)-6H_0(1)+6H_0(2)$
$H_3(0)=H_0(0)-12H_0(1)+30H_0(2)-20H_0(3)$
$H_4(0)=H_0(0)-20H_0(1)+90H_0(2)-140H_0(3)+70H_0(4)$
$H_5(0)=H_0(0)-30H_0(1)+210H_0(2)-560H_0(3)+630H_0(4)-252H_0(5)$
$H_6(0)=H_0(0)-42H_0(1)+420H_0(2)-1680H_0(3)+3150H_0(4)-2772H_0(5)+924H_0(6)$
$H_7(0)=H_0(0)-56H_0(1)+756H_0(2)-4200H_0(3)+11\,550H_0(4)-16\,632H_0(5)+12\,012H_0(6)-3432H_0(7)$
$H_8(0)=H_0(0)-72H_0(1)+1260H_0(2)-9240H_0(3)+34\,650H_0(4)-72\,072H_0(5)+84\,084H_0(6)-51\,480H_0(7)+12\,870H_0(8)$

This leads to

$$H_0(\omega,t)=|\omega|\exp[\omega^2(1+t)^2]\int_{|\omega|(1+t)}^{\infty}\exp(-y^2)dy, \quad (39)$$

which we write

$$H_0(\omega,t)=|\omega|\exp[\omega^2(1+t)^2][\pi^{\frac{1}{2}}/2][1-\Phi(\omega,t)], \quad (40)$$

where

$$\Phi(\omega,t)=2\pi^{-\frac{1}{2}}\int_0^{|\omega|(1+t)}\exp(-y^2)dy \quad (41)$$

is the error function which has been widely tabulated.[14]

With respect to the interference term in (29), viz.,

$$F_A(\text{int})=-(\lambda^2\eta/2)\left\{\int_0^{\pi}\csc^2\theta/2\times\exp\left[-\left(2\ln\sin\frac{\theta}{2}\Big/\ln\eta\right)^2\right]P_A(\cos\theta)\sin\theta d\theta\times\sum_l\sum_j(2j+1)P_l(\cos\theta)\sin\delta_{L,j}\times\cos(2\eta\ln\sin\theta/2+2\psi_l+\delta_{L,j})\right\} \quad (42)$$

we take similar steps. The resulting expression may then be written

$$F_A(\text{int})=\text{R.P.}\Big[-2\lambda^2\eta\sum_{N=|\Lambda-l|}^{|\Lambda+l|}\sum_l\sum_j(\Lambda l00|\Lambda lN0)^2\times(2j+1)\sin\delta_{L,j}\exp[i(2\psi_l+\delta_{L,j})]\times\int_0^{\infty}\exp[(-x/\omega)^2-2i\eta x]\times P_N[1-2\exp(-2x)]dx\Big]. \quad (43)$$

Analogously to the nuclear case, this is expressed as

$$F_A(\text{int})=\text{R.P.}\Big[\sum_{N=|\Lambda-l|}^{|\Lambda+l|}v_NK_N(\omega,\eta)\Big], \quad (44)$$

where

$$v_N=-2\lambda^2\eta\sum_l\sum_j(\Lambda l00|\Lambda lN0)^2\times(2j+1)\sin\delta_{L,j}\exp[i(2\psi_l+\delta_{L,j})] \quad (45)$$

and

$$K_N(\omega,\eta)=\int_0^{\infty}P_N[1-2\exp(-2x)]\times\exp[-(x/\omega)^2-2i\eta x]dx. \quad (46)$$

[14] For example in *Tables of the Error Function and of Its First Twenty Derivatives* (Harvard University Press, Cambridge, 1952). The tables are, however, useless for $|\omega|(1+t)>3$. For those cases the asymptotic expansion of the error function works satisfactorily. It gives the value of $H_0(\omega,t)$ directly:

$$H_0(\omega,t)=2^{-1}(t+1)^{-1}\Big[1+\sum_{k=1}^{\infty}(-1)^k(1\times3\times5\times\cdots\times2k-1)2^{-k}\times\omega^{-2k}(t+1)^{-2k}\Big].$$

As before, we can find the successive K's by using a recursion formula for the more general expression

$$K_N(\omega,\eta,u)=\int_0^{\infty}P_N[1-2\exp(-2x)]\times\exp[-(x/\omega)^2-2(i\eta+u)x]dx. \quad (47)$$

Since here $i\eta+u$ plays the same role as $1+t$ in (35), expression (36) allows us to obtain a recursion scheme for the $K_N(\omega,\eta,0)$ which is completely analogous to that for the $H_N(\omega,0)$ given in Table I. In order to find the value of any desired $K_N(\omega,\eta,0)$ it is thus sufficient to carry out the integrations which yield $K_0(\omega,\eta,u)$ for $u=0, 1, 2, \cdots N$.

The evaluation of

$$K_0(\omega,\eta,u)=\int_0^{\infty}\exp[-(x/\omega)^2-2(i\eta+u)x]dx \quad (48)$$

is accomplished by completing the square in the exponent and by making the substitution

$$y=[x+\omega^2(i\eta+u)]/\omega.$$

This leads to

$$K_0(\omega,\eta,u)=|\omega|\exp[\omega^2(i\eta+u)^2]\times\int_{|\omega|(i\eta+u)}^{\infty}\exp(-y^2)dy. \quad (49)$$

The complex error function which is involved here appears not to have been tabulated. Depending on the value of u, we use two different series for the evaluation of the integral. For $u=0, 1, 2$, we use the converging expansion

$$K_0(\omega,\eta,u)=|\omega^2|\exp[(u^2-\eta^2+2iu\eta)\omega^2]\times\{(\pi^{\frac{1}{2}}/2)-\sum_{k=0}^{\infty}(-1)^k[(i\eta+u)\omega]^{2k+1}\times(k!)^{-1}(2k+1)^{-1}\}. \quad (50)$$

This may be written in the form

$$K_0(\omega,\eta,u)=K_0'(\omega,\eta,u)+iK_0''(\omega,\eta,u), \quad (51)$$

where the $K_0'(\omega,\eta,u)$ and the $K_0''(\omega,\eta,u)$ are both real, by expressing the complex number $i\eta+u$ as $(\eta^2+u^2)^{\frac{1}{2}}\times\cos\tan^{-1}\eta/u+i(\eta^2+u^2)^{\frac{1}{2}}\sin\tan^{-1}(\eta/u)$. Then

$$K_0'(\omega,\eta,u)=|\omega|\exp[(u^2-\eta^2)\omega^2]\{\cos(2u\eta\omega^2)\times[(\pi^{\frac{1}{2}}/2)-(\eta^2+u^2)^{\frac{1}{2}}|\omega|\sum_{k=0}^{\infty}(-1)^k(\eta^2+u^2)^k\omega^{2k}\times\cos[(2k+1)\tan^{-1}\eta/u](k!)^{-1}(2k+1)^{-1}]+\sin(2u\eta\omega^2)(\eta^2+u^2)^{\frac{1}{2}}|\omega|\sum_{k=0}^{\infty}(-1)^k(\eta^2+u^2)^k\omega^{2k}\times\sin[(2k+1)\tan^{-1}\eta/u](k!)^{-1}(2k+1)^{-1}\} \quad (52)$$

and

$$K_0''(\omega,\eta,u)=|\omega|\exp[(u^2-\eta^2)\omega^2]\{\sin(2u\eta\omega^2)\times[\pi^{\frac{1}{2}}/2-(\eta^2+u^2)^{\frac{1}{2}}|\omega|\sum_{k=0}^{\infty}(-1)^k(\eta^2+u^2)^k\omega^{2k}\times\cos[(2k+1)\tan^{-1}\eta/u](k!)^{-1}(2k+1)^{-1}]+\cos(2u\eta\omega^2)(\eta^2+u^2)^{\frac{1}{2}}|\omega|\sum_{k=0}^{\infty}(-1)^k(\eta^2+u^2)^k\omega^{2k}\times\sin[(2k+1)\tan^{-1}\eta/u](k!)^{-1}(2k+1)^{-1}\}. \quad (53)$$

About six terms must be taken in the summation over k to obtain four-digit accuracy. For $u>2$, the simpler asymptotic series may be used:

$$K_0(\omega,\eta,u)=(i\eta+u)^{-1}[1+\sum_{k=1}^{\infty}(-1)^k(1\times3\times5\cdots\times2k-1)\times[2(i\eta+u)^2\omega^2]^{-k}], \quad (54)$$

whence

$$K_0'(\omega,\eta,u)=(\eta^2+u^2)^{-\frac{1}{2}}\cos(\tan^{-1}\eta/u)+\sum_{k=1}^{\infty}(-1)^k(1\times3\times5\cdots\times2k-1)(\eta^2+u^2)^{-(2k+1)/2}\times(2\omega^2)^{-k}\cos[(2k+1)\tan^{-1}\eta/u] \quad (55)$$

and

$$K_0''(\omega,\eta,u)=-(\eta^2+u^2)^{-\frac{1}{2}}\sin(\tan^{-1}\eta/u)-\sum_{k=1}^{\infty}(-1)^k(1\times3\times5\cdots\times2k-1)(\eta^2+u^2)^{-(2k+1)/2}\times(2\omega^2)^{-k}\sin[(2k+1)\tan^{-1}\eta/u]. \quad (56)$$

Equation (44) may now be written

$$F_A(\text{int})=2\lambda^2\eta\sum_{N=|\Lambda-l|}^{|\Lambda+l|}\sum_{l}\sum_{j}(\Lambda l00|\Lambda lN0)^2(2j+1)\times\sin\delta_{Lj}\{\cos(2\psi_l+\delta_{lj})K_N'(\omega,\eta)-\sin(2\psi_l+\delta_{lj})K_N''(\omega,\eta)\}. \quad (57)$$

The $K_N'(\omega,\eta)$ and $K_N''(\omega,\eta)$ are given in terms of the $K_0'(\omega,\eta,u)$ and $K_0''(\omega,\eta,u)$ by the same recursion relations as the unprimed K's, and hence by expressions completely analogous to those of Table I.

TABLE II. Results of numerical integrations of the weighted moments of the modified differential cross section for the experimental data of Kreger *et al* (reference 13).

$\Gamma_0=$	1.745×10^{-25} cm^2
$\Gamma_1=$	0.1160
$\Gamma_2=$	−0.0189
$\Gamma_3=$	−0.2418
$\Gamma_4=$	−0.0694

All the tools are now at hand to calculate the functions F_A from Eqs. (32) and (57) for any given number of nonzero phase shifts. The F_A will be functions in the sines and cosines of the phase-shifts. For the purpose of the numerical solution of Eqs. (29) it is helpful to introduce the double angles $\rho_{Lj}=2\delta_{Lj}$.

Equations (29) then take the form

$$\Gamma_A/\lambda^2=F_A/\lambda^2=\sum_{l=0}^{(n-1)/2}\sum_{j=|l-\frac{1}{2}|}^{l+\frac{1}{2}}[a_A(lj)\sin\rho_{lj}+a_A'(lj)\cos\rho_{lj}]+\sum_{l_1=0}^{(n-1)/2}\sum_{l_2=0}^{(n-1)/2}\sum_{j_1=|l_1-\frac{1}{2}|}^{l_1+\frac{1}{2}}\times\sum_{j_2=|l_2-\frac{1}{2}|}^{l_2+\frac{1}{2}}[b_A(l_1j_1l_2j_2)\sin(\rho_{l_1,j_1}-\rho_{l_2,j_2})\times b_A'(l_1j_1l_2j_2)\cos(\rho_{l_1,j_1}-\rho_{l_2,j_2})]+c_A. \quad (58)$$

The index Λ, which designates the moment with which the integration was performed, runs from 0 to $n-1$. There are thus n such equations, which is also the number $2l-1$ of assumed nonzero phase shifts. The summation in the second term is restricted by the condition $l_1\geq l_2$, with the equality sign holding only for $j_1\neq j_2$. We note in passing that the ratio $a_A'(lj)/a_A(lj)$ is independent of j and that the ratio $b_A'(l_1j_1l_2j_2)/b_A(l_1j_1l_2j_2)$ is independent not only of j_1 and j_2 but also of the order of integration Λ. We have explicitly calculated the coefficients a, a', b, b', and c for one, three and five nonzero phase shifts. Results are given in the Appendix.

V. SOLUTION OF A PROBLEM

We have applied our method to the determination of the phase-shifts in a proton-alpha scattering experiment which was carried out by Kreger, Jentschke, and Kruger[13] at the University of Illinois cyclotron. The energy of the incident protons in the laboratory system was 5.78 Mev. This corresponds to values of the parameters $\eta=0.1314$ and $\lambda=2.731\times10^{-13}$ cm. Five nonzero phase shifts were assumed.

The numerical integrations of the weighted moments of the modified differential cross section were carried out both with a planimeter and with the aid of Simpson's rule, and the results agreed to 1 part in 500. These results, with the last digit representing a mean value of the two methods are given in Table II.

With the substitution of these numbers and of the values of the parameters η and λ into Eqs. (58) and into the appropriate coefficients a, a', b, b', and c, as given in the Appendix, we obtain a set of five simultaneous equations in ρ_0, ρ_{1-}, ρ_{1+}, ρ_{2-}, and ρ_{2+}. (The notation is that of the Appendix.) Since we know that the D-wave

TABLE III. Preliminary phase-shifts iteration for the data of Kreger (reference 13).

Order of iteration	ρ_0	ρ_{1-}	ρ_{1+}
0	−1.629	1.211	3.797
1	−1.645	1.269	3.848
2	−1.625	1.306	3.889
3	−1.629	1.329	3.905
4	−1.627	1.347	3.919
5	−1.624	1.361	3.930
6	−1.623	1.371	3.938
7	−1.622	1.378	3.944
8	−1.622	1.381	3.948
9	−1.621	1.383	3.950
10	−1.621	1.384	3.951

phase shifts are small, we may, as a first approximation, reduce the problem to the solution of three simultaneous equations. This is accomplished by setting aside the equations with $\Lambda=3$ and 4, and by letting ρ_{3-} and $\rho_{3+}=0$ in the equations with $\Gamma=0$, 1, and 2. This gives us three equations of the form (58).

These equations may be solved by an iterative process, in which initial values are assumed for ρ_0, ρ_{1-}, and ρ_{1+}, and successively better values are obtained by substituting the latest values of two of the ρ's into one of the equations, and solving it for a new value of the third ρ. It is of course advantageous to select a zeroth order set of ρ's which is as close as possible to the final values.

For our particular set of parameters the following iteration scheme gives the best convergence: For each order of the iteration we solve the $\Lambda=0$ equation for ρ_{1+}, the $\Lambda=1$ equation for ρ_0, and the $\Lambda=2$ equation for ρ_{1-}, in that order. For our zeroth-order estimate we selected the values obtained by Dodder and Gammel[2] for the neighboring energy of 5.82 Mev for three nonzero phase-shifts. Table III shows the progress of the iteration process.

The 10th and, for this part of the solution, final, order of iteration gives the following values for the phase-shifts: $\delta_0=-46.5°$, $\delta_{1-}=39.7°$, $\delta_{1+}=113.2°$.

TABLE IV. Final phase-shifts iteration for the data of Kreger.

Order of iteration	ρ_0	ρ_{1-}	ρ_{1+}	ρ_{2-}	ρ_{2+}
0	−1.621	1.384	3.951	0	0
1	−1.641	1.371	3.947	−0.021	−0.011
2	−1.658	1.367	3.945	−0.028	−0.015
3	−1.666	1.363	3.944	−0.032	−0.016
4	−1.670	1.359	3.944	−0.036	−0.016
5	−1.670	1.357	3.942	−0.039	−0.016
6	−1.671	1.355	3.942	−0.042	−0.017
7	−1.672	1.352	3.941	−0.044	−0.017
8	−1.672	1.351	3.941	−0.045	−0.017

We now use these results as our zeroth-order estimates for ρ_0, ρ_{1-}, and ρ_{1+} in the full set of five equations (58). As our zeroth-order estimate for ρ_{2-} and ρ_{2+} we still take ρ_{2-} and $\rho_{2+}=0$. The $\Lambda=0$, 1, and 2 equations are solved for the same unknowns as before; the $\Lambda=3$ equation is solved for ρ_{2-} and the $\Lambda=4$ equation is solved for ρ_{2+}. The iteration progresses as shown in Table IV.

The final (8th) order of iteration leads to the following results: $\delta_0=-47.9°$, $\delta_{1-}=38.7°$, $\delta_{1+}=112.9°$, $\delta_{2-}=-1.3°$, $\delta_{2+}=-0.49°$.

ACKNOWLEDGMENTS

We would like to thank Mrs. Jean Kellom and Mr. David Reiner who capably assisted with some of the calculations.

APPENDIX. RESULTS FOR ONE, THREE, AND FIVE PHASE SHIFTS

For one assumed nonzero phase shift (S wave only; all $\rho_{l,j}=0$, except $\rho_{0,\frac{1}{2}}\equiv\rho_0$) there is only one equation of the form (58):

$$\Gamma_0/\lambda^2=a_0(0)\sin\rho_0+a_0'(0)\cos\rho_0+c_0, \tag{59}$$

where

$$a_0(0)=-2\eta K_0'(0),\quad a_0'(0)=-2H_0(0)-2\eta K_0''(0),$$
$$c_0(0)=2H_0(0)+2\eta K_0''(0). \tag{60}$$

The cases which involve more than one nonzero phase-shift are of greater practical interest. We have explicitly calculated the coefficients a, a', b, b', and c as functions of the sole parameter η for the case of three phase-shifts (S, $P_{\frac{1}{2}}$, and $P_{\frac{3}{2}}$ waves) and for the case of five phase-shifts (S, $P_{\frac{1}{2}}$, $P_{\frac{3}{2}}$, $D_{\frac{3}{2}}$, and $D_{\frac{5}{2}}$ waves). The results are given in Table V and Table VI, respectively. For the three phase-shift case, we have put $\rho_{0,\frac{1}{2}}\equiv\rho_0$, $\rho_{1,\frac{1}{2}}\equiv\rho_{1-}$, $\rho_{1,\frac{3}{2}}\equiv\rho_{1+}$, all other $\rho_{l,j}=0$. For the five phase-shifts case, we have set $\rho_{0,\frac{1}{2}}\equiv\rho_0$, $\rho_{1,\frac{1}{2}}\equiv\rho_{1-}$, $\rho_{1,\frac{3}{2}}\equiv\rho_{1+}$, $\rho_{2,\frac{3}{2}}\equiv\rho_{2-}$, $\rho_{2,\frac{5}{2}}\equiv\rho_{2+}$, all other $\rho_{l,j}=0$.

As to the various functions of η which appear in these tables, the $H_0(t)$ are defined by Eq. (41), the $K_0'(u)$ by (52) and (55), and the $K_0''(u)$ by (53) and (56). The meaning of the remaining symbols is as follows:

$$\begin{aligned}
&\alpha=\sin2\psi_1=(2\eta)/(1+\eta^2),\\
&\alpha'=\cos2\psi_1=(1-\eta)^2/(1+\eta^2),\\
&\beta=\sin2\psi_2=(12\eta-6\eta^3)/(4+5\eta^2+\eta^4),\\
&\beta'=\cos2\psi_2=(4-13\eta^2+\eta^4)/(4+5\eta^2+\eta^4),\\
&\gamma=\sin(2\psi_2-2\psi_1)=(4\eta)/(4+\eta^2),\\
&\gamma'=\cos(2\psi_2-2\psi_1)=(4-\eta^2)/(4+\eta^2).
\end{aligned} \tag{61}$$

TABLE V. The coefficients $a_A(lj)$, $a_A'(lj)$, $b_A(l_1j_1l_2j_2)$, $b'(l_1j_1l_2j_2)$, and c_A for three phase shifts ρ_0, ρ_{1-}, ρ_{1+}.

$A=0$

$$a_0(0)=-6\alpha H_0(0)+12\alpha H_0(1)-2\eta K_0'(0)$$
$$a_0'(0)=-(2+6\alpha')H_0(0)+12\alpha' H_0(1)-2\eta K_0''(0)$$
$$a_0(1-)=2\alpha H_0(0)-4\alpha H_0(1)-2\eta\alpha' K_0'(0)+4\eta\alpha' K_0'(1)+2\eta\alpha K_0''(1)$$
$$a_0'(1-)=-(6+2\alpha')H_0(0)+(24+4\alpha')H_0(1)-24H_0(2)-2\eta\alpha K_0'(0)+4\eta\alpha K_0'(1)-2\eta\alpha' K_0''(0)+4\eta\alpha' K_0''(1)$$
$$a_0(1+)=2a_0(1-)$$
$$a_0'(1+)=2a_0'(1-)$$
$$b_0(0,1-)=2\alpha H_0(0)-4\alpha H_0(1)$$
$$b_0'(0,1-)=(\alpha'/\alpha)b_0(0,1-)$$
$$b_0(0,1+)=2b_0(0,1-)$$
$$b_0'(0,1+)=2b_0'(0,1-)$$
$$b_0(1-,1+)=4H_0(0)-24H_0(1)+24H_0(2)$$
$$c_0=(16+6\alpha')H_0(0)-(48+12\alpha')H_0(1)+48H_0(2)+6\eta\alpha K_0'(0)-12\eta\alpha K_0'(1)+(2\eta+6\eta\alpha')K_0''(0)-12\eta\alpha' K_0''(1)$$

$A=1$

$$a_1(0)=-6\alpha H_0(0)+24\alpha H_0(1)-24\alpha H_0(2)-2\eta K_0'(0)+4\eta K_0'(1)$$
$$a_1'(0)=-(2+6\alpha')H_0(0)+(4+24\alpha')H_0(1)-24\alpha' H_0(2)-2\eta K_0''(0)+4\eta K_0''(1)$$
$$a_1(1-)=2\alpha H_0(0)-8\alpha H_0(1)+8\alpha H_0(2)-2\eta\alpha' K_0'(0)+8\eta\alpha' K_0'(1)-8\eta\alpha' K_0'(2)+2\eta\alpha K_0''(0)-8\eta\alpha K_0''(1)+8\eta\alpha K_0''(2)$$
$$a_1'(1-)=-(6+2\alpha')H_0(0)+(36+8\alpha')H_0(1)-(72+8\alpha')H_0(2)+48H_0(3)-2\eta\alpha K_0'(0)+8\eta\alpha K_0'(1)-8\eta\alpha K_0'(2)-2\eta\alpha' K_0''(0)+8\eta\alpha' K_0''(1)-8\eta\alpha' K_0''(2)$$
$$a_1(1+)=2a_1(1-)$$
$$a_1'(1+)=2a_1'(1-)$$
$$b_1(0,1-)=2\alpha H_0(0)-8\alpha H_0(1)+8\alpha H_0(2)$$
$$b_0'(0,1-)=(\alpha'/\alpha)b_1(0,1-)$$
$$b_1'(0,1+)=2b_1(0,1-)$$
$$b_1(0,1+)=2b_1'(0,1-)$$
$$b_1(1-,1+)=0$$

$A=1$

$$b_1'(1-,1+)=4H_0(0)-32H_0(1)+72H_0(2)-48H_0(3)$$
$$c_1=(16+6\alpha')H_0(0)-(80+24\alpha')H_0(1)+(144+24\alpha')\times H_0(2)-96H_0(3)+6\eta\alpha K_0'(0)-24\eta\alpha K_0'(1)+24\eta\alpha K_0'(2)+(2\eta+6\eta\alpha')K_0''(0)-(4\eta+24\eta\alpha')\times K_0''(1)+24\eta\alpha' K_0''(2)$$

$A=2$

$$a_2(0)=-6\alpha H_0(0)+48\alpha H_0(1)-108\alpha H_0(2)+72\alpha H_0(3)-2\eta K_0'(0)+12\eta K_0'(1)-12\eta K_0'(2)$$
$$a_2'(0)=-(2+6\alpha')H_0(0)+(12+48\alpha')H_0(1)-(12+108\alpha')\times H_0(2)+72\alpha' H_0(3)-2\eta K_0''(0)+12\eta K_0''(1)-12\eta K_0''(2)$$
$$a_2(1-)=2\alpha H_0(0)-16\alpha H_0(1)+36\alpha H_0(2)-24\alpha H_0(3)-2\eta\alpha' K_0'(0)+16\eta\alpha' K_0'(1)-36\eta\alpha' K_0'(2)+24\eta\alpha' K_0'(3)+2\eta\alpha K_0''(0)-16\eta\alpha K_0''(1)+36\eta\alpha K_0''(2)-24\eta\alpha K_0''(3)$$
$$a_2'(1-)=-(6+2\alpha')H_0(0)+(60+16\alpha')H_0(1)-(204+36\alpha')\times H_0(2)+(288+24\alpha')H_0(3)-144H_0(4)-2\eta\alpha K_0'(0)+16\eta\alpha K_0'(1)-36\eta\alpha K_0'(2)+24\eta\alpha K_0'(3)-2\eta\alpha' K_0''(0)+16\eta\alpha' K_0''(1)-36\eta\alpha' K_0''(2)+24\eta\alpha' K_0''(3)$$
$$a_2(1+)=2a_2(1-)$$
$$a_2'(1+)=2a_2'(1-)$$
$$b_2(0,1-)=2\alpha H_0(0)-16\alpha H_0(1)+36\alpha H_0(2)-24\alpha H_0(3)$$
$$b_2'(0,1-)=(\alpha'/\alpha)b_2'(0,1-)$$
$$b_2(0,1+)=2b_2(0,1-)$$
$$b_2'(0,1+)=2b_2'(0,1-)$$
$$b_2(1-,1+)=0$$
$$b_2'(1-,1+)=4H_0(0)-48H_0(1)+192H_0(2)-288H_0(3)+144H_0(4)$$
$$c_2=(16+6\alpha')H_0(0)-(144+48\alpha')H_0(1)+(432+108\alpha')\times H_0(2)-(576+72\alpha')H_0(3)+288H_0(4)+6\eta\alpha K_0'(0)-48\eta\alpha K_0'(1)+108\eta\alpha K_0'(2)-72\eta\alpha K_0'(3)+(2\eta+6\eta\alpha')K_0''(0)-(12\eta+48\eta\alpha')K_0''(1)+(12\eta+108\eta\alpha')K_0''(2)-72\eta\alpha' K_0''(3)$$

TABLE VI. The coefficients $a_A(lj)$, $a_A'(lj)$, $b_A(l_1j_1l_2j_2)$, $b_A'(l_1j_1l_2j_2)$, and c_A for five phase shifts ρ_0, ρ_{1-}, ρ_{1+}, ρ_{2-}, ρ_{2+}.

$A=0$

$$a_0(0)=-(6\alpha+10\beta)H_0(0)+(12\alpha+60\beta)H_0(1)-60\beta H_0(2)-2\eta K_0'(0)$$
$$a_0'(0)=-(2+6\alpha'+10\beta')H_0(0)+(12\alpha'+60\beta')H_0(1)-60\beta' H_0(2)-2\eta K_0''(0)$$
$$a_0(1-)=(2\alpha-10\gamma)H_0(0)-(4\alpha-80\gamma)H_0(1)-180\gamma H_0(2)+120\gamma H_0(3)-2\eta\alpha' K_0'(0)+4\eta\alpha' K_0'(1)+2\eta\alpha K_0''(0)-4\eta\alpha K_0''(1)$$
$$a_0'(1-)=-(6+2\alpha'+10\gamma')H_0(0)+(24+4\alpha'+80\gamma')H_0(1)-(24+180\gamma')H_0(2)+120\gamma' H_0(3)-2\eta\alpha K_0'(0)+4\eta\alpha K_0'(1)-2\eta\alpha' K_0''(0)+4\eta\alpha' K_0''(1)$$
$$a_0(1+)=2a_0(1-)$$
$$a_0'(1+)=2a_0'(1-)$$
$$a_0(2-)=(4\beta+12\gamma)H_0(0)-(24\beta+96\gamma)H_0(1)+(24\beta+216\gamma)H_0(2)-144\gamma H_0(3)-4\eta\beta' K_0'(0)+24\eta\beta' K_0'(1)-24\eta\beta' K_0'(2)+4\eta\beta K_0''(0)-24\eta\beta K_0''(1)+24\eta\beta K_0''(2)$$
$$a_0'(2-)=-(20+4\beta'+12\gamma')H_0(0)+(240+24\beta'+96\gamma')H_0(1)-(960+24\beta'+216\gamma')H_0(2)+(1440+144\gamma')H_0(3)-720H_0(4)-4\eta\beta K_0'(0)+24\eta\beta K_0'(1)-24\eta\beta K_0'(2)-4\eta\beta' K_0''(0)+24\eta\beta' K_0''(1)-24\eta\beta' K_0''(2)$$

$A=0$

$$a_0(2+)=\tfrac{1}{3}a_0(2-)$$
$$a_0'(2+)=\tfrac{1}{3}a_0'(2-)$$
$$b_0(0,1-)=2\alpha H_0(0)-4\alpha H_0(1)$$
$$b_0'(0,1-)=(\alpha'/\alpha)b_0(0,1-)$$
$$b_0(0,1+)=2b_0(0,1-)$$
$$b_0'(0,1+)=2b_0'(0,1-)$$
$$b_0(1-,1+)=0$$
$$b_0'(1-,1+)=4H_0(0)-24H_0(1)+24H_0(2)$$
$$b_0(0,2-)=\beta b_0'(1-,1+)$$
$$b_0'(0,2-)=\beta' b_0'(1-,1+)$$
$$b_0(0,2+)=\tfrac{1}{3}b_0(0,2-)$$
$$b_0'(0,2+)=\tfrac{1}{3}b_0'(0,2-)$$
$$b_0(1-,2-)=4\gamma H_0(0)-8\gamma H_0(1)$$
$$b_0'(1-,2-)=(\gamma'/\gamma)b_0(1-,2-)$$
$$b_0(1+,2-)=8\gamma H_0(0)-88\gamma H_0(1)+216\gamma H_0(2)-144\gamma H_0(3)$$
$$b_0'(1+,2-)=(\gamma'/\gamma)b_0(1+,2-)$$
$$b_0(1-,2+)=6\gamma H_0(0)-72\gamma H_0(1)180\gamma H_0(2)-120\gamma H_0(3)$$
$$b_0'(1-,2+)=(\gamma'/\gamma)b_0(1-,2+)$$
$$b_0(1+,2+)=12\gamma H_0(0)-72\gamma H_0(1)+144\gamma H_0(2)-96\gamma H_0(3)$$
$$b_0'(1+,2+)=(\gamma'/\gamma)b_0(1+,2+)$$

TABLE VI.—*Continued.*

$\Lambda=0$

$$b_0(2-,2+)=0$$

$$b_0'(2-,2+)=12H_0(0)-216H_0(1)+936H_0(2)-1440H_0(3)+720H_0(4)$$

$$\begin{aligned}c_0=&(54+6\alpha'+10\beta'+30\gamma')H_0(0)-(432+12\alpha'+60\beta'+240\gamma')H_0(1)+(1512+60\beta'+540\gamma')H_0(2)\\&-(2160+360\gamma')H_0(3)+1080H_0(4)+(6\eta\alpha+10\eta\beta)\times K_0'(0)-(12\eta\alpha+60\eta\beta)K_0'(1)+60\eta\beta K_0'(2)\\&+(2\eta+6\eta\alpha'+10\eta\beta')K_0''(0)-(12\eta\alpha'+60\eta\beta')K_0''(1)+60\eta\beta' K_0''(2)\end{aligned}$$

$\Lambda=1$

$$\begin{aligned}a_1(0)=&-(6\alpha+10\beta)H_0(0)+(24\alpha+80\beta)H_0(1)-(24\alpha+180\beta)H_0(2)+120\beta H_0(3)-2\eta K_0'(0)+4\eta K_0'(1)\\a_1'(0)=&-(2+6\alpha'+10\beta')H_0(0)+(4+24\alpha'+80\beta')H_0(1)-(24\alpha'+180\beta')H_0(2)+120\beta' H_0(3)-2\eta K_0''(0)+4\eta K_0''(1)\\a_1(1-)=&(2\alpha-10\gamma)H_0(0)-(8\alpha-100\gamma)H_1(1)+(8\alpha-340\gamma)\times H_0(2)+480\gamma H_0(3)-240\gamma H_0(4)-2\eta\alpha' K_0'(0)+8\eta\alpha' K_0'(1)-8\eta\alpha' K_0'(2)+2\eta\alpha K_0''(0)-8\eta\alpha K_0''(1)+8\eta\alpha K_0''(2)\\a_1'(1-)=&-(6+2\alpha'+10\gamma')H_0(0)+(36+8\alpha'+100\gamma')H_0(1)-(72+8\alpha'+340\gamma')H_0(2)+(48+480\gamma')H_0(3)-240\gamma' H_0(4)-2\eta\alpha K_0'(0)+8\eta\alpha K_0'(1)-8\eta\alpha K_0'(2)-2\eta\alpha' K_0''(0)+8\eta\alpha' K_0''(1)-8\eta\alpha' K_0''(2)\\a_1(1+)=&2a_1(1-)\\a_1'(1+)=&2a_1'(1-)\\a_1(2-)=&(4\beta+12\gamma)H_0(0)-(32\beta+120\gamma)H_0(1)+(72\beta+408\gamma)\times H_0(2)-(48\beta+576\gamma)H_0(3)+288\gamma H_0(4)-4\eta\beta' K_0'(0)+32\eta\beta' K_0'(1)-72\eta\beta' K_0'(2)+48\eta\beta' K_0'(3)+4\eta\beta K_0''(0)-32\eta\beta K_0''(1)+72\eta\beta K_0''(2)-48\eta\beta K_0''(3)\\a_1'(2-)=&-(20+4\beta'+12\gamma')H_0(0)+(280+32\beta'+120\gamma')H_0(1)-(1440+72\beta'+408\gamma')H_0(2)+(3360+48\beta'+576\gamma')\times H_0(3)-(3600+288\gamma')H_0(4)+1440H_0(5)-4\eta\beta K_0'(0)+32\eta\beta K_0'(1)-72\eta\beta K_0'(2)+48\eta\beta K_0'(3)-4\eta\beta' K_0''(0)+32\eta\beta' K_0''(1)-72\eta\beta' K_0''(2)+48\eta\beta' K_0''(3)\end{aligned}$$

$$\begin{aligned}a_1(2+)=&\tfrac{1}{2}a_1(2-)\\a_1'(2+)=&\tfrac{1}{2}a_1'(2-)\\b_1(0,1-)=&2\alpha H_0(0)-8\alpha H_0(1)+8\alpha H_0(2)\\b_1'(0,1-)=&(\alpha'/\alpha)b_1(0,1-)\\b_1(0,1+)=&2b_1(0,1-)\\b_1'(0,1+)=&2b_1'(0,1-)\\b_1(1-,1+)=&0\\b_1'(1-,1+)=&4H_0(0)-32H_0(1)+72H_0(2)-48H_0(3)\\b_1(0,2-)=&\beta b_1'(1-,1+)\\b_1'(0,2-)=&\beta' b_1'(1-,1+)\\b_1(0,2+)=&\tfrac{1}{2}b_1(0,2-)\\b_1'(0,2+)=&\tfrac{1}{2}b_1'(0,2-)\\b_1(1-,2-)=&4\gamma H_0(0)-16\gamma H_0(1)+16\gamma H_0(2)\\b_1'(1-,2-)=&(\gamma'/\gamma)b_1(1-,2-)\\b_1(1+,2-)=&8\gamma H_0(0)-104\gamma H_0(1)+392\gamma H_0(2)-576\gamma H_0(3)+288\gamma H_0(4)\\b_1'(1+,2-)=&(\gamma'/\gamma)b_1(1+,2-)\\b_1(1-,2+)=&6\gamma H_0(0)-84\gamma H_0(1)+324\gamma H_0(2)-480\gamma H_0(3)+240\gamma H_0(4)\\b_1'(1-,2+)=&(\gamma'/\gamma)b_1(1-,2+)\\b_1(1+,2+)=&12\gamma H_0(0)-96\gamma H_0(1)+288\gamma H_0(2)-384\gamma H_0(3)+192\gamma H_0(4)\\b_1'(1+,2+)=&(\gamma'/\gamma)b_1(1+,2+)\end{aligned}$$

$\Lambda=1$

$$b_1(2-,2+)=0$$

$$b_1'(2-,2+)=12H_0(0)-240H_0(1)+1368H_0(2)-3312H_0(3)+3600H_0(4)-1440H_0(5)$$

$$\begin{aligned}c_1=&(54+6\alpha'+10\beta'+30\gamma')H_0(0)-(540+24\alpha'+80\beta'+300\gamma')H_0(1)+(2376+24\alpha'+180\beta'+1020\gamma')\times H_0(2)-(5184+120\beta'+1440\gamma')H_0(3)+(720\gamma'+5400)H_0(4)-2160H_0(5)+(6\eta\alpha+10\eta\beta)K_0'(0)-(24\eta\alpha+80\eta\beta)K_0'(1)+(24\eta\alpha+180\eta\beta)K_0'(2)-120\eta\beta K_0'(3)+(2\eta+6\eta\alpha'+10\eta\beta')K_0''(0)-(4\eta+24\eta\alpha'+80\eta\beta')K_0''(1)+(24\eta\alpha'+180\eta\beta')\times K_0''(2)-120\eta\beta' K_0''(3)\end{aligned}$$

$\Lambda=2$

$$\begin{aligned}a_2(0)=&-(6\alpha+10\beta)H_0(0)+(48\alpha+120\beta)H_0(1)-(108\alpha+480\beta)H_0(2)+(72\alpha+720\beta)H_0(3)-360\beta H_0(4)-2\eta K_0'(0)+12\eta K_0'(1)-12\eta K_0'(2)\\a_2'(0)=&-(2+6\alpha'+10\beta')H_0(0)+(12+48\alpha'+120\beta')H_0(1)-(12+108\alpha'+480\beta')H_0(2)+(72\alpha'+720\beta')H_0(3)-360\beta' H_0(4)-2\eta K_0''(0)+12\eta K_0''(1)-12\eta K_0''(2)\\a_2(1-)=&(2\alpha-10\gamma)H_0(0)-(16\alpha-140\gamma)H_0(1)+(36\alpha-720\gamma)\times H_0(2)-(24\alpha-1680\gamma)H_0(3)-1800\gamma H_0(4)+720\gamma H_0(5)-2\eta\alpha' K_0'(0)+16\eta\alpha' K_0'(1)-36\eta\alpha' K_0'(2)+24\eta\alpha' K_0'(3)+2\eta\alpha K_0''(0)-16\eta\alpha K_0''(1)+36\eta\alpha K_0''(2)-24\eta\alpha K_0''(3)\\a_2'(1-)=&-(6+2\alpha'+10\gamma')H_0(0)+(60+16\alpha'+140\gamma')H_0(1)-(204+36\alpha'+720\gamma')H_0(2)+(288+24\alpha'+1680\gamma')\times H_0(3)-(144+1800\gamma')H_0(4)+720\gamma' H_0(5)-2\eta\alpha K_0'(0)+16\eta\alpha K_0'(1)-36\eta\alpha K_0'(2)+24\eta\alpha K_0'(3)-2\eta\alpha' K_0''(0)+16\eta\alpha' K_0''(1)-36\eta\alpha' K_0''(2)+24\eta\alpha' K_0''(3)\end{aligned}$$

$$\begin{aligned}a_2(1+)=&2a_2(1-)\\a_2'(1+)=&2a_2'(1-)\\a_2(2-)=&(4\beta+12\gamma)H_0(0)-(48\beta+168\gamma)H_0(1)+(192\beta+864\gamma)H_0(2)-(288\beta+2016\gamma)H_0(3)+(144\beta+2160\gamma)H_0(4)-864\gamma H_0(5)-4\eta\beta' K_0'(0)+48\eta\beta' K_0'(1)-192\eta\beta' K_0'(2)+288\eta\beta' K_0'(3)-144\eta\beta' K_0'(4)+4\eta\beta K_0''(0)-48\eta\beta K_0''(1)+192\eta\beta K_0''(2)-288\eta\beta K_0''(3)+144\eta\beta K_0''(4)\\a_2'(2-)=&-(20+4\beta'+12\gamma')H_0(0)+(360+48\beta'+168\gamma')H_0(1)-(2520+192\beta'+864\gamma')H_0(2)+(8640+288\beta'+2016\gamma')H_0(3)-(15\,120+144\beta'+2160\gamma')H_0(4)+(12\,960+864\gamma')H_0(5)-4320H_0(6)-4\eta\beta K_0'(0)+48\eta\beta K_0'(1)-192\eta\beta K_0'(2)+288\eta\beta K_0'(3)-144\eta\beta K_0'(4)-4\eta\beta' K_0''(0)+48\eta\beta' K_0''(1)-192\eta\beta' K_0''(2)+288\eta\beta' K_0''(3)-144\eta\beta' K_0''(4)\end{aligned}$$

$$\begin{aligned}a_2(2+)=&\tfrac{1}{2}a_2(2-)\\a_2'(2+)=&\tfrac{1}{2}a_2'(2-)\\b_2(0,1-)=&2\alpha H_0(0)-16\alpha H_0(1)+36\alpha H_0(2)-24\alpha H_0(3)\\b_2'(0,1-)=&(\alpha'/\alpha)b_2(0,1-)\\b_2(0,1+)=&2b_2(0,1-)\\b_2'(0,1+)=&2b_2'(0,1-)\\b_2(1-,1+)=&0\\b_2'(1-,1+)=&4H_0(0)-48H_0(1)+192H_0(2)-288H_0(3)+144H_0(4)\\b_2(0,2-)=&\beta b_2'(1-,1+)\\b_2'(0,2-)=&\beta' b_2'(1-,1+)\\b_2(0,2+)=&\tfrac{1}{2}b_2(0,2-)\\b_2'(0,2+)=&\tfrac{1}{2}b_2'(0,2-)\\b_2(1-,2-)=&4\gamma H_0(0)-32\gamma H_0(1)+72\gamma H_0(2)-48\gamma H_0(3)\\b_2'(1-,2-)=&(\gamma'/\gamma)b_2(1-,2-)\end{aligned}$$

TABLE VI.—*Continued.*

A=2

$$b_2(1+,2-)=8\gamma H_0(0)-136\gamma H_0(1)+792\gamma H_0(2)-1968\gamma H_0(3)+2160\gamma H_0(4)-864\gamma H_0(5)$$
$$b_2'(1+,2-)=(\gamma'/\gamma)b_2(1+,2-)$$
$$b_2(1-,2+)=6\gamma H_0(0)-108\gamma H_0(1)+648\gamma H_0(2)-1632\gamma H_0(3)+1800\gamma H_0(4)-720\gamma H_0(5)$$
$$b_2'(1-,2+)=(\gamma'/\gamma)b_2(1-,2+)$$
$$b_2(1+,2+)=12\gamma H_0(0)-144\gamma H_0(1)+648\gamma H_0(2)-1392\gamma H_0(3)+1440\gamma H_0(4)-576\gamma H_0(5)$$
$$b_2'(1+,2+)=(\gamma'/\gamma)b_2(1+,2+)$$
$$b_2(2-,2)=0$$
$$b_2'(2-,2)=12H_0(0)-288H_0(1)+2304H_0(2)-8352H_0(3)\times 14\,976H_0(4)-12\,960H_0(5)+4320H_0(6)$$
$$c_2=(54+6\alpha'+10\beta'+30\gamma')H_0(0)-(756+48\alpha'+120\beta'+420\gamma')H_0(1)+(4428+108\alpha'+480\beta'+2160\gamma')+H_0(2)-(13\,824+72\alpha'+720\beta'+5040\gamma')H_0(3)+(23\,112+360\beta'+5400\gamma')H_0(4)-(19\,440+2160\gamma')H_0(5)+6480H_0(6)+(6\eta\alpha+10\eta\beta)K_0'(0)-(48\eta\alpha+120\eta\beta)K_0'(1)+(108\eta\alpha+480\eta\beta)K_0'(2)-(72\eta\alpha+720\eta\beta)K_0'(3)+360\eta\beta K_0'(4)+(2\eta+6\eta\alpha'+10\eta\beta')K_0''(0)-(12\eta+48\eta\alpha'+120\eta\beta')K_0''(1)+(12\eta+108\eta\alpha'+480\eta\beta')K_0''(2)-(72\eta\alpha'+720\eta\beta')\times K_0''(3)+360\eta\beta'K_0''(4)$$

A=3

$$a_2(0)=-(6\alpha+10\beta)H_0(0)+(84\alpha+180\beta)H_0(1)-(324\alpha+1080\beta)H_0(2)+(480\alpha+2720\beta)H_0(3)-(240\alpha+3000\beta)H_0(4)+1200\beta H_0(5)-2\eta K_0'(0)+24\eta K_0'(1)-60\eta K_0'(2)+40\eta K_0'(3)$$
$$a_2'(0)=-(2+6\alpha'+10\beta')H_0(0)+(24+84\alpha'+180\beta')H_0(1)-(60+324\alpha'+1080\beta')H_0(2)+(40+480\alpha'+2720\beta')H_0(3)-(240\alpha'+3000\beta')H_0(4)+1200\times H_0(5)-2\eta K_0''(0)+24\eta K_0''(1)-60\eta K_0''(2)+40\eta K_0''(3)$$
$$a_2(1-)=(2\alpha-10\gamma)H_0(0)-(28\alpha-200\gamma)H_0(1)+(108\alpha-1440\gamma)H_0(2)-(160\alpha-4880\gamma)H_0(3)+(80\alpha-8440\gamma)H_0(4)+7200\gamma H_0(5)-2400\gamma H_0(6)-2\eta\alpha'K_0'(0)+28\eta\alpha'K_0'(1)-108\eta\alpha'K_0'(2)+160\eta\alpha'K_0'(3)-80\eta\alpha'K_0'(4)+2\eta\alpha K_0''(0)-28\eta\alpha K_0''(1)+108\eta\alpha K_0''(2)-160\eta\alpha K_0''(3)+80\eta\alpha K_0''(4)$$
$$a_2'(1-)=-(6+2\alpha'+10\gamma')H_0(0)+(96+28\alpha'+200\gamma')H_0(1)-(492+108\alpha'+1440\gamma')H_0(2)+(1128+160\alpha'+4880\gamma')H_0(3)-(1200+80\alpha'+8440\gamma')H_0(4)+(480+7200\gamma')H_0(5)-2400\gamma'H_0(6)-2\eta\alpha K_0'(0)+28\eta\alpha K_0'(1)-108\eta\alpha K_0'(2)+160\eta\alpha K_0'(3)-80\eta\alpha K_0'(4)-2\eta\alpha'K_0''(0)+28\eta\alpha'K_0''(1)-108\eta\alpha'K_0''(2)+160\eta\alpha'K_0''(3)-80\eta\alpha'K_0''(4)$$
$$a_2(1+)=2a_2(1-)$$
$$a_2'(1+)=2a_2'(1-)$$
$$a_2(2-)=(4\beta+12\gamma)H_0(0)-(72\beta+240\gamma)H_0(1)+(432\beta+1728\gamma)H_0(2)-(1088\beta+5856\gamma)H_0(3)+(1200\beta+10\,128\gamma)H_0(4)-(480\beta+8640\gamma)H_0(5)+2880\gamma H_0(6)-4\eta\beta'K_0'(0)+72\eta\beta'K_0'(1)-432\eta\beta'K_0'(2)+1088\eta\beta'K_0'(3)-1200\eta\beta'K_0'(4)+480\eta\beta'K_0'(5)+4\eta\beta K_0''(0)-72\eta\beta K_0''(1)+432\eta\beta K_0''(2)-1088\eta\beta K_0''(3)+1200\eta\beta K_0''(4)-480\eta\beta K_0''(5)$$
$$a_2'(2-)=-(20+4\beta'+12\gamma')H_0(0)+(480+72\beta'+240\gamma')\times H_0(1)-(4440+432\beta'+1728\gamma')H_0(2)+(20\,560+1088\beta'+5856\gamma')H_0(3)-(51\,600+1200\beta'+10\,128\gamma')H_0(4)+(71\,040+480\beta'+8640\gamma')H_0(5)-(50\,400+2880\gamma')H_0(6)+14\,400H_0(7)-4\eta\beta K_0'(0)+72\eta\beta K_0'(1)-432\eta\beta K_0'(2)+1088\eta\beta K_0'(3)-1200\eta\beta K_0'(4)+480\eta\beta K_0'(5)-4\eta\beta'K_0''(0)+72\eta\beta'K_0''(1)-432\eta\beta'K_0''(2)+1088\eta\beta'K_0''(3)-1200\eta\beta'K_0''(4)+480\eta\beta'K_0''(5)$$
$$a_3(2+)=\tfrac{4}{5}a_3(2-)$$
$$a_3'(2+)=\tfrac{4}{5}a_3'(2-)$$
$$b_3(0,1-)=2\alpha H_0(0)-28\alpha H_0(1)+108\alpha H_0(2)-160\alpha H_0(3)+80\alpha H_0(4)$$
$$b_3'(0,1-)=(\alpha'/\alpha)b_3(0,1-)$$
$$b_3(0,1+)=2b_3(0,1-)$$
$$b_3'(0,1+)=2b_3'(0,1-)$$
$$b_3(1-,1+)=0$$
$$b_3'(1-,1+)=4H_0(0)-72H_0(1)+432H_0(2)-1088H_0(3)+1200H_0(4)-480H_0(5)$$
$$b_3(0,2-)=\beta b_3'(1-,1+)$$
$$b_3'(0,2-)=\beta'b_3'(1-,1+)$$
$$b_3(0,2+)=\tfrac{1}{5}b_3(0,2-)$$
$$b_3'(0,2+)=\tfrac{1}{5}b_3'(0,2-)$$
$$b_3(1-,2-)=4\gamma H_0(0)-56\gamma H_0(1)+214\gamma H_0(2)-320\gamma H_0(3)+160\gamma H_0(4)$$
$$b_3'(1-,2-)=(\gamma'/\gamma)b_3(1-,2-)$$
$$b_3(1+,2-)=8\gamma H_0(0)-184\gamma H_0(1)+1512\gamma H_0(2)-5536\gamma H_0(3)+9968\gamma H_0(4)-8640\gamma H_0(5)+2880\gamma H_0(6)$$
$$b_3'(1+,2-)=(\gamma'/\gamma)b_3(1+,2-)$$
$$b_3(1-,2+)=6\gamma H_0(0)-144\gamma H_0(1)+1224\gamma H_0(2)-4560\gamma H_0(3)+8280\gamma H_0(4)-7200\gamma H_0(5)+2400\gamma H_0(6)$$
$$b_3'(1-,2+)=(\gamma'/\gamma)b_3(1-,2+)$$
$$b_3(1+,2+)=12\gamma H_0(0)-216\gamma H_0(1)+1368\gamma H_0(2)-4224\gamma H_0(3)+6912\gamma H_0(4)-5760\gamma H_0(5)+1920\gamma H_0(6)$$
$$b_3'(1+,2+)=(\gamma'/\gamma)b_3(1+,2+)$$
$$b_3(2-,2+)=0$$
$$b_3'(2-,2+)=12H_0(0)-360H_0(1)+3888H_0(2)-19\,392H_0(3)+50\,400H_0(4)-70\,560H_0(5)+50\,400H_0(6)-14\,400H_0(7)$$
$$c_3=(54+6\alpha'+10\beta'+30\gamma')H_0(0)-(1080+84\alpha'+180\beta'-600\gamma')H_0(1)+(8316+324\alpha'+1080\beta'+4320\gamma')H_0(2)-(34\,344+480\alpha'+2720\beta'+14\,640\gamma')H_0(3)+(81\,000+240\alpha'+3000\beta'+25\,320\gamma')H_0(4)-(108\,000+1200\beta'+21\,600\gamma')\times H_0(5)+(75\,600+7200\gamma')H_0(6)-21\,600H_0(7)+(6\eta\alpha+10\eta\beta)K_0'(0)-(84\eta\alpha+180\eta\beta)K_0'(1)+(324\eta\alpha+1080\eta\beta)K_0'(2)-(480\eta\alpha+2720\eta\beta)K_0'(3)+(240\eta\alpha+3000\eta\beta)K_0'(4)-1200\eta\beta K_0'(5)+(2\eta+6\eta\alpha'+10\eta\beta')K_0''(0)-(24\eta+84\eta\alpha'+180\eta\beta')K_0''(1)+(60\eta+324\eta\alpha'+1080\eta\beta')\times K_0''(2)-(40\eta+480\eta\alpha'+2720\eta\beta')K_0''(3)+(240\eta\alpha'+3000\eta\beta')K_0''(4)-1200\eta\beta'K_0''(5)$$

A=4

$$a_4(0)=-(6\alpha+10\beta)H_0(0)+(132\alpha+260\beta)H_0(1)-(780\alpha+2160\beta)H_0(2)+(1920\alpha+8000\beta)H_0(3)-(2100\alpha+14\,500\beta)H_0(4)+(840\alpha+12\,600\beta)H_0(5)-4200\beta H_0(6)-2\eta K_0'(0)+40\eta K_0'(1)-180\eta K_0'(2)+280\eta K_0'(3)-140\eta K_0'(4)$$
$$a_4'(0)=-(2+6\alpha'+10\beta')H_0(0)+(40+132\alpha'+260\beta')H_0(1)-(180+780\alpha'+2160\beta')H_0(2)+(280+1920\alpha'+8000\beta')H_0(3)-(140+2100\alpha'+14\,500\beta')H_0(4)+(840\alpha'+12\,600\beta')H_0(5)-4200\beta'H_0(6)$$

TABLE VI.—*Continued.*

A = 4

$$-2\eta K_0''(0)+40\eta K_0''(1)-180\eta K_0''(2)$$
$$+280\eta K_0''(3)-140\eta K_0''(4)$$

$$a_4(1-)=(2\alpha-10\gamma)H_0(0)-(44\alpha-280\gamma)H_0(1)+(260\alpha$$
$$-2680\gamma)H_0(2)-(640\alpha-12\,320\gamma)H_0(3)$$
$$+(700\alpha-30\,500\gamma)H_0(4)-(280\alpha-41\,600\gamma)H_0(5)$$
$$-29\,400\gamma H_0(6)+8400\gamma H_0(7)-2\eta\alpha' K_0'(0)$$
$$+44\eta\alpha' K_0'(1)-260\eta\alpha' K_0'(2)+640\eta\alpha' K_0'(3)$$
$$-700\eta\alpha' K_0'(4)+280\eta\alpha' K_0'(5)+2\eta\alpha K_0''(0)$$
$$-44\eta\alpha K_0''(1)+260\eta\alpha K_0''(2)-640\eta\alpha K_0''(3)$$
$$+700\eta\alpha K_0''(4)-280\eta\alpha K_0''(5)$$

$$a_4'(1-)=-(6+2\alpha'+10\gamma')H_0(0)+(144+44\alpha'+280\gamma')H_0(1)$$
$$-(1044+260\alpha'+2680\gamma')H_0(2)+(3480+640\alpha'$$
$$+12\,320\gamma')H_0(3)-(5940+700\alpha'+30\,500\gamma')H_0(4)$$
$$+(5040+280\alpha'+41\,600\gamma')H_0(5)-(1680$$
$$+29\,400\gamma')H_0(6)+8400\gamma' H_0(7)-2\eta\alpha K_0'(0)$$
$$+44\eta\alpha K_0'(1)-260\eta\alpha K_0'(2)+640\eta\alpha K_0'(3)$$
$$-700\eta\alpha K_0'(4)+280\eta\alpha K_0'(5)-2\eta\alpha' K_0''(0)$$
$$+44\eta\alpha' K_0''(1)-260\eta\alpha' K_0''(2)+640\eta\alpha' K_0''(3)$$
$$-700\eta\alpha' K_0''(4)+280\eta\alpha' K_0''(5)$$

$$a_4(1+)=2a_4(1-)$$
$$a_4'(1+)=2a_4'(1-)$$

$$a_4(2-)=(4\beta+12\gamma)H_0(0)-(104\beta+336\gamma)H_0(1)+(864\beta$$
$$+3216\gamma)H_0(2)-(3200\beta+14\,784\gamma)H_0(3)+(5800\beta$$
$$+36\,600\gamma)H_0(4)-(5040\beta+49\,920\gamma)H_0(5)+(1680\beta$$
$$+35\,280\gamma)H_0(6)-10\,080\gamma H_0(7)-4\eta\beta' K_0'(0)$$
$$+104\eta\beta' K_0'(1)-864\eta\beta' K_0'(2)+3200\eta\beta' K_0'(3)$$
$$-5800\eta\beta' K_0'(4)+5040\eta\beta' K_0'(5)-1680\eta\beta' K_0'(6)$$
$$+4\eta\beta K_0''(0)-104\eta\beta K_0''(1)+864\eta\beta K_0''(2)$$
$$-3200\eta\beta K_0''(3)+5800\eta\beta K_0''(4)-5040\eta\beta K_0''(5)$$
$$+1680\eta\beta K_0''(6)$$

$$a_4'(2-)=-(20+4\beta'+12\gamma')H_0(0)+(640+104\beta'+336\gamma')$$
$$\times H_0(1)-(7560+864\beta'+3216\gamma')H_0(2)$$
$$+(45\,040+3200\beta'+14\,784\gamma')H_0(3)-(150\,920$$
$$+5800\beta'+36\,600\gamma')H_0(4)+(295\,200+5040\beta'$$
$$+49\,920\gamma')H_0(5)-(333\,600+1680\beta'+35\,280\gamma')$$
$$\times H_0(6)+(201\,600+10\,080\gamma')H_0(7)-50\,400H_0(8)$$
$$-4\eta\beta K_0'(0)+104\eta\beta K_0'(1)-864\eta\beta K_0'(2)$$
$$+3200\eta\beta K_0'(3)-5800\eta\beta K_0'(4)+5040\eta\beta K_0'(5)$$
$$-1680\eta\beta K_0'(6)-4\eta\beta' K_0''(0)+104\eta\beta' K_0''(1)$$
$$-864\eta\beta' K_0''(2)+3200\eta\beta' K_0''(3)-5800\eta\beta' K_0''(4)$$
$$+5040\eta\beta' K_0''(5)-1680\eta\beta' K_0''(6)$$

$$a_4(2+)=\tfrac{1}{3}a_4(2-)$$
$$a_4'(2+)=\tfrac{1}{3}a_4'(2-)$$

$$b_4(0,1-)=2\alpha H_0(0)-44\alpha H_0(1)+260\alpha H_0(2)-640\alpha H_0(3)$$
$$+700\alpha H_0(4)-280\alpha H_0(5)$$

A = 4

$$b_4'(0,1-)=(\alpha'/\alpha)b_4(0,1-)$$
$$b_4(0,1+)=2b_4(0,1-)$$
$$b_4'(0,1+)=2b_4'(0,1-)$$
$$b_4(1-,1+)=0$$

$$b_4'(1-,1+)=4H_0(0)-104H_0(1)+864H_0(2)-3200H_0(3)$$
$$+5800H_0(4)-5040H_0(5)+1680H_0(6)$$

$$b_4(0,2-)=\beta b_4'(1-,1+)$$
$$b_4'(0,2-)=\beta' b_4'(1-,1+)$$
$$b_4(0,2+)=\tfrac{1}{3}b_4(0,2-)$$
$$b_4'(0,2+)=\tfrac{1}{3}b_4'(0,2-)$$

$$b_4(1-,2-)=4\gamma H_0(0)-88\gamma H_0(1)+520\gamma H_0(2)-1280\gamma H_0(3)$$
$$+1400\gamma H_0(4)-560\gamma H_0(5)$$

$$b_4'(1-,2-)=(\gamma'/\gamma)b_4(1-,2-)$$

$$b_4(1+,2-)=8\gamma H_0(0)-248\gamma H_0(1)+2696\gamma H_0(2)-13\,504\gamma H_0(3)$$
$$+35\,200\gamma H_0(4)-49\,360\gamma H_0(5)+35\,280\gamma H_0(6)$$
$$-10\,080\gamma H_0(7)$$

$$b_4'(1+,2-)=(\gamma'/\gamma)b_4(1+,2-)$$

$$b_4(1-,2+)=6\gamma H_0(0)-192\gamma H_0(1)+2160\gamma H_0(2)-11\,040\gamma H_0(3)$$
$$+29\,100\gamma H_0(4)-41\,040\gamma H_0(5)+29\,400\gamma H_0(6)$$
$$-8400\gamma H_0(7)$$

$$b_4'(1-,2+)=(\gamma'/\gamma)b_4(1-,2+)$$

$$b_4(1+,2+)=12\gamma H_0(0)-312\gamma H_0(1)+2664\gamma H_0(2)-11\,136\gamma H_0(3)$$
$$+25\,800\gamma H_0(4)-33\,840\gamma H_0(5)+23\,520\gamma H_0(6)$$
$$-6720\gamma H_0(7)$$

$$b_4'(1+,2+)=(\gamma'/\gamma)b_4(1+,2+)$$
$$b_4(2-,2+)=0$$

$$b_4'(2-,2+)=12H(0)-456H_0(1)+6336H_0(2)-41\,280H_0(3)$$
$$+144\,840H_0(4)-290\,160H_0(5)+331\,920H_0(6)$$
$$-201\,600H_0(7)+50\,400H_0(8)$$

$$c_4=(54+6\alpha'+10\beta'+30\gamma')H_0(0)-(1512+132\alpha'+260\beta'$$
$$+840\gamma')H_0(1)+(12\,912+780\alpha'+2160\beta'+8040\gamma')$$
$$\times H_0(2)-(78\,840+1920\alpha'+8000\beta'+36\,960\gamma')$$
$$\times H_0(3)+(244\,620+2100\alpha'+14\,500\beta'+91\,500\gamma')$$
$$\times H_0(4)-(457\,920+840\alpha'+12\,600\beta'+124\,800\gamma')$$
$$\times H_0(5)+(505\,440+4200\beta'+88\,200\gamma')H_0(6)$$
$$-(302\,400+25\,200\gamma')H_0(7)+75\,600H_0(8)$$
$$+(6\eta\alpha+10\eta\beta)K_0'(0)-(132\eta\alpha+260\eta\beta)K_0'(1)$$
$$+(780\eta\alpha+2160\eta\beta)K_0'(2)-(1920\eta\alpha+8000\eta\beta)$$
$$\times K_0'(3)+(2100\eta\alpha+14\,500\eta\beta)K_0'(4)-(840\eta\alpha$$
$$+12\,600\eta\beta)K_0'(5)+4200\eta\beta K_0'(6)+(2\eta+6\eta\alpha'$$
$$+10\eta\beta')K_0''(0)-(40\eta+132\eta\alpha'+260\eta\beta')K_0''(1)$$
$$+(180\eta+780\eta\alpha'+2160\eta\beta')K_0''(2)-(280\eta$$
$$+1920\eta\alpha'+8000\eta\beta')K_0''(3)+(140\eta+2100\eta\alpha'$$
$$+14\,500\eta\beta')K_0''(4)-(840\eta\alpha'+12\,600\eta\beta')K_0''(5)$$
$$+4200\eta\beta' K_0''(6)$$

(γ,p) Reaction in Argon-40*

B. M. SPICER†
Physics Research Laboratory, University of Illinois, Champaign, Illinois
(Received June 3, 1955)

The energy distribution and angular distribution of photoprotons from argon irradiated with 22.5-Mev bremsstrahlung have been measured. The yield of protons was found to be 6.6×10^{4} protons per mole per r, in good agreement with Saskatoon results. The angular distribution of protons indicated that the absorption was predominantly electric dipole, as expected. The energy distribution peaked at 2.6 Mev, and, from its characteristics, it was inferred that the Coulomb barrier for protons plus Cl^{39} was only about 2.5 Mev, and that the level density in Cl^{39} increased with energy approximately as $\exp(E)$. These result are discussed in terms of the compound nucleus model and the direct photoeffect model.

INTRODUCTION

THE abnormally high (γ,p) cross sections in middle-weight nuclei excited with 17.6-Mev γ radiation[1] raised doubts as to the validity of the statistical theory of nuclear reactions, as applied to the nuclear photo-effect. The most successful hypothesis proposed to explain these data was that of Courant,[2] who postulated that a compound nucleus was not formed in all of the cases where a photon was absorbed by the nucleus. In these exceptional cases, the proton was ejected before it could interact with the other nucleons to form a compound nucleus.

In the light nuclei, where the surface-to-volume ratio is large, it might be expected that the direct effect will be emphasised. To test this hypothesis, Wilkinson and Carver[3] used the γ rays from the $Li^{7}(p,\gamma)Be^{8}$ reaction to irradiate an argon gas target. The gas was contained in a proportional counter, and the energy spectrum of the emitted protons was obtained by pulse-height analysis with a 99-channel kick-sorter. The energy distribution of the emitted charged particles had the following characteristics: (a) A large peak was present which was of the same type predicted by the statistical theory of nuclear reactions. This peak occurred at a proton energy of 2.5 Mev, and this energy is lower than is expected on a statistical model, using an exponentially increasing level density in the residual nucleus, and assuming a constant characteristic temperature of 1 Mev. (b) Two small, high-energy peaks were found at proton energies of 6.8 and 5.7 Mev. These were interpreted as being due to transitions to the ground state and the first excited state of Cl^{39}, respectively. However, since the threshold for the reaction, as inferred from these proton energies, is in disagreement with the evidence from other sources, the implications of the existence of these two peaks will not be considered.

Wilkinson and Carver concluded that the reaction did not proceed with any great probability via a surface photoelectric effect since this would have given the main group at high energy. They found a ratio of (γ,p) to (γ,n) cross sections of about $\frac{1}{3}$, instead of 1/25 as expected from the statistical theory.

This abnormally high (γ,p) to (γ,n) cross-section ratio was also found by McPherson, Pederson, and Katz.[4] They measured the activation curves for the $A^{40}(\gamma,n)A^{39}$ and $A^{40}(\gamma,p)Cl^{39}$ reactions by counting the neutrons and measuring the Cl^{39} activity, respectively. The characteristics of the cross-section curves for these two reactions are shown in Table I. The values of the maximum cross sections are even more striking evidence for the abnormally high $\sigma(\gamma,p)/\sigma(\gamma,n)$ ratio. This high ratio is all the more surprising when it is considered that the (γ,p) threshold in argon is 2.5 Mev higher than the (γ,n) threshold. This would lead one to expect that the neutron emission to be energetically favored over proton emission, and that the emission of protons would be further restricted by the Coulomb barrier.

In view of this surprising behavior, it was considered that further investigation of these reactions would be of interest. This paper reports on measurements of the energy distribution and the angular distribution of the protons emitted from argon gas which was irradiated with 22.5-Mev bremsstrahlung.

EXPERIMENTAL PROCEDURE AND TREATMENT OF DATA

The experimental technique used in this experiment was the same as was used in a previously reported

TABLE I. Characteristics of photonuclear cross sections in A^{40}.

Reaction	Energy of peak (Mev)	σ maximum (millibarn)	$\int_0^\infty \sigma dE$ (Mev-millibarn)	Yield at 22 Mev
$A^{40}(\gamma,p)$	$\geqslant 25$	$\geqslant 120$	540	5×10^{4}
$A^{40}(\gamma,n)$	20	38	350	10^{4}

* Supported in part by the joint program of the Office of Naval Research and the U. S. Atomic Energy Commission.
† Fulbright Fellow, on leave from the Physics Department, University of Melbourne, Melbourne, Australia.
[1] O. Hirzel and H. Waffler, Helv. Phys. Acta **20**, 373 (1947).
[2] E. D. Courant, Phys. Rev. **82**, 703 (1951).
[3] D. H. Wilkinson and J. H. Carver, Phys. Rev. **83**, 466 (1951).
[4] McPherson, Pederson, and Katz, Can. J. Phys. **32**, 593 (1954).

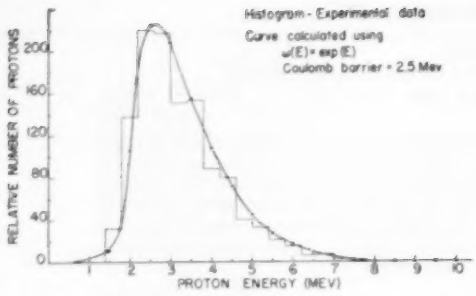

FIG. 1. Energy distribution of photoprotons from argon.

study of the photoprotons from oxygen.[5] An argon gas target, at a pressure of 1.19 atmospheres, was exposed to a collimated 22.5-Mev bremsstrahlung beam from the University of Illinois betatron. The protons emitted were detected in a pair of Ilford E1 emulsions, 100 microns thick.

Background tracks were due almost entirely to neutrons produced in the lead collimator giving rise to recoil protons in the emulsion. This background was estimated as described in reference 5. Background due to the $A^{40}(n,p)Cl^{40}$ reaction is negligible since its threshold, as calculated from the semiempirical mass formula is 8.1 Mev. The background was about 10% of the total number of tracks.

The energy of the proton at the surface of the emulsion was obtained from the range-energy data for Ilford emulsions given by Wilkins.[6] The energy lost by the proton in the gas between target and emulsion was calculated as described in reference 5. In the present experiment, the energy loss formula for argon (at 1.19 standard atmospheres pressure) was approximated by

$$-dE/dx = (0.1361/E)(\ln E + 2.2239) \text{ Mev/cm}.$$

RESULTS AND DISCUSSION

(a) Proton Yield

In an area of 1.56 cm^2 which was scanned, 1350 proton tracks were found and measured. These numbers were substituted into the formula $Y = (4\pi N/d\Omega \cdot R) \times (1/MV)$, where Y is the yield in protons per mole per roentgen, R is the total dose given, in roentgens, as measured by a Victoreen thimble at the center of an 8-cm cube of Lucite, V is the effective volume of the gas target in cm^3, N is the number of tracks found per unit area of the emulsion, M is the number of moles per cm^3 of argon at the gas pressure used, and $d\Omega$ is the mean solid angle at the target subtended by unit area on the emulsion. The figure obtained for the yield of protons at 22.5 Mev was 6.6×10^5 protons per mole per roentgen. This is in very good agreement with McPherson *et al.*'s value of 7.3×10^5 protons per mole per roentgen.[4]

(b) Energy Distribution of Photoprotons

The measured energy distribution is shown in Fig. 1. This distribution has its peak at 2.6 Mev, and there are very few protons having energy greater than 5 Mev. This first statement is in good agreement with the findings of Wilkinson and Carver,[3] who found the peak at 2.5 Mev in their experiment with the Li γ rays. It is perhaps surprising that the energy of the peak is so nearly the same in the two experiments. The Wilkinson-Carver experiment was done at a single energy, 5 Mev above the (γ,p) threshold, whereas the present experiment, although it was done with a continuum of γ-ray energies, detected events which were produced chiefly in the energy range 20 ± 2 Mev.

For comparison, energy distributions were calculated using the statistical theory of nuclear reactions. Now one would not expect a statistical theory to be applicable to a nucleus of only 39 nucleons. However, the results of Diven and Almy[7] on the energy spectrum of photoprotons from aluminum indicated that the statistical theory calculation could reproduce the general features of the observed energy distribution, and lent confidence to the use of the statistical theory to the present case.

The calculations made used the Coulomb barrier penetrabilities given by Feshbach, Shapiro, and Weisskopf,[8] and the cross section for the (γ,p) reaction was taken to be that measured by McPherson *et al.*[4] Three different forms were assumed for the level density in Cl^{39}. Writing the level density as $\omega(E)=\exp(E^n)$, the calculations were done for $n=0, \frac{1}{2}, 1$. The case $n=0$ was used because Diven and Almy[7] had some success with a level density of this form in predicting the energy distribution of photoprotons from aluminum. $n=\frac{1}{2}$ represents a simplification of the usually accepted form of

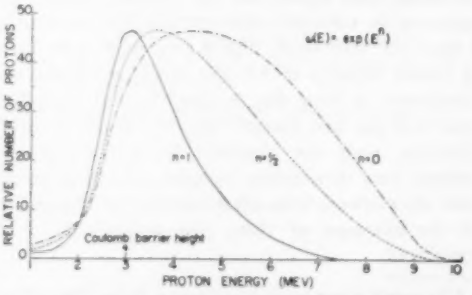

FIG. 2. Energy distribution of photoprotons, calculated using Coulomb barrier height of 3 Mev, level density $=\exp(E^n)$, and McPherson *et al.* measured (γ,p) cross section.[4]

[6] B. M. Spicer, Phys. Rev. **99**, 33 (1955).
[5] J. J. Wilkins, Atomic Energy Research Establishment, Harwell G/R 664 (1951).
[7] B. C. Diven and G. M. Almy, Phys. Rev. **80**, 407 (1950).
[8] Feshbach, Shapiro, and Weisskopf, Nuclear Development Association Report NYO 3077, 1953 (unpublished).

the level density in the statistical theory of nuclear reactions.

The probability of proton emission depends very strongly on the height of the Coulomb barrier. This would not normally be discussed, but Bethe has shown[9] that the peak in the energy distribution should approximate the height of the Coulomb barrier. The classical height for the Coulomb barrier $(Z/A^{\frac{1}{3}})$ is about 5 Mev. Therefore calculations were done for this case and also for the case of the Coulomb barrier being 3 Mev high. This value was suggested by the work of Scott,[10] who discussed the effects arising from consideration of the fact that the nuclear surface is not sharp. He concluded that the effect of a fuzzy surface would be to lower the height of the Coulomb barrier by about 40%.

The results of the calculations for the case of a Coulomb barrier height of 3 Mev are shown in Fig. 2. From the calculations we can draw two conclusions. First, the position of the peak in the energy distribution is controlled primarily by the height of the Coulomb barrier. The peak of the distribution shifts only 0.75 Mev between the two extreme level densities assumed (i.e., $n=0$ and 1). Second, the width at half-maximum of the peak in the energy distribution is determined chiefly by the value of "n" in the level density formula $\omega(E)=\exp(E^n)$. That is, it is determined by the rate of rise of the level density of the residual nucleus. The result of another calculation, using a Coulomb barrier height of 2.5 Mev, and a level density of the form $\omega(E)=\exp(E)$, is shown as the solid line in Fig. 1.

Therefore we conclude that the level density of Cl^{39} rises approximately as fast as $\exp(E)$, and that the effective height of the Coulomb barrier is only about 2.5 Mev instead of the classical value of 5 Mev.

The conclusions of this section support those of Wilkinson and Carver,[3] who noted that the explanation of the low energy of the peak in the energy distribution would require either a drastic modification of the Coulomb barrier or a level density which rises faster than $\exp(E)$. The present experiment apparently demands both of these possibilities.

(c) Angular Distributions

The angular distributions were plotted by grouping the tracks into 20° angular intervals, according to the angle the tracks made with the x-ray beam in the laboratory system. The plot was then corrected for the solid angle subtended by each interval at the position of the track. The solid angle correction factor is very closely $\langle\sin\theta\rangle_{Av}$, where $\langle\sin\theta\rangle_{Av}$ is the average value of $(\sin\theta)$ over the 20° interval.

TABLE II. Values of a, b, and c for the angular distributions.

Distributions	a	b	c
All protons	39	266	1
Protons $\epsilon_p<3$ Mev	2	160	0.5
Protons $\epsilon_p>3$ Mev	45	96	2
Protons $\epsilon_p>4$ Mev	10	52	2

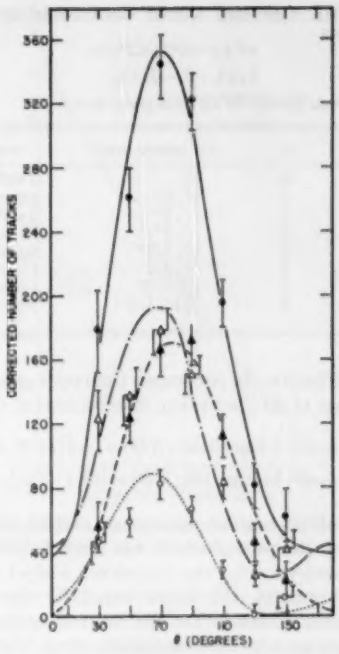

FIG. 3. Angular distributions of photoprotons from argon. ——— all protons, – – – – – – – protons of energy less than 3 Mev, —·—·—·— protons of energy greater than 3 Mev, ... protons of energy greater than 4 Mev.

The angular distributions obtained in this way are shown in Fig. 3. The distributions shown are for all protons, for protons having energy less than 3 Mev, protons having energy greater than 3 Mev, and greater than 4 Mev.

In all cases, the observed distributions could be fitted with curves of the form $a+b\sin^2\theta(1+c\cos\theta)$. This form was suggested by the large anisotropy which was present in all the angular distributions. The constants were determined by making least squares fits to the data. The least squares fits for the four cases are shown on Fig. 3, and the constants as determined are summarized in Table II. In the cases of the high energy protons, the lines have minima at about 130°, as well as the maxima between 60° and 70°. These minima are not to be taken seriously, since the statistics of the measurements at angles greater than 120° are very poor.

The "direct photoelectric effect" models put forward by Courant[2] and Wilkinson[11] predict, for the case of electric dipole absorption, an "$a+b\sin^2\theta$" form for the an-

[9] H. A. Bethe, Revs. Modern Phys. **9**, 69 (1937).
[10] J. M. C. Scott, Phil. Mag. **45**, 441 (1954).
[11] D. H. Wilkinson, Proceedings of the Photonuclear Conference, Philadelphia, May, 1954 (unpublished).

TABLE III. Computed angular distributions for $A^{40}(\gamma,p)$ photoprotons.

$$A^{40}+\gamma \rightarrow A^{40*} \rightarrow Cl^{39}+p.$$

$$J_A+l_\gamma \rightarrow J_B \rightarrow J_c+l_p.$$

$J_A=0^+$, $l_\gamma=1$, $J_B=1^-$ for all cases given here.

l_p	J_c	J of residual state	$N(\theta)$
1	0	$\frac{1}{2}^+$	$3\sin^2\theta$
0	1	$\frac{1}{2}^-$, $\frac{3}{2}^-$	constant
2	1	$\frac{3}{2}^-$, $\frac{5}{2}^-$	$3\sin^2\theta+2$
1	1	$\frac{1}{2}^+$, $\frac{3}{2}^+$	$1+\cos^2\theta$
1	2	$\frac{3}{2}^+$, $5/2^+$	$6+\sin^2\theta$
2	2	$\frac{3}{2}^-$, $5/2^-$	$1+\cos^2\theta$
3	2	$\frac{7}{2}^+$, $5/2^+$	$1+\sin^2\theta$
2	3	$5/2^-$, $7/2^-$	$4+\sin^2\theta$

gular distribution. In particular, Courant's model gives, for the case of $E1$ absorption, distributions of the form:

for the $l \rightarrow l+1$ transition: $N(\theta)=l+\frac{1}{2}(l+2)\sin^2\theta$.

for the $l \rightarrow l-1$ transition: $N(\theta)=(l+1)+\frac{1}{2}(l-1)\sin^2\theta$.

l is the orbital angular momentum carried within the nucleus by the proton which was ejected. Wilkinson's model involves only the transition $l \rightarrow l+1$. If this picture is correct, the forms found for the angular distributions demand that the protons emitted from the A^{40} nucleus are predominantly these which have zero orbital angular momentum within the nucleus. This condition is then difficult to reconcile with the shell model of the nucleus, which is surely correct when applied to the ground states of the nuclei in this region of Z. The last-filled proton shell in A^{40} is indeed a $2s_{\frac{1}{2}}$ shell, but there is also a partially filled $1d_{\frac{3}{2}}$ shell on the proton side. One may then ask, if the protons in the $2s_{\frac{1}{2}}$ shell participate so strongly, why the protons in the $1d_{\frac{3}{2}}$ shell do not participate to any great extent? Courant's model has no answer to this query, but Wilkinson's model gives the result that specially strong transitions occur if the emitted particle was initially in a closed shell, although the increase is not great for an s-shell. If this argument is correct, then one has a case in which a very few particles in the nucleus are responsible for about half of the dipole sum.

Using the method of reference 5, which means using the assumption that a compound nucleus of definite J is formed in the reaction, angular distributions were calculated for the case of electric dipole absorption of photons by the A^{40} nucleus. The results of the calculations are shown in Table III. J_C is the final channel spin, which is obtained by adding vectorially the total angular momentum of the residual state and the intrinsic spin of the outgoing particle. The first impression of the results in Table III is that, even allowing that a compound nucleus theory does apply, and that direct interaction effects are negligible, the experimental results are difficult to explain unless very special conditions are satisfied. One could get an angular distribution of the form "$a+b\sin^2\theta$" quite readily, but to obtain a ratio of "b" to "a" as large as is observed is a much more difficult problem.

The presence of an asymmetry about 90° implies that there must be interference between electric dipole and electric quadrupole absorption of photons. Unfortunately, there is no way of estimating their relative contributions. It should be noted that this interference can occur only if a number of levels of spins 1^- and 2^+ overlap at the excitations in A^{40} which are being considered.

DISCUSSION

McPherson *et al.*'s[4] measurement of the (γ,n) and (γ,p) cross sections showed that the (γ,p) cross section was rising in a region where the (γ,n) cross section was falling. This was not expected on the basis of a simple evaporation theory. Both the experiment of Wilkinson and Carver[3] and the present experiment show that the energy distribution of photoprotons produced in this reaction has its peak at an unexpectedly low energy. Also, this peak is unusually narrow. The angular distributions show a large anisotropy which is difficult to explain. It is the purpose of this section to examine the explanations for these anomalies which are offered by the two models for photonuclear reactions which have been discussed.

(a) The Direct Photoelectric Effect

On this model, the nucleon which absorbs the photon is the one emitted. Thus, there is no competition between neutron and proton emission in the same way as there is on the compound nucleus picture.

The explanation on this model for the energy and angular distributions of the protons is not at all satisfactory quantitatively, but it is certainly plausible qualitatively. It would have to go somewhat as follows: On Wilkinson's model,[11] the emission of protons from the $1d_{\frac{3}{2}}$ shell requires that the outgoing proton have three units of orbital angular momentum. The Coulomb barrier penetration factor for such protons is small even when the protons have several Mev energy. From a photon energy where the direct photoelectric effect is possible on the protons in the closed $2s_{\frac{1}{2}}$ shell, these protons may be the ones which have the greater interaction with the photons and are therefore predominantly emitted. The Coulomb barrier penetration factor would be larger for them. Also the interaction with the protons in the closed $2s_{\frac{1}{2}}$ shell is enhanced by the amount given by the "encouragement factors" discussed by Wilkinson.[11] This then would be a plausible explanation for the relatively sudden upturn of the cross section for the (γ,p) reaction at about 18 Mev. Since most of the events observed in this experiment are induced by photons of energy 20 ± 2 Mev, it would also explain why the peak in the energy distribution appeared at an energy as low as 2.6 Mev for the 22.6-Mev bremsstrahlung irradiation. Thus, we are postulating that the protons in the $2s_{\frac{1}{2}}$ shell are bound by

about 16 Mev. Allowing that the $2s_{\frac{1}{2}}$ proton shell plays the greatest part in the reaction would also mean that the large anisotropy in the angular distributions is also explained. There still remains the difficulty of explaining the steep rise of the cross section between 18 and 23 Mev.

One way of deciding between this picture and the compound nucleus picture would be to repeat the present experiment using bremsstrahlung energies of, say, 16, 18, and 20 Mev. If the model just described is correct, then at the 16- and 18- Mev bremmstrahlung irradiations, the proton angular distribution should have the form of $N(\theta)=1+\sin^2\theta$, since this is the angular distribution characteristic of a $d\rightarrow f$ transition made by the emitted particle. At these energies, it is supposed that a direct photoelectric effect on the protons in the $2s_{\frac{1}{2}}$ shell is energetically impossible. In the 20-Mev irradiation, the contribution of the protons from the direct effect in the $2s_{\frac{1}{2}}$ shell should be becoming important, and its effect on the angular distribution should be observable.

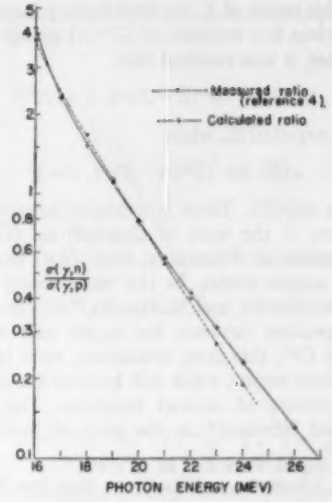

FIG. 4. Comparison with experiment of a rough calculation of the variation with energy of $\sigma(\gamma,n)/\sigma(\gamma,p)$.

(b) Compound Nucleus Theory

Using what was effectively a statistical theory, it was concluded earlier that to produce the observed shape of the energy distribution function, the level density of the residual nucleus, Cl^{39}, must increase with energy approximately as $\exp(E)$.

To get a clue as to the effect that this conclusion has on the ratio of (γ,p) to (γ,n) cross sections, we write down the expression for the ratio, on the statistical theory, of the two cross sections by integrating over the energy distributions. This gives

$$\frac{\sigma(\gamma,n)}{\sigma(\gamma,p)}=\frac{\int_0^{\epsilon_{n\,\max}}\epsilon_n\sigma_c(\epsilon_n)\omega(\epsilon_{n\,\max}-\epsilon_n)d\epsilon_n}{\int_0^{\epsilon_{\max}}e\sigma_c(e)\omega(\epsilon_{\max}-e)de}.$$

Since the (γ,n) threshold is lower than the (γ,p) threshold in A^{40}, and the barrier penetrability for neutrons is always larger than the penetrability for protons of the same energy, there is only one factor in this equation which could be adjusted to allow the ratio of cross sections as given in the equation to become less than unity. This then would say that the energy dependence of the $\sigma(\gamma,n)/\sigma(\gamma,p)$ ratio is due to there being increasingly more proton exit channels than exit channels for neutron emission. This hypothesis was tested very crudely by the following calculation. In the formula given above, put

$$\omega(\epsilon_{n\,\max}-\epsilon_n)=A\exp[B(\epsilon_{n\,\max}-\epsilon_n)],$$
$$\omega(\epsilon_{\max}-e)=C\exp[D(\epsilon_{\max}-e)].$$

Replace the proton barrier penetration function by a step function at 2.5 Mev, in accordance with the conclusion drawn from the shape of the experimental energy distribution. Replace the neutron barrier penetration function by a step function at 0.2 Mev. The integrations may then be performed analytically, giving the result

$$\frac{\sigma(\gamma,n)}{\sigma(\gamma,p)}=\frac{A\left[\left(\frac{1}{B^2}+\frac{0.2}{B}\right)\exp\{B(\epsilon_{n\,\max}-\epsilon_n)\}-\left(\frac{1}{B^2}+\frac{\epsilon_{n\,\max}}{B}\right)\right]}{C\left[\left(\frac{1}{D^2}+\frac{2.5}{D}\right)\exp\{D(\epsilon_{\max}-e)\}-\left(\frac{1}{D^2}+\frac{e_{\max}}{D}\right)\right]}.$$

From this equation it is apparent that, to get any case where the ratio $\sigma(\gamma,n)/\sigma(\gamma,p)<1$, the condition that D be greater than B must be fulfilled. In Fig. 4, the results for $D=1$, $B=0.7$, $A=0.17C$ are shown. The relation between A and C was obtained by normalizing the calculated ratio to the experimental ratio at an energy of 20 Mev.

This rough calculation gives results which are in satisfactory agreement with experiment. It should not be taken as the final answer, however, since it was done merely to show that the existence of more exit channels for protons then for neutrons could explain the observed $\sigma(\gamma,n)/\sigma(\gamma,p)$ cross-section ratio.

This explanation rests explicitly on the assumption

that, in this region of Z, the level density function for a given nucleus is a function of $(N-Z)$ as well as of A. In this case, it was assumed that

$$\omega(E) \text{ for } A^{39}(N-Z=3, J=7/2^-)$$

varied as $\exp(0.07E)$, while

$$\omega(E) \text{ for } Cl^{39}(N-Z=5, J=\tfrac{3}{2})$$

varied as $\exp(E)$. There is evidence supporting this assumption in the work of Gugelot[12] on the nuclear level densities as determined from (p,n) reactions in medium weight nuclei. In the more recent work of Miller, Friedlander, and Markowitz,[13] who investigated the competition between the (α,pn) and $(\alpha,2n)$ reactions in Cr^{50}, this same assumption must be used to explain their results, while still keeping the compound nucleus picture of nuclear reactions. The work of Cohen and Newman[14] on the ratio of the (p,pn) to $(p,2n)$ cross sections in nuclei of mass between 48 and 71 indicated that the ratio of probabilities of proton to neutron emission was much larger than expected on the usual statistical theory of nuclear reactions. These authors considered the explanation that the level density of odd-odd nuclei was very different from that of even-even nuclei of the same mass, which was advanced by Miller *et al.*[13] to explain their results. Cohen and Newman commented that this explanation would introduce difficulties into the explanation of certain results described in their paper. However, the idea is presented here because it does fit the observed facts in the case of the $A^{40}(\gamma,p)$ reaction.

[12] P. C. Gugelot, Phys. Rev. **81**, 51 (1951).
[13] Miller, Friedlander, and Markowitz, Phys. Rev. **98**, 1197(A) (1955).
[14] B. L. Cohen and E. Newman, Phys. Rev. **99**, 718 (1955), and private communication.

ACKNOWLEDGMENTS

The author is indebted to Professor A. O. Hanson and Professor R. B. Duffield for many helpful discussions. Thanks are also due to Mr. H. Moore for his assistance in scanning the plates, and to T. J. Keegan and the crew of the 22-Mev betatron for their assistance in making the irradiations.

PHYSICAL REVIEW VOLUME 100, NUMBER 3 NOVEMBER 1, 1955

Disintegration Schemes of the Te^{127} and Te^{129} Ground States*†

M. C. Day, Jr., G. W. Eakins, and A. F. Voigt
Institute for Atomic Research, and Departments of Chemistry and Physics, Iowa State College, Ames, Iowa
(Received July 11, 1955)

A coincidence scintillation spectrometer was used to study the decay of the 9.3-hour Te^{127} isomer and the 72-minute Te^{129} isomer. The Te^{127} isomer was found to decay by a simple beta ray with an end-point energy of 0.683 ± 0.010 Mev. The beta-ray spectrum of the Te^{129} isomer consists of two beta groups with end-point energies of 1.46 ± 0.01 and 1.01 ± 0.02 Mev. Two gamma rays with energies of 0.450 ± 0.005 and 0.035 Mev were observed, and they were found to be in coincidence. The 0.450-Mev gamma ray was shown to be in coincidence with the 1.01-Mev beta ray, and the 0.035-Mev gamma ray was shown to be in coincidence with the 1.46-Mev beta ray. The results are consistent with level assignments based on the shell model of the nucleus.

INTRODUCTION

THE 9.3 hour isomer of Te^{127} was first studied by Seaborg, Livingood, and Kennedy.[1] Using absorption techniques, they were able to show that it decayed by a simple beta-ray group of ~0.8 Mev. A value of 0.7 Mev. was reported later.[2]

Absorption measurements on the 72-minute isomer of Te^{129} indicated that the radiations consist of two gamma-rays of ~0.3 and ~0.8 Mev and a beta ray of 1.75 Mev.[2] Wilkinson and Rall later reported a beta ray end point of 1.8 Mev as a result of spectrometer studies.[3] Since no coincidence studies on the Te^{129} isomer and no spectrometer measurements of the beta rays from the Te^{127} isomer have been reported, it was felt that further investigation was necessary.

SOURCE PREPARATION

A solution of $H_2TeO_4\cdot 2H_2O$ in 2.4*f* HCl and 1.25*f* HNO_3 was irradiated in the Iowa State College synchrotron. As a result of recoil following the (γ,n) reaction, essentially all of the active tellurium is reduced from the +6 valence state to lower valence states. Since there is no significant electron exchange between tellurate and these lower valence states under ordinary

* Based on a thesis submitted by one of the authors (M.C.D.) to Iowa State College in partial fulfillment of the requirements for a PhD. degree.
† Contribution No. 404. Work was performed in the Ames Laboratory of the U. S. Atomic Energy Commission.
[1] Seaborg, Livingood, and Kennedy, Phys. Rev. **57**, 363 (1940).
[2] The Plutonium Project, Revs. Modern Phys. **18**, 513 (1946).
[3] W. Rall and R. G. Wilkinson, Phys. Rev. **71**, 321 (1947).

conditions,[4] this provides a means of obtaining radioactive tellurium of high specific activity.

After irradiation, 5 mg of Te^{+4} were added as a carrier and precipitated with H_2S.[5] The sources were then prepared by filtration.

EQUIPMENT AND PROCEDURE

The beta-ray and gamma-ray measurements were made with a coincidence scintillation spectrometer similar to that of Johansson.[6] The spectrometer used consists of two scintillation spectrometers that can serve as either beta-ray or gamma-ray detectors, depending on the crystal used.

The beta-ray spectra were determined by the dot method.[7] The pulses displayed on the oscilloscope screen are converted to dots and recorded with a movie camera. The pulse-height distribution is then determined with a multichannel pulse-height analyzer.[8] Gamma transitions were recorded photographically, and their pulse height was determined with a microphotometer.

A pulse generator and step attenuator were used to measure the nonlinearity of the electronic system. For beta-ray spectra Cs^{137}, Pb^{207}, and P^{32} were used as calibration sources. The gamma transitions of Sb^{126} and Cs^{137} were used as calibration points for gamma-ray studies.

Except for the purpose of estimating the approximate relative intensities of the two beta-ray spectra, Kurie plots of only the higher energy beta-ray group of the Te^{129} isomer were made from the total beta spectrum. The end-point energy of the lower energy beta-ray group was obtained by coincidence measurements.

In the study of Te^{129}, half-hour irradiations of 0.898 g of $H_2TeO_4 \cdot 2H_2O$ were obtained and the sources were prepared as described earlier. Three-hour irradiations were obtained for the study of Te^{127}, and the Te^{129} was allowed to decay out before the beta spectrum was run. In all cases, the half-life was followed as a measure of the isotopic purity.

RESULTS

Te^{127}

A typical Kurie plot of the Te^{127} beta ray is shown in Fig. 1. The maximum in the beta-ray distribution was found to be 0.683 ± 0.010 Mev. This is in good agreement with the previously reported values. No gamma transitions were observed.

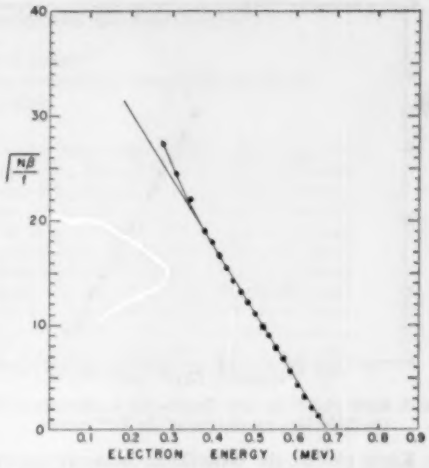

FIG. 1. Typical Kurie plot of the beta spectrum of the 9.3-hour Te^{127} isomer.

Te^{129}

The Te^{129} isomer was found to have two beta-ray groups with maximum energies of 1.46 ± 0.01 and 1.01 ± 0.02 Mev. Figure 2 shows a typical Kurie plot for the high-energy beta ray. Two gamma transitions were observed at 0.450 ± 0.005 Mev and approximately 0.035 Mev. By means of gamma-gamma coincidence measurements, the two gamma rays were determined to be in coincidence. Beta-gamma coincidence studies were made with the high-energy beta-ray group, and it was found to be in coincidence with the 0.035 Mev gamma ray. The 0.450-Mev gamma ray was shown to be in coincidence with the 1.01-Mev beta ray by means of gamma-beta coincidence measurements, and the coincidence beta-ray spectrum obtained was used to determine the end-point energy of the beta-ray group.

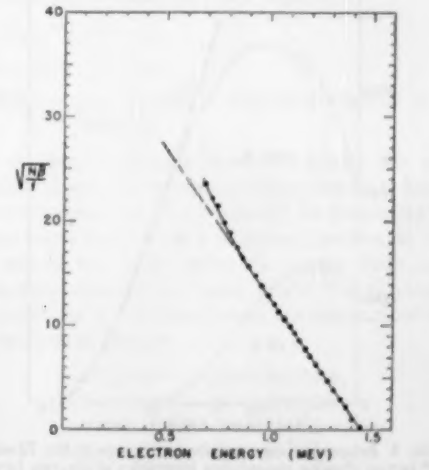

FIG. 2. Typical Kurie plot of the beta spectrum of the 72-minute Te^{129} isomer.

[4] M. Haissinsky and M. Cottin, Anal. Chem. Acta **3**, 226 (1949).
[5] R. Williams, J. Chem. Phys. **16**, 513 (1948).
[6] S. Johansson, U. S. Atomic Energy Commission Report No. ISC 431 (unpublished).
[7] F. T. Boley and D. J. Zaffarano, Phys. Rev. **84**, 1059 (1951).
[8] Hunt, Rhinehart, Weber, and Zaffarano, Rev. Sci. Instr. **25**, 268 (1954).

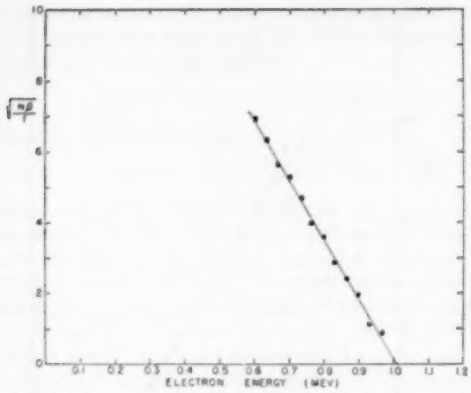

FIG. 3. Kurie plot of the beta distribution in coincidence with the 0.450-Mev gamma ray of the Te^{129} isomer.

The Kurie plot of the coincidence beta-ray spectrum is shown in Fig. 3. The relative intensities of the two beta-ray groups were determined by extrapolating the Kurie plots back to zero energy and reconstructing the energy distribution curves from the Kurie plots. Comparison of the two distribution curves resulted in relative intensities of approximately 80% and 20% respectively for the 1.46- and the 1.01-Mev beta-ray groups, as shown in Fig. 4. The log *ft* values were calculated to be 5.8 for both transitions.

DISCUSSION

The observed simple beta decay of the 9.3-hour Te^{127} isomer is in agreement with the previous studies. The log *ft* value of 5.6 is in the allowed range and is therefore consistent with the proposed level assignments of $d_{3/2}$ for the Te^{127} and $d_{5/2}$ for the I^{127} ground states.[9]

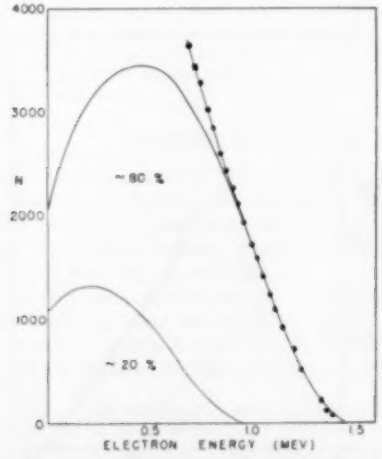

FIG. 4. Beta-ray energy distribution curves of the 72-minute Te^{129} isomer showing the relative intensities of the two beta-ray groups.

[9] M. Goldhaber and R. D. Hill, Revs. Modern Phys. **24**, 179 (1952).

The ground state of I^{129} has been measured as $g_{7/2}$ and Te^{129} has a $d_{3/2}$ ground state.[9] The log *ft* value for the 1.46-Mev beta ray indicates that it is an allowed transition and would not be expected to go directly to the I^{129} ground state, since this would require a spin change, $\Delta I = 2$. In Fig. 5, an energy level diagram for the decay of the 72-minute Te^{129} isomer is presented which is consistent with the reported ground state levels of Te^{129} and I^{129}.

Since no gamma transition was observed from the higher excited state, *A*, to the ground state, *C*, it is possible to make some predictions as to the spins of the two excited levels. If the beta transitions are allowed, there can be no parity changes and any combination of spins 1/2, 3/2, or 5/2 is possible for the excited levels. If *A* is assigned a spin of 5/2, the two possible transitions from *A* would be of comparable intensity for the case of spin assignments of 3/2 and 5/2 for the lower excited level *B*, and they should both be observed. For an assignment of 1/2 to *B*, the low-energy gamma transition (*B*–*C*) would be of the *M*3 class. Such a transition would have a lifetime that is long with respect

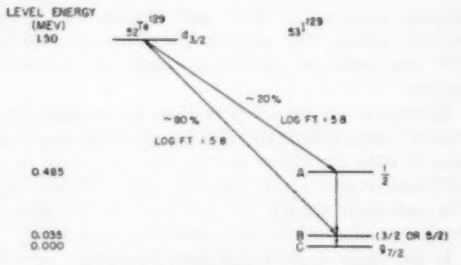

FIG. 5. Proposed decay scheme for the 72-minute Te^{129} isomer.

to the observed 0.450-Mev transition (*A*–*B*), and the two gamma rays would not be in coincidence as was observed. For the case of a spin of 3/2 for *A*, and spin values of 3/2 or 5/2 for *B*, the competition would be between *E*2 and *M*1 type transitions, and both gamma rays might be expected. A spin assignment of 1/2 for *B* is not acceptable for the same reason as before. If a spin assignment of 1/2 is given to *A*, spins of 3/2 or 5/2 for *B* are consistent with the observed data, since the gamma transition from *A* to *C* would be *M*3 and therefore negligible compared to an *M*1 or *E*2 transition to *B*. The two observed transitions would be of comparable lifetimes which would explain the observed coincidence data.

It appears that the spin of *A* is 1/2 and that of *B* either 3/2 or 5/2. According to a single particle model, the higher excited level, *A*, would probably be $s_{1/2}$ and the lower excited level *B*, $d_{3/2}$.

The authors wish to thank Dr. D. J. Zaffarano for the use of the scintillation spectrometer and the Iowa State College synchrotron group for help in obtaining the activities.

Absolute Cross Sections for Deuterons on Beryllium*

ROBERT E. HEFT AND W. F. LIBBY†
Department of Chemistry and Institute for Nuclear Studies, University of Chicago, Chicago, Illinois
(Received March 1, 1955)

The absolute cross section for the reactions of deuterons on beryllium which produce titrium and Be^{10} have been measured up to energies of 17 to 20 million electron volts. Data of Dejong, Endt, and Simons show no threshold which is as expected for exothermic (d,p) and (d,t) processes. For the reaction producing Be^{10}, which is equivalent to the introduction of a neutron into the beryllium nucleus by the bombarding deuteron, the cross section rises to a peak value of about 0.34 barn, at about 4 Mev. It then falls almost linearly to the low value of 0.08 barn at 20 Mev. There are evidences of fine structure in the curve but it is possible that these are not really significant. The reaction producing tritium rises to a peak value of about 0.23 barn at about 5 Mev and then falls to a low value of about 0.03 barn at 13 Mev. The reaction cross section appears to remain essentially constant at this low value although it may rise slightly as the energy is raised to about 20 Mev. A new reaction producing tritium begins at 17.47 Mev, namely one which produces both tritium and Be^7 simultaneously. This corresponds to the ejection of both a triton and a neutron as a result of the deuteron Be^9 collision. This cross section rises from zero at the threshold linearly to a value of 8×10^{-5} barn at 21.5 Mev.

I. INTRODUCTION

DURING the past several years, deuteron-induced reactions of beryllium have been the subject of a number of investigations. In particular the angular distributions of protons and tritons from (d,p) and (d,t) processes have been determined for a number of energies. In the few cases[1] where reaction cross sections have been calculated from the distribution data, the cross sections were determined for a small energy interval only.

No excitation function for the total cross section of the $Be^9(d,p)Be^{10}$ reactions has been reported, and that reported[2] for the (d,t) reaction terminates at 7.7 Mev. In the present work the total cross section for the (d,p) reaction has been measured as a function of energy over the interval 0 to 21.6 Mev, and that for the (d,t) reaction measured for energies up to 18.6 Mev. In the course of the (d,p) investigation it was observed that the reaction $Be^9(d,tn)Be^7$ occurred to a measurable extent above its threshhold energy of 17.47 Mev. Its cross section was also determined for energies up to 21.6 Mev.

The exact nature of the reactions investigated requires further specification. For the (d,p) reaction, the cross section was calculated from the Be^{10} activity produced. Therefore the cross section is a measure of the combined probabilities of production of Be^{10} in its ground state and in such excited states as decay by gamma emission to the ground state. Not included are the transitions to excited states of Be^{10} which decay by particle emission (e.g., $Be^{10*}\rightarrow Be^9+n$).

In the (d,t) reaction investigation, the activity of the tritium itself was measured, therefore the cross section describes the combined probability of all processes in which tritium is produced. These include all transitions of the form $Be^9(d,t)Be^8$ and in addition will include contributions from $Be^9(d,\alpha)Li^{7*}$, where Li^{7*} represents an excited state of Li^7 which may decay to an alpha particle plus a triton. Further contribution to the observed tritium production is made by $Be^9(d,tn)Be^7$ and $Be^9(d,tp)Li^7$ at energies above the threshholds for these reactions which are 17.47 Mev and 15.47 Mev respectively.[1] One further possible source of tritium is from the reaction $Be^9(d,2\alpha)H^3$, however it is not certain that the direct three-body reaction occurs.[1] For the purpose of simplicity of notation the (d,t) reaction will be termed the $Be^9(d,t)Be^8$ reaction, however, one should keep in mind that the other sources of tritium may be present.

In the (d,tn) reaction the cross section was determined from the activity of the Be^7 so that it is a measure of the combined probabilities of the processes:

$Be^9(d,t)Be^{8*}\rightarrow Be^7+n$,

$Be^9(d,n)B^{10*}\rightarrow Be^7+t$,

$Be^9(d,tn)Be^7$ (i.e., the direct three-body reaction if it occurs).

In all cases in which a threshhold energy was not indicated above, the reaction to the ground state has a positive Q value (i.e., is exothermic). In transitions to excited states the Q value is in general positive for the first one or two levels above the ground state and increasingly negative for higher levels. The Q values for transitions to the ground state are summarized for the reactions of interest:

$Be^9(d,p)Be^{10}$	$Q=4.586$ Mev,
$Be^9(d,t)Be^8$	$Q=4.591$ Mev,
$Be^9(d,\alpha)Li^7$	$Q=7.151$ Mev,
$Be^9(d,2\alpha)H^3$	$Q=4.687$ Mev,
$Be^9(d,tn)Be^7$	$Q=17.47$ Mev,
$Be^9(d,tp)Li^7$	$Q=15.47$ Mev.

* Supported by U. S. Air Force, Office of Scientific Research and Development.
† Now at the U. S. Atomic Energy Commission, Washington, D. C.
[1] These are summarized in a review article: F. Ajzenberg and T. Lauritsen, Revs. Modern Phys. 24, 336 (1952).
[2] R. L. Wolfgang and W. F. Libby, Phys. Rev. 85, 437 (1952).

The values given were taken from the review article by Ajzenberg and Lauritsen.[1] References to the original work are given in the article.

It is to be noted that the measurements of the cross section were absolute in the sense that the total production of a given species was determined and not merely the production relative to that at another energy. Measurement of the absolute cross section depends principally upon the determination of the absolute activity of the nuclear species used to monitor the reaction. The method of absolute assay of the activity was different for each of the reactions studied.

Beryllium which is of low atomic mass is of considerable interest as a nuclear reactant. Reactions in which deuterons are used as the bombarding particle are known to proceed by alternative paths involving on the one hand compound nucleus formation and on the other a stripping process in which only one constituent of the deuteron enters the target nucleus. The stripping mechanism may operate in either (d,p) or (d,n) reactions. In the case of (d,t) reactions the analogous process occurs in which a constituent neutron of the target nucleus is picked up by the deuteron without the latter having entered the target nucleus. Compound nucleus formation may be differentiated from the stripping or pick-up processes experimentally by measuring the angular distribution of the emergent protons or tritons. The latter two processes result in characteristic angular distributions which have been theoretically established.[2,3] For the (d,p) reaction, angular distribution measurements of the emergent protons indicates that the stripping process dominates compound nucleus formation over a wide range of energies.[1] For the (d,t) process angular distribution measurements of the emergent tritons indicate that the pick-up process occurs without intervention of a compound nucleus.[1] Since the (d,p) process occurs through the transfer of a neutron from the deuteron to the beryllium while the (d,t) process occurs through the transfer of a neutron from the beryllium to the deuteron, the comparison of the two reactions seemed to be of possible interest.

II. EXPERIMENTAL PROCEDURE

For the reaction producing tritium, the method consists of the bombardment of a beryllium foil with a measured number of deuterons whose energy had been reduced to an appropriate value by passage through aluminum foils, stopping of the emergent tritons in aluminum foils which surround the beryllium target and the subsequent extraction of the tritium in the aluminum foils by heating in a hydrogen atmosphere followed by an absolute determination of the number of tritons formed by a gas counting method.

For the reactions producing Be^{10}, the experimental method consisted of the bombardment of a thick beryllium target with a measured number of deuterons followed by the milling of the target into thin sections and the measurement of the Be^{10} content of each of the thin sections. The activity of the Be^{10} was determined by absolute beta assay of solid beryllium oxide following chemical purification of the beryllium for other radioactivities produced.

Deuteron Range Energy Relationships

Conversion of the experimentally determined range values to the energy values used in construction of the excitation functions was accomplished by the use of the range-energy relationships.

For aluminum, the range-energy relationship used was that given by Smith.[5] The tabulated values of range in aluminum for protons of given energy were converted to deuteron ranges by the relationship: $R_d(E)=2R_p(E/2)$. The coordinate values, plotted to large scale, were used to construct the range-energy curve used in the calculations.

For beryllium, the range-energy relationship used between 0- and 2.7-Mev deuteron energies was determined by graphical integration of the inverse of the measured proton stopping power of beryllium, followed by conversion of the proton range to deuteron range as above. The stopping-power data were those given by Kahn[6] which include a consolidation of the earlier measurements. The behavior of the stopping power near zero energy (i.e., below the 40-kev limit of the measured values) was estimated from the relationship $dE/dx=R\sqrt{E}$ which was obtained from Fermi and Teller's theoretical treatment.[7]

Above 2.7-Mev deuteron energy the calculated range-energy values of Aron[8] were used. These values were adjusted to fit the low-energy values by adding 0.22 mg/cm² Be to each (proton) range value given by Aron. The correction factor was obtained by determining the

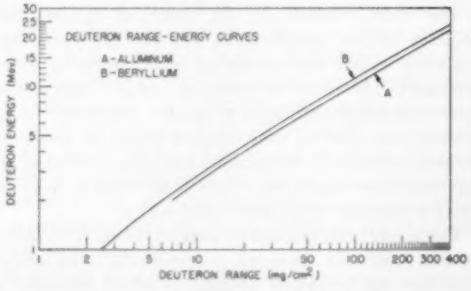

FIG. 1. Range-energy curves for deuterons in aluminum and beryllium.

[2] S. T. Butler, Proc. Roy. Soc. (London) **A208**, 559 (1951).
[3] H. C. Newns, Proc. Phys. Soc. (London) **A65**, 916 (1952).
[5] J. H. Smith, Phys. Rev. **71**, 32 (1947).
[6] D. Kahn, Phys. Rev. **90**, 506 (1953).
[7] E. Fermi and E. Teller, Phys. Rev. **72**, 399 (1947).
[8] W. A. Aron, University of California Radiation Laboratory Report UCRL-1325, 1951 (unpublished), p. 19.

difference in the range value of the two relationships at 1-Mev energy.

A plot of the deuteron range in aluminum and beryllium is shown in Fig. 1.

III. COUNTING METHODS

For the tritium measurements the extraction was done by heating the aluminum or beryllium foil to temperatures of 900° to 1000°C. in the presence of a small amount of hydrogen. Under these conditions very little hydrogen is retained in the metal.[9] The heating was done in an alumina tube two inches long and one cm in diameter, which was lowered into a porcelain tube which was heated by a furnace. The hydrogen gas which was placed in contact with the heated metal foils was introduced into the counter where the tritium content was measured by making a counter mixture of three to four cm of mercury pressure of argon with 1.5 to 2.0 cm of mercury pressure of ethylene, together with hydrogen pressures up to several cm. In most of the present work, however, a few hundredths of a millimeter of mercury pressure of hydrogen was all that was present in the counter. It has been shown[2] that under these conditions the mixture operates as a Geiger counter under conditions of maximum efficiency except for the end loss which is corrected for by methods previously published.[9] The counter used was constructed of one and 15/16th in. inside diameter brass tubing into which Lucite end caps were fitted and sealed with deKhotinsky cement. The active length of the counter, as defined by the flat inner faces of the Lucite caps was seventeen inches. The center wire was made of two-mil tungsten.

The Be^{10} produced by the deuteron bombardment of beryllium was measured by dissolving the beryllium samples resulting from the milling of the thick target and chemically purifying the beryllium. Following this, a BeO powder was produced which was mounted over a small area on a flat surface which constituted a part of the wall of a Geiger counter. The thickness of the BeO sample was measured by weighing and measuring the area of the deposit. It has been shown[10,11] that beta radioactivities which are characterized by single transitions between two levels exhibit exponential absorption curves under conditions of close geometry and that the absorption coefficients or half-thicknesses are functions of the energy such that the range[12] is a slowly varying multiple of the half-thickness. For example, the ratio of the range to the half-thickness falls from a value of 13 for tritium at an energy of 18.9 kev to 9.5 for phosphorous-32 whose beta-ray energy is 17.8 kev. The curve appears to be rather flat out to energies of about 1760 kev though it may fall more gradually than the data obtained so far indicate. Beyond 1760 kev, it seems to decrease to the value quoted for phosphorous-32. In any case, on the basis of the data obtained[12] from this study of the absolute assay of beta radioactive solids it would have been expected that Be^{10}, with its beta spectrum upper limit of 555 kev,[13] would show an aluminum absorption coefficient of 19.7 mg/cm². The remarks made above about the systematics of absorption coefficients are all meant to apply to aluminum absorption coefficients. Experimental measurement of the absorption coefficient of the Be^{10} radiation gave 19.4 ± 0.2 mg/cm². It is further known that the absorption coefficients for beta radiation depend on atomic weight of the absorber,[11,14] with the simple relation that the absorption coefficient or the reciprocal of the half-thickness is directly proportional to the quantity 1 plus the average atomic weight divided by 100. In the case of aluminum, this quantity is 1.27. In the case of BeO, it is 1.125. Therefore, one would expect that the absorption coefficient for the Be^{10} radiation in the BeO would be lower than that in aluminum in the ratio of 1.27 to 1.125 or 1.13 and that the half-thickness should therefore be larger by the same factor or should be 19.4 ± 0.2 mg/cm² $\times 1.13$, or 22.0 ± 0.3 mg/cm² of BeO. Actual direct measurement of this quantity was made by mounting various thicknesses of BeO containing Be^{10} on aluminum foils which were mounted between two geiger counters in close contact, that is under 4π geometry conditions. Several aluminum foils supporting the BeO of various thicknesses were used so that the counting rate could be extrapolated to 0 thickness of supporting foil for various thicknesses of BeO were determined. In this way, the absorption coefficient of the Be^{10} radiation in BeO was determined to be 23.2 ± 0.4 in satisfactory agreement with the calculated value. This number was used in correcting the actual samples resulting from the bombardment for self-absorption in BeO. It is to be noted that in this technique no correction need be made for back-scattering since it assumes that only thick samples be used or that if thin samples be used they be mounted on a backing of the same chemical composition as the thick samples. When this is done the back-scattering correction is automatically included. It is clear from the description above that the geometry factor under the counting conditions used in this research was $\frac{1}{2}$; that is, 2π geometry obtained.

The BeO was mounted by transferring the BeO to the mounting surface with a microspatula where it was tamped into a rectangular shape and then a drop or two of 0.15 percent solution of agar in water was added. The resulting paste-like slurry was then pressed into a rectangular mask which was placed on the mounting surface. The sample was then dried in an oven at 110°C, cooled, and weighed.

[9] A. G. Engelkemeier and W. F. Libby, Rev. Sci. Instr. **21**, 550 (1950).
[10] W. F. Libby, Anal. Chem. **19**, 2 (1947).
[11] A. D. Suttle, Jr., and W. F. Libby, Anal. Chem. **27**, 921 (1955).
[12] L. Katz and A. S. Penfold, Revs. Modern Phys. **24**, 28 (1952).
[13] Hollander, Perlman, and Seaborg, Revs. Modern Phys. **25**, 477 (1953).
[14] P. Lerch, Helv. Phys. Acta **26**, 663 (1953).

In order to determine the number of Be^7 atoms, it was necessary to determine the efficiency with which the emitted gamma rays were counted. This was done by making an absolute assay of one of the samples on a low-level scintillation spectrometer. The method used in the conversion of the spectrum data to total gamma emission rate has been described by Novey.[15] In brief, it consists of the following steps.

(1) The plot of the counting data, which was made in terms of (counts/min)/mv against mv, consisted of two well-defined areas—one due to gammas which were counted as a result of undergoing Compton scattering, and another due to those which had lost their entire energy in the NaI scintillator either by photoelectric process or by multiple scattering. The ratio of the area of the photopeak to the total area gave the fraction of counts in the photopeak. The measured value was 0.445 ± 0.020.

(2) The gamma counting efficiency for the 1-in. thick crystal was calculated for normally incident photons. The total cross section of NaI for the 0.476-Mev gamma was determined by interpolation in the tables of Davisson and Evans[16] to be 23.49×10^{-24} cm^2/atom. From this, the fraction of normally incident gammas stopped in the crystal was calculated to be 0.586 ± 0.005.

(3) The geometrical efficiency was determined from the solid angle subtended at the crystal face by the source on the lowest shelf. This calculated geometry factor was multiplied by the ratio of the area of the photopeak at the upper-shelf position (where the spectrum was run) to that of the photopeak at the lower-shelf position (for which the geometry was calculated). The geometrical efficiency for the upper-shelf position was found to be 0.252 ± 0.020. (Direct calculation of the upper-shelf geometry is difficult because of variation of effective crystal thickness with angle of emission.)

(4) The product of the three factors was used to determine the over-all efficiency of the counter. Thus:

$$(0.445\pm0.020)\times(0.586\pm0.005)\times(0.252\pm0.020)=0.066\pm0.008$$

is the fraction of the gamma counts which appeared in the photopeak at the upper-shelf position. The foregoing omits the effects of self-absorption in the BeO and absorption by the aluminum cover of the crystal, both of which were negligible.

IV. REACTION $Be^9(d,t)Be^8$

The absolute excitation function for $Be^9(d,t)Be^8$ reaction has been determined by Wolfgang and Libby[2] for deuteron energies from 0 to 7.68 Mev. The purpose of the present work was to extend the excitation function measurement to higher energies in order that a comparison with the competing (d,p) process can be made over a wider energy range.

The bombardments were made in the 60-inch cyclotron of the Argonne National Laboratory. In planning the beryllium bombardment, consideration was taken of the energy of the incident deuterons,the angle at which the deuterons traversed the foils, and the temperature to which a given beam current would raise the foils. The measurements required for each of the bombardments were the foil thicknesses and the number of deuterons which traversed the foils.

The initial deuteron energy was determined by measuring the deuteron range in aluminum and then converting the range value to energy by using the range-energy relationship.

The range in aluminum may be found experimentally by measuring the fraction of the beam absorbed by foils of various thicknesses. A plot is then made of the fraction absorbed against foil thickness, and the thickness corresponding to a fraction absorbed of one-half is taken as the mean range.[17] Such measurements have been made by the cyclotron staff, who found the mean range of the deuterons in aluminum to be 358.4 ± 4.0 mg/cm^2 at the position of the target. The error corresponds to the uncertainty in the determination of the mean range. This value was estimated by taking one-half the extreme possible error as being the standard error of the determination. From the range-energy relationship, the energy is found to be 20.84 ± 0.20 Mev. This then is the energy at which the deuterons were incident on the target assembly.

The beam angle determination was made by the cyclotron staff. The method used was to place at the normal target position a thick plate which contained a number of apertures through which beam bundles could pass and traverse a series of aluminum foils referenced to the aperture plate. The foils were then radio-autographed and the beam bundle trajectories plotted. The beam angle relative to the perpendicular to the target surface was found to be $17°30'\pm1°$.

It was necessary to avoid excessive heating of the foils for two reasons. The first was that thermal expansion of the foils would result in an increase in foil area and consequently a decrease in the number of atoms per unit area. Since the atoms per unit area must be known in order to calculate the energy loss, a temperature dependence of this quantity is to be avoided. The second reason was that the tritons could not be expected to remain in the foils if these were at high temperature. Indeed, the tritium extraction procedure used depends on the mobility of the entrapped tritons at temperatures of greater than 450°C.

The deuterons dissipated their entire 21-Mev energy within the foils; therefore, for a current level of 10 microamperes, the heat input was 210 watts. The target assembly was water-cooled but heat transport

[15] T. B. Novey, Phys. Rev. **89**, 672 (1953).
[16] G. M. Davisson and R. Evans, Revs. Modern Phys. **24**, 79 (1952).
[17] M. S. Livingston and H. A. Bethe, Revs. Modern Phys. **9**, 284 (1937).

across the foil surfaces was not efficient so that an experimental determination of the foil temperatures as a function of beam current level was run. A copper-constantan thermocouple junction was pressed between two aluminum foils mounted as for a regular bombardment. The voltage in the thermocouple circuit, with the cold junction at room temperature (22°C), was recorded as a function of the beam current on the target.

On the basis of these data, which showed a temperature of nearly 300°C at 35 μa, a bombardment current level of 10 μa was chosen. At this level the foil temperature could be assumed to be safely below 400°C. At 10 μa, a fifteen-minute bombardment produced 10^3 or more counts per minute of tritium activity in all the targets which were run.

In essence the target assembly consisted of a stack of three foils which were water-cooled and electrically insulated from their surroundings. The deuterons were incident on the topmost foil which was aluminum and which had two functions—first, to diminish the deuteron energy by a predetermined amount and second, to stop the tritons emitted by the beryllium at angles between 90°–180° (laboratory coordinates). The second of the foils was the beryllium one in which the reaction under investigation occurred. The third foil was again aluminum and had the function of stopping the tritons emitted between 0° and 180°.

The energy of a triton formed in a given nuclear reaction is dependent on the energy of the projectile nucleus, and on the angle of emission of the triton with respect to the path of the projectile nucleus. A calculation was made to determine the minimum thickness of aluminum which will de-energize initially 21-Mev deuterons to an energy for which the back-emitted tritons will be just stopped. The thickness value was found to be 52 mg/cm², and hence any de-energizing foil of thickness greater than 52 mg/cm² will completely stop the tritons formed in the beryllium foil. A minimum foil thickness of 64.7 mg/cm² Al was used which de-energized the 20.84-Mev deuterons to 18.85 Mev, and this was the maximum deuteron energy for which the reaction cross section was measured. It was also found that the maximum forward displacement of the tritons is approximately equal to the residual range of the deuterons at the position of reaction so that a foil stack sufficiently thick to stop the deuterons will also stop all tritons formed by the deuterons.

In Fig. 2 is given a schematic diagram of the target assembly used. The foils were pressed against cooling plate *B* by means of screws through the corners of the frame *D*. The beam aperture place *C* was electrically insulated from the remainder of the target assembly by means of an "O" ring. The cooling water flowed in through lead *A* to make contact with the back of plate *B* and then out through lead *A*. Secondary electrons emitted from the foil surface would spiral upward under the action of the magnetic field and be caught

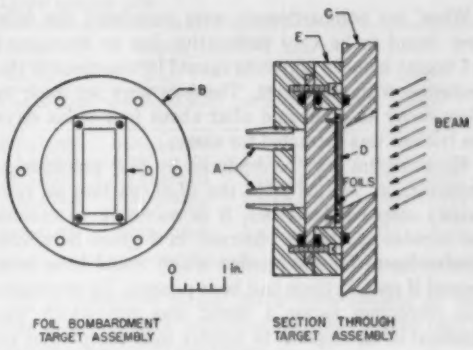

FIG. 2. Target assembly.

by frame *D* or ring *B*, both of which were electrically continuous with the foils.

The beryllium foils were purchased from the Brush Beryllium Company. They contained less than 0.1 percent of any impurity except oxygen (as BeO) which was present to the extent of 0.5 percent. The foils were 0.005 in. thick within a few percent over the foil area. The mean thickness of each foil was individually determined by measuring its weight and area to find its thickness in mg/cm².

The aluminum foils were cold-rolled to specified thicknesses from high-purity aluminum stock (less than 0.01 percent of any impurity) by staff members of the Institute for the Study of Metals of the University of Chicago. After rolling and cutting to size, the foils were annealed at 3000°C for one hour and allowed to cool slowly to room temperature. This treatment served to eliminate any local variations in density which might have resulted from working the metal. The foil thicknesses were determined as above.

Measurement of the number of deuterons incident on the target was made by connecting the target to ground through a current integrator which consisted principally of a condenser connected across a thyratron tube. As deuterons accumulated on the target, electrons would be attracted to the ground side of the condenser and the voltage across the condenser would increase until the firing potential of thyratron was reached. The thyratron would then conduct until the voltage across the condenser dropped below the extinction potential of the thyratron. Each conducting cycle tripped a mechanical register. Calibration of the integrator was routinely made by putting a known current into the circuit with all conditions the same as for bombardment except for the beam. Ordinarily the calibration technique would compensate for the current leak to ground through the water leads of the target as well as any other high-resistance leak source. However, in one of the bombardments, the circuitry was inadvertently changed between calibration and bombardment and a correction for the current leakage had to be made.

When the bombardments were completed the foils were found to be very radioactive due to short-lived (15 hours) induced activities caused by reactions of the deuterons with aluminum. The foils were set aside to allow decay to occur and after about four to six days the tritium was extracted for assay.

Since tritium may be produced by (d,l) processes in aluminum as well as from the (d,d) reaction on previously stopped deuterons, it is necessary to correct the number of tritons observed in a given beryllium bombardment for the number which would have been formed if no beryllium had been present. To determine this correction factor a blank was run which was identical in all respects to regular runs except that no beryllium was used. The total tritium produced in this run amounted to

$$(8.11\pm0.10)\times10^{-2}\frac{\text{(counts/min) of T}}{\mu\text{coul}\times\text{mg/cm}^2\text{ range in Al}}.$$

The beryllium runs were then corrected by subtracting from the total disintegrations/min of tritium produced the quantity $(8.11\pm0.10)\times10^{-2}$ μcoul mg/cm^2 of range in aluminum, where the mg/cm^2 of range in aluminum was taken to be the total range less that part of the range spent in beryllium. The fraction of the total tritium production which was ascribed to aluminum varied from 0.14 to 0.57 in these experiments.

The calculation of the net tritium activity from the beryllium reaction was made by subtracting from the total tritium activity observed the amount produced in the aluminum foils, as described previously. From the observed net counting rate the number of tritons was calculated by multiplying the disintegration rate by the mean lifetime of tritium for decay. The value used was that of Jenks, Sweeton, and Gormley.[18] Their value of the half-life is 12.46 years. The standard error of the calculated value of the number of tritons produced in beryllium was obtained by appropriate combination of the contributing statistical errors. The over-all error was usually in the order of 2 percent.

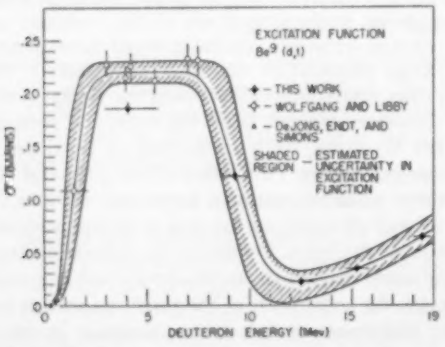

FIG. 3. Absolute excitation curve for tritium production by deuterons on beryllium.

[18] Jenks, Sweeton, and Ghormley, Phys. Rev. **80**, 990 (1950).

The number of microcoulombs of deuterons used during the bombardment was determined from the integrator reading and the calibration factor, as previously described. These, then, were converted into the number of deuterons. The number of atoms of Be/cm^2 of foil were determined by weighing the foil and measuring its area. The obliquity angle of the beam with respect to the foil target was measured as described above and the correction made. With these quantities the absolute cross section for the reaction was calculated simply by dividing the number of tritons produced by the number of Be atoms/cm^2 of area perpendicular to the beam and by the number of deuterons used during the bombardment.

The dependence of the cross section on energy was obtained in graphical form by plotting the cross-section values for the energy interval to which they corresponded and fitting a smooth curve to the data. The energy values were obtained from the range of the deuterons incident on the foil stack, from the effective thickness of the absorbing aluminum foil and from the thickness of the beryllium. In terms of the energy coordinant, the standard error at the maximum energy of 18.85 Mev was 0.20 Mev, while that at the minimum energy of 2.6 Mev was 0.95 Mev.

The numerical results of the various runs are presented in Table I and in Fig. 3.

The experimental data of Wolfgang and Libby[1] are indicated by open circles, those of DeJong, Endt, and Simons[19] by filled triangles, and those obtained in this work by filled circles. The analysis in the low-energy region is essentially that of Wolfgang and Libby. Above 7 Mev the curve of minimum slope which fitted the experimental points was drawn. The shaded area which surrounds the curve represents the estimated standard error in the position of the curve. In addition to the standard error of the measurements, the estimated error includes that due to analysis. For example, between 8 and 11 Mev, a curve of greater slope could be drawn which would still fit the experimental data. This possiblity is indicated by appropriate extension of the shaded area in this region.

One possible source of error in the present work was the production of tritium in the beryllium or aluminum by neutrons produced by (d,n) reactions in the target. Tritons from aluminum formed by neutrons produced by (d,n) on the aluminum would be included in the correction made for (d,t) processes in the aluminum. If one assumes a cross section of 0.25 barn for the (d,n) process in beryllium, then the calculated number of neutrons per deuteron is 3.7×10^{-4}. For aluminum a 0.25-barn cross section would result in the production of 1.4×10^{-3} neutron per deuteron. By using these numbers, the contribution of (n,t) tritons can be estimated by assuming $\sigma(n,t)=\sigma(d,t)$ in which case a 0.18 percent contribution would be made by (n,t)

[19] DeJong, Endt, and Simons, Physica **18**, 676 (1952).

TABLE I. Summary of $Be^9(d,t)Be^8$ reaction data.

Bombardment number (1)	Aluminum foil thickness (mg Al/cm²) (2)	Beryllium foil thickness (mg Be/cm²) (3)	Deuteron energy at incidence on beryllium (Mev) (4)	Deuteron energy on leaving beryllium (Mev) (5)	Number of deuterons (μcoul) (6)	Total tritium activity produced (10^6 counts/min) (7)	Tritium activity from aluminum (10^6 counts/min) (8)	Tritium activity from beryllium (10^6 counts/min) (9)	Cross section (barns) (10)
1	510.0	None	...	...	8946	0.261±0.003	0.261±0.003	...	...
2	321.9	20.6	5.52±0.54	2.67±0.95	9000	1.718±0.006	0.243±0.003	1.475±0.007	0.187±0.004
3	57.5	20.3	18.85±0.20	17.99±0.21	29430	3.28 ±0.03	1.120±0.012	2.16 ±0.03	0.064±0.001
4	136.1	24.6	15.83±0.23	14.65±0.24	8908	0.563±0.005	0.243±0.003	0.320±0.006	0.034±0.001
5	197.8	20.9	13.11±0.27	11.93±0.29	8898	0.424±0.008	0.243±0.003	0.181±0.008	0.023±0.001
6	258.0	20.3	9.99±0.34	8.59±0.39	8995	1.169±0.008	0.243±0.003	0.926±0.008	0.122±0.003

processes. Since all cross-section estimates were in the nature of upper limits, it is seen that no significant error results from ignoring the (n,t) contribution.

Straggling in the range of the deuterons refers to the spread in residual range (and correspondingly in energy) which results when an initially homogenous group of particles traverse a stopping medium. In these experiments the incident beam was inhomogenous to about 1 percent and there was an additional inhomogenity introduced by the straggling to the extent that after traversing a thickness of aluminum equal to the range the total spread was of the order of 2 percent. The result of this spread is to flatten the excitation curve and in portions where σ is changing rapidly with E, the true slope is slightly greater than that observed.

It is believed that the straggling effect was in part responsible for the apparently low value of the cross section obtained for the energy interval 2.67–5.52 Mev. The distribution in range of the deuterons on entering the beryllium was 30.3±4 mg/cm², and on leaving was 9.7±4 mg/cm²; so that there were contributing to the reaction a number of deuterons whose residual range (and corresponding energy) was less than the 7 mg/cm² which corresponds to the beginning of the plateau, and consequently to a lower probability of undergoing a (d,t) reaction. For this reason, the data of Wolfgang and Libby,[1] which were based on deuterons whose distribution in range was only ±1 mg/cm², were given preference in drawing the excitation function over this interval.

V. REACTION $Be^9(d,p)Be^{10}$

Although measurement of the cross section of the $Be^9(d,p)Be^{10}$ reaction has been reported by various workers,[20–22] the values are determined from differential cross section measurements over small energy intervals and often over small angular intervals.[19,20] The present research was undertaken with a view to obtaining a measurement of the total, absolute cross section as a function of energy over the energy interval 0 Mev to 21 Mev. The experimental method may be briefly described as follows:

(1) A beryllium target, thick with respect to the range of the incident deuterons, was bombarded with a measured number of deuterons.

(2) The target was then divided into thin sections by milling, and the resulting samples were chemically treated to obtain pure beryllium oxide.

(3) The activity of the Be^{10} was determined by absolute beta assay of the solid BeO.

(4) The energy at which the Be^{10} was formed was calculated from the thickness of beryllium traversed by the deuterons in reaching the sample level.

The above procedure was carried out for two samples. The first of these was bombarded with 7.78-Mev deuterons of the University of Chicago 30-inch cyclotron and the second was bombarded with 21.5-Mev deuterons of the Argonne National Laboratory cyclotron, Runs I and II respectively.

During the bombardment phase of the experiments determinations were made of the initial deuteron energy, the beam angle, and the number of deuterons used. In both runs, the initial energy was obtained by measuring the range of the incident deuterons in aluminum. In Run I the mean range was found to be 64.83±0.50 mg Al/cm². The error term (0.50 mg/cm²) corresponds to the standard error in the value of the mean range. The error was estimated by taking one-half of the limit of error in the value of the mean range. The mean energy of the incident deuterons was determined from the range energy curve (Fig. 2) to be 7.78±0.03 Mev. Conversion of the energy to range in beryllium gave the value 54.85±0.83 mg Be/cm².

In Run II, the aluminum range was found by the cyclotron staff to be 379±4 mg Al/cm² at the position of the target. Again the error cited represents the uncertainty in the value of the mean range. The corresponding energy value was found to be 21.5±0.2 Mev and the mean range in beryllium obtained from the range energy relationship for beryllium was 331.5±4 mg/cm².

The error in the mean range in beryllium corresponds, in a plot of cross section *versus* the residual deuteron range, to an uncertainty in the position of the entire curve along the horizontal (range) axis. Thus, the entire curve is translated without change in shape by an amount equal to the error in the measurement of the mean. On the other hand, the shape of the curve may

[20] DeJong, Endt, and Simons, Physica **18**, 676 (1953).
[21] F. L. Canavan, Phys. Rev. **87**, 136 (1952).
[22] Fulbright, Bruner, Bromley, and Goldman, Phys. Rev. **88**, 700 (1952).

be dependent on the manner in which the individual deuteron ranges are distributed about the mean.

For Run I the beam angle was found to be $9°\pm1°$ relative to the perpendicular to the target. For Run II it was found to be $10°\pm2°$ relative to the perpendicular to the target.

For Run I the beryllium target was in the shape of a disk, 0.125 in. thick and 3.50 in. in diameter. In it were six 0.125-in. holes equally spaced on a circle of 1.50-in. radius. Through these holes screws were inserted and the disk was fastened (by means of an "O" ring seal) to a hollow brass backing plate through which cooling water was circulated which passed over the back surface of the beryllium. The backing plate was sealed to the cyclotron target chamber, again through an "O" ring connection. The target chamber was separated from the main cyclotron assembly by a phenol fiber plate which served as electrical insulation between the main cyclotron and the target assembly. The backing plate and target chamber were electrically continuous so that secondary electrons expelled by the deuterons from the target surface would be caused to spiral upward by the magnetic field and be stopped in the target chamber whose walls extended an inch or more from the target surface. The beam was collimated prior to entering the target chamber by a 0.25 in.$\times$2.0 in. aperture in a thick copper plate. The target was of high-purity beryllium hot rolled and machined to shape by the Brush Beryllium Company. The target was 99.3 percent beryllium, with oxygen (as BeO) the principle impurity. All other impurities were less than 0.1 percent as determined by spectrographic analysis.

The Run II target was in the shape of a rectangular block whose demensions were 6.25 in.$\times$2.25 in.$\times$0.50 in. It was machined to a smooth finish on both sides, and mounted at the internal[23] target position of the cyclotron, by means of an "O" ring seal to a target support plate. Since the target support plate was cut out to permit passage of the beam and was electrically insulated from the main cyclotron, the walls of its aperture served to catch secondary electrons from the target surface. However, since the plate itself received a small part of the beam current it was not made electrically continuous with the target but instead the current from the target support plate was separately monitored during the bombardment and the secondary electron current was determined by subtracting from the current observed during bombardment that observed when no target was present. The secondary electron current thus determined was found to be of the order of 0.2 percent or less of the total current to the target so that no correction for this effect was applied.

Target cooling for Run II was accomplished by circulating the cooling water within the target itself. The path for the water consisted of a 0.25-in. diameter hole which ran parallel to both of the 6.25-in. edges and to one of the 2.25-in. edges just outside the periphery of the beam area. The target material was stock beryllium of the Argonne National Laboratory; this was of moderate purity and contained less than 0.1 percent of all constituents except oxygen which was present to the extent of 1.0 percent.

For both runs the charge accumulation was measured by a current integrator of the type described in Sec. IV. The calibrations were carried out under simulated bombardment conditions so that the current leakage to ground through the water leads or other high resistances was corrected for in the conversion of integrator reading to microcoulombs. In Run I a slight dependence of the integrator conversion factor on the magnitude of the current was found. However, over the range of current levels used in the bombardment (0 μa to 30 μa) no significant error resulted from this dependence. The number of microcoulombs calculated on the basis of the entire bombardment being made at 30 μa was less then 1 percent greater than the number calculated on the basis of a 10 μa bombardment.

The Run II current level was relatively constant at about 220 μa and the calibration was carried out by using this current level under the metering and leakage conditions which prevailed during bombardment. Six calibrations were carried out during the two day bombardment period. The mean value of the conversion factors obtained from these calibrations was used in the final calculation of the number of deuterons. The individual values all were within one standard error of the mean.

After the bombardments were completed, each of the targets was radio-autographed by placing it in contact with the sheet of x-ray film which was referenced to the target edges. A 20-minute exposure for Run I and a 3-minute exposure for Run II were used. The autographs were made the day following the completion of the bombardments. The radio-autograph served to indicate the extent of tha active area and were used to determine the minimum area which had to be included in the sample to insure complete removal of activity.

The sampling procedure consisted of milling the beryllium into thin sections and determining the thickness removed per cut. The beryllium was then subjected to chemical separation which lead to the preparation of chemically pure beryllium oxide.

Beryllium is a relatively hard metal and in machining it, some lubrication and cooling at the cut surface are to be desired. In addition, it was necessary that the chips resulting from the milling process be quantitatively recovered. Lubrication, cooling, and recovery

[23] The internal target position immediately adjacent to the deflector as opposed to the external mounting position used for the foil bombardments in the (d,p) runs which is separated from the main target chamber by a 3-mil aluminum window. The external chamber may be quickly evacuated and is used when several changes of target over a short period of time are required.

were all obtained by immersing the target in a bath of trichloroethylene during the milling operation.

The individual cuts were 0.001 to 0.003 in. in thickness. It was found in a separate experiment that cuts of less than one mil were liable to be of uneven depth, and that in particular the tool could tend to ride over that portion of the area which had been exposed to the beam without continuously cutting. A lower limit on the resolution obtainable by the milling technique is thus imposed. A single carbide end-mill was used throughout Run I. For Run II a succession of high-speed steel end-mills were used. A single mill was found to last for about 15 to 20 cuts.

The thickness measurement in Run I was made at the time of the milling operation by measuring the depth to which the beryllium was cut away relative to a reference point on the unmilled portion of the sample disk. The measurement was made with a Federal dial gauge which was graduated in units of 0.0001 in. The gauge was calibrated against a milled aluminum block which was cut to various depths which had been accurately measured with a micrometer calipers. The dial gauge was read over a grid pattern of 135 points for each cut. The average depth of cut and the error in the depth of cut were calculated from these data. The weight of the disk before and after milling was measured. The area milled, the total thickness removed, and the weight removed were combined to calculate the density of the beryllium. A separate check on the density was made on an unmilled disk from the same lot and the two values agreed within experimental error. The thicknesses of the individual samples in units of 0.001 in. were converted to centimeters and multiplied by the density to obtain the mg/cm^2 thickness values used in subsequent calculations.

For Run II the beryllium chips resulting from the milling of each layer were caught on a previously weighed filter paper and their weight determined for each cut.

Although the amount of impurity in the beryllium was low, the activity induced in it could amount to several thousand times that of the Be^{10}. The reason for this is that the induced activity is inversely proportional to the half-life of the species and since the Be^{10} half-life is 2.7×10^6 years, any contaminating activity of half-life of the order of several months would, in general, be more active than the Be^{10} itself and in addition would require a considerable time to decay to a negligible level. For this reason an efficient method of separation of beryllium was required.

The method used was that give by Noyes and Bray[24] and it depends upon the solubility in chloroform, of the basic acetate by beryllium. The procedure is given here in summary.

(1) The sample was transferred to a 50-ml centrifuge tube and dissolved in 3*N* HCl.

(2) Concentrated NH_4OH was added in excess to precipitate $Be(OH)_2$ which was centrifuged and washed once with NH_4OH.

(3) The $Be(OH)_2$ was dissolved in 10 ml of 6*N* HAc, transferred to an evaporating dish, and evaporated almost to dryness. Ten ml of glacial acetic acid were added and the mixture was evaporated to dryness.

(4) The resulting basic beryllium acetate, $BeO\cdot3Be(C_2H_3O_2)_2$, was taken up in 40 ml of chloroform and the solution filtered.

(5) The filtrate was caught in a 125-ml separatory funnel, shaken four times with 40 ml of water and the chloroform phase transferred to a platinum evaporating dish.

(6) The chloroform solution was evaporated to dryness and the residue dissolved in 10 ml of 6*N* HNO_3. The nitric acid solution was evaporated to dryness and the residue ignited to the oxide which was mounted for counting.

It was found for the Run I samples that a single extraction cycle resulted in complete removal of contaminating activities. For Run II it was found that an occasional sample contained active impurities so that a complete recycling was carried out on all the Run II samples. The BeO dissolved in aqua regia upon heating in a covered beaker. The resulting solution was treated as above with the exception that the initial $Be(OH)_2$ precipitate was dissolved in HCl, and then reprecipitated before washing. Failure to do this resulted in a glassy residue from the acetic acid evaporation—instead of the crystalline, easily powdered, residue usually obtained.

In determining the absolute cross section from the activity of the product nucleus, the principle experimental difficulty lies in the determination of the absolute disintegration rate of the product. The Be^{10} produced by the (d,p) reaction emits a single beta of 0.555-Mev maximum energy, has no gamma, and has a half-life of 2.7×10^6 years.[18] The method used has been described above. For each milled slice of the bombarded beryllium target the total number of Be^{10} atoms was determined by counting methods and using the 2.7×10^6 year half-life figure. The angle at which the beam hit the target was measured and the correction made for this effect. The cross section then was calculated by dividing the number of Be^{10} atoms produced used by the number of Be atoms/cm^2 of cross section perpendicular to the direction of the beam and the number of deuterons which were used in the bombardment.

The mean energies of the deuterons at the depth of the samples were obtained from the beryllium range energy relationship which is discussed above. The measurements which entered into the energy determination were the initial range and the thickness traversed. These were combined to obtain the residual range which was used to determine the energy.

[24] A. A. Noyes and W. C. Bray, *A System of Qualitative Analysis for the Rare Elements* (The MacMillan Company, New York, 1948), p. 172.

The residual range was determined by subtracting from the incident range (as determined from aluminum absorption), the accumulated thickness of the samples traversed. The incident ranges were, for Run I: 54.85±0.83 mg Be/cm², and for Run II: 331.5±4 mg Be/cm². The thickness traversed in Run I was calculated from the dial gauge measurements of the depth of the cuts. In Run II the individual sample thicknesses were summed to obtain the total thickness between the surface and a given sample layer. Since the total thickness removed was separately determined from the density of the target and the depth of the total cut, it was possible to calculate the thickness values near the end of the range just as accurately as those near the beginning.

The over-all uncertainty in the residual range results from the combination of the uncertainty in the range of the incident deuterons with that of the thickness of beryllium traversed. These uncertainties will be discussed separately and in the order given. The measurement of the mean range of the incident deuterons was subject to an uncertainty of the order of 1 percent. For although in theory the deuteron range is uniquely determined by the magnetic field strength and the radius of the cyclotron, it was observed in both runs that the fraction of the beam transmitted by a given foil depended to a small extent on the beam current level, which is independent of these parameters. Furthermore, repeated runs at the same current level gave some spread in the transmission fraction for a given foil thickness. The limit of error of the measured mean range in aluminum was divided by two to obtain an estimate of the standard error of the determination. The mean range in aluminum was found to be 64.83 ±0.50 mg/cm² for Run I and 379.0±4.0 mg/cm² for Run II. In the determination of residual range, the uncertainty in the mean range applies identically to all sample points so that the entire curve is translated by the amount of the error.

The individual ranges of the incident deuterons are distributed about the mean value in roughly a Gaussian distribution. The spread in range results from two effects of almost equal magnitude. The first is that there is a finite energy interval over which deuterons can maintain resonance and emerge from the dees. The second is that the energy loss process in traversing the foil consists of a large number of small steps which result in a statistical distribution in the distance traversed for a given energy loss. The combined magnitude of these effects may be determined from the slope of the transmission curve at the mean thickness value. Thus, in Run I the total deviation was found to be 1.4 mg/cm², which was attributed to contributions of 0.7 mg/cm² and 1.2 mg/cm² by the stopping and inhomogenity effects, respectively. (The deviations combine as the square root of the sum of the squares.) In terms of beryllium thickness the total deviation was 1.2 mg/cm² and since the thickness of the individual samples were of the order of 5 mg/cm², the spread in range had much less effect on the interval of range to which a given cross-section measurement applied than did the finite sample thickness. For this reason cross section coordinates were plotted as average values over the sample thicknesses.

In Run II, however, the standard deviation of the individual ranges about the mean was found to be 5.6 mg Be/cm². This was attributed to contributions of 2.9 mg Be/cm² by the stopping effect and 4.7 mg Be/cm² by the inhomogenity of the beam. In this run also, the samples were milled at a slight angle to the target surface which resulted in a spread in the distances traversed by the deuterons reaching any given level. The standard deviation in the distance traversed was found from the deuteron distribution and the geometry to be 2.0 mg Be/cm². This deviation was combined with that due to the beam inhomogenity to obtain a standard deviation of 5.1 mg Be/cm² for the residual range of the deuterons about the mean residual range.

For Run I the value of the thickness traversed was known to be within about 2 percent. This was the accuracy with which the depth of cut was measured by the dial gauge. For Run II the individual sample weights were of the order of 150±3 mg and the area milled was 30.00±0.04 cm² so that the sample thicknesses were known to ±0.1 mg/cm². The cumulative uncertainty in the thickness traversed was of the order of ±0.5 mg/cm². Therefore, the uncertainty in the residual range was essentially that due the uncertainty in the initial range. The final determination of the spread in energy values to which give cross section measurement applied was made by multiplying the spread in the residual range, q_R, by the stopping power.

The results of the runs are presented in Table II.

In Fig. 4 is presented a plot of the excitation function. The effect of straggling on the shape of the curve is to diminish the rate of change of the cross section with energy. For this reason the Run I data, in which strag-

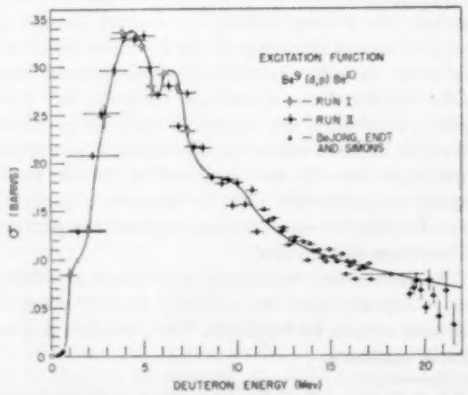

FIG. 4. Absolute excitation function for Be^{10} production by deuterons on beryllium.

gling was much less than Run II, were given greater weight in the region of rapidly changing cross section. From 14 Mev the 21.6 Mev. the curve drawn fits the equation $\sigma = 1.5/E_D$. The data plotted between 0.25 and 0.62 Mev are those of DeJong, Endt, and Simons,[18] and were obtained by them by integration of their differential cross-section data.

In deciding whether the excitation function obtained represents an accurate measurement of the variation of σ with E, consideration must be taken of the possibility of systematic errors.

Since the reaction $Be^9(d,n)B^{10}$ is used for neutron production it is possible that $Be^9(n,\gamma)Be^{10}$ may have contributed significantly to the observed Be^{10} production. However, sample layers taken beyond the extreme deuteron range showed zero Be^{10} activity. Since neutrons had traversed these layers, it was concluded that the (n,γ) contribution was negligible. There exists a question as to whether the Be^{10} found in a given sample was formed in that layer or whether the ranges of the recoiling Be^{10} nuclei were of a magnitude comparable with the sample thicknesses. The maximum recoil energy obtained in the present experiments was that resulting from the interaction at 21.5-Mev deuteron energy. At this energy the Be^{10} recoil energy was calculated to be 10.8 Mev using a method given by Libby.[25] Although there is no range energy relationship for Be^{10} in beryllium, there are available range energy relationships for Be^9 and Be^{10} in Ilford emulsions.[26] The measured values extend to 5.5 Mev where, for the Be^9 ion, a range of 8.5 microns is reported. Since a 1-mil cut corresponds to 25 microns, it would appear that there would be some contribution to the straggling by the movement of Be^{10} atoms from their place of formation; however, the standard deviation due to straggling was of the order of 1 mil and since these deviations combine as the root mean square of the components, no significant increase in total straggling would be anticipated except for the highest energy samples.

There is a question as to what effect the straggling of the deuterons used in Run II might have on the calculation of the cross section. In the calculations presented, the number of deuterons was assumed constant over the residual range interval of the sample. A calculation of the magnitude of the error introduced by neglect of the distribution of residual range showed that for the most part the effect was 1 percent or less, however, where σ was changing rapidly the effect amounted to about 2 percent. Since this was of the order of the uncertainty in σ no correction was made. Near zero energy, where the effect was most pronounced, the Run I data could be used to obtain the excitation function.

One further possible source of error lay in the tendency of the milling tool to cut unevenly in thin cuts. A number of the samples in which the thickness removed was of the order of 3.3 mg/cm² or less were observed to be significantly lower in cross section value than the mean of their neighboring samples. In a few cases the following sample appeared to be high in value, as if the metal which the mill had missed in the first cut were added to the second. However, the effect was not always observed for thin samples and a few of the apparently low results were from thicker samples so that no attempt was made to compensate for this source of error other than to give the thicker sample data preference over the thin in positioning the curve in regions of abundant data.

VI. REACTION $Be^9(d,tn)Be^7$

In the course of measuring the Be^{10} activity for the determination of the $Be^9(d,p)Be^{10}$ cross section, it was observed that samples corresponding to high deuteron energy contained a gamma activity which could not be chemically separated from Be^{10}. The activity was identified as that of Be^7 which decays by K capture to Li^7, 11 percent of the decay is through the 0.476-Mev excited state of Li^7 and the lithium gamma is observed.[13] The threshhold energies for the production of this isotope were determined. The (d,tn) reaction, whose threshhold energy is 17.47 Mev, proved to be the only reaction which was energetically possible. The $(d,p3n)$ reaction threshold is at 30.3 Mev and that for the $(d,d2n)$ reaction is at 25.1 Mev.

The Be^7 activity was obtained along with the Be^{10} activity whose treatment was given in the previous chapter. All the details of experimental procedure up to and including the mounting of the samples were identical for the two species. For samples in which Be^7 activity was present an additional counting rate determination was made using a 250 mg Al/cm² absorber to eliminate the Be^{10} beta activity. The calculation of the absolute disintegration rate of the Be^7 required that the counting efficiency of the gammas under this condition be determined.

Since the counting rate of the samples under the 250 mg/cm² aluminum absorber was that of the gamma activity only, this counting rate served to measure the relative yield of Be^7. The individual sample rates were divided by the weight of BeO to obtain counts per minute of gamma per milligram of BeO. This procedure involves the assumption that self-absorption of the gamma by the BeO was negligible, which was well justified.

The absence of contaminating activities was checked for all samples by recounting them after approximately two half-lives. In all cases the observed decay rate was within the counting error of 53.7 days. In addition, the spectrum of one of the samples was run on a scintillation spectrometer and found to be free from observable contamination.

The total counting rate of the sample was converted to the absolute number of Be^7 atoms by using the

[25] W. F. Libby, J. Am. Chem. Soc. **69**, 2523 (1947).
[26] C. H. Miller and A. G. W. Cameron, Can. J. Phys. **31**, 723 (1953).

TABLE II. Summary of $Be^9(d,p)Be^{10}$ reaction data.

Sample number (1)	Sample thickness (mg/cm^2) (2)	Mean thickness traversed (mg/cm^2) (3)	Residual range (mg/cm^2) (4)	Be^{10} activity (counts/min) (5)	BeO weight (mg) (6)	BeO area (cm^2) (7)	Cross section (barns) (8)	Mean energy (Mev) (9)
I-1	9.0	4.5	50.3	71.8	90.2	1.18	0.233±0.005	7.39±0.38
I-2	5.1	11.5	43.8	71.2	68.9	1.01	0.278±0.005	6.82±0.22
I-4	6.0	19.0	35.8	122.5	98.2	1.79	0.292±0.006	6.06±0.25
I-5	6.8	25.8	29.4	39.0	42.9	0.53	0.280±0.012	5.43±0.30
I-6	2.3	30.4	24.8	116.5	99.3	1.42	0.322±0.005	4.91±0.15
I-7	6.9	38.1	16.6	204.7	169.8	2.38	0.336±0.005	3.82±0.50
I-9	4.9	43.8	11.0	25.5	28.6	0.40	0.249±0.013	2.90±0.42
I-10	5.0	47.5	66.3	72.0	118.4	2.52	0.130±0.004	2.01±1.00
I-11	2.5	52.2	2.6	11.8	58.9	0.50	0.084±0.007	1.05±0.50
I-12	9.1	58.1	−3.2	0.0	78.4	1.23	0.000±0.007	0.00
II-1	11.31	4.3	332.2	6.0	64.8	0.75	0.030±0.002	21.56±0.17
II-2	9.35	14.9	321.6	17.1	84.0	0.93	0.066±0.021	21.16±0.17
II-3	10.39	25.0	311.5	9.6	79.5	0.91	0.039±0.017	20.80±0.17
II-4	8.62	34.1	302.1	16.3	89.3	0.97	0.061±0.009	20.48±0.18
II-5	2.96	40.4	296.1	22.7	95.4	1.11	0.077±0.011	20.26±0.18
II-6	7.68	45.8	290.7	17.5	93.0	1.34	0.048±0.007	20.07±0.18
II-7	5.75	52.6	283.9	18.3	84.4	1.06	0.066±0.010	19.80±0.19
II-8	3.96	58.5	278.0	22.1	102.1	1.06	0.076±0.009	19.56±0.19
II-9	4.50	61.8	274.7	17.9	85.7	0.99	0.068±0.007	19.42±0.19
II-10	4.76	66.5	270.0	23.2	126.4	1.35	0.063±0.006	19.24±0.20
II-11	40.97	89.8	246.7	46.4	212.1	2.01	0.083±0.001	18.26±1.68
II-12	3.66	112.3	224.2	38.8	169.0	1.82	0.078±0.002	17.16±0.21
II-13	3.58	116.1	220.4	51.7	184.6	2.06	0.094±0.002	17.06±0.21
II-14	4.02	120.1	216.4	44.9	177.9	1.82	0.090±0.002	16.88±0.21
II-15	3.03	123.7	212.8	38.5	169.5	1.53	0.091±0.002	16.72±0.22
II-16	3.90	127.2	209.3	35.0	132.6	1.46	0.089±0.002	16.56±0.22
II-17	3.02	130.7	205.8	28.2	127.3	1.34	0.078±0.002	16.36±0.22
II-18	4.05	134.3	202.2	49.2	167.1	1.93	0.096±0.002	16.22±0.22
II-19	4.40	138.6	197.9	38.5	129.5	1.54	0.092±0.002	16.04±0.22
II-20	4.00	142.9	193.6	45.8	163.9	1.74	0.097±0.002	15.96±0.22
II-21	2.52	146.2	190.3	24.5	93.2	1.12	0.083±0.002	15.82±0.23
II-22	5.60	150.3	186.2	58.2	180.9	2.09	0.104±0.002	15.62±0.23
II-23	5.21	155.8	180.7	36.2	119.7	1.40	0.097±0.002	15.36±0.23
II-24	3.84	160.4	176.1	54.7	185.4	1.99	0.101±0.002	15.14±0.23
II-25	4.10	164.4	172.1	58.1	179.7	1.98	0.109±0.002	14.94±0.24
II-26	3.66	168.4	168.1	47.0	165.7	1.80	0.097±0.002	14.75±0.24
II-27	3.73	172.1	164.4	45.4	146.1	1.69	0.101±0.002	14.56±0.24
II-28	4.74	176.4	160.1	51.3	156.2	1.74	0.109±0.002	14.38±0.24
II-29	3.77	180.7	155.8	47.3	144.4	1.63	0.108±0.002	14.12±0.25
II-30	3.48	184.4	152.1	61.9	182.3	1.98	0.115±0.002	13.92±0.25
II-31	2.50	187.4	149.1	30.4	98.8	1.17	0.098±0.002	13.76±0.26

calibration described above in Sec. II. The over-all gamma counting efficiency in the 2π counts was 0.214 percent.

The cross section for the $Be^9(d,tn)Be^7$ reaction was calculated as the ratio of the number of Be^7 atoms produced to the number of Be^9 atoms per cm^2 of beam and the number of deuterons used.

The uncertainty in the cross section may be considered as a resultant of two components, that which changes from sample to sample and that which applies to all samples. The nonsystematic errors amounted to approximately 2 percent in all samples. While the systematic amounted to about 12 percent and was chiefly attributable to the counting efficiency uncertainty. The shape of the excitation function depends only on the nonsystematic error so that only this was indicated in the plotted data. The uncertainty in the mean value of the energy was of the order of -0.2 Mev. The quantity plotted was the standard deviation of the mean energy due to the straggling effect and finite sample thickness.

Experimental Results

In Table III is given a summary of the experimental values and the calculated values of the cross section.

In Fig. 5 is given the excitation function of the reaction of the reaction $Be^9(d,tn)Be^7$. It will be noted that the point corresponding to the energy 20.2 Mev does not fall on a smooth curve through the remaining points. However, this value was obtained from the data of sample II-5 which was a thin cut. As was noted in the preceding chapter, the thin cuts had been observed occasionally to produce inhomogeneous samples as a result of the cutting tool riding over a part of the area milled. Therefore, this point was not drawn explicitly and its weighted mean cross-section value with the succeeding sample II-6 was used in the construction of the curve.

It will be noted that a small residual Be^7 activity was found below the threshhold energy of 17.47 Mev. This was attributed to the straggling of the deuterons and was not drawn in.

TABLE II.—*Continued.*

Sample number (1)	Sample thickness (mg/cm²) (2)	Mean thickness traversed (mg/cm²) (3)	Residual range (mg/cm²) (4)	Be^{11} activity (counts/min) (5)	BeO weight (mg) (6)	BeO area (cm²) (7)	Cross section (barns) (8)	Mean energy (Mev) (9)
II-32	5.64	191.6	144.9	64.6	190.2	2.02	0.118±0.002	13.54±0.26
II-33	4.95	197.0	139.5	48.3	131.8	1.49	0.122±0.002	13.06±0.27
II-34	4.74	201.8	134.7	49.3	163.8	1.50	0.118±0.002	13.00±0.27
II-35	3.13	205.7	130.8	39.6	115.3	1.30	0.114±0.002	12.78±0.28
II-36	3.03	208.8	127.7	60.5	153.4	1.70	0.132±0.003	12.50±0.28
II-37	6.60	212.6	123.9	61.1	170.9	1.75	0.128±0.003	12.40±0.28
II-38	6.40	220.3	116.2	74.8	181.4	1.94	0.142±0.002	11.98±0.29
II-39	3.95	225.5	111.0	65.9	148.8	1.78	0.139±0.003	11.66±0.30
II-40	5.90	229.5	107.0	76.6	155.3	1.94	0.151±0.003	11.42±0.30
II-41	3.18	235.2	101.3	48.2	142.3	1.36	0.128±0.003	11.06±0.31
II-42	5.85	239.7	96.8	89.8	177.7	1.95	0.171±0.003	10.80±0.32
II-43	5.65	245.5	91.0	46.2	178.5	1.82	0.156±0.003	10.42±0.32
II-44	4.51	251.7	84.8	94.4	184.3	1.93	0.179±0.004	10.00±0.32
II-45	4.81	255.5	81.0	67.3	166.9	1.58	0.155±0.003	9.74±0.34
II-46	2.91	259.3	77.2	91.8	160.7	1.90	0.182±0.004	9.48±0.35
II-47	5.25	263.5	73.0	81.3	181.5	1.64	0.178±0.004	9.20±0.36
II-48	7.85	270.4	65.1	101.4	180.8	2.04	0.185±0.004	8.62±0.38
II-49	5.65	277.0	59.5	86.1	139.3	1.46	0.216±0.005	8.18±0.40
II-50	5.68	282.9	53.6	92.0	181.6	1.54	0.217±0.004	7.68±0.42
II-51	4.34	287.1	49.4	126.5	164.5	1.74	0.272±0.005	7.32±0.43
II-52	4.16	292.4	44.1	125.7	178.4	1.94	0.238±0.003	6.84±0.46
II-53	6.75	297.9	38.6	133.1	171.8	1.70	0.280±0.004	6.34±0.48
II-54	5.07	303.9	32.6	149.4	194.6	2.02	0.271±0.005	5.76±0.53
II-55	2.40	307.8	28.7	103.9	108.5	1.32	0.300±0.005	5.35±0.56
II-56	3.82	310.9	25.6	168.4	174.5	1.84	0.332±0.005	5.00±0.59
II-57	4.33	315.0	21.5	95.0	173.9	1.80	0.328±0.006	4.51±0.63
II-58	3.82	319.1	17.4	167.0	176.2	1.87	0.330±0.004	3.94±0.69
II-59	3.17	322.7	13.8	118.6	144.6	1.45	0.296±0.006	3.40±0.75
II-60	2.54	325.6	10.9	55.7	71.4	0.82	0.252±0.006	2.75±1.00
II-61	3.68	328.8	7.7	91.6	147.8	1.62	0.208±0.003	2.30±1.50
II-62	3.96	332.6	4.1	60.5	165.3	1.70	0.129±0.002	1.49±2.50
II-63	4.55	337.0	−0.5	26.1	138.1	1.55	0.062±0.002	···
II-64	4.25	341.4	−4.5	7.0	148.1	1.56	0.016±0.002	···
II-65	5.35	345.4	−8.9	5.3	158.3	1.54	0.012±0.002	···

It is interesting to compare the total tritium production with that due to the (d,tn) process. At 18.4 Mev for example, the (d,t) cross section was found to be 0.06 barn, the (d,tn) cross section at this energy has been found to be 0.02×10^{-3} barn. One may therefore conclude that the Be^8 excited states which result from the $Be^9(d,t)Be^8$ process decay principally by alpha emission rather than neutron. However, since the pick-up process results in the production of Be^8 in all states which are energetically possible, it is not surprising that the two states[1] for which Be^7+n decay is observed should constitute only a small part of the total. The states are those observed by means of resonances in the $Li^7(p,n)Be^7$ excitation curve. They are found at 19.18 and 21.4 Mev above the Be^8 ground state and hence correspond to deuteron energies of 17.65 Mev and 20.50 Mev. An intermediate level which corresponds to an 18.66-Mev deuteron energy has a very pronounced resonance for the competing reaction $Li^7(p,\alpha)\alpha$.

VII. DISCUSSION OF (d,p) AND (d,t) EXCITATION FUNCTIONS

Theory of (d,p) *reactions.*—A theory which gives the excitation function for the total cross section was given by Peaslee.[27] The observed excitation function was considered to be the product of two energy-dependent probabilities, the first was the probability of a neutron of the deuteron being at the nuclear surface. The second was the probability that a captured neutron would be in a negative energy state in the compound nucleus. Neutrons which were captured but in a positive energy

TABLE III. Summary of $Be^9(d,tn)Be^7$ reaction data.

Sample number	$\frac{I}{W}\exp\left(\frac{0.693\Delta t}{53.7}\right)$ $\left(\frac{\text{counts/min}}{\text{mg BeO}}\right)$	Cross section (10^{-28} cm²)	Mean energy (Mev)
II-1	58.1±1.0	77.8±1.3	21.56±0.17
II-2	52.2±1.0	69.8±1.3	21.16±0.17
II-3	46.9±0.8	62.9±1.0	20.80±0.18
II-4	35.8±0.8	47.9±1.0	20.48±0.18
II-5	37.7±0.8	50.4±1.0	20.26±0.18
II-6	28.1±0.5	37.6±0.7	20.07±0.19
II-7	22.7±0.5	30.1±0.7	19.80±0.19
II-8	18.6±0.4	24.8±0.6	19.56±0.19
II-9	14.5±0.3	19.4±0.5	19.42±0.20
II-10	10.9±0.3	13.5±0.5	19.24±0.20
II-11	2.0±0.1	2.7±0.1	18.26±1.68
II-12	0.6±0.1	0.8±0.1	17.16±0.21
II-13	0.0±0.1	0.0±0.1	17.06±0.21

[27] D. C. Peaslee, Phys. Rev. 74, 1001 (1948).

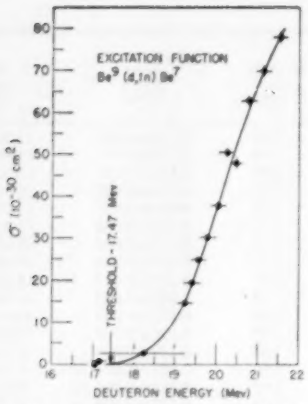

FIG. 5. Excitation function for $Be^9(d,tn)Be^7$.

state were subject to re-emission and the reaction did not contribute to the (d,p) reactions. The product of these two curves was adjusted to the absolute value of a given experimental curve by assignment of a sticking probability for the neutron. Very satisfactory fits to the experimental shape were found for reactions cited which were all for target nuclei of atomic mass greater than twenty-four. In all cases the excitation function was smoothly changing in agreement with the theory. An assumption of the theory which is not met in the present work is that incident neutrons of all possible angular momenta may react. In the light of the discussion to follow, this assumes a large number of available states for the entering neutrons.

The theory of Butler,[3] which predicts the angular distribution of the protons from stripping reactions to a single level of the product nucleus, has been the subject of numerous experimental investigations. The great interest in it resulted from the prediction that the positions of maxima in the angular distribution were determined by the angular momentum of the reacting neutron with respect to the target nucleus. Selection rules for the angular momenta—that the vector sum of the neutron angular momentum, neutron spin and target spin must equal the spin of the product nucleus—permitted the determination of limits on the spin of the product excited state once the neutron angular momentum, l_n, was established. It has been shown by measurements on the $Be^9(d,p)Be^{10}$ proton distribution[22] that the ground state and first excited state of Be^{10} are both formed through p neutron capture ($l_n=1$). The observed angular distributions for the two states indicate that the stripping process predominates over compound nucleus formation up to the maximum energy at which the distribution was studied, 14.5 Mev.[23]

Theory of (d,t) *reactions.*—Although no theory of (d,t) excitation functions for total cross sections has been developed, a theory for the angular distribution of the emergent tritons from pick-up processes has been developed.[4] It is completely analogous to the (d,p) angular distribution theory. The angular momentum of the target-emitted neutron determines the position of the maxima in the angular distribution. The selection rules for allowed transitions are the same as above. It has been shown that the transition to the ground state of Be^8 occurs through the pickup of p-wave neutrons ($l_n=1$). Examination of the proton and triton distribution of the same author[22] indicate that the compound nucleus contribution in the (d,t) process is less than that in the (d,p).

In considering the characteristics of the excitation functions, it is necessary to take into account the predominant mode of reaction. Thus, if compound nucleus formation were predominant one would expect the energy levels of the B^{11} nucleus to be significant in determining the shape of the excitation curve. This follows from the generally accepted viewpoint that the reaction probability in compound nucleus processes may be expressed as the product of the probability of compound nucleus formation and the probability of a given mode of decay. In many cases, the first of these is the shape determining factor since its energy dependence may be much greater than that of the second.

In stripping (or pickup) however, the compound nucleus formation probability does not appear, and the reaction might profitably be considered to be made up of a number of completely unrelated reactions, namely, those leading to each excited state of the Be^{10} (or Be^9) nucleus. Thus, as the deuteron energy increased to the threshold value for a particular state one would expect a perturbation in the excitation curve due to contribution by a new reaction. The maximum effect of each new level would be observed not at the energy of the level itself, but some 1 or 2 Mev higher since at the threshhold, the reaction probability is zero.

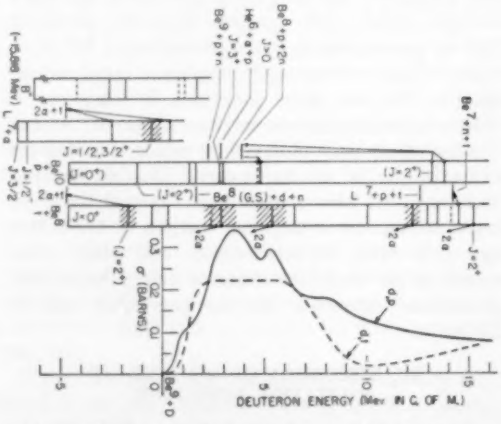

FIG. 6. Energy level scheme and excitation functions for $Be^9(d,p)Be^{10}$ and $Be^9(d,t)$.

[23] C. F. Black, Phys. Rev. 87, 205(A) (1952).

In considering the excitation functions from this point of view, it is helpful to have available an energy level scheme for the isotopes involved. Such a scheme has been presented in Fig. 6. It was adapted from the values given in the very comprehensive review of energy levels of light nuclei given by Ajzenberg and Lauritsen.[1] All the indicated levels are plotted at energies relative to the ground state energy of Be^9 plus a deuteron. The energies indicated are those in the center-of-mass system.

A plot of the two excitation functions drawn to the same energy scale has been included in the figure.

ACKNOWLEDGMENTS

The authors are very anxious to acknowledge the great assistance given by the Argonne National Laboratory and the crew of its cyclotron is providing the bombardments. They wish to thank Mr. Melvin Fielding for operation of the 8-Mev Chicago cyclotron, Dr. James R. Arnold for the use of his scintillation sysectrometer and Dr. Kay K. Chenye for the preparation of special foils. Finally, they wish to thank the U. S. Air Force, Office of Scientific Research and Development, for financial support.

PHYSICAL REVIEW VOLUME 100, NUMBER 3 NOVEMBER 1, 1955

Electric Excitation of Certain Rare-Earth Nuclei by Protons*

HANS MARK† AND GEORGE T. PAULISSEN
Department of Physics and Laboratory for Nuclear Science, Massachusetts Institute of Technology, Cambridge, Massachusetts
(Received July 28, 1955)

Sixteen energy levels have been observed in thirteen isotopes of samarium, europium, gadolinium, and terbium. Electric quadrupole transition probabilities have been determined for some of these energy levels from the measured electric excitation cross sections. For the even-A isotopes of Gd, the properties of the low-lying energy levels are in good agreement with the expectations of the "strong coupling" rotational model. The first energy levels in the even isotopes of samarium show the sharp break in the position of the first excited level which has recently been pointed out by Scharff-Goldhaber. In general, the results are in good qualitative agreement with the predictions of the collective model; however, the moments of inertia for the rotational levels observed in this region are substantially larger than those expected from the intrinsic deformations obtained from the radiative transition probabilities.

I. INTRODUCTION

SINCE the discovery of electric excitation nearly three years ago,[1,2] a large amount of information concerning nuclear energy level structure has been collected by means of this process. Over one hundred isotopes, ranging from F^{19} to U^{238}, have been bombarded by α particles (see publications of G. M. Temmer and N. P. Heydenburg; Sherr, Li, and Christy; and Torben Huus and collaborators) or protons (see publications of Eisinger, Cook, and Class; R. M. Williamson and W. I. Goldburg; P. H. Stelson and F. K. McGowan; Simmons, Van Patter, Famularo, and Stuart; Torben Huus and collaborators; and McClelland, Mark, and Goodman) and in most isotopes, the existence of one or more energy levels has been established. Most workers have observed the γ rays emitted after the excitation of the nucleus while others (see Torben Huus and collaborators and W. I. Goldburg and R. M. Williamson) have detected the internal conversion electrons which, in most cases, also follow the nuclear excitation. For some nuclei, the angular distribution of γ rays following electric excitation has also been determined (see Eisinger, Cook and Class; W. I. Goldburg and R. M. Williamson; P. H. Stelson and F. K. McGowan; and Simmons *et al.*).

An electric excitation event is said to occur when an energetic charged particle passes by a nucleus and exchanges some of its kinetic energy with the nucleus through the agency of the electric field existing between the projectile and the nucleus. In the vast majority of the cases observed so far it is the quadrupole term of this field which gives rise to the excitation but it is of course possible, in principle, to excite energy levels having other multipole orders as well.[3,4] The energy levels of the nucleus being bombarded are then studied by observing the energies of the γ rays which are emitted upon the decay of the excited nucleus. The number of γ rays per charged particle (i.e., the electric excitation cross section) is related to the radiative transition probability of the energy level under investigation. Since large radiative transition probabilities give rise to large electric excitation cross sections, the process has been particularly useful for the study of the

* Supported in part by the joint program of the Office of Naval Research and the U. S. Atomic Energy Commission.
† Now at the Department of Physics, University of California, Berkeley, California.
[1] C. L. McClelland and Clark Goodman, Phys. Rev. **91**, 760 (1953).
[2] T. Huus and C. Zupančič, Kgl. Danske Videnskab. Selskab, Mat.-fys. Medd. **28**, No. 1 (1953).
[3] Sherr, Li, and Christy, Phys. Rev. **94**, 1076 (1954).
[4] G. M. Temmer and N. P. Heydenburg, Phys. Rev. **94**, 1252 (1954).

so-called "collective" transitions in nuclei. The great abundance of these "collective" levels throughout the periodic table has served as an excellent qualitative confirmation of the validity of Aage Bohr's "collective" model of nuclear structure.[5]

In general, there is remarkably good agreement among the experimental workers in the field regarding the position of energy levels in the many isotopes which have been studied. However, quite serious discrepancies exist in the measured electric excitation cross sections and hence in the measured values of the radiative transition probabilities. These discrepancies are caused by the difficulties in measuring absolute γ-ray yields with presently available techniques and will be discussed in detail in the following section. It has been suggested[6] that many of the existing uncertainties in the measured cross sections (such as uncertainties in stopping power, detector efficiency, etc.) would disappear if the ratio of elastically to inelastically scattered particles from a given level were measured rather than the number of γ rays (or internal conversion electrons) which are emitted per bombarding particle. In such experiments, any uncertainties, due to internal conversion, in the radiative transition probabilities calculated from the cross sections would also be absent. Experiments of this type have recently been performed[7] at the Massachusetts Institute of Technology using the new high-resolution, charged-particle spectrograph of the MIT-ONR generator group with very promising results.

II. EXPERIMENTAL METHODS

The experimental procedures used in the series of measurements to be described are substantially the same as those which have been used previously[8,9] in similar experiments. Some changes have been made which were designed to improve the γ-ray yield measurements. The basic problem of measuring the number of γ rays per proton can be conveniently divided into three parts: the determination of the proton beam current, the determination of the attenuation suffered by the γ rays as they travel from the target to the detector, and the determination of the efficiency of the detector for γ rays of a given energy for the experimental geometry used. The proton beam current was measured with a standard beam current integrator which consists of a condenser in parallel with a relay which closes whenever the voltage across the condenser reaches a certain point. This instrument was calibrated with a standard battery to within 2%. It is improbable, however, that the actual beam current is known this accurately since there is considerable secondary electron emission when targets are bombarded with high-energy protons. Several tests with targets at different positive voltages were made to estimate the size of this effect, and as a result of these studies, the estimated error in the beam current is of the order of 10%.

The attenuation of the γ rays between the target and the detector arises from self-absorption in the target, absorption in the aluminum target holder tube, absorption in the aluminum housing and the magnesium oxide layer of the crystal, and absorption in the tin sheets which were used to reduce the background of characteristic x-rays from each target. All of these effects except the last are reasonably small even for γ rays of energies of the order of 80 kev ($\sim$20% attenuation), and therefore the expected attenuation was calculated using published values of absorption coefficients.[10] The attenuation of the γ rays in the tin absorbers is quite large ($\sim$60%) for the lowest energy γ rays, and hence the absorption in the tin was determined experimentally by measuring the attenuation for a given γ ray as a function of absorber thickness. The error in γ-ray yield per proton due to attenuation of the γ rays will be a function of γ-ray energy. The smallest errors ($\sim$5%) will occur for the γ rays with the highest energies (i.e., smallest attenuation) and larger errors ($\sim$15%) are expected for the lowest energy γ rays.

By far the most troublesome problem encountered in the determination of absolute γ-ray yields is the determination of the absolute efficiency of the detector. In all cases, the γ-ray intensity was determined by graphical integration of the photopeak in the pulse-height spectrum (see Figs. 2, 3, 4, 5, 6, and 7). The proton bremsstrahlung[11,12] background was subtracted out experimentally. The error in the yield due to background subtraction is roughly 5%. Since the area of the photo-peak is used as a measure of the γ-ray intensity, the efficiency of the crystal for the production of pulses in the photo-peak must be determined. For γ rays with energies below 100 kev, large (2 in.$\times$2 in.) NaI crystals are substantially 100% efficient detectors—that is, almost every γ ray which strikes the face of the crystal gives rise to a pulse in the photopeak. For higher energy γ rays this is no longer the case, and therefore the efficiency must either be calculated theoretically or measured. Pulses in the photopeak arise from two sources: a γ ray may be absorbed by an atom emitting a photo-electron which carries off the entire energy of the γ ray; or a γ ray may undergo one or more Compton collisions with almost free electrons in the crystal, and then the final degraded photon ultimately is absorbed in a photoelectric event. Both of these events give rise to pulses in the photopeak and hence both must be included in a theoretical calculation of the efficiency.

[5] A. Bohr and B. R. Mottelson, Kgl. Danske Videnskab. Selskab, Mat.-fys. Medd. **27**, No. 16 (1953).
[6] H. Mark, Phys. Rev. **94**, 1436(A) (1954).
[7] W. W. Buechner and C. K. Bockelman (private communication).
[8] McClelland, Mark, and Goodman, Phys. Rev. **97**, 1191 (1955).
[9] Mark, McClelland, and Goodman, Phys. Rev. **98**, 1245 (1955).
[10] C. M. Davisson and R. D. Evans, Revs. Modern Phys. **24**, 79 (1952).
[11] C. Zupančič and T. Huus, Phys. Rev. **94**, 205 (1954).
[12] Mark, McClelland, and Goodman, Phys. Rev. **98**, 279(A) (1955).

Meader, Muller, and Wintersteiger[13] have made extensive calculations of NaI photopeak efficiency and their results have been used to interpolate the photopeak efficiency curve between experimental points.

The photopeak efficiency of the crystal was determined for annihilation radiation (510 kev) from a Na^{22} source by a γ-γ coincidence experiment and for 279-kev γ rays from a Hg^{203} source by a β-γ coincidence experiment, using the equipment shown in Fig. 1. For the β-γ coincidence experiment one of the γ counters was replaced by a pilot B plastic scintillator 0.05 in. thick mounted on a du Mont 6292 photomultiplier tube. This counter was sensitive only to the β particles emitted by the source. In both cases measurements were made for several different geometries including the one actually used in the experiment. For the annihilation radiation, counter B was set so that only the photopeak pulses were large enough to trip the coincidence circuit. Because of the back-to-back correlation of the annihilation quanta, the photopeak efficiency of counter B is then just the ratio of the number of counts in the photopeak observed at the coincidence output to the number of counts in the photopeak at the analyzer output. For the geometry used in the electric excitation experiments (i.e., crystal faces $\frac{5}{16}$ in. from the target and perpendicular to proton beam) this number is 0.25 ± 0.02. Assuming that the effective range of a 510-kev photon in the crystal is 0.9 in., the photopeak efficiency for the geometry used in these experiments can be obtained by multiplying 0.25 by the effective solid angle subtended by the counter B at the target. The photopeak efficiency for the experimental geometry determined in this manner is 0.033. The error in this number may be as large as 30% or more because of the uncertainty in determining the effective solid angle. In the case of the 279-kev radiation from Hg^{203}, counter B was again set so that only photopulses of the γ rays tripped the coincidence circuit and counter A was replaced by the electron counter. Since the β and γ rays from the source are essentially directionally uncorrelated, the ratio of counts at the coincidence output to those at the analyzer output is a direct measure of the photopeak efficiency for the experimental geometry. For the experimental geometry used in the cross-section measurements, this ratio was 0.15. It should be pointed out, however, that this result may also be in error by 30% or more because of scattered low-energy electrons from the source and because the 279-kev γ ray is quite highly internally converted[14] giving rise to electrons which are not accompanied by γ rays. (It was possible with the pilot B scintillator to observe both the K and L conversion lines from the 279-kev transition. The resolution was roughly 35%. The actual coincidence ratios were taken at an energy near the maximum of the β spectrum—between 50 and 80 kev. The background from the internal conversion lines and from scattered electrons at this energy was unfortunately still considerable.) In view of the many uncertainties in the theoretical interpolations and in the calibration measurements themselves, the errors in the γ-ray yield are of the order of 50% due to uncertainties in detector calibration alone. The error from this source will of course be a function of γ-ray energy with the largest errors occurring for the γ rays with the highest energy. However, as has been pointed out, the uncertainties in the attenuation of the γ rays behave in the opposite manner with the largest errors occurring for the lowest-energy γ rays. It is probable, therefore, that the absolute error in the number of γ rays per proton stays reasonably constant as a function of γ-ray energy.

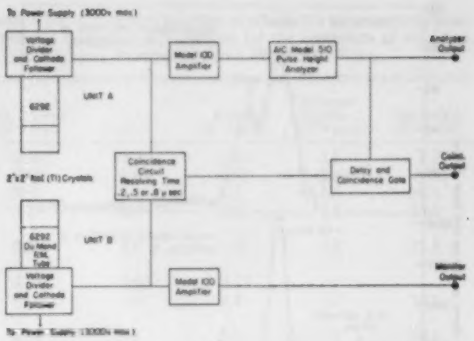

FIG. 1. Experimental equipment. The equipment used for the detection of the γ rays is shown in this figure. A signal appears at the coincidence output whenever a pulse in crystal B is in coincidence with a pulse in crystal A which is within the window of the single-channel analyzer. The coincidence circuit is not activated by pulses from the counters which are below a certain voltage, and hence the system possesses a cut-off point below which it will not work. The position of the cut-off point can be adjusted by varying the high voltage across unit B. The pulses observed at the analyzer output represent the pulse spectrum in unit A while the monitor output registers all pulses in unit B.

The experimental geometry employed is also somewhat different from that which has been described previously.[6] The crystals were placed, one on each side of the target holder, with their axes perpendicular to the proton beam and their faces $\frac{5}{16}$ in. from the target. The beam was focused on the target on a spot roughly 0.5 mm square. In this way, errors in the total γ yield due to the angular distribution of the emitted γ rays are reduced to less than 5%. The aluminum target holder tube was 0.5 in. in diameter and the walls were $\frac{1}{16}$ in. thick. The targets in all cases were made of the metallic oxide powder ($\sim$30 mg) compressed on a small ($\frac{1}{4}$-in. diameter) aluminum plug which was held in position between the crystals on a thin brass rod. The inside of the holder tube was lined with 0.002-in. tin sheet to eliminate background radiations arising from scattered protons striking the aluminum tube.

There are two reasons for using both crystals in coincidence during the electric excitation experiments.

[13] Maeder, Muller, and Wintersteiger, Helv. Phys. Acta **27**, 3 (1954).
[14] D. Saxon, Phys. Rev. **74**, 849 (1948).

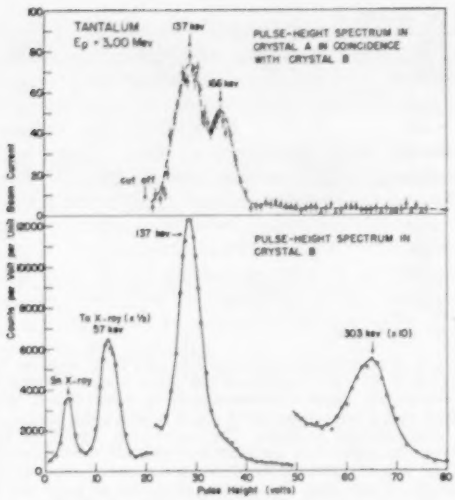

FIG. 2. Pulse-height spectrum observed from tantalum target during bombardment with 3-Mev protons. The lower panel shows the spectrum observed at the analyzer output and the upper panel shows the spectrum at the coincidence output. The peak corresponding to the tin x-ray seen in the singles spectrum comes from fluorescence radiation of the tin absorber between the target and the detector. The voltage across counter *B* is adjusted so that the coincidence circuit is not tripped by the x-ray pulses and therefore they do not contribute to the random background. The 137-kev peak observed in the coincidence spectrum is slightly larger than the 166-kev peak because of the large random background at this point due to the excitation of the 137-kev level alone.

One is to observe cascade transitions in odd A nuclei where it is often possible to excite the first two energy levels. Figure 2 shows the pulse-height spectrum obtained when a thick tantalum metal target is bombarded with 3-Mev protons. The unbroken curve shows the spectrum obtained in one crystal in coincidence with pulses in the other. In the singles spectrum, peaks corresponding to energies of 137 and 303 kev are observed. These peaks are caused by γ rays coming from the decay of the first two energy levels in this isotope. The coincidence spectrum shows peaks at 166 kev and 137 kev which come from the cascade decay of the 303-kev level and are therefore in coincidence. From such measurements it is possible to determine the ratio of the number of cascade to crossover γ rays for the second energy level. Such measurements have been made for a number of odd A nuclei[15] and are presently being extended. The other reason for using the coincidence spectrometer in the electric excitation experiments is that it aids in the identification of impurity γ rays. A γ ray at 510 kev is observed from all oxide targets which is accompanied by a high coincidence counting rate characteristic of annihilation radiation (see Fig. 3). It is very probable that this γ ray arises from annihilation radiation emitted[16] in the decay of F^{17} which is produced in the target by the reaction $O^{16}(p,\gamma)F^{17}$. The continuous coincidence background observed from oxide targets is of the order of 5 times larger than that observed from metallic targets which indicates the presence of high-energy capture γ rays emitted in cascade transitions between highly excited states in F^{17}.

In all cases, the yield of γ rays was measured from targets which were thick to 3-Mev protons. The energy calibration of the scintillation spectrometer was carried out by using the methods which have been described in reference 9. The γ-ray energies quoted in column 2 of Table I are considered accurate to 5% except for some special cases which will be discussed in the next section. Column 5 in the table of results shows the

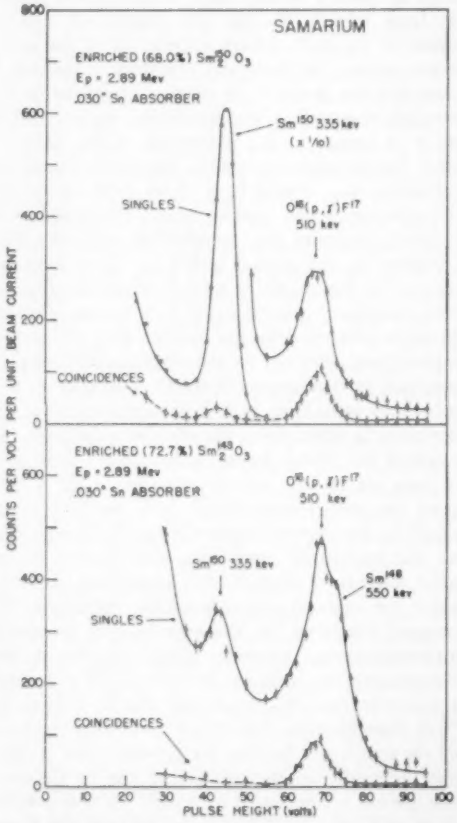

FIG. 3. Pulse-height spectra observed from $(Sm^{148})_2O_3$ and $(Sm^{150})_2O_3$ targets during bombardment with 2.89-Mev protons. This figure shows the peaks corresponding to γ rays of 335 kev and 550 kev which arise from the excitation of energy levels in Sm^{150} and Sm^{148} respectively. The peak at 510 kev is due to annihilation radiation which probably comes from the decay of F^{17} produced in the oxide target by the reaction $O^{16}(p,\gamma)F^{17}$.

[15] H. Mark and G. Paulissen, Phys. Rev. **99**, 1654 (A) (1955).

[16] F. Ajzenberg and T. Lauritsen, Revs. Modern Phys. **27**, 77 (1955).

TABLE I. The experimental results are summarized in this table. Column 4 lists the proton energies at which the cross section measurements were made. The values of $B(E2)$ listed in column 8 are the reduced transition probabilities for the excitation of the level. The values of Q_0 (energy) listed in column 10 are calculated from Eq. (2) in reference 8 assuming $R_0 = 1.44A^{1/3} \times 10^{-13}$ cm.

Nuclide	E_γ(kev)	$I_0 \to I$	E_p(Mev)	N_γ/proton (10^{-9})	$B(E2)/(\alpha r+1)$ (10^{-48} cm^4)	αr	$B(E2)$ (10^{-48} cm^4)	Q_0(cross section) (10^{-24} cm^2)	Q_0(energy) (10^{-24} cm^2)
Sm^{148}	550[a]	0→2	2.88	4.8	0.74	10^{-3}	0.74	2.7	7.39
Sm^{150}	335	0→2	2.88	13.9	0.51	0.03	0.52	2.3	9.45
Sm^{152}	125	0→2	2.88	53.9	0.43	1.6	1.1	3.3	15.4
Sm^{154}	84	0→2	2.88	41.2	0.27	6.3	2.0	4.5	18.8
Eu^{151}	300	5/2→?	2.88	2.0	...	...	...	...	...
Eu^{153}	85	5/2→7/2	2.88	15.8	0.20[b]	4.0	1.0	5.0	21.8
	115	...	2.88	2.5	...	...	...	...	...
	200	5/2→9/2	2.88	6.5	0.14	0.05	0.15	...	...
Gd^{154}	123[c]	0→2	1.88	8.8	1.0	1.6	2.6	5.1	16.0
Gd^{154}	140[a]	7/2→?	2.88	...	...	...	...	...	...
Gd^{156}	89	0→2	1.88	2.2	0.74	5.7	5.0	7.1	18.8
Gd^{157}	127[a]	7/2→?	2.88	...	...	...	...	...	...
Gd^{158}	80	0→2	1.88	2.4	0.63	8.6	6.0	7.7	19.8
Gd^{160}	76	0→2	1.88	3.0	0.73	12.0	9.5	9.7	20.2
Tb^{159}	77	3/2→?	2.88	...	...	...	...	...	...
	167[d]	3/2→?	2.88	...	...	...	...	...	...

[a] Error ±10%.
[b] Calculated assuming no contribution from cascade.
[c] Composite line.
[d] Probable impurity line.

number of γ rays per proton obtained from each target. The absolute error in this number from all the sources discussed in this section is of the order of 75% and in some special cases, which will be discussed in the next section, may be even larger. However, the relative errors between yields from different isotopes of the same element are much smaller (of the order of 15%) since many of the factors which contribute to the large absolute error tend to cancel out. The conversion of the measured yield to the electric excitation cross section will be discussed in the final section.

III. EXPERIMENTAL RESULTS

Sixteen γ rays have been observed in thirteen isotopes of samarium, europium, gadolinium, and terbium. Many of these γ rays have already been observed by other workers following the β decay of unstable isotopes in the same region of the periodic table and all of them have also been observed by Temmer and Heydenburg[17] by electric excitation with α particles and by Huus, Bjerregard, and Elbek[18] who have studied the internal conversion electrons emitted from many of these materials upon bombardment with protons. (The authors are indebted to Dr. Temmer for sending us a preprint of his results prior to publication and also to Dr. Elbek who supplied us with a rough draft copy of his paper.) In most cases, the isotopic assignments of the γ rays were determined by bombarding samples of enriched isotopes. For those elements where enriched samples were not available, the most probable assignment was made on the basis of previously published work.

[17] G. M. Temmer and N. P. Heydenburg (private communication).
[18] Huus, Bjerregard, and Elbek, Kgl. Danske Videnskab. Selskab, Mat.-fys. Medd. (to be published).

Sm^{148}

The pulse-height spectrum obtained when an enriched (72.7%) $(Sm^{148})_2O_3$ target is bombarded with 2.89-Mev protons is shown in the lower panel of Fig. 3. A γ ray at 550 kev is observed which comes from the excitation of an energy level in Sm^{148}. Unfortunately, the 510-kev annihilation radiation of roughly equal intensity from the $O^{16}(p,\gamma)F^{17}$ reaction partially obscures the 550-kev radiation. The upper panel of Fig. 3 shows the pulse-height spectrum obtained from an enriched $(Sm^{150})_2O_3$ target obtained under similar conditions. This target contained only 2.54% Sm^{148}, and therefore the peak at 510 kev in this spectrum is caused entirely by the annihilation radiation. The intensity and energy of the 550-kev line were estimated by subtracting the curve in the upper panel from the lower one. The errors in both the energy and the intensity of this γ ray are unusually large because of this background effect.

Sm^{150}

The upper panel in Fig. 3 shows the pulse-height spectrum obtained when an enriched (68.0%) $(Sm^{150})_2O_3$ target is bombarded with 2.89-Mev protons. The strong γ ray at 335 kev comes from the excitation of an energy level in Sm^{150} at about this energy (336.7 kev) which is also observed[19] following the β decay of Pm^{150}.

Sm^{152}

The pulse-height spectrum obtained when enriched (96.0%) $(Sm^{152})_2O_3$ is bombarded with 2.89-Mev protons is shown by the dashed curve in Fig. 4. A strong γ ray at 125 kev is observed which comes from the excitation of a level at this energy in Sm^{152} which is also observed[20] following the positron decay of Eu^{152}.

[19] V. K. Fischer, Phys. Rev. **96**, 1549 (1954).
[20] Slattery, Lu, and Wiedenbeck, Phys. Rev. **96**, 465 (1954).

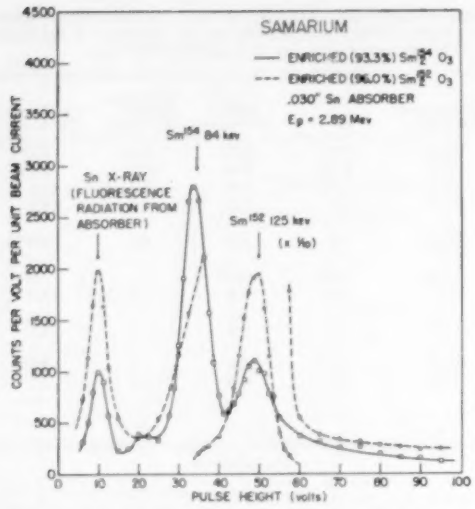

FIG. 4. Pulse-height spectra observed from $(Sm^{152})_2O_3$ and $(Sm^{154})_2O_3$ targets during bombardment with 2.89-Mev protons. This figure shows peaks corresponding to γ rays of 125 kev and 84 kev which arise from the excitation of energy levels in Sm^{152} and Sm^{154}, respectively.

Sm^{154}

The solid line in Fig. 4 shows the pulse-height spectrum when enriched (93.3%) $(Sm^{154})_2O_3$ is bombarded with 2.89-Mev protons. A γ ray at 84 kev is observed which comes from the excitation of a level in Sm^{154}. The peak at 125 kev observed in this spectrum comes from the 3.2% Sm^{152} present in this sample.

Eu^{151}

No enriched isotopes of europium were available for these experiments. Four γ rays (300 kev, 200 kev, 115 kev, and 85 kev) are observed when a natural Eu_2O_3 target is bombarded with protons. The γ ray at 300 kev has been tentatively assigned to the 47.8% abundant Eu^{151} by Temmer and Heydenburg.[17] This assignment is probably correct because no γ ray of this energy is observed[20] following the β decays of Gd^{153} and Sm^{153}.

Eu^{153}

The other three γ rays which are observed when the natural Eu_2O_3 is bombarded with 2.89-Mev protons are shown in the upper panel in Fig. 5. The three γ rays at 200 kev, 115 kev, and 85 kev probably arise from the excitation of the first two energy levels at 85 kev and 200 kev in 52.2% abundant Eu^{153}. There is some evidence that the 115-kev γ ray is always in coincidence with an 85-kev γ ray, indicating that the 115-kev γ ray arises from the cascade decay of the 200-kev level in this isotope. However, this scheme cannot be definitely established from our data because of the large coincidence background from oxide targets. Several γ rays of similar energies are observed[21] in the β decay of Sm^{153}; however, the level schemes proposed in references 21 and 22 are not in agreement with our data or the data of Temmer and Heydenburg.[17]

Gd^{154}

The pulse-height spectrum obtained when an enriched (33%) target of $(Gd^{154})_2O_3$ is bombarded with 2.89-Mev protons is shown by the dotted curve in Fig. 6.

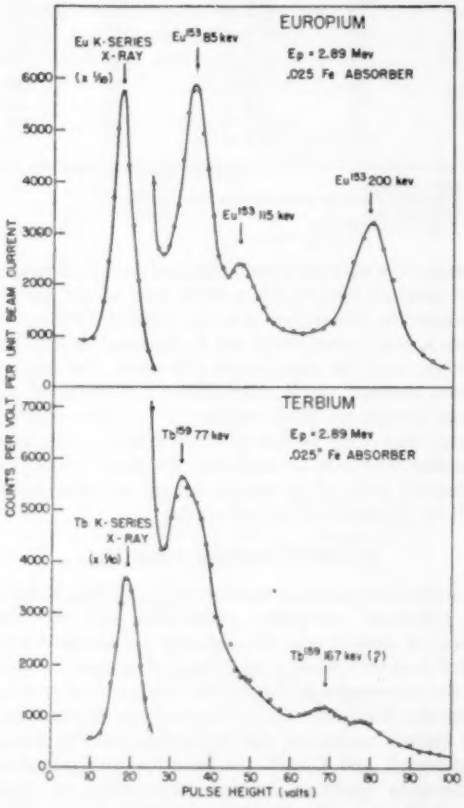

FIG. 5. Pulse-height spectra observed during the bombardment of Eu_2O_3 and Tb_2O_3 targets with 2.89-Mev protons. The peaks corresponding to γ rays at 85, 115, and 200 kev in the upper panel probably arise from the excitation of the first two rotational levels in Eu^{153}. This drawing is a good example of a rotational spectrum observed in an electric excitation process. There is some evidence that every 115-kev γ ray is always in coincidence with an 85-kev γ ray. A γ ray at 300 kev is observed from the europium targets which has roughly the intensity of the 200-kev peaks and probably arises from the excitation of a level in Eu^{151}. The terbium spectrum shown in the lower panel is not considered too reliable for reasons which are explained in the text.

[20] *Nuclear Data*, National Bureau of Standards Circular Report No. 499 (U. S. Government Printing Office, Washington, D. C., 1950).

[21] Cork, Leblanc, Nester, and Stumpf, Phys. Rev. **88**, 685 (1952).

A strong γ ray at 123 kev is observed which is also seen[20] in the β decay of Eu^{154}. The small peak at 85 kev in this spectrum is caused by the presence of 16% of Gd^{156} in the sample.

$Gd^{155,157}$

The pulse-height spectrum obtained when natural Gd_2O_3 targets are bombarded with 2.89-Mev protons is shown by the unbroken curve in Fig. 6. The γ rays corresponding to the two peaks at ~127 and ~140 kev have been assigned by Temmer and Heydenburg[17] to energy levels in 15.7% abundant Gd^{157} and 14.7% abundant Gd^{155}, respectively. No cross-section measurements were made for these lines since their intensities are so low. The peak at 127 kev is certainly composite, with the 123-kev line in 2.15% abundant Gd^{154} contributing to the observed intensity.

Gd^{156}

Figure 7 shows the pulse-height spectrum obtained when enriched (80.22%) $(Gd^{156})_2O_3$ is bombarded with 1.71-Mev protons. A peak corresponding to a γ ray of 89 kev is observed which comes from the excitation of an energy level in this isotope.

Gd^{158}

The dotted curve in Fig. 7 shows the pulse-height spectrum when enriched (92.9%) $(Gd^{158})_2O_3$ targets are bombarded with 1.71-Mev protons. A peak is observed corresponding to a γ ray of 80 kev which comes from the excitation of an energy level in this isotope.

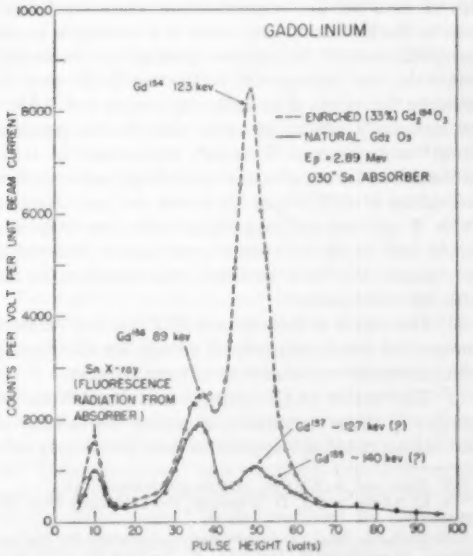

FIG. 6. Pulse-height spectra observed during the bombardment of enriched $(Gd^{154})_2O_3$ and natural Gd_2O_3 bombarded with 2.89-Mev protons. The strong peak corresponding to a γ ray at 123 kev is due to excitation of a level in Gd^{154} and the two bumps on the curve at about 127 and 140 kev are probably caused by the excitation of levels in Gd^{157} and Gd^{155}, respectively.

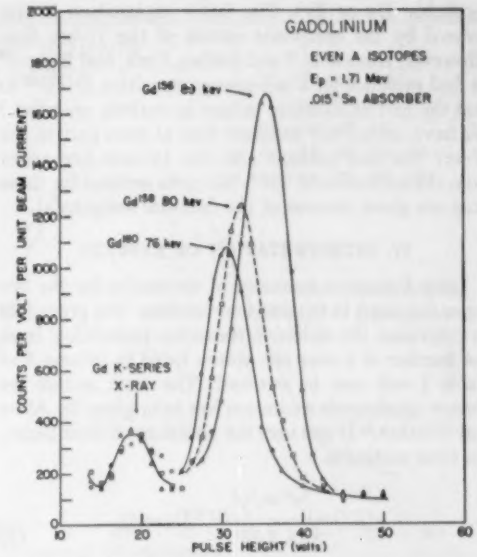

FIG. 7. Pulse-height spectra observed during the bombardment of $(Gd^{156})_2O_3$, $(Gd^{158})_2O_3$, and $(Gd^{160})_2O_3$ targets by 1.71-Mev protons. The peaks observed at 89, 80, and 76 kev arise from the excitation of energy levels in Gd^{156}, Gd^{158}, and Gd^{160}, respectively.

Gd^{160}

The pulse-height spectrum observed when an enriched (95.4%) $(Gd^{160})_2O_3$ target is bombarded with protons is shown in Fig. 7. A peak is observed at 76 kev which corresponds to a γ ray coming from the excitation of a level in Gd^{160}.

Tb^{159}

The lower panel in Fig. 5 shows the pulse-height spectrum when a Tb_2O_3 target is bombarded with 2.89-Mev protons. Peaks corresponding to γ rays of 77 kev and 167 kev are observed. In addition, a small rise in the curve at about 210 kev is also present. It is quite difficult to interpret this spectrum since the samples used in these experiments were most probably contaminated with other rare-earth materials. Furthermore, since the sample available to us consisted of $(NH_4)Tb(SO_4)_2$ the oxide had to be obtained by precipitation with NH_4OH. It is possible therefore that the high continuous background and perhaps some of the observed lines are due to light impurities. It should also be noted that both the K x-ray and the 77-kev lines are broader than the corresponding lines observed from europium. The width of the K x-ray line could be explained either by the existence of an energy level near this energy in Tb^{159} or—more likely—a rare-earth contamination in the target with a slightly larger Z

(probably Dy or Er). The latter explanation is also favored by the composite nature of the 77-kev line. (However, Huus *et al.*[18] and Jordan, Cork, and Burson[23] do find evidence for a low-energy transition in Tb^{159} so that the first explanation cannot be entirely excluded.) We have tentatively assumed that at least part of the 77-kev line and perhaps also the 167-kev line arises from the excitation of Tb^{159}. No cross sections for these lines are given because of the doubtful assignment.

IV. INTERPRETATION OF RESULTS

Table I shows a summary of the results for the isotopes discussed in the previous sections. The procedure to determine the radiative transition probability from the number of γ rays per proton listed in column 5 of Table I will now be outlined. The cross section for electric quadrupole excitation has been given by Alder and Winther.[24] If one uses the notations of their paper, the cross section is

$$\sigma(E2)=\frac{2\pi^2}{25}\frac{m_1^2v_f^2}{Z_2^2h^2}B(E2)g_{E2}(\xi) \tag{1}$$

$$=\psi(E)B(E2),$$

where

$$\xi=\frac{Z_1Z_2e^2}{h^2}\left[\frac{1}{v_f}-\frac{1}{v_i}\right]. \tag{2}$$

The definition of $B(E2)$ in Eq. (1) has been changed slightly from that used by Alder and Winther. Our $B(E2)$ is equal to their $B(E2)$ divided by e^2. The electric excitation cross section is related to the number of γ rays per proton emitted from a thick target (N_γ) by:

$$N_\gamma=\frac{N_A a}{\alpha_T+1}\int_0^{E_p}\frac{\sigma(E2)}{S(E)}dE, \tag{3}$$

where N_A is the number of atoms per gram, a is the isotopic abundance of the material under investigation, $S(E)$ is the stopping power of the target material in Mev/(g/cm^2), α_T is the total internal conversion coefficient of the level and $\sigma(E2)$ is the electric excitation cross section given in Eq. (2). The upper limit of the integration is the initial energy of the proton. The electric excitation cross section is the product of two factors, one depending on proton energy and the dynamics of the collision [$\psi(E)$ in formula (1)] and the other depending only the radiative transition probability of the energy level under consideration [$B(E2)$ in formula (1)]. The quantity of interest is $B(E2)/(\alpha_T+1)$. Inserting (1) into (3) and solving for $B(E2)/(\alpha_T+1)$ gives

$$\frac{B(E_2)}{\alpha_T+1}=\frac{N_\gamma}{N_A a I(E_p)}, \tag{4}$$

where

$$I(E_p)=\int_0^{E_p}\frac{\psi(E)}{S(E)}dE. \tag{5}$$

Once N_γ is measured, the evaluation of the radiative transition probability depends upon the evaluation of (5). The functions $\psi(E)$ have been tabulated[25] for a wide range of values of proton energies. The stopping powers $S(E)$ for the various oxide targets were obtained from the experimental values for gold and oxygen given by Allison and Warshaw[26] by using interpolation procedures previously[27] described. The functions $\psi(E)/S(E)$ were then plotted against proton energy (E) and the numbers $I(E_p)$ were determined by graphical integration from these curves. The probable error introduced in the value of $B(E2)/(\alpha_T+1)$ by uncertainties in the value of the stopping power and by the interpolation procedure is of the order of 15%. The values of $B(E2)/(\alpha_T+1)$ are listed in column 6. The cumulative errors from the values in N_γ and from the integration of the stopping power make it probable that the absolute values of $B(E2)/(\alpha_T+1)$ quoted are reliable to roughly a factor of two. The relative values of the $B(E2)/(\alpha_T+1)$ in any series of isotopes which have roughly similar energy level schemes are very much more reliable (~15%).

In order to calculate the actual radiative transition probabilities, $B(E2)$, from the values of $B(E2)/(\alpha_T+1)$, values for the total internal conversion coefficient, α_T, must be obtained for each transition. Very little experimental data on the magnitudes of these coefficients exist in the literature, and hence it is necessary to use extrapolations of the rather inadequate theoretical values in the literature.[28–30] The methods used to calculate the values of α_T shown in column 7 of Table I are essentially similar to those used in our previous report[8] and those of Sunyar.[31] The errors in these estimated values are of course quite large, and therefore the values of $B(E2)$ and Q_0 (cross section) listed in Table I are order-of-magnitude estimates only and should not be used to draw quantitative theoretical conclusions. We have included these numbers in the table for two reasons:

(1) The trends in the values of $B(E2)$ in any series of isotopes are considered reliable enough for comparison with theory and are therefore of some interest.

(2) The values of Q_0 (energy) calculated from the energies of these transitions, assuming the validity of the "strong coupling" approximation, are all very sub-

[23] Jordan, Cork, and Burson, Phys. Rev. **92**, 315 (1953).
[24] K. Alder and A. Winther, Phys. Rev. **96**, 237 (1954).
[25] K. Alder and A. Winther (private communication).
[26] S. K. Allison and S. D. Warshaw, Revs. Modern Phys. **25**, 779 (1953).
[27] McClelland, Mark, and Goodman, Laboratory for Nuclear Science, Massachusetts Institute of Technology LNS-MIT Technical Report No. 66, 1954 (unpublished).
[28] Rose, Goertzel, Spinrad, Harr, and Strong, Phys. Rev. **83**, 79 (1951).
[29] Gellman, Griffith, and Stanley, Phys. Rev. **85**, 944 (1952).
[30] B. I. Spinrad, Phys. Rev. **98**, 1302 (1955).
[31] A. W. Sunyar, Phys. Rev. **98**, 653 (1955).

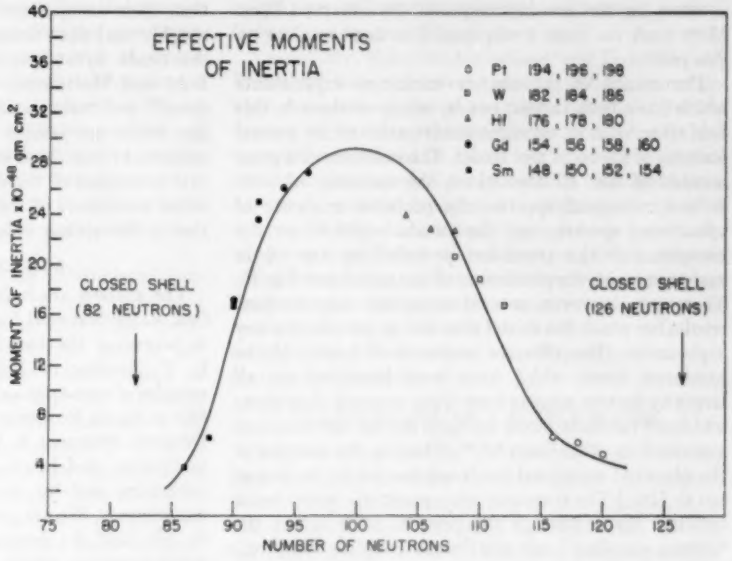

FIG. 8. Effective moments of inertia of even-A nuclei as a function of neutron number. The effective moment of inertia is calculated from the energy of the first excited level in each isotope by using the formula:

$$E=(\hbar^2/2\mathcal{I})I(I+1).$$

The trends exhibited by $\mathcal{I}$ are the same as those shown by known nuclear electric quadrupole moments. There is some doubt whether this formula is applicable for the observed levels in Sm^{148}, Sm^{150}, and the platinum isotopes.

stantially larger (outside experimental errors in either number) than those obtained from the cross sections—a fact which is also of some theoretical interest. (See reference 8.)

Several remarks regarding the experimental results are in order. The trends in the values of the energies and radiative transition probabilities for the even-A isotopes of gadolinium are in good agreement with the expectations of the "strong coupling" picture of Bohr and Mottelson.[5] The energies increase as the closed shell at 82 neutrons is approached while the transition probabilities decrease, which is a reflection of the fact that the largest intrinsic nuclear deformations are to be expected at a neutron number of about 96. It should be pointed out that the trends in the even-A isotopes of tungsten and hafnium[8,17] are the reverse of those observed in gadolinium because the closed shell at 126 neutrons apparently dominates their behavior.

The behavior of the even-A isotopes of samarium is more difficult to understand. In the neutron-rich isotopes Sm^{154} and Sm^{152}, the energies of the first excited levels are very close to those in the neighboring gadolinium isotopes, but in the isotopes Sm^{150} and Sm^{148} the energies are 3 and 5 times larger, respectively. It has been suggested[32] that, at this point in the periodic table, the "strong coupling" approximation breaks down and that the fast $E2$ transitions observed below this point are the "vibrational" levels predicted by the "weak coupling" approximation. A strong argument in favor of this interpretation is that the even-A nuclei below this point have second excited levels at roughly twice the energy of the first level which is what would be expected for vibrational spectra (see the summary of data in reference 32). Furthermore, in odd-A nuclei below this point in the periodic table, electric excitation experiments have not revealed a single case[9,33] where the first two energy levels fit into a good "strong coupling" (i.e., rotational) spectrum; whereas above this point many examples[2,8,17] of well-developed rotational spectra are known.

The odd-A isotopes, for which results are given in Table I, also show some interesting properties. The three low-energy γ rays observed from the europium target fit into the proper rotational sequence for a nucleus with ground level spin 5/2. These energy levels have been tentatively assigned to Eu^{153}. It is somewhat difficult to understand why the isotope Eu^{151} does not also exhibit a good rotational spectrum, since several examples of neighboring odd-A isotopes where both numbers have proper rotational spectra are in existence.[8,17] The energy levels observed in the odd-A isotopes of gadolinium also raise some interesting questions. The situation here should be roughly similar to the one encountered in the hafnium[8,17] isotopes where both the odd- and even-A isotopes have strongly excited first energy levels at roughly similar energies. In the case of the odd-A gadolinium isotopes the energy levels observed have transition probabilities which are of the order of 30 times smaller than those observed in the neighboring odd-A isotopes (see Fig. 3). Temmer and Heydenburg[17] have suggested that these γ rays arise from the second excited levels in these nuclei and actually have some evidence for the existence of energy levels in these isotopes at about 48 kev. This would

[32] G. Scharff-Goldhaber and J. Weneser, Phys. Rev. 98, 212 (1955).

[33] G. M. Temmer and N. P. Heydenburg, Phys. Rev. 98, 1308 (1955).

account for the low intensities of the observed lines. More work on these levels should be done to clear up this point.

The results of the electric excitation experiments which have been carried out by many workers in this field all serve as an excellent confirmation of the general features of the collective model. The existence of a great number of fast $E2$ transitions, the existence of well-defined rotational spectra, the probable existence of vibrational spectra, and the trends exhibited by the energies and the transition probabilities are all in agreement with the predictions of the model (see Fig. 8). There are, however, several important experimental results for which the model does not as yet provide any explanation. The effective moments of inertia of the rotational levels which have been identified are all larger by factors ranging from three to seven than those which are calculated from intrinsic nuclear deformations measured in other ways.[8,17,34] (That is, the energies of the observed rotational levels are too low by factors of ten to fifty.) The reason for the apparently sharp break between the regions in the periodic table where the "strong coupling" and the "weak coupling" approximations are applicable is also not well understood. Finally, if the energy levels which are observed in the "weak coupling" region are indeed "vibrational" levels, then their energies are also much lower[9,33] (factors of roughly ten) than those which would be expected from the crude hydrodynamical estimates worked out in Bohr and Mottelson.[6] The fact that both the "rotational" and "vibrational" levels apparently have energies which are smaller by roughly the same order of magnitude than those expected from the model suggests that a revision of the fundamental assumptions about either the nature of the nuclear "fluid" or its distribution in the nuclear volume may be necessary.

[34] K. W. Ford, Phys. Rev. **95**, 1250 (1954).

ACKNOWLEDGMENTS

The authors are indebted to Dr. C. P. Keim of the Oak Ridge National Laboratory for his very kind help in procuring the enriched isotopes, and to Professor L. C. Bradley of MIT for providing some of the samples of rare-earth oxides used in this work. We would like to thank Professor V. F. Weisskopf, Professor M. Deutsch, Professor S. D. Drell, Dr. Gertrude Scharff-Goldhaber, and Dr. G. Goldring for many useful conversations and for their continued interest in these experiments. We are grateful to many of our colleagues in this field for keeping us informed of their latest results, some of which were invaluable in the preparation of this report. Finally it is a pleasure to acknowledge the help of Mr. Matti K. Salomaa, who designed and built much of the electronic equipment and Mr. Allen Lenchek who performed many of the calculations.

PHYSICAL REVIEW VOLUME 100, NUMBER 3 NOVEMBER 1, 1955

Empirical Correlation of Nuclear Magnetic Moments

R. K. Osborn and E. D. Klema
Oak Ridge National Laboratory, Oak Ridge, Tennessee

(Received April 18, 1955)

A simple generalization of the extreme shell model, based upon the kinematics of the collective model, is proposed for the correlation of nuclear magnetic moments. It is shown that, if the concept of a rotating core is adjoined to that of the single-particle model, largely in disregard of dynamical considerations, then by the aid of three simple empirical rules ground-state wave functions may be easily constructed which correctly express the parities, spins, and magnetic moments of all nuclei for which $A \geq 7$, with the exception of W^{183}.

The choice of a particular set of empirical rules was dictated primarily by the twofold desire to keep their number to a minimum and at the same time restrict the consequent wave function to but two components; hence, considerable oversimplification of the true state of affairs is inevitable. However, the internal consistency of the results does point up strikingly the previously observed, but not explicitly investigated, possibility that the nature of the variable degrees of freedom required for generalization of the single-particle model may differ fundamentally for $j=l+1/2$ in contrast to $j=l-1/2$ single-particle configurations —being predominantly those of the core in the former instance and those of the single particle in the latter.

I. INTRODUCTION

THE single-particle model of the nucleus, which assumes that the relevant degrees of freedom required for a description of the nuclear ground state are those of the last odd particle (for even-even and odd-even nuclei, and hence no degrees of freedom for the former), leads to the well-known Schmidt values for magnetic moments. Presumably the deviations of the experimental moments from the Schmidt limits are to be accounted for through the interplay of some other degrees of freedom of the nuclear system than those of the last odd particle. One of three main lines of endeavor have usually been followed in the attempt to uncover the nature and significance of these extra degrees of freedom required for an understanding of nuclear ground-state properties.

One approach has been predicated upon the assumption that these extra degrees of freedom are representable as appropriately restricted sets of single-particle degrees of freedom. According to this view, a wave function for the ground state is presumed to be a superposition of properly symmetrized products of single-particle wave functions which satisfy the requirement of fixed parity and spin. So far as magnetic moments are concerned, a reasonably tractable scheme for configurational mixing has had considerable success.[1,2]

A second approach is based upon fundamental considerations concerning the nature of nucleon-nucleon interactions. Upon the assumption that these interactions include charge-exchange forces, one is led immediately to the expectation of contributions to nuclear magnetic moments arising from the exchange currents.[3] This concept was exploited successfully by Villars[4] in accounting for the moments of H^3-He^3 in terms of a pseudoscalar meson theory employing a charge exchange potential. Such an approach, of course, exhibits explicitly the mechanism of charge exchange in terms of charged meson currents. The same concept was employed in a phenomenological sense[5,6] by Russek and Spruch[7] to odd-A nuclei in general. Their results indicated that deviations from the Schmidt limits might well be largely accounted for in terms of exchange current effects.

The third main line of attack has proceeded from the opposite extreme, namely on the idea that the motions of all the particles with the exception of the last odd one are characterized by some small set of collective degrees of freedom. Various investigators have associated these degrees of freedom with one or the other or both of two quite different types of collective core motions—oscillations or rotations. Foldy and Milford[8,9] have examined the magnetic moments to be expected on the basis of an oscillator-plus-particle model, in which it was assumed that the single-particle quantum numbers were good quantum numbers. The model appears qualitatively successful for nuclei with total spin $I \geqslant 3/2$ and for which the single-particle configuration is characterized by $j=l+1/2$. The remaining nuclei are, however, not satisfactorily accounted for.

Employing the same model but including the possibility of configurational mixing as well as surfon mixing, Kerman[10] computed magnetic moments and found the situation somewhat improved, especially for spin-1/2 nuclei, but still not completely satisfactory, particularly in the regions of high spin.

Conversely, Bohr and Mottelson[11] and Davidson and Feenberg[12] have extensively investigated nuclear magnetic moments on the assumption that the collective degrees of freedom relevant for the ground state are essentially rotational in character. These investigators also took into account the possibility that more than one single-particle configuration might participate in the ground state. Such a model appears to be potentially adequate to correlate all nuclear magnetic moments within a relatively simple scheme. However, restrictions imposed upon the allowable ranges for the degrees of freedom chosen to characterize the system, primarily dictated by considerations of energetics, somewhat obscure this potentiality.

II. KINEMATICS OF A SIMPLE MODEL

As there appears to be considerable evidence[11] that degrees of freedom characteristic of an asymmetric rotator play an important role in the description of nuclear ground and low-lying excited states, we felt that it would be worthwhile to introduce them kinematically, rather than dynamically, as a simple, but purely empirical, generalization of the single-particle model. Such an approach is suggested by the fact that the best-known properties of nuclear ground states—parity, spin, and magnetic moment—are predominantly determined by the kinematics of the system; whereas, conversely, those properties which appear to depend to a greater extent upon details of interactions are the least well known.

Thus we reject at the outset any detailed attempt to tie conclusions obtainable from the model to energy considerations. We simply postulate that a nucleus can, for some purposes at least, be regarded as a permanently deformed core (if even-even and not doubly magic); a permanently deformed core plus a single particle (if odd-even); or a permanently deformed core plus two particles (if odd-odd). We seek a small set of empirical rules to guide us in the determination of whatever deformation parameters are needed in order to correlate the measurements of nuclear ground-state properties.

In the first place, the shell model is to be invoked for the principal ordering of the nuclear ground states, and for the spin and parity assignments for the single-particle configurations. We further assume that the nuclear parity is that of the single particle, and that the core deformation is axially symmetric. The assumption that the shell configuration of the last odd particle should determine the parity of the nucleus requires evenness of the core parity. Such a rotator exhibits generally three degrees of freedom which may conveniently be characterized by the projection of the

[1] R. J. Blin-Stoyle, Proc. Phys. Soc. (London) **A66**, 1158 (1953).
[2] R. J. Blin-Stoyle and M. A. Perks, Proc. Phys. Soc. (London) **A67**, 885 (1954).
[3] A. F. Siegert, Phys. Rev. **52**, 787 (1937).
[4] F. Villars, Helv. Phys. Acta **20**, 476 (1947).
[5] R. G. Sachs, Phys. Rev. **74**, 433 (1948).
[6] R. K. Osborn and L. Foldy, Phys. Rev. **79**, 795 (1950).
[7] A. Russek and L. Spruch, Phys. Rev. **87**, 111 (1952).
[8] L. L. Foldy and F. J. Milford, Phys. Rev. **80**, 751 (1950).
[9] F. J. Milford, Phys. Rev. **93**, 1297 (1954).
[10] A. K. Kerman, Phys. Rev. **92**, 1176 (1953).
[11] A. Bohr and B. R. Mottelson, Kgl. Danske Videnskab. Selskab, Mat.-fys. Medd. **27**, No. 14 (1953).
[12] J. P. Davidson and E. Feenberg, Phys. Rev. **89**, 856 (1953).

total angular momentum upon the space z-axis, the magnitude of the total angular momentum, and its projection on the symmetry axis fixed in the rotating body.

The appropriate operator representatives of these degrees of freedom are $\mathfrak{Q}_z$, $\mathfrak{Q}^2$, and $\mathfrak{Q}_z'$, respectively. Primes will be used whenever quantities referred to body axes are to be indicated. The usual commutation rules for the components of angular momentum of a "rigid body" are invoked; i.e.,

$$[\mathfrak{Q}_i,\mathfrak{Q}_j]=i\epsilon_{ijk}\mathfrak{Q}_k \tag{1a}$$

and

$$[\mathfrak{Q}_i',\mathfrak{Q}_j']=-i\epsilon_{ijk}\mathfrak{Q}_k'. \tag{1b}$$

Operators characterized by these commutation rules possess the usual diagonalizing representation[11] of the axially symmetric top,

$$D_{MK}^{\lambda*}(\theta_i)$$

where the $\theta_i=(\alpha,\beta,\gamma)$ are the Euler angles employed in the specification of the orientation of the deformed core relative to a space-fixed set of axes. In this representation,

$$\mathfrak{Q}_z D_{MK}^{\lambda*}=MD_{MK}^{\lambda*}, \tag{2a}$$

$$\mathfrak{Q}^2 D_{MK}^{\lambda*}=\lambda(\lambda+1)D_{MK}^{\lambda*}, \tag{2b}$$

$$\mathfrak{Q}_z' D_{MK}^{\lambda*}=KD_{MK}^{\lambda*}. \tag{2c}$$

It is useful also to note that

$$\mathfrak{Q}_\mu D_{MK}^{\lambda*}=[\lambda(\lambda+1)]^{\frac{1}{2}}C(\lambda 1\lambda;M,\mu)D_{M+\mu,K}^{\lambda*}, \tag{3a}$$

$$\mathfrak{Q}_\mu' D_{MK}^{\lambda*}=(-1)^\mu[\lambda(\lambda+1)]^{\frac{1}{2}} \times C(\lambda 1\lambda;K,-\mu)D_{M,K-\mu}^{\lambda*}, \tag{3b}$$

where $\mathfrak{Q}_{\pm1}=\mp(1/\sqrt{2})(\mathfrak{Q}_x\pm i\mathfrak{Q}_y)$ and $\mathfrak{Q}_0=\mathfrak{Q}_z$, and where the C's are Clebsch-Gordan coefficients. The parity operation on these wave functions leads to

$$\begin{aligned}\Pi D_{MK}^{\lambda*}(\gamma\beta\alpha)&=D_{MK}^{\lambda*}(\pi-\gamma,\pi-\beta,\pi+\alpha)\\&=(-1)^{\lambda+K}D_{M,-K}^{\lambda*}(\gamma\beta\alpha)\end{aligned} \tag{4}$$

and consequently the requirement that the core functions be of even parity demands that they appear only in the combination

$$D_{MK}^{\lambda*}+(-1)^{\lambda+K}D_{M,-K}^{\lambda*}.$$

We here invoke another greatly simplifying assumption, namely that $K=0$.[11] This provides immediately the additional consequence that λ must always be even.

The relevant degrees of freedom for the description of the odd nucleon (if there is one) are presumed to be characterized by the operators $\mathbf{L}^2$, orbital angular momentum, $\mathbf{S}^2$, intrinsic spin, $\mathbf{J}^2$, total particle angular momentum, and $\mathbf{J}_z$ (or $\mathbf{J}_z'$), projection of total particle angular momentum on the space (or body) z-axis. In the representation we have chosen in which to investigate the consequences of the model, it does not matter whether the particle motions are quantized in the body system—strong coupling—or in the space system—weak coupling. The choice of a system of quantization must ultimately be determined by the form of the Hamiltonian for the system, but in the present work such considerations are avoided.

The appropriate diagonalizing representation for these operators is

$$\chi_{jl}^m=\sum_\tau C(\tfrac{1}{2}lj;\tau,m-\tau)\chi_{\frac{1}{2}}^\tau Y_l^{m-\tau}. \tag{5}$$

Both representations have been chosen so that they transform under rotations of the coordinate system according to

$$\psi_j^m(e')=\sum_{m'}\psi_j^{m'}(e)D_{m'm}^j(R_{e\to e'}). \tag{6}$$

We now simply assert that the appropriate nuclear wave function shall transform under rotations according to D^I, where I is the magnitude of the total nuclear angular momentum, consisting in general of a sum of that for the odd particle, or particles, and the core. This leads us directly to at least three possible representations for the system as a whole:

$$\begin{aligned}\Psi_{I\lambda jl}^M(e,\theta_i)=&\sqrt{2}N_\lambda\sum_m C(j\lambda I;m,M-m)\\&\times\chi_{jl}^m(e)D_{M-m,0}^{\lambda*}(\theta_i)\end{aligned} \tag{7a}$$

if the particle is quantized in space,

$$\begin{aligned}\Psi_{I\lambda jl}^M(e',\theta_i)=&N_\lambda\sum_m C(j\lambda I;m0)[\chi_{jl}^m(e')D_{M,m}^{I*}(\theta_i)\\&+(-1)^{j-I}\chi_{jl}^{-m}(e')D_{M,-m}^{I*}(\theta_i)]\end{aligned} \tag{7b}$$

if the particle is quantized in the body;

$$\begin{aligned}B_{jl}^{Mm}(e',\theta_i)=&N_I[\chi_{jl}^m(e')D_{M,m}^{I*}(\theta_i)\\&+(-1)^{j-I}\chi_{jl}^{-m}(e')D_{M,-m}^{I*}(\theta_i)]\end{aligned} \tag{7c}$$

and

$$\begin{aligned}\Phi_{I\lambda\rho l}^M(e,\theta_i)=&\sum_j(-1)^{l-\rho-j+I}[(2\rho+1)(2j+1)]^{\frac{1}{2}}\\&\times W(\lambda lI\tfrac{1}{2};\rho j)\Psi_{I\lambda jl}^M(e,\theta_i)\end{aligned} \tag{7d}$$

where the W-function is a Racah coefficient.

As stated above, the representations (7a) and (7b) in which the normalizing coefficient N_λ is defined by $N_\lambda=[(2\lambda+1)/(16\pi^2)]^{\frac{1}{2}}$, are essentially the same for our present purpose. They are the representations in which $\mathfrak{J}^2=(\mathfrak{Q}+\mathbf{J})^2$, $\mathfrak{Q}^2$, $\mathbf{J}^2$, $\mathbf{L}^2$ and $\mathfrak{J}_z$ are the constants of the motion. Hereafter we shall designate them as the λ representation. The simple, but important, connection between the two λ representations for particle quantization in space and body coordinate systems should be pointed out here. As is to be expected, they are related by a rotation of *particle* wave functions. Since

$$\chi_{jl}^m(e')=\sum_{m'}\chi_{jl}^{m'}(e)D_{m'm}^j(\theta_i),$$

we have

$$\sum_m C(j\lambda I;m,0)\chi_{ji}{}^m(e')D_{M,m}{}^{I*}(\theta_i)$$
$$=\sum_{mm'} C(j\lambda I;m,0)\chi_{ji}{}^{m'}(e)D_{m',m}{}^{j}(\theta_i)D_{M,m}{}^{I*}(\theta_i)$$
$$=\sum_{m'L} C(jIL;m',-M)\chi_{ji}{}^{m'}(e)D_{M-m',0}{}^{L*}(\theta_i)$$
$$\times\sum_m(-1)^{m'-m}C(j\lambda I;m,0)C(jIL;m,-m)$$
$$=\sum_m C(j\lambda I;m,M-m)\chi_{ji}{}^m(e)D_{M-m,0}{}^{\lambda*}(\theta_i); \quad (8a)$$

and similarly for the symmetrization term. The identity of the two representations is a simple consequence of the fact that regardless of the quantization coordinate system, both $\mathbf{J}$ and $\mathfrak{L}$ are presumed to precess about the same fixed vector, $\mathfrak{I}$.

The representation (7c) is the one employed by Bohr and Mottelson[11] and by Davidson and Feenberg[12] and is distinguished from the λ representation in that it exhibits the z component (m) of the angular momentum of the particle in the body system as a constant of the motion. We shall call this the m representation. Both of these representations employ the same angular momentum coupling schemes; i.e.,

$$\mathbf{J}=\mathbf{L}+\mathbf{S},$$

and $\mathfrak{I}=\mathbf{J}+\mathfrak{L}$. As is to be expected, the λ and m-representations in the body system are connected by a unitary transformation; explicitly,

$$\Psi_{I\lambda jl}{}^M(e',\theta_i)$$
$$=\sum_m(-1)^{j-m}C(jI\lambda;m,-m)B_{Ijl}{}^{Mm}(e',\theta_i). \quad (9)$$

The representation (7d) is given little consideration herein, but is listed simply for completeness. It is the representation for the particle quantized in the space coordinate system which employs the alternative coupling scheme

$$\mathbf{R}=\mathfrak{L}+\mathbf{L}, \quad \mathfrak{I}=\mathbf{R}+\mathbf{S},$$

where

$$\mathbf{R}^2\Phi_{I\lambda\rho l}{}^M=\rho(\rho+1)\Phi_{I\lambda\rho l}{}^M. \quad (10)$$

This would be a natural representation if it were assumed that the particle-core coupling was very strong compared to the spin-orbit coupling. However, such an assumption somewhat obscures the significance of shell theory, and since we wish to build upon shell theory as a foundation, we choose to ignore the implications of this coupling scheme.

We have found from empirical considerations that the λ representation is more satisfactory than any of the others listed above for the correlation of nuclear magnetic moments. Primarily for this reason, but supplemented by some other considerations to be discussed below, we have settled upon the representation in which $\mathfrak{I}^2$, $\mathfrak{L}^2$, $\mathbf{J}^2$, $\mathbf{L}^2$, and $\mathfrak{I}_z$ are commuting, diagonal operators as the one with which, by the aid of a few rules of superposition, to attempt to describe nuclear ground states.

At this point we postulate the empirical rules which guide us in the choice of a wave function:

(1) The ground states of nuclei are predominantly determined by the degrees of freedom associated with the last odd particle, or particles, in the nucleus and those associated with the rotation of an axially symmetric core consisting of all but the last odd particle, or particles.

(2) The predominant single-particle configuration in the ground state is that assigned by the single-particle model.

(3) The quantum numbers required to specify these degrees of freedom are taken to be: I, magnitude of total angular momentum; M, space z-component of total angular momentum; l, magnitude of orbital angular momentum of odd particle; s, magnitude of intrinsic spin of odd particle; $j=l\pm s$, magnitude of total angular momentum of odd particle; λ, magnitude of core angular momentum; and $K=0$, projection of core angular momentum upon body system of axes. It is further assumed that the core states shall be of even parity—hence in connection with $K=0$, λ must be even.

(4) a. All nuclei with spin greater than 1/2 and for which $j=l+1/2$ are characterized by the good quantum numbers I, M, l, and j; and by a superposition of at most two interacting core states.

b. All nuclei with spin greater than 1/2 and for which $j=l-1/2$ are characterized by the good quantum numbers I, M, and λ; and by a superposition of at most two interacting single-particle configurations within the same major shell.

c. Nuclei with spin 1/2 are characterized by the single-particle configuration assigned by shell theory and the nearest interacting core-plus-particle configuration.

The concept of interacting states implies, of course, some consideration of the nature of the particle-core interaction. Assuming that the predominant part of this intereaction is independent of velocities, we may express it as

$$\sum_{Lmm'} T_L{}^{m'}D_{m',m}{}^L(\theta_i)\varphi_m,$$

where $T_L{}^{m'}$ is the m' component of an Lth rank irreducible tensor in the space of the particle and φ_m is an empirical scalar coefficient. The matrix elements of such an interaction operator in the representation characterized by the quantum numbers indicated above are

$$E_L(I;\lambda jl;\lambda' j'l')$$
$$=(2L+1/4\pi)(-1)^{I+l+\lambda'-\frac{1}{2}}[(2l'+1)(2\lambda'+1)(2j+1)$$
$$\times(2j'+1)]^{\frac{1}{2}}C(l'Ll;0,0)C(\lambda'L\lambda;0,0)W(ljl'j';\tfrac{1}{2}L)$$
$$\times W(jj'\lambda\lambda';LI)\varphi_0. \quad (11)$$

If we now take as a convenient, though hardly critical, assumption that the interaction is characterized primarily by $L=2$ (suggested by the usual form of the

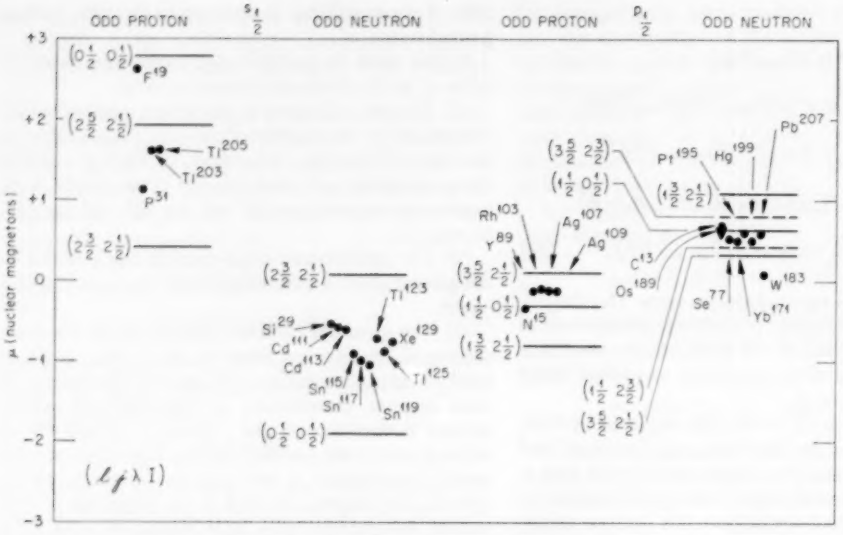

FIG. 1. Experimentally observed and calculated magnetic moments for $j=1/2$ nuclei. The solic circles and triangle represent the measured values and the solid and dashed lines represent the calculated moments for the indicated values of (l, j, λ, I) as defined in the text.

particle-core interaction in the hydrodynamical model[11]), we see immediately that the concept of interacting states contains the selection rules $\Delta(jj'2)$, $\Delta(ll'2)$, and $\Delta(\lambda\lambda'2)$, where the symbol Δ implies the usual restriction on the magnitudes of three vectors which form a triangle.

It is a consequence of assumption 4(b) above that particle configurations which mix are usually characterized by $l\neq l'$; hence the contributions to the magnetic moment from the assumed mixtures of states will rarely include cross terms. However, for the sake of completeness, we give all of the matrix elements of the magnetic moment operator; i.e.,

$$\mu(Ij\lambda l) = \left[g_{jl}+(g_c-g_{jl})\frac{I(I+1)-j(j+1)+\lambda(\lambda+1)}{2I(I+1)}\right]I \quad (12a)$$

for the diagonal elements, and

$$\mu(I\lambda l;\ j=l+\tfrac{1}{2},\ j'=l-\tfrac{1}{2}) = \frac{(g_l-g_s)[(I+l+\lambda+\frac{3}{2})(I+l-\lambda+\frac{1}{2}) \times(l-I+\lambda+\frac{1}{2})(I-l+\lambda+\frac{1}{2})]^{\frac{1}{2}}}{2(I+1)(2l+1)}, \quad \lambda=\lambda'\neq 0 \quad (12b)$$

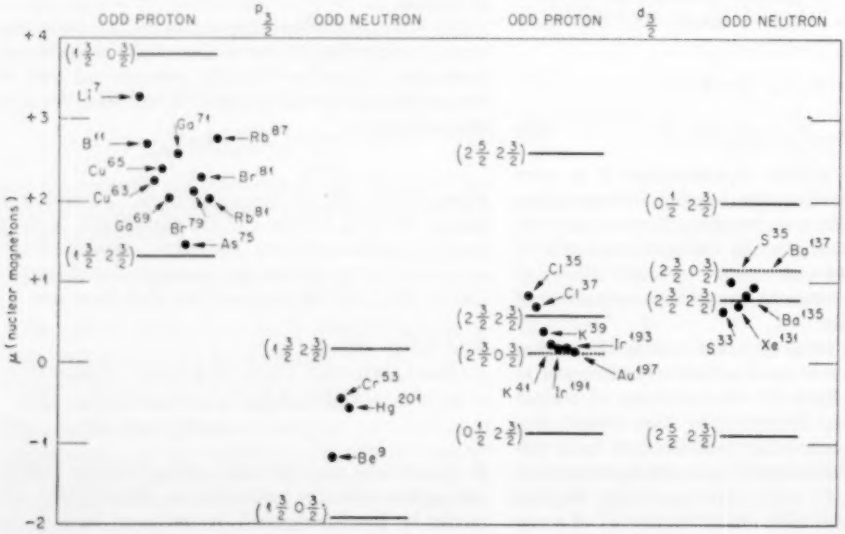

FIG. 2. Experimentally observed and calculated magnetic moments for $j=3/2$ nuclei. The solid circles represent the measured values and the solid and dotted lines represent the calculated moments for the indicated values of (l, j, λ, I) as defined in the text.

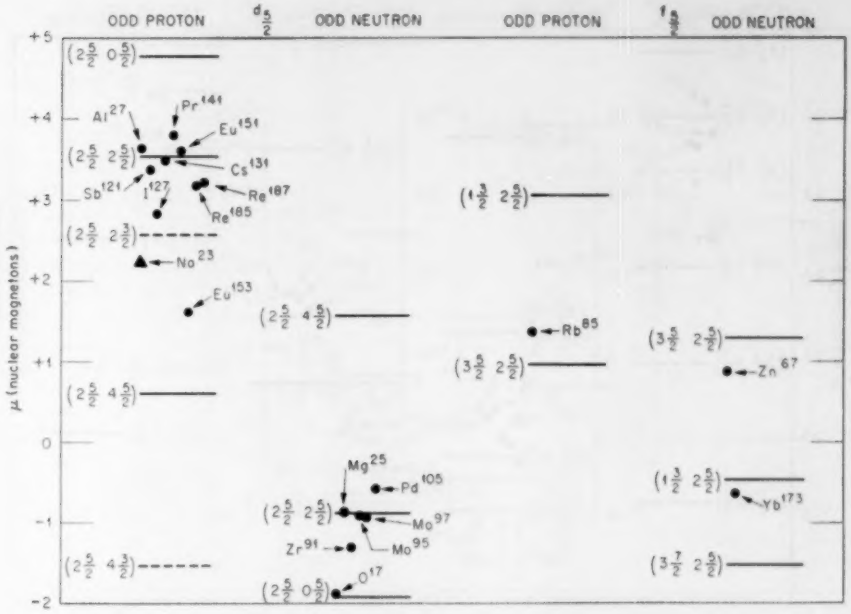

FIG. 3. Experimentally observed and calculated magnetic moments for $j=5/2$ nuclei. The solid circles and triangle represent the measured values and the solid and dashed lines represent the calculated moments for the indicated values of (l, j, λ, I) as defined in the text.

for the nondiagonal elements. We have taken throughout $g_c=0.45\sim Z/A$. The quantity g_{jl} is the usual single-particle theory gyromagnetic ratio; thus the Schmidt limiting values for the magnetic moments follow immediately upon setting $j=I$ and $\lambda=0$.

The contribution to the magnetic moment from a particular state in the m-representation is given by

$$\mu(I\,jlm)=\left[g_{jl}+(g_c-g_{jl})\times\frac{2I(I+1)-2m^2-(-1)^{j-l}(j+\tfrac{1}{2})(I+\tfrac{1}{2})\delta_{m\frac{1}{2}}}{2I(I+1)}\right]I. \quad (13)$$

For $I=m>1/2$, this becomes $\mu(I\,jlI)=[Ig_{jl}+g_c]I/(I+1)$, and for $I=m=1/2$ we have $\mu(\frac{1}{2}\,jl\frac{1}{2})=\frac{1}{6}[3g_c+(g_{jl}-g_c)\{1+(-1)^{j-l}(2j+1)\}]$ as noted previously by Davidson and Feenberg.[12]

In accordance with the ideas presented above, the ground-state wave function can be taken to be (to within a single-particle radial factor)

$$(1-a^2)^{\frac{1}{2}}\Psi_{I\lambda jl}{}^M+a\Psi_{I\lambda' j'l'}{}^M$$

where $(jl)=(j'l')$ and $\lambda\neq\lambda'$ for $l+1/2$ nuclei, and $\lambda=\lambda'$ but $(jl)\neq(j'l')$ for $l-1/2$ nuclei. The mixing coefficient a is to be determined by the relation

$$a^2=[\mu(\text{obs})-\mu(I\,j\lambda l)]/[\mu(I\,j'\lambda'l')-\mu(I\,j\lambda l)], \quad (14)$$

except in the rare cases in which $l-1/2$ nuclei admix with the spin-orbit partner. For such cases, of course, the cross terms in the magnetic moment relation must be considered.

It is not our intention here to suggest that the extremely simple scheme outlined above should supplant more sophisticated calculations whenever they have been successfully carried through. In particular, the detailed examinations of the many-particle model for light nuclei conducted by Mizushima and Umezawa[13] and Flowers[14] probably render the extension of at least the dynamical aspects of the deformed-core model into the region of light nuclei superfluous, if not dubious. Furthermore, so far as heavy nuclei are concerned, the scheme should be regarded simply as an alternative explanation to that proposed by Blin-Stoyle and Perks[1,2]—an alternative which hitherto has not been explicitly recognized as adequate. Demonstration of the alternative is pertinent since for heavy nuclei at least it is expected that a collective model will be far more tractible for correlating quadrupole moments. Thus, though in many special instances and for light nuclei generally, it may seem objectionable to do so, we shall nevertheless extend consideration of the scheme practically without restriction.

All odd-even nuclei from Li^7 on whose spins and magnetic moments have been measured have been considered from the standpoint of the model described above. The results are presented in graphical form in Figs. 1 to 5. On these figures the nuclei are grouped according to the single-particle assignment of the last odd particle, and the values of the calculated magnetic moments for states characterized by the quantum numbers (l, j, λ, I) are shown as either solid or dashed

[13] M. Mizushima and M. Umezawa, Phys. Rev. **85**, 37 (1952).
[14] B. H. Flowers (private communication).

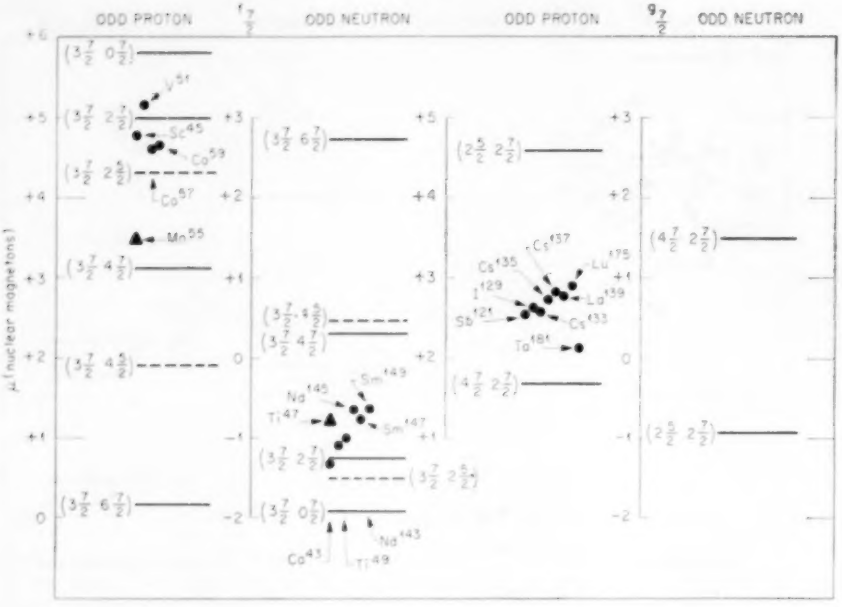

FIG. 4. Experimentally observed and calculated magnetic moments for $j=7/2$ nuclei. The solid circles and triangles represent the measured values and the solid and dashed lines represent the calculated moments for the indicated values of $(l,\ j,\ \lambda,\ I)$ as defined in the text.

lines. The experimentally measured magnetic moments are indicated by solid circles or triangles.

The results are also given numerically in the corresponding Tables I to X. The sources of the data are Klinkenberg's compilation,[15] designated by K; Bohr and Mottelson's compilation,[11] designated by B-M; or other sources, designated by the reference to the published paper describing the measurement. These tables give the calculated values of the magnetic moments of the pure states, the experimentally measured moments, and the experimentally measured spins of the ground states of the nuclei in question. In those cases in which the spin listed is not that given in Klinkenberg's paper,[15] the reference to the later measurement of the spin has been given.

TABLE I. Experimentally observed and calculated magnetic moments for $s_{1/2}$ nuclei.

Calculated magnetic moments, $(l,\ j,\ \lambda,\ I)$					
Odd proton			Odd neutron		
$(0\ 1/2\ 0\ 1/2)$ $\mu=2.79$			$(0\ 1/2\ 0\ 1/2)$ $\mu=-1.91$		
$(2\ 5/2\ 2\ 1/2)$ $\mu=1.94$			$(2\ 5/2\ 2\ 1/2)$ $\mu=-1.19$		
$(2\ 3/2\ 2\ 1/2)$ $\mu=0.41$			$(2\ 3/2\ 2\ 1/2)$ $\mu=0.067$		
Nucleus	Observed I	Observed[a] μ	Nucleus	Observed I	Observed[a] μ
F^{19}	1/2	2.63 (K)	Si^{29}	1/2	−0.56 (B-M)
P^{31}	1/2	1.13 (B-M)	Cd^{111}	1/2	−0.59 (K)
Tl^{203}	1/2	1.61 (K)	Cd^{113}	1/2	−0.62 (K)
Tl^{205}	1/2	1.63 (K)	Sn^{115}	1/2	−0.92 (K)
			Sn^{117}	1/2	−1.00 (K)
			Sn^{119}	1/2	−1.05 (K)
			Te^{123}	1/2	−0.74 (K)
			Te^{125}	1/2	−0.89 (K)
			Xe^{129}	1/2	−0.78 (K)

[a] Values labeled (K) are taken from Klinkenberg's compilation (reference 15). Values labeled (B-M) are taken from Bohr and Mottelson's compilation (reference 11).

[15] P. F. A. Klinkenberg, Revs. Modern Phys. **24**, 63 (1952).

An examination of Figs. 1 to 5 reveals that the magnetic moments of nearly all the odd-even nuclei are correlated by the present model in a reasonably consistent fashion. The results are discussed in detail below.

The $s_{1/2}$ Nuclei

The pattern of configurational mixing exhibited by these nuclei is particularly interesting. The three nuclei $_9F^{19}$, $_{15}P^{31}$, and $_{14}Si^{29}$, which appear in the early $2s$ shell, seem to behave quite differently from the other members of this group. In the case of $_9F^{19}$, an admixture of either $d_{3/2}$ or $d_{5/2}$ will account for the observed moment, though considerably less of the $d_{3/2}$ is needed, a fact which might well be a criterion of preference. However, both $_{15}P^{31}$ and $_{14}Si^{29}$ must be admixed with the $d_{3/2}$. But it is to be noted that in both of these instances the preceding $d_{5/2}$ subshell has been filled.[16] (Unless explicitly stated to the contrary, we have accepted Klinkenberg's single-particle configuration assignments.) Hence for $d_{5/2}$ admixture one must postulate the configurations $(d_{5/2})^6(s_{1/2})^1+(d_{5/2})^5(s_{1/2})^2$. But because the pairing energy[16,17] for nucleons paired in a subshell is proportional to $(2j+1)$, it is quite possible that there is an energy discrimination against the $d_{5/2}$ admixture. It is noteworthy, in fact, that this phenomenon of an apparent pairing energy discrimination against certain

[16] M. G. Mayer, Phys. Rev. **78**, 16 (1950).
[17] G. Racah and I. Talmi, Physica **18**, 1097 (1952).

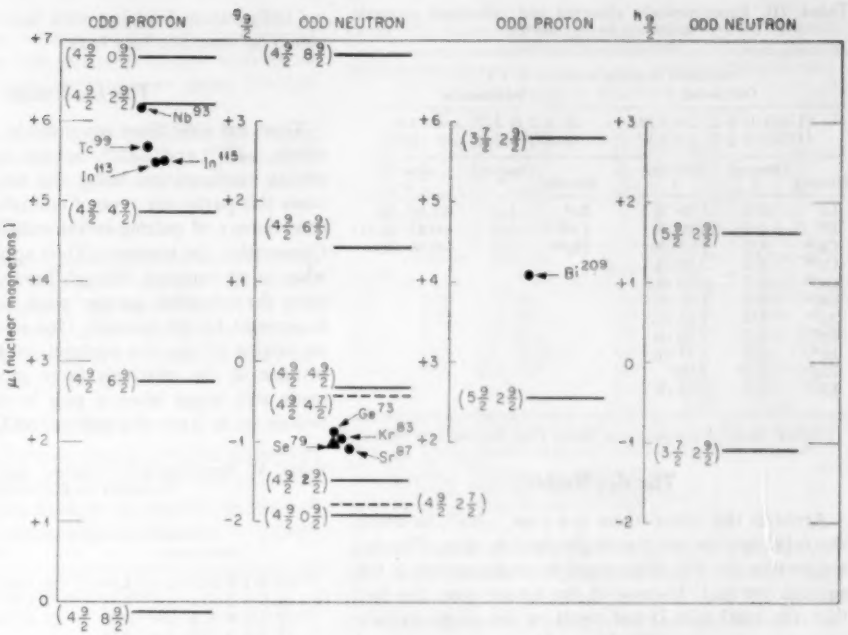

FIG. 5. Experimentally observed and calculated magnetic moments for $j=9/2$ nuclei. The solid circles and triangle represent the measured values and the solid and dashed lines represent the calculated moments for the indicated values of (l, j, λ, I) as defined in the text.

configurational admixtures is encountered frequently. The remaining $s_{1/2}$ nuclei all appear in the later $3s$ subshell which is presumably preceded by the $4d_{3/2}$ subshell. In all of these cases $d_{3/2}$ admixture is required. This s-d mixing was also noted by Davidson and Feenberg[12] and Bohr and Mottelson.[11]

The $p_{1/2}$ Nuclei

It is expected that $_7N^{15}$ and $_6C^{13}$ would both require $p_{3/2}$ admixture, as indeed they do. But it is most interesting to observe that none of the moments of the remaining nuclei—all of which apparently have an $f_{5/2}$ subshell as a nearer neighbor than $p_{3/2}$—could be accounted for by $p_{3/2}$ admixture; whereas the $f_{5/2}$ does very well. The nucleus $_{76}Os^{189}$ is the one case found so far of configurational mixing in which the observed spin is not that of the single particle. Its moment is accounted for by mixing with the $f_{5/2}$, just as in the case with the other members of this group. In Fig. 1 the moments for the two pure states required for this nucleus are shown by the dashed lines and the experimentally observed moment is indicated by the solid triangle. The only true exception found so far on the basis of the present model, $_{74}W^{183}$, appears in this group. Its observed moment cannot be fitted.

The $p_{3/2}$ Nuclei

The assumption of but one single-particle state and two core states is very satisfactory here. It is to be observed that configurational mixing with fixed λ would not adequately account for these moments.

The $d_{3/2}$ Nuclei

Four nuclei in this group, $_{16}S^{33}$, $_{17}Cl^{35}$, $_{17}Cl^{37}$, and $_{54}Xe^{131}$, exhibit anomalous, but not exceptional, behavior. Their moments require admixture of the spin-orbit partner instead of the s state as might be expected. It is to be noted that in all four cases the amount of admixture is small. The moments of the remaining members of the group are satisfactorily accounted for by s-state mixing. It should be pointed out that the latter cases could also be accounted for by λ mixing.

TABLE II. Experimentally observed and calculated magnetic moments for $p_{1/2}$ nuclei.

Calculated magnetic moments, (l, j, λ, I)	
Odd proton	Odd neutron
(1 1/2 0 1/2) $\mu=-0.26$	(1 1/2 0 1/2) $\mu=0.64$
(3 5/2 2 1/2) $\mu=0.10$	(3 5/2 2 1/2) $\mu=0.34$
(1 3/2 2 1/2) $\mu=-0.81$	(1 3/2 2 1/2) $\mu=1.09$
	(3 5/2 2 3/2) $\mu=0.80$
	(1 1/2 2 3/2) $\mu=0.43$

Nucleus	Observed I	Observed μ	Nucleus	Observed I	Observed μ
N^{15}	1/2	−0.28 (K)	C^{13}	1/2	0.70 (K)
Y^{89}	1/2	−0.14 (K)	Se^{77}	1/2	0.53 (B-M)
Rh^{103}	1/2	−0.10 (B-M)	Yb^{171}	1/2	0.5 (B-M)
Ag^{107}	1/2	−0.11 (K)	W^{183}	1/2	0.08[b]
Ag^{109}	1/2	−0.13 (K)	Os^{189}	3/2[a]	0.65[a]
			Pt^{195}	1/2	0.60 (K)
			Hg^{199}	1/2	0.50 (K)
			Pb^{207}	1/2	0.59 (K)

[a] H. R. Loeliger and L. R. Sarles, Phys. Rev. **95**, 291 (1954).
[b] J. A. Vreeland and K. Murakawa, Phys. Rev. **83**, 229(A) (1951).

TABLE III. Experimentally observed and calculated magnetic moments for $p_{3/2}$ nuclei.

Calculated magnetic moments, (l, j, λ, I) Odd proton			Odd neutron		
(1 3/2 0 3/2) $\mu=3.79$			(1 3/2 0 3/2) $\mu=-1.91$		
(1 3/2 2 3/2) $\mu=1.30$			(1 3/2 2 3/2) $\mu=0.16$		
Nucleus	Observed I	Observed μ	Nucleus	Observed I	Observed μ
Li^{7}	3/2	3.26 (K)	Be^{9}	3/2	−1.18 (K)
B^{11}	3/2	2.69 (K)	Cr^{53}	3/2	−0.47 (B-M)
Cu^{63}	3/2	2.23 (K)	Hg^{201}	3/2	−0.56 (K)
Cu^{65}	3/2	2.38 (K)			
Ga^{69}	3/2	2.02 (K)			
Ga^{71}	3/2	2.56 (K)			
As^{75}	3/2	1.44 (K)			
Br^{79}	3/2	2.10 (K)			
Br^{81}	3/2	2.27 (K)			
Rb^{85}	3/2[a]	2.00[a]			
Rb^{87}	3/2	2.75 (K)			

[a] Hobson, Hubbs, Nierenberg, and Silsbee, Phys. Rev. **96**, 1450 (1954).

The $d_{5/2}$ Nuclei

Again in this group there is a case, $_{11}Na^{23}$, in which the total spin is not the single-particle spin. The $d_{5/2}$ assignment for the single-particle configuration is the natural one and, because of the active core, the fact that the total spin is not equal to the single-particle spin presents no difficulties. Again the calculated moments for this case have been shown as dashed lines and the observed moment as a solid triangle in Fig. 3. It is seen that this magnetic moment is quite consistent with the general pattern.

It is clear that the moments of all of the nuclei in this group are satisfactorily accommodated by one single-particle configuration and two core states. If one invokes the selection rule $\Delta(\lambda\lambda'2)$ consequent upon the assumption of predominantly quadrupole interaction between particle and core, one notices there is some correlation between a preference for higher spin core-state admixtures ($\lambda=2,4$), rather than the lower ($\lambda=0,2$), and increasing mass.

TABLE IV. Experimentally observed and calculated magnetic moments for $d_{3/2}$ nuclei.

Calculated magnetic moments, (l, j, λ, I) Odd proton			Odd neutron		
(2 3/2 2 3/2) $\mu=0.56$			(2 3/2 2 3/2) $\mu=0.77$		
(0 1/2 2 3/2) $\mu=-0.87$			(0 1/2 2 3/2) $\mu=1.96$		
(2 5/2 2 3/2) $\mu=2.58$			(2 5/2 2 3/2) $\mu=-0.90$		
(2 3/2 0 3/2) $\mu=0.12$			(2 3/2 0 3/2) $\mu=1.15$		
Nucleus	Observed I	Observed μ	Nucleus	Observed I	Observed μ
Cl^{35}	3/2	0.82 (K)	S^{33}	3/2	0.64 (K)
Cl^{37}	3/2	0.68 (K)	S^{33}	3/2	1.00[a]
K^{39}	3/2	0.39 (K)	Xe^{131}	3/2	0.68 (B-M)
K^{41}	3/2	0.22 (K)	Ba^{135}	3/2	0.83 (K)
Ir^{191}	3/2	0.16 (B-M)	Ba^{137}	3/2	0.94 (K)
Ir^{193}	3/2	0.17 (B-M)			
Au^{197}	3/2	0.14 (B-M)			

[a] Burke, Strandberg, Cohen, and Koski, Phys. Rev. **93**, 193 (1954).

Configurational mixing with but a single core state would be unsatisfactory here.

The $f_{5/2}$ Nuclei

There are only three examples in this group, two of which, $_{37}Rb^{85}$ and $_{30}Zn^{67}$, behave quite regularly, the mixing configuration being the nearby $p_{3/2}$. In both cases this particular type of admixture is favored as a consequence of pairing in the subshell of higher spin. Conversely, the nucleus $_{70}Yb^{173}$ appears here as somewhat of an anomaly (though hardly as an exception), since the spin-orbit partner must be admixed in order to account for its moment. One would expect little or no mixing of $f_{7/2}$ (in contrast to $p_{3/2}$) with the $f_{5/2}$, because of the relatively large spin-orbit separation, made still larger when a pair in the 7/2 subshell is broken up in favor of a pair in the 5/2 subshell.

TABLE V. Experimentally observed and calculated magnetic moments for $d_{5/2}$ nuclei.

Calculated magnetic moments, (l, j, λ, I) Odd proton			Odd neutron		
(2 5/2 0 5/2) $\mu=4.79$			(2 5/2 0 5/2) $\mu=-1.91$		
(2 5/2 2 5/2) $\mu=3.54$			(2 5/2 2 5/2) $\mu=-0.87$		
(2 5/2 4 5/2) $\mu=0.60$			(2 5/2 4 5/2) $\mu=1.56$		
(2 5/2 2 3/2) $\mu=2.58$					
(2 5/2 4 3/2) $\mu=-1.53$					
Nucleus	Observed I	Observed μ	Nucleus	Observed I	Observed μ
Na^{23}	3/2	2.22 (K)	O^{17}	5/2	−1.89 (K)
Al^{27}	5/2	3.64 (K)	Mg^{25}	5/2	−0.86 (K)
Sb^{121}	5/2	3.36 (K)	Zr^{91}	5/2	−1.3[b]
I^{127}	5/2	2.81 (K)	Mo^{95}	5/2	−0.91 (K)
Cs^{133}	5/2[a]	3.48 (B-M)	Mo^{97}	5/2	−0.93 (K)
Pr^{141}	5/2	3.9 (B-M)	Pd^{105}	5/2	−0.57[c]
Eu^{151}	5/2	3.6 (K)			
Eu^{153}	5/2	1.6 (K)			
Re^{185}	5/2	3.17 (K)			
Re^{187}	5/2	3.20 (K)			

[a] E. H. Bellamy and K. F. Smith, Phil. Mag. **44**, 33 (1953).
[b] S. Suwa, J. Phys. Soc. Japan **8**, 734 (1953).
[c] A. Steudel, Z. Physik **132**, 429 (1952).

The $f_{7/2}$ Nuclei

All of the odd-proton nuclei in this group and three of the odd-neutron members, $_{20}Ca^{43}$, $_{22}Ti^{47}$, and $_{22}Ti^{49}$, appear between the major-shell closings at 20 and 28. Thus, in terms of a rotating core-plus-single-particle model, one might expect little likelihood of configurational mixing here, as the degrees of freedom associated with single-particle configurations lying below closed shells should presumably exhibit little or no independence. However, admixture of core states quite satisfactorily accounts for all of the magnetic moments in this group.

It is especially to be noted that we have here two more examples ($_{25}Mn^{55}$ and $_{22}Ti^{47}$) of the situation in which the single-particle spin and nuclear spin are not the same, but that again core activity provides a simple accounting for boths pins and moments. If the selection

rule $\Delta(\lambda\lambda'2)$ is to be invoked for the core-state mixing for the members of this group, it is seen that in all cases except $_{23}V^{51}$ and $_{20}Ca^{43}$ the core states ($\lambda=2,4$) are required.

Again for some members of this group configurational mixing to account for the moments is possible only if core-state admixture is simultaneously invoked.

The $g_{7/2}$ Nuclei

All of the single-particle configurations for this group lie between the major shells at 50 and 82. The natural interacting configuration is the nearby $d_{3/2}$, and it is apparent from Fig. 4 that admixture of this configuration satisfactorily accommodates all of the magnetic moments of these nuclei.

The $g_{9/2}$ Nuclei

The $g_{9/2}$ level lies between the major-shell closings at 28 and 50, and is the only subshell of even parity in this major shell. Thus here, as in the case of some of the $f_{7/2}$ nuclei, the model exhibits marked correspondence to the expectation of little or no configurational mixing, in that it demands core admixture for the ground state. It is clear from Fig. 5 that such admixture successfully accounts for all of the magnetic moments of this group. On the assumption that the ground state consists of but two core states, it is seen that in all cases the core states involved are those for $\lambda=2$ and $\lambda=4$.

It is to be noted that in this group there appears another nucleus, $_{34}Se^{79}$, whose measured spin does not correspond to the spin of the single-particle configuration to which it has been assigned.

TABLE VI. Experimentally observed and calculated magnetic moments for $f_{5/2}$ nuclei.

Calculated magnetic moments, (l, j, λ, I) Odd proton			Odd neutron		
(3 5/2 2 5/2) $\mu=0.95$			(3 5/2 2 5/2) $\mu=$ 1.28		
(1 3/2 2 5/2) $\mu=3.05$			(1 3/2 2 5/2) $\mu=-0.48$		
(3 7/2 2 5/2) $\mu=4.31$			(3 7/2 2 5/2) $\mu=-1.51$		
(3 5/2 0 5/2) $\mu=0.86$			(3 5/2 0 5/2) $\mu=$ 1.37		
Nucleus	Observed I	Observed μ	Nucleus	Observed I	Observed μ
Rb^{85}	5/2	1.35 (K)	Zn^{67}	5/2	0.88 (B-M)
			Yb^{173}	5/2	−0.65 (K)

The $h_{9/2}$ Nuclei

This group is important because of the presence in it of $_{83}Bi^{209}$. Though Blin-Stoyle and Perks[2] have been able to account for the magnetic moment of this nucleus by their procedure of pure configurational mixing, it has remained anomalously large within the context of the collective model according to the investigations of Bohr and Mottelson[11] and Kerman.[10] However, the latter authors predicated their assumptions as to the character of the ground state upon energy considerations. Thus if the collective degrees of freedom associated with the core are presumed to be predominantly rotational, and if it is further presumed that the motion of the single particle relative to the core is such that the projection of its total angular momentum on the body symmetry axis is maximal and a constant of the motion, then one is led to selection rules which forbid the admixture of the nearby $f_{7/2}$ single-particle configuration. Alternatively, if the core degrees of freedom are presumed to be representable as the normal modes of surface oscillations, the admixture of $f_{7/2}$ with $h_{9/2}$ to form the ground state of $_{83}Bi^{209}$ occurs naturally, but quite inadequately. However, if the appeal to an explicit model for the energy is abandoned, it is seen that $h_{9/2}-f_{7/2}$ admixture for $\lambda=2$ successfully accounts for the magnetic moment of $_{83}Bi^{209}$.

TABLE VII. Experimentally observed and calculated magnetic moments for $f_{7/2}$ nuclei.

Calculated magnetic moments, (l, j, λ, I) Odd proton			Odd neutron		
(3 7/2 0 7/2) $\mu=5.79$			(3 7/2 0 7/2) $\mu=-1.91$		
(3 7/2 2 7/2) $\mu=4.99$			(3 7/2 2 7/2) $\mu=-1.25$		
(3 7/2 4 7/2) $\mu=3.12$			(3 7/2 4 7/2) $\mu=$ 0.30		
(3 7/2 6 7/2) $\mu=0.17$			(3 7/2 6 7/2) $\mu=$ 2.74		
(3 7/2 2 5/2) $\mu=4.31$			(3 7/2 2 5/2) $\mu=-1.51$		
(3 7/2 4 5/2) $\mu=1.90$			(3 7/2 4 5/2) $\mu=$ 0.48		
Nucleus	Observed I	Observed μ	Nucleus	Observed I	Observed μ
Sc^{45}	7/2	4.76 (K)	Ca^{43}	7/2[b]	−1.32 (B-M)
V^{51}	7/2	5.15 (K)	Ti^{47}	5/2[c]	−0.79[c]
Mn^{55}	5/2	3.47 (K)	Ti^{49}	7/2[c]	−1.10 (B-M)
Co^{57}	7/2[a]	4.6 (B-M)	Nd^{149}	7/2	−1.0 (K)
Co^{59}	7/2	4.65 (K)	Nd^{145}	7/2	−0.65 (K)
			Sm^{147}	7/2[d]	−0.76[d]
			Sm^{149}	7/2[d]	−0.64[d]

[a] Baker, Bleaney, Bowers, Shaw, and Trenham, Proc. Phys. Soc. (London) **A66**, 305 (1953).
[b] C. D. Jeffries, Phys. Rev. **90**, 1130 (1953).
[c] C. D. Jeffries, Phys. Rev. **92**, 1096(A) (1953).
[d] K. Murakawa, Phys. Rev. **93**, 1232 (1954).

III. DISCUSSION

It is clear that, though no explicit model was employed to define the interdependence of the variables

TABLE VIII. Experimentally observed and calculated magnetic moments for $g_{7/2}$ nuclei.

Calculated magnetic moments, (l, j, λ, I) Odd proton			Odd neutron		
(4 7/2 2 7/2) $\mu=1.69$			(4 7/2 2 7/2) $\mu=$ 1.50		
(2 5/2 2 7/2) $\mu=4.59$			(2 5/2 2 7/2) $\mu=-0.92$		
(4 7/2 0 7/2) $\mu=1.72$			(4 7/2 0 7/2) $\mu=$ 1.49		
Nucleus	Observed I	Observed μ			
Sb^{121}	7/2	2.55 (K)			
I^{235}	7/2	2.62 (B-M)			
Cs^{131}	7/2	2.58 (K)			
Cs^{135}	7/2	2.73 (K)			
Cs^{137}	7/2	2.84 (K)			
La^{139}	7/2	2.78 (K)			
Lu^{175}	7/2	2.9 (K)			
Ta^{181}	7/2	2.1 (K)			

TABLE IX. Experimentally observed and calculated magnetic moments for $g_{9/2}$ nuclei.

Calculated magnetic moments, (l, j, λ, I) Odd proton	Odd neutron
(4 9/2 0 9/2) $\mu=$ 6.79	(4 9/2 0 9/2) $\mu=-1.91$
(4 9/2 2 9/2) $\mu=$ 6.21	(4 9/2 2 9/2) $\mu=-1.48$
(4 9/2 4 9/2) $\mu=$ 4.87	(4 9/2 4 9/2) $\mu=-0.32$
(4 9/2 6 9/2) $\mu=$ 2.75	(4 9/2 6 9/2) $\mu=$ 1.43
(4 9/2 8 9/2) $\mu=-0.14$	(4 9/2 8 9/2) $\mu=$ 3.82
	(4 9/2 2 7/2) $\mu=-1.78$
	(4 9/2 4 7/2) $\mu=-0.42$

Nucleus	Observed I	Observed μ	Nucleus	Observed I	Observed μ
Nb^{90}	9/2	6.16 (K)	Ge^{73}	9/2	-0.88[a]
Tc^{99}	9/2	5.68 (B-M)	Se^{79}	7/2[b]	-1.02[b]
In^{113}	9/2	5.49 (K)	Kr^{83}	9/2	-0.97 (K)
In^{115}	9/2	5.50 (K)	Sr^{87}	9/2	-1.1 (K)

[a] C. D. Jeffries, Phys. Rev. **92**, 1262 (1953).
[b] Hardy, Silvey, Townes, Burke, Strandberg, Parker, and Cohen, Phys. Rev. **92**, 1532 (1953).

chosen to describe the nuclear system (which would in principle completely determine the relative importance of these degrees of freedom for a particular ground state), considerable appeal to somewhat gross energy considerations was made for guidance in the construction and application of the rules discussed above.

First of all, heavy reliance was placed upon the extreme shell model for the specification of single-particle configurations. Such reliance contains the implication that nuclear ground-state energies are predominantly determined by the dynamics of the single particle. Thus though it is assumed that core degrees of freedom play a critical role in the determination of some ground state properties—spins in a few cases and magnetic moments in all cases—their role so far as the energy is concerned is considerably less significant.

Secondly, it has been assumed that the single-particle degrees of freedom associated with configurations lying below closed shells are so tightly bound into the core that these levels are no longer available for configurational mixing. Accordingly the $4f_{7/2}$ and $5g_{9/2}$ ground states must be characterized by an admixture of different core states rather than of different single-particle states.

The first of these considerations was employed primarily as a guide in the selection of single-particle parameters to characterize the ground state. The second was invoked as an empirical rule. There is thirdly a consideration of major interest and importance which, however, was ignored in the construction of the rules and arises rather as a consequence of the application of the model than as a guide to its application. This is the question of the relative energy separation of the pair of levels employed in the construction of the ground-state wave function to that of other possible pairs. In accordance with the assumption that the ground-state energies are predominantly determined by the dynamics of the single particle, one would expect configurational mixing to be characterized by a relatively small admixture of that configuration which lies nearest to the single-particle-state assignment for a particular nucleus. Since the core must be active ($\lambda \neq 0$) in either the case of configurational admixture—in which case it is the mechanism that makes possible the combination of different single-particle-spin states into a state of fixed total spin—or the case of core-state mixing, by definition; the question of the relative energy separation of pure particle states to that of pure core states is not of dominant importance. Thus, the fact that the single-particle quantum numbers are good in the case of $l+1/2$ particle assignments, whereas conversely the core quantum numbers are good for $l-1/2$ particle assignments, is apparently primarily a consequence of the presence or absence of interacting single-particle states lying close to a given $l+1/2$ or $l-1/2$ configuration, respectively.

The situation is most strikingly illustrated by the high-spin nuclei. The configurations $5g_{9/2}$ and $4f_{7/2}$ lie between major-shell closings which enclose no interacting single-particle configurations. Conversely the levels $6h_{9/2}$, $5g_{7/2}$, and $4f_{5/2}$ all have interacting nearby levels. The odd neutrons in the $5f_{7/2}$ level do lie close to the $6h_{9/2}$, and indeed an appropriate admixture of the $h_{9/2}$ with the $f_{7/2}$ will account for the magnetic moments of this group; but if the $h_{9/2}-f_{7/2}$ separation is sufficiently great, core-state admixing in the ground states of these nuclei would be preferred.

The assumption of core-state admixture for the $d_{5/2}$ and $p_{3/2}$ nuclei and configurational mixing for the $d_{3/2}$ acquires less clear-cut *a posteriori* justification from attempts to estimate the energy contributions from admixed single-particle configurations, the rearrangement of pairs, and admixed core states. It is often possible, by treating each nucleus in these groups as a special case, to choose a different characterization of particular ground states than was employed herein and still account for the magnetic moment while simultaneously improving the situation in the light of the crude energy considerations indicated above. However, this investigation was predicated upon the assumption that present knowledge of nuclear ground-state energies was the least valid basis for determining ground-state wave functions. Hence, since the proposed rules are simple, relatively unambiguous in application, and extremely successful in correlating nuclear magnetic moments, we have chosen to ignore the alternatives mentioned above.

Of course, there is no question of pure core-state admixture in the $p_{1/2}$ and $s_{1/2}$ ground states. For these

TABLE X. Experimentally observed and calculated magnetic moments for $h_{9/2}$ nuclei.

Calculated magnetic moments, (l, j, λ, I) Odd proton	Odd neutron
(5 9/2 2 9/2) $\mu=2.55$	(5 9/2 2 9/2) $\mu=$ 1.62
(3 7/2 2 9/2) $\mu=5.80$	(3 7/2 2 9/2) $\mu=-1.10$
(5 9/2 0 9/2) $\mu=2.62$	(5 9/2 0 9/2) $\mu=$ 1.56

Nucleus	Observed I	Observed μ
Bi^{209}	9/2	4.08 (K)

nuclei the major question is the choice of admixing single-particle configurations. Correlation of the moments of these nuclei permits very little latitude as regards the above choice, and one notes that usually the state required corresponds to the one that would be expected to admix from simple energy considerations.

It is interesting to observe that in nearly all cases the state of minimal core activity characterized by $\lambda=2$ is of major importance in the correlation of the moments. The core admixture required for $l+1/2$ nuclei usually consists of either the pair $\lambda=0$ and 2, or the pair $\lambda=2$ and 4. In either event it is almost always the case that the core state $\lambda=2$ predominates. Furthermore, the core good quantum number for all of the $l-1/2$ nuclei is $\lambda=2$. It is further noteworthy that for nearly all of the $l-1/2$ cases the amount of admixed single-particle configuration is small. However, the assumption that the core quantum number is good for $l-1/2$ nuclei may well be indefensible; and, as inspection of the tables reveals, is certainly not necessary. For all $l-1/2$ nuclei with $I>3/2$ it is seen that, in fact, it makes practically no difference empirically whether the shell theory single-particle configuration is admixed with $\lambda=0$ or 2. However, considerable difference is indicated for the $d_{3/2}$ cases, as is shown by the dotted lines in Fig. 2.

The application of these rules to the odd-odd nuclei can be carried out in a straightforward manner and their magnetic moments satisfactorily accounted for, but in general the situation is quite nonunique. If one takes as the coupling scheme

$$\mathbf{J}_p+\mathbf{J}_n=\mathbf{J}, \quad \mathbf{J}+\mathfrak{L}=\mathfrak{J},$$

where $\mathbf{J}_p$ and $\mathbf{J}_n$ are the total angular momentum operators for the proton and neutron, respectively, it is apparent that there is still an unspecified quantum number; i.e., j, the eigenvalue of $\mathbf{J}$ representing the resultant angular momentum of the two single-particle configurations. Furthermore there does not appear to be any simple criterion by means of which one might even restrict the range of values available to this quantum number—other than the not very restrictive requirements that

$$|I-\lambda|\leqslant j\leqslant|I+\lambda|, \quad |j_p-j_n|\leqslant j\leqslant|j_p+j_n|.$$

Noting, however, the consistent predominance of the core state $\lambda=2$ in the ground states of the odd-even nuclei, we have taken as starting assumptions that $j\sim I$ and $\lambda=2$ will be of major importance in the construction of the ground states here also. The particle quantum numbers are again taken to be those associated with the single-particle configuration assignments of the extreme shell model. Although configurational mixing might be expected in those cases in which one or both of the single-particle assignments is $l-1/2$, it is found that pure core-state admixture successfully accounts for all of the moments of the odd-odd nuclei. The significance of this apparently simpler situation's obtaining for these nuclei in comparison to the odd-even is not clear.

TABLE XI. Experimentally observed and calculated magnetic moments for odd-odd nuclei.

Nucleus	Observed I	Observed μ	$(l_p, j_p, l_n, j_n, j, \lambda, I)$	Calculated μ
B^{10}	3	1.80 (K)[b]	(1 3/2 1 3/2 3 0 3)	1.88
			(1 3/2 1 3/2 3 2 3)	1.75
N^{14}	1	0.40 (K)	(1 1/2 1 1/2 1 2 1)	0.49
			(1 3/2 1 3/2 1 2 1)	0.36
Na^{22}	3	1.74 (K)	(2 5/2 2 5/2 3 0 3)	1.73
Na^{24}	4	1.69 (B-M)	(2 5/2 2 5/2 2 4 4)	1.88
			(2 5/2 2 5/2 2 6 4)	1.60
K^{40}	4	−1.29 (K)	(2 3/2 3 7/2 4 0 4)	−1.68
			(2 3/2 3 7/2 4 2 4)	−1.16
K^{42}	2[a]	−1.14 (B-M)	(2 3/2 3 7/2 2 0 2)	−1.72
			(2 3/2 3 7/2 2 2 2)	−0.41
V^{50}	6 (B-M)[b]	3.35 (B-M)	(3 7/2 3 7/2 6 0 6)	3.32
Rb^{86}	2	−1.69 (B-M)	(3 5/2 4 9/2 2 0 2)	−2.13
			(3 5/2 4 9/2 2 2 2)	−0.62
Cs^{134}	4[a]	2.96 (B-M)	(2 5/2 2 3/2 2 2 4)	4.54
			(2 5/2 2 3/2 2 4 4)	2.62

[a] E. H. Bellamy and K. F. Smith, Phil. Mag. 44, 33 (1953).
[b] See reference a of Table I.

As a consequence of the above considerations, we shall not enter into any detailed discussion of these nuclei. Table XI lists the members of this group for which the spins and magnetic moments have been measured and indicates for each a reasonable set of quantum numbers defining ground states which satisfactorily correlate these moments. The diagonal elements of the magnetic moment operator are given by

$$\mu(Ij\lambda j_p j_n)=\left\{\left[g_{j_p l_p}\frac{j(j+1)+j_p(j_p+1)-j_n(j_n+1)}{2j(j+1)}+g_{j_n l_n}\frac{j(j+1)+j_n(j_n+1)-j_p(j_p+1)}{2j(j+1)}\right]\times\frac{I(I+1)+j(j+1)-\lambda(\lambda+1)}{2I(I+1)}+g_c\frac{I(I+1)-j(j+1)+\lambda(\lambda+1)}{2I(I+1)}\right\}I. \quad (15)$$

For $\lambda=0$ and $j=I$, this reduces to

$$\mu(Ij_p j_n)=\left[\tfrac{1}{2}(g_{j_p l_p}+g_{j_n l_n})+(g_{j_p l_p}-g_{j_n l_n})\frac{j_p(j_p+1)-j_n(j_n+1)}{2I(I+1)}\right]I. \quad (16)$$

It is finally to be noted that in the main a somewhat analogous scheme can be developed in the m-representation (strong-coupling representation), in which admixture of different single-particle projection states replaces pure core-state admixture, and configurational mixing occurs in principle the same as in the λ repre-

sentation. It is found, however, that the development of this scheme demands somewhat greater complication in order to accommodate the $I=3/2$ nuclei. As it is one of our principal motives to attempt to find the scheme with the minimal set of arbitrary rules, we have chosen the λ representation, in which the $I=3/2$ nuclei present unexceptional behavior. The fact that the m- and λ representations differ unambiguously when examined in the light of the empirical model discussed herein may possibly be significant. The principal difference lies, so far as magnetic moments are concerned, in the fact that in the m-representation $p_{3/2}$ ground states require an admixture of other single-particle configurations, usually $f_{5/2}$. Thus, if there is independent evidence for strong admixture of this type for these nuclei,[18] a preference for the m-representation might well be indicated in spite of its greater complexity empirically.

Though the investigations necessary for a detailed discussion of the significance of the model relative to electric quadrupole moments are not completed, a few comments on the matter are relevant here. It is clear, of course, that quadrupole moments cannot be completely determined within the context of the present model, as they depend sensitively upon the magnitude of the distortion of the core which in turn depends upon nuclear degrees of freedom which have been explicitly excluded from consideration. However, in those cases for which the quadrupole moments have been experimentally determined, it is possible to estimate the magnitude and sign of the quantity which contains the dependence of the theoretical quadrupole moment upon the dynamics of the core shape.

The appropriate quadrupole moment operator for a system consisting of a single particle plus a deformed core is

$$Q_{0p}=\sum_{m'} D_{mm'}^{2*}(\theta_i)Q_{m'}+2(\tfrac{1}{5}\pi)^{\frac{1}{2}}e_p r_p^2 Y_2^m(\hat{r}_p), \quad (17a)$$

where $D(\theta_i)$ is as previously defined and $Y(\hat{r}_p)$ is a spherical harmonic in the space of the particle. For axially symmetric deformations this reduces to

$$Q_{0p}=(\tfrac{1}{5}\pi)^{\frac{1}{2}}Q_m Y_2^m(\theta_i)+2(\tfrac{1}{5}\pi)^{\frac{1}{2}}e_p r_p^2 Y_2^m(\hat{r}_p). \quad (17b)$$

The pertinent matrix elements of this operator are

$$\begin{aligned} Q(I,\lambda jl,\lambda' j'l') &= (\Psi_{I\lambda jl}{}^I, Q_{0p}\Psi_{I\lambda' j'l'}{}^I) \\ &= \delta_{jj'}\delta_{ll'}Q_0 P_c(Ij;\lambda\lambda') \\ &\quad +\delta_{\lambda\lambda'}\langle e_p r_p^2\rangle P_p(I\lambda;jlj'l') \end{aligned} \quad (18)$$

where

$$Q_0=e\int \rho r^2(3\cos^2\theta-1)d\tau_c, \quad (19)$$

$$P_c(Ij;\lambda\lambda')=\left[\frac{(2\lambda'+1)I(2I-1)(2I+1)}{(I+1)(2I+3)}\right]^{\frac{1}{2}} \times C(\lambda' 2\lambda;0,0)W(jI\lambda 2;\lambda' I), \quad (20)$$

$$P_p(I\lambda;jlj'l')=2(-1)^{l+i'-1} \times\left[\frac{(2l'+1)(2j+1)(2j'+1)I(2I-1)(2I+1)}{(I+1)(2I+3)}\right]^{\frac{1}{2}} \times C(l'2l;0,0)W(ljl'j';\tfrac{1}{2}2)W(2j'I\lambda;jI). \quad (21)$$

P_c is a projection factor for the core and P_p a projection factor for the particle, both of which vanish for $I=0$ or $1/2$. For $\lambda=\lambda'=0$, it follows that $j=I$, $P_c=0$, and $P_p=-(2j-1)/2(j+1)$.

The quantity Q_0 contains all of the dependence upon the dynamics of the deformation. For the hydrodynamical model[11] one has

$$Q_0=\frac{3}{(5\pi)^{\frac{1}{2}}}ZeR_0^2\langle\beta\cos\gamma\rangle,$$

where R_0 is the nuclear radius; and for a rigid rotator it may conveniently be expressed as

$$Q_0=(6/5)ZeR_0^2(I_s-I_a)/I_a,$$

where I_s and I_a are the spherical moment of inertia and the moment of inertia of the deformed object about the symmetry axis, respectively. It is obvious from the latter expression that Q_0 is positive for a prolate deformation and negative for an oblate deformation.

The first point relevant to the present discussion is that the quantity $\langle\beta\cos\gamma\rangle$, which for axial symmetry is simply $\pm\langle\beta\rangle$, has been computed for the nucleus ${}_{83}Bi^{209}$ employing the wave function determined by its magnetic moment and found to be ~-0.06. Thus both sign and magnitude correspond reasonably to expectation. Secondly, because of the not-inconsiderable nondiagonal contribution to the quadrupole moment for the $l+1/2$ nuclei whose ground states contain core-state admixtures, calculation of nuclear distortions from measured quadrupole moments provides the possibility of a determination of the sign of the mixing coefficient. Thirdly, the calculation of the core distortions may provide a test of the selection rule $\Delta(\lambda\lambda'2)$ in the construction of the $l+1/2$ ground-state wave functions. It will be remembered that the admixing core states for the heavier nuclei were generally characterized by $\lambda=2$ and $\lambda=4$. But in all of these cases, as far as fitting magnetic moments is concerned, the states with $\lambda=0$ and 4 would have been equally satisfactory. However, the core contribution to the quadrupole moment changes sign in going from the admixture (0,4) to (2,4) for $I=5/2$, and changes substantially in magnitude but not in sign for $I>5/2$.

IV. ACKNOWLEDGMENTS

The authors wish to express their gratitude to Dr. A. H. Snell for his sustained interest and encouragement throughout the course of this work and to Professor L. W. Nordheim for reading and commenting on this manuscript. They wish also to thank Virginia Klema for her assistance in carrying out and checking calculations.

[18] The existence of such evidence has been suggested to us by L. W. Nordheim (private communication).

Rotational States in Tm^{169}

SVEN A. E. JOHANSSON
Department of Physics, University of Lund, Lund, Sweden
(Received July 11, 1955)

The decay of Yb^{169} has been investigated by means of a coincidence scintillation spectrometer. Eleven gamma rays have been arranged in a level scheme with levels at 10, 120, 142, 318, 336, 382, and 476 kev. The multipolarity of the strongest gamma rays has been determined and spin values assigned to some of the levels. It is found that five of the levels form a rotational band with $K=\frac{1}{2}$. In this case the Bohr-Mottelson unified model predicts an anomalous rotational spectrum. The experimental spectrum agrees very well with the theory. The gamma-ray intensities are discussed and there is a good agreement with the unified model also in this respect.

INTRODUCTION

THE ytterbium isotope of mass 169 decays by electron capture to Tm^{169}. The half-life is 32 days. The radiation emitted in this decay has been studied by several investigators[1,2] and is fairly well known. No consistent decay scheme seems to have been established, however.

The level scheme of Tm^{169} is of interest for a special reason. This nucleus lies in a region where the Bohr-Mottelson unified model[3,4] should be applicable. The lowest levels are expected to form a rotational band. The spin of the ground state is found to be $\frac{1}{2}$.[5,6] In this case the unified model predicts an anomalous spacing of the rotational levels. A determination of the level scheme will thus provide a rather detailed test of this model.

In the present work the decay of Yb^{169} has been investigated by means of a coincidence scintillation spectrometer. The experimental results make it possible to set up a consistent level scheme for Tm^{169}. This scheme is compared with the predictions of the unified model.

MEASUREMENTS

Radioactive ytterbium was obtained by pile irradiation of ytterbium oxide. The irradiated material (supplied by Johnson, Matthey and Company, Ltd., London) was of very high purity and had been tested by spectrophotometric and spectrographic examination. Foreign elements other than the rare earths were estimated to amount to less than 0.004% of the product. No other rare earth elements could be detected and the upper limit for the most likely impurities was estimated to be 0.02%. The ytterbium oxide was irradiated for one month and the sample was allowed to age for one month to allow the short-lived ytterbium activities to decay.

The coincidence scintillation spectrometer has been described in detail elsewhere.[7,8] It consists of two scintillation spectrometers coupled in coincidence. A certain radiation component is selected in the spectrum from one of the spectrometers and the corresponding coincidence spectrum from the other spectrometer is recorded. The resolving time of the coincidence circuit is 0.2 μsec. The scintillation spectrometer consists of sodium iodide crystals mounted on DuMont photomultipliers, type 6292. The resolution of the spectrometers is 6.2% full width at half-maximum for the Cs^{137} 662-kev line.

Figure 1 shows the gamma spectrum of Yb^{169}. The statistical errors in this spectrum as well as in all the following are small and have not been drawn in the figures. Most spectra comprise more than 10 000 pulses. The resolution of the spectrum in its main components is also shown. The highest peak is due to the K_α and K_β x-rays of thulium. They are emitted in the electron capture process and in the internal conversion of the gamma rays. The spectrum also contains gamma rays of the energies 64, 94, 110, 133, 178, 198, and 308 kev. These values are in excellent agreement with those reported by Cork *et al.*[1] and by Martin *et al.*[2]

The spectrum has a small bump at 250 kev. A possible reason for this is the addition of peaks when two gamma rays or x-rays are absorbed simultaneously in the same crystal. The 198-kev gamma ray and part of the K x-rays are in coincidence and they will therefore give a small peak at about 250 kev. The size of the peak depends on the solid angle subtended by the crystal at the source. In the coincidence measurements, where it is necessary to use large solid angles, this effect sometimes is of importance. For the spectrum shown in Fig. 1, however, it is very small. The bump at 250 kev must therefore be attributed to one or several gamma-rays. When the spectrum is analyzed more in detail it is found that the 250-kev peak is broader than can be accounted for by a single gamma ray. It must therefore be concluded that the spectrum contains two or more weak gamma rays in the range 240–260 kev.

[1] Cork, Keller, Rutledge, and Stoddard, Phys. Rev. **78**, 95 (1950).
[2] Martin, Jensen, Hughes, and Nichols, Phys. Rev. **82**, 579 (1951).
[3] A. Bohr, Kgl. Danske Videnskab. Selskab, Mat.-fys. Medd. **26**, No. 14 (1952).
[4] A. Bohr and B. R. Mottelson, Kgl. Danske Videnskab. Selskab, Mat.-fys. Medd. **27**, No. 16 (1953).
[5] H. Schüler and T. Schmidt, Naturwiss. **22**, 838 (1934).
[6] K. H. Lindenberger and A. Steudel, Naturwiss. **42**, 41 (1955).
[7] Sven A. E. Johansson and S. Almquist, Arkiv Fysik **5**, 427 (1953).
[8] Sven A. E. Johansson, Iowa State College Report, ISC-431 (unpublished).

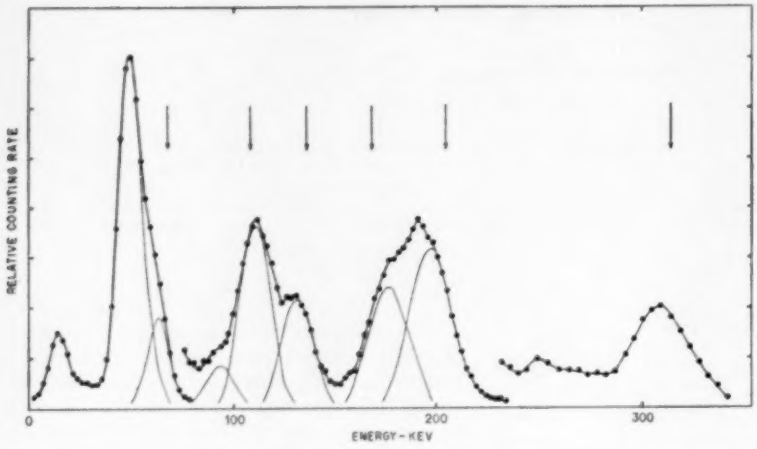

FIG. 1. Gamma-ray spectrum of Yb^{169}. The fine lines show the resolution of the spectrum into its main components.

The decay of Yb^{169} is known to proceed via a metastable state with a half-life of 0.7 μsec.[2,9] The coincidence spectrometer makes it possible to record spectra of the radiation preceding and following the metastable state. First a delay of 0.4 μsec was introduced after the spectrometer which is connected to the single-channel analyzer. The channel was set at the x-ray peak. The coincidence spectrometer will then record the spectrum of the radiation following the metastable state. It is shown in Fig. 2(a). The greater part of the radiation apparently follows the metastable state. The 64-kev gamma ray is missing, however. The broad distribution around 250 kev can be accounted for by accidental addition of the 198-kev and K x-ray peaks. Hence the weak gamma rays at 250 kev are presumably missing too.

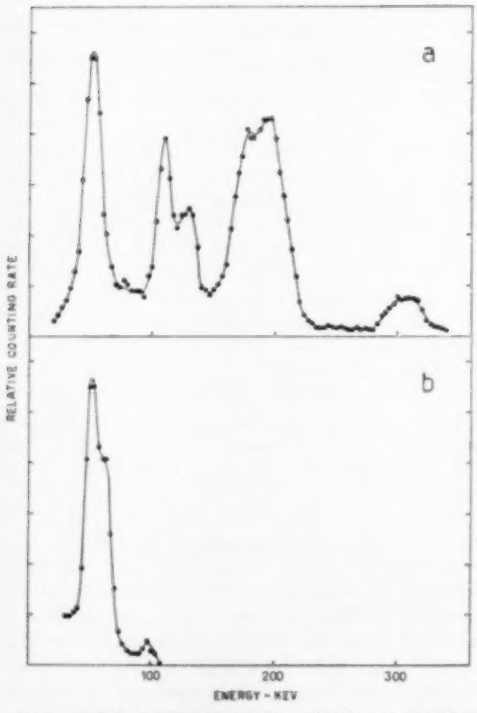

FIG. 2. (a) Spectrum of the radiation following the metastable state. (b) Spectrum of the radiation preceding the metastable state.

Next a 0.4-μsec delay was introduced after the other spectrometer in order to study the radiation preceding the metastable state. The channel of the analyzer was set on the 110-kev peak. The resulting coincidence spectrum is shown in Fig. 2(b). The only gamma rays preceding the metastable state are the ones at 64 and 94 kev.

In order to investigate the coincidence relationships a series of coincidence spectra were recorded with the analyzer channel set to select various gamma rays. Even if most of the gamma rays are not completely resolved, it is in most cases possible to find a channel position where a certain gamma ray can be practically completely separated from the adjacent rays. The various channel settings used in the present investigation are shown with arrows in Fig. 1.

First the channel was set on the 64-kev peak. The corresponding coincidence spectrum is shown in Fig. 3(a). Besides the K x-rays this spectrum contains the 94, 110, 133, 178, 198, and 308-kev gamma rays. The relative intensities are about the same as in the total spectrum with one exception: the 94-kev peak is much stronger. The only way to account for this fact is to assume that the 64-kev and 94-kev gamma rays are in prompt coincidence but that the 64-kev ray is separated from the other rays by the metastable state.

[9] S. DeBenedetti and F. K. McGowan, Phys. Rev. 74, 728 (1948).

Since the resolving time of the coincidence circuit is shorter than the lifetime of the metastable state, the coincidence rate will be lower in the latter case. The bump at 250 kev is due to accidental coincidences in the same crystal between the 198- and 178-kev gamma rays and the K x-rays.

The channel was then set on the 110-kev peak. The coincidence spectrum is shown in Fig. 3(b). The 64-, 94-, and 178-kev gamma rays are relatively weaker than the 198-kev ray. The 110- and 133-kev rays are very weak; their presence is very likely due to secondary effects like accidental coincidences and backscattering. The spectrum also shows a bump at 260 kev. It cannot be explained as an effect of accidental coincidences as in the previous spectrum. It must therefore be assumed that the 110-kev gamma-ray is in coincidence with a weak gamma ray at about 260 kev.

Next the channel was set on the 133-kev peak. The coincidence spectrum, shown in Fig. 3(c), is similar to the previous one except that the 178-kev peak is the strongest. It is asymmetric because of the presence of a small peak at about 195 kev. If the channel setting had allowed a certain part of the 110-kev peak to fall into the channel, then the 198-kev gamma ray would have appeared in the spectrum. However, with the channel setting used, only a small part of the 195-kev peak can be due to the 198-kev gamma ray. Furthermore, if the peak is analyzed more carefully, it turns out that the small peak definitely lies lower than 198 kev, at about 194 kev. It is therefore tentatively assumed that the 133-kev gamma ray is in coincidence with a gamma ray of 194 kev. At higher energies there is a weak bump at 240 kev. As in the previous spectrum it cannot be explained as an effect of accidental coincidences. It is therefore assumed that there also exists a 240-kev gamma ray.

With the channel set on the 178-kev peak, the spectrum of Fig. 4(a) was recorded. The main gamma-ray peak is due to the 133-kev gamma ray. The 64-, 94-, and 110-kev gamma rays are relatively weaker.

Figure 4(b) shows the spectrum recorded with the channel set on the 198-kev peak. Peaks due to the 64- and 110-kev gamma rays can be seen. The 110-kev peak has a tail on the high-energy side, which must be due to a gamma ray with an energy slightly higher than 110 kev. A detailed analysis of the peak shows that the tail can be only partly ascribed to the 133-kev gamma ray. There is also a component of lower energy, which may be the 120-kev gamma ray reported by Martin *et al.*

Finally the channel was set on the 308-kev peak. The spectrum, shown in Fig. 4(c), contains the 64- and 94-kev gamma rays.

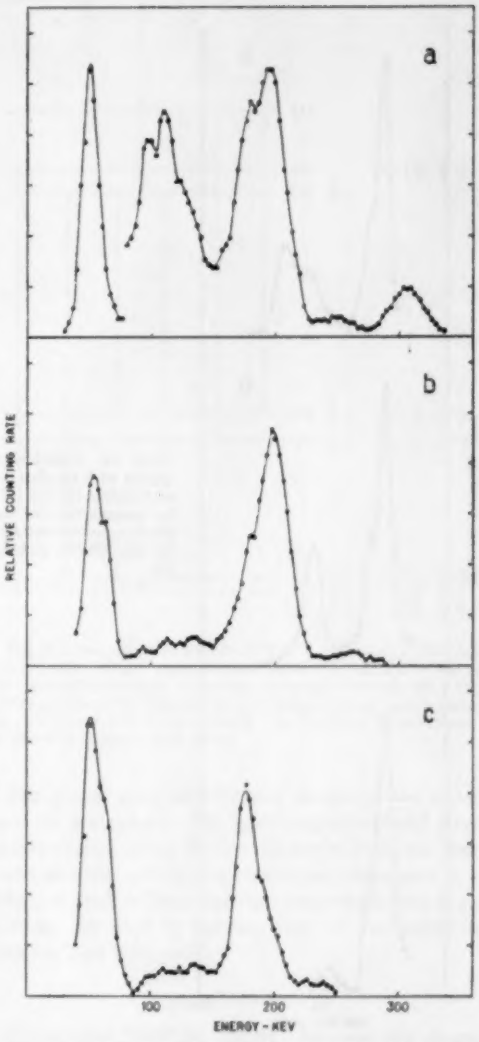

FIG. 3. Coincidence spectra with the channel set to select (a) the 64-kev gamma ray, (b) the 110-kev gamma ray, and (c) the 133-kev gamma ray.

LEVEL SCHEME

The coincidence experiments establish the level scheme shown in Fig. 5. All spectra are in agreement with this scheme. A few points warrant some discussion.

A level has been placed at 10 kev for the following reasons. The coincidence spectrum in Fig. 4(b) shows coincidences between the 198- and 120-kev gamma rays. The spectrum of the radiation preceding the metastable state at 318 kev does not contain a 120-kev gamma ray. Hence this gamma ray must follow the 198-kev gamma ray. This requires a level at 10 kev. Additional support for this interpretation is provided by the Coulomb excitation of thulium.[19] In that experiment a single

[19] T. Huus (private communication).

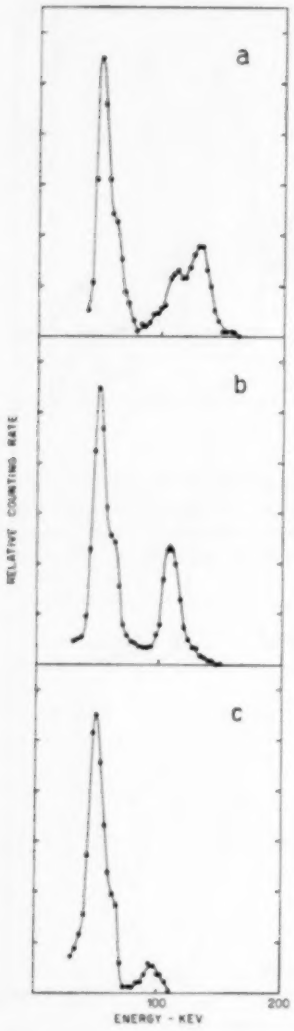

FIG. 4. Coincidence spectra with the channel set to select (a) the 178-kev gamma ray, (b) the 198-kev gamma ray, and (c) the 308-kev gamma ray.

level is excited which decays by emission of two gamma rays of 110- and 120-kev. Hence, even though the 10-kev gamma ray leading to the ground state has not been detected, there seems to be enough experimental evidence for postulating a level at 10 kev.

A gamma ray is expected to go from the 142-kev to the 120-kev level. Due to its low energy it has not been detected in the present experiment, but it is very likely the 22.8-kev gamma ray reported by Martin *et al.* This gamma ray explains some features in the coincidence experiments. Figure 3(b) shows that the 178-kev gamma ray to some extent is in coincidence with the 110-kev gamma ray. The level scheme shows that this can be explained as a cascade via the 23-kev transition. The spectrum in Fig. 4(a) gives another example of the existence of this cascade. These spectra allow a calculation of the intensity of the 23-kev transition, as will be discussed below.

The order of the 64-kev and 94-kev transitions can be determined from their relative intensities. The intensity of the corresponding gamma rays are listed in Table I. The intensity of the conversion electrons can not be determined accurately from the conversion spectrum of Martin *et al.*, but it can be seen that the 94-kev gamma ray is not especially highly converted. Hence the 94-kev transition must be considerably weaker than the 64-kev transition. The former is therefore the preceding one.

The coincidence spectra in Figs. 3(b) and 3(c) indicate that there exist two weak gamma rays at 240 kev and 260 kev in coincidence with the 133-kev and 110-kev gamma rays, respectively. These two gamma rays fit very well into the level scheme, both starting from the 382-kev level. This agreement supports the correctness of the proposed interpretation of the coincidence spectra.

All gamma rays reported are included in the level scheme, except the 142-kev and 160-kev rays. It is interesting to note that they fit well into the scheme as transitions from the 476-kev level to the 336-kev and 318-kev levels, respectively. They are so weak, however, that the coincidence measurements give no information and therefore they are not included in the scheme.

It is interesting to note that the relative intensities of the gamma rays are the same in the spectrum of the total radiation (Fig. 1) as in the spectrum of the delayed radiation. This means that no electron capture branches go to the 120-kev or 142-kev levels. It follows from the subsequent discussion that no branches go to the ground state or the first excited state.

The spectrum in Fig. 1 is used to determine the relative intensities of the gamma rays. The photoelectric efficiency of the scintillation spectrometer is calculated for the various energies, taking into account the photoelectric absorption coefficient, secondary absorption processes, K x-ray and electron escape, and absorption of the gamma rays in the material surrounding the crystal. The efficiency varies fairly slowly from about 95% at 100 kev to about 40% at 300 kev. The area of the peak times the efficiency then gives the relative intensities.

The relative intensity of the K-conversion lines has been determined by Martin *et al.* The absolute intensity, i.e., the intensity relative to the number of disintegrations, can be determined in the following way: The K x-rays are produced in two different processes, namely in the K-capture decay and in the internal conversion of the gamma rays. Hence the total intensity of the x-rays is equal to the intensity of the x-rays following the K-capture plus the intensity of the internal conversion x-rays. The total intensity of the x-rays is known relative to the gamma-ray intensities from Fig. 1. The number of disintegrations is assumed

to be equal to the sum of the intensities of the transitions to the ground state and the first excited state. This assumption follows from the fact that no K-capture branches are going to these states. The only unknown quantity in the equation is then the ratio between the relative scales for the intensities of the gamma rays and internal conversion lines. When this ratio is determined by solving the equation, all intensity values can be expressed on the same relative scale. The absolute intensities and K-conversion coefficients can then be easily obtained.

This calculation is necessarily fairly approximate. Errors in the relative intensities will cause a considerable uncertainty in the absolute values. The intensities of the K-conversion electrons from the 94-kev and 64-kev gamma rays are not known and they are therefore not included in the calculation. The calculated electron intensities and conversion coefficients are for this reason somewhat too high. This calculation, however, is mainly of interest for determining the multipolarity of the gamma rays. The accuracy is certainly enough for this purpose.

Table I shows the intensities and conversion coefficients of the main gamma rays. The multipolarities are listed in column five and the corresponding theoretical conversion coefficients[11] in column six. A comparison shows that the multipole assignments can be made without any ambiguity.

The intensity of the 23-kev transition can be calculated from the coincidence spectra in Figs. 3(b) and 4(a) as discussed above. It turns out to be 0.20. It is then possible to check the intensity values by comparing the sum of the intensities of the transitions going to a certain level with the sum of the intensities of the transitions starting from that level. Satisfactory agreement is obtained for the 120-kev and 142-kev levels, the only ones where this check is possible.

The experimental data make it possible to assign spin values to most of the levels. The only values which give agreement with the experiments are the ones shown in Fig. 5.

TABLE I. Intensity values relative to the disintegration rate, approximate K-conversion coefficients, multipole assignments, and the corresponding theoretical conversion coefficients.

Energy kev	Gamma-ray intensity	K-electron intensity	K-conversion coefficient	Multipole assignment	Theoretical conversion coefficient
K x-rays	1.13				
64	0.25				
94	0.034				
110	0.144	0.47	3	$M1$	2.4
133	0.091	0.05	0.5	$E2$	0.48
178	0.146	0.12	0.8	$M1$	0.60
198	0.214	0.09	0.4	$M1$	0.45
308	0.060	0.004	0.06	$E2$	0.05

[11] Rose, Goertzel, Spinrad, Harr, and Strong, Phys. Rev. 83, 79 (1951).

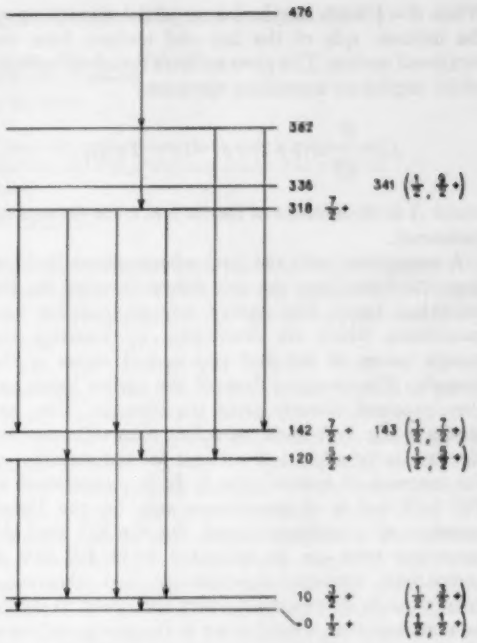

FIG. 5. Proposed level scheme of Tm^{169}. The energy and spin values to the left are experimental values. The energy values to the right are calculated from the theoretical formula with the energy values of the first two excited states inserted to determine the two parameters of the formula. The numbers in parentheses are theoretical values of K and I.

The ground state and the four lowest excited states have the same parity. The experimental material gives no information about its sign. However, both the shell model and the calculations on the wave functions in a deformed nucleus[12] indicate that the ground state is an $s_{\frac{1}{2}}$ state. Hence it is assumed that all the levels in question have even parity.

DISCUSSION

The nucleus Tm^{169} lies halfway between two closed shells and is expected to be strongly deformed. According to the unified model, the intrinsic motion of the nucleus can be separated from the collective rotational motion. Each intrinsic state is then the first member of a rotational band having states of spin

$$I=K, K+1, K+2, \cdots,$$

where K is the component of the total angular momentum along the nuclear symmetry axis. In the case of Tm^{169}, $K=\frac{1}{2}$ and there will be a rotational band with

$$I=1/2, 3/2, 5/2, \cdots.$$

[12] S. G. Nilsson, Kgl. Danske Videnskab. Selskab, Mat.-fys. Medd. (to be published).

When $K=\frac{1}{2}$ there may occur a partial decoupling of the intrinsic spin of the last odd nucleon from the rotational motion. This gives an extra rotational energy, which implies an anomalous spectrum:

$$E_I=\frac{\hbar^2}{2\Im}\{I(I+1)+a(-1)^{I+\frac{1}{2}}(I+\tfrac{1}{2})\},$$

where $\Im$ is the moment of inertia and a the decoupling parameter.

A comparison with the level scheme shows that the four first levels have the spin values expected for the rotational band. The energy formula contains two parameters which are determined by inserting the energy values of the first two excited states in the formula. The energy values of the higher levels are then obtained directly from the formula. They are shown in Fig. 5. A small correction term with negative sign has to be applied to account for the variation of the moment of inertia with I. It is proportional to $I^2(I+1)^2$ and is of importance only for the higher members of a rotational band. For the 9/2 level the correction term can be estimated to be 1–2 kev. A comparison between experimental and theoretical energy values shows a satisfactory agreement. It should be remarked that a small error in the energy values of the first two excited states can account for the small difference between experiment and theory. A better agreement is obtained by adjusting the formula to all levels by the least-squares method.

Hence the properties of the rotational band are correctly predicted by the unified model. The rotational energy quantum $\hbar^2/2\Im$ has the value 12.66 kev. Approximately the same value has been found for rotational bands in neighboring nuclei. The decoupling parameter a is equal to -0.74. A theoretical value has been calculated by Mottelson and Nilsson[13] based on wave functions obtained by considering particle motion in an axially symmetric deformed potential with the inclusion of an appropriate spin-orbit force.[12] The theoretical value is -0.8, a very satisfactory agreement.

The levels at 318, 383, and 476 kev apparently do not belong to the rotational band. The radiation probability of these levels shows a peculiar behavior. The 318-kev level decays by $M1$ and $E2$ emission but the lifetime is as long as 0.7 μsec. The 382-kev level decays mainly to the 318-kev level. One would expect that the transition probability for a transition to the 142-kev level would be considerably greater than to the 318-kev level. Similarily the 476-kev level decays to the 382-kev level but not to the lower levels. This can be explained as cases of K-forbiddenness, which means that the change in K is greater than the multipolarity of the transition.[14] In the decay of the 318-kev level, K is changed by 3 units. The lifetime according to the single-particle formula[15] is about 5×10^{-12}. Hence the retardation due to K-forbiddenness is 10^6. In the decay of the 382-kev level, one expects the intensity ratio between the 240-kev and 64-kev gamma transitions to be 100 or higher, depending on the multipolarity of the two gamma rays. Instead the 64-kev gamma ray is about 50 times as intense as the 240-kev gamma ray. The forbiddenness factor is in this case of the order 10^4 or higher.

Another possible example of K-forbiddenness is provided by the branching ratios of the K-capture. There is no branching to the 142-kev level or lower levels. The great change in K implied in transitions to those levels may account for this retardation.

The reduced transition probability for $M1$ radiation within a rotational band with $K=\frac{1}{2}$ depends on the intrinsic structure of the nucleus. When the wave functions are known the transition probabilities can be calculated and compared with the experimental values. Mottelson and Nilsson[13] have made such a calculation for the intensity ratio of the 133-kev and 23-kev gamma rays, which is found to be 20. The total intensity of the 23-kev transition has been determined as described above. With the use of the theoretical L-conversion coefficients of Rose and Goertzel,[16] one can calculate the intensity of the gamma-radiation. The intensity ratio between the 133-kev and 23-kev gamma rays then turns out to be 14, in very satisfactory agreement with the theory.

Hence the conclusion of the present work is that the level scheme of Tm^{169} makes possible a very detailed test of the unified model. There is very good agreement between theory and experiment.

ACKNOWLEDGMENTS

The author is greatly indebted to Dr. A. Bohr, Dr. B. R. Mottelson, and Dr. S. G. Nilsson for interesting discussions.

[12] B. R. Mottelson and S. G. Nilsson, Z. Physik 141, 217 (1955).

[14] Alaga, Alder, Bohr, and Mottelson, Kgl. Danske Videnskab. Selskab, Mat.-fys. Medd. (to be published).

[15] V. F. Weisskopf, Phys. Rev. 83, 1073 (1951).

[16] M. E. Rose and G. H. Goertzel, *Beta- and Gamma-ray Spectroscopy*, edited by K. Siegbahn (North-Holland Publishing Company, Amsterdam, 1955), Chap. 14.

K-Series Fluorescence Yields of Argon, Copper-65, and Indium-113†

G. R. HARRISON, R. C. CRAWFORD, AND J. I. HOPKINS
Vanderbilt University, Nashville, Tennessee

(Received June 20, 1955)

K-series fluorescence yield measurements have been made for A, Cu^{65}, and In^{113} with a proportional counter spectrometer and found to be 0.081 ± 0.006, 0.39 ± 0.02, and 0.82 ± 0.02, respectively. The method is discussed and a comparison with theoretical values is noted.

I. INTRODUCTION

FLUORESCENCE radiation is the result of primary ionization in the inner shells of atoms. For the purpose of determining *K*-fluorescence yield values, this inner shell ionization has most commonly been produced by x-ray excitation.[1,2] When radioactive nuclei decay, vacancies are frequently created in the *K* shell by internal conversion of gamma radiation and by *K* capture. The fluorescence yield (w_K) of the *K* shell is defined as the number of *K* x-rays emitted per *K* shell vacancy, and can be calculated if the rate of emission either of characteristic x-rays or of Auger electrons can be measured, and if the number of *K*-shell vacancies is known.

The recent development of proportional counter techniques for electron and x-ray detection has provided another method with considerable merit for the determination of fluorescence yield of gases as well as for substances which are undergoing nuclear transformations.[3] This method has been used to determine the fluorescence yields of argon gas, copper-65 and indium-113.

II. EXPERIMENTAL PROCEDURE

A. Proportional Counter Spectrometer

The proportional counter used was constructed of one-eighth inch thick cylindrical brass tubing, 17 inches in length and 4 inches in diameter. The central electrode was a 2-mil stainless steel wire soldered to brass needles which in turn were mounted at each end of the counter through kovar seals. At one end of the counter a piece of brass in the form of a Y was screwed into the counter and the kovar seal mounted to it rather than the end plate; this enables the end plate to be removed for cleaning and adjustment purposes. The source opening was $\frac{3}{4}$ inch in diameter and tapered so that when a source ring was in place, the inner surface of the ring was flush with the inside wall of the counter. The source opening was closed by a cylindrical aluminum cup $\frac{1}{16}$ inch thick, 3 inches high, and 3 inches in diameter. The counting gas was a 99.9% purity mixture of 90% argon and 10% methane and the counter was operated at one atmosphere of pressure.

The high voltage was supplied from an Atomic Instrument Company Model 1040*A* regulated power supply and was filtered further before being applied to the counter. The voltage was constantly monitored to within 5/100 of 1% with a Type *K* potentiometer.

The voltage pulses from the counter were amplified by an Atomic Instrument Company Model 205*B* Preamplifier, which was directly coupled to the counter, and a Model 205*A*-1 type Linear Amplifier. The pulses were fed to a single channel differential pulse height analyzer of the type designed by Francis and Bell.[4] The output pulses of the pulse-height analyzer were recorded by two standard scalers in series which were arranged for timing a predetermined number of counts.

A voltage *versus* output pulse study of the counter for 8-kev x-rays from radioactive Zn^{65} showed a proportionality from 1600 to 2300 volts.

B. Sources and Preparation

The radioactive sources Zn^{65} and Sn^{113}, both of which decay by the electron capture process and both of which exhibit internal conversion of the gamma ray, though very slight in the case of Zn^{65}, were obtained from the Oak Ridge National Laboratory. The radioactive Zn^{65} was produced by deuteron bombardment of copper Cu^{65}. Fluorescence yield studies were made for Cu^{65} as well as argon since the fluorescence of the argon gas in the chamber was excited by the 8-kev x-ray. The radioactive Sn^{113} was produced by neutron capture from enriched Sn^{112}.[5] The Zn^{65} was vacuum evaporated onto an aluminum coated $10\mu g\ cm^{-2}$ Zapon film. The Sn^{113} was vacuum evaporated onto a $140\mu g\ cm^{-2}$ Al foil.

III. EXPERIMENTAL RESULTS

The observed Cu^{65} x-ray spectrum is shown in Fig. 1. The spectrum was taken with a $5.16\ mg\ cm^{-2}$ aluminum absorber placed over the source to absorb the Auger electrons; the counter was filled to atmospheric pressure

† Work supported by an Atomic Energy Commission Research Grant.

[1] A. H. Compton and S. K. Allison, *X-Rays in Theory and Experiment* (D. Van Nostrand Company, Inc., New York, 1935).

[2] E. H. S. Burhop, *The Auger Effect* (Cambridge University Press, Cambridge, 1952).

[3] Curran, Angus, and Cockcroft, Phil Mag. **40**, 36 (1939); P. Rothwell and D. West, Proc. Phys. Soc. (London) **A63**, 539 (1950); S. C. Curran, Advances in Physics, Phil. Mag. Suppl. **2**, 411 (1953).

[4] J. A. Francis and P. R. Bell, Oak Ridge National Laboratory Report ORNL-1470 (unpublished).

[5] Loaned by the Stable Isotopes Division of the Oak Ridge National Laboratory.

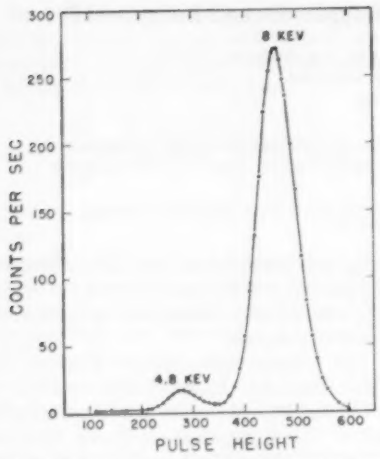

FIG. 1. Zn^{65} source with a 5.16-mg/cm² absorber showing the Cu^{65} x-ray and the argon x-ray escape peak.

with the argon gas mixture. The absorption due to methane is assumed to be negligible.

There are two clearly defined peaks occurring in the spectrum, corresponding to energies of 4.8 kev and 8.0 kev. These two peaks can be explained by examining the interaction of the Cu^{65} x-rays with the argon atoms in the counter. Since the photoelectric process of x-ray absorption is predominant in this energy range, the Cu^{65} x-rays ionize the argon atoms in their inner electron shells. If this shell happens to be the K shell, the energy of the ejected photoelectron is the energy of the incident x-ray (8.0 kev) minus the binding energy of the argon K electron (3.2 kev). This photoelectron is immediately absorbed in the counter. There is now a positive energy of 3.2 kev in the ionized argon atom. If this atom reorganizes with the emission of an Auger electron, the electron is immediately absorbed in the counter. Since Auger electron reorganization occurs within 10^{-10} second after the original ionization, a pulse corresponding to the full 8.0 kev is recorded. If the argon atom reorganizes with the emission of the 3.0 kev argon x-ray, there is a large probability that this x-ray will escape from the counter. Since the argon K x-ray does not have enough energy to ionize surrounding argon atoms in the K shell, it must interact with L and M electrons if it is to be absorbed in the counter. Consequently the absorption coefficient of argon for its own x-rays is relatively small. If the argon K–L x-ray does escape from the counter, there will be a pulse formed corresponding to the energy of the initial photoelectron plus Auger electrons and x-rays from the L or M shells, thus giving the 4.8-kev peak. Any photoelectrons originating in the L or M shells are immediately absorbed in the counter producing a pulse corresponding to the full absorption of the 8.0-kev x-ray.

With the Zn^{65} source mounted in the source opening without an absorber, the spectrum in Fig. 2 was obtained. Here two peaks are present, the 6.8-kev peak due to the Cu^{65} Auger electrons and the 8.0-kev peak due to the Cu^{65} K–L x-rays. These assignments were made from absorption experiments but further evidence for their identification was established by noting no change in the Auger electron intensity with a reduction in gas pressure. This was to be expected since the electron path length would still be much less than the counter diameter. In the case of the 8.0-kev x-radiation, however, a reduction in gas pressure did result in an observed decrease in intensity.

Spectrum A of Fig. 3 shows the energy spectrum of In^{113} arising from the Sn^{113} source. The voltage applied to the counter in this case was 1800 volts. Spectrum B of Fig. 3 shows the same energy region with a 5.16-mg/cm² aluminum absorber placed between the source and the counter. With the use of an energy calibration curve and the different spectra shown, the types and energies of the different transitions can be established.

In the decay of In^{113*} a number of different transitions may occur. There are vacancies in the K and L electron shells of the In^{113} due to electron capture as well as the internal conversion of the gamma ray. If first a vacancy in the K shell is considered, the atom is said to have a positive energy of 27.9 kev which is the binding energy of the K electron orbit. If the atom reorganizes with the emission of a K–L x-ray, this x-ray will have an energy corresponding to 24.0 kev. If the atom reorganizes with the emission of the K–LL Auger electron, this electron will have energy corresponding to approximately 20 kev. The vacancies in the L shells give rise to an x-ray of approximately 3.3 kev of energy. Any Auger reorganizations due to vacancies in the L shells would have too low an energy to detect. The K–M x-ray which has an energy of 27.3 kev and the K–LM Auger electron an energy of 23.5 kev can be detected by the counter.

It is apparent by observing the spectra in Fig. 3 that the peaks occurring at 120 and 370 pulse-height units

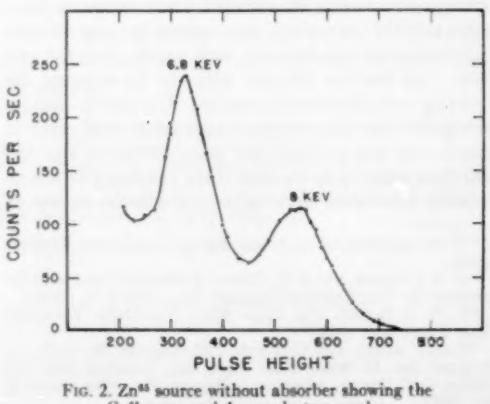

FIG. 2. Zn^{65} source without absorber showing the Cu^{65} x-ray and Auger electron peaks.

must be due to x-rays. The peak at 375 corresponds to the 24.0-kev K–L x-ray from In^{113} and the peak at 120 corresponds to 8.0 kev in energy and is due to the fluorescence radiation produced in the brass counter walls by the indium x- and gamma radiation. The small bump at 420 pulse-height units on the high-energy side of the 24.0-kev peak is the 27.3-kev K–M x-ray from In^{113}. If an examination is made of the peak occurring at 260 pulse height units, it is seen immediately that this peak is due to electrons. This peak corresponds to the 20-kev K–LL Auger electron transition from In^{113}. The bulge on the high-energy side of the Auger electron peak occurring at 320 pulse-height units is due to the 23.5-kev K–LM Auger electron reorganization of the In^{113} and the argon gas fluorescence produced by the indium x-ray. A breakdown of the Sn^{113} spectrum is shown in Fig. 4.

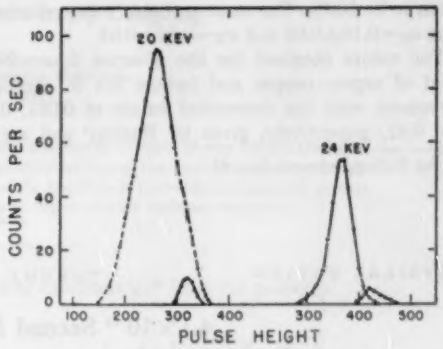

FIG. 4. Auger electron and K x-ray lines of In^{113}.

IV. ANALYSIS OF RESULTS

The data used in evaluating the fluorescence yield of argon, Cu^{65}, and In^{113} in this research are reproducible to within $\pm 1\%$. Background was taken from time to time and found to be negligible in the regions where the important peaks occurred. Certain base-line interpretations were necessary but these do not introduce large errors.

A. Argon

To determine the K-series fluorescence yield of argon (w_K), it is necessary to examine the spectrum of Fig. 1. As explained previously, the high-energy peak is produced by the combined photoelectric and Auger process occurring in the argon gas and the lower peak is produced when the argon K x-ray escapes from the counter following the photoelectric process. Correction has to be made for the reabsorption of the K x-rays of argon in the counter gas and can be estimated from absorption data[6] and the mass of the gas per cm^2 as seen by the x-rays. Also a correction has to be made to account for the incident radiation absorbed in the L, M, $N\cdots$ shells, and can be determined from "K jump" data.[7] With an estimated error of no more than 5% in each correction, the most probable value for the K-series fluorescence yield of argon was found to be $w_K=0.081\pm0.006$.

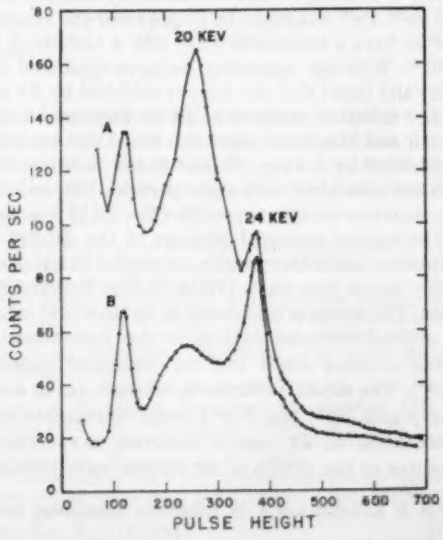

FIG. 3. Sn^{113} source showing (A) In^{113} K x-ray and K-LL Auger electron peak without absorber and (B) Sn^{113} source with 5.16-mg/cm^2 absorber.

B. $Zn^{65}-Cu^{65}$

A proportional counter is especially useful in measuring the fluorescence yield of atoms undergoing nuclear transformation since Auger reorganizations as well as x-ray emission can be detected. In determining the K-series fluoresence yield of Cu^{65}(w_K) from Fig. 2, the K-series Auger yield (a_K) is first computed, then $w_K=1-a_K$. In order to compare the relative intensity of the Auger electrons to the total intensity of the x-rays plus the Auger electron intensity, it was necessary to determine the counter efficiency for 8-kev x-rays. This was done by comparing areas under the x-ray peaks when the counter was operated at two different gas pressures. The efficiency for 8-kev x-rays was found to be approximately $97\pm1\%$. The efficiency for the Auger electrons was taken to be 100%. The most probable values obtained were $a_K=0.61\pm0.02$ and $w_K=0.39\pm0.02$.

C. $Sn^{113}-In^{113}$

The K-series Auger yield for In^{113} was determined from Fig. 3, the breakdown of which is shown in Fig. 4. The efficiency for the 24-kev In^{113} x-ray was measured to be $7.7\pm0.7\%$ and again the Auger electron efficiency

[6] Margaret Lewis, National Bureau of Standards Report 2457, April, 1953 (unpublished).

[7] B. Woernle, Ann. Physik 5, 475 (1930); R. G. Spencer, Phys. Rev. 38, 1943 (1931); Compton and Allison, reference 1, pp. 536–542.

taken to be 100%. The most probable values obtained were $a_K=0.18\pm0.02$ and $w_K=0.82\pm0.02$.

The values obtained for the K-series fluorescence yield of argon, copper and indium are in excellent agreement with the theoretical values of 0.081, 0.37 and 0.82, respectively, given by Burhop[8] and are in good agreement with the experimental values appearing in a summary of fluorescence yield measurements given by Broyles, Thomas, and Haynes.[9] The authors believe that a liberal allowance has been made in estimating the probable errors and because of good agreement with other data, the usefulness of the method is indicated.

[8] See Burhop, reference 2, p. 45.

[9] Broyles, Thomas, and Haynes, Phys. Rev. **89**, 715, 1953.

PHYSICAL REVIEW VOLUME 100, NUMBER 3 NOVEMBER 1, 1955

4.1×10^{-8} Second Metastable State in Pa^{231}†

D. STROMINGER AND J. O. RASMUSSEN
Radiation Laboratory and Department of Chemistry, University of California, Berkeley, California

(Received July 25, 1955)

A metastable state of Pa^{231} with a half-life of $(4.1\pm0.4)\times10^{-8}$ second has been observed. This half-life is exhibited by both 26- and 85-kev $E1$ gamma transitions. A comparison is made with the metastable state in Pa^{233}. Upper limits on lifetimes are given for the $E1$ gamma transitions in Np^{239} and Ac^{225}. The erratic variation in the lifetimes for $E1$ transitions is discussed.

A METASTABLE state of Pa^{231} with a half-life of $(4.1\pm0.4)\times10^{-8}$ second was observed by a coincidence study of delayed gamma transitions following the beta decay of Th^{231}, using a sample chemically separated from uranium enriched in U^{235}.

An anthracene crystal was used to detect the beta particles from the decay of Th^{231} and a sodium iodide (thallium iodide activated) crystal was used to detect the gamma radiation accompanying the decay of the excited daughter nucleus. A single-channel pulse-height analyzer was used to discriminate against noise in the electron detector. A 50-channel differential pulse-height analyzer was used to analyze the energy of the coincident gamma radiation. A fast-slow coincidence arrangement was used at a resolving time of 5×10^{-8} second.

Beta emitter Th^{231} has been studied intensively by Freedman *et al.*[1] and by Stephens.[2] The decay is quite complex, and no wholly satisfactory decay scheme has yet been established. The most prominent gamma radiation is found at 26- and 85-kev energy. Stephens found these gamma rays to be not in coincidence with one another, in contradiction to the suggested decay scheme of Freedman *et al.* Stephens assigned these gamma rays a multipolarity $E1$ on the basis of their low conversion coefficients.

In the present studies both the 26- and the 85-kev gamma transitions were seen to be delayed, and both appeared to have the same half-life. Some higher energy gamma radiation of low intensity was also seen and showed no delay ($T_{\frac{1}{2}}<3\times10^{-9}$ second). The intensity of these higher energy gamma transitions is so low that their energies could not be determined in the coincidence spectra.

A sample of Ra^{225} was also run and the 40-kev $E1$ gamma ray[3] in Ac^{225} following the beta decay appeared to be prompt ($T_{\frac{1}{2}}<4\times10^{-9}$ second). The 75-kev gamma radiation in Np^{239} following alpha decay of Am^{243} [3] and following beta decay of U^{239} [3,4] has also been shown to be prompt ($<2\times10^{-9}$ second).

It is interesting to note the similarity between Pa^{231} and Pa^{233}. Pa^{233} was shown by Engelkemeir and Magnusson[5] to have a metastable state with a half-life of 3.7×10^{-8}. With our apparatus we have confirmed this delay and found that the delay is exhibited by 30- and 87-kev radiation, assigned as $E1$ by Stephens.[2] Engelkemeir and Magnusson have also found that the delay is exhibited by L x-ray, 30- and 86-kev radiation.[4] We also saw coincident with alpha particles 140- and 200-kev radiation which was prompt ($T_{\frac{1}{2}}<2\times19^{-9}$ second).

The various measured lifetimes of the delayed $E1$ transitions in the heavy region correspond to transitions vastly slower than single proton lifetime formulas estimate. This slowness is probably to be attributed largely to a j-forbiddenness ($\Delta j\geq2$) in the Bohr-Mottelson strong coupling model (see the discussion[6] regarding Np^{237}). The erratic variation in lifetimes (as in analogous nuclei Np^{237} and Np^{239}) probably indicates some cancellation of $E1$ matrix elements, a cancellation sensitive to fine details of the nuclear wave functions.

† This work was performed under the auspices of the U. S. Atomic Energy Commission.

[1] Freedman, Jaffey, Wagner, and May, Phys. Rev. **89**, 302 (1952).

[2] Frank S. Stephens, Jr., Ph.D. thesis, University of California Radiation Laboratory Unclassified Report UCRL-2970, June, 1955 (unpublished).

[3] M. I. Kalkstein and J. O. Rasmussen (unpublished results, 1952).

[4] D. Engelkemeir (private communication, 1955).

[5] D. Engelkemeir and L. B. Magnusson, Phys. Rev. **94**, 1395 (1954).

[6] J. O. Rasmussen, Arkiv Fysik **7**, 185 (1953).

Electric Multipole Moments in j-j Coupling*

R. D. LAWSON
University of California, Berkeley, California
(Received July 5, 1955)

It is possible to derive a simple expression for the electric quadrupole moment of any I-state arising in j-j coupling, from the proton configuration $(l_j)^n$, without explicitly setting up the wave function in question. If the given I-state occurs more than once, only the sum of the quadrupole moments is obtainable by this method. In principle, it is possible to generalize the theory to higher electric multipole moments.

THE success of the shell model[1] has led one to calculate various nuclear properties assuming that the nucleons outside a closed shell move in some sort of average nuclear potential. These extra-core nucleons are assumed to have their individual j's coupled together by j-j coupling to form a resultant I state. In this note we shall show that it is possible to give a simple expression for the electric quadrupole moment of any I-state, consistent with the exclusion principle, derivable from the configuration[2] $(l_j)^n$, without explicitly writing down the wave function of the state in question. Throughout our calculations we shall neglect: (a) interparticle interactions, so that all I states are degenerate[3]; (b) the neutrons outside the closed shell; (i.e., our calculations will be valid for nuclei with an even number of neutrons whose spins pair off)[4]; (c) any contribution to the quadrupole moment due to distortion of the core.[5]

THEORY

In j-j coupling the eigenfunction of n identical particles coupling their spins to I, $(I_z=M)$, is given by

$$\psi_I{}^M=\sum_k a_{Ik}{}^M\chi_k{}^M, \tag{1}$$

where

$$\chi_k{}^M=(n!)^{-\frac{1}{2}}|\phi_j{}^{m_{k1}}\phi_j{}^{m_{k2}}\cdots\phi_j{}^{m_{kn}}|. \tag{2}$$

$\phi_j{}^m$ is a normalized single-particle wave function representing a state with total angular momentum j and z component m, the symbol $|\cdots|$ stands for the Slater determinant, the factor $1/\sqrt{n!}$ comes from normalization, and $\sum_{i=1}^n m_{ki}=M$.

The functions $\chi_k{}^M$ have the property

$$J_z\chi_k{}^M=\sum_{i=1}^n j_{iz}\chi_k{}^M=M\chi_k{}^M. \tag{3}$$

In general if there are λ linearly independent χ^M's, there will be λ linearly independent ψ's which can be formed from them. The expansion coefficients are determined from the condition that

$$\mathbf{J}^2\psi_I{}^M=(\sum_{i=1}^n \mathbf{j}_i)^2\psi_I{}^M=I(I+1)\psi_I{}^M, \tag{4}$$

where the possible eigenvalues of $\mathbf{J}^2$ will range from[6] $I=M$ to $I=I_{\max}=n[j-\frac{1}{2}(n-1)]$.

Because of the orthonormality of the $\psi_I{}^M$'s and the $\chi_k{}^M$'s, it follows that

$$\sum_k a_{Ik}{}^{M*}a_{I'k}{}^M=\delta_{II'}, \tag{5}$$

$$\sum_I a_{Ik}{}^{M*}a_{Ik'}{}^M=\delta_{kk'}, \tag{6}$$

where $a_{Ik}{}^{M*}$ is the complex conjugate of $a_{Ik}{}^M$.

The quadrupole moment in the state I, $(I_z=M)$, is defined as

$$\begin{aligned}Q_I{}^M&=\int\psi_I{}^{M*}\sum_{i=1}^n(3z_i^2-r_i^2)\psi_I{}^M d\tau_1\cdots d\tau_n\\&=\int(\sum_k a_{Ik}{}^{M*}\chi_k{}^{M*})\sum_{i=1}^n(3z_i^2-r_i^2)\\&\qquad\times(\sum_{k'}a_{Ik'}{}^M\chi_{k'}{}^M)d\tau_1\cdots d\tau_n.\end{aligned} \tag{7}$$

Since $\chi_k{}^M$ is orthogonal to $\chi_{k'}{}^M$ $(k\neq k')$, and since they are both eigenfunctions of J_z with eigenvalue M, it follows that at least two of the $m_{k'i}$'s must be different from the m_{ki}'s. Further, in the ith term of the sum in Eq. (7), if we integrate over all coordinates except $d\tau_i$, we see that $m_{kj}=m_{k'j}$ $(j\neq i)$, therefore, in Eq. (7), $k=k'$. Using this fact together with Eq. (6), we see

* Work supported by the Office of Ordnance Research.

[1] M. G. Mayer, Phys. Rev. **75**, 1969 (1949); Haxel, Jensen, and Seuss, Phys. Rev. **75**, 1766 (1949).

[2] We neglect the possibility of the particles making up the configuration being in different l states. A particular case of this is considered by S. Sengupta, Phys. Rev. **96**, 235 (1954), who assumes the configuration $[(d_{5/2})^2s_{1/2}]_{J=3/2}$ to explain the quadrupole moment of Na^{23}.

[3] D. Kurath, Phys. Rev. **80**, 98 (1950); **88**, 804 (1952); **91**, 1430 (1953); B. H. Flowers, Proc. Roy. Soc. (London) **A212**, 248 (1952); **A215**, 398 (1952); A. R. Edmonds and B. H. Flowers, Proc. Roy. Soc. (London) **A214**, 515 (1952); **A215**, 120 (1952); I. Talmi, Helv. Phys. Acta **25**, 185 (1952).

[4] Calculations in which both neutrons and protons outside the closed shell are combined to give a resultant I-state are considered by B. H. Flowers, Phil. Mag. **43**, 1330 (1952); M. F. Scharff, Phys. Rev. **95**, 1114 (1954).

[5] J. Rainwater, Phys. Rev. **79**, 432 (1951); A. Bohr and B. R. Mottelson, Kgl. Danske Videnskab. Selskab, Mat.-fys. Medd. **27**, No. 16 (1953).

[6] Because of the exclusion principle all I values will not be allowed. In particular, the state $I=I_{\max}-1$ is always forbidden. However, for these states the expansion coefficients will vanish identically.

that

$$\sum_{I=I_{\max}}^{M} Q_I{}^M=\sum_k \int \chi_k{}^{M*} \sum_{i=1}^{n}(3z_i^2-r_i^2) \times \chi_k{}^M d\tau_1 \cdots d\tau_n = A_M, \quad (8)$$

where A_M, as we shall show later, may be easily evaluated from the single-particle quadrupole moments.

It is well known that $Q_I{}^M$ is simply related[7] to $Q_I{}^I \equiv Q_I$:

$$Q_I{}^M = T_{MI} Q_I,$$

where

$$T_{MI}=\frac{3M^2-I(I+1)}{I(2I-1)}, \quad |M| \leqslant I$$
$$T_{MI}=0, \quad |M|>I. \quad (9)$$

Thus, Eq. (8) may be written as $\sum_I T_{MI} Q_I = A_M$, or, in matrix notation,

$$TQ=A, \quad (10)$$

where the elements of the matrix T are the T_{MI}; and Q and A are column matrices.

Thus, in order to find a simple expression for Q it is necessary to find the inverse of the matrix T. By a straightforward but tedious calculation, one can show that $(T^{-1})_{\alpha\beta}$ $(\alpha, \beta \geqslant 1)$ is

$$(T^{-1})_{\alpha\beta}=0 \quad \text{if } \beta>\alpha$$
$$=1 \quad \text{if } \beta=\alpha$$
$$=\frac{\alpha+1-I_M}{I_M+2-\alpha} \quad \text{if } \beta=\alpha-1$$
$$=\frac{6}{(2I_M+5-2\alpha)(I_M+2-\alpha)} \quad \text{if } \beta=\alpha-s, \quad s \geqslant 2 \quad (11)$$

where I_M is the maximum I value obtainable from the configuration[8]

$$I_M=n\left[j-\tfrac{1}{2}(n-1)\right]. \quad (12)$$

Using these expressions for T^{-1}, it follows that the quadrupole moment in the state I $(I_z=I)$, is

$$Q_I=\frac{6}{(I+1)(2I+3)} \sum_{\alpha=I+2}^{I_M} A_\alpha+\frac{2-I}{I+1}A_{I+1}+A_I. \quad (13)$$

To evaluate the A_M's, Eq. (8), we use the form of the wave function $\chi_k{}^M$, Eq. (2). In the ith terms of the sum, integrate over all coordinates except $d\tau_i$. Because of the orthonormality of the $\phi_j{}^m$'s this gives a factor $(n-1)!$ so that[9]

$$A_M=\sum_k\left\{\frac{1}{n}\sum_{i=1}^{n}\int (3z_i^2-r_i^2) \times\left[|\phi_j{}^{m_{k1}}(i)|^2+\cdots+|\phi_j{}^{m_{kn}}(i)|^2\right]d\tau_i\right.$$
$$\left.=\sum_k\{q_j{}^{m_{k1}}+q_j{}^{m_{k2}}+\cdots+q_j{}^{m_{kn}}\}\right., \quad (14)$$

where

$$\sum_{i=1}^{n} m_{ki}=M$$

and $q_j{}^m$ is the quadrupole moment of a single particle in the state j $(j_z=m)$. One may easily drive an expression[10] for $q_j{}^j \equiv q_j$

$$q_j=-\left[(2j-1)/(2j+2)\right]\langle r^2\rangle. \quad (16)$$

Combining this result with Eq. (13) we may immediately calculate the quadrupole moment of any state arising from the configuration $(l_j)^n$.

APPLICATION

Let us apply the above theory to the $(f_{7/2})^3$ configuration and determine the quadrupole moment of the state $I=5/2$. Making use of the fact that $q_j{}^m=q_j{}^{-m}$ and that $\sum_{m=-j}^{j} q_j{}^m=0$, we see that

$$A_{3/2}=-q_{7/2}{}^{1/2}; \quad A_{7/2}=0; \quad A_{9/2}=q_{7/2}{}^{3/2};$$
$$A_{11/2}=q_{7/2}{}^{7/2}+q_{7/2}{}^{1/2}; \quad A_{13/2}=q_{7/2}{}^{7/2}+q_{7/2}{}^{5/2}+q_{7/2}{}^{1/2};$$
$$A_{15/2}=q_{7/2}{}^{7/2}+q_{7/2}{}^{5/2}+q_{7/2}{}^{3/2}; \quad q_{7/2}=-\tfrac{3}{7}\langle r^2\rangle;$$

so that

$$Q_{5/2}=-(13/21)\langle r^2\rangle=-0.62\langle r^2\rangle, \quad (17)$$

which agrees with the value given by Mayer and Jensen.[10]

DISCUSSION

We have succeeded in finding a simple expression for the quadrupole moment of any I state derivable from the configuration $(l_j)^n$ without recourse to the somewhat tedious task of setting up the wave function for the state in question. The theory has, however, the disadvantage that if the given I state occurs more than once, the expression for Q_I which we derive, gives only the sum of the quadrupole moments calculated from the two or more linearly independent eigenfunctions which describe the state.

The method can in principle be generalized to give higher electric multipole moments.

We should like to thank Dr. R. H. Huddlestone, Dr. W. A. Nierenberg, Dr. M. A. Ruderman, and Dr. E. Teller for interesting discussions.

[7] See for example J. M. Blatt and V. F. Weisskopf, *Theoretical Nuclear Physics* (John Wiley and Sons, Inc., New York, 1952).

[8] In the expression for T^{-1}, all I states ranging from $I=I_M$ to $I=0$ or $\frac{1}{2}$, depending on whether there are an even or odd number of particles, have been included. Some of these states may be forbidden by the exclusion principle. However, Q_I for these forbidden states will vanish identically.

[9] It follows from this equation that the maximum electric multipole moment a state may have is not determined by the I value of the state in question, but rather by the j value of the particles making up the state (i.e., the maximum electric multipole moment obtainable from the configuration $(l_j)^n$ is a 2^{2j} moment).

[10] See for example M. G. Mayer and J. H. D. Jensen, *Elementary Theory of Nuclear Shell Structure* (John Wiley and Sons, Inc., New York, 1955).

(d,n) Reactions on Boron and Carbon*

J. B. MARION†, T. W. BONNER, AND C. F. COOK‡
The Rice Institute, Houston, Texas

(Received July 21, 1955)

The counter ratio method has been used to investigate neutron thresholds in the (d,n) reactions on B^{10}, B^{11}, C^{12}, and C^{13}. Thresholds were found corresponding to excited states in C^{11*} at 8.107, 8.430, and 8.660 Mev; in $^{*}C^{13*}$ at 15.100 Mev; in N^{14*} at 2.37 Mev; and in N^{14*} at 5.683 Mev. Resonances in the reaction $C^{12}(d,n)$ were found at 3.01 and 3.36 Mev and in the reaction $C^{13}(d,n)$ at 1.80, 2.45, and 3.46 Mev. The absolute cross sections for the reactions $B^{10}(d,n)$, $B^{11}(d,n)$, and $C^{13}(d,n)$ were measured.

INTRODUCTION

ACCURATE measurements of the energies of excited states of nuclei have been made by detecting thresholds for the emission of neutrons to excited states of the residual nuclei in (p,n) and (d,n) reactions on light- and medium-weight nuclei.[1–5] Since such measurements provide precise information concerning nuclear energy states that are not usually accessible to measurement by means of magnetic analysis techniques, these data are important for the comparison of corresponding levels of isotopic spin multiplets. Furthermore, this method allows the investigation with good resolution of regions of excitation in some nuclei which cannot be easily reached in other types of reactions.

Increased sensitivity over other techniques for the detection of threshold neutrons[6] is provided by measuring, as a function of bombarding energy, the counting rates in two paraffin-moderated BF_3 counters. One of these counters is preferentially sensitive to low-energy neutrons ("slow counter") and the other is almost energy-insensitive ("modified long counter"). The ratio of the counting rate in the slow counter to that in the modified long counter gives a measure of the number of slow neutrons emitted at a particular bombarding energy. As the energy is increased, sharp rises in the "counter ratio" indicate the emission of threshold neutrons to an energy level of the residual nucleus. The increase of the counter ratio is made even more pronounced by the fact that the efficiency of the modified long counter, in its position behind the slow counter, decreases rapidly for neutrons of energy less than about 0.3 Mev.[4] The precise determination of the energy of the excited state is provided by an accurate measurement of the energy of the bombarding particles at the point at which the emission of threshold neutrons is first possible. The technique of measuring the bombarding energy entails the use of a proton (or lithium) moment magnetometer. The details have been given previously.[3]

The absolute cross sections for the reactions $B^{10}(d,n)$, $B^{11}(d,n)$, and $C^{13}(d,n)$ are also of interest. The relative yield curves, which were measured with the modified long counter, were calibrated by comparing the counting rates from the targets (which contained weighed amounts of material) with that from a calibrated Ra-Be source. The comparisons were made at a deuteron energy of 2.98 Mev. A "long counter" of the type described by Hanson and McKibben[7] was used. Backgrounds, obtained by bombarding a blank of the metal onto which the target materials had been deposited, have been subtracted.

$B^{10}(d,n)C^{11}$

The energies of the excited states of B^{11} below 10 Mev have been measured[8,9] with an accuracy of about 8 kev by the magnetic analysis of the proton groups from the reaction $B^{10}(d,p)B^{11}$. Therefore, it is of interest to obtain measurements with comparable accuracy of the energies of the excited states of the mirror nucleus, C^{11}. The best information previously available concerning these levels was obtained by Johnson,[10] who measured the energies of the neutron groups from the reaction $B^{10}(d,n)C^{11}$ using a photographic plate technique. Although the existence of several levels below 8.8 Mev was well established, these measurements did not permit an accuracy greater than 20 kev in the most favorable cases, nor greater than 60 kev in the event that the group was weak. An alternative method of measuring the energies of these states is by the observation of the γ radiation accompanying the $B^{10}(d,n)C^{11}$ reaction. A γ ray of 6.50 ± 0.04 Mev has been observed in a pair spectrometer investigation of the γ radiation from the deuteron bombardment of B^{10}. However, no γ rays of measurable intensity attributable to the decay of states

* Supported by the U. S. Atomic Energy Commission.
† National Science Foundation Predoctoral Fellow; now Postdoctoral Fellow at Kellogg Radiation Laboratory, California Institute of Technology, Pasadena, California.
‡ Now at Convair, Fort Worth, Texas.
[1] T. W. Bonner and C. F. Cook, Phys. Rev. **94**, 807 (A) (1954); C. F. Cook and T. W. Bonner, Phys. Rev. **94**, 807 (A) (1954); Marion, Cook, and Bonner, Phys. Rev. **94**, 807 (A) (1954); Cook, Bonner, and Marion, Phys. Rev. **95**, 639 (A) (1954).
[2] T. W. Bonner and C. F. Cook, Phys. Rev. **96**, 122 (1954).
[3] Marion, Brugger, and Bonner, Phys. Rev. **100**, 46 (1955).
[4] Brugger, Bonner, and Marion, Phys. Rev. **100**, 84 (1955).
[5] Marion, Bonner, and Cook, Phys. Rev. **100**, 91 (1955).
[6] T. W. Bonner and J. W. Butler, Phys. Rev. **83**, 1091 (1951).
[7] A. O. Hanson and J. L. McKibben, Phys. Rev. **72**, 673 (1947).
[8] Van Patter, Buechner, and Sperduto, Phys. Rev. **82**, 248 (1951).
[9] M. M. Elkind, Phys. Rev. **92**, 127 (1953).
[10] V. R. Johnson, Phys. Rev. **86**, 302 (1952).

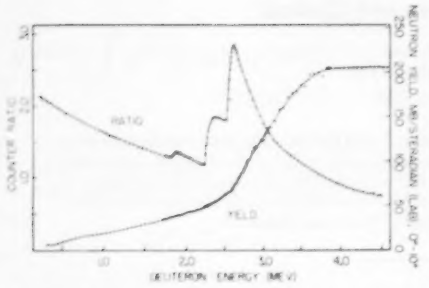

FIG. 1. $B^{10}(d,n)C^{11}$. Counter ratio and yield of neutrons in the forward direction as a function of bombarding energy. An evaporated target of boron metal, enriched to 96% B^{10}, was used.

in C^{11} above an excitation of 7.5 Mev were found.[11] Presumably, this is due to the fact that such states are unstable to the emission of an α particle, a process that is orders of magnitude faster than γ radiation.

In order to examine the level structure of C^{11} above 6.5 Mev, the Q-value for the $B^{10}(d,n)C^{11}$ reaction, the counter ratio technique was applied to this reaction. A target of about 35-kev thickness at a deuteron energy of 2 Mev was prepared by evaporating boron metal, enriched to 96% B^{10}, onto a tantalum blank. Measurements of the counter ratio and the yield of neutrons in the forward direction were made over the range of deuteron energies from 0.35 to 4.5 Mev. The results are presented in Fig. 1. Pronounced thresholds were observed at bombarding energies of 2.351 ± 0.004 and 2.628 ± 0.004 Mev, and a weak threshold were observed at 1.964 ± 0.004 Mev. All of these thresholds rise to peak value in approximately target thickness. The corresponding excited states in C^{11} are located at 8.107, 8.430, and 8.660 Mev. These values are consistently higher than those obtained by Johnson,[10] who found the energies to be 8.08, 8.39, and 8.62 Mev. The relative intensity of neutron emission to the 8.430- and 8.660-Mev states is approximately the same near threshold as was found by Johnson at 3.6 Mev. However, the yield of neutrons emitted to the 8.107-Mev level, relative to the intensity of emission to the 8.430-Mev state, is about a factor of 4 more intense near threshold than at the higher bombarding energy. Table I summarizes the information concerning these states in C^{11}.

A careful search was made over the range of deuteron energies from 0.35 to 1.2 Mev in an attempt to detect thresholds corresponding to the C^{11} states which were observed by Johnson[10] at 6.87 and 7.39 Mev. These thresholds should occur at deuteron energies of 0.48 and 1.10 Mev. No deviation from a smooth curve was found between 0.35 and 1.95 Mev. Therefore, the emission of neutrons to these states is strongly suppressed near threshold, although at a bombarding energy of 3.6 Mev, these neutron groups have intensities comparable with those emitted to states for which thresholds were observed.[10] The ratio curve was extended to a bombarding energy of 4.5 Mev, corresponding to an excitation in C^{11} of 10.2 Mev. In this energy region, states are known to exist at 9.70 and 10.06 Mev,[12] and possibly exist at 8.97 and 9.13 Mev.[10] No evidence was found for the emission of neutrons to these levels near threshold.

The excitation function for neutron emission in the forward direction shows some indication of a broad resonance near 0.9 Mev; a similar result was obtained by Burke, Risser, and Phillips.[13] At an energy of about 2.4 Mev, a sudden increase in the yield accompanies the two intense thresholds. It is probable, therefore, that a large fraction of the yield above this energy consists of neutrons emitted to the C^{11} states at 8.430 and 8.660 Mev. This interpretation is consistent with the relative intensities of the various neutron groups at a bombarding energy of 3.6 Mev, observed by Johnson.[10] The yield becomes approximately constant above about 4 Mev, and no indication of a further increase was observed up to the maximum bombarding energy used.

The cross section for the emission of neutrons into the forward cone of half-angle 10° is given in Fig. 1, in units of millbarns per steradian in the laboratory system. No correction has been applied for the presence of 4 percent of B^{11} in the target material. Since the $B^{11}(d,n)$ cross section is about 50% higher than that for the $B^{10}(d,n)$ reaction in this energy region, the effect of such a correction would be to lower the observed yield curve by about 6%. Oxygen contamination on the target may arise from the evaporation of B_2O_3 instead of boron metal; however, no thresholds corresponding to those observed in the $O^{16}(d,n)F^{17}$ reaction[3] were observed, and it was assumed that the amount of oxygen contamination was negligible. At 2.0 Mev, the cross section is 42 mb/sterad, which is to be compared with a value of 40 mb/sterad, obtained by Burke, Risser, and Phillips.[13]

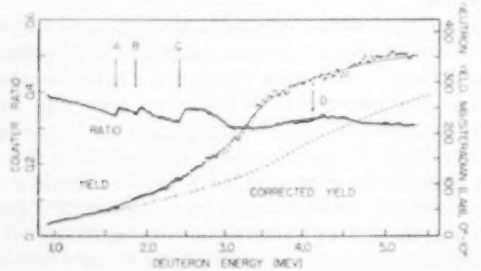

FIG. 2. $B^{11}(d,n)C^{12}$. Counter ratio and yield of neutrons in the forward direction as a function of bombarding energy. The "corrected yield" curve has been corrected for the effects of O^{16} and B^{10} on the target.

[11] Bent, Bonner, McCrary, Ranken, and Sippel, Phys. Rev. **99**, 710 (1955).

[12] Brown, Snyder, Fowler, and Lauritsen, Phys. Rev. **82**, 159 (1951).

[13] Burke, Risser, and Phillips, Phys. Rev. **93**, 188 (1954).

TABLE I. Neutron thresholds in the reaction $B^{10}(d,n)C^{11}$.

Threshold energy (Mev)	Q-value (Mev)	Present work C^{11}	Present work Intensity at 0° (threshold)	Other measurements[a] C^{11}	Other measurements[a] Intensity at 0° (E_d = 3.6 Mev)
1.964±0.004	−1.635±0.004	8.107±0.008[b]	0.18	8.08±0.02	0.04
2.351±0.004	−1.958±0.004	8.430±0.008[b]	1.0	8.39±0.02	1.0
2.628±0.004	−2.188±0.004	8.660±0.008[b]	1.6	8.62±0.02	1.8

[a] See reference 10.
[b] The error assignment includes the uncertainty in the ground-state Q-value calculated from the mass defect uncertainties listed by Drummond (reference 14).

$B^{11}(d,n)C^{12}$

The level structure of the C^{12} nucleus is accessible to investigation by a number of nuclear reactions; however, the region of excitation from 10 to 16 Mev has been studied only through the $B^{11}(d,n)C^{12}$ reaction. Johnson[10] measured the energy of the neutron groups from this reaction with a photographic plate technique and obtained the energies of a number of excited states of C^{12} up to an energy of 16.1 Mev. In order to further investigate the C^{12} states in the energy region above the Q-value for the $B^{11}(d,n)C^{12}$ reaction (13.724 Mev), the counter ratio technique was used to study this reaction. For bombarding energies from 1.0 to 5.5 Mev, the range of excitation in C^{12} from 14.5 to 18.4 Mev may be investigated.

A target of normal boron metal, evaporated onto a tungsten blank, was used in this experiment; it was approximately 50-kev thick at a deuteron energy of 2.5 Mev. The results obtained by measuring the counter ratio and the yield of neutrons in the forward direction over the range of bombarding energies from 1.0 to 5.5 Mev are shown in Fig. 2. The various thresholds that were observed are indicated by the arrows and letters.

The first threshold detected, indicated by *A* in Fig. 2, occurs at a bombarding energy of 1.627±0.004 Mev. The rise in the ratio takes place in target thickness. The corresponding Q-value is −1.376±0.004 Mev, and the energy of the C^{12} excited state is 15.100±0.006 Mev, where the error assignment includes the uncertainty in the ground-state Q-value, calculated from the mass defect uncertainties listed by Drummond.[14] This is in good agreement with the value of 15.09±0.03 Mev, obtained by Johnson.[10]

A broad maximum in the ratio curve, indicated by *D* in Fig. 2, was found near an energy of 4.1 Mev and is probably due to the emission of neutrons to the state in C^{12} at 17.22 Mev (Γ=1.27 Mev), that is observed[15] in the yield of 16-Mev γ radiation from proton capture in B^{11}. Other nearby states could contribute to this rise if neutrons of only high angular momentum could be emitted near threshold.

The thresholds marked *B* and *C* are due to the ground and first excited states of F^{17}, resulting from the reaction $O^{16}(d,n)F^{17}$. From the intensity of these thresholds, relative to those observed with an oxygen target,[3] it was estimated that there were approximately equal numbers of boron and oxygen atoms on the target used in this experiment. This suggests that a large part of the evaporated boron was in the form B_2O_3.

The yield curve, shown by the experimental points and the curve in Fig. 2, includes the effects of the oxygen contamination and of the 19% B^{10} present in the normal boron. The dashed curve results when a correction for these effects is applied. The cross section is given in units of millibarns per steradian in the laboratory system for the emission of neutrons into the forward cone of half-angle 10°. The uncorrected cross section at 2.0 Mev is 76 mb/sterad, which is to be compared with a value of 80 mb/sterad for normal boron, obtained by Burke, Risser, and Phillips.[13]

$C^{13}(d,n)N^{13}$

The level structure of the N^{13} nucleus in the energy region which is accessible to investigation with the counter ratio technique has been well studied by a number of investigators.[15] Therefore, this reaction was not studied as thoroughly as the other reactions reported in this paper. The range of bombarding energies from 2.8 to 3.9 Mev is of interest since it includes the region in which a threshold for neutron emission leaving N^{13} in the first excited state occurs.

The results obtained in an investigation of this region are shown in Fig. 3. The target used in this experiment was prepared by cracking methyl iodide onto a tantalum blank heated in an indication heater and was approxi-

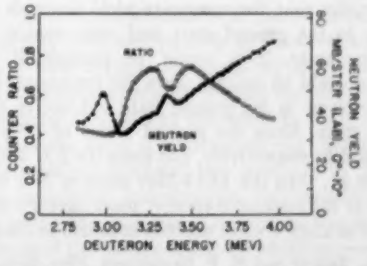

FIG. 3. $C^{13}(d,n)N^{13}$. Counter ratio and yield of neutrons in the forward direction as a function of bombarding energy. The cross section is from reference 17.

[14] J. E. Drummond, Phys. Rev. **97**, 1004 (1955).
[15] F. Ajzenberg and T. Lauritsen, Revs. Modern Phys. **27**, 77 (1955).

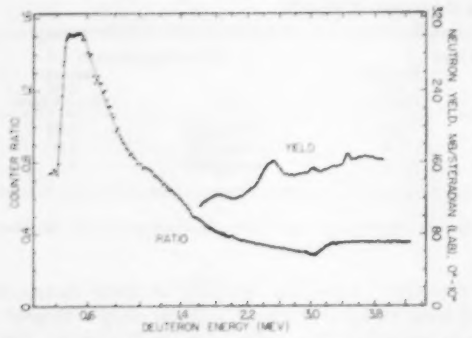

FIG. 4. $C^{13}(d,n)N^{14}$. Counter ratio and yield of neutrons in the forward direction as a function of bombarding energy. A carbon target, enriched to 68% C^{13}, was used.

mately 65-kev thick at a deuteron energy of 3 Mev. The resonance at 3.01 Mev probably corresponds to the combined effects of the unresolved levels in N^{14} at 12.79, 12.82, and 12.92 Mev.[16,18] The resonance at 3.36 Mev probably is due to the level at 13.16 Mev. Resonances in the yield of long-range protons from the deuteron bombarding of C^{13} have also been observed from these compound nucleus states.[17] The expected rise in the counter ratio begins at a bombarding energy of 3.07 $\pm$0.02 Mev and requires an appreciable energy interval to reach its peak value. To obtain the true threshold energy, however, the width of this N^{13} level must be taken into account. This increases the observed threshold energy by approximately one-half of the level width of 40 kev.[16] The resulting threshold energy is 3.09$\pm$0.02 Mev, corresponding to an energy for the first excited state of N^{13} of 2.37$\pm$0.02 Mev, in agreement with previous measurements[16] on the scattering and capture of protons by C^{13}. The ratio rises to its peak value in approximately 200 kev, or 3 times target thickness, suggesting that p-wave neutrons form the dominant part of the yield near threshold. Near the peak of the curve, there is a dip in the ratio, corresponding in energy and width to the 3.36-Mev resonance in the yield. This decrease in the ratio at resonance is caused, not by a decrease in the number of slow neutrons, but by an increase in the number of fast neutrons. This implies that the resonance yield proceeds almost entirely to the ground state and only weakly to the 2.37-Mev state. This would be possible if s-wave neutrons could be emitted from the compound nucleus state involved to the ground state but not to the first excited state. Since the ground states of C^{13} and N^{13} are 0^+ and $\frac{1}{2}^-$ respectively, and since the 2.37-Mev state of N^{13} is $\frac{1}{2}^+$, then the 13.14-Mev state of N^{14}, which is formed at the resonance energy, must have $J=0^-$ or 1^- in order to allow s-wave neutron emission to the ground state but not to the first excited state. Deuterons with $l=1$ are required to form this compound state.

The cross section for the $C^{13}(d,n)N^{13}$ reaction is given in Fig. 3 in units of millibarns per steradian in the laboratory system for neutron emission into the forward cone of half-angle 10°. The details of the measurement of the absolute cross section are given elsewhere.[17]

$C^{13}(d,n)N^{14}$

The reaction $C^{13}(d,n)N^{14}$ is another example of a reaction which allows a counter ratio investigation of an energy region in the residual nucleus which has been studied previously only by observing either the various energy groups of neutrons from this reaction or the γ radiation from the decay of the levels. It is possible to study a region of excitation in N^{14} from 5.5 to 8.8 Mev with the counter ratio method with deuteron bombarding energies up to 4 Mev. A number of states have been reported in this energy region.[15]

Carbon targets were prepared by cracking methyl iodide, enriched to 68% C^{13}, onto hot tantalum blanks. The target used in this experiment was approximately 15-kev thick at a deuteron energy of 0.6 Mev and approximately 5-kev thick at 3 Mev. The results obtained by measuring the counter ratio and the forward yield of neutrons over the range of bombarding energies from 0.4 to 4.2 Mev are shown in Fig. 4. An intense threshold, due to an excited state in N^{14} at 5.683$\pm$0.007 Mev, occurs at a bombarding energy of 0.422$\pm$0.005 Mev. Both the neutron group emitted to this level[19] and the γ radiation from its decay[19,20] have been observed in the deuteron bombardment of C^{13}. The counter ratio at this threshold requires an energy interval of approximately 4 times target thickness to rise to its peak value, suggesting that p-wave neutrons are responsible for most of the yield near threshold. If it is assumed that this state in N^{14} has $J=1$,[15] then, since the incoming deuterons probably have zero angular momentum due to their low energy, the parity of this state must be even in order to account for the emission of p-wave neutrons. The emission of neutrons with angular momentum of 1 or greater is probably responsible for the fact that the ratio does not decrease immediately following the initial rise at the 0.422-Mev threshold.

The ratio curve decreases smoothly from the peak of the first threshold to an energy of 1.0 Mev, with no indication of thresholds due to the known levels in N^{14} at 5.83 and 5.98 Mev, which should occur at bombarding energies of 0.59 and 0.76 Mev. Thresholds corresponding to the states at 6.23 and 6.44 Mev should occur at energies of 1.05 and 1.29 Mev. The irregularity in the ratio near 1.0 Mev probably is the result of the weak emission of neutrons to these levels.

A second pronounced threshold, due to the reaction

[16] F. L. Talbott and N. P. Heydenburg, Phys. Rev. **90**, 186 (1953).
[17] Bonner, Eisinger, Kraus, and Marion, Phys. Rev. (to be published).
[18] R. E. Benenson, Phys. Rev. **90**, 420 (1953).
[19] Bent, Bonner, and Sippel, Phys. Rev. **98**, 1237 (1955).
[20] R. G. Thomas and T. Lauritsen, Phys. Rev. **88**, 969 (1952).

TABLE II. Neutron threshold in the reaction $C^{13}(d,n)N^{14}$.

Threshold energy (Mev)	Q-value (Mev)	Excitation in N^{14} (Mev) Present work	Other measurements
0.422±0.005	−0.365±0.005	5.683±0.007[a]	5.76±0.05[b] 5.72±0.04[c] 5.66±0.05[d]

[a] The error assignment includes the uncertainty in the ground-state Q-value, calculated from the mass defect uncertainties listed by Drummond (reference 14).
[b] See reference 18.
[c] γ-ray measurement corrected for Doppler shift; see reference 19.
[d] γ-ray measurement corrected for Doppler shift; see reference 20.

$C^{12}(d,n)N^{13}$, occurs at a bombarding energy of 3.07 Mev. A portion of the rise at this threshold and the fact that the ratio curve does not decrease appreciably for energies above 3.2 Mev are probably the result of neutron emission to the broad state in N^{14} at 8.06 Mev, which would be expected to begin at 3.16 Mev.

Table II summarizes the results of the investigation of thresholds in the $C^{13}(d,n)N^{14}$ reaction.

The excitation function measured with the carbon target, enriched to 68% C^{13}, is shown in Fig. 4. The cross section is given in units of millibarns per steradian in the laboratory system for the emission of neutrons into the forward cone of half-angle 10°. Resonances in the yield occur at bombarding energies of 1.80, 2.45, 3.01, and 3.46 Mev. Only the peak at 3.01 Mev is due to the $C^{12}(d,n)N^{13}$ reaction. Because of the reduced concentration of C^{12} in the target material and the smaller cross section for the $C^{12}(d,n)$ reaction as compared with that for the $C^{13}(d,n)$ reaction, the number of counts due to C^{12} is smaller by a factor of 5 than the number from C^{13}. Therefore, the resonances in the $C^{12}(d,n)$ reaction either appear as weak effects or are not observed. The broad resonance at 1.80 Mev, due to the $C^{13}(d,n)$ reaction, was also observed by Richardson.[21] The resonance energies, estimated widths, and excitation energies in N^{15} are summarized in Table III.

TABLE III. Resonances in the reaction $C^{13}(d,n)N^{14}$.

Deuteron energy (Mev)	Γ (Mev)	N^{15} (Mev)
1.80±0.05	≈0.6	17.80±0.05
2.45±0.03	≈0.4	18.27±0.03
3.46±0.03	≈0.15	19.15±0.03

[21] J. E. Richardson, Phys. Rev. **80**, 850 (1950).

PHYSICAL REVIEW VOLUME 100, NUMBER 3 NOVEMBER 1, 1955

Reactions $Be^9(\alpha,\alpha')$, $Be^9(\alpha,d)$, and $Be^9(d,d')$†

V. K. RASMUSSEN*, D. W. MILLER, M. B. SAMPSON, AND U. C. GUPTA
Department of Physics, Indiana University, Bloomington, Indiana

(Received July 19, 1955)

The existence of a level in Be^9 at 3.01±0.1 Mev has been verified by the inelastic scattering of 21.6-Mev alpha particles and 10.8-Mev deuterons. Some evidence has also been found for a level in Be^9 at 1.74±0.1 Mev. However, it is shown that the present experimental data are most simply explained by a three-body break-up of the compound nucleus with a final-state potential-scattering interaction between the outgoing neutron and Be^8. The previously-reported occurrence of the reaction $Be^9(\alpha,d)B^{11}$ to the ground state and 2.14-Mev excited state of B^{11} is verified.

I. INTRODUCTION

RECENT work on the $Li^7(He^3,p)Be^9$ and $B^{10}(l,\alpha)Be^9$ reactions[1] has indicated that there are levels in Be^9 at 1.8 and 3.1 Mev, and the behavior of the $Be^9(\gamma,n)Be^8$ cross section also suggests a level at ~1.6 Mev.[2] These levels have not previously been observed in other reactions or in the inelastic scattering of protons, deuterons or electrons.[3] It seemed of interest, therefore, to look for them by inelastic alpha scattering, although the small mass of the target nucleus results in poor effective resolution with the experimental arrangement available.

Some time ago McMinn[4] observed the $Be^9(\alpha,d)B^{11}$ reaction to the ground state of B^{11}, to a known excited state at 2.14 Mev, and possibly to a state at 0.63 Mev. McMinn used a range measurement technique which did not distinguish between protons and deuterons, the groups being identified as deuterons by their variation in range as the angle of observation was changed. With the magnetic spectrometer now available in this laboratory completely unambiguous identification of reaction products is possible. A reinvestigation was therefore made of the groups found by McMinn.

† Supported by the joint program of the Office of Naval Research and the U. S. Atomic Energy Commission.
* Now at the Bartol Research Foundation, Swarthmore, Pennsylvania.
[1] Kunz, Moak, and Good, Phys. Rev. **95**, 640 (1954); Almqvist, Allen, and Bigham, Phys. Rev. **99**, 631 (A) (1955).
[2] E. Guth and C. J. Mullin, Phys. Rev. **76**, 234 (1949).
[3] F. Ajzenberg and T. Lauritsen, Revs. Modern Phys. **27**, 77 (1955).
[4] McMinn, Sampson, and Rasmussen, Phys. Rev. **84**, 963 (1951).

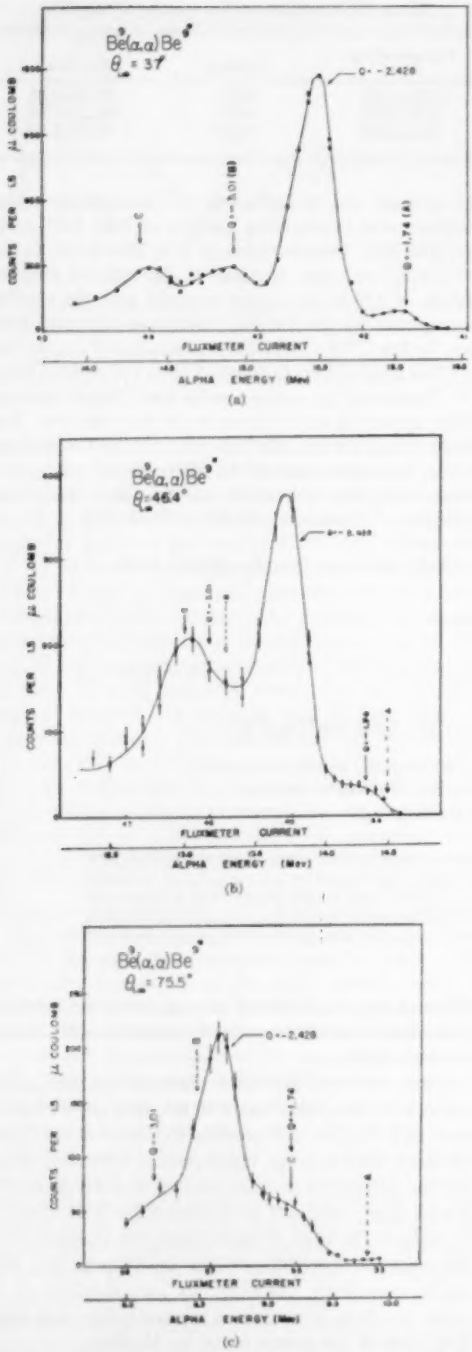

FIG. 1. Portions of the spectrum of 21.6-Mev alphas inelastically scattered by Be^9 at three laboratory angles. The arrows labeled *A* and *B* illustrate how the shift of a group with angle may be used to identify the mass number of the scattering nucleus. At 37° it is assumed that the peaks labeled *A* and *B* represent alpha-groups leaving a hypothetical contaminant of mass 10 excited to hypothetical levels at 2.10 and 3.35 Mev. At 46.4° and 75.5° the groups would then shift to the positions shown. The arrow labeled *C* represents the predicted location of a contaminant group exciting C^{13} to 4.43-Mev. Since the targets contained some carbon, part of the counting rate at *C* probably comes from this source. The *Q* values assigned to the Be^9 groups were calculated from Figs. 2 and 5 (see also Sec. IV) and are shown here only for comparison purposes.

II. EXPERIMENTAL ARRANGEMENT

The arrangement of the cyclotron and magnetic spectrometer was the same as that used previously,[5] except that a CsI(Tl) scintillation counter was substituted for the proportional counter to enable particles of smaller specific ionization than alpha-particles to be counted easily. There are two reasons for difficulty in counting such particles with a proportional counter, the electrical noise from the cyclotron and the large neutron-induced background. The scintillation counter represented a considerable improvement, although the neutron background became troublesome for protons below about 4-Mev energy. The CsI(Tl) showed "saturation," so that 6-Mev alpha-particles gave about the same pulse height as 4-Mev protons. Pulses from heavier ions were much further reduced, being detectable only under the most favorable circumstances. At a given spectrometer field, protons and alphas of the same energy, and deuterons of one-half their energy, are focused simultaneously. The "saturation" of the crystal for alphas was thus very convenient for the separation of the alphas and the protons. For deuterons, the proportionality constant between energy and pulse height is (approximately) the same as for protons, so that deuterons could also be easily identified. This identification was frequently verified by noting the energy loss of a group in question in aluminum foils inserted in front of the counter. To obtain more intense "samples" of various particles for identification purposes, the beryllium target could be replaced by a thick aluminum target. With an alpha particle beam, a large number of alphas and protons and a few deuterons were obtained in this way. A deuteron beam, easily obtained from residual deuterium in the ion source, also produced large numbers of deuterons and protons and a few alpha particles in the aluminum target. For the first part of this experiment, only an integral discriminator was available. As a result, to count deuterons in the presence of protons and alphas, it was necessary to run a curve first for deuterons plus alphas plus protons and then for alphas plus protons alone. A differential discriminator was used in the latter part of the experiment.

The target employed was an evaporated, unbacked beryllium metal foil 100 kev thick for 8.78-Mev ThC′ alphas, which contained some carbon and oxygen contamination.

[5] Rasmussen, Miller, and Sampson, Phys. Rev. **100**, 181 (1955).

III. RESULTS

A. $Be^9(\alpha,\alpha')Be^{9*}$

The spectrum of inelastically-scattered alpha particles leaving Be^9 excited to the neighborhood of 2.4 Mev was obtained at laboratory angles of 37.0°, 46.4°, 60.9°, 75.5°, and 90°. Results at three of these angles are shown in Fig. 1. All of these curves were taken with a reduced spectrometer acceptance angle in an effort to improve the effective resolution.[6] Although the figure shows that states at 1.8 and 3.1 Mev cannot be located with any accuracy, it is clear that there is a definite grouping of particles both at higher and lower energies than the group due to the well-known 2.43-Mev state. The elastic group was also run to make certain that the satellite groups were not instrumental or target effects. The 60.9° data are similar to those shown in the figure, but at 90° the intensity was too low compared to the background to obtain significant results. Because of the continuous alpha-particle background (discussed in some detail in Sec. IV) it did not seem profitable to attempt to resolve the three peaks of Fig. 1 graphically.

At angles of 46.4° and 60.9° this continuum was examined down to an energy corresponding to excitation of Be^9 to around 8 Mev. The continuum starts rising just below the lowest alpha energy shown in Fig. 1, and eventually reaches a counting rate comparable to the group caused by inelastic excitation of Be^9 to 2.43 Mev. No further states in Be^9 are observed; if they exist they are excited with less than 10% of the intensity of the group from the 2.43-Mev state.

B. $Be^9(d,d')Be^{9*}$

The region of excitation in Be^9 around 2.43 Mev was also investigated by the (d,d') reaction. Since deuterons from the cyclotron have ½ the mass and ½ the energy of alpha particles, the effective resolution is considerably improved. However, it was found that with an external deuteron beam the general laboratory neutron background was too high to permit as detailed an investigation as was desirable.

Figure 2 shows the spectrum of inelastic deuterons obtained at a laboratory angle of 37°, with the differential discriminator set to count deuterons only. That the continuum of deuterons is real, and not an instrumental effect, was shown by examining the deuteron spectrum in the neighborhood of the elastic group. This comparison revealed that the small number of counts above the main group in Fig. 2 is at least five times background. A level around 3.0 Mev is clearly indicated by Fig. 2. There is also a slight rise where a deuteron group leaving Be^9 excited to 1.8 Mev should fall. Before the differential discriminator was available, this spectrum was obtained with an integral discriminator and subtraction techniques, yielding a curve very similar to Fig. 2. Alpha-particle and proton groups from other reactions made observation of the deuteron group to the 3.0-Mev level somewhat uncertain in the run with the integral discriminator, but the region just above the main deuteron group was fortunately free of extraneous alphas and protons, allowing the rise near 1.8 Mev to be seen. Subtraction curves at 46.4° and 75.5° also gave evidence for a rise in this region, but the extraneous groups were too intense to allow any definite conclusions to be drawn concerning a possible weak deuteron group to a 3.0-Mev level.

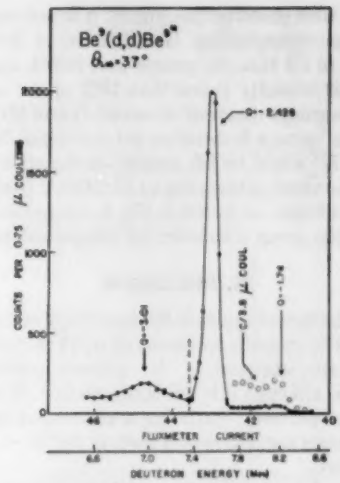

FIG. 2. Portion of the spectrum of 10.8-Mev deuterons inelastically scattered by Be^9. The beam energy was slightly different for the parts of the spectrum on the left and on the right of the dashed vertical line at fluxmeter 43.6, as indicated by another run (not shown) over the $Q=-2.428$-Mev group. On the basis of these data, the group labeled $Q=-1.74$ represents a discrete state in Be^9 only if an uncorrelated three-body breakup of the compound nucleus occurs (see Sec. IV and Fig. 5).

If these deuteron groups are correctly[7] attributed to inelastic scattering by Be^9, and if the group leaving Be^9 excited to 2.428 Mev is used to establish the beam energy, then the deuteron group at lower energy corresponds to a Be^9 level at 3.01±0.1 Mev. This group seems to be wider than it should be, possibly indicating a natural width for the level of the order of 0.3 Mev. If the theoretical (uncorrelated) background discussed in Sec. IV and shown in Fig. 5(a) is subtracted, the weak deuteron peak at higher energy gives a Be^9 excitation of 1.74±0.1 Mev.

C. $Be^9(\alpha,d)B^{11}$

Deuterons corresponding to the reaction $Be^9(\alpha,d)B^{11}$ leading to the ground state of B^{11} and to the state at

[6] At a given spectrometer angle, alphas scattered over a finite angular range, determined both by the spectrometer acceptance angle and the cross section of the beam, enter the spectrometer. With a target nucleus as light as beryllium, this spread in scattering angle gives a considerable spread in energy.

[7] The data obtained are not quite sufficient to rule out the possibility that they result from contaminants, although this seems very unlikely in view of the (α,α') results.

2.14 Mev were observed (see Fig. 3). A search was made for groups corresponding to excitation of B^{11} in the range 0.4 to 1.0 Mev. No groups were found, and if any exist, their intensity is less than 10% of the intensity of the two groups that were observed. One of McMinn's[4] "deuteron" groups is therefore not deuterons. If it were protons, B^{12} would be left excited to the state at 3.38 Mev (discovered subsequent to McMinn's work). This group was found, as shown in Fig. 4, where the ground-state proton group is included for comparison purposes.

IV. DISCUSSION

The existence of a state in Be^9 near 3.0-Mev excitation is verified by inelastic scattering of alpha particles. This state is also observed in the inelastic scattering of deuterons, although it is less easily excited. In both the alpha and deuteron scattering a continuous spectrum with features suggestive of a level in Be^9 at ~1.8 Mev is observed.

In the alpha bombardment, this continuum could result from the reactions

$$Be^9+\alpha \rightarrow C^{12*}+n$$

$$C^{12*} \rightarrow Be^{8}+\alpha' \quad (1)$$

$$\rightarrow Be^{8}+n+\alpha' \quad (2)$$

$$\rightarrow Be^{8}+He^{5}$$

$$He^{5} \rightarrow n+\alpha', \quad (3)$$

in addition to contributions from possible broad excited states of Be^9. At a given angle of observation, the maximum possible alpha energy from any of the three reactions is the same, and corresponds to the Be^8 and neutron having the same (vector) velocity. Thus the maximum energy is the same as that resulting from inelastic scattering leaving Be^9 just unstable to neutron emission ($Q=-1.666$ Mev). From Fig. 1, it seems probable that the alpha spectrum extends to this point.

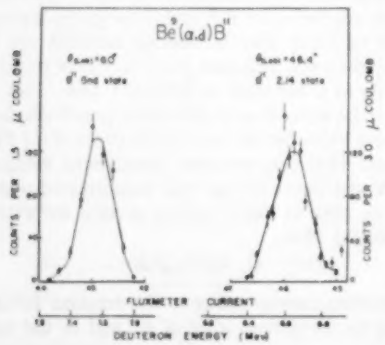

FIG. 3. Deuteron groups from the bombardment of Be^9 by 21.6-Mev alpha particles leaving B^{11} in its ground state and the known 2.14-Mev excited state.

In the deuteron scattering, the continuum could result from

$$Be^9+d \rightarrow Be^{8}+n+d' \quad (4)$$

$$\rightarrow B^{10*}+n$$

$$B^{10*} \rightarrow Be^{8}+d', \quad (5)$$

or from broad states of Be^9. The maximum energy deuteron in this continuum results when the neutron and Be^8 have the same velocity, and may be calculated in the same way as for the alpha scattering.

Since the deuteron peaks are better resolved than the alpha peaks, it seemed feasible in this case to consider possible shapes for the continuum. For a direct three-body breakup [reaction (4)] in which there are no correlations between outgoing particles, the deuteron

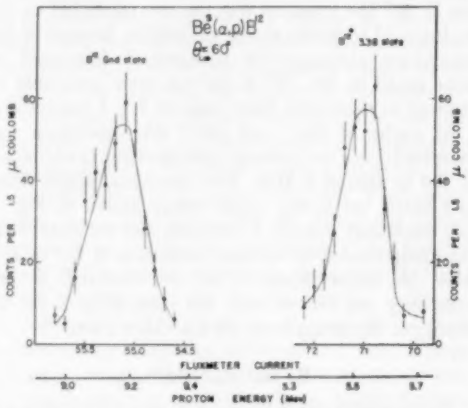

Fig. 4. Two of the proton groups resulting from the bombardment of Be^9 by 21.6-Mev alphas. The group leaving B^{12} excited to 3.38 Mev is the one that was incorrectly identified as a deuteron group in the range-measurement work of reference 4.

spectrum may be calculated by the method given by Fermi[5] or by Watson.[5] In the compound nucleus (B^{11*}) rest system, one finds

$$dN/dp_1 \sim p_1^2 q, \quad (6)$$

where p_1 is the deuteron momentum and q is the relative momentum of the neutron and Be^8: i.e.,

$$q=\mu(\mathbf{v}_2-\mathbf{v}_3), \quad (7)$$

where μ is the reduced mass for the system Be^8 and neutron. The energy available for the breakup of B^{11*} is $W=7.2$ Mev. If M is the nucleon mass, then

$$q^2=\frac{16}{9}MW-\frac{44}{81}p_1^2. \quad (8)$$

[5] E. Fermi, *Elementary Particles* (Yale University Press, New Haven, 1951), p. 56.

[5] K. M. Watson, Phys. Rev. **88**, 1163 (1952).

The spectrum given by Eq. (6) is shown in Fig. 5(a). No corrections were made for the solid-angle transformation to the laboratory system nor for the experimental resolution. However, an estimated experimental background of 25 counts was added to the theoretical spectrum. Equation (6) was reduced to a form that could be compared directly with the experimental results by using the relations that the fluxmeter current $I\sim 1/p$ and $dp/p=-dI/I=$a constant independent of p. Subtraction of the theoretical curve from the experimental curve between $I=41$ and 43 gives a peak of the shape and width expected for a discrete deuteron group. Thus, *if* there are no correlations, a state in Be^9 at 1.74 ± 0.1 Mev excitation is indicated. At much lower deuteron energies (around $I=46$), the theoretical uncorrelated spectrum predicts only about 0.6 the observed yield. This difference may be the effect of a broad state in the Be^9 or of states in B^{10}(B^{10} excitation ≈ 12.0 Mev) involved in reaction (5).

Neglect of interactions between the outgoing particles may be an especially poor approximation near the upper end of the deuteron spectrum, however, where the neutron and the Be^8 nucleus spend a long time together. Two possible theoretical spectra, which represent the effect of two particular types of final-state interactions, were therefore investigated. Two basic assumptions were made, aside from the particular forms of the final-state interactions. First, neither the Be^8 nor the neutron was assumed to interact with the deuteron, because near the upper end of the deuteron continuum they both recoil in a direction nearly opposite to the deuteron. On the other hand, in this region the relative velocity of neutron and Be^8 is small, and they were assumed to interact, but only in an S state.

If the Be^8+ neutron interaction is taken as S-wave potential scattering with scattering length $a=\hbar/\alpha$, then the spectrum assumes the form[9]:

$$dN/dp_1\sim p_1{}^2q/(\alpha^2+q^2), \tag{9}$$

where q, as before, is the relative momentum of Be^8 and the neutron. If the interaction is represented by a single-level Breit-Wigner formula (no potential scattering), where $E=q^2/2\mu$ is the relative kinetic energy of the neutron and Be^8, then[9]

$$\frac{dN}{dp_1}\sim\frac{p_1{}^2q}{(E_0-E)^2+(\Gamma^2/4)}. \tag{10}$$

Here E_0 represents the resonance energy, $\Gamma=2(q/\hbar)\gamma^2$ the total level width, and γ^2 the reduced width.

Within the appreciable statistical errors, the experimental curve may be fitted by Eq. (9) [see Fig. 5(b)] with a value of the scattering length a from 1 to 1.3 $\times 10^{-12}$ cm, which seems to be reasonable.[10] On the other hand, the pure resonance (no potential) scattering of Eq. (10) will also fit the data within the statistical errors involved [see Fig. 5(c)], although rather unreasonable parameters are required (reduced width $\gamma^2=$ Wigner limit $\hbar^2/\mu R$, $E_0=840$ kev). However, one would always expect some potential scattering contribution, and it seems probable that the relative amounts of potential and resonance scattering could be varied over a considerable range and still yield agreement with the present data.[11] Data taken under more favorable experimental conditions should allow definite conclusions to be drawn. At present, it may only be said that the experimental evidence reported here is consistent with pure potential scattering, although a level in Be^9 at around 1.74 Mev cannot be ruled out.

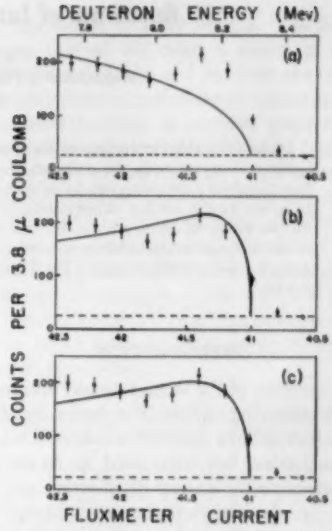

FIG. 5. Three theoretical spectra for $Be^9+d\rightarrow Be^9+n+d'-1.666$ Mev as compared with experimental points from Fig. 2. The center-of-mass to laboratory solid-angle transformation has been neglected, as has the effect of finite experimental resolution (see the main group in Fig. 2). The location of the end point has been calculated from the accepted Q value of -1.666 Mev using the 2.428 group to obtain the beam energy. Curve (a) is for no interaction between the out-going particles, curve (b) is for a neutron-Be^9 potential-scattering final-state interaction with scattering length $a=1.3\times 10^{-12}$ cm, and curve (c) is for a pure neutron-Be^9 resonance-scattering final-state interaction with parameters given in the text.

V. ACKNOWLEDGMENTS

The authors would like to express their appreciation to Professor E. J. Konopinski for a great deal of help with the theoretical aspects of the problem, and to Mr. J. R. Rees for assistance in construction of the CsI counter.

[10] C. G. Shull and E. O. Wollan, Phys. Rev. **81**, 527 (1951); K. W. Ford and D. Bohm, Phys. Rev. **79**, 745 (1950).

[11] Actual calculations for this more complicated case, with interference terms added to Eqs. (9) and (10), have not been carried out.

Spectrum of Internal Bremsstrahlung from Cr^{51}

S. G. Cohen and S. Ofer
Department of Physics, Hebrew Univ -sity, Jerusalem, Israel
(Received July 14, 1955)

Under favorable circumstances the spectrum of internal bremsstrahlung can be detected from K-capture isotopes decaying with the emission of γ rays. The high-energy part of the ground to ground internal bremsstrahlung spectrum can be detected in Cr^{51}, in the presence of 320-kev γ rays, if suitable precautions to minimize the random superposition of small pulses are taken. A value of 780 ± 50 kev has been found for the energy of disintegration. By using the theoretical expression of Morrison and Schiff for the intensity of the internal bremsstrahlung spectrum, a value of 7% was obtained for the percentage of disintegrations decaying to the 320-kev level of V^{51}. These results are in good agreement with measurements by independent methods.

INTRODUCTION

THE emission of the weak internal bremsstrahlung accompanying radioactive decay by K-capture has been observed in a number of isotopes. Scintillation counter technique has been used in recent years in order to measure the energy distribution and absolute intensity of the internal bremsstrahlung.[1–5] Good agreement (especially in shape) of the high-energy part of the distribution with the approximate theory of Morrison and Schiff[6] has been obtained in all the examples investigated. Measurements of the low-energy spectrum in Fe^{55} [3] and Cs^{131},[4,5] however, has shown that there are considerably more low-energy photons than predicted by theory. Recently, more refined calculations of the spectrum have been carried out by Glauber and Martin,[7] taking into account L-capture and using proper Coulomb modified wave functions. A measurement of the end point of the internal bremsstrahlung spectrum gives the energy of disintegration directly. In decay by orbital electron capture, this can only otherwise be obtained by a measurement of the threshold for the (p,n) reaction.

Because of the weak intensity of the internal bremsstrahlung spectrum no observations of this spectrum have been reported in cases where K-capture is accompanied by discrete γ rays, in particular when the product nucleus may be formed in excited states. In this work, it will be shown that under favorable circumstances the internal bremsstrahlung spectrum can be observed even in such cases, and that at least the higher-energy form of the spectrum can be measured. Such measurements may also permit one to obtain an independent measurement of branching ratios, if the theoretical expressions for the intensity of the spectrum are relied upon.

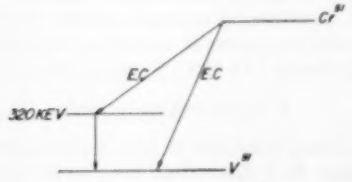

FIG. 1. Decay scheme of Cr^{51}.

The measurements were carried out on Cr^{51} (half-life, 26.5 days), which decays solely by K-capture, according to the decay scheme shown in Fig. 1. According to the most recent measurements,[8,9] the product nucleus V^{51} is formed in an excited state, leading the emission of 320-kev γ rays in approximately 10% of the disintegrations.

The experiments were carried out using a NaI scintillation counter. The essential experimental problem was to minimize the extent of superposition of low-energy pulses due to the 320-kev γ rays—a process which would give rise to an apparent high-energy spectrum and thus obscure the internal bremsstrahlung spectrum.

EXPERIMENTAL METHOD AND RESULTS

A source of high purity was used, free from contamination of β-ray sources, which might give rise to external bremsstrahlung. The source was prepared through a Szilard-Chalmers process in the irradiation of solid potassium chromate in the Harwell pile. A NaI crystal, $1\frac{1}{2}$-in. diameter and 1-in. long, provided with a magnesium oxide reflector, and coupled to a 6260 E.M.I. photomultiplier was used as the γ-ray detector.

A single-channel analyzer was used to analyze the pulses. Figure 2(a) shows a differential pulse spectrum corresponding to the most intense part of the spectrum, and displays clearly the photoelectric and Compton peaks of the 320-kev γ rays.

The energetic part of the internal bremsstrahlung spectrum (greater than 320 kev) associated with the ground to ground transition should appear as a low-intensity tail on the high-energy side of the photopeak shown in Fig. 2(a). In order to observe such a low-

[1] D. Maeder and P. Preiswerk, Phys. Rev. **84**, 595 (1951).
[2] Bell, Jauch, and Cassidy, Science **115**, 12 (1952).
[3] L. Madansky and F. Rasetti, Phys. Rev. **94**, 407 (1954).
[4] B. Saraf, Phys. Rev. **94**, 642 (1954).
[5] B. Saraf, Phys. Rev. **95**, 97 (1954).
[6] P. Morrison and L. Schiff, Phys. Rev. **58**, 24 (1940).
[7] R. J. Glauber and P. C. Martin, Phys. Rev. **95**, 572 (1954).
[8] W. S. Lyon, Phys. Rev. **87**, 1126 (1952).
[9] T. S. Bunker and J. W. Starner, Phys. Rev. **97**, 1272 (1955).

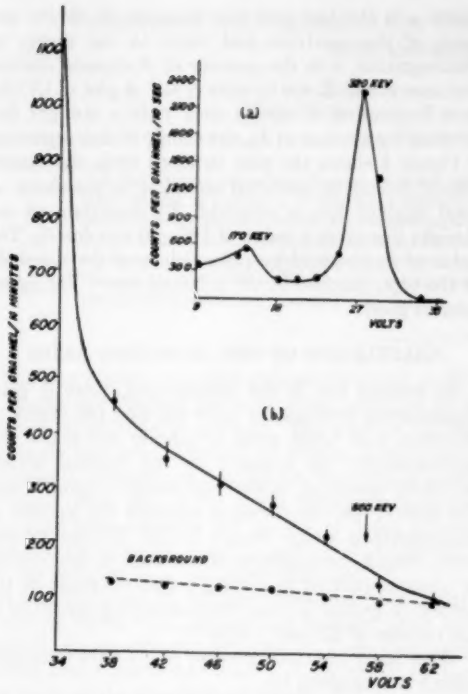

FIG. 2. (a) Differential pulse spectrum from Cr^{51} showing photo and Compton peaks of 320-kev γ ray. (b) Differential pulse spectrum resulting from emission of internal bremsstrahlung from Cr^{51} between 400 kev and 700 kev.

intensity tail unambiguously, it is clearly necessary to reduce as far as possible the extent of random superposition of the pulses resulting from the discrete γ rays. To this end, the following steps were taken:

(1) Low resolving times in the amplifier and pulse analyzer were used (about 0.8 microsecond); (2) low source intensities were used since the number of chance superpositions varies as the square of the counting rate; (3) a 3-mm lead filter was placed between the source and the scintillation crystal in order to reduce the intensity of the 320-kev γ rays reaching the crystal, relative to the intensity of the more energetic part of the bremsstrahlung spectrum. Such a filter distorts, of course, the form of the continuous internal bremsstrahlung spectrum arriving at the crystal. But on the other hand, this distortion is to a large extent compensated by the variation of efficiency of the NaI crystal with energy. In fact, the recorded pulse spectrum bears a much closer resemblance to the true energy spectrum when the filter is used.

In order to make certain that chance superpositions could be disregarded, the ratio of the number of pulses corresponding to energies greater than 400 kev to the number of pulses in the 320-kev photopeak was measured and found to be independent of the distance between the source and the crystal. The final experiments were carried out using a source of about 100 microcuries at a distance of 7 cm from the crystal.

Figure 2(b) shows a typical set of results for the pulse spectrum corresponding to energies greater than 400 kev. The counting rates were rather low, but nevertheless reproducible results were obtained after due care was taken to stabilize the electronics. Because of the low counting rate, it was essential to determine the spectrum of the background. The latter was also reduced by using a lead shield. The γ-ray spectrometer was calibrated at energies of 320 kev (Cr^{51}), 411 kev (Au^{198}), and 660 kev (Cs^{137}). Cs^{137} provided a convenient calibration point near the end point of the internal bremsstrahlung spectrum.

SHAPE AND END POINT OF THE INTERNAL BREMSSTRAHLUNG SPECTRUM

In order to obtain the form of the internal bremsstrahlung spectrum from the experimental pulse distribution, the following corrections and considerations were taken into account:

(1) Subtraction of the background counting rate.

(2) The variation of the efficiency of the system—lead absorber plus NaI crystal—as a function of the energy of incident photons must be known. The transmission of the lead filter under the conditions of the experiment was measured at the energies of 320 kev, 411 kev, and 660 kev by measuring the intensities of the photopeaks of these lines with and without the filter. The variation of "full peak" efficiency of the NaI crystal was obtained from the data of Kahn and Lyon.[10] The variation of the product of the transmission of the lead filter with the efficiency of the NaI crystal as a function of photon energy is shown in Fig. 3. It is

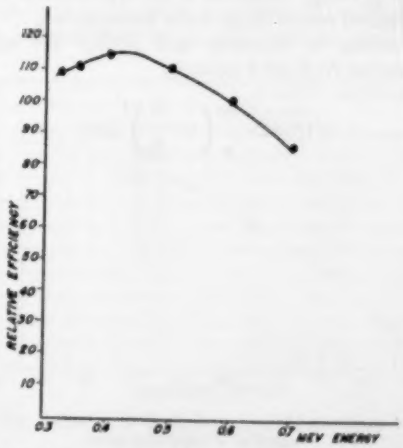

FIG. 3. Variation of γ-ray detector efficiency (lead filter plus NaI crystal) as a function of γ-ray energy.

[10] B. Kahn and W. S. Lyon, Nucleonics 11, No. 11, 61 (1953).

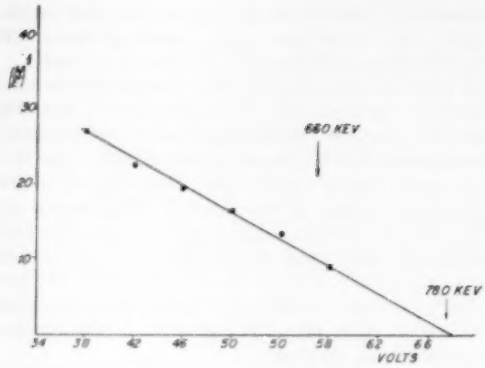

FIG. 4. Plot of $(N/E)^{\frac{1}{2}}$ as a function of E. A straight line intercepting the abscissa at the energy of disintegration E_0 is predicted by the theory of Morrison and Schiff.

seen that the change of over-all efficiency in the range of interest is not large.

(3) In principle, the Compton pulse distribution in the NaI crystal should also be taken into account in computing the spectrum of incident photons from the experimental results. Most of the Compton pulses, however, fall below 400 kev. There is indeed a small Compton contribution above 400 kev resulting from γ rays above 600 kev, but the intensity of the internal bremsstrahlung spectrum above 600 kev is itself small. It was estimated that the corrections involved are very small compared to other errors—mainly statistical, resulting from the low counting rate. Similarly, it was estimated that errors not more than about 2% were introduced by the Compton γ rays created in the lead filter and detected by the crystal.

(4) No corrections were considered necessary for the change of energy resolution of the spectrometer in the very limited energy range under investigation.

According to Morrison and Schiff,[6] the energy distribution $N(E)dE$ is given by

$$N(E)dE=\frac{n\alpha}{\pi}\left(1-\frac{E}{E_0}\right)^2 EdE,$$

where α is the fine structure constant, E_0 is the end point of the spectrum and equal to the energy of disintegration, n is the number of K-capture disintegrations. E and E_0 are in units of mc^2. A plot of $(N/E)^{\frac{1}{2}}$ as a function of E should thus yield a straight line crossing the abscissa at E_0, the energy of disintegration.

Figure 4 shows the plot obtained from the experimental intensities corrected according to the above. A good straight line is obtained. Extrapolation of the straight line gives a value of 780±50 kev for E_0. The value of E_0 obtained by observations of the threshold of the (p,n) reaction in V^{51} is 750±6 kev.[11] The agreement is good.

CALCULATION OF THE BRANCHING RATIO

As pointed out in the introduction, there is good experimental evidence for believing that the theory of Morrison and Schiff gives accurately the shape and approximately the intensity of the internal bremsstrahlung spectrum in the high-energy region. Using the theory, one can therefore estimate the fraction of disintegrations which branch to the 320-kev excited state, from a measurement of the ratio of the number of photons emitted in a certain spectral range of the ground to ground internal bremsstrahlung spectrum to the number of 320-kev γ rays.

If the latter ratio is denoted by N_B/N_γ, the branching ratio β is then given by

$$\frac{\beta}{1-\beta}=\frac{N_\gamma}{N_B}\frac{\alpha}{\pi}\int_{E_1}^{E_2}\left(1-\frac{E}{E_0}\right)^2 EdE,$$

where E_1 and E_2 are the limits of energy between which the number of internal bremsstrahlung photons are measured. Since the internal conversion coefficient of the 320-kev γ ray is very small (3×10^{-3}),[9] the process of internal conversion may be neglected in the calculation. By this method we obtained a value of 7% for the branching ratio in Cr^{51}. This agrees well with the recent measurements of 10%[8] and 9.8%[9] obtained by K x-ray—gamma coincidence methods.

[11] Richards, Smith, and Browne, Phys. Rev. **80**, 524 (1950).

Variation of the Position of the Cosmic-Ray Neutron Intensity Maximum with Geomagnetic Latitude*

R. K. Soberman, A. Beiser, and S. A. Korff
New York University, University Heights, New York, New York

(Received June 14, 1955)

It has been experimentally demonstrated that there exists a maximum in the cosmic-ray neutron intensity when plotted as a function of altitude or pressure. The position of this maximum at various geomagnetic latitudes in the northern hemisphere has been measured by experiments which used balloon-borne unshielded BF_3 counters with various enrichments of the B^{10} isotope. It has been found that the position of the maximum varies approximately parabolically when plotted as a function of geomagnetic latitude. The range of variation is from about 120 millibars at the equator to about 70 millibars at the north geomagnetic pole. The experimental results are compared with theory.

IT is now known that there exists a maximum in the cosmic-ray neutron intensity when measured as a function of altitude or pressure. The position of this maximum has been measured at various geomagnetic latitudes in the northern hemisphere. The experimental technique used was to fly boron trifluoride counters and associated circuitry by means of large plastic balloons. This apparatus and the method of interpreting the raw data has been previously described.[1-5]

It was found that the position of the neutron intensity maximum varies with geomagnetic latitude. Data are available for six different latitudes.[2-6] These data were plotted and a curve was sought which would be the best fit to all the experimental points.

Messel[7] has calculated the dependence of the atmospheric depth of the maximum number of nucleons involved in a nucleonic cascade on the minimum energy of the incident primaries. He obtained a relation of the form:

$$\theta_{max}=\alpha \ln(\beta E_{min}), \tag{1}$$

where θ_{max} is the atmospheric depth of the maximum of the cascade; E_{min} is the minimum energy of the incident primaries; and α and β are constants which depend on the type of cascade being considered. From the papers of Johnson[8] and Alpher[9] on the geomagnetic cutoff values for primaries incident at various angles, it was found that these cutoff values can be reasonably approximated for protons and alpha particles which are incident at almost any particular angle by a Gaussian distribution of the form:

$$E_{min}=\gamma \exp(-\delta\lambda^2), \tag{2}$$

where λ is the geomagnetic latitude, and γ and δ are constants which depend upon the type of primary considered and also upon the angle of incidence assumed. If we now substitute this approximation into Eq. (1), we obtain a relation between the depth of the cascade maximum and the geomagnetic latitude. That is,

$$\theta_{max}=C-D\lambda^2, \tag{3}$$

where C and D are constants which are determined by α, β, γ, and δ. This is the equation for a parabola.

At first glance it appears difficult to relate the neutron intensity which is detected by a $1/v$ detector such as an unshielded BF_3 counter with the nucleons involved in a nucleonic cascade whose energies may be of the order of several Bev. However, as Cocconi *et al.*[10] have shown, in every nuclear process, disintegration nucelons which result from evaporations and slow recoils are produced, and these can be used as indicators of the development of the nucleonic cascade. Since the average distance that an evaporation neutron will diffuse in the atmosphere is equivalent to only about 100 millibars,[2,11] it can be seen that the neutron intensity maximum

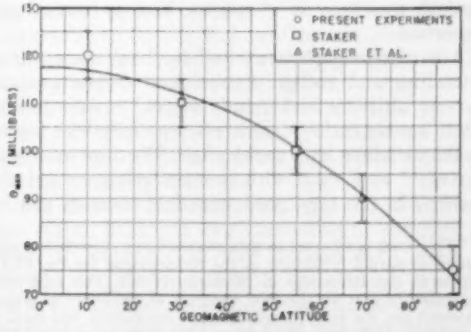

FIG. 1. Position of the neutron intensity maximum *versus* geomagnetic latitude.

* Supported by the Office of Naval Research.

[1] Pavalow, Davis, and Staker, Rev. Sci. Instr. **21**, 529 (1950).
[2] W. O. Davis, Phys. Rev. **80**, 150 (1950).
[3] W. P. Staker, Phys. Rev. **80**, 52 (1950).
[4] Neuburg, Soberman, Swetnick, and Korff, Phys. Rev. **97**, 1276 (1955).
[5] Staker, Pavalow, and Korff, Phys. Rev. **81**, 889 (1951).
[6] R. K. Soberman, New York University thesis (to be published).
[7] H. Messel, *Progress in Cosmic Ray Physics*, edited by J. G. Wilson (Interscience Publishers, New York, 1954), Vol. II, Chap. 4.
[8] T. H. Johnson, Revs. Modern Phys. **10**, 193 (1938).
[9] R. A. Alpher, J. Geophys. Research **55**, 437 (1950).
[10] Cocconi, Cocconi-Tongiorgi, and Widgoff, Phys. Rev. **79**, 768 (1950).
[11] Bethe, Korff, and Placzek, Phys. Rev. **57**, 573 (1940).

which would be measured by a $1/v$ detector would occur not far from the maximum of the nucleonic cascade and would be expected to vary in the same way, with geomagnetic latitude. With the above reasoning in mind, a parabola was fitted to the six points by the method of least squares (see Fig. 1). It can be seen that the curve falls within all of the estimated probable errors.

An interesting point about the above theory is that the geomagnetic cutoff (E_{min}) is different for primary protons than for alpha particles. This might seem to predict the existence of a double maximum in the neutron intensity curves due to nucleonic cascades which are originated by these different primaries. A close look at the experimental data, particularly those which were obtained at $\lambda=10.1°$ where the effect would be more pronounced, indicates that perhaps such an effect does exist and what we commonly think of as the neutron intensity maximum may be the composite of two such maxima. More accurate data in the vicinity of 100 mb are needed before anything further can be said about this point.

PHYSICAL REVIEW VOLUME 100, NUMBER 3 NOVEMBER 1, 1955

Cosmic-Ray Electrons Near Sea Level and at Mountain Altitudes*

PAUL R. BARKER
Department of Physics, University of Michigan, Ann Arbor, Michigan
(Received June 13, 1955)

A cloud chamber containing aluminum and lead plates has been used to study the intensities and energies of cosmic-ray electrons as a function of altitude and zenith angle. The energy distribution is found to be approximately independent of altitude and zenith angle. The decrease of electron intensity with zenith angle is found to be much less than has been reported by investigators using counter telescopes. The increase of the vertical intensity with altitude is found to be slightly smaller than previously reported. The numbers of electrons resulting from decay and collision processes of μ mesons have been calculated and subtracted from the observed numbers. The residual electrons have an exponential altitude dependence with an absorption length of 135 ± 15 g cm^{-2}, and a zenith-angle dependence which is much less steep than would be expected if they preserved the directions of the primary particles from which they originate.

INTRODUCTION

OBSERVATIONS of cosmic-ray electrons are of interest in order to provide information for comparison with suppositions concerning the origin of electrons in the atmosphere. At sea level, most of the observed electrons can be explained in terms of decay and collision processes of μ mesons. At higher altitudes electrons resulting from nuclear interactions, primarily through the decay of π^0 mesons, become increasingly important.

A number of measurements have been made of the intensities and energy distributions of electrons at various altitudes and zenith angles,[1–5] with results which are not entirely consistent, especially with regard to the variations with zenith angle. The most extensive surveys[1,2] were made with counter telescopes and absorbers. In this way, good statistical accuracy can be obtained but accurate identification of individual events is not possible. In order to obtain better information about the electron intensities, the present experiment was undertaken. A cloud chamber containing metal plates and triggered by a narrow-angle telescope was used. This method has several advantages over methods using counters alone. All electrons which reach the visible region of the chamber can be counted, regardless of how they scatter in the plates. Side showers can easily be recognized. Energetic electrons can be distinguished from heavier particles by the showers they produce in a series of lead plates, and their energies can be estimated from the development of the showers. A few aluminum plates, above the lead plates, serve to stop slow electrons, whose energies can be determined from their ranges. Stopped heavy particles can be recognized by their large ionization. With this type of apparatus, measurements were made at Ann Arbor (altitude 280 m), Echo Lake (3260 m), and Mt. Evans (4300 m).

APPARATUS

The main body of the cloud chamber was a Pyrex cylinder of inside diameter 29 cm. The average thickness in the region below the counters was 0.63 cm. Eight absorbing plates were used in the chamber. The top plate was 0.32 cm of aluminum (alloy 24S), the

* This work is reported in greater detail in a dissertation submitted in partial fulfillment of the requirements for the Ph.D. degree at the University of Michigan (1952). The work was supported in part by the joint program of the Office of Naval Research and the U. S. Atomic Energy Commission, and most of it was done while the author held an AEC Predoctoral Fellowship.

[1] K. I. Greisen, Phys. Rev. **61**, 212 (1942).
[2] K. I. Greisen, Phys. Rev. **63**, 323 (1943).
[3] E. D. Palmatier, Phys. Rev. **88**, 761 (1952).
[4] Lovati, Mura, Succi, and Tagliaferri, Nuovo cimento **12**, 526 (1954).
[5] C. N. Chou and M. Schein, Phys. Rev. **98**, 162 (1955).

next two were each 0.64 cm of aluminum, the fourth was 0.66 cm of brass, and the bottom four were each 0.64 cm of lead. A thin bronze foil was fastened to the top plate and four short vertical wires were soldered to the foil. These wires formed a rectangle outlining the region which could be traversed by particles passing through the counters and upper wall of the chamber without scattering. The rectangle measured 4.0 by 10.5 cm, with the short dimension along the line of sight of the camera. The depth of focus of the camera was about 10 cm. The region of good illumination was considerably larger than the region which could be traversed by unscattered particles.

The chamber was triggered by an array of nine Victoreen 1B85 counters. These counters are made of aluminum, with wall thickness 0.030 g cm^{-2}, active length 6.4 cm, and diameter 1.9 cm. In order to keep the beam defined by the counters as close as possible to the focal plane of the camera, the counters were arranged as indicated in Fig. 1, with their axes parallel to the front of the chamber. The three counters on the right were connected to one triple-coincidence circuit, the three in the middle to another, and the three on the left to a third. The resolving time was about 35 μsec. The counters were mounted on a light-weight wooden framework, all of which was well outside the beam. The experiments were performed in wooden buildings beneath slots covered with thin aluminum (0.09 cm at Ann Arbor, 0.05 cm in Colorado).

The camera, cloud chamber, and counters were all fixed rigidly to a frame which could be rotated about an axis parallel to the axis of the chamber and could be clamped solidly at any angle up to 60° from the vertical. Measurements were made at angles of 0°, 45°, and 60°. At Ann Arbor, the apparatus was tilted toward the east, at Echo Lake toward the north, and at Mt. Evans toward the southeast. These directions were determined by the orientations of the buildings used.

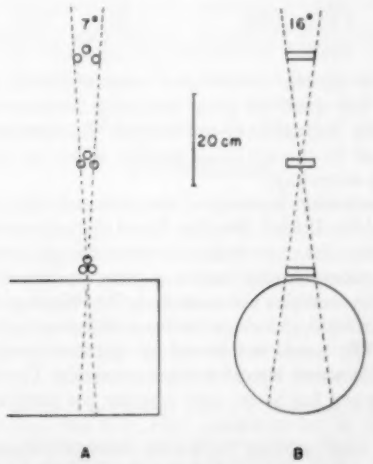

FIG. 1. Arrangement of counters and cloud chamber. A. Side view. B. Front view.

EXPERIMENTAL RESULTS

The negative of each photograph was examined carefully through a stereoscopic viewer. Those pictures in which conditions were not suitable for the formation of tracks in all sections of the chamber were rejected. The only exception is a series taken at 0° on Mt. Evans, in which the uppermost section showed an excessive amount of fog but conditions were good in the rest of the chamber. In these pictures, particles penetrating the top plate were counted but no attempt was made to count those stopping in the top plate.

Each of the acceptable photographs was assigned to one of the following classifications:

Blank pictures show no tracks entering the chamber. Besides events caused by random coincidences and diffuse side-showers, this group includes particles of very low energy which cannot penetrate the wall of the chamber, and electrons which are scattered through large angles in the wall.

Side showers include all events in which two or more particles enter the chamber from a direction other than that defined by the counter telescope.

Extraneous particles include all single particles which do not emerge from the chamber wall within the allowed area beneath the counters and all particles except slow electrons which enter through the allowed area but do not have the right direction. The allowed area is defined by assuming that there is no scattering in the counters.

Penetrating particles pass through the absorbing plates without producing showers, and therefore must be mesons or heavier particles. A penetrating particle, in traversing the lead, frequently produces one or more collision electrons, but such events are easily distinguished from electron-induced showers by the fact that the heavy particle continues on its way without appreciable scattering. Events where the identification is uncertain are extremely rare. To penetrate all the plates μ mesons must have a minimum momentum of 150 Mev/c and protons a minimum of 600 Mev/c.

Stopped heavy particles can be distinguished from electrons by ionization greater than twice minimum with no scattering in the gas.

Slow electrons are those stopping in one of the first four plates. Each was listed according to the plate in which it stopped, and was counted even when it emerged from the top wall of the chamber in a direction different from that defined by the counters. The rms angles of scattering in the chamber wall were estimated from the formula given by Rossi and Greisen[6] for thin layers. Electrons which entered at angles much larger than the expected rms values were recorded as

[6] B. Rossi and K. Greisen, Revs. Modern Phys. 13, 240 (1941).

TABLE I. Observed numbers of electrons and other events. N_s is the total number of track segments beneath the bottom five plates. Numbers followed by the symbol (?) indicate events whose identification is uncertain.

	Ann Arbor			Echo Lake			Mt. Evans			
	0°	45°	60°	0°	45°	60°	$0_{(1)}$°	$0_{(2)}$°	45°	60°
Electrons										
Entering chamber	323 19?	324 18?	285 20?	504 16?	428 14?	341 19?	···	453 12?	491 20?	398 19?
Penetrating 1st plate	301 15?	294 12?	267 15?	486 14?	402 10?	301 14?	348 16?	435 10?	466 15?	373 10?
Penetrating 2nd plate	269 13?	253 12?	234 11?	443 13?	342 9?	261 12?	327 6?	408 9?	420 15?	320 10?
Penetrating 3rd plate	248 12?	220 10?	202 10?	396 13?	304 9?	227 10?	284 6?	373 9?	364 14?	273 6?
Penetrating 4th plate	158 8?	132 8?	128 9?	271 11?	198 6?	147 7?	182 6?	263 8?	243 9?	176 2?
$N_s \geq 4$	69 4?	54 2?	51 5?	100 6?	82 2?	57 2?	63 3?	113 5?	98 4?	66 1?
$N_s \geq 6$	39 2?	37 1?	37 5?	73 3?	55	32	35 1?	81 4?	64 3?	50
$N_s \geq 10$	23	20	19 4?	37 1?	30	23	15 1?	49 3?	35 1?	21
$N_s \geq 16$	12	12	8 2?	21	13	10	4	22 2?	15	8
Multiple el.	36	3	0	50	8	0	31	95	19	3
Other events										
Penetrating particles	1022 2?	1116 3?	905 6?	622 1?	759 1?	625 2?	349 5?	464 8?	607 2?	579 3?
Total acceptable pictures	1466	1625	1393	1312	1463	1453	878	1114	1436	1443
Blank pictures	58	83	114	70	119	152	93	67	137	169
Side showers	13	30	30	34	84	222	18	27	90	177
Extraneous particles	5	37	24	25	19	31	8	20	36	43
Stopped heavy particles	13	9	9	19	32	56	32	34	41	47
Total counting rate (min^{-1})	0.158	0.066	0.0374	0.400	0.179	0.095	0.560		0.288	0.127

questionable. The error caused by missing electrons which scatter through large angles was estimated to be negligible for those which penetrate the second plate.

Fast electrons include all those penetrating the first four plates. For each of these the total number of track segments beneath the brass plate and beneath each of the lead plates was recorded. In cases where a track was obviously scattered back from the upper surface of a lead plate, it was counted only once. In doubtful cases such tracks were frequently counted twice.

Multiple electrons occurred when air showers were incident in the direction defined by the counters. In such cases several electrons generally enter the chamber within the allowed region, and it is impossible to determine how many of them passed through the counters. The best that can be done in counting these electrons is to set an upper limit by including all those which might be allowable.

A few nuclear interactions were observed in the plates, but these are of no particular interest since it was often impossible to tell whether the counters were triggered by the initiating particle or by an upward-moving secondary.

The observed numbers of electrons and other events are listed in Table I. For Mt. Evans the column headed $0_{(1)}$° gives the data obtained while the top section of the chamber was foggy and $0_{(2)}$° gives the data obtained after this condition was corrected. The "blank pictures" listed under $0_{(1)}$° include electrons stopping in the first plate. The numbers followed by question marks refer to events whose identification is uncertain. Usually the uncertainty has to do with whether the particle went through all the counters.

The total counting rates were measured during part of each run and are included in Table I. The standard deviations are about 3%.

ENERGY CALIBRATION

Slow Electrons

In determining the relationship between range and energy for the slow electrons, it was desired to take into account the fact that, when an electron transfers most of its energy to a photon, the photon may materialize in one of the lead plates and produce one or more observable electrons. In such cases, the electron was counted as having emerged from the plate in which it stopped, and as having traveled a further distance which was estimated by observing the secondary electrons. A rough estimate indicates that a 20-Mev photon passing vertically through the lead plates would have a probability slightly over 0.5 of producing an observable secondary. Therefore, only that part of the radiation loss was counted which involves energy transfers of less than 20 Mev. This partial radiation loss was calculated from the cross sections given by Heitler[7] and by Wheeler and Lamb,[8] with corrections for incomplete screening as indicated by Heitler. The inverse of the sum of this radiation loss and the corresponding collision loss was integrated graphically to give the partial range down to 5 Mev. From the data of Fowler *et al.*[9] and of Hereford and Swann,[10] the average range of a 5-Mev electron, including the effects of multiple scattering, was taken to be 0.72 cm in aluminum and 0.20 cm in brass. The total ranges, obtained by adding the partial ranges to the ranges at 5 Mev, are not corrected for the effect of scattering at energies above 5 Mev because no experimental evidence could be found concerning the penetration probabilities when the electrons are not considered as lost after scattering through small angles. The ranges obtained for aluminum agree to within a few percent with the average ranges given by Fowler *et al.*[9] on the basis of a semiempirical calculation of the effects of scattering.

Table II gives the total amount of material traversed by electrons penetrating the various absorbing plates and the corresponding energies as derived from the above considerations. The Pyrex of the chamber wall was converted to an equivalent thickness of aluminum by comparison of the total energy loss at 15 Mev.

Fast Electrons

A common way of estimating the initiating energy of a shower produced in a series of lead plates has been by counting the number of electrons at the maximum of the shower, making no use of information which might be derived from observation at points other than the maximum. This method is not very satisfactory for energies where the maximum number of electrons is small and therefore subject to large fluctuations. The ideal quantity to observe would be the area under the shower curve which gives the number of electrons as a function of depth. Neglecting the effect of scattering, this area is proportional to the initiating energy. The area cannot be determined exactly by experimental methods, but the integral from zero to a depth corresponding to the total amount of absorber present can be approximated by adding together the numbers of electrons observed in each of the spaces between the plates.

TABLE II. Energy required by electrons to penetrate absorbers.

Penetration	Material traversed	Energy (Mev)
Chamber wall	0.73 cm Al	5.1
1st plate	1.08 cm Al	6.9
2nd plate	1.70 cm Al	10.4
3rd plate	2.32 cm Al	14.4
4th plate	2.32 cm Al+0.66 cm brass	30

The expected average development of showers in lead was obtained from Wilson's Monte Carlo results.[11] Wilson gives two measures of the number of electrons at a given depth: n_{si}, the number observed near the shower axis and within 30° of the original direction, and n_s, the number observed when all electron paths between successive lead plates are counted. The electrons counted in the present experiment were essentially those scattered by less than 90°, and a value halfway between n_{si} and n_s was used. The material above the lead was considered equivalent to 0.5 radiation lengths of lead, and the numbers of electrons expected beneath the brass plate and beneath each of the lead plates were obtained from the Monte Carlo curves and added together. The results were plotted as a function of energy from 50 Mev to 500 Mev, and the energies corresponding to various integral numbers of track segments (Table III) were obtained from the graph.

A recent study of showers produced by photons from π^0 decay[12] indicates that the Monte Carlo calculations are more accurate when used with a higher cutoff, giving smaller numbers of electrons. Therefore it is probable that the energies listed in Table III are too small. Other unpublished observations[13] also indicate that these energies may be too small.

ERRORS AND CORRECTIONS

Scattering

For electrons of energy greater than about 10 Mev, the effect of scattering in the chamber wall is negligible. Scattering in the roof, the top counters, and the bottom counters has a negligible effect at even smaller energies. The most serious source of error is scattering in the central counters. Electrons which should be counted will be eliminated if they scatter through small angles

[7] W. Heitler, *The Quantum Theory of Radiation* (Oxford University Press, New York, 1947), p. 172.
[8] J. A. Wheeler and W. E. Lamb, Phys. Rev. **55**, 858 (1939).
[9] Fowler, Lauritson, and Lauritson, Revs. Modern Phys. **20**, 236 (1948).
[10] F. L. Hereford and C. P. Swann, Phys. Rev. **78**, 727 (1950).
[11] R. R. Wilson, Phys. Rev. **86**, 261 (1952).
[12] P. A. Bender, Nuovo cimento (to be published).
[13] A. M. Shapiro, private communication, 1951.

TABLE III. Energies of showers in the lead plates. A shower of n track segments corresponds to an energy of E Mev.

n	4	6	10	16
E	80	125	230	395

in such a way that they miss the bottom counter. There is only partial compensation by others scattered in, because these are required to pass through the top counter. Comparison of the rms angle of scattering and the angle intercepted by the diameter of one of the bottom counters viewed from the position of the central counters indicates that the two are equal at about 10 Mev. Therefore it may be expected that the effect becomes negligible only at energies considerably above 10 Mev. Unfortunately, the importance of this effect was not realized at the time the apparatus was designed.

The effect of scattering in the central counters was calculated in an approximate way by considering the counters as flat plates of thickness πd, where d is the thickness of the counter walls and πd is the average path length through the two walls for particles distributed uniformly in space and moving perpendicular to the axis of the counter. This approximation gives an over-correction because most of the trajectories of unscattered particles pass through the middle of the central counters where the thickness is less than πd, while most of the trajectories of particles that can be scattered into the bottom counter pass near the sides where the thickness is greater.

The results of the calculation can be expressed in terms of the tabulated[14] functions $h_0(x)=\int_x^\infty \exp(-y^2/2)dy$, $h_1(x)=\int_x^\infty h_0(y)dy$, and $h_2(x)=\int_x^\infty h_1(y)dy$. A Gaussian angular-distribution function, as given by Rossi and Greisen[6] was used. It was found that in a plane perpendicular to the axes of the counters the fraction of electrons of energy E which are scattered out is

$$F_1=2(\lambda E)^{-1}(2\pi)^{-\frac{1}{2}}[h_1(0)-h_1(\lambda E)],$$

where $\lambda=4a(2\pi d)^{-\frac{1}{2}}(21L)^{-1}$, a is the diameter of a counter, L is the distance between the top and bottom counters, and d is the thickness of a counter wall in radiation lengths. It is assumed that $a \ll L$. In the present case, $\lambda=0.0936$ Mev^{-1}. The number of electrons which, after entering along trajectories that do not pass through the bottom counter, are deflected into the bottom counter is given, in terms of the number entering along allowed trajectories, by

$$F_2=F_1-2(\lambda E)^{-2}(2\pi)^{-\frac{1}{2}}[h_2(0)-2h_2(\lambda E)+h_2(2\lambda E)].$$

Thus, the number of electrons counted is reduced by the fraction (F_1-F_2). There is a small loss due to scattering in the perpendicular plane, past the ends of the counters, but above 10 Mev the effect is negligible in the present case. The observed differential energy distribution should be multiplied by the correction factor $C(E)=(1-F_1+F_2)^{-1}$. If $S_0(E)$ is the observed integral distribution, the corrected integral distribution is given by $S(E)=S_0(E)+\int_E^\infty S_0(U)C'(U)dU$. In general, the integral must be evaluated numerically.

[14] *Mathematical Tables* (British Association for the Advancement of Science, London, 1931), Vol. 1.

Other Experimental Errors

Since the counting rates were not determined with great accuracy, the data were analyzed in terms of the ratios of the numbers of electrons and penetrating particles observed. Accurate values of the intensities of penetrating particles are known from other experiments.[1,15] With this method of analysis the small errors due to counter inefficiency and meteorological variations are completely eliminated.

A particle which passes through only two of the counters may, by collision in the roof or one of the counters, produce a secondary electron capable of triggering the third counter. By comparison with the measurements of Brown *et al.*[16] it is estimated that the number of such events in which an electron enters the chamber in such a way as to be counted is completely negligible.

It is estimated that one or two percent of the measured electron intensity may consist of photons which materialize in the roof or in the top counters. This error is small compared to the statistical errors and no correction has been made for it.

Another possible source of error is the appearance in the cloud chamber of electrons which did not pass through the counters. To find how many of these might originate from random coincidences, 500 pictures of penetrating particles (where it is quite certain what triggered the counters) were examined, and only one electron was found. Comparison with the observed numbers of blank pictures and extraneous particles indicates that errors due to random coincidences are negligible. The number of false events where the observed electrons are related to the particles that triggered the counters is difficult to determine but should be only a small fraction of the number of blank pictures and extraneous particles. Because of the possibility of this type of event, it is necessary to use a triple- rather than a double-coincidence telescope, although the latter appears more desirable in order to reduce the effects of scattering. A preliminary run at Ann Arbor, without the central counters, gave eight times the rate of blank pictures reported here and indicated an energy distribution with relatively more electrons of low energy. This surplus of slow electrons is interpreted as the result of including events where the observed electron did not pass through the whole telescope. Such errors are most likely among the electrons of very low energy, which were counted even when they entered the chamber at large angles.

[15] W. L. Kraushaar, Phys. Rev. **76**, 1045 (1949).

[16] Brown, McKay, and Palmatier, Phys. Rev. **76**, 506 (1949).

RELATION BETWEEN COUNTING RATE AND INTENSITY

The relation between the observed counting rates and the directional intensities depends on the variation of zenith angle over the telescope. The arrangement here is different from usual in that the axes of the counters remain in a vertical plane when the telescope is tilted. The relation was calculated under the assumption that the variation of intensity with zenith angle is given by $I(\theta)=I_0\cos^n\theta$. With two counters of diameter a and length b, separated by a distance L ($L\gg a$), one can show that the counting rate when the axis of the telescope is at an angle θ to the vertical is $N(\theta)=I(\theta)a^2\alpha^2(1+C\alpha^2)$, where $\tan\alpha=b/L$ and $C=1/3-n/12+[n(n-1)/12]\tan^2\theta$. Terms involving higher powers of α have been neglected. With the three sets of counters used in the present experiment, the ratio of counting rate to absolute intensity is $3a^2\alpha^2(1+C\alpha^2)$, where $3a^2\alpha^2=0.21$ cm² sterad. For $n=3$, the correction factor, $1+C\alpha^2$, is 1.002 at 0°, and 1.031 at 60°. The effect is less for smaller values of n. No components with $n>3$ were observed. Since the statistical uncertainties are rather large, the above correction factor has been neglected.

INTENSITIES OF PENETRATING PARTICLES

The counting rates of penetrating particles, obtained by multiplying the numbers of penetrating particles by the total counting rates and dividing by the numbers of acceptable pictures, are given in Fig. 2. The lines are drawn with a slope corresponding to $\cos^{2.1}\theta$, in agreement with the results obtained by other investigators.[1,18] The agreement is satisfactory since the counting rates were not measured with extreme care. The determination of counting rate for 45° at Ann Arbor exhibits poor internal consistency and may include a systematic error.

The vertical intensity of penetrating particles at Ann Arbor is found to be 0.0087 ± 0.0003 cm^{-2} sterad^{-1} sec^{-1}. The best measurement of this quantity is probably that of Kraushaar[16] who found the vertical intensity at Ithaca to be 0.00904 ± 0.00005 cm^{-2} sterad^{-1} sec^{-1} (corrected to a minimum range of 23 g cm^{-2} of air by means of Kraushaar's range spectrum).

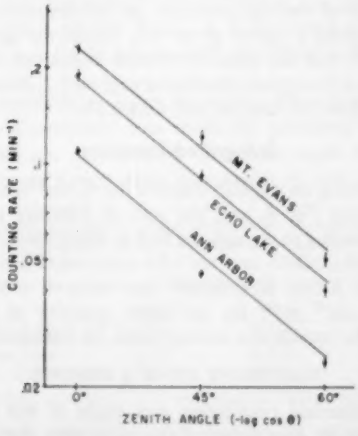

FIG. 2. Zenith-angle dependence of penetrating particles. The straight lines are proportional to $\cos^{2.1}\theta$.

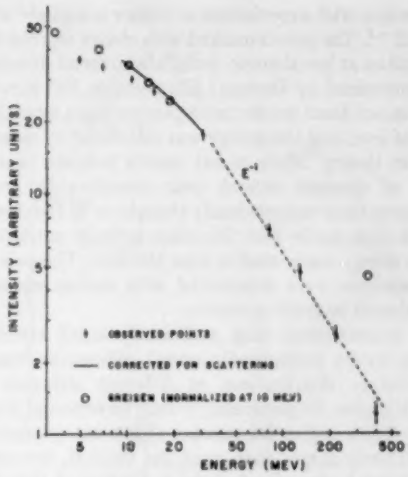

FIG. 3. Integral energy distribution of electrons.

The observed ratio of vertical intensities at Echo Lake and Ann Arbor is 1.72 ± 0.085, and the ratio for Mt. Evans and Echo Lake is 1.22 ± 0.065. Kraushaar found a ratio of 1.71 ± 0.02 for Echo Lake and Ithaca. Rossi *et al.*[17] found 1.22 ± 0.009 for Mt. Evans and Echo Lake.

The good agreement with other observations of penetrating particles indicates that if there are any significant systematic errors they must be of such a nature as to affect only the electrons.

ENERGY DISTRIBUTION OF ELECTRONS

The energy distributions of electrons observed at the various altitudes and zenith angles do not differ by amounts appreciably greater than the statistical errors. Therefore, they can all be represented approximately by the average distribution of Fig. 3, which was obtained by adding together all the electrons of each energy range, exclusive of the Mt. Evans $0_{(1)}°$ column. Half of the questionable electrons were counted and the errors indicated are the arithmetical sums of the statistical standard deviations and half the numbers of questionable electrons. The correction for scattering in the central counters was computed in the manner described previously and the corrected distribution is indicated by the solid line extending between 9 and 30 Mev. Between 30 and 400 Mev, the distribution can be represented by E^{-1}. At the high-energy end there is an indication that it is falling off more rapidly, in

[17] Rossi, Hilberry, and Hoag, Phys. Rev. 57, 461 (1940).

agreement with experiments at higher energies[4,5] which give $E^{-1.5}$. The points marked with circles represent the intensities at low altitude, integrated over all directions, as determined by Greisen.[2] His point at 350 Mev was determined from the electrons penetrating a large thickness of iron, and the energy was calculated by means of shower theory. More recent results indicate that the tails of showers extend over considerably greater distances than was previously thought to be the case,[11,18] and it is probable that this point actually corresponds to an energy much smaller than 350 Mev. The points at low energies were determined with carbon absorbers and should be quite accurate.

A measurement with sufficiently small statistical errors would undoubtedly reveal differences between the energy distributions at different altitudes and zenith angles. In particular, it may be expected that at large zenith angles the number of low-energy electrons is relatively larger than near the vertical, because of scattering in the air. A slight indication of this effect was found, but it is hardly significant statistically.

INTENSITIES OF ELECTRONS

Zenith-Angle Variation

The ratios of electrons to penetrating particles are given in Fig. 4 for electrons with $E>10$ Mev and $E>80$ Mev. The numbers for $E>10$ Mev were obtained by multiplying the number penetrating the second plate by 34/30, in agreement with the corrected curve of Fig. 3. At Mt. Evans, the zenith-angle dependence of the ratios can be represented by $\cos^{0.5}\theta$ for $E>80$ Mev, and by $\cos^{0.7}\theta$ for $E>10$ Mev, giving $\cos^{2.5}\theta$ and $\cos^{2.1}\theta$ for the electron intensities. At Echo Lake, the angular dependence is not very different from that at Mt. Evans, but at Ann Arbor the ratios are approximately independent of the zenith angle, and the electron intensities can be represented roughly by $\cos^{2.1}\theta$ for $E>10$ Mev and $\cos^{2.7}\theta$ for $E>80$ Mev.

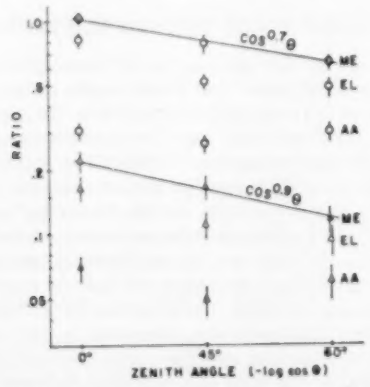

FIG. 4. Ratio of electrons to penetrating particles as a function of zenith angle at Ann Arbor, Echo Lake, and Mt. Evans. The circles represent electrons with $E>10$ Mev and the triangles represent electrons with $E>80$ Mev.

It should be noted that the limits of error indicated in Fig. 4 represent extremely generous estimates when the angular dependence is under consideration. Since the particles of uncertain identification occur in a similar way at all angles, the fraction of them which should be counted is surely about the same in each case. Neglecting this effect, we find the maximum statistical error in the exponent of $\cos\theta$ to be about 0.4.

Experiments using counter telescopes have given much steeper distributions. In particular, Palmatier[3] found $\cos^{3.5}\theta$ for electrons of $E>30$ Mev at Ithaca and $\cos^{4.7}\theta$ at Echo Lake. It is to be expected that the angular distribution will be slightly steeper at higher energies due to smaller scattering in the air, and thus our data for $E>80$ Mev are in strong disagreement with Palmatier's results.

A recent experiment using random expansions of a cloud chamber at 3500 m altitude[4] indicates that both electrons of $E>300$ Mev and penetrating particles have angular distributions of $\cos^2\theta$. However, the statistical uncertainties are large and the data are consistent with a somewhat steeper distribution for the electrons as suggested by an extrapolation of our results to higher energies.

Vertical Intensity

Taking the vertical intensity of penetrating particles as 0.0090 cm^{-2} sterad^{-1} sec^{-1} at Ann Arbor, we find that the vertical intensity of electrons with $E>10$ Mev is 0.0028 ± 0.00025 cm^{-2} sterad^{-1} sec^{-1}. The curve deduced by Rossi[19] for the vertical intensities of electrons gives 0.0022 at the altitude of Ann Arbor. Rossi assigns a lower limit of 10 Mev to these electrons, but it is probable that, due to scattering, not all electrons above this energy were included. The vertical intensity found by Palmatier[3] at Ithaca is 0.0031 for $E>13$ Mev. For the ratio of vertical intensities at Mt. Evans and Ann Arbor Rossi's curve gives 9.5, while we find only 7.1 ± 0.8. For the ratio of vertical intensities at Echo Lake and Ann Arbor, Rossi's curve gives 5.2, Palmatier's results give 5.0, and we find 4.6 ± 0.55.

Integrated Intensity

Assuming an angular distribution of $\cos^{2.1}\theta$, in agreement with Fig. 4, and the vertical intensity given in the preceding paragraph, we find an integrated intensity of 0.0056 ± 0.0005 cm^{-2} sec^{-1} for electrons of $E>10$ Mev at Ann Arbor. Kraushaar[15] has deduced a value of 0.0060 cm^{-2} sec^{-1} for the same quantity at Ithaca, using the results of a measurement by Greisen.[2]

ELECTRONS FROM μ MESONS

A numerical calculation was made of the vertical intensity at Ann Arbor of electrons with $E>10$ Mev

[18] I. B. Bernstein, Phys. Rev. **80**, 995 (1950).

[19] B. Rossi, Revs. Modern Phys. **20**, 537 (1948).

originating from the decay of μ mesons. The energy distribution of the decay electron in the rest system and the altitude variation of the shape of the meson spectrum were taken into account. The track-length calculations of Rossi and Klapman[20] were used. The greatest uncertainty in the result appears to be due to insufficient information about the momentum spectrum of mesons as a function of altitude. The meson spectra of Sands[21] were used and values for intermediate atmospheric depths obtained by linear interpolation on a semi-logarithmic plot (equivalent to assuming exponential variation with depth for a given momentum). The ratio of electrons with $E>10$ Mev to mesons with $p>150$ Mev/c was found to be 0.183.

The same quantity was calculated in a simplified way, using the method developed by Rossi *et al.*[20,22] This method assumes that in the rest system of the meson the electron always receives 1/3 of the energy, and that the meson spectrum does not vary with altitude. Considering fast mesons only, it is found that the ratio of electrons to mesons at depth h is given by the expression $(1.69\times10^{-4}/N_h)(N/\rho)_{h-113}$. N is the intensity of fast mesons and ρ is the density of air. N_h is to be evaluated at the point of observation and $(N/\rho)_{h-113}$ at a point 113 g cm^{-2} higher. Taking N and ρ from the curves given by Rossi,[19] we find that at Ann Arbor ($h=1000$ g cm^{-2}) the ratio is 0.188, in good agreement with the value obtained by the more complicated method.

For other altitudes and zenith angles the computation was made only by the simplified method, and the results were multiplied by 183/188. Assuming that the shape of the meson spectrum is the same at all altitudes and zenith angles, the ratio for zenith angle θ can be obtained by letting N represent the vertical intensity of fast mesons and evaluating N/ρ at a point 113 cosθ g cm^{-2} above the point of observation.

The number of collision electrons, as calculated by Rossi and Klapman,[20] is 0.064 times the number of mesons with $p>150$ Mev/c. It is reasonable to assume that this ratio is independent of altitude and zenith angle.

An approximate correction for the effect of scattering in the atmosphere was made by assuming that all electrons are deflected by the same angle from the direction of production. This angle, α, was taken as

TABLE IV. Calculated ratios of intensity of electrons ($E>10$ Mev) from decay and collision of μ-mesons to intensity of μ mesons ($p>150$ Mev/c).

	0°	45°	60°
Ann Arbor	0.232	0.222	0.227
Echo Lake	0.324	0.302	0.302
Mt. Evans	0.369	0.338	0.336

[20] B. Rossi and S. J. Klapman, Phys. Rev. **61**, 414 (1942).
[21] M. Sands, Phys. Rev. **77**, 180 (1950).
[22] B. Rossi and K. Greisen, Phys. Rev. **61**, 121 (1942).

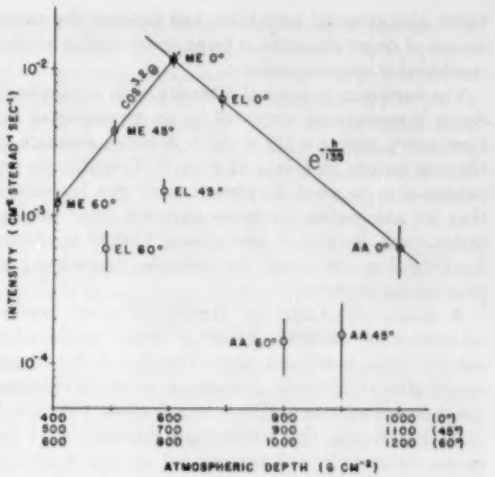

FIG. 5. Intensities of electrons with $E>10$ Mev resulting from nuclear interactions, plotted against atmospheric depth. The points for zenith angle 45° are offset by 100 g cm^{-2} to the left, and the points for 60° are offset by another 100 g cm^{-2}. For a given altitude the graph may be considered as a plot of intensity against $-\log\cos\theta$.

0.25 radian from the calculations of Roberg and Nordheim[23] for the rms deflection of shower electrons with $E>10$ Mev. Under the assumption that the electrons are produced with an angular distribution of $\cos^2\theta$, it can be proved that the distribution including scattering is $\cos^2\theta[1-\sin^2\alpha(1-\frac{1}{2}\tan^2\theta)]$. The correction factor is 0.938 at 0°, 0.969 at 45°, and 1.031 at 60°. The calculated numbers of electrons from decay and collision, including this correction, are given in Table IV.

ELECTRONS FROM NUCLEAR INTERACTIONS

The numbers of electrons calculated to originate from μ mesons were subtracted from the observed numbers, and the intensities of the residual electrons are indicated in Fig. 5. To convert the ratios of electrons to mesons into absolute intensities, it was assumed that the intensities of penetrating particles are proportional to $\cos^{2.3}\theta$ and that the intensity at Echo Lake is 1.72 times that at Ann Arbor and at Mt. Evans 1.22 times that at Echo Lake. A correction was made for the protons included in the penetrating particles, taking the proportion of protons as 0.06 at Mt. Evans, 0.04 at Echo Lake, and 0.0075 at Ann Arbor.[24] At large zenith angles the proportion of protons is certainly smaller, but this fact was not taken into account because the correction for protons affects the electron intensity by a maximum of only three percent.

The limits of error in Fig. 5 are the same as those of Fig. 4. The points for 45° and 60° at Ann Arbor are very uncertain because they represent differences be-

[23] J. Roberg and L. W. Nordheim, Phys. Rev. **75**, 444 (1949).
[24] M. C. Mylroi and J. G. Wilson, Proc. Phys. Soc. (London) **A64**, 404 (1951).

tween almost equal quantities and because the calculations of decay electrons at large zenith angles involve considerable approximation.

The variation of vertical intensity with atmospheric depth is represented very well by an expression of the form $e^{-h/L}$, with $L=135$ g cm^{-2}. A rough estimate of the uncertainty in L is ± 15 g cm^{-2}. This altitude dependence is in good agreement with the hypothesis that all the excess electrons originate from nuclear interactions. By way of comparison, Tinlot[25] has found $L=118\pm 2$ g cm^{-2} for the altitude dependence of penetrating showers.

A recent calculation by Stroffolini[26] gives vertical intensities of electrons from μ decay considerably smaller than were used here. The use of his results would give an altitude dependence of excess electrons which is still exponential, but with L about 150 g cm^{-2}.

At Mt. Evans, the zenith-angle dependence of the excess electrons is well represented by $\cos^{3.2}\theta$, and at Echo Lake it is approximately the same. Miller *et al.*[27] found a similar dependence for slow protons at 3300 meters. There is little other evidence available concerning the angular variation of particles associated with nuclear interactions.

Palmatier, following a procedure similar to that used here, subtracted a calculated contribution by electrons due to μ mesons from the measured intensities.[3] He found that the residual intensities, at Ithaca and Echo Lake, are proportional to the expression $e^{-h/100\cos\theta}$. This is a much steeper angular variation than that indicated in Fig. 5. He used a lower energy limit of 30 Mev, but the difference in energy limit should have only a small effect on the zenith-angle variation.

MULTIPLE-ELECTRON EVENTS

In all the preceding analysis, only electrons occurring singly have been included. The numbers given in Table I for electrons occurring multiply are upper limits and must include many which did not pass through the counter telescope. A reasonable guess for the number of allowable electrons capable of penetrating the second plate is half the number listed. This is probably a large overestimate since the angular opening of the telescope is so small. Including half of the listed numbers increases the total vertical intensities by less than 10%. The altitude dependence is not appreciably affected. The change in angular distribution is equivalent to an increase of about 0.1 in the exponent of $\cos\theta$. For the electrons from nuclear interactions, the vertical intensities are increased by 15 or 20% and the exponent of $\cos\theta$ is increased by 0.2.

SUMMARY AND DISCUSSION

Almost all investigations, including the one reported here, give substantial agreement regarding the directional intensities of penetrating particles and their variation with altitude and zenith angle.[1,3,4,15,17]

We find the energy distribution of electrons to be approximately independent of altitude and zenith angle. An average energy spectrum, corrected for scattering in the counters, is presented in Fig. 3. The shape of this spectrum, in the region of low energies, is in good agreement with that determined by Greisen in measurements of the integrated intensity near sea level.[2] There are indications that the points above 50 Mev actually correspond to energies somewhat higher than those given.[12]

We find the zenith-angle dependence of the electron component to be approximately the same as that of the penetrating particles near sea level, and only slightly steeper at mountain altitudes. The observations of Lovati *et al.*[4] with random expansions of a cloud chamber support this conclusion, but Palmatier's counter measurements[3] give a much steeper angular distribution. We have endeavored without success to find a satisfactory explanation for this discrepancy. It is possible that at low energies our results may contain errors due to scattering or to counting electrons which did not pass through the counter telescope, but it is difficult to conceive that such errors could be appreciable at energies above 80 Mev. The only obvious criticism of Palmatier's work is that he does not appear to have made adequate correction for scattering in the central counter. The relation between wall-thickness and spacing of his counters was such that the correction should be almost exactly the same as in the present experiment. However, this correction could have only a negligible effect on the angular distributions.

We find the vertical intensity at Ann Arbor of electrons with $E>10$ Mev to be 0.0028 ± 0.00025 cm^{-2} sterad^{-1} sec^{-1}, in rough agreement with Rossi's data.[19] Palmatier[3] gives a higher vertical intensity, but it is difficult to make exact comparisons because of uncertainties involved in setting the energy limit. Our data give a somewhat slower increase of vertical intensity with altitude than has been indicated by Rossi.

Subtracting the numbers of electrons produced by μ mesons from the observed numbers, we find that the residual electrons have a zenith-angle dependence of about $\cos^{3.2}\theta$ at mountain altitudes. Near sea level, the errors are very large and the angular variation is not well determined. The vertical intensity of these electrons varies exponentially with altitude, with an absorption length of 135 ± 15 g cm^{-2}. This is approximately the form of altitude variation that is to be expected if the electrons originate from nuclear interactions through intermediary steps of very short lifetime, such as the π^0 meson. The expression given by Palmatier[3] for the dependence of the residual electrons on altitude and zenith angle, $e^{-h/L\cos\theta}$, is of the form that would be obtained under the assumption that there are no angular deviations in the production of the electrons or in the

[25] J. Tinlot, Phys. Rev. **74**, 1197 (1948).
[26] R. Stroffolini, Nuovo cimento **10**, 300 (1953).
[27] Miller, Henderson, Garrison, and Sandstrom, Phys. Rev. **85**, 723 (1952).

development of the showers. This assumption is not very realistic and it is to be expected that, because of angular deviations, the zenith-angle distribution will actually be less steep.

The zenith-angle distribution of residual electrons found in the present experiment is much less steep than could be explained under the assumption that the electrons preserve the directions of the primary particles from which they originate. In deriving the numbers of electrons due to μ mesons we found that the scattering of shower electrons has a relatively small effect on the zenith-angle distribution. With a steeper initial distribution the effect is larger, but it does not appear sufficient to explain the small observed zenith-angle variation. The indications are, therefore, that there are appreciable angular deviations in the production and decay processes of the π^0 mesons, and, consequently, that their average energy is not large.

In comparing the results of experiments using counters alone and those using cloud chambers, one might consider the latter as more reliable, in spite of poorer statistics, because each event can be considered individually and the various components can be identified with greater accuracy. In a measurement using only counters it is usual to determine the total counting rate and then subtract the counting rates of all unwanted types of events, and there is always the possibility of overlooking or wrongly estimating some of the extraneous events. We feel that further investigations are required to determine the reasons for the disagreements in the results obtained by the two methods.

ACKNOWLEDGMENTS

The author wishes to express his appreciation to Professor W. E. Hazen for suggesting and encouraging this work, and to Professors Byron Cohn and Mario Iona for their cooperation at the Inter-University High Altitude Laboratory.

PHYSICAL REVIEW VOLUME 100, NUMBER 3 NOVEMBER 1, 1955

Measurement of the High-Energy End of the Bremsstrahlung Spectrum*†

DONALD C. HAGERMAN‡ AND K. M. CROWE
High-Energy Physics Laboratory, Stanford University, Stanford, California

(Received July 13, 1955)

Results of a differential measurement of the upper six percent of the bremsstrahlung photon spectrum produced by 500±25 Mev electrons agree with the Bethe-Heitler formula within the combined experimental errors of approximately 25%. The measurement was made by running a collimated beam of 10^9 electrons per pulse through a diffusion cloud chamber and observing the electrons degraded in energy by the production of a gamma ray. Observation of electron-electron scattering events provided a normalization in the center of the energy region investigated. A total of 330 events was observed. The performance of a diffusion cloud chamber under these conditions is discussed.

INTRODUCTION

THE differential cross section for the production of bremsstrahlung by high-energy electrons was first calculated by Bethe and Heitler[1] on the basis of the Born approximation. If one includes the various corrections to this formula—such as the screening effect—the final result should provide an accurate description of the radiation produced by a beam of electrons striking a thin, low-Z target. For a high-Z target, which is commonly used as a radiator, the Born approximation introduces an error.

Experimentally, the cross section has been checked for several primary energies in the medium energy range (10 to 300 Mev). Absolute measurements have been made by observing the initial and final energies of the electron in a cloud chamber, the energy of the gamma ray being determined by subtraction. Curtis[2] found that the shape of the theoretical spectrum agrees quite well with the experimental shape, but that the experimental cross section in lead is about 7% lower than the theoretical value. His primary energy was 60 Mev with a half-width of 10 to 13 Mev in the primary energy spectrum. In the upper 5% of the spectrum he shows one point with an error of ±15%. Fisher[3] did the same sort of experiment using a primary beam whose average energy was 247 Mev; the half-width of his primary energy spectrum was approximately 80 Mev. In the upper 5% of the spectrum Fisher shows two points with approximately 5% errors. He concludes that the experimental cross section is 9% lower than the theoretical.

At this time, investigators are using the photon-

* Supported by the joint program of the Office of Naval Research and the U. S. Atomic Energy Commission.

† This paper is a summary of a thesis submitted in partial fulfillment of the requirements for the Ph.D. degree at Stanford University.

‡ Now at the Los Alamos Scientific Laboratory of the University of California, Los Alamos, New Mexico.

[1] W. Heitler, *The Quantum Theory of Radiation* (Clarendon Press, Oxford, 1954), third edition.

[2] C. D. Curtis, Phys. Rev. **89**, 123 (1953).

[3] P. C. Fisher, Phys. Rev. **92**, 420 (1953).

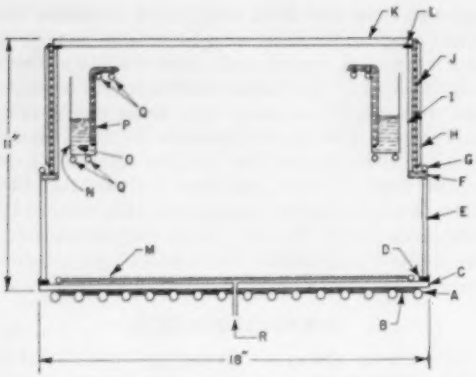

FIG. 1. Diagram of the diffusion cloud chamber. *Legend: A*—Copper tubing through which coolant is circulated to regulate the temperature of the cloud-chamber base. *B*—Solder to increase heat transfer between *A* and *C*. *C*—¼-in. copper base plate. *D*—Sponge rubber to seal walls to base. *E*—Polystyrene wall. *F*—Brass ring. *G*—Tubing through which coolant may be circulated to control temperature of *F*. *H*—Water jacket used to insulate thermally the chamber from the magnet. *I*—Polystyrene wall. *J*—Styrafoam insulation. *K*—Plate-glass top. *L*—Rubber gasket. *M*—Black velvet to provide background for photography. *N*—Alcohol tray. *O*—Alcohol mixture (1:1:1 mixture of ethyl alcohol, methyl alcohol and distilled water). *P*—Felt wick to increase effective area of alcohol. *Q*—Tubing through which coolant may be circulated to control temperature of *O*. *R*—Drain.

difference method at high energies to investigate various photonuclear reactions; the accurate analysis of these results by this method depends critically on the high-energy tip of the bremsstrahlung spectrum. Neither of the cloud-chamber measurements cited shows many points in the upper 5% of the spectrum; further, their work was done at comparatively low energies, and extrapolation of their results might allow additional effects not as yet seen to be overlooked. Therefore, it was decided to make a measurement of this part of the spectrum using a primary beam of as high an energy as available and with the highest resolution possible. A cloud chamber was used to do this in much the same way as Curtis[2] and Fisher[3] did their work. However, one major change in the experimental technique was made: Instead of sending just a few electrons through the chamber per picture, 10^3–10^4 electrons were sent through in a single pulse. This produced an average of one event per picture in the energy region of interest. This method also increased the data-taking rate, but it introduced certain problems regarding the operation of the chamber and the separation of *e-e* scattering events that might be confused with bremsstrahlung.

CLOUD-CHAMBER EQUIPMENT

A diagram of the diffusion cloud chamber used is shown in Fig. 1. This chamber operates at atmospheric pressure and is air-filled. Under our operating conditions, the duty cycle is 30–60 sec. The base is cooled by a dry-ice refrigerating system using trichlorethylene-*D* as the circulating coolant. The chamber in this experiment was operated in a magnetic field of ~2100 gauss. The target (19 mg/cm² of tantalum) was placed in the center of the chamber.

The primary electron beam was produced by the Stanford Mark III linear accelerator.[4] For this experiment, the beam was sent through a double-deflection magnet system;[5] the electron optics of the magnet system was adjusted so that the beam reaching the cloud chamber was less than 0.3 cm in diameter, had an energy of 500 Mev with an energy spectrum of half-width less than 1 Mev, and had a negligible gamma-ray contamination. The accuracy of the beam energy is $\sim\pm 3\%$.

The stereo camera with which the pictures were taken has two lenses and uses 35-mm unperforated film. All pictures were taken on Eastman Linagraph Ortho film. The pictures were measured using a space table consisting of a translucent glass plate mounted so that it had two rotational degrees of freedom corresponding to the angles θ and ϕ in Fig. 2. The reprojector uses the optical system of the camera. Illumination is provided by Sylvania 300 ac arc lamps.

CLOUD-CHAMBER OPERATING CONDITIONS

It was found while operating the chamber to observe cosmic rays that the depth of the active volume was 5–8 cm, and that as long as temperature equilibrium was maintained the operation of the chamber was quite stable. The condition of the chamber is markedly changed when a heavy electron beam is periodically sent through the chamber. These effects of the beam on the operation of the chamber can be described in terms of the additional insensitive regions or dead spots that appear in the normally-active volume of the chamber.

The dead regions in the chamber which existed during the experiment are listed below. (See Fig. 3 for a schematic view of these dead spots. Note that not all are caused by the beam.) (1) The beam decreases the active volume of the chamber to an average depth of 3 cm. This was discovered when it was observed that

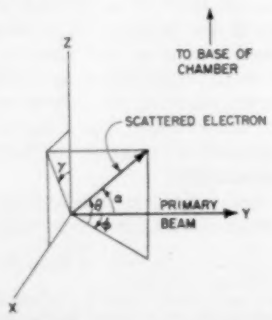

FIG. 2. Coordinate system used.

[4] Chodorow, Ginzton, Hansen, Kyhl, Neal, Panofsky, and the staff, Rev. Sci. Instr. **26**, 134 (1955).

[5] W. K. H. Panofsky and J. A. McIntyre, Rev. Sci. Instr. **25**, 287 (1954).

most of the events seen had positive values of θ (see Fig. 2). Enough events with negative θ were seen to assure us that the beam was within the active volume; however, events with a large negative value of θ were rare. (2) The beam creates a dead space whose boundaries are parallel to and several centimeters away from the beam. This insensitive region is caused by the intense ionization produced by the beam which depletes the vapor in the region adjacent to the beam. The boundary of this dead region was found by measuring the apparent origin of 165 tracks (by apparent origin is meant that point at which a track leaves a dead region; the actual origin of the track is at the intersection of the primary beam and the target). The number of tracks *vs* the perpendicular distance from the beam is shown in Fig. 4. At a distance of 5 cm from the beam, 85% of all of the tracks were in the active volume, so this distance was taken as an edge of the active volume. The exact position of the edge of the

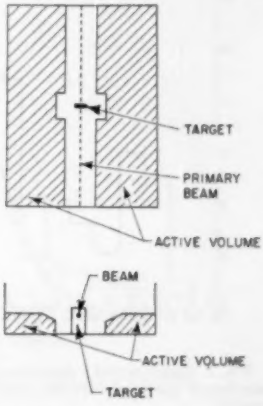

FIG. 3. Active volume in the cloud chamber under normal operating conditions.

active volume affects the efficiency appreciably only for high-energy secondary electrons. (3) A dead region is caused by the target: in its immediate vicinity the chamber is completely dead and further from the target the active-volume height is reduced. This seems to be partly caused by the disturbance introduced in the temperature gradient of the chamber by the presence of the target; vapor also condenses onto the target leaving nearby regions depleted. This completely dead region does not affect the results since all of the events studied were sufficiently energetic that their orbits left this region. The reduced height around the target discriminates against wide-angle, low-energy events. The effect is observed by plotting the low-energy events on the θ–ϕ plane.

These dead regions in the chamber seemed to be approximately the same size from picture to picture. If all the tracks that do not fall within the average active volume are rejected, the effect of the insensitive regions can be corrected for in a purely geometrical manner.

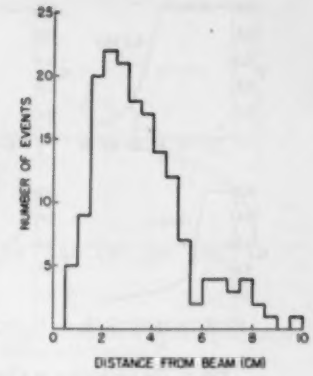

FIG. 4. Apparent origin of tracks *vs* their perpendicular distance from the beam.

The uncertainty introduced can be calculated from the estimates of the variations of the volume, and it is clear that the error can be reduced to an arbitrary value by sacrificing events.

EFFICIENCY CALCULATIONS

The geometrical boundaries of the active volume as described above were defined in relation to the coordinate system of the events by means of a sighting device similar to a transit mounted on the space table. Tracks were then simulated on the viewing plate of the space table and the allowed regions for various event energies were determined in terms of the θ–ϕ coordinates. The results of these measurements for several typical electron energies are shown in Fig. 5. The allowed regions lie within the area defined by the curve and the ϕ axis. Note that the 5.2-Mev graph has an additional line A on it: this is caused by the decrease in height of the active volume around the target [see the discussion of region (3), above]. On this graph the allowed region lies under the upper curve and above the ϕ axis, or line A. These acceptance criteria are also a slowly varying function of the minimum track length allowed. Two centimeters was chosen as this minimum length; this is long enough so that the angles can be measured accurately; the curvature of such an apparently short track can be determined since the origin of the track is

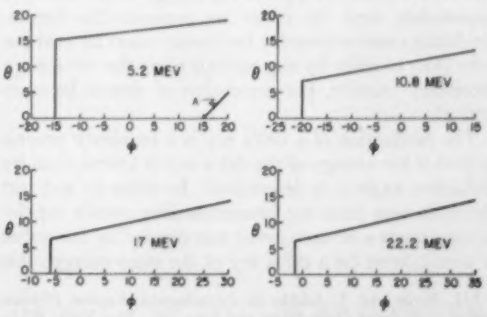

FIG. 5. Allowed regions in the θ–ϕ plane.

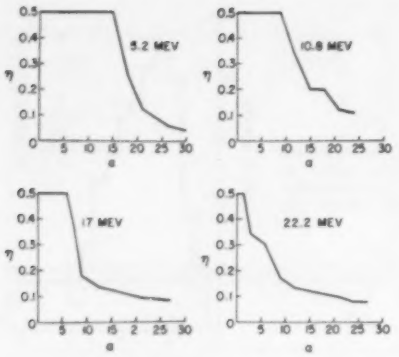

FIG. 6. The efficiency η as a function of α.

accurately known. In practice, most of the tracks are much longer than this 2-cm minimum.

The efficiency as a function of energy and the deflection angle α is determined by these allowed regions. The efficiency is the ratio of the total azimuthal angle that lies within the allowed region to 360°; efficiency curves as calculated in this manner are shown for representative energies in Fig. 6.

REDUCTION OF DATA

The data were first reduced by testing each event to see if it fell within the allowed region in the θ-ϕ plane. In practice, this rejected ~40% of the events. In the final analysis of the data, events of energy between 3 and 30 Mev were retained (for bremsstrahlung events this corresponds to fractional quantum energies of 0.997 to 0.940). These were sorted into energy bins 5-Mev wide, with the exception of the lowest-energy bin which was 2-Mev wide.

Other low-energy secondary electrons that are seen in this type of experiment are caused by the formation of high-energy delta rays. These delta rays can be used to provide a beam normalization since in principle they are separable in their angular distribution from the bremsstrahlung events. The cross section for the production of delta rays is given by the Møller formula;[6] this cross section diverges as the energy of the delta ray approaches zero. In order to measure the bremsstrahlung cross section for fractional quantum energies very close to unity by any method using the low-energy secondary particle, the separation of events becomes critical.

The production of a delta ray is a two-body process so that if the energy of the delta ray is known then its deflection angle α is determined. In order to sort out the delta rays from the bremsstrahlung events the deflection angle α of each event was divided by the value of α calculated for a delta ray of the same energy; this ratio of angles is called x. The experimental inaccuracies change the delta-ray spectrum as a function of x into something similar to a Gaussian distribution, and the multiple scattering broadens this distribution.

The scattering spectrum was calculated on the basis of the Molière theory of scattering.[6,7] To a sufficient accuracy the single and plural scattering can be neglected, leaving only the multiple scattering. In the figures and in reducing the data, we have used a distribution corresponding to particles produced at the center of the target. The deviation introduced by this simplification is reflected by a normalization error of only ten percent, which has been included in the assigned normalization error.

RESULTS

All of the experimental results were plotted as a function of x for the various energy bins. When this

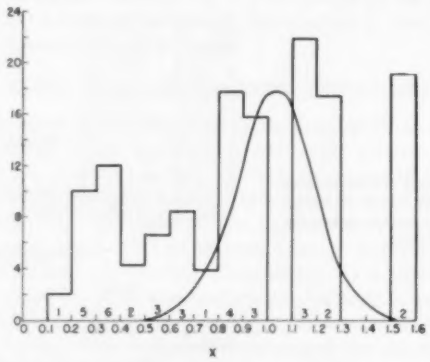

FIG. 7. Experimental x spectrum for 10–15 Mev electrons. The numbers at the base of the histogram are the observed numbers of events.

was done it was noticed that between 10 and 25 Mev the delta-ray events were evidently separated from the bremsstrahlung events and the normalization was based on these events alone. In Fig. 7, the x-spectrum for 10–15 Mev electrons is shown. In Fig. 8, the theoretical delta-ray spectrum and the experimental spectrum as a function of energy are shown. The normalization was determined from a weighted average of the measured values for the 10- to 25-Mev groups. For the lower-energy electrons this shows that not as many delta rays are seen as would be expected; this loss is caused by the decrease in the active height around the target [see discussion of region (3), above]. This loss does not affect the bremsstrahlung results since they tend to be emitted with small values of the deflection angle.

The bremsstrahlung results are shown in Fig. 9. The theoretical curve was calculated from the Bethe-Heitler formula (including screening and the contribution due

[6] H. Bethe and J. Ashkin in *Experimental Nuclear Physics*, edited by E. Segrè (John Wiley and Sons, Inc., New York, 1953), Vol. I.

[7] G. Molière, Z. Naturforsch. **3a**, 78 (1948).

to e–e bremsstrahlung).[6] The errors indicated by the inner bars on the probable-error brackets for fractional quantum energies greater than 0.97 are those due to the subtraction of delta-ray events; to determine these errors the probable error of normalization was taken as 25%. The total error for these points is the statistical combination of the statistical error and the subtraction error. Between fractional quantum energies of 0.950 and 0.970 the probable error is due to statistics alone. For the point at the fractional quantum energy of 0.945 the half-bars indicate the statistical error. The total error at this point is larger than indicated by statistics since it contains a 25% correction that does not appear in any of the other points. This correction is caused by the fact that the electrons of this energy emitted with an α of less than 2° stay entirely within the beam dead spot and are not seen [see the discussion of dead spot (2), above]. The correction is determined from the percentage of events that occur within a similar cone

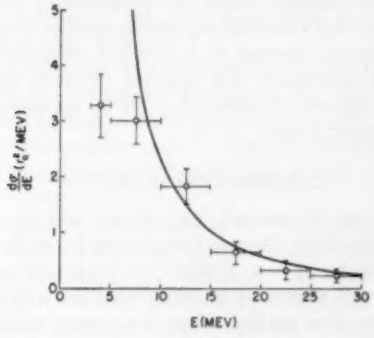

FIG. 8. Differential cross section for e–e scattering.

in the next lower energy bin. The errors in the correction come from the statistical errors in the angular distribution of the next lower bin and uncertainty in the dead region boundary which is ~0.6° in the figure of 2°.

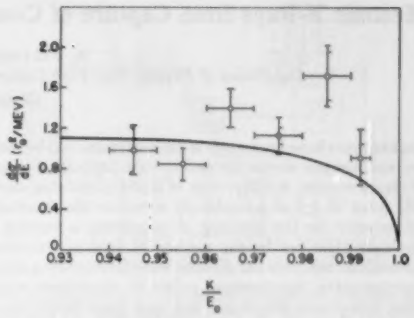

FIG. 9. Differential bremsstrahlung cross section. (The errors are discussed in the text.)

CONCLUSIONS

The high-energy tip of the bremsstrahlung spectrum as measured in this manner agrees with the theoretical spectrum within the experimental uncertainties. If the average of the measurements is taken, it is found to be 22% higher than the theoretical value; this is within the normalization error of these results. It apparently would be extremely difficult to measure the finite end point of the bremsstrahlung spectrum by this method because of the difficulty of separating out the delta-ray background. It does seem feasible, however, to make other cloud-chamber measurements using this method in which a heavy beam of ionizing particles is run directly through the chamber. In any experiment of this sort, the limits of the active volume must be established accurately to eliminate uncertainties in the efficiency.

ACKNOWLEDGMENTS

We wish to thank G. Rawitscher, Dr. D. R. Yennie, and Professor W. K. H. Panofsky for valuable discussions concerning the theory of this experiment. K. Sherwin, D. D. Lloyd, and R. M. Friedman were of great assistance in the construction and operation of the equipment. The operators of the Mark III accelerator were most helpful in the performance of the experiment.

Mesonic X-Rays from Capture of Cosmic-Ray μ Mesons in a Chemical Compound*†

A. Fafarman‡ and M. H. Shamos
Department of Physics, New York University, Washington Square College, New York, New York

(Received June 7, 1955)

Measurements have been made of the x-rays emitted by mesonic carbon and oxygen atoms formed by the capture of negative cosmic ray μ mesons. A 4-liter tank of liquid scintillator, dioxane, $C_4O_2H_8$ (plus 10 g/l of p-terphenyl) served as the absorber and as the detector for the stopping of cosmic-ray μ mesons. The mesons were identified by the method of delayed coincidences. The mesonic x-rays from the dioxane were detected by a scintillation spectrometer. Spectrometer pulses in coincidence with the stopping meson were lengthened and their pulse height recorded on a recording milliammeter. The time distribution of the delayed coincidences was recorded over the delay interval 0.5 to 8.0 μsec. The measured $2p-1s$ transition energies of 82 kev and 145 kev, for carbon and oxygen respectively, agree with the simple Bohr orbit calculations within the precision of the measurement. The observed ratio of captures by oxygen and carbon (0.33 ± 0.04) does not agree with the Z-dependence predicted by Fermi and Teller for mesonic atom formation by chemical compounds (0.67) nor with the simple stopping power calculation (0.50); however, in view of the thick absorber (14 cm depth of dioxane), the above experimental ratio is uncertain because of Compton degradation of the oxygen $2p-1s$ radiation which shifts some events from the oxygen to the carbon peak. The observed distribution of delays is consistent with the assignment of the observed radiation to μ-meson capture.

I. INTRODUCTION

FOLLOWING the suggestions of Wheeler[1,2] on the applications of the negative μ meson as a probe for nuclear electric and magnetic fields, the spectroscopy of μ mesonic atoms has been applied to several problems. Fitch and Rainwater[3] have made accurate determinations of nuclear radii in absorbers of high Z. Conversely, by using materials of low Z, and the precisely known K x-ray absorption edges of absorbing foils, several investigators[4,5] have determined the μ-meson mass with high precision, permitting a comparison with the mass obtained by other methods.[6]

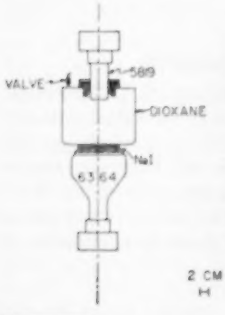

FIG. 1. Apparatus for the study of the capture of negative μ mesons in carbon and oxygen. A 5819 photomultiplier views the tank of dioxane (or toluene) scintillator in which the stopping mesons are detected by the method of delayed coincidences. Mesonic x-rays are detected by a coincidence scintillation spectrometer which includes the NaI crystal and the 6364 photomultiplier; (the photomultipliers are attached to their respective preamplifiers; apparatus supports and photomultiplier mu metal shields are not shown).

However, the slowing down and capture of the negative μ meson into a mesonic Bohr orbit requires further study. For example, the present experimental evidence does not establish clearly the Z-dependence predicted by Fermi and Teller[7] for the relative number of captures on different elements of a chemical compound. The present experiment was intended to study this and related aspects of μ-meson capture by spectroscopy of the mesonic x-rays.

II. EXPERIMENTAL METHOD[8]

For low Z materials, e.g., carbon and oxygen, in which the life of the negative μ meson is not shortened appreciably, it was possible to study the mesonic x-rays with essentially no background and with no contribution from nuclear absorption gamma radiation or from (decay beta particle) bremsstrahlung. A large volume organic liquid scintillator was used as the absorber and as the detector for the stopping of μ

* Assisted in part by the U. S. Atomic Energy Commission and by the Office of Naval Research.

† A brief description of this research has been given at the 1955 Washington meeting of the American Physical Society [Phys. Rev. **99**, 623(A) (1955)].

‡ Submitted by A. Fafarman in partial fulfillment of the requirements for the degree of Doctor of Philosophy in the Graduate School of Arts and Science at New York University.

[1] J. A. Wheeler, Revs. Modern Phys. **21**, 133 (1949).

[2] J. A. Wheeler, Phys. Rev. **92**, 812 (1953).

[3] V. L. Fitch and J. Rainwater, Phys. Rev. **92**, 789 (1953). These measurements hold forth the possibility of resolving the $2p_{\frac{1}{2}}-2p_{\frac{3}{2}}$ to ground-state doublet of the Pb mesonic atom.

[4] Koslov, Fitch, and Rainwater, Phys. Rev. **95**, 291 (1954).

[5] S. DeBenedetti *et al.*, Phys. Rev. **94**, 766(A) (1954).

[6] Hydrogen constitutes a special case; see R. E. Marshak, *Meson Physics* (McGraw-Hill Book Company, Inc., New York, 1952), pp. 171, 172.

[7] E. Fermi and E. Teller, Phys. Rev. **72**, 399 (1947).

[8] Some earlier experiments on Pb mesonic atoms were performed in this laboratory using a different experimental method than that described above. [A. Fafarman and M. H. Shamos, Phys. Rev. **87**, 219(A) (1952)]. These experiments are summarized here. A conventional coincidence-anticoincidence GM counter telescope was used to select cosmic-ray mesons stopping in a Pb absorber. Gamma radiation coincident in time with the stopped meson ($\mu\gamma$ coincidence) was detected by a scintillation spectrometer which was placed outside of the direct meson beam and guarded by a double ring of anticoincidence GM counters. The measurements showed (continuous) gamma radiation of maximum energy 5.5 ± 1.5 Mev. The interpretation of the results was complicated by a high background. The rate of background events (Pb absorber removed) in the energy interval 1 to 10 Mev was 0.09 ± 0.03/hr, while the corresponding rate with the Pb absorber in place (foreground rate) was 0.25 ± 0.04/hr. The high background was due principally to photon secondaries of fast mesons and of decay positrons. The difference between the foreground and background included (in addition to the mesonic x-rays of Pb), the gamma radiation resulting from the nuclear absorption of the negative mesons and the bremsstrahlung of a fraction of the decay positrons which result from the decay of positive μ mesons in the absorber; (the resolving time for $\mu\gamma$ coincidences was 0.9 μsec and bremsstrahlung from positrons appearing within this interval could contribute to the foreground minus background rate).

mesons[9–11]; the μ mesons were identified by the method of delayed coincidences. The mesonic x-rays were detected by a NaI scintillation spectrometer in time coincidence with the stopped meson; i.e., the measurement was made of the energy of the associated *prompt* radiation without measuring radiation associated with the *delayed* meson decay beta particle or *delayed* nuclear radiation.

The apparatus for the measurement of the mesonic x-rays from carbon and oxygen consisted essentially of two scintillation detectors together with the associated electronics. The detectors are illustrated in Fig. 1. The upper detector was a 4-liter tank of liquid scintillator 19 cm in diameter $\times$14 cm high, viewed by a single 5819 photomultiplier. The tank was filled with toluene (plus 10 g/l p-terphenyl) or with dioxane (plus 10 g/l p-terphenyl) for measurements on carbon and on carbon plus oxygen respectively. The dioxane was comparable to toluene in scintillation efficiency[12] although some dioxane had to be dehydrated for satisfactory performance.[13] The tank was constructed from a thin-walled aluminum pot; the joints were sealed with Sauereisen No. 31 cement.[14]

A threaded ring was cemented to the 5819 tube and screwed into a threaded bushing on the tank, sealing against it by means of a corrugated lead gasket. A valve was used to vent the tank. Delayed coincidences in this tank (with a delay of 0.5 to 8.0 μsec) will be identified as μ-β events.

The gamma detector was a 4-in. diameter $\times$ $\frac{1}{2}$-in. thick sodium iodide crystal, hermetically sealed in a 0.025-in. wall aluminum container. The inner surface was a fired aluminum oxide coating of negligible absorption which served as a diffuse reflector to secure more uniform light collection in various parts of the crystal. A type 6364, 5-in. photomultiplier was used with the crystal; this combination gave a pulse height distribution curve for the Cs^{137} photopeak (663 kev) having a full width (at half-maximum) of 17%. Events occuring in this crystal will be identified as γ events.

Figure 2 is a block diagram of the electronics. The scintillation pulses are amplified in moderately fast amplifiers (rise time $1–2\times10^{-7}$ sec) and fed to a gated beam tube coincidence circuit. The width of the time resolution curve for the coincidence circuit is about 3×10^{-7} sec. A $\mu\gamma$ coincidence followed by a second pulse in the tank with a delay of 0.5 to 8.0 μsec (β pulse) is selected by the delay discriminator and sorted into one

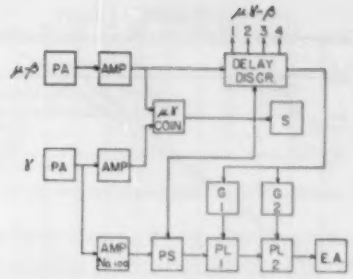

FIG. 2. Electronics for the study of negative μ meson capture. Pulses from the tank (μ-β) and from the NaI (γ) are amplified by preamplifiers, PA, and fast amplifiers, AMP. The γ pulse is amplified also in a slow amplifier, AMP No. 100; the pulse in this channel is stretched to 20 μsec by a pulse stretcher, PS, whenever a $\mu\gamma$ coincidence occurs. The stretched pulse is further lengthened by a doubly gated, G1G2, pulse lengthener, PL1 PL2, and recorded on an Esterline Angus recording milliammeter EA, only if the γ is accompanied by a delayed β event ($\mu\gamma$-β) as selected by the delay discriminator.

of four channels.

(1) $\mu\gamma$-β (delayed 0.5 to 2.5 μsec),
(2) $\mu\gamma$-β (delayed 2.5 to 4.4 μsec),
(3) $\mu\gamma$-β (delayed 4.4 to 6.3 μsec),
(4) $\mu\gamma$-β (delayed 6.3 to 8.0 μsec).

The delay discriminator furnishes a master pulse $(\mu\gamma\text{-}\beta)_{1234}$ whenever any of the four channels is actuated. The master pulse gates a two-stage pulse lengthener which lengthens the γ pulse to 2 seconds in duration and permits the amplitude of the γ pulse to be recorded on an Esterline Angus recording milliammeter.

The γ pulse which is used in the pulse height measurement is derived from the γ preamplifier, delay-line-shaped for a duration of 4 μsec and amplified with a rise time of 0.5 μsec and gain of 700 by a Los Alamos Model 100 amplifier. The pulse output of the amplifier is stretched to a duration of 20 μsec whenever a $\mu\gamma$ coincidence occurs, so that, if it proves to be a $\mu\gamma$-β event, the response of the pulse lengthener will be independent of the delay of the master output pulse from the delay discriminator.

III. CALIBRATION PROCEDURE

The following calibration procedure was used. Artificial pulses were supplied to the input of the preamplifier and plots of chart deflection, D', *vs* millivolts input were made (e.g., Fig. 3). The calibration pulse was a negative step signal with a 1000-μsec exponential decay (to minimize undershoot of the amplifier) and was generated by a Hg switch generator; the pulse amplitude was determined by a Helipot across a calibrated voltage source. Following this, a plot of the output pulse height, E, of the No. 100 amplifier *vs* millivolts input was made (see Fig. 3). The output pulse height in volts is measured by the E (voltage) setting of the differential discriminator which is used for

[9] F. D. S. Butement, Phil. Mag. **349**, 208 (1953).
[10] J. V. Jelley and W. J. Whitehouse, Proc. Phys. Soc. (London) **A66**, 454 (1953).
[11] C. L. Cowen *et al.*, Phys. Rev. **90**, 493 (1953).
[12] H. Kallmann (private communication).
[13] See L. F. Fieser, *Experiments in Organic Chemistry* (D. C. Heath, Boston, 1941), second edition, p. 368.
[14] Joints made with this cement were somewhat permeable for toluene and dioxane—aluminum welds should be used for permanent tanks.

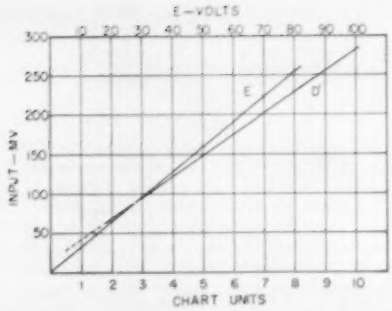

FIG. 3. Amplifier and pulse-lengthener calibrations. The ordinate is the amplitude in millivolts of the calibration pulse input. The abscissa (upper scale) gives the pulse output of the amplifier No. 100 as measured by the differential discriminator, E volts. The abscissa (lower scale) gives the chart deflection D'. The slight nonlinearity in the D' plot at small deflections is characteristic of diode pulse lengtheners.

analyzing the calibrating radioactive sources. The repetition rate of the Hg switch pulse generator is about 4/second in this part of the calibration, whereas single pulse operation is used for the chart deflection calibration.

The energy scale was determined by differential pulse-height analysis of the spectra of artificial radioactive sources (e.g., Figs. 4 and 5 for Cs^{137} and Ce^{144}).[15] Essentially the E (volts) scale of the differential discriminator served as the fiducial mark in these three calibrations, which had the end purpose of relating a particular chart deflection to a corresponding energy loss in the NaI crystal. The tank of scintillating liquid was removed during the calibrations.

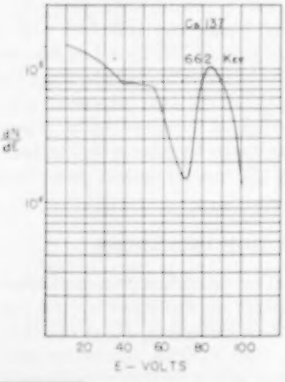

FIG. 4. Cs^{137} calibration curve. The ordinates are counts (per 20 seconds) for a 3 volt window; the abscissa is the pulse height in volts. The amplifier attenuation (Model 100 amplifier) is about 3 times the attenuation used for Fig. 5.

[15] The characteristic peaks in these spectra must be corrected by $-dE/2$ where dE is the differential discriminator window. This is seen easily by a graphical analysis for a differential discriminator which selects pulses in the voltage interval E to $(E-dE)$. The same analysis shows, incidentally, that the width of the pulse-height distribution curve is

$$\delta E/E \cong [(\delta E/E)_0^2 + (dE/E)^2]^{\frac{1}{2}},$$

where $(\delta E/E)_0$ is the width for vanishingly small window, dE. The dE used here was 3 volts. The broadening of the distribution curves due to this window is negligible.

IV. RESULTS

A test run was made using a three-liter tank of toluene (15 cm diameter×20 cm deep). The more significant counting rates are listed in Table I. Figure 6 is a differential pulse-height distribution of $\mu\gamma$-β events; the energy calibrations are estimated from a Cs^{137} calibration. The distribution is roughly Gaussian with a peak at approximately 90 kev and a full width of 50%. This peak is to be attributed to the $2p-1s$ mesonic x-ray of carbon.

The 4-liter tank of dioxane (Fig. 1) was substituted for the toluene and the measurements were continued. The more important counting rates (for a portion of these measurements) are shown in Table II. Energy calibrations were performed periodically using the photopeaks of the 663-kev gamma ray of Cs^{137} and the 134- and 80-kev gamma radiation from Ce^{144}. The extrapolation from the higher energy gamma rays (i.e., the 663-kev gamma ray of Cs^{137}) was not suitable because of a nonlinearity in the response of the 6364 photomultiplier.[16]

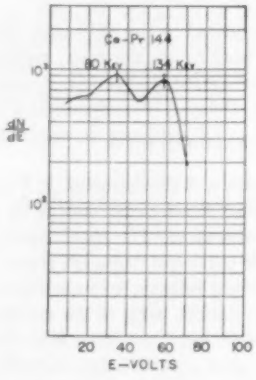

FIG. 5. Ce-Pr^{144} calibration curve. The ordinates are counts (per 10 seconds) for a 3-volt window; the abscissa is the pulse height in volts.

Figure 7 is the pulse-height distribution of 335 $\mu\gamma$-β (on scale) events.[17] The energies for carbon and oxygen are 83 kev and 146 kev. The full widths are 81% for the carbon peak and 53% for the oxygen peak. Some broadening of the carbon peak is anticipated because of Compton degradation of the oxygen $2p-1s$ peak. The suggestion of low-energy radiation at the lower edge

[16] Nonlinearity in a photomultiplier of similar construction has been reported [see R. W. Pringle and S. Standil, Phys. Rev. **80**, 762 (1950)]. S. Koslov (private communication) has observed that the combination of a NaI crystal used with a 5819 photomultiplier was linear over a wide range of energies, whereas the same NaI crystal with a type 6292 photomultiplier was nonlinear. In the present apparatus, using a NaI crystal and type 6364 photomultiplier, the calibration constant in kev/millivolt was 12% higher at 663 kev as compared to 134 kev. This nonlinearity may be related to the biasing of the photomultiplier shield element relative to the cathode and first dynode.

[17] Several different gain settings are represented in this distribution. The data have been corrected and plotted to the calibrated energy scale. The data listed in Tables II and III apply to a portion of these measurements at a given (constant) gain setting.

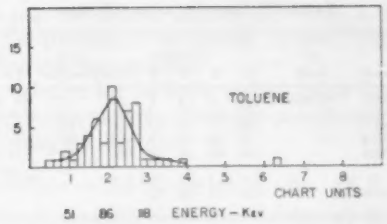

FIG. 6. Mesonic x-ray spectrum from carbon (toluene). The ordinate is the number of events per 0.2 chart division interval. The abscissa (upper number) is the chart division; the lower values are the corresponding energies in kev as estimated from a Cs^{137} calibration.

of the carbon peak is attributable to the combined effects of the oxygen $3d-2p$ radiation and the carbon $2p-1s$ escape peak.[18]

It is possible to extrapolate the carbon and oxygen curves to appropriate half-widths and to determine the areas under each curve. After corrections for detector efficiency and for the loss due to nuclear absorption, this procedure yields a ratio for captures on oxygen to those on carbon of 0.29 ± 0.04.

The time distribution of delayed coincidence μ-β events in toluene for the natural mixture of cosmic ray μ mesons is plotted in Fig. 8. A sufficient number of events are represented to yield a value of 2.13 ± 0.07 μsec for the mean life.[19] The time distribution of a portion of the $\mu\gamma$-β events in dioxane is listed in Table III and also plotted in Fig. 8 superimposed on a 2.13 μsec decay curve. The mean life of the negative μ mesons in oxygen is 1.9 μsec[20] (as compared to 2.0 μsec in carbon[21]). However, the diluting effect of the off-scale $\mu\gamma$-β events[22] would be expected to nullify the significance

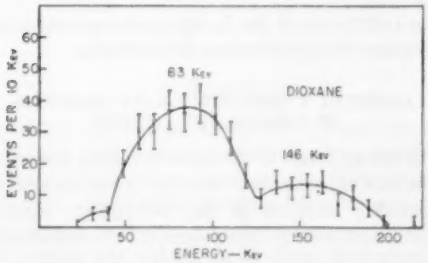

FIG. 7. Mesonic x-ray spectrum from carbon and oxygen (dioxane). The ordinate is the number of events per 10-kev energy interval; the abscissa is the energy as estimated from a Ce-Pr^{144} calibration.

[18] In the measurement of low-energy gamma radiation by NaI, the photoelectric peak is usually accompanied by a subsidiary peak (escape peak) lying below the main peak by the K shell binding energy of iodine (33 kev). This is due to events in which the iodine x-ray resulting from the photoelectric effect is not absorbed in the crystal.

[19] A. Fafarman and M. H. Shamos, Phys. Rev. **96**, 1096 (1954).

[20] H. K. Ticho, Phys. Rev. **74**, 1343 (1948).

[21] H. A. Morewitz and M. H. Shamos, Phys. Rev. **92**, 134 (1953).

[22] These usually correspond to the stopping of positive μ mesons n the NaI crystal.

TABLE I. Toluene (3-liter tank).

Running time	138 hr
$\mu\gamma$-β events (101, 40, 16, 4)	161
$\mu\gamma$-β events (on-scale; <370 kev)	54
$\mu\gamma$-β rate	1.20±0.09/hr
μ-β rate	12±2/hr
$\mu\gamma$ rate	64/min

of the slightly shortened mean life in oxygen on the delay distribution of the $\mu\gamma$-β events in dioxane.[22]

V. POSSIBLE SOURCES OF ERROR

A. Energy Measurement

The energy resolution at this energy (100 kev) is only ~40%.[24] Periodic energy calibrations showed an average deviation of ±2%.[25] The low resolution, together with the statistical uncertainties, makes it difficult to determine the position of the photoelectric peaks for the experimental curves. The calibrations showed the type 6364 photomultiplier to be nonlinear; the ratio of the calibration constants (kev/millivolt) at 660 kev and at 100 kev was 1.14±0.02. There is a small error attributable to the nonzero slope or irregularity of the stretched pulse.[26] The maximum correction for this is −2%. The pulse lengthener baseline showed a slight dependence on the counting rate which was less than 2% of full scale. The data in Fig 7 have been corrected for the nonlinearity of the photomultiplier and for the nonzero slope of the stretched γ pulse.

B. Accidental and Other Events

From the values in Table III, the calculated $N_{\mu\gamma}$ (accidental) = 0.008/min, which is negligible in relation to the $\mu\gamma$ rate of 76/min.

However, $N_{\mu\gamma\text{-}\beta}$ (accidental) = 0.17/hr. This is 10% of the observed rate; since the usual $\mu\gamma$ event is a meson passing completely through the NaI crystal, these accidentals will be off-scale events of several Mev.

TABLE II. Dioxane (4-liter tank).

Running time	266 hr
$\mu\gamma$-β events	401
$\mu\gamma$-β events (on-scale; <250 kev)	142
$\mu\gamma$-β rate	1.51+0.08/hr
μ-β rate	20±6/hr
$\mu\gamma$ rate	76/min

[23] In addition roughly twice as many captures of negative μ mesons occur on the carbon as on the oxygen. However, the predominant contribution is that of the off-scale events.

[24] Although better resolution would have been obtained with a smaller detector, a large area detector was chosen because of the low intensity of events.

[25] Based on the internal consistency of the various calibrations (i.e., no allowance is made for possible systematic errors).

[26] This refers to the γ pulse which is stretched from a duration of 4 μsec to one of 20 μsec whenever a $\mu\gamma$ coincidence occurs.

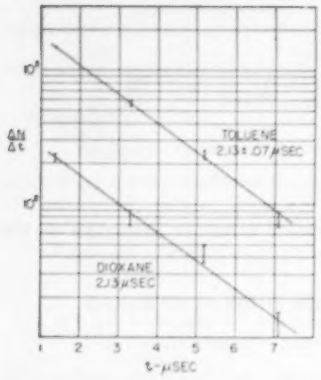

FIG. 8. Differential delay distributions for toluene and dioxane. The ordinate is the differential channel count, the abscissa the delay in μsec.

The above accidentals are attributable to random coincidences. However, the largest component of the $\mu\gamma$-β rate is due to positive mesons passing through the tank which stop and decay in the NaI crystal. Estimating the probability for the decay positron to pass through the tank giving an apparent $\mu\gamma$-β event, leads to a calculated rate which is 2 to 3 times as great as the calculated rate for the events under study; this calculation is in good accord with the experimental data (Table II); such events corresponding to the stopping and decay of positive mesons in the NaI crystal will, of course, be very energetic and off-scale (>10 Mev).

C. Capture Ratio

The experimental value for the ratio of captures in mesonic atom formation by oxygen and carbon was computed by two methods:

(a) measurement of the areas under the carbon and oxygen peaks.
(b) comparison of the peak values.

After correction for the detection efficiency and for the loss due to nuclear absorption, values of 0.29 ± 0.04 and 0.36 ± 0.04 were obtained. These values are in error because of Compton degradation of the oxygen $2p-1s$ radiation in the tank (~14 cm depth) and the escape peak (in the NaI crystal) of the oxygen $2p-1s$ radiation; both of these effects appear under the carbon peak. The expected result is a broadening of the carbon peak and this is in fact observed.

VI. DISCUSSION

An approximate calculation based on the known rate of meson stoppings in the tank and on the computed detection efficiency, indicates that almost every stopping meson makes a radiative transition to the ground ($1s$) state of a carbon or of an oxygen mesonic atom. The energy resolution is not sufficient to distinguish the presence of a small admixture of higher orbital transitions (e.g., $3p-1s$) in addition to the $2p-1s$ radiation.[27] However, the discrepancy between the measured energies and the computed values (Appendix I) for the $2p-1s$ carbon and oxygen mesonic x-rays, while not outside the experimental errors, indicate the presence of some transitions with $n>2$ to $n=1$.

TABLE III. Counting rates—dioxane.

Hours	$\mu\gamma$ Rate	Channel 1	2	3	4	$\mu\gamma$-β Total	$\mu\gamma$-β On-scale	$\mu\gamma$-β Total rate
18.7	74/min	18	4	4	1	27	7	1.4 ±0.3/hr
91.4	74	62	28	16	5	111	40	1.21±0.12
85.1	77	86	27	13	13	139	48	1.63±0.14
70.4	77	67	30	22	5	124	47	1.76±0.16
Totals 265.6		233	89	55	24	401	142	1.51±0.08
								on-scale 0.53±0.05
Totals corrected[a]		221	77	43	12			

[a] Corrected for accidental counts 0.044/hr in each channel.

The validity of the Z-dependence law for the probability of forming mesonic atoms on the various elements of a chemical compound remains obscure. The results in this experiment are vitiated partly because of the incomplete resolution of the carbon and oxygen curves, and because of Compton degradation of the energy of the oxygen mesonic x-ray, which shifts oxygen events to the carbon peak.[28] The surmounting of these difficulties involves the use of a thin dioxane absorber as opposed to the thick dioxane absorber used in the present experiment. The use of a thin absorber virtually rules out cosmic ray mesons as the source; however, an artificial μ-meson beam should be suitable, provided that a delayed coincidence method is used to eliminate the low-energy background radiation often present in accelerator experiments.

VII. ACKNOWLEDGMENTS

We wish to thank Dr. L. Spruch for several helpful suggestions during the course of this work.

APPENDIX I. MESONIC X-RAYS ENERGIES IN CARBON AND OXYGEN

The energy levels of the mesonic carbon and oxygen atoms can be computed from the point nucleus (hydrogen-like) solutions of the Schrödinger equation. The solutions (energy eigenvalues) for this equation are:

$$E_n=-\tfrac{1}{2}\mu c^2(\alpha Z/n)^2,$$

[27] This admixture should be small because of the greater statistical weight of the circular orbits, $l=n-1$, in the meson capture process. See G. R. Burbridge and A. H. DeBorde, Phys. Rev. 89, 189 (1953).

[28] *Note added in proof.*—To check the effect of the Compton scattering, a separate calibration has been performed using a "phantom," i.e., a container of water geometrically similar to the dioxane tank and having a weak Ce-Pr[144] source dispersed uniformly throughout. The observed spectrum did not differ markedly from that obtained with the bulk source; an upper limit of about 10% could be set on events lost from the 134-kev peak to lower energies. Hence it does not appear that Compton degradation of the oxygen $2p-1s$ radiation is responsible for the discrepancy.

where μ is the reduced mass of the meson, α the fine structure constant, Z the atomic number, and n the principal quantum number.

The solution for the finite nuclear radius (nonpoint source) is obtained by a first-order perturbation calculation using the potential.[29]

$$V(r) = -(Ze^2/R)(\tfrac{3}{2} - \tfrac{1}{2}r^2/R^2) \quad \text{for} \quad r \leq R$$
$$= -Ze^2/r \quad \text{for} \quad r \geq R,$$

where $R = 1.2 \times 10^{-13} A^{\frac{1}{3}}$ cm (nuclear radius).

It suffices for low-Z materials to calculate the perturbation of the $1s$ level. The higher levels $n \geq 2$, except in the heaviest elements, satisfy the point nucleus solutions. The fractional energy shift due to the perturbation is[30]

$$\Delta E/E_{1s} = -\tfrac{4}{3}Z^2(R/a_0)^2,$$

where $a_0 = \hbar^2/\mu e^2 = 2.52 \times 10^{-11}$ cm (radius of the first Bohr orbit of the mesonic hydrogen atom).

The K and L shell energies obtained from the point nucleus solutions of the Schrödinger and the Dirac[31] wave equations are shown in Table IV. The perturbation correction has been applied to the $1s$ level.

TABLE IV. μ-mesonic atoms—lowest energy levels (in Mev).

Z	$1s_{\frac{1}{2}}$	$2p_{\frac{1}{2}}$	$2p_{\frac{3}{2}}$ $2s_{\frac{1}{2}}$	$2p_{\frac{1}{2}} - 1s_{\frac{1}{2}}$	Computed from
6	−0.1018	−0.0254	⟶	0.0764	Schrödinger
	−0.1019	−0.0254	($2p_{\frac{3}{2}} - 12$ kev)	0.0765	Dirac
	−0.1015			0.0761	Perturbation of Dirac solution
8	−0.1823	−0.0456	⟶	0.1367	Schrödinger
	−0.1824	−0.0456	($2p_{\frac{3}{2}} - 47$ kev)	0.1368	Dirac
	−0.1807			0.1351	Perturbation of Dirac solution

[29] See reference 6, footnote on p. 173.

[30] This result is obtained also by L. N. Cooper and E. M. Henley, Phys. Rev. **92**, 801 (1953), their Eq. (11).

[31] $E_{n,j} = \mu c^2 \left[1 + \dfrac{(\alpha Z)^2}{\{n - |k| - (k^2 - \alpha^2 Z^2)^{\frac{1}{2}}\}^2}\right]^{-\frac{1}{2}}$
$\cong \mu c^2 \left[1 - \dfrac{(\alpha Z)^2}{2n^2} - \dfrac{(\alpha Z)^4}{2n^4}\left(\dfrac{n}{|k|} - \dfrac{3}{4}\right)\right]$, $k = -\ell - 1$ for $j = \ell + \frac{1}{2}$, $k = \ell$ for $j = \ell - \frac{1}{2}$.

PHYSICAL REVIEW VOLUME 100, NUMBER 3 NOVEMBER 1, 1955

Angular Correlation Effects in V-Particle Decay

S. B. TREIMAN AND H. W. WYLD, JR.
Palmer Physical Laboratory, Princeton University, Princeton, New Jersey

(Received June 6; revised manuscript received September 16, 1955)

In decay processes of the types: hyperon→nucleon+pion; or K-meson→pion+pion, the most general distribution function in η—the angle between the decay plane normal and a reference direction **N** normal to the line of flight of the unstable particle—has the form of a finite Fourier series. The degree of the highest harmonic is simply related to the spin of the unstable particle. The coefficients in the series depend on the state of polarization of the spin with respect to the reference direction **N**. It is possible however to set upper limits on the coefficients; this may prove useful in any attempt to analyze angular correlation data, particularly in the case of hyperon decay. The upper limits for various low spin values are computed, and other consequences of the angular momentum and parity conservation laws are discussed.

I. INTRODUCTION

ANGULAR correlation effects in V-particle decay have been investigated recently by a number of workers,[1–5] in an attempt to learn something about the spins of the new unstable particles. For reasons of parity and angular momentum conservation, a particle of spin zero or spin one-half must decay isotropically in its rest frame. In the case of particles which undergo two-body decay, this means that the distribution in η—the angle between the decay plane normal **n** and any reference direction **N** which is normal to the line of flight of the unstable particle and which is defined independently of **n**—must be uniform.[6] A nonuniform distribution in η would automatically imply spin greater than one-half; and from the form of the distribution (see below) one could set a lower limit to the value of the spin.

Even for particles of very large spin, however, angular correlation effects would show up only if the spins were somehow polarized (i.e., nonrandomly distributed) with respect to the reference direction **N**. This suggests that the effect, if it exists at all, would be most likely to manifest itself with unstable particles produced in low-energy interactions of elementary particles, e.g., the reaction $\pi^- + p \rightarrow$hyperon$+K$-meson observed at Brookhaven. Nevertheless, early Princeton work[1] on V^0-particles produced in generally complex

[1] Ballam, Hodson, Martin, Rau, Reynolds, and Treiman, Phys. Rev. **97**, 245 (1955); see also *Proceedings of the Fifth Annual Rochester Conference on High-Energy Physics* (Interscience Publishers, Inc., New York, 1955).

[2] Report by C. D. Anderson, *Proceedings of the Fifth Annual Rochester Conference on High-Energy Physics* (Interscience Publishers, Inc., New York, 1955).

[3] G. D. James and R. A. Salmeron, Phil. Mag. **46**, 571 (1955).

[4] Sreekantan, Pevsner, and Sandri, Phys. Rev. **98**, 642 (*A*) (1955).

[5] Fowler, Shutt, Thorndike, and Whittemore, Phys. Rev. **98**, 121 (1955).

[6] Treiman, Reynolds, and Hodson, Phys. Rev. **97**, 244 (1955).

cosmic-ray interactions gave some indication of angular correlation effects for events involving a pair of V^0-particles which have a common origin. However, other groups,[2-4] also working with cosmic-rays, found no appreciable effect. But recently, the Brookhaven workers[5] have reported results on the distribution in angle η between the decay and production planes of unstable particles, and they find a marked correlation effect for the hyperons, the angle η tending toward small values. They conclude that the spins of the hyperons are probably greater than one-half.

In view of the affirmative Brookhaven results, we consider it worthwhile to present a further discussion of the relationship of angular correlation effects and spin. The discussion does not involve any detailed model of the unstable particles but is instead based solely on the conservation laws of parity and angular momentum.

II. ANGULAR DISTRIBUTION FUNCTION

In a recent note it was shown that for a particle of given spin j, which undergoes two-body decay, the most general form of the angular distribution in η is given by[7]

$$p(\eta)=\frac{1}{2\pi}\times\left\{1+\sum_{M=2,4,\cdots}^{M_{max}}(A_M\cos M\eta+B_M\sin M\eta)\right\}; \quad (1)$$

where

$$M_{max}=\begin{cases}2j, & \text{(integral } j\text{)}\\ 2j-1, & \text{(half-odd integral } j\text{).}\end{cases} \quad (1')$$

In the derivation of this equation, it is assumed that the decay plane normal $\mathbf{n}$ is a vector with a well-defined *sense* as well as direction and that the angle η between $\mathbf{n}$ and the reference vector $\mathbf{N}$ ranges from 0 to 2π. (One could, for example, take $\mathbf{n}$ to have the sense of the vector product of the two final particle momenta, taken in a prescribed order.) In practice, however, one has not thus far associated a sense with $\mathbf{n}$, so that one in fact measures the smaller of the two angles between the directions of $\mathbf{n}$ and $\mathbf{N}$. For the sake of clarity we denote by η' the angle so defined ($0\leq\eta'\leq\frac{1}{2}\pi$). The distribution $p'(\eta')$ in η' is then related to the distribution in η by

$$p'(\eta')=p(\eta')+p(\pi-\eta')+p(\pi+\eta')+p(2\pi-\eta')=\frac{2}{\pi}\left\{1+\sum_{M=2,4,\cdots}^{M_{max}}A_M\cos M\eta'\right\},\quad\left(0\leq\eta'\leq\frac{\pi}{2}\right). \quad (2)$$

The equation for $p'(\eta')$ is more restricted in form than that for $p(\eta)$ because of the lumping together of probabilities from the four quadrants of η. Some information is then necessarily lost.

The angular momentum and parity conservation laws not only prescribe the above forms for $p(\eta)$ and $p'(\eta')$, however, but also impose other restrictions on the angular distribution. For one thing, the conservation laws can be used to set upper limits on the magnitudes of the Fourier coefficients A_M and B_M; and in any attempt to fit data to expressions of the above form it will be very helpful to take these limits into account. This is especially true in the case of hyperon decay, where, as it turns out, the upper limits on the coefficients are fairly small in certain cases (see Table I). The main purpose of the present work is to compute the limits on the Fourier coefficients. We shall also briefly discuss other consequences of the conservation laws.

Equation (1) is derived by forming the expression $|\psi|^2$—where ψ is the final state wave function in the rest system of the unstable particle—and integrating over all variables except for the azimuthal angle η of the relative momentum vector of the decay products (the z-axis lies along the line of flight of the unstable particle and the y-axis along the reference direction $\mathbf{N}$).[6] The Fourier coefficients A_M and B_M are evidently then the respective expectation values with respect to ψ of the operators $2\cos M\eta$ and $2\sin M\eta$[8]:

$$A_M=2\langle\psi|\cos M\eta|\psi\rangle,\qquad B_M=2\langle\psi|\sin M\eta|\psi\rangle. \quad (3)$$

The wave function ψ contains as a factor an angular momentum eigenfunction corresponding to j and having definite parity, determined by the parity of the unstable particle. This function can be expressed as a linear combination of the eigenfunctions φ_j^m of the operator $J_z(-j\leq m\leq j)$. We take the φ_j^m as our basis functions.

TABLE I. Maximum possible value of Fourier coefficient A_M (or B_M) in angular distribution $p(\eta)$ or $p'(\eta')$—for decay process of type: hyperon→nucleon+pion. The spin of the hyperon is denoted by j.

j	M	
3/2	2	0.577
5/2	2	0.775
	4	0.447
7/2	2	0.914
	4	0.577
	6	0.378
9/2	2	1.019
	4	0.655
	6	0.500
	8	0.333

[7] See reference 6. The equations are written here in a slightly different notation.

[8] Angular correlations effects must properly be discussed in terms of mixtures of states ψ; and expectation values must correspondingly be taken with respect to density matrices. For the present purposes, however, it is enough to consider only pure states.

We can then form the matrix elements of $\cos M\eta$ and $\sin M\eta$ with respect to the φ_j^m; and it is then evident from Eq. (3) that the maximum possible value of A_M, for example, is just equal to the largest eigenvalue of the resulting matrix $2\langle jm'|\cos M\eta|jm\rangle$. (Since the upper limits on A_M and B_M are clearly identical, we discuss the former only.)

III. LIMITS ON THE FOURIER COEFFICIENTS

For decay processes of both types: (a) hyperon→nucleon+pion; and (b) K-meson→pion+pion, one can show that the matrix elements are given by[9]

$$2\langle jm'|\cos M\eta|jm\rangle = \begin{cases} (-1)^{\frac{1}{2}M}\left[\dfrac{(j-m)!(j+m)!}{(j-m')!(j+m')!}\right]^{\frac{1}{2}}, & (m'=m\pm M) \\ 0, & \text{(otherwise)} \end{cases} \quad (4)$$

where

$$\epsilon=\pm 1 \quad \text{for} \quad |m'|\gtrless|m|.$$

As we have already seen, the maximum eigenvalue of the above matrix is just equal to the maximum possible value of the coefficient A_M in Eqs. (1) and (2). Under certain circumstances, mentioned below, it is possible to give a simple formula for the largest eigenvalue for given j and M. In other cases, we have determined the eigenvalues by numerical procedures. Results are set forth in Tables I and II, which refer to hyperon and K-meson decay, respectively.

In the case of hyperon decay (half-odd integral j), whenever $M\geq j+\frac{1}{2}$ the matrix takes the simple form in which nonvanishing elements occur only within the upper-right and lower-left quadrants. The maximum eigenvalue is then simply equal to the magnitude of the largest matrix element. For this, one finds from Eq. (4)

$$A_M{}^{\max}=\left(\frac{2j+1-M}{2j+1+M}\right)^{\frac{1}{2}}. \quad (5)$$

In particular, for the largest permissible value of M, $M=2j-1$, we have

$$A_{2j-1}{}^{\max}=(1/2j)^{\frac{1}{2}}. \quad (6)$$

It is apparent from these equations that for the larger values of M, the upper limits on the Fourier coefficients fall off with increasing j; whereas, from Table I we see that $A_M{}^{\max}$ increases with j for the smaller values of M.

In the case of K-meson decay (integral j), we note that the particular matrix element

$$2\langle j,\tfrac{1}{2}M|\cos M\eta|j,-\tfrac{1}{2}M\rangle$$

has absolute value unity. This means that there is always a state, namely $(1/\sqrt{2})(Y_j^{\frac{1}{2}M}\pm Y_j^{-\frac{1}{2}M})$, for which $A_M=1$. Thus, the upper limit on A_M is always at least unity. In fact, whenever $M\geq j$, the upper limit is precisely equal to unity. For $M<j$, the upper limit exceeds unity, although not by very much when the spin is fairly small (see Table II).

TABLE II. Maximum possible value of Fourier coefficient A_M (or B_M) in angular distribution $\rho(\eta)$ or $\rho'(\eta')$—for decay process of type: K-meson→pion+pion. The spin of the K-meson is denoted by j.

j	M	
1	2	1.00
2	2	1.00
	4	1.00
3	2	1.06
	4	1.00
	6	1.00
4	2	1.13
	4	1.00
	6	1.00
	8	1.00

IV. DISCUSSION AND FURTHER APPLICATIONS

It is perhaps worth emphasizing again that on the basis of the angular distribution data taken alone, there is no way to determine the exact value of the spin. As has already been pointed out, even if the spin were very large, the distribution in η might under the experimental conditions be uniform (unpolarized spins). The best one can do is determine a lower limit on the spin. There are many procedures which can be used for this purpose, all of them based on angular momentum and parity conservation and all, in part, independent of one another. The problem is to find the best procedure with respect to a given set of data, i.e., the procedure which leads to the largest lower bound on the spin j.

We have discussed two methods, which are partly independent of each other. The angular distribution $\rho'(\eta')$ can be expressed as a finite Fourier series. The degree of the highest harmonic required to fit a set of data automatically determines a lower limit on j. However, if any one of the Fourier coefficients A_M required to fit the data exceeds the limit imposed by angular momentum and parity conservation, one obtains a larger lower bound on j. For example, it could happen that the experimental data for a set of Λ^0-particle decay events is perfectly consistent with an angular distribution of the form $\rho'(\eta')=(2/\pi)(1+A_2\cos 2\eta')$, so that one has immediately $j\geq\frac{3}{2}$. But if the required value of A_2 is say 0.70, then from Table I it follows that in fact $j\geq 5/2$. Furthermore, it should be noted that there is no state for which two or more of the coefficients A_M have their maximum values simultaneously. Thus, when A_2 has its maximum value for given j, A_4 is certain to have a value less than its maximum.

[9] We would like to thank R. K. Adair and R. Dalitz for calling to our attention an error in our original expression for the matrix element.

TABLE III. Maximum possible value of $P'(\frac{1}{4}\pi)$, the probability that $\eta' \leq \frac{1}{4}\pi$—for decay process of type: hyperon→nucleon +pion.

j	
3/2	0.684
5/2	0.747
7/2	0.788
9/2	0.817

TABLE IV. Maximum possible value of $P'(\frac{1}{4}\pi)$, the probability that $\eta' \leq \frac{1}{4}\pi$—for decay process of type: K-meson→pion +pion.

j	
1	0.818
2	0.818
3	0.834
4	0.850

The number of Fourier terms, and the limits on their coefficients, by no means exhausts the limitations imposed by the conservation laws on the shape of $p'(\eta')$ for a given spin. We have emphasized these features because they are simple from a computational point of view and because they provide a useful basis for a first survey of experimental data. One could go on, however, and calculate for example the limits on the various moments of the angular distribution; or the limits on the actual value of $p'(\eta')$ itself for any specified angle η'. In such procedures one maximizes not the individual Fourier coefficients taken one at a time but rather a suitable sum of coefficients. Thus, the state which maximizes A_2, for example, is not the same as the state which maximizes the value of $p'(\eta')$ for η' equal to say 50°. It could happen that a given set of data is perfectly consistent with a certain j value on the basis of the tests described above but that the experimental value of $p'(50°)$, say, exceeds the limit for that value of j.

We mention one particular test which seems to be especially suited to analyzing quickly a limited amount of data and which occurred to us in connection with the Brookhaven results.[4] The Brookhaven workers find that in seven examples of hyperon decay ($4\Lambda^0; 3Y^{\pm}$) the angle η' between the decay and production planes is less than ~45° in all cases. We therefore ask: for given spin of the hyperon, what is the maximum possible value for the fraction of cases in which $\eta' < \frac{1}{4}\pi$? We denote the integral distribution by $P'(\eta')$, where

$$P'(\eta') = \int_0^{\eta'} p'(\eta'')d\eta''. \tag{7}$$

From Eq. (2), it follows that

$$P'(\tfrac{1}{4}\pi) = \frac{1}{2} + \frac{1}{\pi} \times \sum_{M=2,4,\cdots}^{M_{max}} \frac{1}{M} A_M(-1)^{\frac{1}{2}(M-2)}[1-(-1)^{\frac{1}{2}M}] = \frac{1}{2} + \frac{1}{\pi}\{A_2 - \tfrac{1}{3}A_6 + \cdots\}. \tag{8}$$

Just as before, we form the matrices A_M with respect to the basis function φ_j^m; and then, summing these matrices according to Eq. (8), we find the matrix for $P'(\frac{1}{4}\pi)$. The maximum eigenvalue gives the largest possible value of $P'(\frac{1}{4}\pi)$. We have carried out this procedure for the case of hyperon decay, for spins up to $j=9/2$ inclusive; and K-meson decay, for spins up to $j=4$ inclusive. The results are given in Tables III and IV, respectively. It should be noted, incidentally, that because of the symmetry about $\frac{1}{4}\pi$, these results also represent the upper limits on the probability that η' lies between $\frac{1}{4}\pi$ and $\frac{1}{2}\pi$.

Comparison of Tables I and III on the one hand with Tables II and IV on the other indicates that the maximum possible deviations from isotropy are much more restricted in the case of hyperon decay than in the case of K-meson decay. Pronounced angular correlations in the case of hyperon decay would immediately force one to a high spin assignment for the hyperon. Although the experimental situation is far from clear as yet, the results reported from Brookhaven seem to point in this direction.

Diffusion Chamber Study of Very Slow Mesons. III. Scattering of Negative Pions in Hydrogen*

M. C. RINEHART,† K. C. ROGERS, AND L. M. LEDERMAN
Department of Physics, Columbia University, New York, New York

(Received July 1, 1955)

The elastic scattering in hydrogen of negative pions near 15 Mev is studied. In a path length represented by 8300 π-μ decays, twenty-six events were observed. At these low energies, the S-wave dominates the scattering. Treating the small P-wave and large Coulomb contributions as known, the data is found to be well represented by an S-wave phase shift proportional to momentum. Under this assumption, the phase shift parameters are given by the relation: $\alpha_3+2\alpha_1=(0.25\pm0.05)p/\mu c$ in radians.

A. INTRODUCTION

THE experimental arrangement previously described[1,2] has been employed in a search for pion-hydrogen scatterings. This investigation was motivated by the promising simplification that, at sufficiently low energy, only S-wave and Coulomb effects determine the scattering. Interest in the S-wave has been generated by ambiguities in the sign of the phase shift, by the apparently anomalous energy dependence[3] and the theoretical speculations thereby inspired,[4–6] and by the fact that the same low-energy S-wave parameters are contained in other phenomena: The Panofsky effect and the pi-mesonic x-rays.[7]

B. EXPERIMENTAL PROCEDURE

The 60-Mev π^- beam of the Nevis Cyclotron was moderated and allowed to spiral into the high-pressure hydrogen gas (density=0.002 g/cm³) of the diffusion cloud chamber. The pion spectrum obtained (Table I) is a compromise between pion flux per photograph and background. The problem of obtaining a reasonable flux of very low-energy pions is complicated by the low stopping power of the gas, the enormous straggling and scattering of the moderated beam and by the geometry and magnetic field of the cloud chamber.

Scanning involved the counting of $\pi\to\mu$ decays in flight, these being characterized by a deflection of $\geq 5°$ in either of the stereo views. This data together with the known lifetime and decay kinematics leads to a knowledge of the total pion path length as a function of momentum. The gas density is determined from continuous monitoring of pressure and temperature distribution in the gas. The latter data is obtained from thermistors which are embedded in the stainless walls of the chamber. Wall and gas temperatures at the same height were correlated by a run in which horizontal thermometers were suspended in the gas. The temperature at the center of the sensitive layer was −40°C. Corrections to the flux count are detailed in Table I.

TABLE I. Flux determination.

Interval (Mev, lab)	2.5–5	5–10	10–15	15–20	20–25	25–30
Uncorrected number decays counted	1290	2080	2000	1470	880	580
Coulomb scattering correction	−11%	−4%	−2%	−1.1%	−8%	−0.9%
Fraction of scatterings counted using 5° cutoff	0.98	0.96	0.95	0.94	0.93	0.92
5° cutoff flux correction[a]	6.5%	8.5%	10.5%	13%	15%	16.5%
Corrected number decays counted[b]	1230	2190	2160	1620	970	640
Pion path length kilometers	2.16	5.47	7.09	6.36	4.36	3.22

[a] The number of π-μ decays which project to less than 5° is deduced from the decay kinematics.
[b] An additional very small geometric correction is included here. Also considered is the small effect of scatterings which are above the cut-off angle but which project to less than 5°.

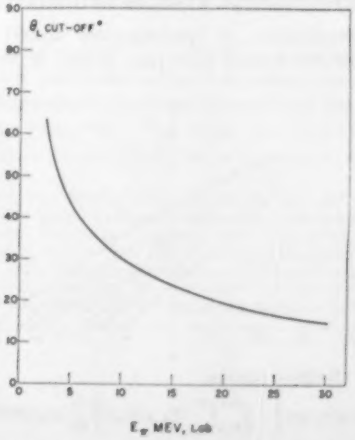

FIG. 1. Minimum acceptable scattering angle as determined from criterion that recoil proton have a range ≥1 mm.

* This research is supported in part by the joint program of the Office of Naval Research and the U. S. Atomic Energy Commission.
† Now at Hudson Laboratories, Dobbs Ferry, New York.
[1] Sargent, Cornelius, Rinehart, Lederman, and Rogers, Phys. Rev. **98**, 1349 (1955).
[2] Sargent, Rinehart, Rogers, and Lederman, Phys. Rev. **99**, 885 (1955).
[3] de Hoffmann, Metropolis, Alei, and Bethe, Phys. Rev. **95**, 1586 (1954).
[4] R. Marshak, Phys. Rev. **88**, 1208 (1954).
[5] H. P. Noyes and A. E. Woodruff, Phys. Rev. **94**, 1401 (1954).
[6] M. Ross, Phys. Rev. **95**, 1687 (1955).
[7] Deser, Goldberger, Baumann, and Thirring, Phys. Rev. **96**, 773 (1954); K. A. Brueckner, Phys. Rev. **98**, 769 (1955).

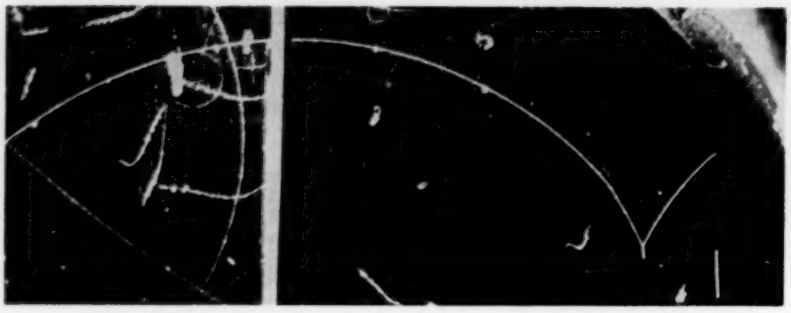

FIG. 2. Diffusion chamber photograph of a 3-Mev meson scattering in hydrogen. Both recoil proton and scattered meson come to rest in the gas.

All deflections are examined closely for correlated recoils at the vertex. Events with recoil tracks are measured and the results compared with the predictions of pion-hydrogen kinematics. The decay and scattering kinematics are not sufficiently different over the entire range of angles to distinguish a scattering event from a decay with accidental association of a blob or with a delta ray at the vertex. This circumstance forced the adoption of a minimum proton recoil length criterion of 1.0 mm. The remaining accidental coincidence rate was then negligible. Figure 1 gives the minimum scattering angle (a function of pion energy) inferred from the recoil criterion. Figure 2 illustrates a "typical" pion-hydrogen collision.

The scanning efficiency was determined by independent rescanning of the film. The scanning was considered satisfactory when the second scanning was 90% efficient in the π-μ decay count relative to the first. The greatest contribution to error in cross section arises from the counting of small-angle π-μ decays. The projected angular distribution of π-μ decay angles is a check that these errors are small compared to statistical errors.

C. EXPERIMENTAL RESULTS AND ANALYSES

The examination of approximately 45 000 photographs yielded a total pion path length of 30 km as inferred from about 8000 π-μ decays. (The total scanning time amounted to about 300 scanning days). A total of twenty-six acceptable scattering events were counted. The relevant data is presented in Table II.

The large spread in energy of the flux and of the events together with the limited statistics makes the method of maximum likelihood the appropriate tool for the most efficient utilization of the data.[8]

The π^--proton elastic scattering cross section, for sufficiently low energy, is[9]

$$\frac{d\sigma}{d\Omega}=\lambda\left[\left(\frac{e^2/\hbar v_r}{2\sin^2(\theta/2)}+\frac{2\alpha_1+\alpha_3}{3}+\frac{2\alpha_{33}}{3}\cos\theta\right)^2+\frac{\alpha_{33}^2}{9}\sin^2\theta\right]. \quad (1)$$

In the maximum likelihood procedure the P-wave (α_{33}) and Coulomb contributions are treated as known functions of momentum[10] and the likelihood function is maximized to obtain the best value for the S-wave parameter, $2\alpha_1+\alpha_3$. The first assumption made is that this quantity varies linearly over the momentum interval $(0.2\leqq p/\mu c\leqq 0.6)$:

$$2\alpha_1+\alpha_3=m+q\eta \text{ (radians)}, \quad (2)$$

where $\eta=p/\mu c$.

The likelihood function is plotted in Fig. 3. The result of the statistical analysis is:

$$m=0 \text{ radian}, \quad q=0.25 \text{ radian}. \quad (3)$$

Permissible variations may be read from Fig. 3.

The momentum interval was next split in an attempt to observe a change in slope between the 2.5–10 Mev interval and 10–30 Mev interval. The best fit in each region turned out to be identical to (3). However, within the very poor statistics which resulted, the data

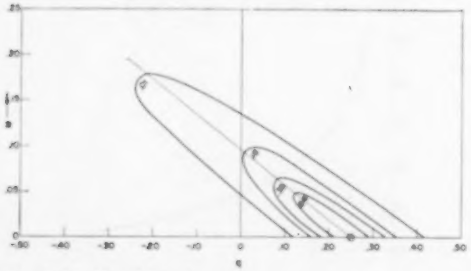

FIG. 3. Likelihood function

$$L(m,q)=\exp\left[-\int_{E_1}^{E_2}\int_{\theta_{\min}}^{\pi}N_{\theta,E}(m,q)\prod_1^{26}\frac{d\sigma}{d\Omega}(m,q)d\theta dE\right]$$

for S-wave scattering parameters: $\alpha_1+2\alpha_3=m+q\eta$. The likelihood is normalized to unity at the maximum value. N is the expected number of events at θ, E, using parameters m, q.

[8] F. Solmitz (unpublished mimeographed note). The authors wish to thank Dr. J. Orear for calling our attention to this note and for suggestions on the application of maximum likelihood to this problem.

[9] L. Van Hove, Phys. Rev. **88**, 1358 (1952); F. Solmitz, Phys. Rev., **94**, 1799 (1954). Here we assume that we neglect all but the largest P-wave phase shift.

[10] See reference 3 and J. Orear, Phys. Rev. **96**, 176 (1954).

could tolerate a change in slope as large from 0.30η in the high-momentum interval to 0.10η in the low-momentum interval. Under the assumption that $m=0$, a standard error may be assigned to the average best fit slope over the entire interval:

$$2\alpha_1+\alpha_3=(0.25\pm0.05)\eta, \quad (4)$$

where the error arises wholly from the statistics of 26 events. The result is not very sensitive to reasonable uncertainties in the P-wave extrapolation, assuming an initial η^3 dependence. Systematic errors due to scanning, flux count etc., are estimated to be less than 20 percent of the statistical error. The small amount of P-wave eliminates the possibility of sign ambiguity which appears at higher energies.[11]

D. DISCUSSION

In order to obtain α_1 and α_3 separately, this result must be combined with those of other experiments. These are either π^+ scattering which yields α_3 directly or π^- charge-exchange scattering which yields $\alpha_1-\alpha_3$. At present the π^+ scattering data below 30 Mev are quite preliminary.[12,13] The charge exchange scattering at 42, 30, and 20 Mev has been studied by Spry[14] and by Tinlot and Roberts.[15] We take as the best value

$$\alpha_1-\alpha_3=(0.27\pm0.03)\eta. \quad (5)$$

The combination of (4) and (5) leads to the solution:

$$\alpha_1=(+0.17\pm0.04)\eta, \quad \alpha_3=(-0.10\pm0.02)\eta \quad (6)$$

It is interesting to note that this solution is essentially that obtained by Orear[10] from an analysis which weighted data above 30 Mev most heavily. The solutions (6) for α_3 are also in agreement with the available π^+ data.[12,13] Recent experiments with pi-mesonic x-rays[16] give convincing evidence that the nuclear potential is repulsive for S-wave mesons. This has been interpreted[7] as establishing at least the sign of $(\alpha_1+2\alpha_3)$ as negative, in agreement with (6), but not in agreement with solutions which make use of these results together with the Panofsky effect, photomeson production, and detailed balancing arguments.[17]

[11] Bodansky, Sachs, and Steinberger, Phys. Rev. **93**, 1367 (1954).
[12] J. Orear, Phys. Rev. **98**, 239A (1955).
[13] S. Whetstone and D. Stork, Phys. Rev. **99**, 673(A) (1955).
[14] W. Spry, Phys. Rev. **95**, 1295 (1954).
[15] J. Tinlot and A. Roberts, Phys. Rev. **95**, 137 (1954).
[16] Stearns, Stearns, Di Benedetti, and Leipuner, Phys. Rev. **96**, 804 (1955); Camac, McGuire, Platt, and Schulte, Phys. Rev. **99**, 897 (1955).
[17] A nonlinear extrapolation to zero which would give agreement with the Panofsky effect and the condition $\alpha_1+2\alpha_3<0$ implies $d^2\alpha_1/d\eta^2>0$. For detailed objections to this behavior see H. P. Noyes, *Fifth Annual Rochester Conference on High Energy Physics* (Interscience Publishing Company, New York, 1955). A crude verification of the Panofsky ratio is obtained from reference 1 on internal pairs by assuming the validity of the theoretical branching ratios. This yields $(\pi^-+p\to\pi^0+n)/(\pi^-+p\to n+\gamma)=1.0\pm0.5$, where the uncertainty is in the nature of a maximum error.

TABLE II. Pion-proton scattering events.

C.m. energy Mev	C.m. scattering angle (degrees)
2.1	81
2.1	130
3.2	79
3.3	121
4.0	72
4.8	120
5.8	52
6.4	52
6.5	41
7.4	64
7.8	42
8.1	46
8.4	95
10	131
10.5	65
11.3	57
11.5	29
11.9	94
12	39
12.7	38
13	32
13	101
18.4	109
19	43
20	24
22	124

A much more detailed study of meson scattering at even lower energies would be of great interest but will be achieved only with enormous labor, using this technique. The new liquid hydrogen bubble chamber device is an ideal instrument for this type of study and will probably account for the next advance in this domain.

ACKNOWLEDGMENTS

The authors wish to acknowledge the contributions of Dr. C. P. Sargent to the early phases of this investigation. Miss Kate Lien of the Scandinavian-American trainee program contributed strongly to the scanning effort.

Note added in proof.—A new result for the minus-plus photo pion production ratio in deuterium was reported by G. Bernardini at the Pisa Conference on Elementary Particles, June, 1955. This raises the Panofsky effect result to $\alpha_1-\alpha_3=0.23\pm0.02\eta$ in agreement with (5).

Polarization of Protons Elastically Scattered from Nuclei*

R. M. STERNHEIMER
Brookhaven National Laboratory, Upton, New York
(Received July 12, 1955)

The polarization of 130-Mev protons elastically scattered from Be, C, Al, and Fe has been calculated by means of the optical model of the nucleus, including a spin-orbit coupling term. The results are in reasonable agreement with the measurements of Dickson, Rose, and Salter. Calculations were also carried out for proton energies of 50 Mev and 90 Mev, in order to explain the rapid decrease of the polarization as the energy is decreased below 130 Mev. By using a central potential whose real part decreases with increasing proton energy between 50 Mev and 130 Mev, reasonably good agreement was obtained for the dependence of the polarization on energy for Be and C.

I. INTRODUCTION

SEVERAL experiments[1] have shown that high-energy protons elastically scattered from nuclei have a large spin polarization. Both the magnitude and the direction[2] of the observed polarization can be accounted for by the spin-orbit coupling introduced by Mayer and Jensen for the nuclear shell model.[3] Dickson, Rose, and Salter[4] have recently measured the polarization of 130-Mev protons elastically scattered from various nuclei. These authors[4] have also shown that the polarization P for Be and C at scattering angles of 20° and 30° decreases rapidly as the proton energy is decreased below 130 Mev. The purpose of this paper is to present calculations of P for energies of 50–130 Mev, using the optical model of the nucleus.[5] It was suggested by Rose[6] that the rapid decrease of P as the energy T is decreased may be due to the increase of the magnitude of the real potential V_r with decreasing T, which was found by Taylor[7] and by Mandl and Skyrme.[8] This expectation was verified in the present calculations in which reasonable agreement has been obtained for the variation of P with energy, by assuming values for the parameters of the optical model which reproduce approximately the measured total cross sections as a function of energy. The phase shifts were obtained by means of the WKB approximation, using a Woods-Saxon[9] type of radial dependence for the central potential V, i.e., a uniform potential well near the center of the nucleus, which goes over into an exponential tail at large distances. The spin-orbit coupling U was taken proportional to $(1/r)(dV/dr)$.

II. RESULTS OF THE CALCULATIONS

The calculations of P were carried out by the same procedure as in the earlier work[10] on the polarization of 300-Mev protons[11] scattered from Al. The central potential was taken as[9]

$$V=\frac{V_r+iV_i}{1+\exp[(r-r_0)/a]}, \tag{1}$$

where V_r and V_i determine the real and imaginary parts of V, respectively; r_0 is the nuclear radius and a determines the length of the exponential tail. In most of the calculations, a was taken as 0.49×10^{-13} cm, which is the value used by Woods and Saxon[9] for the scattering of 22-Mev protons by Pt. In the work of I, r_0 was taken as $1.07\times10^{-13}A^{\frac{1}{3}}$ cm. Preliminary calculations for energies of 50–130 Mev were carried out with this r_0, but it was found that the calculated total neutron cross sections[12] and absorption cross sections[13] are appreciably smaller than the experimental values for any reasonable choice of V_r and V_i. For this reason, r_0 was increased to $1.23\times10^{-13}A^{\frac{1}{3}}$ cm. It should be noted that the calculated polarization is not sensitive to the choice of r_0. With the present choice of r_0 and a, $\langle r^2\rangle^{\frac{1}{2}}$ as given by Eq. (25) of I is 2.83, 3.39, and 4.07×10^{-13} cm for C, Al, and Fe, respectively. These values are somewhat higher than $\langle r^2\rangle^{\frac{1}{2}}$

* Work performed under the auspices of the U. S. Atomic Energy Commission.

[1] Oxley, Cartwright, and Rouvina, Phys. Rev. **93**, 806 (1954); Chamberlain, Segrè, Tripp, Wiegand, and Ypsilantis, Phys. Rev. **93**, 1430 (1954); Marshall, Marshall, and de Carvalho, Phys. Rev. **93**, 1431 (1954); J. M. Dickson and D. C. Salter, Nature **173**, 946 (1954); de Carvalho, Marshall, and Marshall, Phys. Rev. **96**, 1081 (1954).

[2] L. Marshall and J. Marshall, Nature **174**, 1184 (1954); Phys. Rev. **98**, 1398 (1955).

[3] E. Fermi, Nuovo cimento **11**, 407 (1954); W. Heckrotte and J. V. Lepore, Phys. Rev. **94**, 500 (1954); **95**, 1109 (1954); Snow, Sternheimer, and Yang, Phys. Rev. **94**, 1073 (1954); B. J. Malenka, Phys. Rev. **95**, 522 (1954); R. M. Sternheimer, Phys. Rev. **95**, 587 (1954).

[4] Dickson, Rose, and Salter, Proc. Phys. Soc. (London) **68**, 361 (1955).

[5] Fernbach, Serber, and Taylor, Phys. Rev. **75**, 1352 (1949).

[6] B. Rose (private communication). I would like to thank Dr. Rose for this suggestion and for showing me some data in advance of publication.

[7] T. B. Taylor, Phys. Rev. **92**, 831 (1953), and thesis, Cornell University, 1954 (unpublished).

[8] F. Mandl and T. H. R. Skyrme, Phil. Mag. **44**, 1028 (1953).

[9] R. D. Woods and D. S. Saxon, Phys. Rev. **95**, 577 (1954).

[10] R. M. Sternheimer, Phys. Rev. **97**, 1314 (1955). This paper will be referred to as I. In Eq. (4) of I, the contribution of $Ul\cdot\sigma$ is correctly given for the plus sign (σ parallel to l), but for the minus sign, $-kbl/(2T)$ should be replaced by $-kb(l+1)/(2T)$. The omission of the term 1 has a negligible effect on the results of I since the important phase shifts have l values of order 10.

[11] Chamberlain, Segrè, Tripp, Wiegand, and Ypsilantis, Phys. Rev. **95**, 1105 (1954).

[12] A. E. Taylor and E. Wood, Phil. Mag. **44**, 95 (1953).

[13] A survey of absorption cross sections for protons of various energies is given by Millburn, Birnbaum, Crandall, and Schecter, Phys. Rev. **95**, 1268 (1954).

for the nuclear charge distribution[14,15] which is $\approx 0.95 \times 10^{-13} A^{\frac{1}{3}}$ cm. The difference can be accounted for by the finite range of the nuclear forces. The potential (1) used in the present work corresponds to an effective square well of radius $\sim 1.4 \times 10^{-13} A^{\frac{1}{3}}$ cm. This value is close to the nuclear radius used in the calculations of Taylor[7] and of Mandl and Skyrme.[8]

The calculations were carried out for Be, C, Al, and Fe. The total absorption cross section σ_a is given by Eq. (24) of I. The total neutron cross section σ_t (absorption + diffraction scattering) is obtained from the imaginary part of the forward scattering amplitude. One finds

$$\sigma_t = \frac{2\pi}{k^2} \sum_{l=0}^{l_m} \left\{ (l+1)\left[1-\exp\left(-KA\left(\frac{l+\frac{1}{2}}{k}\right)\right) \times \cos 2\delta_{l,n,r}^{+}\right] + l\left[1-\exp\left(-KA\left(\frac{l+\frac{1}{2}}{k}\right)\right) \times \cos 2\delta_{l,n,r}^{-}\right]\right\}, \quad (2)$$

where k = wave number of incident proton, K = reciprocal absorption mean free path at the center of the nucleus, A is the integral over V defined by Eq. (3) of I; $\delta_{l,n,r}^{\pm}$ is the real part of the nuclear phase shift $\delta_{l,n}^{\pm}$ for the angular momentum l; l_m is the maximum l which contributes. $\delta_{l,n}^{\pm}$ is given by Eq. (5) of I; the optical parameter k_1 for the center of the nucleus is obtained from $|V_r|$ by means of[5]

$$k_1 = k[(1+|V_r|/T)^{\frac{1}{2}} - 1]. \quad (3)$$

At $T = 130$ Mev, Eq. (3) is practically equivalent to the relation $k_1 = k|V_r|/(2T)$ used in I. We note that σ_t depends on the spin-orbit coupling $U(r)\mathbf{l}\cdot\boldsymbol{\sigma}$ since it involves separately the $\delta_{l,n}^{+}$ and $\delta_{l,n}^{-}$. As explained below, $U(r)$ was taken such that its maximum value $U_{\max}$ (occurring near $r = r_0$) is 1 Mev for each element and independent of energy. σ_t and σ_a were calculated for various values of V_r and K. It was found that agreement within ~ 20 percent for σ_t and σ_a can be obtained by assuming that $|V_r|$ decreases from 55 Mev at $T = 50$ Mev to 35 Mev at $T = 90$ Mev and 15 Mev at $T = 130$ Mev. As previously shown by Taylor[7] and by Mandl and Skyrme,[8] this decrease is necessary in order to account for the decrease of σ_t with T. K was assumed to decrease from 4.5×10^{12} cm^{-1} at $T = 50$ Mev to 4.0×10^{12} cm^{-1} at $T = 90$ Mev and 3.5×10^{12} cm^{-1} at $T = 130$ Mev.[16] As an indication of the agreement obtained, we note that for Al, the calculated σ_t is 730, 1090 and 1310 mb at $T = 130$, 90, and 50 Mev, respectively, as compared to the experimental values[12] 770, 1090, and 1630 mb. The calculated σ_a is 450, 480, and 500 mb at $T = 130$, 90, and 50 Mev, respectively, as compared to the measured values[13] 430, 470, and 500 mb. For the other elements the agreement is similar to that obtained for Al. For C, σ_t agrees with experiment within 10 percent, but the calculated σ_a is ~ 20 percent too high. For Fe, the calculated σ_t is ~ 10 percent too low at 130 Mev, and ~ 20 percent too low at 50 Mev; the calculated σ_a is correct within 10 percent. We note that a small change of V_r and K would not affect significantly the behavior of the polarization.

The values of K given above may be compared with the corresponding values of $\eta\rho(0)\bar{\sigma}$, where $\rho(0)$ is the density of nucleons at the center of the nucleus, $\bar{\sigma}$ is the average of the p-p and n-p cross sections at the energy $T_n = T + |V_r|$ of the proton inside the nucleus; η is a factor giving the reduction of the cross sections in the nucleus due to the Pauli principle. Following Goldberger[17] we used $\eta = 1 - (7/5)(E_F/T_n)$, where E_F is the Fermi energy which was taken as 22 Mev. Assuming that the nucleon density is proportional to $1/\{1+\exp[(r-r_0)/a]\}$, one finds $\rho(0) = 1.09 \times 10^{38}$ cm^{-3} for Al. Using the measured values of[18] $\bar{\sigma}$, one obtains $\eta\rho(0)\bar{\sigma} = 4.0$, 3.8, and 3.5×10^{12} cm^{-1} for $T = 50$, 90, and 130 Mev, respectively. These values are quite close to the constants K used in the calculations.

Concerning the dependence of $|V_r|$ on T, we note that at $T = 0$, V_r can be determined from the requirement that the neutron scattering length be zero for lithium ($A = 7$) and for vanadium ($A = 50$).[19] Using the potential (1), s wave functions were obtained for various values of V_r (with $V_s = 0$, $a = 0.49 \times 10^{-13}$ cm) for both Li ($r_0 = 2.35 \times 10^{-13}$ cm) and V ($r_0 = 4.53 \times 10^{-13}$ cm). V_r was varied until an s function was found which gives zero scattering length. This wave function has one node for Li and two nodes for V. The appropriate values of V_r are -53.3 Mev for Li and -51.3 Mev for V. This result together with the choice $V_r = -55$ Mev at $T = 50$ Mev indicates that $|V_r|$ may remain approximately constant for $T \leqq 50$ Mev before decreasing to the small value of ~ 15 Mev at 130 Mev.[7,8,20]

With the above values of $|V_r|$, Eq. (3) gives $k_1 = 1.4 \times 10^{12}$ cm^{-1} at $T = 130$ Mev, 3.8×10^{12} cm^{-1} at $T = 90$ Mev, and 7.1×10^{12} cm^{-1} at $T = 50$ Mev. These constants, together with the values of K given above, were used in evaluating P by means of Eqs. (3)–(19) of I. It may be noted that the integrals A and B of I were evaluated numerically for each nucleus, i.e., for each set of values r_0 and a. In these calculations, the Coulomb scattering was taken as that of a uniform charge distribution of radius r_0.

[14] Hofstadter, Fechter, and McIntyre, Phys. Rev. **92**, 978 (1953); D. G. Ravenhall and D. R. Yennie, Phys. Rev. **96**, 239 (1954).

[15] V. L. Fitch and J. Rainwater, Phys. Rev. **92**, 789 (1953); L. N. Cooper and E. M. Henley, Phys. Rev. **92**, 801 (1953).

[16] This value of K corresponds to an imaginary potential $V_i = -18$ Mev.

[17] M. L. Goldberger, Phys. Rev. **74**, 1269 (1948).

[18] B. Rossi, *High Energy Particles* (Prentice-Hall, Inc., New York, 1952), p. 347.

[19] R. K. Adair, Phys. Rev. **94**, 737 (1954); Feshbach, Porter, and Weisskopf, Phys. Rev. **96**, 448 (1954).

[20] R. Jastrow, Phys. Rev. **82**, 261 (1951).

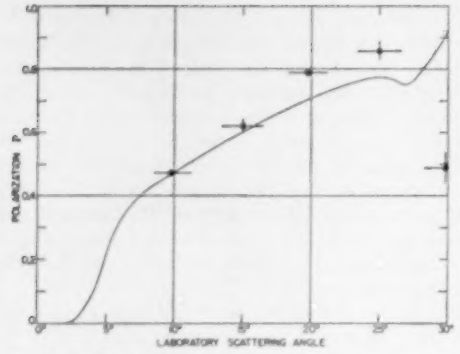

FIG. 1. Polarization P for 130-Mev protons scattered from C, calculated for the Woods-Saxon potential with $a=0.49\times10^{-13}$ cm. The circles represent the experimental values of Dickson, Rose, and Salter.[4]

The spin-orbit coupling $U(r)$ was taken proportional to $(1/r)(dV/dr)$ and is given by

$$U(r)=-\frac{b\exp[(r-r_0)/a]}{r\{1+\exp[(r-r_0)/a]\}^2}, \tag{4}$$

where b=constant. The maximum of U occurs near $r=r_0$[21]; its magnitude will be called U_{max}. The parameter b was so adjusted that U_{max} is the same for each element. This value of U_{max} was obtained from the calculations of P for C at 130 Mev. Upon taking $r_0=2.81\times10^{-13}$ cm, $a=0.49\times10^{-13}$ cm, $V_r=-15$ Mev, and $K=3.5\times10^{12}$ cm^{-1}, it was found that for $U_{max}=1.0$ Mev, one obtains reasonable agreement with the experimental points,[4] as shown in Fig. 1. The corresponding curve of P for Be at 130 Mev is not shown; the agreement obtained is about the same as for C.

Figure 2 shows the results of the calculations for Al at 130 Mev. Curve A was obtained for $r_0=3.68\times10^{-13}$ cm, $a=0.49\times10^{-13}$ cm, $V_r=-15$ Mev, $K=3.5\times10^{12}$ cm^{-1}, and $U_{max}=1.0$ Mev. The agreement with experiment is reasonably good for scattering angles $\theta<18°$. At 23°, P has a minimum which occurs at the same angle as the diffraction minimum of the differential cross section $d\sigma/d\Omega$. Neither minimum is observed, although the slope of the measured $d\sigma/d\Omega$ *vs* θ curves[4] changes abruptly at this angle. This discrepancy is probably due in part to the limited angular resolution of the apparatus which was[4] ±1.5°. As shown by Fig. 2, the calculated P drops below 0.6 only between $\theta=20°$ and 23°. In order to determine whether the minimum of P could be removed by assuming a more gradual drop of V at the nuclear boundary, P was recalculated with a larger value of a. The results of this calculation are shown as curve B. The constants used were: $r_0=3.68\times10^{-13}$ cm, $a=0.80\times10^{-13}$ cm, $V_r=-15$ Mev, $K=2.5\times10^{12}$ cm^{-1}, and $U_{max}=0.45$ Mev. Because of the increase of a, it was necessary to use lower values of K and U_{max} than for curve A in order to fit the observed σ_s and P. It is seen that curve B does not have a minimum and is thus in better agreement near $\theta=20°$. We note that at large angles ($\gtrsim23°$) both curves A and B lie above the experimental points. There are two possible reasons for this discrepancy. (1) For $\theta\gtrsim20°$, the inelastic scattering in which the nucleus is excited to a low-lying level is probably comparable with the elastic scattering. The polarization for the inelastic scattering is expected to be smaller than for the elastic scattering. Hence if an appreciable number of slightly inelastic events are included in the measurements, this would decrease the observed values of P. (2) The present calculations become less accurate at large angles ($\theta\gtrsim25°$) because of the angular dependence of the nucleon-nucleon scattering amplitudes which is not taken into account in the optical model. It has been pointed out by Fernbach, Heckrotte, and Lepore[22] that inclusion of this effect would probably decrease the calculated polarization at large angles.

Figure 3 shows the results obtained for 130-Mev protons scattered from Fe. Curve A was calculated from potential (1) with $r_0=4.68\times10^{-13}$ cm, $a=0.49\times10^{-13}$ cm, $V_r=-15$ Mev, $K=3.5\times10^{12}$ cm^{-1}, and $U_{max}=1.0$ Mev. This curve gives somewhat too much polarization inside the main diffraction peak. A decrease of U_{max} with increasing atomic number would be compatible with the spin-orbit coupling required for the nuclear shell model.[23] Therefore, P was also calculated

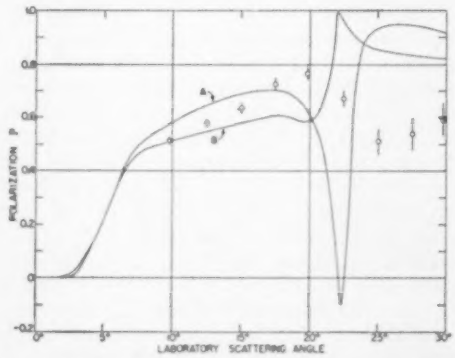

FIG. 2. Polarization P for 130-Mev protons scattered from Al, calculated for the Woods-Saxon potential. Curve A was obtained for $a=0.49\times10^{-13}$ cm. Curve B was calculated for $a=0.80\times10^{-13}$ cm. The circles represent the experimental values of Dickson, Rose, and Salter.[4]

[21] The singularity of Eq. (4) at $r=0$ due to the $1/r$ factor has no physical meaning and was effectively removed in the calculations (in the present work and in I) by assuming that U remains constant for $r\lesssim0.5\times10^{-13}$ cm. This behavior arises because V does not have zero derivative at $r=0$. Due to the smallness of $\exp[(r-r_0)/a]$ in the numerator of U, the factor $1/r$ becomes effective only for $r\lesssim0.5\times10^{-13}$ cm, and in this region U was taken as constant.

[22] Fernbach, Heckrotte, and Lepore, Phys. Rev. **97**, 1059 (1955).

[23] D. R. Inglis, Revs. Modern Phys. **25**, 390 (1953).

for potential (1) with $U_{max}=0.75$ Mev (curve B) and 0.6 Mev (curve C); the constants r_0, a, V_r, and K were the same as for curve A. It is seen that B and C give lower polarization than A for $\theta<16°$. There is a deep minimum of P for curves A, B, and C at the angle of the first diffraction minimum $\theta=18°$. In view of the result obtained by increasing a for Al, calculations were carried out for $a=0.8\times10^{-13}$ cm and 1.0×10^{-13} cm. However, the resulting P still has a deep (negative) minimum, so that in contrast to Al, a moderate increase of a is not adequate. We note that the minimum of P is primarily due to the interference with the Coulomb scattering, since it was found that for neutron scattering from Fe with the same parameters as for case A, the curve of P *vs* θ has no minimum at 18° and is qualitatively similar to curve B in Fig. 2 for Al. The fact that the Coulomb scattering decreases the value of P at the diffraction minimum has been pointed out by Fernbach, Heckrotte, and Lepore.[22] This also explains why the effect is more pronounced for Fe than for Al.

Curve D of Fig. 3 was obtained for a Gaussian well $V=(V_r+iV_i)\exp(-r^2/r_g^2)$, with $r_g=3.83\times10^{-13}$ cm, $V_r=-35$ Mev, $K=4\times10^{12}$ cm^{-1} at the center of the nucleus, and $U=-2\exp(-r^2/r_g^2)$ Mev. These values of r_g, V_r, and K were chosen in order to fit σ_t and σ_a. It is seen that the minimum of P is higher than for curves A–C. Curve D has a negative region for $\theta<3°$, which is associated with the interference between Coulomb and nuclear scattering. This negative region was also found for cases A–C for Fe, and for C and Al (Figs. 1, 2), but the negative values of P for these cases are too small to be shown in the figures ($|P|<0.01$).

Concerning the discrepancy of P at the diffraction minimum, it is possible that a well shape different from the ones considered above would give better agreement with the observed polarization in this region. It should also be mentioned that the use of the WKB approximation may introduce some inaccuracies. In addition, part

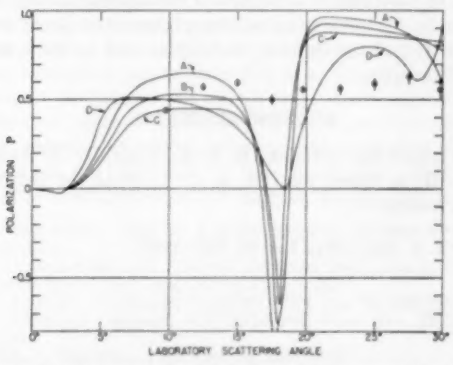

FIG. 3. Polarization P for 130-Mev protons scattered from Fe. Curves A, B, and C were calculated for $U_{max}=1$ Mev, 0.75 Mev, and 0.6 Mev, respectively, using the Woods-Saxon potential with $a=0.49\times10^{-13}$ cm. Curve D was obtained for a Gaussian well shape. The circles represent the experimental values of Dickson, Rose, and Salter.[4]

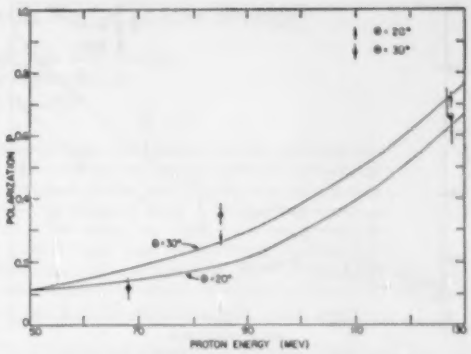

FIG. 4. Polarization P for protons scattered from Be as a function of proton energy for scattering angles $\theta=20°$ and 30°. The calculated curves were obtained for the Woods-Saxon potential with $a=0.49\times10^{-13}$ cm. The experimental values of Dickson, Rose, and Salter[4] are represented by crosses for $\theta=20°$ and by circles for $\theta=30°$.

of the discrepancy may be due to experimental difficulties such as the limited angular resolution and multiple scattering in the target. Thus if θ_s is the root-mean-square angle for multiple scattering, particles observed at an angle θ to the incident beam have undergone nuclear scattering over a range of angles extending approximately from $\theta-\theta_s$ to $\theta+\theta_s$. If θ_s is of order 2°, this effect would increase the measured values of P at the diffraction minimum.

Dickson, Rose, and Salter[4] have presented results for the differential cross sections $d\sigma^+/d\Omega$ and $d\sigma^-/d\Omega$ for scattering to the left and to the right, respectively, from the second target. Since the incident beam was scattered to the left and its polarization is 0.68, $d\sigma^\pm/d\Omega$ is given by $\langle d\sigma/d\Omega\rangle(1\pm0.68P)$ where $\langle d\sigma/d\Omega\rangle$ is the differential scattering cross section averaged over spin directions. The calculated values of $d\sigma^\pm/d\Omega$ are appreciably smaller than those given by Dickson *et al.*,[4] presumably because the latter include some inelastic scattering. In this connection, we note that the present calculations reproduce approximately the total diffraction scattering cross section for neutrons, which is given by $\sigma_t-\sigma_a$. The calculated curves of $d\sigma^\pm/d\Omega$ for the potential (1) have a noticeable diffraction minimum at an angle which is 30° for Be, 27° for C, 23° for Al, and 18° for Fe. This minimum was not observed[4] for Be and C, while for Al and Fe, there is a pronounced change of slope of the $d\sigma^\pm/d\Omega$ curves at 22° and 18°, respectively, which is due to the diffraction effect. We note that for Al and Fe the calculated angle agrees with the data. Dickson *et al.*[4] have suggested that for Be and C there is, in fact, no diffraction minimum, whereas for Al and heavier nuclei the elastic cross section has maxima and minima which are partly smeared out by the angular resolution, multiple scattering in the target, and the presence of some inelastic events. It should be noted that the depth of the calculated minimum of $d\sigma^\pm/d\Omega$ depends rather

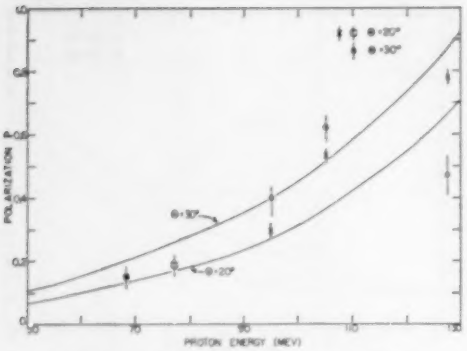

FIG. 5. Polarization P for protons scattered from C as a function of proton energy for scattering angles $\theta=20°$ and 30°. The calculated curves were obtained for the Woods-Saxon potential with $a=0.49\times10^{-13}$ cm. The experimental values of Dickson, Rose, and Salter[4] are represented by crosses for $\theta=20°$ and by circles for $\theta=30°$. The square shows the value obtained by Strauch[25] at $\theta=20°$.

strongly on the shape of the nuclear potential well. Thus for the Gaussian well used for Fe (see curve D in Fig. 3.) the calculated curve of $d\sigma^-/d\Omega$ decreases uniformly with θ, while $d\sigma^+/d\Omega$ has only a shallow minimum at $\theta=19°$.

Figures 4 and 5 show the polarization as a function of proton energy T for Be and C at $\theta=20°$ and 30°. The calculations were done for $T=50$, 90, and 130 Mev, using potential (1) and the spin-orbit coupling (4) with $U_{max}=1.0$ Mev. For Be, we took $r_0=2.56\times10^{-13}$ cm and $a=0.49\times10^{-13}$ cm; for C: $r_0=2.81\times10^{-13}$ cm and $a=0.49\times10^{-13}$ cm. The values of V_r and K were as follows: (a) at $T=50$ Mev[24]: $V_r=-55$ Mev, $K=4.5\times10^{12}$ cm^{-1}; (b) at $T=90$ Mev: $V_r=-35$ Mev, $K=4.0\times10^{12}$ cm^{-1}; (c) at $T=130$ Mev: $V_r=-15$ Mev, $K=3.5\times10^{12}$ cm^{-1}. The experimental points are those obtained by Dickson, Rose, and Salter[4] for Be and C, and the value found by Strauch[25] for protons of average energy 77 Mev scattered from C at 20°. It is seen that the present calculations are in agreement with the rapid rise of P with increasing energy. The increase of P with T can be explained qualitatively as follows. The polarization is determined by the relative difference between the effective potentials for the two spin directions which is given by $(2l+1)U_{max}/|V_r|$. If U_{max} remains approximately constant, while $|V_r|$ decreases, the ratio will increase, resulting in a rapid rise of the polarization.

Concerning the value $U_{max}=1$ Mev used in the present calculations, we note that the U_{max} required for the nuclear shell model is of the same order of magnitude. An estimate of this value of U_{max} can be made from the energy levels of O^{17}. According to Adair,[26] the 5.08-Mev level of O^{17} is the $^2D_{\frac{3}{2}}$ state corresponding to the $^2D_{\frac{5}{2}}$ ground state. Although the excited state is only $\sim$50 percent pure, one obtains in this manner an estimate of 1.02 Mev for the average value of $|U(r)|$ for a $1d$ neutron in the field of O^{16}. The $1d$ wave function was calculated for the potential (1) with $V_r=-53$ Mev, $V_i=0$, $r_0=3.08\times10^{-13}$ cm, $a=0.49\times10^{-13}$ cm. By averaging $U(r)$ over the $1d$ density, one finds that $\langle|U(r)|\rangle_{1d}=1.02$ Mev corresponds to $U_{max}=1.53$ Mev. Hence it appears that the required U_{max} for the light nuclei does not change appreciably over the range 0–130 Mev.

III. CONCLUSIONS

Optical model calculations have been carried out for the polarization of protons of energy 50–130 Mev elastically scattered from Be, C, Al, and Fe. The calculated results are in reasonable agreement with the data obtained by Dickson, Rose, and Salter[4] and by Strauch.[25] The rapid decrease of P as the proton energy is decreased below 130 Mev is attributed to the increase of the real part of the central potential with decreasing energy. The spin-orbit coupling $U(r)\mathbf{l}\cdot\boldsymbol{\sigma}$ was assumed to be concentrated on the nuclear surface. Reasonable agreement with the measured values of P inside the first diffraction peak was obtained by taking $U_{max}=1$ Mev for the maximum U occurring on the nuclear surface. It can be concluded that a study of the polarization at low energies ($\lesssim$130 Mev) gives direct information about the real part of the central potential as well as the spin-orbit coupling.

ACKNOWLEDGMENTS

I would like to thank Dr. R. K. Adair, Dr. B. Rose, Dr. G. A. Snow, and Dr. L. C. L. Yuan for helpful discussions.

[24] It is expected that the case of Be and C at 50 Mev is near the limit of validity of the WKB approximation. The l values which contribute extend up to $l_m=7$. However only the phase shifts for $l\lesssim3$ correspond to particle paths for which the closest distance from the center of the nucleus is less than r_0. Nevertheless, the present calculations probably still give reasonable results at this energy. This limitation is expected to become unimportant for $T\gtrsim90$ Mev.

[25] K. Strauch, Phys. Rev. **98**, 234 (1955).

[26] R. K. Adair, Phys. Rev. **92**, 1491 (1953).

Theory of Neutron Reactions with Nuclei at Low Energy*

K. A. Brueckner, R. J. Eden,† and N. C. Francis
Indiana University, Bloomington, Indiana

(Received April 11, 1955)

A theory of the interaction of low-energy neutrons with nuclei has been developed using methods previously applied to the study of the nuclear ground state. It is show that an average potential is predicted by the theory which very closely resembles that used by Feshbach, Porter, and Weisskopf in their studies of the neutron cross sections. The calculated parameters for scattering at a few Mev are a real depth of 41 Mev and an imaginary part somewhat less than 1 Mev. The theory also predicts the appearance of characteristic narrow compound-state resonances in the cross section; these are the result of sharp fluctuations in the real and imaginary part of the equivalent potential acting on a neutron which are the result of appreciable coupling between the single-particle and compound-nucleus states. An estimate of the level width is given for a simple class of compound-state levels and is of the order of typical widths observed experimentally.

A comparison of these results is made with a theory of Wigner, Lane, and Thomas; the principal difference is in the much smaller imaginary part of the potential determined by this theory.

I. INTRODUCTION

FESHBACH, Porter, and Weisskopf[1] have shown that certain average cross sections for neutron-nuclear reactions can be represented by a model consisting of a single neutron scattering on a complex neutron scattering on a complex square well. It is the primary aim of this paper to show how this model may be derived and the complex potential calculated from the Schrodinger equation for many nucleons in strong interaction with each other. The secondary aim is to examine the finer detail of the resonance structure which will be seen if one does not average cross sections over finite energy ranges.

The basis of the method is the construction of a transformation operator which relates the independent particle model of the nucleus to the actual nuclear state. This operator has to be constructed so that not only the stationary states of the nucleus are accurately described but also so that in the model a single neutron scatters on a potential well in the same way as it would on the actual nucleus. It is found that the methods developed for discussing the gross properties[2-5] and also the detailed properties[6-8] of the nuclear ground-state wave function can be extended so as to apply to the present problem in the energy range under discussion (incident neutron 0 to 5 Mev). In Sec. II, an equivalent one particle potential for the incident neutron is constructed and is found to be complex and strongly energy dependent at certain energies. An approximation related to smoothing out this energy dependence enables us to calculate this potential which is found to have a real part of about 41 Mev and an imaginary part of about 1 Mev which increases slowly with energy.

The method can be described also in terms of shell model language which gives a useful interpretation of the collision process and approximations though of course it is a picture which must not be taken too literally. If the neutron was bound it would appear to move simply in the shell-model potential which is real and can be calculated[2-4] from two-body interactions within the nuclear medium. An incident neutron above zero energy sees a formally similar potential well, however, there are two important differences: (1) the incident wave when matched on to the single-particle wave functions in the real well leads to a broad resonance; (2) at these energies there are, in addition to excited states of one independent particle in the well, also excited states of the same energy of two (or more) independent particle modes of motion. The potential seen by the incident neutron contains an imaginary part which is the result of coupling between the single particle and two (or more) particle levels. These two particle levels themselves are also broadened by similar coupling. The imaginary part of the potential appears in a term containing a sum over discrete states; if this sum is replaced by an integration one no longer obtains the strong effects of the individual levels as the energy is varied but rather obtains an average effective potential; it is this which corresponds to the imaginary term in the model of Feshbach, Porter, and Weisskopf.

Certain simple aspects of the resonance fine structure are examined in Sec. III using a different approximation for the potential in which the neutron scatters. We consider a somewhat idealized case in that we suppose that at neutron energies of two or three Mev, where the single particle levels are very broad and overlap many more complicated compound nucleus levels, we can fix our attention on the sharp resonance resulting from a particularly simple type of excitation. This is possible

* Supported in part by a grant from the National Science Foundation.

† Smithson Research Fellow of the Royal Society, on leave of absence from Clare College, Cambridge, England.

[1] Feshbach, Porter, and Weisskopf, Phys. Rev. **96**, 448 (1954).
[2] Brueckner, Levinson, and Mahmoud, Phys. Rev. **95**, 217 (1954).
[3] K. A. Brueckner, Phys. Rev. **96**, 508 (1954).
[4] K. A. Brueckner, Phys. Rev. **97**, 1353 (1955).
[5] K. A. Brueckner and C. A. Levinson, Phys. Rev. **97**, 1344 (1955).
[6] R. J. Eden and N. C. Francis, Phys. Rev. **97**, 1366 (1955).
[7] Brueckner, Eden, and Francis, Phys. Rev. **98**, 1445 (1955).
[8] Brueckner, Eden, and Francis, Phys. Rev. **99**, 76 (1955).

only if we assume that the overlap in energy of the compound nucleus levels can be neglected; a consequence is that broadening of the levels occurs only because of transitions to the single-particle level. It is found that if two particles are in excited states, there is an imaginary part to the effective potential acting on this state which arises from tranisitions to single-particle excited states. On the evarage the imaginary part is of the order of 10 kev at excitations corresponding to the incident neutron energies of a few Mev; it corresponds to the width of a type of sharp "compound state" resonance. It is also found that the real part of the equivalent potential well seen by the neutron changes rapidly in this narrow energy range. The fluctuation in the real potential is the same order of magnitude ($\sim$2 Mev) as the width of the giant neutron resonance. It is this fluctuation which is responsible for the narrow resonance may give either a peak or a peak followed by a sharp dip in the cross section as a function of energy.

In Sec. IV, the results of Secs. II and III are summarized and a comparison is made with a theory recently developed by Wigner, Lane, and Thomas.[9] Finally some concluding remarks are made in Sec. V.

II. EQUIVALENT SCATTERING POTENTIAL

A. Real Part of the Potential

We consider the matrix element for elastic scattering of a neutron on a nucleus. The wave function of the particles in the nucleus is antisymmetrized, and we will also later introduce a device which takes account of the indistinguishability of the incoming neutron and the neutrons in the nucleus.

The equivalent potential for elastic scattering has been derived by Francis and Watson,[10] neglecting exchange effects and assuming knowledge of the nuclear wave functions. Adopting their formula to the notation used in references 2–8, this potential is

$$V_0=\sum_{i=1}^{A}(\Psi(A),t_{1i}F_{1i}\Psi(A)), \tag{1}$$

where $\Psi(A)$ is the ground-state wave function of the target nucleus (which contains A nucleons), t_{1i} is the two-body scattering matrix evaluated in the nuclear medium, F_{1i} is an operator which allows for the effects of incoherent scattering in the nuclear medium.

The difficulty of using the formula (1) for V_0 lies in the fact that the ground-state wave function $\Psi(A)$ has a very complicated form, and further this formula does not take account of the identity of the scattered neutron with the other neutrons in the system so it is not directly applicable at the energies (0 to 5 Mev) which we wish to consider. We must therefore modify the form (1) of the potential to overcome these difficulties. This we shall do by making use of the extensive knowledge of the nuclear ground-state wave function given us by the results of references 2–8. We could in principle do this by introducing a second transformation of the wave function $\Psi(A)$ of Eq. (1); this method, however, is inconvenient since the treatment of the $A+1$ nucleons is unsymmetrical and the effects of the identity of the particles, for example, cannot easily be taken into account. Consequently we shall use a method closely related to that of references 2–6 which treats all nucleons symmetrically.[11] This we do by solving not Eq. (1) for the potential, but instead by considering the problem of determining the potential acting on a shell model particle in a stationary state with the same energy as the energy of the actual problem. That is we shall neglect the fact that we are actually dealing with a scattering problem and consider instead a stationary problem with boundary conditions such that the wave functions vanish at the nuclear surface. This clearly is a good approximation if in the actual scattering problem the reflection coefficient at the nuclear surface is sufficiently close to unity so that the nonstationary character of the state due to flux loss through the nuclear surface can be treated as a perturbation. In this approximation we have replaced the scattering problem by a stationary problem which we can solve using the technique developed by dealing with the ground-state problem.

An additional advantage of this method is that it allows us easily to take into account the identity of the scattered particle with the nuclear particles since the methods we have developed[5] treat all particles in an equivalent way using the powerful and convenient formalism of second quantization. Here as in other papers we shall use the somewhat more compact and intuitive language of particle description but keep in mind that in actual quantitative evaluation, the quite simple translation to the language of second quantization must be made.

In this approximation we determine V_0 by considering the excited states of the nucleus containing $A+1$ nucleus. It has been shown in previous papers[2–6] that these states can be related to a model of equal energy which describes independent particle motion. The nuclear wave function $\Psi(A+1)$ is given in terms of the model wave function $\Phi(A+1)$ by the relation

$$\Psi(A+1)=F\Phi(A+1), \tag{2}$$

where

$$F=1+\frac{1}{e}\sum_{ij}{}' I_{ij}F_{ij},$$
$$F_{ij}=1+\frac{1}{e}\sum_{lm\neq ij}{}' I_{lm}F_{lm}. \tag{3}$$

[9] Lane, Thomas, and Wigner, Phys. Rev. **98**, 693 (1955).
[10] N. C. Francis and K. M. Watson, Phys. Rev. **92**, 291 (1953).
[11] The same method was used in reference 2 and a result nearly identical with the following was obtained.

The operators here are labeled by the independent-particle states of the model. The two-body operator t_{ij} is defined in terms of the two-body potential v_{ij} by the integral equation

$$t_{ij}=v_{ij}+v_{ij}\frac{1}{e}{}'t_{ij}. \tag{4}$$

The operator t_{ij} is then separated into

$$t_{eij}=\text{diagonal part of } t_{ij}, \tag{5}$$

and

$$I_{ij}=\text{nondiagonal part of } t_{ij}. \tag{6}$$

The propagator e^{-1} is the reciprocal of

$$e=E-\sum_{i=1}^{A+1}T_i-\sum_{i<j=1}^{A}t_{eij}. \tag{7}$$

In these expressions a prime to the left of an operator means that matrix elements to the state $\Phi(A+1)$ must be omitted. The independent particle or model wave function $\Phi(A+1)$ is a product of single-particle wave functions which are eigenfunctions of the kinetic energy operator satisfying boundary conditions appropriate to the model. The energy of the system is in the first approximation characteristic of this method:

$$E=\sum_{i=1}^{A+1}T_i+\sum_{i<j=1}^{A}t_{eij}. \tag{8}$$

It will be seen that the Eqs. (4) and (7) for t_{ij} and e form a coupled set for which a self-consistent solution has to be sought. This has been done by one of us (K.A.B.)[4] and leads to an energy-dependent potential $V_e(k)$ where the wave number k specifies the state of the particle. The higher approximations to this equivalent potential involve higher order terms in the incoherent reaction matrices I_{ij} and can be disregarded[1,8] since they have a very small effect on the energy.

Next we determine the potential energy of a particle moving with such a wave number that the total energy of the nucleus plus one neutron is equal to the energy of the nucleus in its ground state together with a separated neutron of energy E_n. In the present approximation, the energy of the excited nucleus of $A+1$ nucleons differs from the ground-state energy by

$$E(A+1)=E(A)+k^2/2M+V_e(k), \tag{9}$$

where k is the wave number of the particle moving in the nucleus. Thus, to determine the wave number and hence the potential, we have

$$k^2/2M+V_e(k)=E_n. \tag{10}$$

In the energy range of interest, a good approximation to the potential is

$$V_e(k)=-68\text{ Mev}+(1/2\sigma)k^2, \tag{11}$$

where $(1/M+1/\sigma)^{-1}=M^*\cong 0.60M$. Using this result, we find

$$k^2=2M^*(E_n+68\text{ Mev}), \tag{12}$$

and

$$V_e(k)=-\frac{M^*}{M}(68\text{ Mev})+\left(1-\frac{M^*}{M}\right)E_n. \tag{13}$$

Using $M^*/M=0.60$, which is an approximate value valid at energies near the Fermi energy, we find

$$V=-41\text{ Mev}+0.40E_n. \tag{14}$$

Consequently the potential is slowly energy-dependent decreasing in strength by a few percent as the neutron energy is increased from 0 to 5 Mev. This is the equivalent well depth experienced by a particle having neutron mass, and determines the wave function which has to be matched on to the incoming neutron wave.

B. Imaginary Part of the Potential

The real well depth 41 Mev has been calculated on the assumption that the independent particle states are stable. This assumption will not be valid if the incident neutron has energy greater than zero. However, it is reasonable that the variation of the real potential V_1 with energy will be correctly given by Eq. (14) for low neutron energies where as mentioned before the neutron wave function inside the nucleus can still be approximately represented by that of a stationary state. The main change will come from the appearance of an imaginary part in the equivalent potential encountered by the neutron. Physically this imaginary part of the potential comes from the existence of states of the compound $(A+1)$ nucleus which are coupled to and have a larger lifetime than the single-particle (positive energy) states. Mathematically it comes from the change in the equation for t_{1j} where the subscript 1 refers to the particle excited above zero energy. In deriving the real part of the potential, we have not fully taken into account the change from discrete states to the continuum scattering states. The principal effect is the appearance of excited states of the system with the same energy as the initial state. Consequently the singularity in the propagator can no longer be specified by eliminating matrix elements to the ground state. We must instead change the nature of the singularity by introducing a small imaginary part to correspond to the fact that the scattering wave function contains outgoing scattered waves.[12] This we do in the usual way by replacing Eq. (4) for the reaction matrix by the modified equation for the scattering operator

$$t_{ij}'=v_{ij}+v_{ij}\frac{1}{e+i\eta}t_{ij}'. \tag{15}$$

[12] B. Lippman and J. Schwinger, Phys. Rev. 79, 469 (1950).

We see now that t_{ij}' must have an imaginary part, hence

$$V_a'=\sum_i\sum_j t_{ai,j}' \tag{16}$$

must also have an imaginary part which in turn must be inserted in the propagator e^{-1}. This means that the self consistent solution which we are seeking is constructed to correspond to a set of states within the nuclear volume which are moving in a complex potential.

We introduce a device here to allow us to treat the scattering single-particle state in a manner symmetrical with the compound-nucleus states. The stationary single-particle state which would exist if the boundary conditions appropriate to a stationary state were imposed at the nuclear surface is in fact considerably broadened by the possibility of actual penetration of the nuclear surface and particle loss. At low energies the state is quite long-lived, however, since the reflection factor at the surface is nearly unity; consequently it is a good approximation to replace the effects of particle loss through the nuclear surface by the effects of a uniform imaginary part to the potential. Thus we use an approximate wave function for the single-particle state inside the nucleus which corresponds to a potential with imaginary part

$$W=W_a+W_b, \tag{17}$$

where W_a is the result of transitions to other compound nucleus states and W_b is adjusted to give the same attenuation of the state that would result from surface penetration. We shall use this approximation only in the derivation of the imaginary part of the potential associated with absorption processes and in actually solving the scattering problem we will need to work with a potential having only iW_a for its imaginary part. In this approximation we can write for the potential acting on particle i:

$$V_{ai}'=V_i+iW_i. \tag{18}$$

Both the real and imaginary parts of the potential will in general depend on the state of the particle, particularly the imaginary part which will increase rapidly with the excitation energy. The solution of Eq. (15) for all of the relevant t's will determine the V_a's; consequently a problem of self-consistency arises. Although in determining the real part of the potential we have solved the problem following a self-consistent procedure, we shall work with less rigor in determining the imaginary part of the potential. This is possible since the states and energies are only slightly perturbed by the transition processes and the imaginary part of the well is very small. This we shall determine only approximately; the result will then be self-consistent in first order. The precise approximations to be made will be evident as we proceed.

The imaginary part of the potential due to absorption for particle 1 is given by (writing the diagonal matrix element explicitly)

$$W_a=\mathrm{Im}\sum_{j=1}^{A}(\Phi_0(A+1),t_{1j}'\Phi_0(A+1)), \tag{19}$$

where by Im { } we mean the imaginary part of { }. We will estimate this by replacing the repulsive core potential V_{ij} in the equation for t_{ij}' by a regular potential[13] and work to second order in this potential. This gives

$$W_a=\mathrm{Im}\sum_{j=1}^{A}\sum_{\lambda}(\Phi_0(1,j),v_{1j}\Phi_\lambda(1,j))$$
$$\times(E-T_\lambda-V_\lambda-iW_\lambda)^{-1}(\Phi_\lambda(1,j),v_{1j}\Phi_0(1,j)), \tag{20}$$

where we have made the matrix product explicit by inserting the intermediate states $\Phi_\lambda(1,\gamma)$. T_λ is the kinetic energy in this state, $V_\lambda+iW_\lambda$ is the complex potential acting on this state. We next write this sum in more compact form, combining the summations over j and λ,

$$W_a=\sum_\lambda(0|v|\lambda)^2\frac{W_\lambda}{(E-E_\lambda)^2+W_\lambda^2}, \tag{21}$$

where $E_\lambda=T_\lambda+V_\lambda$ is the real energy which determines the positions of the energy levels of the compound nucleus and

$$(0|v|\lambda)=(\lambda|v|0)=(\Phi_0(1,j),v_{1j}\Phi_\lambda(1,j)). \tag{22}$$

C. Evaluation of the Imaginary Part of the Potential

We shall determine the value of W_a by two quite different methods, both of which give only an average value and neglect fluctuation due to the discreteness of the sum over states. We shall not attempt to give a precise determination of W_a although such an evaluation is in principle straightforward in the approximation of Eq. (21).

We first evaluate the average value of W_a over an energy interval Δ. Such an average is related to the averaging process used by Barschall *et al.*[14] in their analysis of the neutron scattering data. The average is

$$\bar{W}_a^{(1)}=\frac{1}{\Delta}\int_{E_0-\frac{1}{2}\Delta}^{E_0+\frac{1}{2}\Delta}\sum_\lambda(\lambda|v|0)^2\frac{W_\lambda}{(E-E_\lambda)^2+W_\lambda^2}dE. \tag{23}$$

This we evaluate making use of several simplifying approximations. We will assume that Δ is large enough so that the number of states λ with energies E_λ in Δ always includes many levels, i.e.,

$$\Delta\gg D, \tag{24}$$

[13] This approximation derives its validity from the fact that for low momentum values the correct t_{ij}' closely resemble the scattering from a regular well of correct depth and range.

[14] H. H. Barschall, Phys. Rev. **86**, 431 (1952); Am. J. Phys. **22**, 517 (1954); N. Nereson and S. Darden, Phys. Rev. **94**, 1678 (1954); M. Walt and H. H. Barschall, Phys. Rev. **93**, 1062 (1954).

where D is the mean spacing of the levels E_λ. We then can approximate to the results of the integration of Eq. (23) by

$$\bar{W}_a^{(1)}=\pi\sum_\lambda(\lambda|v|0)^2\Gamma_\Delta(E_0,E_\lambda), \tag{25}$$

where

$$\Gamma_\Delta(E_0,E_\lambda)=\frac{1}{\pi\Delta}\int_{E_0-\Delta/2}^{E_0+\Delta/2}\frac{W_\lambda dE}{(E-E_\lambda)^2+W_\lambda^2}$$
$$\cong 1/\Delta \text{ if } |E_0-E_\lambda|<\tfrac{1}{2}\Delta$$
$$\cong 0 \quad \text{if } |E_0-E_\lambda|>\tfrac{1}{2}\Delta. \tag{26}$$

This function Γ_Δ is analogous to a spread-out delta function; it is independent of the level widths W_λ as long as $\Delta\gg W_\lambda$ which will be satisfied if

$$D>W_\lambda. \tag{27}$$

Using this approximation to the integral, we have

$$\bar{W}_a^{(1)}=\pi\sum_{E_\lambda \text{ in } \Delta}\frac{1}{\Delta}|(\lambda|v|0)|^2. \tag{28}$$

Now making use of our assumption that many levels λ lie in Δ, it is reasonable to replace $(\lambda|v|0)^2$ by its average value, giving us

$$\bar{W}_a^{(1)}=\pi(\lambda|v|0)_{Av}^2\frac{1}{\Delta}\sum_{E_\lambda \text{ in } \Delta}'=\frac{\pi}{D}(\lambda|v|0)_{Av}^2, \tag{29}$$

where Δ/D is the number of levels in Δ. Thus we have a simple relationship between the level width, the matrix elements for transitions between the states 0 and λ, and the level spacing. Before evaluating this, we shall give another way of estimating $\bar{W}_a$.

We make another approximation suggested by the result we have just derived. This is to make use of the fact that $\bar{W}_a$ does not depend on the level widths or on the value of E but rather on the density of levels. Consequently, it is reasonable to estimate $\bar{W}_a$ by replacing the discrete states λ by continuum states and letting $\Delta\gg W_\lambda$ approach zero. In this case we find the result of ordinary perturbation theory[15]

$$\bar{W}_a^{(2)}=\pi\int d\lambda(\lambda|v|0)^2\delta(E_0-E_\lambda), \tag{30}$$

where the integral over λ has replaced the discrete state sum.

For simplicity we shall in evaluating the two values of W_a given by Eqs. (29) and (30) use a simple representation of the nuclear states, i.e., we shall represent the model ground state by a degenerate Fermi gas and the excited states by plane waves of definite momenta. This approximation is accurate for large nuclei as long as we are not interested in precise details such as the exact positions and widths of resonances, for example. It is to be noted that this approximation is not equivalent to assuming that the actual nuclear wave function Ψ is a Fermi gas, Ψ being related to the model wave function Φ by the transformation operator F (Eq. 3).

We first evaluate $(0|v|\lambda)_{Av}^2$ in this representation. For v we use a Yukawa well with Serber exchange mixture. Introducing the momentum states explicitly, we find

$$(\mathbf{k}_1'\mathbf{k}_2'|v|\mathbf{k}_1\mathbf{k}_2)=\left(\frac{2\pi V_0}{\mu v}\right)\left[\frac{1}{\mu^2+(\mathbf{k}_1-\mathbf{k}_1')^2}+\frac{1}{\mu^2+(\mathbf{k}_1+\mathbf{k}_1')^2}\right]\delta_{\mathbf{k}_1+\mathbf{k}_2,\mathbf{k}_1'+\mathbf{k}_2'}. \tag{31}$$

The average over states λ is equivalent to averaging over states of excitation E_λ in Δ and also to averaging over the angles of $\mathbf{k}_1'$. Making use of the fact that the states which interest us are of low excitation so that the vectors $\mathbf{k}_1$ and $\mathbf{k}_1'$ are both approximately equal to k_F in magnitude, the average gives

$$(0|v|\lambda)_{Av}^2\cong\left(\frac{2\pi V_0}{\mu v}\right)^2\frac{1}{\mu^2k_F^2} \tag{32}$$

where we have dropped a small term using $k_F^2/\mu^2\gg 1$. Taking $V_0=0.252\mu$, $v=(4/3)\pi A/\mu^3$, $k_F\simeq 1.8\mu$, and inserting the results in Eq. (29) for W_a, we find

$$\bar{W}_a(1)\cong(200/A)^2\times 68 \text{ Mev}/D(\text{kev}). \tag{33}$$

Thus, for a typical heavy nucleus ($A=200$) and for a level spacing $D=100$ kev, this gives $W_a=0.68$ Mev. It will be noted that the level spacing D will decrease with energy so that the predicted imaginary potential W_a will increase as the energy of the incident neutron increases.

To evaluate the continuum approximation given by Eq. (30) for the level width, we re-insert explicitly the sums over the relevant momentum indicies and replace the summations by integrals. The result

$$\bar{W}_a^{(2)}=\frac{\pi}{(2\pi)^6}\left(\frac{2\pi V_0}{\mu}\right)^2\int d\mathbf{k}_i\int d\mathbf{k}_i'\left|\frac{1}{\mu^2+(\mathbf{k}_1-\mathbf{k}_i')^2}+\frac{1}{\mu^2+(\mathbf{k}_1+\mathbf{k}_1')^2}\right|^2\delta(E_1+E_i-E_1'-E_i'). \tag{34}$$

This integration must be carried out in such a way that the exclusion principle is not violated; the requirement is that

$$|\mathbf{k}_1'|\geq k_F, \quad |\mathbf{k}_i'|=|\mathbf{k}_1+\mathbf{k}_i-\mathbf{k}_1'|\geq k_F. \tag{35}$$

In addition the integration over $\mathbf{k}_i$ runs only over the unexcited states of the core, i.e., over the Fermi gas.

[15] This approximation to Eq. (19) for the imaginary part of the potential is formally similar to an approximation used by Lane (unpublished). His method differs in that he replaces the correct combination $v(1/\epsilon)i$ of Eq. (4) by $i(1/\epsilon)i$ instead of our replacement by $v(1/\epsilon)v$. He also supposes that the actual nuclear wave function can be represented as a degenerate Fermi gas; we regard this approximation as valid only in describing the model wave function (see also the remarks at the beginning of Sec. III).

To remove the delta function on momentum, we make use of the reduced mass approximation[4] for the energies

$$E=k^2/2M^*. \tag{36}$$

Consequently the integral over $\mathbf{k}_1'$ becomes

$$\int d\mathbf{k}_1'\delta(E_1+E_i-E_1'-E_i')=M^*\int\frac{k_1'dk_1'}{|\mathbf{k}_1+\mathbf{k}_i|}, \tag{37}$$

where we have used

$$\frac{\partial E}{\partial\cos\theta_1'}=\frac{\partial}{\partial\cos\theta_1'}\left[\frac{k_1'^2}{2M^*}+\frac{(\mathbf{k}_1+\mathbf{k}_i-\mathbf{k}_1')^2}{2M^*}\right]$$
$$=|\mathbf{k}_1+\mathbf{k}_i|k_1'/M^*, \tag{38}$$

where θ_1' is the angle between $\mathbf{k}_1+\mathbf{k}_i$ and $\mathbf{k}_1'$.

To evaluate the integral we shall use the fact that the restrictions due to the exclusion principle severely limit the range of interaction, and make an expansion valid for k_1 near k_F. That is, we let

$$\mathbf{k}_1=\mathbf{k}_F+\mathbf{x},\quad \mathbf{k}_1'=\mathbf{k}_F'+\mathbf{x}',\quad \mathbf{k}_i=\mathbf{k}_F''-\mathbf{x}_i, \tag{39}$$

and keep only terms linear in the x's. The integral then becomes

$$\left(\frac{2\pi V_0}{\mu}\right)^2\frac{1}{(2\pi)^3}\frac{k_F{}^3M^*}{\mu^4}\int\frac{dx_i d\mu_i dx_1'}{|\mathbf{k}_1+\mathbf{k}_i|}, \tag{40}$$

where μ_i is the cosine of the angle between $\mathbf{k}_1$ and $\mathbf{k}_i$. We have simplified the result by taking terms in the square of the potential which are large when the approximations $\mathbf{k}_1\cong\mathbf{k}_1'$ and $\mathbf{k}_1\cong-\mathbf{k}_1'$ are made, these being the values of $\mathbf{k}_1'$ which give the principal contribution for transitions near the Fermi momentum. We also correct for our neglect of the exclusion principle by multiplying by a factor of $\frac{3}{4}$ which corrects for the apriori probability for interactions in even states to occur. The restrictions on the integration now are that

$$x_1'\geqq 0,\quad x_1+x_i-x_1'\geqq 0, \tag{41}$$

where we have made use of the energy conservation condition in simplifying the second of these. We shall finally make another approximation in relaxing the conditions of energy conservation on the integration. These have only the effect of somewhat decreasing the range of integration so that we shall in neglecting them overestimate the integral. Estimates of the error made in this approximation indicate that it is rather small. Using these restrictions, we find

$$W_a^{(2)}=\frac{3}{8\pi}\left(\frac{V_0}{\mu}\right)^2\frac{k_F{}^3M^*}{\mu^4}\int_0^{x_1}dx_i\times\int_0^{x_1-x_i}dx_1'\int_{-1}^{1}\frac{d\mu}{(2k_F{}^2-2k_F{}^2\mu)^{\frac{1}{2}}}$$
$$=\frac{3}{8\pi}\left(\frac{V_0}{\mu}\right)^2\left(\frac{k_F}{\mu}\right)^2\frac{M^*}{\mu}\frac{x_1^2}{\mu}. \tag{42}$$

This we bring to final form by using the approximation

$$x=k_1-k_F\cong(k_1^2-k_F^2)/2k_F=(E_1-E_F)M^*/K_F. \tag{43}$$

The result is

$$W_a^{(2)}=\frac{3}{8\pi}\left(\frac{V_0}{\mu}\right)^2\left(\frac{M^*}{\mu}\right)^2\left(\frac{E_1-E_F}{\mu}\right)^2\mu. \tag{44}$$

This is an overestimate of the original integral since both approximations made have increased the result. $W_a^{(2)}$ shows a quadratic dependence on the excitation energy measured relative to the energy E_F of the particle in the highest Fermi level. The magnitude predicted is

$$W_a^{(2)}=\left(\frac{M^*}{M}\right)^2\left(\frac{E_1-E_F}{8.4}\right)^2\text{ Mev}, \tag{45}$$

where E_1 and E_F are measured in Mev. Thus, at excitations of 10 Mev corresponding to scattering states of low energy, W_a is a few tenths of a Mev (taking $M^*/M\sim 0.6$). This agrees with the previous estimate; we conclude that the imaginary part of the potential for a single particle is roughly one Mev and probably somewhat less.[16] However, it should be noted that there will in addition be (smaller) contributions from more complicated forms of compound states which will tend to increase the imaginary part of the mean potential which has been estimated here.

III. RESONANCE FINE STRUCTURE

In the previous section, we have been primarily concerned with an approximation appropriate to determining the average effective potential for the scattering of a neutron on a nucleus. The average was defined over an energy range which was required to contain many two-particle excited states for the equivalent shell-model problem. It is to be emphasized that although these shell-model states are used to define corresponding nuclear states and are used also in computation of the average potentials, the method does not assume weak interactions between nucleons. The apparent paradox is explained by considering the complicated relation between the actual nuclear wave function and the model wave function [see for example Eqs. (2) and (3)]. It will be noted that the transformation operator which changes a shell model state into a nuclear state introduces strong correlations into the nuclear wave function which correspond to strong forces between nucleons. The great value of the shell model lies in its use in determining observables which do not depend strongly on short-distance correlations between nucleons, and it is in this connotation that we have used it in the previous section.

In the present section we shall investigate not the average equivalent potential acting on the neutron over

[16] The result obtained by Lane (see reference 15) is larger than this, primarily due to the appearance of $(M^*/M)^2\sim\frac{1}{4}$ in our formula [Eq. (45)]. This is a consequence of the strong momentum dependence of the self-consistent potential predicted by our methods.[4]

a fairly wide energy interval, but we will consider instead the detailed behavior of the equivalent potential in the neighborhood of a two-particle excited state of the nuclear model. It is clear that such an excited state will correspond to a much more complicated compound state of the system, target nucleus plus neutron, and the fluctuation in the equivalent potential which we will derive will correspond to some complicated change with energy of the compound nuclear state. There are two aspects of the problem; the first we shall consider is the level width of the two-particle excited states, and the second is the manner in which the resonances arise in terms of the scattering of a neutron on the equivalent potential.

A. Compound Nucleus Level Widths

In Sec. II, we have seen that there are terms in the equivalent potential which result from the incoming neutron interacting with a single shell-model particle in the target nucleus and forming a two-particle excited state. We will examine the broadening of these two-particle levels which arises because they are energetically capable of decaying by the inverse process. This process can be represented as a transition to a single-particle excited state of the nucleus followed by a decay of this state through absorption to other compound states or through penetration of the nuclear surface. In this evaluation we will neglect direct transitions to nearby two- and many-particle excited states, assuming that these levels in contrast to the broad single-particle levels do not overlap appreciably with the two-particle level we are considering.

To evaluate the broadening of the two-particle level, we use a generalization of the result for the imaginary part of the potential given in Eq. (21), i.e.,

$$W_\lambda = \mathrm{Im}\sum_{\lambda'}(\lambda|v|\lambda')\frac{1}{E_\lambda - T_{\lambda'} - V_{\lambda'} - iW_{\lambda'}}(\lambda'|v|\lambda), \quad (46)$$

where λ is the excited two-particle state and the sum over λ' is over all other excited states of the system. We have in Eq. (46) taken the energy E to be the energy E_λ which determines the position of the level. We make use of the approximation just described which assumes that all of the level broadening is due to transitions to the single-particle excited state. Thus in the sum over λ' we include only the state "0". Furthermore we write for this state $T_{\lambda'}+V_{\lambda'}=E_1$ and $W_{\lambda'}=W$. The result is

$$W_\lambda = (\lambda|v|0)^2\frac{W}{(E_1-E_\lambda)^2+W^2}. \quad (47)$$

To estimate $(\lambda|v|0)$, we use the expression for v used before [Eq. (31)] and find

$$W_\lambda \approx \left(\frac{2\pi V_0}{\mu v}\right)^2 \frac{1}{\mu^4 W}\frac{1}{(1+\Delta k^2/\mu^2)^2}\frac{1}{[1+(\Delta E/W)^2]}, \quad (48)$$

where Δk is the momentum transfer and ΔE is the energy difference. Taking the nuclear volume

$$v=(4/3)\pi A/\mu^3$$

and the Yukawa well strength $V_0=0.25\mu$, this expression becomes

$$W_\lambda = 0.070\ \mathrm{Mev}\left(\frac{200}{A}\right)^2\frac{1}{W\ (\mathrm{Mev})} \times\frac{1}{(1+\Delta k^2/\mu^2)^2}\frac{1}{[1+(\Delta E/W)^2]}. \quad (49)$$

For a typical case, with good energy and momentum overlap ($\Delta k\sim\Delta E\sim 0$), if one takes $A=200$ and $W=3$ Mev, this gives $W_\lambda=23$ kev.

There obviously can be great fluctuations in the widths of these two-particle levels, particularly as a result of the great possible variations in Δk, the momentum transfer. Since the momentum in a low excited state is quite large ($k\sim k_F\sim 1.8\mu$), $(\Delta k^2/\mu^2)$ can range from zero to about four, leading to variations in width from 23 kev to about 1 kev. In spite of the roughness of our approximations, it is apparent that level broadening of these two-particle excited states of the model (which correspond to excited compound states of the nucleus) is comparable with the broadening of the detailed resonances which are observed in neutron scattering at energies of one or two Mev.[17]

In addition to these two-particle excited states, there will be more complicated excited states corresponding to three or more particles not in the lowest unoccupied levels. For the initial single-particle state to couple to a state with three particles excited, the incoherent scattering operator I_{ij} [Eq. (6)] will have to act twice on successive pairs of particles to bring about the necessary changes in excitation. This more indirect coupling will tend to make the levels narrower than the simple two-particle excited states. In order to investigate them in the present formalism, it is necessary to use the more exact form for the equivalent potential given by

$$(\Phi_0, \textstyle\sum_{ij} t_{ij}F_{ij}\Phi_0). \quad (50)$$

To see explicitly how a resonance associated with a three-particle excited state can arise, consider a typical term of third order in the incoherent scattering matrices I_{ij}. This is

$$\sum_{i\neq j\neq k}\left(\Phi_0, I_{ij}\frac{1}{e}I_{\mu\kappa}\frac{1}{e}I_{lh}\Phi_0\right). \quad (51)$$

[17] It should be emphasized that the determination of resonance widths which we have made here is valid only when the single-particle levels are sufficiently broad to overlap in energy the compound nucleus levels. This condition is not well satisfied at low energies where all levels become very narrow as the metastable states of the bound system are approached. This restriction is evident in Eq. (49) since if $\Delta E \gg W$ as is the case at very low energy, the level widths become very small.

To evaluate a typical matrix element, let the operator act on an initial system with particles a,b in the ground state and particle c in the single-particle excited state. Under the action of the incoherent operators, the following transitions can occur in succession:

$$\begin{aligned} ab(c) &\rightarrow a'b'(c), \\ a'(b')c &\rightarrow a(b')c', \\ (a)b'c' &\rightarrow (a)bc, \end{aligned} \tag{52}$$

where we have indicated the particle unaffected in a transition by parentheses. For such a possible series of transitions, the contribution is

$$I_{bc,\,b'c'}(E_b+E_c-E_{b'}-E_{c'})^{-1} \times I_{ac',\,a'c}(E_a+E_b-E_{a'}-E_{b'})^{-1}I_{a'b',\,ab}, \tag{53}$$

where we write explicitly the matrix elements of e^{-1}. The three-particle excited state reached in this process are a', b', c and a, b', c'; if either of these states has the same energy as the initial state, then the matrix element of Eq. (53) will be markedly increased and a fluctuation in the potential strength will occur. This is of course a consequence of transitions occurring between the single-particle and the three-particle states. These terms are expected to be considerable smaller than those resulting from simpler types of excitation since they are of higher order in the interaction operators t_{ij} or I_{ij}. We shall not proceed farther in considering these more complicated excitations.

Before considering the way in which the resonances arise there is one further point to be noted about the width of the two particle resonances. According to the formula of Eq. (49), the width W_λ depends on the energy of the levels relative to the single-particle levels in a simple way, namely

$$W_\lambda \sim [1+(\Delta E/W)^2]^{-1}. \tag{54}$$

This dependence will be considerably masked by the strong fluctuations in the matrix elements of v and also by the fact that the experiments do not serve to distinguish whether a particular resonance corresponds to a two- or three- (or more-) particle excitation.

B. Resonances

In order to show how it is that resonances in the scattering cross section occur at energies which correspond to the two-particle excited states we consider the behavior of the equivalent potential near these energies. In the approximation of Eqs. (8) the equivalent potential is

$$V_e(1)=\sum_i(\Phi_0,t_{1i}\Phi_0)=\sum_i\Big[(\Phi_0,v_{1i}\Phi_0) + \sum_\lambda(\Phi_0,v_{1i}\Phi_\lambda)\frac{1}{E-E_\lambda-iW_\lambda}(\Phi_\lambda,t_{1i}\Phi_0)\Big]. \tag{55}$$

We wish to exhibit the fluctuation in $V_e(1)$ which occurs for energies near the energy of a particular two-particle excited state Φ_λ; thus we break the expression for $V_e(1)$ up into two terms:

$$V_e(1)=V_e'(1)+(\Phi_0,v_{1i}\Phi_\lambda)\frac{1}{E-E_\lambda-iW_\lambda}(\Phi_\lambda,t_{1i}\Phi_0). \tag{56}$$

We can now expect that if E is close to E_λ the term $V_e'(1)$ will be slowly varying, partly because it is mainly determined by contributions from far off states and partly because the rapidly varying term depending on the state Φ_λ has been omitted. The remaining term will be rapidly varying and we will consider its variation by approximating v and t with a Yukawa well. This gives a term:

$$\Delta V_e(1)=(0|v|\lambda)^2\frac{1}{E-E_\lambda-iW_\lambda}. \tag{57}$$

It is clear that the real and imaginary parts of this part of the equivalent potential will vary rapidly as E is varied near E_λ. The variation can be estimated by using the relation of Eq. (47) for the width of a level λ. Substituting the potential matrix element $(\lambda|v|0)^2$ given by this equation into Eq. (57) we obtain

$$\Delta V_e(1)=\frac{W_\lambda}{W}[(E_\lambda-E_1)^2+W^2]\frac{E-E_\lambda+iW_\lambda}{(E-E_\lambda)^2+W_\lambda^2}. \tag{58}$$

For E_λ near E_1 so that $(E_\lambda-E_1)<W$, this simplifies to

$$\Delta V_e(1)\cong WW_\lambda\frac{E-E_\lambda+iW_\lambda}{(E-E_\lambda)^2+W_\lambda^2}. \tag{59}$$

We see that both the real and imaginary parts of ΔV_e change by amounts of order W, W being the width of the single-particle level (absorption plus surface penetration). Thus W is the width of the giant resonance and is of order 3 Mev. The sharp variation in V_e occurs over energy interval determined by W_λ which we have shown in the first part of this section to be of the order of tens of kev.

A variation in the real part of the equivalent potential V_e of the order of 3 Mev is of course quite sufficient to lead to a pronounced resonance in the scattering cross section, particularly if the energy E is separated from the giant (single particle) resonance by an energy less than the variation. Although it is rather an oversimplification to regard this change in real well depth as equivalent to a change in the incident energy, this comparison is certainly adequate to show that either a true resonance or a resonance followed by a sharp dip in the cross section can arise from a fluctuation in V_e of the order of 3 Mev.

IV. DISCUSSION AND COMPARISON WITH THE THEORY OF WIGNER, LANE, AND THOMAS

The results we have obtained can be described qualitatively in the following way: the average scattering of a neutron by a nucleus can be represented by the scattering by a complex well, the real part being given by Eq. (14) and the imaginary part by Eqs. (33) and (45). Such an interaction leads to giant resonances in the cross section at the position of the independent-particle states; the general behavior of the cross section is due almost entirely to the real part of the potential, the imaginary part giving only a slight broadening of the resonances and a general smoothing of the cross section. Consequently, the appearance of the giant resonances is a manifestation primarily of the representation of the neutron-nucleus interaction by a uniform-potential-well small imaginary part.

It is possible to derive an interesting relationship between the average level width of the compound nucleus and the parameters of the single-particle levels. Combining Eqs. (29) and (47) we find

$$\frac{(W_\lambda)_{Av}}{D}\cong\frac{W_a W}{(E-E_1)^2+W^2}, \tag{60}$$

where W_a is that part of the single-particle level width due to absorption, W is the total single-particle level width, and E_1 is the energy of the single-particle state. This result shows similarity to a result used by Wigner *et al.*,[9]

$$(\gamma_\lambda^2)_{Av}/D=S(E), \tag{61}$$

where $S(E)$ is a "strength function" which is assumed to have a dependence on energy similar to Eq. (60). Consequently, both in this work and in Wigner's, the average compound-state level width is governed by its proximity to the single-particle state. It is to be noted, however, that very great fluctuations of the widths of individual levels are to be expected due to the range of variation of the matrix elements of the operator connecting the single particle and compound nucleus states. In addition, on our work the strength function $S(E)$ does not play a dominant role in the determination of the scattering. We instead transfer our emphasis to the determination of an equivalent uniform and constant potential which will automatically lead to the giant resonances.

Another departure of our results from those of Wigner *et al.*, is in the determination of the real and imaginary part of the single particle equivalent potential. The most important qualitative departure is in the imaginary part which in our formalism is given by Eq. (21), repeated here for convenience,

$$W_a=\mathrm{Im}\sum_\lambda\sum_j(0|v_{1j}|\lambda)\frac{1}{E-E_\lambda-iW_\lambda}(\lambda|v_{1j}|0). \tag{62}$$

This formula, as we have shown, predicts correctly the approximate magnitude of the average imaginary well strength. It is possible to show that Wigner's result[18]

$$W_a^2=\sum_j(0|v_{1j}^2|0) \tag{63}$$

corresponds to a certain approximation to Eq. (62). Suppose that it is assumed that W_λ is constant and equal to W_a, i.e., that the imaginary part of the potential is the same for all states. Further suppose that the important contributions to the sum over λ come from such states that $|E-E_\lambda|\ll W_\lambda$. In this approximation

$$W_a=\mathrm{Im}\sum_\lambda\sum_\lambda(0|v_{1j}|\lambda)\frac{i}{W_a}(\lambda|v_{1j}|0), \tag{64}$$

or

$$W_a^2=\sum_\lambda\sum_j(0|v_{1j}|\lambda)(\lambda|v_{1j}|0)=\sum_j(0|v_{1j}^2|0), \tag{65}$$

which is Wigner's result. This approximation, however, is not a good representation of the summation of Eq. (62) since the widths W_λ are not constant and, more important, the summation over λ includes states very different in energy from E so that, over most of the sum, $|E_\lambda-E|\gg W_\lambda$. Consequently, a different approximation such as we have used in Sec. II must be used and as shown there gives a much smaller value for W_a than Eq. (65).

V. CONCLUSIONS

We have applied to the neutron reaction problem methods[3-8] which are based on a detailed study of the problem of many nucleons in strong interaction. These methods have in other applications given detailed and quantitative insight into many aspects of the ground and low excited states of nuclei. In extending them to the study of the neutron reactions at low energy, we have shown that the "cloudy crystal ball" model of Weisskopf *et al.*,[1] appears in a natural way and that the predicted parameters of the interaction agree closely with those determined empirically.[19] The methods also show the origin of the sharp compound-nucleus resonances as a manifestation of coupling between the single-particle states and the two- (or more-) particle excited states of the compound nucleus.

It is apparent from these results that the simplicities of nuclear structure which are evidenced in the shell model also persist strongly in the behavior of the nucleus in low-energy scattering. The very small imaginary part of the equivalent potential acting on a particle in a scattering state at low energy reflects the close relationship which exists between the low excited

[18] We have not inserted the effects of the exclusion principle explicitly; these automatically included if, as we have remarked in the introduction, we interpret the v's as appropriately second quantized operators.

[19] The calculated imaginary part of the potential is somewhat smaller than that determined in the empirical analysis; the discrepancy is perhaps due to our omission of the effects of transitions to more complicated (than two-particle) states of the compound nucleus.

states and the ground state where the shell model behavior is most apparent and the single-particle orbits best defined.

It is to be emphasized that the equivalent potential which we have determined is constructed to give the correct scattering of the neutron by the nucleus, i.e., to predict correctly the asymptotic behavior of the wave function. This does not imply that the actual wave function for the system is also given correctly everywhere by this interaction. The actual strongly correlated and highly mixed wave function is instead given in terms of the wave function determined by the equivalent uniform potential by an extremely complicated transformation [Eq. (3)]. Thus we expect that the Weisskopf complex potential can be used to predict only the asymptotic behavior of the scattering wave function, any more detailed information being available only if the transformation is explicitly constructed. This situation is analogous to that which exists in the shell model theory of the nucleus where again predictions of the detailed behavior of the nuclear ground state can be made only if the departures of the nuclear wave function from the shell model wave function due to the strong particle-particle forces are determined.

PHYSICAL REVIEW VOLUME 100, NUMBER 3 NOVEMBER 1, 1955

Two-Nucleon Potential from the Cut-Off Yukawa Theory*

SOLOMON GARTENHAUS†
University of Illinois, Urbana, Illinois
(Received June 8, 1955)

Using the Yukawa theory with cutoff, the two-nucleon interaction is calculated up to fourth order in the coupling constant. The resulting potential at large distances ($\gtrsim 10^{-13}$ cm) is similar to the well-known potential with no cutoff. At small distances, however, the tensor potential approaches zero, and the central potential is strongly repulsive. The details are essentially determined by two parameters, the coupling constant and cutoff. The Schrödinger equation for the two-nucleon problem at low energies is solved numerically, and values are obtained for the binding energy, the quadrupole moment, and the four n-p scattering parameters. It is found that the triplet experimental values are reproduced quite well, and the singlet parameters reasonably well by the same coupling constant and cutoff required to explain pion-nucleon scattering and photoproduction.

I. INTRODUCTION

SINCE the time that Yukawa first proposed to explain nuclear forces as a manifestation of the exchange of field quanta by nucleons, numerous papers have been published on the predicted properties of nuclear systems due to this exchange of pions by nucleons.[1-3] To make any sort of progress, utilization has usually been made of perturbation expansions in the coupling constant as well as the so-called static approximation in which nuclear recoil is almost completely neglected. It has been found that with a local theory (no cutoff) the resulting two-nucleon potential has a strong singularity at small distances, and that this singularity is aggravated by including higher order terms in the expansion. The Schrödinger equation for a two nucleon system is not soluble with such a potential, and the tendency has been to replace the interaction at small distances with a phenomenological, infinite repulsive core. Thus, Brueckner and Watson[2] were able to fit most of the low-energy n-p data, treating the widths of the repulsive cores in the singlet and triplet states as adjustable parameters. Similarly, Taketani[1] utilizing the depth of the cores as an additional parameter, found that best agreement was obtained to the low energy n-p data with infinite repulsive cores. Neglect of nucleon recoil has been justified by the argument that one was interested primarily in low-energy phenomena, where the nucleon velocity is small. Attempts to include recoil terms,[2,3] have not led to conclusive results.

Recently, Chew[4] has shown that reasonable predictions for photo-meson production, pion-nucleon scattering etc. are obtained by the cut-off form of the Yukawa theory. There are two adjustable parameters in this theory, the renormalized coupling constant, f^2, and the cut-off energy of virtual mesons, ω_m. The purpose of the present paper is to show that all of the low energy n-p parameters (i.e., the binding energy, the quadrupole moment as well as the four scattering parameters) can be produced with reasonable accuracy by the above theory with the same values for f^2 and ω_m as are required by pion-nucleon scattering and photoproduction.

* Submitted in partial fulfillment of the requirements for the Ph.D. degree at the University of Illinois.

† Part of this work was done while the author held a General Electric fellowship.

[1] M. Taketani *et al.*, Progr. Theoret. Phys. **7**, 45 (1952).

[2] K. A. Brueckner and K. M. Watson, Phys. Rev. **92**, 1023 (1953).

[3] E. M. Henley and M. A. Ruderman, Phys. Rev. **92**, 1036 (1953).

[4] G. F. Chew, Phys. Rev. **95**, 1669 (1954).

Since the interaction Hamiltonian of reference 4 assumes that the motion of the nucleons can be neglected during the transit times of the pions, for purposes of computing the potential, we consider a physical situation in which two very slowly moving nucleons approach each other and are scattered. (By very "slowly" it is meant that the *kinetic* energy of the nucleons is small compared to the average *total* energy of an exchanged pion.) In the standard way, we separate out those diagrams of the transition matrix which do not have two simultaneous bare nucleon lines between two exchanged-meson lines. The sum of such diagrams is then called the potential V. The justification for this procedure is that if we use this V in the Schrödinger equation to solve the nucleon-nucleon scattering problem, we obtain exactly all of the diagrams included in the original transition matrix. The approximation considered here then, is that terms involving $\omega \pm k^2/M$ where ω is the meson energy and k^2/M is the nucleon energy, are consistently replaced by ω, while energy denominators, such as occur in the solution of the two nucleon Schrödinger equation, k^2/M, are kept intact. Further, we utilize the potential to calculate the deuteron properties on the assumption that the mean velocity of the nucleons in the deuteron is small.

II. DISCUSSION OF THE POTENTIAL

Using the above outlined technique, the calculation of the potentials is straightforward. For the interaction between pions and nucleons, we take[4]

$$H_{\text{int}}=(4\pi)^{\frac{1}{2}}\frac{f_0}{\mu}\sum_{N=1}^{2}\sum_{\lambda}\int d\mathbf{r}\rho(\mathbf{r}-\mathbf{r}_N)\tau_\lambda{}^N\boldsymbol{\sigma}^N\cdot\nabla\phi_\lambda(\mathbf{r}), \quad (1)$$

where f_0 is the dimensionless, unrationalized, unrenormalized coupling constant ($\hbar=c=1$), μ is the pion mass, $\rho(\mathbf{r})$ is the "source function," with the property $\int\rho(\mathbf{r})d\mathbf{r}=1$, $\boldsymbol{\sigma}^N$, $\boldsymbol{\tau}^N$ are the Pauli spin and isotopic spin operators for the Nth nucleon respectively, $\phi_\lambda(\mathbf{r})$ are the three real components of the pion field and $\mathbf{r}_N$ is the position vector of the Nth nucleon. It is useful to introduce the function $v(k)$ which is the Fourier transform of $\rho(\mathbf{r})$,

$$v(\mathbf{k})=\int e^{i\mathbf{k}\cdot\mathbf{r}}\rho(\mathbf{r})d\mathbf{r} \quad (2)$$

and the parameter k_m, defined by

$$\omega_m=(k_m{}^2+\mu^2)^{\frac{1}{2}},$$

where ω_m is the maximum energy for which $v(k)$ differs appreciably from zero. Using (1) we obtain for the second- and fourth-order potentials

$$V_2(r)=-\frac{4\pi}{(2\pi)^3}\left(\frac{f}{\mu}\right)^2\boldsymbol{\tau}^1\cdot\boldsymbol{\tau}^2\int\frac{d\mathbf{k}v^2(k)e^{i\mathbf{k}\cdot\mathbf{r}}}{\omega_k{}^2}\boldsymbol{\sigma}^1\cdot\mathbf{k}\boldsymbol{\sigma}^2\cdot\mathbf{k}, \quad (3)$$

$$V_4(r)=-\frac{(4\pi)^2}{(2\pi)^6}\left(\frac{f}{\mu}\right)^4\int\int\frac{d\mathbf{k}_1d\mathbf{k}_2}{\omega_1{}^3\omega_2}e^{i(\mathbf{k}_1+\mathbf{k}_2)\cdot\mathbf{r}}$$
$$\times\left[\left(\frac{3}{\omega_2}+\frac{2\boldsymbol{\tau}^1\cdot\boldsymbol{\tau}^2}{\omega_1+\omega_2}\right)(\mathbf{k}_1\cdot\mathbf{k}_2)^2\right.$$
$$+\boldsymbol{\sigma}^1\cdot(\mathbf{k}_1\times\mathbf{k}_2)\boldsymbol{\sigma}^2\cdot(\mathbf{k}_1\times\mathbf{k}_2)$$
$$\left.\times\left(\frac{3}{\omega_1+\omega_2}+\frac{2\boldsymbol{\tau}^1\cdot\boldsymbol{\tau}^2}{\omega_2}\right)\right]v^2(k_1)v^2(k_2), \quad (4)$$

($\mathbf{r}$ is the internucleon distance) which except for the $v(k)$ factors are identical to the corresponding terms of formula (60) of reference 2. If $\rho(\mathbf{r})$ is spherically symmetric, it follows from Eq. (2) that $v(k)$ is also angle independent. The angular integrations are then elementary but tedious and ultimately yield:

$$V_2(r)=-\frac{2}{3\pi}\left(\frac{f}{\mu}\right)^2\boldsymbol{\tau}^1\cdot\boldsymbol{\tau}^2\left\{\frac{\boldsymbol{\sigma}^1\cdot\boldsymbol{\sigma}^2}{r}\int_0^\infty\frac{k^3dkv^2(k)}{\omega_k{}^2}\sin kr\right.$$
$$+3S_{12}\int_0^\infty\frac{kdkv^2(k)}{\omega_k{}^2}$$
$$\left.\times\left[\left(\frac{k^2}{3r}-\frac{1}{r^3}\right)\sin kr+\frac{k}{r^2}\cos kr\right]\right\}, \quad (5)$$

and

$$V_4(r)=-\frac{2}{\pi^2}\left(\frac{f}{\mu}\right)^4\int_0^\infty\int_0^\infty\frac{k_1k_2dk_1dk_2v^2(k_1)v^2(k_2)}{\omega_1\omega_2(\omega_1+\omega_2)}$$
$$\times\left\{\left[\frac{6}{\omega_1\omega_2}+(3+2\boldsymbol{\tau}^1\cdot\boldsymbol{\tau}^2)\left(\frac{1}{\omega_1{}^2}+\frac{1}{\omega_2{}^2}\right)\right]\right.$$
$$\times\left[f_1''f_2''+\frac{2f_1'f_2'}{r^2}\right]$$
$$+\tfrac{2}{3}S_{12}\left[\frac{4\boldsymbol{\tau}^1\cdot\boldsymbol{\tau}^2}{\omega_1\omega_2}+(3+2\boldsymbol{\tau}^1\cdot\boldsymbol{\tau}^2)\right.$$
$$\times\left.\left(\frac{1}{\omega_1{}^2}+\frac{1}{\omega_2{}^2}\right)\right]\left[\frac{f_1'f_2'}{r^2}-\frac{f_1''f_2'}{r}\right]$$
$$+\tfrac{2}{3}\boldsymbol{\sigma}^1\cdot\boldsymbol{\sigma}^2\left[\frac{4\boldsymbol{\tau}^1\cdot\boldsymbol{\tau}^2}{\omega_1\omega_2}+(3+2\boldsymbol{\tau}^1\cdot\boldsymbol{\tau}^2)\right.$$
$$\left.\left.\times\left(\frac{1}{\omega_1{}^2}+\frac{1}{\omega_2{}^2}\right)\right]\left[2\frac{f_1''f_2'}{r}+\frac{f_1'f_2'}{r^2}\right]\right\}, \quad (6)$$

where $f_i=\sin(kr)/r$; $i=1, 2$, the prime means differentiation with respect to r, and $S_{12}=(3\sigma^1\cdot\mathbf{r}\sigma^2\cdot\mathbf{r}/r^2)-\sigma^1\cdot\sigma^2$ as usual.

In the formulas (3) to (6), the unrenormalized coupling constant, f_0, does not appear; instead the renormalized coupling constant, f, appears. This replacement, as is well known, has the effect of including many seemingly higher-order terms in the expansion of the potential. Thus, for example, if the coupling constant in the second order potential, Eq. (5), were f_0 instead of f, then this term would correspond to the exchange of a single meson by two "bare" nucleons. If one modifies this term to include also those diagrams in which various numbers of mesons are emitted and reabsorbed by the same nucleon while a single meson is exchanged, then the sum of this series is equal to the one-meson exchange term provided only that we replace f_0 by f. This in turn means that one may speak of a single meson being exchanged between two physical nucleons, i.e., nucleons which are modified by their associated mesonic clouds. Similarly, in the case of two-meson exchange, one can speak of the crossing of two mesons between two physical nucleons. In this situation, however, one may not so simply state that the effect of the nucleons not actually being bare is equivalent to replacing f_0 by f. For there are the well-known multiple-scattering corrections[2,3] which will not be included in the potential by this method. Thus, use of the renormalized coupling constant in the potential enables us to include many seemingly higher-order terms. However, radiative corrections, which go at worst like f^4, have been completely left out; this neglect is further discussed below.

The effect which the factor $v^2(k)$ has on the behavior of the above potentials is worthy of notice. To observe the small-r dependence one may expand the integrands of (5) and (6) in powers of r and keep only the first term. It is easily shown that there are no singularities in the potentials, that at small r the second- and fourth-order central potentials are strongly repulsive in singlet as well as in triplet even states, and that the second- and fourth-order tensor potentials approach zero with r. All the details in this region are completely determined by $v(k)$ and f^2. Further, it can be shown that for sufficiently small r the behavior of the potentials, to a good approximation, is given by a certain function of the argument, $k_m r$, which means that a change in k_m is equivalent to changing the scale of r in this region. For large r, on the other hand, the potentials, (5) and (6) coincide with the corresponding formulas of reference 2, showing that, as expected, $v(k)$ has little effect in this region.

To see the functional dependence of the potentials on $v(k)$ more clearly, let us examine (3) or (5) more closely in the absence and presence of $v(k)$. To be specific, let us concentrate on the central part of the force and in order to be able to evaluate integrals analytically, let us select

$$v(k)=k_m^2/(k^2+k_m^2). \tag{7}$$

The central part of Eq. (3) in even states can be written in general as

$$V_{2c}(r)=\frac{4\pi}{(2\pi)^3}\left(\frac{f}{\mu}\right)^2\int d\mathbf{k}e^{i\mathbf{k}\cdot\mathbf{r}}v^2(k) - \frac{4\pi}{(2\pi)^3}\mu^2\left(\frac{f}{\mu}\right)^2\int\frac{d\mathbf{k}e^{i\mathbf{k}\cdot\mathbf{r}}v^2(k)}{\omega_k^2}. \tag{8}$$

In the no-cutoff theory, $v^2(k)=1$ and (8) becomes

$$V_{2c}(r)=4\pi\left(\frac{f}{\mu}\right)^2\delta(\mathbf{r})-\mu f^2\frac{e^{-\mu r}}{\mu r}, \tag{9}$$

which corresponds to a delta-function repulsion at the origin and Yukawa attraction for $r\neq 0$. If now, however, we use $v(k)$ as given by (7), there results

$$V_{2c}(r)=\mu f^2\frac{1}{2}\left(\frac{k_m}{\mu}\right)^3 e^{-k_m r}-\frac{\mu f^2}{(1-\mu^2/k_m^2)^2} \times\left\{\frac{e^{-\mu r}}{\mu r}-e^{-k_m r}\left[\frac{1}{\mu r}+\frac{1}{2}\frac{k_m}{\mu}\left(1-\frac{\mu^2}{k_m^2}\right)\right]\right\}, \tag{10}$$

in which the first term on the right corresponds to the delta function in Eq. (9) and the second term to the Yukawa potential. In the cut-off theory, since $\omega_m\cong 6\mu$, (10) approaches the Yukawa potential for large $r(\gtrsim 1/\mu)$ but remains finite for $r=0$. Specifically in the limit of small r, equation (10) becomes

$$V_{2c}(0)=1+\frac{1}{2}\left(\frac{k_m}{\mu}\right)^3-\frac{3}{2}\left(\frac{k_m}{\mu}\right)$$

and approaches plus infinity as $(k_m/\mu)\to\infty$, which is identical to the result of (9). Also, it is clear from Eq. (10) that if for $r\neq 0$ one takes the limit as $(k_m/\mu)\to\infty$, then one obtains the usual result, namely, (9). However, in our case, where k_m is finite, the delta-function repulsion of (8) becomes spread out away from the origin and gives a repulsive core of nonzero width which is determined by the values of k_m and f^2.

In evaluating the potentials (5) and (6) one has substantial freedom in selecting the function, $v(k)$. A basic feature of the cut-off theory is that the precise functional form of $v(k)$ is irrelevant as far as predictions of the theory are concerned; the only requirements on $v(k)$ being that it be close to unity for values of k less than k_m and be effectively zero for k greater than k_m. This invariance of the theory does not mean, for example, that the potentials themselves are independent of the form of $v(k)$ but only that physical quantities which are predicted by these potentials are. The numerical value of k_m was obtained by the comparison of the

theory to pion-nucleon scattering data.[5] Specifically, the quantities which were compared to experiment were integrals of the approximate form:

$$\text{(a)} \quad \int_0^\infty v^2(k)d(k^2)$$

and

$$\text{(b)} \quad \int_0^\infty v^2(k)dk.$$

Selecting $v(k)$ as a square cutoff, the first of these integrals was defined to be k_m^2 and the second, k_m. If now a different functional form for $v(k)$ is selected we impose the condition on $v(k)$ that

$$\int_0^\infty v^2(k)d(k^2)=k_m^2$$

and check the consistency by seeing how close the integral (b) is to k_m.

The first evaluation of the potentials was done with a square cut-off function. This forcing of the integrands of (5) and (6) to become zero very abruptly, led to oscillations in the potentials for large values of r, and as such was not convenient for the numerical solution of the n-p differential equations. On the other hand, a $v(k)$ with a long tail makes evaluation of the potentials themselves difficult. As a compromise between these two extremes it was decided to select a Gaussian cut-off function,

$$v(k)=\exp(-k^2/2k_m^2).$$

This choice of $v(k)$ is satisfactory since with it the integral (a) becomes k_m^2 and the integral (b) is equal to $\frac{1}{2}(\pi)^{\frac{1}{2}}k_m$ which is within 10% of k_m. The potentials (5) and (6) were evaluated numerically with this choice of $v(k)$ and are plotted in Figs. 1 and 2.

Evaluation of (5) and (6) in the case of $\omega_m=6\mu$ and $f^2=0.089$, brings out the following characteristics. The second-order tensor force approaches zero at the origin, is then attractive all the way out, and has its maximum attraction of about 140 Mev near $r=0.6/\mu$. The fourth-order tensor potential also approaches zero with r, but on the other hand, is only about one-third as large and of the opposite sign, thus yielding an over-all attractive tensor force of about 100 Mev at max. As for the second-order central force, the possibility of subtracting out the delta function repulsion [Eq. (8)] leaves the attractive part of this potential smaller than "normal" by a factor of $\sim(\mu/k_m)^2$. Evaluation of the central part of Eq. (5) for $\omega_m=6\mu$, $f^2=0.089$, shows that although in close the repulsion is of order 1 Bev, the maximum attraction is only about 5 Mev; this is not nearly enough attraction to give the large singlet scattering length required by experiment. The fourth-order singlet potential, on the other hand, has a maximum attraction of about 70 Mev for the same choice of f^2 and k_m. Thus, in the singlet state, the second-order attractive force is effectively zero and the major contribution to it comes from the fourth and possibly higher orders. Similarly, in the triplet state, the fourth-order central potential is substantially larger than the second order. The large-

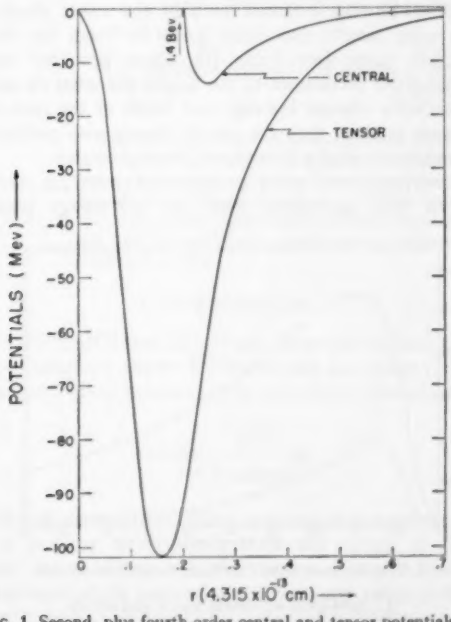

FIG. 1. Second- plus fourth-order central and tensor potentials in even angular momentum states for $f^2=0.089$ and $\omega_m=6\mu$.

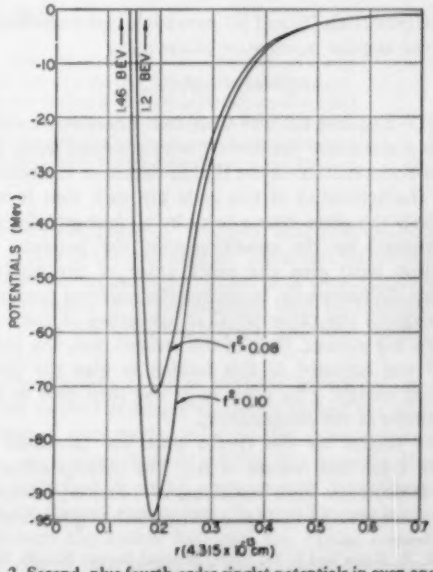

FIG. 2. Second- plus fourth-order singlet potentials in even angular momentum states for $\omega_m=6\mu$, $f^2=0.089$ and $f^2=0.10$.

[5] G. F. Chew, Phys. Rev. 95, 285 (1954).

TABLE I. Triplet parameters obtained with the potentials using the indicated values of f^2 and ω_m.

f^2	$\omega_m(\mu)$	P_D (%)	Q (10^{-27} cm^2)	r_{1t} (10^{-13} cm)	a_t (10^{-13} cm)
0.089	6.00	6.80	2.90	1.75	5.42
0.093	5.60	7.00	3.08	1.81	5.47
Experimental		2–8	2.74	1.70	5.39

ness of the tensor potential, however, leads one to feel that higher-order corrections to the triplet potentials will not be as important as those to the singlet.

The accuracy with which the second- and fourth-order terms alone represent the potential is difficult to gauge. As of now, no attempts have been made to derive the higher-order corrections to the potential within the cut-off theory. Indication from other considerations makes the author feel that these corrections will not radically change the potentials computed here. Brueckner and Watson[2] have concluded as a result of their studies that for $r \gtrsim 0.6/\mu$ the second- and fourth-order terms are good approximations to the potential, in that multiple scattering corrections are unimportant in this region, amounting to about 30% at maximum and decreasing very rapidly with r. In the present case, the maximum attraction of the triplet potential is very near to $r=0.6/\mu$ and thus the central potential computed here should be a reasonable approximation. The core of the singlet potential, on the other hand, occurs at about $r=0.5/\mu$ and thus may require some higher order corrections in this region. In any event, a very strong assumption made here is that higher-order corrections will not remove the repulsive core.

III. COMPARISON TO EXPERIMENT

The potentials (5) and (6) were evaluated numerically for even angular momentum states using

$$v(k)=\exp(-k^2/2k_m^2)$$

for $\omega_m=5.6\mu$ and 6μ. The deuteron characteristics and the n-p scattering parameters were obtained using the Blatt-Kalos routine on the Illinois electronic computer.[6] The characteristics of this code are such that it will multiply the given tensor force by a constant which is determined by the condition that the potential in question shall give the exact value of the binding energy. Subsequently, it utilizes the resulting potential to compute the other physical properties of the low-energy n-p system. Now in the present case, the value of f^2 was adjusted in this fashion to give the exact binding energy. This value of f^2 was then used in the remainder of the computation.

The results for the triplet state are tabulated in Table I for both values of ω_m. The corresponding S and D deuteron wave functions, $u(r)$ and $w(r)$ respectively are plotted in Fig. 3. Remarkably good results were obtained for $\omega_m=6\mu$ and $f^2=0.089$. The agreement for $\omega_m=5.6\mu$, although not as good as the other case, still gives results which probably lie within errors due to the approximations made in neglecting higher-order terms (e.g., the f^8 and higher terms are neglected). We conclude thus, that all the triplet parameters of the n-p system can be obtained, via the cut-off meson theory, provided only that higher-order corrections do not appreciably change the qualitative features of the potentials, which have been obtained here.

With the above values of ω_m and f^2, the singlet parameters were ostensibly not in as good agreement with experiment. The singlet potential, even though it has about three times the depth of the triplet central potential, does not have enough attraction with $f^2=0.089$, to give the large singlet scattering length which is observed. However, the conclusions of Brueckner and Watson,[2] that corrections to the potential due to multiple scatterings are *attractive* and of the order of 30% near $r=0.6/\mu$ tends to make the lack of agreement appear not too unreasonable. Since for a value of $f^2=0.089$, the maximum attraction in the singlet potential occurs at about $r=0.6/\mu$, it seems plausible to simulate some of these higher-order multiple scattering effects by an increase in the coupling constant. Thus it is found that for $\omega_m=6\mu$, a value of $f^2=0.10$ (this differs by 12%, from the value of f^2 required in the triplet state) gives the correct singlet scattering length and yields 2.54×10^{-13} cm for the value of the singlet effective range. Similarly, for $\omega_m=5.6\mu$, a value of $f^2=0.11$ was required to give the exact singlet scattering length and yield 2.65×10^{-13} cm for the effective range (see Table II). Thus, provided the higher-order corrections to the singlet potential do not appreciably change the sign and width of the core, it appears hopeful that the cut-off theory also predicts correctly the singlet behavior of the n-p system.

Chew and Low,[7] using an improved technique, have shown that agreement with the low-energy pion-

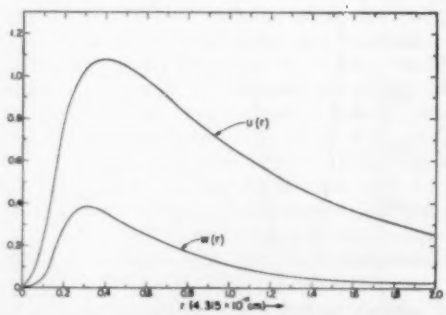

FIG. 3. The deuteron wave functions, normalized so that $\int_0^\infty (u^2+w^2)dr=1$, where $u(r)/r$ and $w(r)/r$ correspond to the S and D states respectively.

[6] M. H. Kalos and J. M. Blatt, Internal Report No. 50, University of Illinois, Digital Computer Laboratory, 1953 (unpublished).

[7] G. F. Chew and F. E. Low (to be published).

phenomena is obtained by a coupling constant in the neighborhood of 0.07–0.08 and a cut-off energy near 6μ. These values are quite close to those used here to give best agreement for the low-energy n-p system. Thus, except possibly for peculiarities which may appear in higher orders, it seems that the low-energy n-p system can be predicted without recourse to adjustable parameters.

The application of these potentials to problems at higher energies has not yet been considered by the present author. In making the calculation here, nucleon kinetic energies have been consistently ignored relative to total meson energies. How large the nucleon energies may become before the calculation breaks down is a question which is difficult to answer without further work. Since the depth of the attractive part of the triplet central force is of the order 15 Mev, it is expected that the nucleon kinetic energies in the deuteron also are of this magnitude. The agreement obtained for the deuteron thus leads one to speculate that the potentials may be reliable for nucleon energies beyond the range of reliability of the effective range theory. Indeed, Fujii *et al.*[8] have applied their potentials to n-p scattering at 40 and 90 Mev and have concluded that the characteristic features of the high-energy nucleon-nucleon scattering are reproduced quite well. It seems reasonable, therefore, that the potentials derived here may also apply at these higher energies.

[8] S. Fujii *et al.*, Progr. Theoret. Phys. **11**, No. 1 (1954).

TABLE II. The singlet effective ranges obtained by adjusting f^2 to give the exact singlet scattering length.

f^2	$\alpha_m(\mu)$	r_{0s} (10^{-13} cm)
0.10	6	2.54
0.11	5.6	2.65

ACKNOWLEDGMENTS

The author would like to express his deepest gratitude to Professor G. F. Chew for his suggesting this problem and his constant help throughout. Without his guidance and encouragement this work would not have been possible. He would also like to thank Professor F. E. Low and Dr. Y. Yamaguchi for many helpful discussions. Also, thanks are due Professors R. E. Meagher and J. P. Nash at the Illinois computer laboratory for the liberal machine time allocated for this problem.

PHYSICAL REVIEW VOLUME 100, NUMBER 3 NOVEMBER 1, 1955

State-Vector Normalization in Formal Scattering Theory*

BRYCE S. DEWITT
Radiation Laboratory, Department of Physics, University of California, Berkeley, California
(Received June 13, 1955)

The familiar problem of state-vector normalization and, in field theories, the related problem of charge renormalization are shown to arise in a natural manner in the formal scattering theory introduced by Lippmann and Schwinger. The mathematical arguments necessary for dealing with these problems are developed entirely within the framework of the formal theory and lead to the customary rules for the construction of the renormalized S-matrix and reactance operator, provided mass renormalization is simultaneously carried out and the one-to-one correspondence between perturbed and unperturbed eigenstates is set up in a "natural" fashion.

I. INTRODUCTION

LIPPMANN and Schwinger[1] have shown that the stationary states which describe scattering processes for a given system may be represented formally by

$$\psi^{\pm}=\lim_{\epsilon\to 0}\frac{\pm i\epsilon}{E-H\pm i\epsilon}\phi, \qquad (1)$$

where H is the Hamiltonian operator of the system, ϵ is a positive infinitesimal, E is the energy of the state in question, and the vector ϕ represents a plane wave of the same energy. The $+$ sign refers to the states with outgoing or "retarded" scattered waves, and the $-$ sign to the incoming or "advanced" wave states. That $\psi^{\pm}$ are indeed eigenvectors of H corresponding to the eigenvalue E is immediately seen by multiplying Eq. (1) on the left by $E-H\pm i\epsilon$ and then passing to the limit.

Although Eq. (1) was initially introduced in the limited context of simple scattering theory, its use as a method of constructing eigenvectors of an operator H has a much wider range of validity. For example, H may be a finite matrix, or an operator with discrete rather than continuous eigenvalues. In a review article (to be published) the author has used Eq. (1) as a starting point for a discussion of bound-state perturbation theory. It is the purpose of the present note, however,

* This work was performed under the auspices of the U. S. Atomic Energy Commission.
[1] B. A. Lippmann and J. Schwinger, Phys. Rev. **79**, 469 (1950).

to point out that Eq. (1) may also be used as a basis for a connected description of scattering theory as it appears in the complicated context of the renormalization program for quantized fields. It is easy to see, in fact, that the normalization (or renormalization) problem arises quite naturally in a formalism based on Eq. (1); for, when E is an eigenvalue of H then the operator $\pm i\epsilon(E-H\pm i\epsilon)^{-1}$ projects out only that portion of ϕ which lies in the corresponding eigen-subspace. Therefore $\psi^{\pm}$ as given by Eq. (1) is not generally normalized. The fact that it *is* normalized in simple scattering problems is due to special circumstances.

In dealing with discrete spectra one may use almost any vector ϕ on the right of Eq. (1) in order to construct an eigenvector of H. When continuous spectra are involved, however, it appears to be not only a convenience for physical interpretation but a practical mathematical necessity to choose ϕ in a special way, namely, to be an eigenvector of an "unperturbed" Hamiltonian operator H_0 which is obtained from H by subtracting a portion H_1 which has an obvious significance as a scattering potential, an interaction, or a "coupling":

$$H_0=H-H_1. \tag{2}$$

One then sets up a one-to-one correspondence between the eigenvectors $\psi_a^{\pm}$ of H and the eigenvectors ϕ_a of H_0 in such a way that the $\psi_a^{\pm}$ approach the ϕ_a as $H_1\to 0$, where the vanishing of H_1 is assumed to take place in a *linear* fashion; i.e., $g\to 0$ where $H_1=g\mathfrak{C}$, g being often referred to as a "coupling constant." This, of course, involves some sort of assumption about quantities being analytic in g at the origin, which may or may not be justified but which nevertheless underlies all proposals for dealing with quantized field problems which have had any success to date. If the criterion of analyticity in g is satisfied, then, as will presently become apparent, Eq. (1) becomes an adequate vehicle with which to express the one-to-one correspondence between the $\psi_a^{\pm}$ and the ϕ_a.

We shall follow the accepted practice of rendering the continuous spectrum discrete by imposing periodic boundary conditions with respect to a fundamental volume $V=L^3$ upon the eigenfunctions of H_0 so that the uniform orthonormalization,

$$(\phi_b,\phi_a)=\delta_{ba}, \tag{3}$$

may be employed for all the eigenvectors ϕ_a. When V is very large we shall speak of the resulting spectrum as "quasi-continuous."

II. THE NORMALIZATION CONSTANTS

In order that normalization be properly taken into account in contexts more general than simple scattering theory, Eq. (1) must be modified by the insertion of an appropriate normalization constant. For compactness of notation let us introduce the Green's function[2]

$$G^{\pm}(E)=G^{\mp}(E)^{\dagger}=(E-H\pm i\epsilon)^{-1} \tag{4a}$$

$$=G_0^{\pm}(E)[1+H_1G^{\pm}(E)]$$
$$=[1+G^{\pm}(E)H_1]G_0^{\pm}(E) \tag{4b}$$

$$=G_0^{\pm}(E)[1-H_1G_0^{\pm}(E)]^{-1}$$
$$=[1-G_0^{\pm}(E)H_1]^{-1}G_0^{\pm}(E), \tag{4c}$$

where

$$G_0^{\pm}(E)=G_0^{\mp}(E)^{\dagger}=(E-H_0\pm i\epsilon)^{-1}, \tag{5}$$

and then write

$$Z_a^{\frac{1}{2}}\psi_a^{\pm}=\pm i\epsilon G^{\pm}(E_a)\phi_a, \tag{6}$$

where the Z_a are the normalization constants and the E_a are the eigenvalues of H. Here (and from now on) the limit $\epsilon\to 0$ is to be understood.

In the case of quantized fields, as in bound-state theory, the spectra of H and H_0 are not generally identical. We shall therefore redefine H_0 and H_1 according to the scheme[3]

$$\begin{aligned} H_0&\to H_0+\textstyle\sum_a|\phi_a\rangle\Delta E_a\langle\phi_a|,\\ H_1&\to H_1-\textstyle\sum_a|\phi_a\rangle\Delta E_a\langle\phi_a|,\end{aligned} \tag{7}$$

where the ΔE_a are the *level shifts* which may be computed later in the course of solving the problem (if desired). The ΔE_a evidently play a role in the definition of the one-to-one correspondence between the $\psi_a^{\pm}$ and the ϕ_a, for it must be assumed that $\Delta E_a\to 0$ as $g\to 0$. It is to be observed that the switching off of the "perturbation" ($H_1\to 0$) is no longer a linear process, since H_1 now involves not only $g\mathfrak{C}$ but also the ΔE_a which are complicated functions of g assumed to be analytic at the origin.

With these modification one has

$$H\psi_a^{\pm}=E_a\psi_a^{\pm}, \quad H_0\phi_a=E_a\phi_a, \tag{8}$$

so that Eq. (6) may be rewritten in the form

$$Z_a^{\frac{1}{2}}\psi_a^{\pm}=G^{\pm}(E_a)[G_0^{\pm}(E_a)]^{-1}\phi_a$$
$$=[1+G_0^{\pm}(E_a)R^{\pm}(E_a)]\phi_a, \tag{9}$$

where

$$R^{\pm}(E)=R^{\mp}(E)^{\dagger}$$

$$=[G_0^{\pm}(E)]^{-1}G^{\pm}(E)H_1=H_1G^{\pm}(E)[G_0^{\pm}(E)]^{-1} \tag{10a}$$

$$=H_1+H_1G^{\pm}(E)H_1 \tag{10b}$$

$$=H_1[1+G_0^{\pm}(E)R^{\pm}(E)]$$
$$=[1+R^{\pm}(E)G_0^{\pm}(E)]H_1 \tag{10c}$$

$$=H_1[1-G_0^{\pm}(E)H_1]^{-1}=[1-H_1G_0^{\pm}(E)]^{-1}H_1. \tag{10d}$$

[2] The Fourier transform of $G^{\pm}(E)$, namely

$$G^{\pm}(t)=(2\pi)^{-1}\textstyle\int_{-\infty}^{\infty}G^{\pm}(E)e^{-iEt}dE,$$

satisfies the differential equation $(i\partial/\partial t-H)G^{\pm}(t)=\delta(t)$ in the limit $\epsilon\to 0$.

[3] In relativistic field theories the customary redefinition of H_0 and H_1 is slightly different from this. Equation (7) amounts to a renormalization of energy, which is not relativistically invariant. The invariant *mass* renormalization, however, involves only a trivial modification.

Equation (9) now shows explicitly the correspondence $\psi_a^{\pm} \to \phi_a$, $Z_a \to 1$, as the perturbation is switched off, since $R^{\pm}(E) \to 0$ as $H_1 \to 0$.[4]

The $Z_a^{\frac{1}{2}}$, as has already been intimated, are projection coefficients and hence have a simple physical significance. To see this, take the scalar product of Eq. (6) with $\psi_a^{\pm}$ and impose the condition $(\psi_a^{\pm}, \psi_a^{\pm}) = 1$, obtaining

$$Z_a^{\frac{1}{2}} = (\psi_a^{\pm}, \pm i\epsilon G^{\pm}(E_a)\phi_a) = (\mp i\epsilon G^{\mp}(E_a)\psi_a^{\pm}, \phi_a) = (\psi_a^{\pm}, \phi_a). \quad (11)$$

The phases of the $\psi_a^{\pm}$ will be assumed to be defined by taking the $Z_a^{\frac{1}{2}}$ to be positive real numbers. Then Z_a *is the probability of finding the state* ϕ_a *in the state* $\psi_a^{\pm}$, and hence

$$0 \leq Z_a \leq 1. \quad (12)$$

The nondependence of the Z_a on the $\pm$ signs may be inferred by taking the scalar product of Eq. (6) with itself.

III. ORTHOGONALITY

We have now to investigate the orthogonality of the $\psi_a^{\pm}$. It will be convenient at this point to record three identities satisfied by the operators $R^{\pm}(E)$:

$$R^{\mp}(E_b) - R^{\pm}(E_a) \equiv (E_a - E_b \pm 2i\epsilon) R^{\mp}(E_b) \times G_0^{\mp}(E_b) G_0^{\pm}(E_a) R^{\pm}(E_a), \quad (13)$$

$$R^{\pm}(E_b) - R^{\pm}(E_a) \equiv (E_a - E_b) R^{\pm}(E_b) \times G_0^{\pm}(E_b) G_0^{\pm}(E_a) R^{\pm}(E_a), \quad (14)$$

$$\partial R^{\pm}(E)/\partial E \equiv -R^{\pm}(E)[G_0^{\pm}(E)]^2 R^{\pm}(E). \quad (15)$$

The first two identities follow from Eqs. (10a, b) and the third is obtained from the second by passing to the limit $E_b \to E_a$.

Using Eqs. (3), (9), and (13), one may write[5]

$$\begin{aligned}(Z_b Z_a)^{\frac{1}{2}}(\psi_b^{\pm}, \psi_a^{\pm}) &= (\phi_b, [1 + R^{\mp}(E_b) G_0^{\mp}(E_b)][1 + G_0^{\pm}(E_a) R^{\pm}(E_a)]\phi_a) \\ &= \delta_{ba} + \left(-\frac{1}{E_a - E_b \pm i\epsilon} + \frac{1}{E_a - E_b \pm 2i\epsilon} \right) \times (\phi_b, [R^{\mp}(E_b) - R^{\pm}(E_a)]\phi_a) \\ &\underset{\epsilon \to 0}{\to} \begin{cases} 0, & E_b \neq E_a, \\ \delta_{ba} \pm \epsilon^{-1}(\phi_b, \mathrm{Im} R^{\pm} \phi_a), & E_b = E_a, \end{cases} \end{aligned} \quad (16)$$

where

$$R^{\pm} = \sum_a R^{\pm}(E_a) |\phi_a\rangle\langle\phi_a|. \quad (17)$$

In simple scattering problems the operator H_0 is chosen in such a way that H_1 refers to a scattering force which is *confined to a limited region of space*. The vectors ϕ_a are usually taken to correspond to (1) plane waves, (2) spherical harmonics of plane waves, or (3) Coulomb wave functions if part of the scattering force is inverse-square. The matrix elements $(\phi_b, H_1 \phi_a)$, and hence $(\phi_b, R^{\pm}\phi_a)$, are then of order V^{-1} in magnitude, owing to the normalization condition Eq. (3). Gell-Mann and Goldberger[5] have argued that the limiting process $\epsilon \to 0$ must be accompanied by a simultaneous limiting process $V \to \infty$ of such a nature that $(\epsilon V)^{-1} \to 0$, and hence that the term involving $\mathrm{Im} R^{\pm}$ in Eq. (16) vanishes, implying the orthonormality of the $\psi_a^{\pm}$ with $Z_a = 1$. As the argument given by these authors is rather obscure we feel it advisable to restate it in a different form. The matter is really quite simple. With the imposition of the periodic boundary conditions the level separation in the quasi-continuous spectrum is of order L^{-1}. In order that the imaginary parts $\pm i\epsilon$ of the energy denominators of the Green's functions give the correct causal description of the scattering process (i.e., be able to make the distinction between retarded and advanced waves), ϵ must be much larger than the level spacing so that the summation over intermediate states will take on a *fine-grained* aspect with respect to ϵ and be representable as an integral over a contour which passes definitely to one side or the other of the energy pole. Therefore $L^{-1}/\epsilon \to 0$ and *a fortiori* $(\epsilon V)^{-1} \to 0$.[6]

In cases in which the Z_a are not simply equal to unity Eq. (16) may be used to compute their values. A problem evidently arises if the spectrum of H is degenerate. It is necessary to show that the quantity $(\phi_b, \mathrm{Im} R^{\pm}\phi_a)$ is diagonal in a and b when $E_b = E_a$, in order to insure the orthogonality of the $\psi_a^{\pm}$ within degenerate subsets. It is useful to consider first the situation as it occurs in simple bound-state (discrete spectrum) theory. If we exclude the possibility of accidental degeneracy, then the degeneracy in question persists for all values of g, and in particular when the perturbation is switched off. This type of "nonremovable" degeneracy has its origin in special symmetry properties possessed by H_1, and it is well known that the ϕ_a can then be chosen in such a way that $(\phi_b, \psi_a^{\pm}) = 0$ if $a \neq b$ with $E_a = E_b$. The combination of this result with Eqs. (9) and (11) implies $(\phi_b, R^{\pm}\phi_a) = \pm i\epsilon(Z_a - 1)\delta_{ba}$ for $E_a = E_b$, and hence the orthogonality of the $\psi_a^{\pm}$ via Eq. (16). The nonremovability of the degeneracy also implies $Z_a = Z_b$ for $E_a = E_b$.

The situation in field theory is quite similar. Again

[4] If H possesses eigenstates (e.g., extra bound states) which have no counterparts among the ϕ_a, then these states and their corresponding eigenvalues are to be excluded from the present discussion. Also to be excluded are unstable eigenstates of H_0, since these have no counterparts among the eigenvectors of H. In passing from H_0 to H these latter states undergo a mathematical as well as physical decay, and their renormalization constants Z_a vanish rigorously.

[5] M. Gell-Mann and M. L. Goldberger, Phys. Rev. **91**, 398 (1953).

[6] A more physical argument involves the recognition that the use of ϵ is related to an adiabatic switching procedure in which the perturbation H_1 is "turned on" for a length of time of order ϵ^{-1}. If this mathematical trick is to provide an adequate substitute for an actual physical process involving a wave packet which moves unperturbed both before and after scattering, then ϵ^{-1} must be much shorter than the length of time L/v taken by the packet to traverse the fundamental volume, v being the packet velocity.

nonremovable degeneracy arises from the symmetry properties of H_1. Let us suppose that the ϕ_a represent free-particle momentum states, the operator H_0 describing the noninteracting fields. The closest analogs of the states of discrete-spectrum theory are the 1-particle states and the vacuum state. For these states the result $(\phi_b, R^{\pm}\phi_a) = \pm i\epsilon(Z_a - 1)\delta_{ba}$ again holds. Here, moreover, on account of the symmetries of H_1 and the relativistic invariance of the theory, Z_a depends not just solely on the energy but solely on the particle in question. As in discrete-spectrum theory the constants Z_a, and hence $(\phi_b, R^{\pm}\phi_a)$ for these states, are independent of the normalization volume V.

For many-particle states the operator $R^{\pm}$ may be separated into two parts, one which is dependent on and the other which is independent of V. We shall call the latter the "singular part" and the former part the "remainder," writing

$$R^{\pm} = \mathrm{Sing}R^{\pm} + \mathrm{Rem}R^{\pm}. \tag{18}$$

The structure of these parts is easily visualized in terms of Feynman diagrams. $\mathrm{Rem}R^{\pm}$ corresponds to all those diagrams in which at least two real particles (as opposed to virtual particles) interact. The contribution to $R^{\pm}$ from such a diagram is of order $V^{-N/2}$ where N is the number of irreducible vertex parts leading to external real particles. Therefore $\mathrm{Rem}R^{\pm}$ makes no contribution to the normalization of the $\psi_a{}^{\pm}$. The normalization is completely determined by $\mathrm{Sing}R^{\pm}$, whereas the physically observed scattering is completely described by $\mathrm{Rem}R^{\pm}$.

$\mathrm{Sing}R^{\pm}$ corresponds to the diagrams in which the real particles involved (as well as the vacuum) undergo self-energy interactions with virtual quanta but otherwise suffer no change of state. One may therefore write generally

$$\mathrm{Sing}(\phi_b, \psi_a{}^{\pm}) = Z_a{}^{\frac{1}{2}}\delta_{ba} \tag{19}$$

and

$$(\phi_b, \mathrm{Sing}R^{\pm}\phi_a) = \pm i\epsilon(Z_a - 1)\delta_{ba}, \tag{20}$$

it being here not even necessary to specify $E_a = E_b$.[7] This completes the proof that

$$(\psi_b{}^{\pm}, \psi_a{}^{\pm}) = \delta_{ba}. \tag{21}$$

IV. MISCELLANEOUS RELATIONS

It is useful to have alternative statements of the facts expressed by Eqs. (19) and (20). We first introduce the convenient abbreviation

$$F_{ba} \equiv (\phi_b, F\phi_a) \tag{22}$$

for an arbitrary operator F, and then expand the Green's function of H in terms of the $\psi_a{}^{\pm}$:

$$G_{ba}{}^{\pm}(E) = \sum_c \frac{(\phi_b, \psi_c{}^{\pm})(\psi_c{}^{\pm}, \phi_a)}{E - E_c \pm i\epsilon}. \tag{23}$$

[7] If H possesses any nonrelativistic features, such as in the problem where it describes a particle which is bound by a fixed potential but which scatters incident radiation, then the specification $E_a = E_b$ must be retained. Moreover Z_a will then generally vary from one stable bound level to another.

Taking the singular part of this equation one gets, with Eq. (19),

$$\mathrm{Sing}G_{ba}{}^{\pm}(E) = (E - E_a \pm i\epsilon)^{-1} Z_a \delta_{ba}. \tag{24}$$

This implies

$$\pm i\epsilon\, \mathrm{Sing}G_{ba}{}^{\pm}(E_a) = Z_a \delta_{ba}, \tag{25}$$

a result which could also be inferred from Eq. (6).

Using Eqs. (4b) and (10a), one may write

$$R^{\pm}(E) = [G_0{}^{\pm}(E)]^{-1} G^{\pm}(E) [G_0{}^{\pm}(E)]^{-1} - [G_0{}^{\pm}(E)]^{-1}, \tag{26}$$

and hence

$$R_{ba}{}^{\pm}(E) = (E - E_b \pm i\epsilon)(E - E_a \pm i\epsilon) \times \sum_c \frac{(\phi_b, \psi_c{}^{\pm})(\psi_c{}^{\pm}, \phi_a)}{E - E_c \pm i\epsilon} - (E - E_c \pm i\epsilon)\delta_{ba}. \tag{27}$$

The singular part of this equation, with $E = E_a$, leads directly to Eq. (20). Differentiation of this equation with respect to E gives

$$\frac{\partial R_{ba}{}^{\pm}(E)}{\partial E} = \sum_c \left[1 - \frac{(E_a - E_c)(E_b - E_c)}{(E - E_c \pm i\epsilon)^2}\right] \times (\phi_b, \psi_c{}^{\pm})(\psi_c{}^{\pm}, \phi_a) - \delta_{ba} \tag{28}$$

and hence

$$\mathrm{Sing}[\partial R_{ba}{}^{\pm}(E)/\partial E]_{E=E_a} = (Z_a - 1)\delta_{ba}, \tag{29}$$

a result which will be needed later.

Equations (25) and (29) also hold in discrete-spectrum theory provided the specification $E_a = E_b$ is added.

V. THE S-MATRIX

The elements of the S-matrix are defined by

$$(S^{\pm 1})_{ba} = (\psi_b{}^{\mp}, \psi_a{}^{\pm}). \tag{30}$$

Using Eqs. (9), (14), and (15), one may write

$$\begin{aligned}
&(Z_b Z_a)^{\frac{1}{2}}(S^{\pm 1})_{ba} \\
&= (\phi_b, [1 + R^{\pm}(E_b)G_0{}^{\pm}(E_b)][1 + G_0{}^{\pm}(E_a)R^{\pm}(E_a)]\phi_a) \\
&= \delta_{ba} + (\phi_b, R^{\pm}(E_b)G_0{}^{\pm}(E_b)G_0{}^{\pm}(E_a)R^{\pm}(E_a)\phi_a) \\
&\quad + \frac{\frac{1}{2}}{E_b - E_a \pm i\epsilon}(\phi_b, [R^{\pm}(E_b) + R^{\pm}(E_a) \\
&\quad + (E_a - E_b)R^{\pm}(E_b)G_0{}^{\pm}(E_b)G_0{}^{\pm}(E_a)R^{\pm}(E_a)]\phi_a) \\
&\quad + \frac{\frac{1}{2}}{E_a - E_b \pm i\epsilon}(\phi_b, [R^{\pm}(E_a) + R^{\pm}(E_b) \\
&\quad + (E_b - E_a)R^{\pm}(E_b)G_0{}^{\pm}(E_b)G_0{}^{\pm}(E_a)R^{\pm}(E_a)]\phi_a) \\
&= \delta_{ba} \mp i\frac{\epsilon}{(E_b - E_a)^2 + \epsilon^2}(\phi_b, [R^{\pm}(E_b) + R^{\pm}(E_a)]\phi_a) \\
&\quad + \frac{\epsilon^2}{(E_b - E_a)^2 + \epsilon^2}(\phi_b, R^{\pm}(E_b)G_0{}^{\pm}(E_b)G_0{}^{\pm}(E_a)R^{\pm}(E_a)\phi_a) \\
&\xrightarrow[\epsilon \to 0]{} \delta_{ba} \mp 2\pi i\delta(E_b - E_a) \\
&\quad \times \{R_{ba}{}^{\pm} \mp \tfrac{1}{2}i\epsilon[\partial R_{ba}{}^{\pm}(E)/\partial E]_{E=E_a}\},
\end{aligned} \tag{31}$$

where the representation

$$\delta(E)=\frac{1}{\pi}\frac{\epsilon}{E^2+\epsilon^2} \tag{32}$$

for the delta function has been used. Only the singular part of the term in $\partial R_{ba}{}^{\pm}(E)/\partial E$ contributes to the S-matrix in the limit $\epsilon\to 0$. Hence, use of Eqs. (20) and (29) and the formal identity $\delta(E_b-E_a)\delta_{ba}=(\pi\epsilon)^{-1}\delta_{ba}$ gives

$$\begin{aligned}(S^{\pm 1})_{ba}&=(Z_bZ_a)^{-1}\{[1\mp 2i\epsilon^{-1}(\pm i\epsilon\mp\tfrac{1}{2}i\epsilon)(Z_a-1)]\delta_{ba}\\&\qquad\mp 2\pi i\delta(E_b-E_a)\,\mathrm{Rem}R_{ba}{}^{\pm}\}\\&=\delta_{ba}\mp i\mathfrak{R}_{ba}{}^{\pm},\end{aligned} \tag{33}$$

where

$$\mathfrak{R}_{ba}{}^{\pm}=(Z_bZ_a)^{-\frac{1}{2}}\,\mathrm{Rem}\mathbf{R}_{ba}{}^{\pm} \tag{34}$$

and where boldface type is used to denote, for any operator, the energy shell operation

$$\mathbf{F}_{ba}\equiv 2\pi\delta(E_b-E_a)F_{ba}. \tag{35}$$

$\mathfrak{R}^{\pm}$ is the *renormalized* transition operator which describes physically observable scattering processes. Owing to the orthonormality conditions (21) the S-matrix, as defined by Eq. (30), is unitary.[8] $\mathfrak{R}^{\pm}$ therefore satisfies the probability conservation law

$$\mathfrak{R}^{\pm}\mathfrak{R}^{\mp}=\mathfrak{R}^{\mp}\mathfrak{R}^{\pm}=\pm i(\mathfrak{R}^{\pm}-\mathfrak{R}^{\mp}) \tag{36}$$

or, since $\mathfrak{R}^{\mp}=\mathfrak{R}^{\pm\dagger}$,

$$\mathfrak{R}^{\pm}\mathfrak{R}^{\pm\dagger}=\mathfrak{R}^{\pm\dagger}\mathfrak{R}^{\pm}=\mp 2\,\mathrm{Im}\mathfrak{R}^{\pm}. \tag{37}$$

In discrete-spectrum theory $R^{\pm}$ has no nonsingular part; hence $\mathfrak{R}^{\pm}=0$, $\psi_a{}^{+}=\psi_a{}^{-}$, and the S-matrix reduces to the triviality $S=1$.

VI. THE PARTICLE PROPAGATION FUNCTIONS AND THE RENORMALIZATION PROGRAM

The demonstration of the internal consistency of the renormalization program in quantum field theory is conveniently carried out in terms of irreducible diagrams, each of which is used as a replacement for an infinite class of diagrams.[9] In the computations for a given scattering process only irreducible diagrams need be considered, provided the products of diagonal one-particle matrix elements of the unperturbed Green's function $G_0{}^{\pm}(E)$ occurring in the expansion of Eq. (10d) are replaced by corresponding products of diagonal one-particle matrix elements of the perturbed Green's function $G^{\pm}(E)$:

$$G_{aa}{}^{\pm}(E)=\sum_c\frac{|(\phi_a,\psi_c{}^{\pm})|^2}{E-E_c\pm i\epsilon}. \tag{38}$$

When ϕ_a is a one-particle state the only terms which contribute to the above sum, other than $c=a$, are those for which $\psi_c{}^{\pm}$ involves two or more real particles with $E_c>E_a$. Expression (38) is then called the *modified propagation function* of the particle in question. Its structure may be displayed by writing it in the form

$$G_{aa}{}^{\pm}(E)=\frac{Z_a}{E-E_a\pm i\epsilon}+\sum_{E_c>E_a}\frac{|(\phi_a,\psi_c{}^{\pm})|^2}{E-E_c\pm i\epsilon}, \tag{39}$$

from which it is seen to have a behavior similar to Z_a times the unmodified propagation function $G_{0aa}{}^{\pm}(E)$ in the neighborhood of $E=E_a$. The *renormalized* propagation function is defined in such a way as to remove the factor Z_a:

$$\bar{G}_{aa}{}^{\pm}(E)\equiv Z_a{}^{-1}G_{aa}{}^{\pm}(E). \tag{40}$$

The practical computation of the modified propagation functions is conveniently carried out in terms of the *self-energy functions*. These functions are introduced by separating the right-hand side of Eq. (4b) into diagonal and off-diagonal parts:

$$\begin{aligned}&G_{ba}{}^{\pm}(E)\\&=\frac{1}{E-E_b\pm i\epsilon}[\delta_{ba}+H_{1ba}G_{aa}{}^{\pm}(E)+\textstyle\sum_{c\neq a}H_{1bc}G_{ca}{}^{\pm}(E)]\\&=\frac{1}{E-E_b\pm i\epsilon}[\delta_{ba}+\Sigma_{ba}{}^{\pm}(E)G_{aa}(E)],\end{aligned} \tag{41}$$

where

$$\Sigma_{ba}{}^{\pm}(E)=H_{1ba}+\sum_{c\neq a}H_{1bc}\frac{1}{E-E_c\pm i\epsilon}\Sigma_{ca}{}^{\pm}(E). \tag{42}$$

Iteration of Eq. (42) gives

$$\Sigma_{ba}{}^{\pm}(E)=(\phi_b,H_1[1-1_aG_0{}^{\pm}(E)H_1]^{-1}\phi_a), \tag{43}$$

where

$$1_a\equiv 1-\phi_a\rangle\langle\phi_a. \tag{44}$$

The diagonal one-particle elements $\Sigma_{aa}{}^{\pm}(E)$ are the self-energy functions, in terms of which one may write

$$G_{aa}{}^{\pm}(E)=\frac{1}{E-E_a-\Sigma_{aa}{}^{\pm}(E)\pm i\epsilon} \tag{45a}$$

$$=G_{0aa}{}^{\pm}(E)[1-\Sigma_{aa}{}^{\pm}(E)G_{0ca}{}^{\pm}(E)]^{-1}. \tag{45b}$$

Comparison of Eqs. (45a) and (39) allows one to infer[10]

$$[\Sigma_{aa}{}^{\pm}(E)]_{E=E_a\mp i\epsilon}=0, \tag{46}$$

$$[\partial\Sigma_{aa}{}^{\pm}(E)/\partial E]_{E=E_a\mp i\epsilon}=-\zeta_a, \tag{47}$$

$$Z_a=(1+\zeta_a)^{-1}. \tag{48}$$

An evaluation of the diagrams corresponding to Eq. (25) readily shows that the normalization constant Z_a associated with a many-particle state is simply the

[8] For the proof of unitarity when bound states are present see reference 5.

[9] F. J. Dyson, Phys. Rev. 75, 1736 (1949).

[10] If the redefinition (7) of H_0 and H_1 had not been carried out initially then one would have obtained, in the limit $\epsilon\to 0$,

$$\Delta E_a=\Sigma_{aa}{}^{+}(E_a)=(\phi_a,H_1[1-1_aG_0{}^{+}(H_{0aa}+\Delta E_a)H_1]^{-1}\phi_a),$$

from which the level shifts can be computed.

product of the normalization constants associated with the individual particles in that state. Strictly speaking, a vacuum normalization constant should also be included, but since it is uniformly present in all states it is uniformly ignored. In a typical boson-fermion two-field theory in which the coupling is linear in the boson field and bilinear in the fermion field, the fermion and boson normalization constants are customarily called Z_2 and Z_3 respectively.

Let us consider the contribution to the operator $\mathfrak{R}^{\pm}$ from a given irreducible diagram. Suppose the numbers of initial fermions and bosons for this diagram are F_a and B_a respectively, and suppose the corresponding final numbers are F_b and B_b. Then

$$Z_a=Z_2^{F_a}Z_3^{B_a}, \quad Z_b=Z_2^{F_b}Z_3^{B_b}, \quad Z_bZ_a=Z_2^{F}Z_3^{B}, \tag{49}$$

where

$$F=F_a+F_b, \quad B=B_a+B_b. \tag{50}$$

Let V be the number of vertices in the diagram. Then the number of internal fermion lines is $V-\frac{1}{2}F$ (F must be an even number), and the number of internal boson lines is $\frac{1}{2}(V-B)$. Each internal fermion line contributes a modified fermion propagation function G_2, each internal boson line contributes a modified boson propagation function G_3, and each vertex contributes a modified vertex operator Γ (sum of all proper vertex diagrams) times the coupling constant g. Here we omit the $\pm$ signs and the energy dependence of these functions. Ignoring also the order in which these quantities must appear and the momentum-energy integrations in which they are involved, we may write the total contribution from the internal parts of the diagram schematically as $g^V\Gamma^V G_2^{V-\frac{1}{2}F}G_3^{\frac{1}{2}(V-B)}$.

The external lines do not contribute propagation functions since, as may be seen from the expansion of Eq. (10d), scattering diagrams must begin and end with vertices. Instead, each external line contributes a quantity

$$G_{cc}^{\pm}(E)[G_{0cc}^{\pm}(E)]^{-1}=[1-\Sigma_{cc}^{\pm}(E)G_{0cc}^{\pm}(E)]^{-1}, \tag{51}$$

in which the dangling unmodified propagator has been cancelled out by its inverse, and in which the subscript c refers to the particle in question. When this quantity is evaluated on the energy shell, with $E=E_c$, it reduces to Z_c. Therefore each external line contributes simply a normalization constant, the total external contribution being $Z_2^FZ_3^B$. Combining these results with Eqs. (34) and (49), one gets for the renormalized transition operator the schematic expression

$$\mathfrak{R}=T\sum(Z_2^FZ_3^B)^{\frac{1}{2}}g^V\Gamma^VG_2^{V-\frac{1}{2}F}G_3^{\frac{1}{2}(V-B)}, \tag{52}$$

where the summation is over all irreducible diagrams and where T is a formal symbol replacing the weight factor $2\pi\delta(E_b-E_a)$ on the energy shell.

The well-known result that $\mathfrak{R}$ can be expressed entirely in terms of renormalized quantities[9] follows immediately. The renormalized particle propagation functions are

$$\bar{G}_2=Z_2^{-1}G_2, \quad \bar{G}_3=Z_3^{-1}G_3. \tag{53}$$

One may also include the vertex renormalization, although it plays no role in state-vector normalization:

$$\bar{\Gamma}=Z_1\Gamma \tag{54}$$

where

$$Z_1=(1+\zeta_1)^{-1}, \tag{55}$$

$$\zeta_1\gamma=g^{-1}[\partial\Sigma_2^{\pm}(E)/\partial A]_{E=E_2\mp i\epsilon,\,A=0}, \tag{56}$$

the latter quantity denoting a derivative of the fermion self-energy function with respect to a constant external boson field A, and γ denoting the unmodified vertex operator.[11] If now the renormalized coupling constant is introduced, namely

$$\bar{g}=Z_1^{-1}Z_2Z_3^{\frac{1}{2}}g, \tag{57}$$

one may write

$$\mathfrak{R}=T\sum\bar{g}^V\bar{\Gamma}^V\bar{G}_2^{V-\frac{1}{2}F}\bar{G}_3^{\frac{1}{2}(V-B)}. \tag{58}$$

VII. THE REACTANCE OPERATOR

In simple scattering theory the reactance operator is introduced by splitting up Eq. (10c) in the form

$$\left[1-H_1\mathcal{P}\frac{1}{E-H_0}\right]R^{\pm}(E) =H_1[1\mp\pi i\delta(E-H_0)R^{\pm}(E)] \tag{59}$$

with the use of the representation

$$1/(E\pm i\epsilon)=\mathcal{P}(1/E)\mp\pi i\delta(E), \tag{60}$$

the symbol $\mathcal{P}$ denoting the "principal value" when appearing in an integral. Equation (59) yields

$$R^{\pm}=K(1\mp\tfrac{1}{2}i\mathbf{R}^{\pm}), \tag{61}$$

where

$$K=\sum_a\left[1-H_1\mathcal{P}\frac{1}{E_a-H_0}\right]^{-1}H_1|\phi_a\rangle\langle\phi_a|. \tag{62}$$

The same procedure is valid in field theory provided a certain amount of caution is exercised in performing the energy-shell operation (35) which appears in Eq. (61). In simple scattering theory the matrix elements of the operator $R^{\pm}$ vary smoothly across the energy shell. In field theory, on the other hand, the singular part of this operator varies abruptly across the energy shell. Multiplying the singular part by $2\pi\delta(E_b-E_a)$ is equivalent to multiplication by $2/\epsilon$, but not so for the smooth nonsingular remainder. Since the quasi-continuous spec-

[11] As is well known, the modified vertex operator itself may be expressed as $\Gamma=\gamma+g^{-1}\delta\Sigma_2/\delta A$, where the derivative is now a variational one with respect to an arbitrary external field. Therefore the renormalized vertex operator reduces to γ in the neighborhood of $E=E_2$ and $k=0$, k being the momentum energy of the associated boson line. In a gauge-invariant theory, or in a theory in which the vertex operators commute, the differetiation in Eq. (56) becomes equivalent to the energy differentiation in Eq. (47) and $Z_1=Z_2$. [J. C. Ward, Phys. Rev. 78, 182 (1950).]

trum is fine-grained with respect to ϵ there are many states lying on the energy shell, and not just a single state with E_b *exactly* equal to E_a. These closely packed states may be replaced by a single state with $E_b=E_a$ only if $2\pi\delta(E_b-E_a)$ is replaced in $\mathrm{Rem}\mathbf{R}^{\pm}$ by a factor much larger than $2/\epsilon$. This factor is the formal T-symbol of Eqs. (52) and (58).[13]

Using Eq. (20), one may write in the case of field theories

$$R_{ba}^{\pm}=\pm i\epsilon(Z_a-1)\delta_{ba}+\mathrm{Rem}R_{ba}^{\pm}, \tag{63}$$

$$\mathbf{R}_{ba}^{\pm}=\pm 2i(Z_a-1)\delta_{ba}+\mathrm{Rem}\mathbf{R}_{ba}^{\pm} \tag{64}$$

and hence, from Eq. (61),

$$\pm i\epsilon(Z_a-1)\delta_{ba}+\mathrm{Rem}R_{ba}^{\pm} = K_{ba}Z_a\mp\tfrac{1}{2}i\sum_c K_{bc}\,\mathrm{Rem}\mathbf{R}_{ca}^{\pm}. \tag{65}$$

The reactance operator is obtained by performing the energy-shell operation on K. It will appear presently that this operator has no singular part, and hence the limit $\epsilon\to 0$ may be taken at once in Eq. (65) with consequent elimination of the first term on the left. Multiplying the result by $(Z_bZ_a)^{-\frac{1}{2}}$ and performing the energy shell operation, one gets the renormalized Heitler integral equation

$$\mathfrak{R}^{\pm}=\mathfrak{K}(1\mp\tfrac{1}{2}i\mathfrak{R}^{\pm}), \tag{66}$$

where

$$\mathfrak{K}_{ba}=Z_b^{-\frac{1}{2}}Z_a^{\frac{1}{2}}\mathbf{K}_{ba}. \tag{67}$$

A contrast between Eqs. (34) and (67) is immediately apparent. The reactance operator $\mathbf{K}$ may be analyzed in terms of exactly the same diagrams as the transition operator $\mathbf{R}^{\pm}$, as comparison of Eqs. (10d) and (62) clearly shows. The propagation functions, modified vertex operators, and self-energy functions may all be again introduced, the only difference being that the imaginary parts $\pm i\epsilon$ are to be omitted and all integrals evaluated in the sense of the principal value. And yet the renormalization factors now appear with different exponents.

The explanation of the apparent contradiction is quite easy and has to do with the values to be assigned to the external lines associated with the particles in the *initial* state. These values are

$$G_{cc}(E_c)[G_{0cc}(E_c)]^{-1}=[1-\Sigma_{cc}(E_c)G_{0cc}(E_c)]^{-1}, \tag{68}$$

the $\pm$ signs being now omitted. Unlike the situation in Eq. (51), the energy evaluation is here taken directly at the pole of the modified propagation function rather than immediately above or below it. When $\pm$ signs are inserted expression (68) has the value Z_c. However, when they are omitted it is to be interpreted as having the value 1, because $\Sigma_{cc}(E_c)$ vanishes owing to the redefinition (7) of the unperturbed Hamiltonian. That is to say, the iterated self-energy diagrams which expression (68) evaluates are to be regarded as making no contribution since the particle self-energies (level shifts) have been adjusted to zero. For the same reason, the diagrams which contribute to the singular part of $\mathbf{R}^{\pm}$ make no contribution to $\mathbf{K}$.

The values to be assigned to the final particle lines, however, are determined by the requirement of smoothness for K across the energy shell, which demands an evaluation of the form

$$\lim_{E\to E_c} G_{cc}(E)[G_{0cc}(E)]^{-1}=Z_c. \tag{69}$$

The total external contribution in the present case is therefore $Z_2^{F_b}Z_2^{B_b}=Z_b$. Combination of this result with Eq. (67) leads once again to Eq. (52) with $\mathfrak{R}$ now replaced by $\mathfrak{K}$, and one sees that the renormalized reactance operator, like the renormalized transition operator, can be computed entirely in terms of renormalized quantities.

ACKNOWLEDGMENTS

The author would like to acknowledge several interesting discussions with members of the Radiation Laboratory Theoretical Group and with members of the physics department.

[13] The meaning of the T-symbol is expressed by the identity $2\pi=T\Delta E$, where ΔE is the level separation of the quasi-continuous spectrum. For a single particle $\Delta E=v\Delta p=2\pi v/L$, where $\Delta p=2\pi/L$ is the momentum interval and v is the velocity of the particle. Therefore T may be regarded as the time L/v for the particle to traverse the fundamental volume. (The units here are such that $\hbar=1$.) In the computation of cross sections the square of the absolute value of the transition operator is needed. The square of of the delta function is therefore encountered on the energy shell. Division by T cancels one delta function and gives the transition *rate*, while the remaining delta function has the effect of introducing a "density of final states."

Spectrum and Nonrelativistic Limit of a Bethe-Salpeter Equation*†

FREDERICK L. SCARF
Department of Physics and Laboratory for Nuclear Science, Massachusetts Institute of Technology, Cambridge, Massachusetts
(Received June 20, 1955)

The eigenvalue spectrum of the relativistic two-body equation introduced by Wick is investigated in detail for arbitrary binding energy. It is verified that for any nonzero binding energy there is a complete discrete spectrum of allowed coupling constants and that this spectrum is labeled by the four quantum numbers n, l, m, *and* κ. In the limit of zero binding energy, it is shown that all eigenvalues tend to zero. The set of coupling constants with $\kappa=0$ correspond best to the Balmer formula. The wave functions are also investigated with respect to certain proposed boundary conditions and are compared with the nonrelativistic hydrogen atom wave functions. Again it is found that all states with $\kappa=0$ correspond best to the nonrelativistic states, but that the "spurious" states with $\kappa>0$ are not unacceptable. Possible generalizations of these results are discussed.

I. INTRODUCTION

EVER since the development from field theory of the relativistic two-body or Bethe-Salpeter equation[1] many questions about its significance and consistency have been raised. These points have been summarized in a recent paper by Wick[2] (hereafter referred to as W). However, in the same paper and in subsequent work by Cutkosky[3] (hereafter referred to as C), very important and illuminating answers were given to many of these questions. In the first part of W, the definition of the Bethe-Salpeter (B.S.) wave function is used together with certain "stability" conditions to derive a particular functional form for physically acceptable solutions of the complete B.S. equation. This argument at once gives a boundary condition on the exact wave function and also shows that one may transform the equation to a Euclidean space. The important simplifications introduced by the use of Euclidean variables are vividly illustrated in the remaining sections of these papers.

The B.S. equation for two scalar particles interacting through a massless scalar field is considered in the ladder approximation. It is shown that a remarkable integral representation introduced by Wick and generalized by Cutkowsky can be used to reduce this particular B.S. equation to a one-dimensional integral equation for a kernel function $g(s)$. The eigenvalues of this equation are the eigenvalues of the original B.S. equation. This integral equation is solved exactly for zero total energy and approximately for zero binding energy with a few numerical calculations in the intermediate region. It is found that the eigenvalues and eigenfunctions can be labeled by four quantum numbers, m, l, n, κ, where m, l, n have their usual N.R. meaning and κ is the "relative time" quantum number.[4] It is shown in W and C that in the N.R. limit the states with $\kappa=0$ have eigenvalues which approximate the Balmer formula and wave functions on a spacelike surface roughly like the hydrogen atom wave functions. Their approximation for small binding energy indicates that the states with $\kappa\neq 0$ do not tend to an acceptable N.R. limit and, in fact, that they will have zero binding energy with a finite and fairly large coupling constant.

These results about the spectrum would be extremely satisfying since they suggest that even in the ladder approximation, as long as the coupling constant is small, one obtains only those solutions which are physically sensible and indeed have approximately the correct N.R. limit. However, the analysis in W and C raises several new and interesting points.

As we shall show below, the one-dimensional differential equation resulting from the integral equation is of a type which has solutions not completely specified by stating the positions of the singularities and their exponents. Also the limit of zero binding energy represents a confluence of singularities which complicates the discussion considerably. For these reasons one must be extremely careful in discussing the solutions for zero binding energy. Since the behavior of the solutions in this customarily unimportant limit will be used to decide just which of these solutions are acceptable, it is of great importance to investigate the eigenvalue spectrum in this region. Furthermore, since the differential equation is actually singular for arbitrary binding energy, it is of interest to prove rigorously that there is a complete discrete spectrum.

Secondly, we wish to investigate just which boundary condition should be imposed on the B.S. wave function and what effect this boundary condition has. Wick's boundary condition is derived for the exact solution of the full B.S. equation, and it is certainly not clear whether it is appropriate to impose this on an exact solution of the ladder equation.

Finally, we propose to investigate the resultant wave

* Assisted in part by the joint program of the Office of Naval Research and the U. S. Atomic Energy Commission.
† Based in part on sections of a doctoral thesis submitted to the Physics Department at the Massachusetts Institute of Technology.
[1] E. E. Salpeter and H. A. Bethe, Phys. Rev. **84**, 1232 (1951); J. Schwinger, Proc. Natl. Acad. Sci. U. S. **37**, 455 (1951).
[2] G. C. Wick, Phys. Rev. **96**, 1124 (1954).
[3] R. E. Cutkosky, Phys. Rev. **96**, 1135 (1954).
[4] The energy is taken to be a parameter and the coupling constant is considered to be the eigenvalue.

functions on a spacelike surface for $\kappa=0$, 1, 2, etc., in the region of small binding energy.

In the next section we present the relevant equations from W and C and illustrate the singularities and complications which we have mentioned.

II. INTEGRAL REPRESENTATION

The B.S. wave function $\phi(\mathbf{p},p_0)$ is a function of the relative momentum $\mathbf{p}$ and the "relative energy" p_0. Wick has shown that as a consequence of the field theoretical definition of ϕ and certain stability conditions, one may express ϕ as

$$\phi(\mathbf{p},p_0)=\frac{1}{2\pi i}\int_{\omega_M}^{\infty}d\omega \times[f_1(\mathbf{p},\omega)(p_0+\omega-i\epsilon)^{-1}+f_2(\mathbf{p},\omega)(p_0-\omega+i\epsilon)^{-1}], \quad (1)$$

where for scalar particles with equal masses m and total energy E we may write

$$\omega_M=E_p-\tfrac{1}{2}E=(\mathbf{p}^2+m^2)^{\frac{1}{2}}-\tfrac{1}{2}E.$$

Wick observes that (1) implies

$$\phi(\mathbf{x},x_4)\to 0 \quad \text{as} \quad |x_4|\to\infty, \quad (2)$$

and suggests that (2) be adopted as a boundary condition for the exact wave function. We note that the condition that a wave function be exactly expressible in the form (1) is more restrictive than (2) and suggest that (1) be interpreted as the boundary condition on the solution of the complete B.S. equation.[6] It is not immediately clear just what role either (1) or (2) play in determining acceptable solutions of the ladder equation. It is worth noting that all previous systematic approximations[6] to ϕ can be written in the form (1). Below we shall investigate the behavior of the exact solutions of the ladder equation with regard to (1) and (2).

Using (1) Wick transforms the ladder equation for equal-mass scalar particles interacting through a scalar massless field to obtain

$$[(p-i\eta)^2+1][(p+i\eta)^2+1]\phi(p)=\frac{\lambda}{\pi^2}\int\frac{d^4k\phi(k)}{(p-k)^2}, \quad (3)$$

where $p=(\mathbf{p},p_4)$, $\eta=(0,\frac{1}{2}E)$, $m=\hbar=c=1$ and λ is the coupling constant. Then as shown in W and C, the general solution of (3) can be written

$$\phi_n^{l,m}(p)=\int_{-1}^{1}\frac{dz g_n(z)\mathcal{Y}_l^m(\mathbf{p})R^{n-l-1}C_{n-l-1}^{l+1}(X/R)}{[p^2+1-\eta^2+2i\eta pz]^{n+2}}, \quad (4)$$

with

$$X=1-\eta^2-p^2, \quad R^2=(p^2+1-\eta^2)^2-4p_4^2(1-\eta^2),$$

and C_{n-l-1}^{l+1} is a Gegenbauer polynomial. With this integral representation of (4), $g_n(z)$ is given by

$$g_n(z)=\frac{\lambda}{2n}\int_1^1\frac{[R(z,\zeta)]^n g_n(\zeta)d\zeta}{(1-\eta^2+\eta^2\zeta^2)}, \quad (5)$$

$$R(z,\zeta)=(1\pm z)/(1\pm\zeta) \quad \zeta\gtrless z.$$

Equation (5) can be converted into a differential equation

$$(1-z^2)g_n''(z)+2(n-1)zg_n'(z)-n(n-1)g_n(z) +\lambda(1-\eta^2+\eta^2z^2)^{-1}g_n(z)=0, \quad (6)$$

with the following boundary conditions

$$g_n(\pm 1)=0, \quad (7)$$

$$g_n(0)=0 \text{ (odd)}, \quad g_n'(0)=0 \text{ (even)}. \quad (8)$$

It is this set of equations, (5)–(8), with which we shall be primarily concerned. If we wish to write (6) in standard Sturm-Liouville form,

$$\frac{d}{dz}\left(p\frac{dg}{dz}\right)+(q+\lambda r)g=0, \quad (9)$$

we readily find

$$p(z)=(1-z^2)^{1-n}, \quad q(z)=-n(n-1)(1-z^2)^{-n}$$
$$r(z)=(1-\eta^2+\eta^2z^2)^{-1}(1-z^2)^{-n}. \quad (10)$$

Thus for any value of η, r, and p are singular at the end points $z^2=1$ and in fact, the "effective interval length" r/p is also singular there. Equations (6), (7), and (8) form a singular-end-point boundary value problem which could have a continuous spectrum, a finite discrete spectrum or a complete discrete spectrum. Such problems are frequently encountered in mathematical physics but it has been emphasized by Kemble[7] that the solutions must be rigorously examined in each case.

We note furthermore that when $\eta\to 1$ (zero binding energy) the kernel in (5) becomes unbounded and the equation becomes intrinsically singular. We must certainly investigate to what extent the boundary conditions (8) remain significant. We also see that while the limit of zero binding energy certainly has a definite physical meaning we must use care in defining the contour of integration in (5) in order to insure that we approach this limit from the negative energy side.

Because of these complications and since the limit as $\eta\to 1$ will decide which solutions are acceptable, we feel that it is necessary to examine the exact solutions for arbitrary η and to investigate these exact solutions in the $\lim \eta\to 1$ in order to determine the nonrelativistic behavior. As we shall see below, this assertion is justified.

[6] This type of boundary condition is also implicitly suggested in recent work by Nishijima. K. Nishijima, Progr. Theoret. Phys. (Japan) **12**, 279 (1954), and **10**, 549 (1953).

[6] E. E. Salpeter, Phys. Rev. **87**, 328 (1952); R. Karplus and A. Klein, Phys. Rev. **87**, 848 (1952).

[7] E. C. Kemble, *Principles of Quantum Mechanics* (McGraw-Hill Book Company, Inc., New York, 1937), p. 127.

III. EXACT SOLUTIONS

It is convenient to transform (6) by letting $u=(1-z^2)$ and we obtain

$$4u(1-u)(1/\eta^2-u)g_n''-[2u+4(n-1)(1-u)](1/\eta^2-u)g_n'+[\lambda/\eta^2-n(n-1)(1/\eta^2-u)]g_n=0. \quad (11)$$

It can be seen that (11) is an equation of Fuchsian type with four regular singular points located at 0, 1, $1/\eta^2$, ∞. The general equation of this type was first studied by Heun[8] and has been called Heun's equation. Since the solutions of this equation are used rarely and have several distinctive properties, we shall quote some of the relevant information about them.

Snow[9] gives the differential equation in normal form as

$$y''+\left[\frac{\gamma}{u}+\frac{1+\alpha+\beta-\gamma-\delta}{u-1}+\frac{\delta}{u-a}\right]y'+\frac{[\alpha\beta u+b]}{u(u-1)(u-a)}y=0. \quad (12)$$

It can be seen that the general Fuchsian equation with four singularities is not completely specified by the position of the singularities and their exponents, but contains an accessory parameter, b. We shall see the effect of this below. In general, the two linearly independent power series solutions around $u=0$ are given by

$$y_1(u)=F(a,b;\alpha,\beta,\gamma,\delta;u),$$
$$y_2(u)=u^{1-\gamma}F(a,b';1+\alpha-\gamma,1+\beta-\gamma,2-\gamma,\delta;u), \quad (13)$$

where

$$b'=b-(1-\gamma)[\delta+a(1+\alpha+\beta-\gamma-\delta)],$$

and

$$F(a,b;\alpha,\beta,\gamma,\delta;u)\equiv 1-\frac{bu}{\gamma a}+\sum_{s=2}^{\infty}a_s u^s.$$

The three-term recursion formula is

$$a(s+2)(s+\gamma+1)a_{s+2}=-(s+\alpha)(s+\beta)a_s+\{(s+1)^2(1+a)+(s+1)\times[\gamma+\delta-1+(\alpha+\beta-\delta)a]-b\}a_{s+1}.$$

Comparing (11), (12), and (13), we find two solutions,

$$g_n^{(1)}(z)=(1-z^2)^n\times F\left(\frac{1}{\eta^2},\frac{\lambda-n(n+1)}{4\eta^2};\frac{1+n}{2},\frac{n}{2},n+1,0;1-z^2\right), \quad (14)$$

$$g_n^{(2)}(z)=F\left(\frac{1}{\eta^2},\frac{\lambda-n(n-1)}{4\eta^2};\frac{1-n}{2},-\frac{n}{2},1-n,0;1-z^2\right) \quad (15)$$

[8] K. Heun, Math. Ann. **33**, 161 (1889).
[9] C. Snow, National Bureau of Standards, Applied Mathematics Series 19, 1952 (unpublished), Chap. VII.

It can be shown that $g_n^{(1)}(z)$ is not linearly independent of $g_n^{(2)}(z)$ when n is integral as it is here. However, since $g_n^{(1)}(\pm 1)$ is nonzero, the second independent solution constructed from it will also be nonzero when $z^2=1$. Therefore, we can say that $g_n(z)=g_n^{(2)}(z)$ is the most general solution of (6) which obeys (7).

We are now in a position to investigate the spectrum rigorously. There are definite general tests which may be applied to singular-end-point boundary value problems in order to determine what kind of spectrum results. A straightforward treatment which suffices for our purposes is given by Kemble.[7] In essence, one must examine integrals of the form [see (9), (10)]

$$\int_a^x \rho(y)|g(y)|^2dy$$

and limits of the form $p(z)|g(z)|^2(z-a)^{-m}$ and $p(z)\times|g'(z)|^2(z-a)^{m-1}$ in the neighborhood of the end points ($z^2=0$, $z^2=1$). If these integrals and limits are bounded for given ϵ and m independent of λ for *all* λ, then one can show that, subject to some additional regularity restrictions, there is a complete normal Sturm-Liouville spectrum. The critical point in this proof concerns the radius of convergence of the solution around $z^2=0$, and around $z^2=1$.

It can be shown from the recursion formula that the series (13) converges up to the smallest of $(a, 1)$. It can also be shown that the power series converges *at* $u=1$ if $a>1$ and $\mathrm{Re}(\gamma+\delta-\alpha-\beta)>0$.

If we apply these tests to $g_n(z)$, (14), we find that $g_n(z)$ converges out to and including the point $z=0$, independent of λ or η. Carrying out a term-by-term differentiation, one can easily show that $g_n(z)$ satisfies Kemble's singular end point boundary conditions at the boundary $z^2=1$ for all λ and all η. In order to examine the behavior at the end point $z=0$, we transform to expansions of $g_n(z)$ about $z=0$.

$$g_n(z)=(1-z^2)^n\times F\left(\frac{1}{\eta^2},\frac{\lambda-n(n+1)}{4\eta^2};\frac{1+n}{2},\frac{n}{2},1+n,0;1-z^2\right)$$
$$=AF\left(1-\frac{1}{\eta^2},\frac{n(n+1)(1-\eta^2)-\lambda}{4\eta^2};\frac{n+1}{2},\frac{n}{2},\tfrac{1}{2},0;z^2\right)+BzF\left(1-\frac{1}{\eta^2},\frac{(n+1)(n+2)(1-\eta^2)-\lambda}{4\eta^2};\frac{n+2}{2},\frac{n+1}{2},\tfrac{3}{2},0;z^2\right). \quad (16)$$

Applying the arguments of the previous paragraphs, we find that the series representation around $z=0$ converges up to but *not* including the point $z=(1-\eta^2)^{\frac{1}{2}}/\eta$. (See Fig. 1.) Again we can examine Kemble's singular-

end-point boundary conditions and we find that they are satisfied for all λ except when $\eta=1$. We conclude that except for $\eta=1$, we have a complete discrete spectrum of Sturm-Liouville type and following Wick we label the eigenvalues with the quantum number κ.

In the mathematical literature the solutions for which the branch regular at $u=0$ and that regular at $u=1$ coincide are commonly called Heun's *functions*. More explicitly the Heun's function is frequently defined by stating that it belongs to the exponent zero at $u=0$ and at $u=1$. By examining (16) we see that $g_{n,\kappa}(z)\times(1-z^2)^{-n}$ and $g_{n,\kappa}(z)(1-z^2)^{-n}z^{-1}$ ($g_{n,\kappa}$ even and odd, respectively) are Heun's functions of $(1-z^2)$. We may then find the spectrum by requiring that the above products $[g_{n,\kappa}(z)(1-z^2)^{-n}$, etc.] be Heun's *functions*. We now indicate the difficulty in finding exact values for λ.

We may first note that the power series for the solution of Heun's equation cannot in general be uniformly convergent in the domain including its circle of convergence. For if this were true we could differentiate the series representation of (14) term by term and if the resultant series converged, we would have $g_n'(0)=0$ for all λ. Thus since $g_n(\pm1)=0$ for all λ, we would have a continuum. It is therefore impractical to work with the power series representation in order to find the eigenvalues since no one has been able to sum the series. No definite integral representation of a solution of Heun's equation has been found and it has been conjectured that none exist.[10]

In recent years, however, several other expansions with more useful regions of convergence have been presented. It was shown by Erdélyi[11] that any solution of Heun's equation can be represented by a hypergeometric function expansion, convergent outside an ellipse with foci at $u=0$, $u=1$ and containing $u=a$ on its circumference (Fig. 1). For the special case of Heun's functions it has been shown by Svartholm[12] that one may expand

$$F(a,b;\alpha,\beta,\gamma,\delta;u)=\sum_{s=0}^{\infty}b_s\,{}_2F_1(-s,s+\alpha+\beta-\delta;\gamma;u), \quad (17)$$

where this expansion is absolutely convergent for

$$\left|\frac{1+(1-1/u)^{\frac{1}{2}}}{1-(1-1/u)^{\frac{1}{2}}}\right|<\left|\frac{1+(1-1/a)^{\frac{1}{2}}}{1-(1-1/a)^{\frac{1}{2}}}\right|, \quad (18)$$

or *inside* the ellipse mentioned above. Furthermore, this expansion is absolutely convergent *on* the ellipse if $\mathrm{Re}(1-\delta)>0$. The recursion formula is given in the reference cited. If we compare (17), (18), and (14),

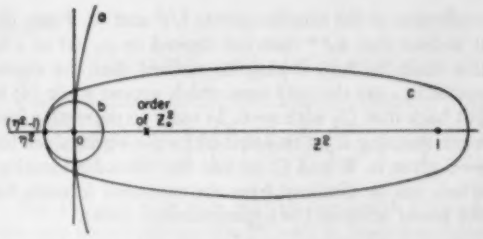

FIG. 1. The finite singularities of Eq. (6) in the complex z^2 plane. (a) Circle of convergence of series around $z^2=1$. (b) Circle of convergence of series around $z^2=0$. (c) Ellipse of convergence of hypergeometric function series. For $(1-\eta^2)\ll1$, Wick matches his approximate solutions at z_0^2, $1\gg\eta^2z_0^2\gg(1-\eta^2)$, or outside b.

we see that we may write

$$g_{n,\kappa}(z)(\text{even})=(1-z^2)^n\sum_{s=0}^{\infty}b_s\times{}_2F_1(-s,s+n+\tfrac{1}{2};n+1;1-z^2), \quad (19)$$

and $g_{n,\kappa}(z)$ may be written as a series of orthogonal Jacobi polynomials absolutely convergent in the closed region bounded by (18). This expansion would seem to be the best starting place for an attempt to find exact or approximate eigenvalues for arbitrary $\eta\neq1$ since it could be inserted into the integral equation and the orthogonality relations could be applied. We shall not pursue this line of attack any further since our primary concern is the spectrum in the limit as $\eta\to1$.

For this reason we mention another more convenient series representation introduced by Erdélyi.[13] It can be shown that for Heun's functions either of the following representations is valid:

$$F(a,b;\alpha,\beta,\gamma,\delta;u)=\sum_{s=0}^{\infty}\frac{c_s(-1)^s\Gamma(\nu+s)}{\Gamma(1-\mu+s)}\,{}_2F_1(\nu+s,\mu-s;\gamma;u), \quad (20)$$

where

$$\nu=\alpha,\quad \mu=\beta-\delta, \quad (21)$$

or

$$\nu=\beta,\quad \mu=\alpha-\delta. \quad (22)$$

The virtue of this representation is that for a Heun's function the series converges in the whole u plane except for a possible branch cut along the axis. The Heun's function, and hence (20), is still irregular at infinity and at $u=a$. The recursion formula for the c_s in (20) is given in the last reference cited. It may be noted that the Heun's function for $u>1$ is given by (20) with the analytic continuations of the hypergeometric functions inserted.

We are now in a position to investigate carefully the spectrum as $\eta\to1$. Before we do so we wish to clarify the results obtained in the other irregular limit, $\eta\to0$. It may be seen from (11) that $\lim\eta\to0$ represents a

[10] C. G. Lambe and D. R. Ward, Quart. J. Math. 5, 81 (1934).
[11] A. Erdélyi, Duke Math. J. 9, 48 (1942).
[12] N. Svartholm, Math. Ann. 116, 413 (1939).
[13] A. Erdélyi, Quart. J. Math. 15, 64 (1944).

confluence of the singular points $1/\eta^2$ and ∞. From (4) it is clear that $\phi_{n,\kappa}^{l,m}$ does not depend on $g_{n,\kappa}(z)$ or κ in this limit. In fact, it may be verified that the eigenvalues $\lambda_{n,0}$ are the only ones which appear when (4) is put back into (3) with $\eta=0$. In order to determine just what meaning is to be ascribed to the eigenvalues for $\eta=0$ given in W and C, we use the following identity, which can be obtained from the recursion formula for the power series or the hypergeometric series.

$$\lim_{\alpha\to\infty} F(a,ac;\alpha,\beta,\gamma,\delta;u) = {}_2F_1(\mu+(\mu^2+c)^{\frac{1}{2}},\mu-(\mu^2+c)^{\frac{1}{2}};\gamma;u) \quad (23)$$

$$\mu=\tfrac{1}{2}(\alpha+\beta-\delta).$$

In our case we find

$$\lim_{\eta\to 0} g_{n,\kappa}(z) = (1-z^2)^n\, {}_2F_1\left(\frac{2n+1}{4}+(\tfrac{1}{4}+\lambda_{n,\kappa})^{\frac{1}{2}}, \frac{2n+1}{4}-(\tfrac{1}{4}+\lambda_{n,\kappa})^{\frac{1}{2}}; n+1; 1-z^2\right). \quad (24)$$

Choosing even and odd functions we find

$$\lim_{\eta\to 0} g_{n,\kappa}(z) = (1-z^2)^n C_\kappa^{n+\frac{1}{2}}(z),$$

$$\lim_{\eta\to 0}\lambda_{n,\kappa} = (n+\kappa)(n+\kappa+1);\ \kappa=0,\ 1,\ 2,\ \cdots. \quad (25)$$

These are just the results obtained in W and C by solving (6) *in* the limit $\eta=0$ and we see that these are the correct solutions.

In the next section, we investigate in detail the spectrum in the "nonrelativistic" limit as $\eta\to 1$.

IV. LIMIT OF ZERO BINDING ENERGY

The limit of $g_{n,\kappa}(z)$ at $\eta=1$ can be obtained by regarding this limit as the confluence of the singularities $1/\eta^2$ and 1. From the recursion formula one can verify that

$$F(1,b;\alpha,\beta,\gamma,\delta;u) = (1-u)^{\frac{1}{2}(\gamma-\alpha-\beta)+\rho}\times {}_2F_1\left(\frac{\gamma+\alpha+\beta}{2}+\mu, \frac{\gamma+\beta-\alpha}{2}+\mu;\gamma;u\right), \quad (26)$$

$$\mu^2=\left[\tfrac{1}{2}(\gamma-\alpha-\beta)-\alpha\beta-b\right].$$

From (14) we have

$$\lim_{\eta\to 1} g_{n,\kappa}(z) = (1-z^2)^n z^{l+\rho}\times {}_2F_1\left(\frac{3}{4}+\frac{n}{2}+\frac{\rho}{2}, \frac{1}{4}+\frac{n}{2}+\frac{\rho}{2}; n+1; 1-z^2\right) \quad (27)$$

$$\rho^2=(\tfrac{1}{4}-\lambda).$$

It can be shown that (27) is the general solution of (6) which obeys (7) when η is set equal to one in the differential equation. We can see that $\rho=\pm\frac{1}{2}$ for $\lambda=0$, $-\frac{1}{2}<\rho<\frac{1}{2}$ for $0<\lambda\leq\frac{1}{4}$ and $\rho=i\sigma$ (σ real) for $\lambda>\frac{1}{4}$. Thus the only solutions regular at $z=0$ are those for $\lambda=0$ ($\rho=\pm\frac{1}{2}$) with exponents 0 and 1. However, the boundary conditions (8) at $z=0$ are formally satisfied for all λ. That is, if we define $2g(0)=\lim_{\delta\to 0}[g(0+\delta)+g(0-\delta)]$, etc., we find $g(0)=0$ for all odd functions and $g'(0)=0$ for all even functions. For $\lambda\neq 0$, these (even) solutions have an infinite discontinuity in slope at the origin, but we cannot rule this out *a priori* since (5) has an unbounded kernel in this limit. The fact that we have an infinite set of solutions all of which formally satisfy the boundary conditions is, in a sense, the effect of the accessory parameter mentioned above.

Two distinct approximation methods were used in W and C. For the lowest nodeless eigenfunction ($\kappa=0$), the following substitution was made in (5)

$$(1-\eta^2+\eta^2z^2)^{-1}\simeq\pi(1-\eta^2)^{-\frac{1}{2}}\delta(z). \quad (28)$$

This immediately yields

$$\lim_{\eta\to 1} g_{n,0}(z) = (1-|z|)^n \quad (29)$$

$$\lambda_{n,0}\simeq(2n/\pi)(1-\eta^2)^{\frac{1}{2}}. \quad (30)$$

One can see that in the region of small binding energy $[(1-\eta^2)\ll 1]$, (30) is in good agreement with the Balmer formula given by $\lambda=2n(2-2\eta)^{\frac{1}{2}}/\pi$. [Binding energy is equal to $(2-2\eta)$.]

For the higher eigenfunctions Wick suggests a different procedure since all nodes in these functions shrink to the origin as $\eta\to 1$. The interval $0\leq z\leq 1$ is divided into an outside interval $z_0\leq z\leq 1$, and an inside interval $0\leq z\leq z_0$. Choosing z_0 so that

$$(1-\eta^2)^{\frac{1}{2}}\ll z_0\ll 1,$$

Wick then neglects $(1-\eta^2)$ compared to z^2 in the outside interval. In the inside interval z^2 is neglected compared to one and thus terms of "order" $\leq(1-\eta^2)^{\frac{1}{2}}$ have been dropped. The appropriate solutions of these approximate equations are easily obtained in terms of hypergeometric functions. These solutions are analytically continued to the neighborhood of z_0 and matched there. It is found that this matching can be made smoothly only for $\lambda>\frac{1}{4}$, and the conclusion in W and C is that

$$\lim_{\eta\to 1}\lambda_{n,\kappa}=\tfrac{1}{4};\ \kappa\neq 0.$$

This type of approximation, which is so frequently used in solving boundary value problems, is based on several implicit assumptions. The important point here is the assumption that $g_{n,\kappa}(z)$ is representable by a convergent power series around the origin out to z_0. If we refer back to (16), the exact solution around $z=0$ (see Fig. 1), we find that this *diverges at* $\eta^2z^2=(1-\eta^2)$ (or $x=1$). Thus by neglecting terms of order $\leq(1-\eta^2)^{\frac{1}{2}}$, we have essentially neglected the actual radius of convergence of the exact solution. In Appendix I, the rela-

tion of Wick's inside solution to the exact one is discussed. It is shown that Wick's hypergeometric function is a good approximation to the exact solution for $0\leq z\leq(1-\eta^2)^{\frac{1}{2}}$; however, the analytic continuation of this function past $(1-\eta^2)^{\frac{1}{2}}$ (and out to z_0) has no definite correspondence to the actual solution.

In view of the above considerations we assert that no methods based on approximate power series solutions such as the above will reliably give the spectrum as $\eta\to 1$. The possibility of using numerical calculations is also eliminated, since the results in C show that the higher eigenvalues ($\kappa\neq 0$) decrease very slowly as $\eta\to 1$ and one could not determine from this whether or not they stop at a finite value. In order to obtain unambiguous information about the spectrum in the limit of zero binding energy, we must examine the continuum of solutions (27) to see which of these could possibly be the limit of an eigenfunction.

A program such as this does give meaningful results even though a bound state with zero binding energy is unphysical. That is, in any quantum mechanics problem we obtain a definite limiting set of eigenfunctions and eigenvalues as we let the binding energy tend to zero. This limiting set, in general, depends on whether we approach zero binding energy from positive or negative energies. Our case is not an exception. We must remember that $(1-\eta^2)^{\frac{1}{2}}$ really stands for $m(1-\eta^2)^{\frac{1}{2}}$ where m is to be understood as having a small negative imaginary part. Thus if we were to approach zero binding energy from the positive energy side, we would have

$$[(1-\eta^2+\eta^2z^2)^{-1}]_{\eta=1}=2\pi i\delta_+(z^2). \tag{31}$$

However, we are interested in the limit as $\eta\to 1$ from the bound state and we must require

$$[(1-\eta^2+\eta^2z^2)^{-1}]_{\eta=1}=\lim_{\epsilon\to 0}(z^2+\epsilon^2)^{-1}. \tag{32}$$

With (32) in mind, we can obtain unambiguous information by looking at the limit $\eta=1$.

Let us consider an even *eigenfunction* for any η. If we turn to Erdélyi's expansion and choose (22) we have

$$g_{n,\kappa}(z)=(1-z^2)^n\sum_{s=0}^{\infty}c_s\frac{(-1)^s\Gamma\left(\frac{n}{2}+\frac{1}{2}+s\right)}{\Gamma\left(1-\frac{n}{2}+s\right)}\times{}_2F_1\left(\frac{n}{2}+\frac{1}{2}+s,\frac{n}{2}-s;n+1;1-z^2\right). \tag{33}$$

This series representation converges in the finite z^2 plane. $g_{n,\kappa}$ has a logarithmic branch point when $\eta^2z^2=-(1-\eta^2)$ but $g_{n,\kappa}$ is finite there. Using the value for the hypergeometric function on its circle of convergence we have

$$g_{n,\kappa}(0)=\sum_{s=0}^{\infty}\frac{c_s(-1)^s\Gamma\left(\frac{n}{2}+\frac{1}{2}+s\right)\Gamma(n+1)\Gamma(\frac{1}{2})}{\Gamma\left(1-\frac{n}{2}+s\right)\Gamma\left(\frac{n}{2}+s+1\right)\Gamma\left(\frac{n}{2}+\frac{1}{2}-s\right)}. \tag{34}$$

For any odd n we note that all terms with $s\geq\frac{1}{2}+\frac{1}{2}n$ are zero since they contain $\Gamma(-m)$ in their denominators. Therefore

$$g_{n,\kappa}(0)=\sum_{s=0}^{\frac{1}{2}(n-1)}\frac{c_s(-1)^s\Gamma\left(\frac{n}{2}+\frac{1}{2}+s\right)\Gamma(n+1)\Gamma(\frac{1}{2})}{\Gamma\left(1-\frac{n}{2}+s\right)\Gamma\left(\frac{n}{2}+s+1\right)\Gamma\left(\frac{n}{2}+\frac{1}{2}-s\right)},\qquad n\text{ odd}. \tag{35}$$

We note that (35) is true for all η even when $\eta=1$. This is so since all c_s must be bounded for *all* η in order that points between zero and one remain ordinary points. This can also be seen by examining the recursion formula for the c_s given in reference 13. For $n=1$ we have

$$g_{1,\kappa}(0)=2c_0/3\pi^{\frac{1}{2}}. \tag{36}$$

For the higher odd values of n we find (36) multiplied by simple nonsingular functions of η.[14] We always find, however, that $g_{n,\kappa}(0)$ is proportional to the arbitrary constant c_0 (κ even) and hence that $g_{n,\kappa}$ has exponent 1 at $z=0$ if κ is even. This result is true for eigenfunctions with η arbitrary, and it remains valid even in the limit where we set η *equal* to one. Thus

$$g_{n,\kappa}(0)\neq 0\ (\kappa\text{ even, all }\eta). \tag{37}$$

If we compare (36), (37), with (27) we find that only the value $\rho=-\frac{1}{2}$ can represent the even eigenfunctions in the limit $\eta=1$.

$$\lim_{\eta\to 1}\lambda_{n,\kappa}=0;\ \kappa\text{ even}, \tag{38}$$

$$\lim_{\eta\to 1}g_{n,\kappa}(z)_{\text{even}}=(1-z^2)^n\,{}_2F_1\left(\frac{n}{2}+\frac{1}{2},\frac{n}{2};n+1;1-z^2\right). \tag{39}$$

It is noteworthy that (39) is just the first term of Erdélyi's expansion (33). Using the fact that an odd eigenvalue must be between any two even ones, we have

$$\lim_{\eta\to 1}\lambda_{n,\kappa}=0;\ \kappa\text{ odd}, \tag{40}$$

$$\lim_{\eta\to 1}g_{n,\kappa}(z)_{\text{odd}}=(1-z^2)^n z\,{}_2F_1\left(\frac{n}{2}+1,\frac{n}{2}+\frac{1}{2};n+1;1-z^2\right). \tag{41}$$

[14] A corresponding analysis may be carried out for even n by using Eq. (21) for the expansion.

The series (39) and (41) can be summed and we obtain

$$\lim_{\eta\to 1} g_{n,\kappa}(z)=\begin{cases}(1-|z|)^n, & \kappa \text{ even},\\ \dfrac{z}{|z|}(1-|z|)^n, & \kappa \text{ odd}.\end{cases} \tag{42}$$

Thus all even solutions degenerate into the ones found in W and C as the nodes shrink together.

Since we have invoked the limit $\eta=1$ in discussing the solutions of the differential equation, it is of interest to see just how (42) satisfies the integral equation (5) in this limit since (5) is more directly connected with the original problem. We may also see again in this way that (42) represents the only part of the set (27) which is acceptable. Furthermore, since it is known that an ambiguity exists concerning the integral equation satisfied by a solution of Heun's equation,[15] this point is worth investigating.

We again consider κ even and $n=1$ for simplicity. Then (5) may be rewritten as a Volterra equation:

$$g_{1,\kappa}(z)=g_{1,\kappa}(0)-\lambda\int_0^z \frac{dy\,g_{1,\kappa}(y)(z-y)}{(1-\eta^2+\eta^2y^2)(1-y^2)}, \tag{43}$$

$$g_{1,\kappa}(0)=\lambda\int_0^1 \frac{dy\,g_{1,\kappa}(y)}{(1-\eta^2+\eta^2y^2)(1+y)}. \tag{44}$$

In the limit $\eta=1$ this becomes [see (32)]

$$g_{1,\kappa}(z)=g_{1,\kappa}(0)-\lambda\lim_{\epsilon\to 0}\int_0^z \frac{dy\,g_{1,\kappa}(y)(z-y)}{(y^2+\epsilon^2)(1-y^2)}, \tag{45}$$

$$g_{1,\kappa}(0)=\lambda\lim_{\epsilon\to 0}\int_0^1 \frac{dy\,g_{1,\kappa}(y)}{(y^2+\epsilon^2)(1+y)}. \tag{46}$$

Let us consider which solutions (27) can obey (45) and (46). If ρ is not equal to $-\frac{1}{2}$ ($\lambda\neq 0$), then $g_{1,\kappa}(0)\equiv 0$. We can easily see that for $-\frac{1}{2}<\rho\leq\frac{1}{2}$, every term in the series (27) is real and positive. Thus the integral (46) diverges, and we have a contradiction. We may therefore state that $0<\lambda\leq\frac{1}{4}$ cannot be an eigenvalue of (45), (46) in this limit.

If $\lambda>\frac{1}{4}$, $\rho=i\sigma$ (σ real) and (27) becomes

$$\lim_{\eta\to 1} g_{1,\kappa}(z)$$

$$=(1-z^2)^n z^{\frac{1}{2}+i\sigma}\,{}_2F_1\left(\frac{5}{4}+i\frac{\sigma}{2},\frac{3}{4}+\frac{i\sigma}{2};2;1-z^2\right). \tag{47}$$

This function, which is real, has an essential singularity at $z=0$ and for small z we may write

$$\lim_{\eta\to 1} g_{1,\kappa}(z)=z^{\frac{1}{2}}\cos(\sigma\ln z-\alpha)[1+\cdots]. \tag{48}$$

Because of the rapid oscillation of (47) near the origin one might expect that the effect of the z^{-2} singularity is canceled out so that the integrals in (45) and (46) are finite. If we assert that neither integral is to become infinite, we have essentially two cases to consider:

(a) If we assume that the kernel in (45) is only apparently singular because of the rapid oscillation near the origin, (48), then we may transform (45) so that the kernel is manifestly nonsingular. However, in this case we have a homogeneous Volterra equation [$g_{1,\kappa}(0)\equiv 0$] with a bounded kernel, and there are no nontrivial solutions.

(b) If the kernel cannot be transformed to a nonsingular one, then any solution (47) which obeys (46) must do so because of an exact cancellation of infinite contributions. If this is so, it is clear that there will be at least one value of z (near $z=0$) such that the integral in (45) will be infinite and again we have a contradiction. We conclude that no value $\lambda>0$ can be an eigenvalue of (45), (46), and hence (5) in the limit $\eta=1$. It remains to be shown that the value $\lambda=0$ is an eigenvalue of (5) *in* the limit $\eta=1$. It is easiest to insert the set (42) into (5) and integrate the R.H.S. Keeping (32) in mind we obtain

$$\lim_{\eta\to 1} g_{n,\kappa}(z)=\begin{cases}A_{n,\kappa}\left[\lambda\lim_{\epsilon\to 0}\left(\frac{1}{\epsilon}+\cdots\right)\right](1-|z|)^n\\ \qquad +\lambda f_{n,\kappa}(z);\ \kappa \text{ even}\\ A_{n,\kappa}[\lambda\lim_{\epsilon\to 0}(\log\epsilon+\cdots)]\dfrac{z}{|z|}(1-|z|)^n\\ \qquad +\lambda f_{n,\kappa}(z);\ \kappa \text{ odd},\end{cases} \tag{49}$$

where $A_{n,\kappa}$ is nonzero and $f_{n,\kappa}$ is bounded. It is clear that this equation has one and only one eigenvalue

$$\lim_{\eta\to 1}\lambda_{n,\kappa}=0. \tag{50}$$

In the next section we explain just how this degeneracy arises and obtain rough formulas for $\lambda_{n,\kappa}(\eta)$, $(1-\eta^2)\ll 1$.

V. DISCUSSION OF THE SPECTRUM

In one-dimensional bound quantum mechanical systems we find, in general, two kinds of behavior as the potential strength is reduced to zero. In the first type all eigenvalues remain in the spectrum for any finite coupling constant and become degenerate in the limit of zero potential strength. In systems of the second kind we find that we have fewer energy levels as we reduce the coupling constant until we come to a certain critical strength and below this value of the coupling constant we have only one bound state. It has been suggested that it is surprising that a differential equation such as (6) should have a spectrum of the first type.

This point can be understood by looking at the first odd eigenfunction for $(1-\eta^2)\ll 1$ but not equal to zero. We must have $g_{n,1}(0)=0$ and if λ is small, this eigen-

[15] A. Erdélyi, Quart. J. Math. **13**, 107 (1942).

function must begin to rise very rapidly as z increases as shown by (27). However, the curvature must be great enough to turn $g_{n,1}(z)$ around, since $g_{n,1}'(z)$ must be positive near $z=0$ and negative for $z^2 \gg (1-\eta^2)$. This would indicate a large curvature and hence a large λ. We shall find below that this objection can be resolved since in fact the eigenvalues $\lambda_{n,\kappa}$ tend to zero very slowly as $\eta \to 1$ if $\kappa > 0$.

We introduce the following familiar nonlinear transformation[16] in order to write (6) as a Schrödinger equation and in order to display a sensitive expression for the eigenvalues. If for simplicity we again restrict our attention to $n=1$, we let

$$2K(\eta)=\frac{1}{\pi}\int_{-1}^{1}\frac{d\zeta}{(1-\zeta^2)^{\frac{1}{2}}(1-\eta^2+\eta^2\zeta^2)^{\frac{1}{2}}},$$

$$x=\frac{1}{2K}\int_{-1}^{z}\frac{d\zeta}{(1-\zeta^2)^{\frac{1}{2}}(1-\eta^2+\eta^2\zeta^2)^{\frac{1}{2}}}, \tag{51}$$

$$y_\kappa=(1-z^2)^{-\frac{1}{4}}(1-\eta^2+\eta^2z^2)^{-\frac{1}{4}}g_{1,\kappa}(z),$$

$$\lambda_{1,\kappa}=\tfrac{1}{4}\Lambda_\kappa^2K^{-2}(\eta)-(2\eta^2-1)/2.$$

Then (6) becomes

$$y_\kappa''(x)+[\Lambda_\kappa^2-Q(x)]y_\kappa(x)=0, \tag{52}$$

with

$$Q(x)=(1-z^2[x])^{\frac{1}{2}}(1-\eta^2+\eta^2z^2[x])^{\frac{1}{2}}$$

$$\times\frac{d^2}{dx^2}\{(1-z^2[x])^{-\frac{1}{2}}(1-\eta^2+\eta^2z^2[x])^{-\frac{1}{2}}\}+\tfrac{1}{2}-\eta^2. \tag{53a}$$

In order to evaluate $Q(x)$, we would have to express z in terms of x and substitute in (53a). Unfortunately the transformation from z to x, Eq. (51), involves elliptic integrals and we cannot write a simple algebraic form for $Q(x)$. We can obtain the behavior of $Q(x)$ by the following argument: writing $(df/dx)=(dx/dz)\times(df/dz)$, we can write $Q(x)=Q(z[x])$ as a function of $z[x]$ and we arrive at a simple algebraic expression.

$$Q(z[x])=6K^2(\eta)\eta^2$$

$$\times\left[z^2+\frac{z^2(1-z^2)\eta^2}{2(1-\eta^2+\eta^2z^2)}+\frac{z^2(1-\eta^2+\eta^2z^2)}{2\eta^2(1-z^2)}\right]. \tag{53b}$$

Knowing how Q varies with z, we may obtain $Q(x)$ by noting how z varies with x. In particular, by observing dx/dz which has a simple form, we can make a graphical transformation from $Q(z[x])$ as a function of z to $Q(x)$ as a function of x.

We note the following points about this transformation of the differential equation:

(a) $K=K(\eta)$ is the complete elliptic integral and it has the following expansions[17]

$$K(\eta)=\begin{cases}\frac{1}{2}\pi+\frac{1}{8}\pi\eta^2+\cdots, & \eta\ll 1\\ 1/\pi\ln 4(1-\eta^2)^{-\frac{1}{2}}+\cdots, & (1-\eta^2)^{\frac{1}{2}}\ll 1.\end{cases}$$

(b) We see from (51) that $z=-1$, 0, 1 are transformed into $x=0$, $\frac{1}{2}\pi$, π, respectively, for all η including $\eta=1$. By examining dx/dz we see that for $\eta\neq 1$ this is a smooth transformation with $(dx/dz)(z^2=1)=\infty$. In the limit $\eta=1$ we have $dx/dz=0$, $-1<z<1$ and $dx/dz=\infty$, $z^2=1$.

(c) $Q(z=\pm 1)=\infty$ and $Q(z=0)=0$ for all η including $\eta=1$. From (b) above we see that $Q(x)$ is a smooth potential well, broader than $Q(z)$ with $Q(x=0,\pi)=\infty$, $Q(x=\pi/2)=0$ for all η. As η tends to one, $Q(z)$ become steeper and the transformation $z\to x$ becomes broader. Thus the limit as $\eta\to 1$ of $Q(x)$ is an indeterminate form. We can, however, obtain a considerable amount of information since the formula for $\lambda_{1,\kappa}$ is very sensitive.

Let us consider one extreme—that in which the limit of $Q(x)$ has a finite base, i.e., the limit of $Q(x)$ touches the zero line over a finite region. In this case all Λ_κ would remain finite and we see that this would require $\lim\lambda_{1,\kappa}=-\frac{1}{2}$. We therefore rule this out and state that even in the limit $\eta=1$, $Q(x)$ is zero only at the point $x=\frac{1}{2}\pi$.

The other extreme case would require that $\lim Q(x)$ as $\eta\to 1$ tends to a square of vanishing width a. We know that eigenvalues of such a system tend to $\Lambda_\kappa^2\to\pi^2(\kappa+\frac{1}{2})^2/a^2$. If we fix $\lambda_{1,0}$ so that it tends to zero, we find that in this extreme we have a complete discrete λ spectrum tending to infinity. Ruling this out we conclude that:

(a) $\mathrm{Lim}Q(x)=0$ only for $x=\pi/2$.

(b) $\mathrm{Lim}Q(x)=\infty$ when $x=0$, π.

(c) Since $\lambda_{1,0}\to 0$, Λ_0^2 must tend to $K^2(\eta)$ [see (51)], and hence all Λ_κ^2 must tend to infinity as fast as $K^2(\eta)$.

(d) $\mathrm{Lim}Q(x)$ does not tend to a square well of vanishing width and hence $\lim(\Lambda_{\kappa+1}^2-\Lambda_\kappa^2)$ goes slower than $K^2(\eta)$ for large κ. Therefore, all eigenvalues become degenerate for large κ.

From this discussion the difference between our limiting spectrum and the results indicated by Wick's approximation can easily be seen. A spectrum with all eigenvalues, $\lambda_{1,\kappa}$, tending to zero in the limit $\eta\to 1$ merely means that $\lim Q(x)$ is a smooth function. On the other hand, a result such as Wick's would require $\lim(\Lambda_1^2-\Lambda_0^2)=O(K^2)$, while $\lim(\Lambda_{\kappa+1}^2-\Lambda_\kappa^2)<O(K^2)$ for $\kappa>0$. In other words, the limiting form of $Q(x)$ would have to be a potential well shaped somewhat like an inverted wine bottle with the neck shrinking faster than the upper part.

Using the knowledge that $Q(x)$ is a smooth function with the properties mentioned above, we may make a

[16] E. L. Ince, *Ordinary Differential Equations* (Dover Publications, New York, 1948), p. 270.

[17] E. Jahnke and F. Emde, *Tables of Functions* (Dover Publications, New York, 1945), p. 73.

correspondence between $Q(x)$ and another potential well which has the above properties. Knowing the spectrum of the comparison potential, we obtain an approximate formula for $\lambda_{l,\kappa}$. This is done in Appendix II and the result is

$$\lambda_{l,\kappa}(\eta)\simeq\begin{cases}(1-\eta^2)^{\frac{1}{2}}+\cdots\kappa=0\\ \alpha\kappa[\ln 2(1-\eta^2)^{-1}]^{-1}+\cdots\kappa>0\end{cases},\quad (1-\eta^2)^{\frac{1}{2}}\ll 1. \tag{54}$$

The important feature of (54) is that λ is a power of $(1-\eta^2)^{\frac{1}{2}}$ for $\kappa=0$ and that λ tends to zero more slowly, as a logarithm of $(1-\eta^2)^{\frac{1}{2}}$, for $\kappa>0$. This result meets the objection raised in the first part of this section and also joins well with Cutkosky's numerical results for $\eta\neq 1$.

In Sec. VI, we shall investigate the original B.S. wave functions with these results in mind.

VI. B.S. WAVE FUNCTIONS

In this section, we wish to investigate the B.S. wave functions on a space-like surface. These are given by

$$\Phi_{n,\kappa}{}^{l,m}(\mathbf{p})=\int_{-\infty}^{\infty}dp_4\phi_{n,\kappa}{}^{l,m}(p). \tag{55}$$

We immediately see from (4), the definition of $\phi(p)$, that since $R^{n-l-1}C_{n-l-1}^{l+1}$ is an even function of p_4, the B.S. wave functions have the symmetry of $g_{n,\kappa}(z)$. Therefore

$$\Phi_{n,\kappa}{}^{l,m}(\mathbf{p})\equiv 0,\ \kappa \text{ odd},$$

and we can restrict our discussion to functions with even κ. We shall attempt to determine how $\Phi(\mathbf{p})$ changes as we vary n, l, κ. Let us begin this discussion by considering those states with $l=n-1$. Then from (4) and (55) we have

$$\Phi_{n,\kappa}{}^{n-1,m}(\mathbf{p})=\mathcal{Y}_{n-1}{}^{m}(\mathbf{p})\int_{-1}^{1}\frac{g_{n,\kappa}(z)dz}{[\mathbf{p}^2+1-\eta^2+\eta^2z^2]^{n+1}}. \tag{56}$$

If we let $z^2=(\mathbf{p}^2+1-\eta^2)s^2$, (56) becomes

$$\Phi_{n,\kappa}{}^{n-1,m}(\mathbf{p})=\mathcal{Y}_{n-1}{}^{m}(\mathbf{p})[\mathbf{p}^2+1-\eta^2]^{-n-1}D_{n,\kappa}(\mathbf{p},\eta), \tag{57}$$

$$D_{n,\kappa}(\mathbf{p},\eta)=\int_0^{(\mathbf{p}^2+1-\eta^2)^{-\frac{1}{2}}}\frac{dsg_{n,\kappa}[(\mathbf{p}^2+1-\eta^2)^{\frac{1}{2}}s]}{[\eta^2s^2+1]^{n+1}}. \tag{58}$$

We observe that if $D_{n,\kappa}$ were constant, (57) would be precisely equal to the hydrogen atom wave function with $l=(n-1)$.[18] Therefore our study of the nonrelativistic behavior of the B.S. wave functions is reduced to a study of the deviation from constancy of (58) in the region $(\mathbf{p}^2+1-\eta^2)\ll 1$. In particular, we wish to know how $D_{n,\kappa}$ varies with $\mathbf{p}^2$ for $(1-\eta^2)\ll 1$. In order to discuss this point, we may obtain a considerable amount of information by using the fact that $g_{n,\kappa}$ obeys the integral equation (5). Thus, for any even κ, (5) yields

$$ng_{n,\kappa}(0)/\lambda_{n,\kappa}(\eta)=\int_0^1\frac{g_{n,\kappa}(z)dz}{(1+z^2)^n(1-\eta^2+\eta^2z^2)}. \tag{59}$$

We make the same transformation in (59) as was done in (56) and we obtain

$$n(\mathbf{p}^2+1-\eta^2)^{\frac{1}{2}}g_{n,\kappa}(0)/\lambda_{n,\kappa}(\eta)=\int_0^{(\mathbf{p}^2+1-\eta^2)^{-\frac{1}{2}}}$$

$$\times\frac{dsg_{n,\kappa}[(\mathbf{p}^2+1-\eta^2)^{\frac{1}{2}}s]}{[1+(\mathbf{p}^2+1-\eta^2)^{\frac{1}{2}}s]^n[1+\eta^2s^2-\mathbf{p}^2(\mathbf{p}^2+1-\eta^2)^{-1}]}. \tag{60}$$

It is of interest to compare (58) and (60). Let us first consider $\mathbf{p}^2=0$ and $(1-\eta^2)\ll 1$. [It is of no significance to consider the limit $\eta=1$ for this discussion since (58) and (60) have quite different behavior at zero binding energy.] The denominators in both integrals are rather sharply peaked around $s=0$. In (58) the peaking effect is much stronger than in (60), if $\mathbf{p}^2=0$ and η is near one. However, if we consider $g_{n,\kappa}$ for $\kappa=2$, for instance, we see that even here the main contribution to the integral (60) comes from the central peak since the integral in (60) has the same sign as this central peak. Thus, for any η, the peaking effect of the denominator in (59) or (60) (with $\mathbf{p}^2=0$) is so great that the main contribution comes from the center. This is even more pronounced for $D_{n,\kappa}(0,\eta)$ since the denominator in (58) is more sharply peaked around the origin.

This indicates that $D_{n,\kappa}(0,\eta)$ is a less sensitive function of η (for η fairly near one) than is $[(1-\eta^2)^{\frac{1}{2}}\times g_{n,\kappa}(0)\lambda_{n,\kappa}(\eta)]$. From our discussion of the approximate values for $\lambda_{n,\kappa}$ we know that $\lambda_{n,0}\to(1-\eta^2)^{\frac{1}{2}}$, while $\lambda_{n,\kappa}$, $\kappa>0$ tends to a slowly varying logarithmic function of $(1-\eta^2)^{\frac{1}{2}}$ in this region. We conclude therefore that in the region of small binding energies $D_{n,0}(0,\eta)$ is sensibly constant while $D_{n,\kappa}(0,\eta)$ is a slowly varying function of η. The first part of this statement may be checked by inserting $g_{n,0}(z)\simeq(1-|z|)^n$ and integrating the R.H.S. of (58).

It is of more interest to consider η fixed at some value $(1-\eta^2)^{\frac{1}{2}}\ll 1$, and to investigate how $D_{n,\kappa}(\mathbf{p},\eta)$ varies with $\mathbf{p}^2$. Again for $\kappa=0$ we may insert $(1-|z|)^n$ for $g_{n,\kappa}$ and integrate. We find

$$D_{n,0}(\mathbf{p},\eta)=1+O(\mathbf{p}^2+1-\eta^2). \tag{61}$$

Therefore, in the nonrelativistic region, $(\mathbf{p}^2+1-\eta^2)\ll 1$, $D_{n,0}$ is roughly constant and the B.S. wave function $\Phi_{n,0}{}^{n-1,m}(\mathbf{p})$ is a good approximation to the corresponding nonrelativistic wave function. We expect this, since $g_{n,0}(z)$ is a broad smooth function of z; also, the transformation $z^2=(\mathbf{p}^2+1-\eta^2)s^2$ has stretched out the origin in a nonlinear manner such that $D_{n,0}$ is not a sensitive function of $\mathbf{p}$ in the N.R. region.

One might expect that the rapid oscillation of g for

[18] L. Pauling and B. Podolsky, Phys. Rev. **34**, 109 (1929).

$\kappa>0$ might completely change this smooth functional dependence of $D_{n,\kappa}(\mathbf{p},\eta)$ on $\mathbf{p}$. Let us consider the first "anomalous" solution with $\kappa=2$. We see that an integral such as the R.H.S. of (60) is actually a slowly varying function of $\mathbf{p}^2$ compared to the rapid variation in the B.S. wave function itself (57). Comparing (60) with (57) we see that $D_{n,2}(\mathbf{p},\eta)$ varies even more slowly than $(\mathbf{p}^2+1-\eta^2)^{\frac{1}{2}}$ at least until $\mathbf{p}^2$ is several times greater than $(1-\eta^2)$. The most that could occur to $D_{n,2}(\mathbf{p},\eta)$ as we increased $\mathbf{p}^2$ would be the occurrence of a node and a change of sign. This would, however, not happen in the N.R. region. Generalizing these results, we can state:

(a) For $l=n-1$ the B.S. wave function on a space-like surface can be given by the N.R. wave function times a factor $D_{n,\kappa}(\mathbf{p},\eta)$. The function $D_{n,\kappa}(\mathbf{p},\eta)$ can have at most $\frac{1}{2}\kappa$ nodes.

(b) In the region $(1-\eta^2)\ll 1$, $\mathbf{p}^2=O(1-\eta^2)$, all $D_{n,\kappa}$ are roughly constant with respect to $\mathbf{p}^2$. $D_{n,\kappa}$ can be taken as constant over a greater region in $\mathbf{p}^2$ space than can $D_{n,\kappa+2}$.

(c) Since $D_{n,0}(\mathbf{p},\eta)$ has no nodes, $\Phi_{n,0}{}^{n-1,m}(\mathbf{p})$ is the best approximation to the nonrelativistic wave function. However, all $\Phi_{n,\kappa}{}^{n-1,m}(\mathbf{p})$ for κ small (κ of the order of several times n) will be reasonable approximations to the N.R. wave functions in the region $(\mathbf{p}^2+1-\eta^2)\ll 1$ and none of these show unacceptable behavior.

By partial integration of (4), we can extend these results to include lower values of l. For instance,

$$\Phi_{n,\kappa}{}^{n-2,m}(\mathbf{p})=\mathcal{Y}_{n-2}{}^{m}(\mathbf{p})D_{n,\kappa}(\mathbf{p},\eta)[\mathbf{p}^2+1-\eta^2]^{-n}\times\left[1+\frac{\mathbf{p}^2}{n[\mathbf{p}^2+1-\eta^2]}\right]C_2{}^{n-1}\left(\frac{1-\eta^2-\mathbf{p}^2\left(1+\frac{1}{n}\right)}{1-\eta^2+\mathbf{p}^2\left(1+\frac{1}{n}\right)}\right), \quad (62)$$

while the hydrogen atom wave function is given by

$$\Phi_n{}^{n-2,m}(\mathbf{p})=\mathcal{Y}_{n-2}{}^{m}(\mathbf{p})[\mathbf{p}^2+1-\eta^2]^{n}\times C_2{}^{n-1}\left(\frac{1-\eta^2-\mathbf{p}^2}{1-\eta^2+\mathbf{p}^2}\right). \quad (63)$$

In general, we find best agreement for large n and large l where the particles move in roughly classical orbits.

VII. BOUNDARY CONDITIONS

At this point we must consider the effect of the boundary conditions (1), (2) on ϕ. The B.S. wave function $\phi_{n,\kappa}{}^{l,m}(p)$ is given by (4). As defined above, $g_{n,\kappa}(z)$ is a bounded continuous function of z over the range $-1\leq z\leq 1$. By inspection of (4) we see that $\phi_{n,\kappa}{}^{l,m}(p)$ is a continuous function of $\mathbf{p}$, p_4, bounded on the real p_4 axis and tending rapidly to zero as p_4 tends to infinity. Therefore, the configuration space transform $\phi_{n,\kappa}{}^{l,m}(x)$ exists. Since ϕ is a smooth decreasing function of p_4 which is regular near $p_4=0$, the rapid oscillation of the exponential in the transform implies

$$\phi_{n,\kappa}{}^{l,m}(\mathbf{x},x_4)\to 0 \quad \text{as} \quad |x_4|\to\infty \ (\text{all } l,m,n,\kappa).$$

We conclude that *all* eigenfunctions of (3) obey the weak condition, (2).

The strong boundary condition, (1), contains (2). Equation (1) also requires that all poles in the B.S. wave function be located beyond $p_4=\pm i\omega_M$ and that any pole *at* $p_4=\pm i\omega_M$ be of first order. By inspecting the denominator $[p_4{}^2+\mathbf{p}^2+1-\eta^2+2i\eta p_4 z]$, where z ranges over $-1\leq z\leq 1$, we find that all poles of $\phi_{n,\kappa}{}^{l,m}(p)$ are at or beyond $p_4=\pm i\omega_M$. If we note that $g_{n,\kappa}(z)=(1-z^2)^n f_{n,\kappa}(z)$ where $f_{n,\kappa}(1)=1$, we may perform an integration by parts in Eq. (4). Observing that

$$\left.\frac{d^s g_{n,\kappa}}{dz^s}\right]_{(z^2=1)}=0, \quad s<n,$$

we have

$$\phi_{n,\kappa}{}^{l,m}(\mathbf{p},p_4)=\psi_{n,\kappa}{}^{l,m}(\mathbf{p},p_4)+\{[\mathbf{p}^2+1-\eta^2+p_4{}^2+2i\eta p_4]^{-1}\pm[\mathbf{p}^2+1-\eta^2+p_4{}^2-2i\eta p_4]^{-1}\}\times R^{n-l-1}C_{n-l-1}{}^{l+1}(X/R)\mathcal{Y}_l{}^m(\mathbf{p}),$$

where $\psi_{n,\kappa}{}^{l,m}(\mathbf{p},p_4)$ can have at most a logarithmic singularity at $p_4=\pm i(E_p-\eta)=\pm i\omega_M$. Thus the wave functions $\phi_{n,\kappa}{}^{l,m}(p)$ for *all* n, l, m, κ obey both boundary conditions (1) and (2) with no additional restrictions. It may be worth noting that the second solution of Eq. (6), given by (15), does not obey the strong boundary condition. Therefore, if in some other B.S. equation it is not immediately clear that solutions of the second type, (15) are unacceptable, the strong boundary conditions may be invoked to eliminate them and yield a discrete spectrum.

Finally we consider orthonormalization conditions which may be obtained from the B.S. equation itself. Wick has observed that the product of the propagation terms is self-adjoint only for $m_a=m_b$. Therefore in the case we are dealing with, we can derive a set of "orthonormalization" conditions since we are working with equal mass particles and Euclidean variables. That is, we need not consider the change in sign in $(m-i\epsilon)$ upon taking the adjoint of (3). From Eq. (3) we find

$$(\eta_{n,\kappa}{}^2-\eta_{n',\kappa'}{}^2)\int d^4p\,\phi_{n',\kappa'}{}^{l,m*}(p)\phi_{n,\kappa}{}^{l,m}(p)\times[2-\eta_{n,\kappa}{}^2-\eta_{n',\kappa'}{}^2+2\mathbf{p}^2-2p_4{}^2]=0, \quad (64)$$

if

$$\lambda_{n,\kappa}=\lambda_{n',\kappa'},$$

and

$$(\lambda_{n,\kappa}-\lambda_{n',\kappa'})\int d^4p\int d^4k\times\phi_{n',\kappa'}{}^{l,m*}(p)\phi_{n,\kappa}{}^{l,m}(k)(p-k)^{-2}=0, \quad (65)$$

if

$$\eta_{n,\kappa}=\eta_{n',\kappa'}.$$

Equation (64) applies to the *complete* B.S. equation while (65) is obtained only from the ladder approximation. The significance of conditions like these is not immediately clear. Analogs of (64) and (65) can also be obtained when the two masses differ, but they reduce to the same form only if κ and κ' are both even or both odd. This is so because the non-self-adjoint term in the product of the propagators is an odd function of p_4. Furthermore, it is difficult to determine whether or not the B.S. wave functions obey these "orthogonality" conditions. In (64), for instance, if $\eta \neq \eta'$, the arguments of ϕ'^* and ϕ are different and it would only be practical to try to examine (64) in configuration space. It seems that a further investigation of (64) and (65) in the N.R. limit is necessary in order to understand the possible significance of these conditions. On the other hand, some conditions similar to (64), (65) would seem to be necessary to reduce the continuum found by Goldstein[19] in his examination of the corresponding problem of two Fermi-Dirac particles interacting with zero total energy. The whole problem of orthogonality of B.S. wave functions and the extension of any orthogonality conditions to singular "potentials" or non-Hermitian operators needs to be investigated further.[20]

VIII. CONCLUSIONS

We have rigorously examined the spectrum of a Bethe-Salpeter equation in the ladder approximation. For equal-mass scalar particles with a scalar massless field we have found a complete discrete eigenvalue spectrum labeled by quantum numbers n, l, m, κ. In the limit of zero binding energy it is found that all eigenvalues $\lambda_{n,\kappa}$ tend to zero. While the set of eigenvalues $\lambda_{n,0}$ give the best fit to the N.R. spectrum, the eigenvalues for $\kappa > 0$ are not unacceptable in this limit. The B.S. wave functions are examined on a space-like surface. Again it is found that the set $\Phi_{n,0}{}^{l,m}(\mathbf{p})$ yield the best fit to the hydrogen atom wave functions but that the $\Phi_{n,\kappa}{}^{l,m}(\mathbf{p})$, $\kappa > 0$, are not unacceptable. It is shown that all B.S. wave functions obey certain proposed boundary conditions. We believe that these results are disturbing for the following reasons:

(a) Any more realistic approach to the two-body problem will very likely utilize some form of truncated interaction kernel, and we would expect our solutions to have many features in common with these. Therefore, we may expect the appearance of "spurious" solutions in the N.R. limit for many, if not all problems.

(b) Our conclusions remain true even if the particle masses are different. In this case it has been shown in C that an equation analogous to (5) results. The denominator $[1-\eta^2+\eta^2 z^2]^{-1}$ in (5) is replaced by $[(1-\eta^2)\times(1+\Delta^2+2\Delta z)+\eta^2(\Delta+z)^2]^{-1}$ where $m_a=1+\Delta$, $m_b=1-\Delta$. In the limit $\eta \to 1$, this denominator gives a singularity (at $z=-\Delta$) which is in the region of integration. Thus, the analog of (5) also becomes intrinsically singular in this limit. Again we find all $\lambda_{n,\kappa} \to 0$ as $\eta \to 1$. The actual eigenfunctions and approximate eigenvalues in this problem may immediately be obtained from our results by applying the similarity transformation introduced in C.

(c) If a finite quantum mass is used we would expect even more complications. At zero binding energy even the actual N.R. eigenvalues do not tend to zero and for $\eta \neq 1$, it would be difficult to distinguish the various solutions.

(d) Most important is the fact that one wishes to apply the B.S. equation to systems with no simple N.R. limit. Even in the problem we have discussed, if $\eta \leq \Delta$, the various eigenvalue curves cross and there is no clear distinction between n and κ. It would seem that further investigations concerning orthogonality, extra boundary conditions such as (64) and (65) above, etc., are necessary in order to understand the role of the "spurious" solutions of the B.S. equation.

ACKNOWLEDGMENTS

I wish to express my gratitude to Professor F. Villars for his valuable advice and guidance while this work was being carried out. I am deeply indebted to Professor C. G. Wick and to Dr. R. E. Cutkosky for making available to me their results before publication. I would also like to thank Professor Wick for several stimulating and informative discussions on certain aspects of this work.

APPENDIX I

Wick's inside solution [that is, the solution of Wick's approximate Eq. (61)] may conveniently be taken as

$$g_{l,\kappa}(z) \simeq \begin{cases} {}_2F_1\left(-\tfrac{1}{4}+\frac{\rho}{2}, -\tfrac{1}{4}-\frac{\rho}{2}; \tfrac{1}{2}; \eta^2 z^2(\eta^2-1)^{-1}\right), \\ \qquad\qquad \kappa \text{ even} \\ z\ {}_2F_1\left(\tfrac{1}{4}+\frac{\rho}{2}, \tfrac{1}{4}-\frac{\rho}{2}; \tfrac{3}{2}; \eta^2 z^2(\eta^2-1)^{-1}\right), \\ \qquad\qquad \kappa \text{ odd}, \end{cases} \tag{I.1}$$

where $z^2 < z_0^2 \ll 1$, $\rho = (\tfrac{1}{4}-\lambda)^{\frac{1}{2}}$.

From Eq. (16) above we see that the exact solution around the origin may be written

$$g_{l,\kappa}(z) = \begin{cases} F\left(1-\frac{1}{\eta^2}, \frac{2(1-\eta^2)-\lambda}{4\eta^2}; \tfrac{1}{2}, 1, \tfrac{1}{2}, 0; z^2\right), \kappa \text{ even} \\ zF\left(1-\frac{1}{\eta^2}, \frac{6(1-\eta^2)-\lambda}{4\eta^2}; \tfrac{3}{2}, 1, \tfrac{3}{2}, 0; z^2\right), \kappa \text{ odd}. \end{cases} \tag{I.2}$$

[19] J. S. Goldstein, Phys. Rev. **91**, 1516 (1953); H. S. Green, Phys. Rev. **97**, 540 (1955).

[20] We refer here to an extension of the work in reference 5 and a generalization of the requirements for a physically acceptable operator. See K. M. Case, Phys. Rev. **80**, 797 (1950).

We use the identity

$$F(a,b;\alpha,\beta,\gamma,\delta;u) = F\left(\begin{matrix}1 & b\\ -, & -\\ a & a\end{matrix};\alpha,\beta,\gamma,\ 1+\alpha+\beta-\gamma-\delta;\ \frac{u}{a}\right), \quad \text{(I.3)}$$

in order to obtain the following for the *exact* solutions

$$g_{L,\kappa}(z) = \begin{cases} F\left(\dfrac{-\eta^2}{1-\eta^2}, \dfrac{-[2(1-\eta^2)-\lambda]}{4(1-\eta^2)}; 1, \tfrac{1}{2}, \tfrac{1}{2}, 2;\right. \\ \qquad\qquad \left.\eta^2z^2(\eta^2-1)^{-1}\right), \ \kappa \text{ even} \\ zF\left(\dfrac{-\eta^2}{1-\eta^2}, \dfrac{-[6(1-\eta^2)-\lambda]}{4(1-\eta^2)}; \tfrac{3}{2}, 1, \tfrac{3}{2}, 2;\right. \\ \qquad\qquad \left.\eta^2z^2(\eta^2-1)^{-1}\right), \ \kappa \text{ odd.} \end{cases} \quad \text{(I.4)}$$

Both sets of series (I.1) and (I.4) converge up to $\eta^2z^2=(1-\eta^2)$ (see Fig. 1). Therefore, we might expect (I.1) to be a reasonable approximation to (I.4) in this interval. However, we note that neither Erdélyi's nor Svartholm's expansions yield (I.1) as leading terms. In order to see the relation between (I.1) and (I.4), we take the limit $\eta\to 1$. Using Eq. (23) above we find from (I.4)

$$\lim_{\eta\to 1} g_{L,\kappa}(z) = \begin{cases} {}_2F_1\left(-\tfrac{1}{4}+\dfrac{\rho}{2}, -\tfrac{1}{4}-\dfrac{\rho}{2}; \tfrac{1}{2};\right. \\ \qquad\qquad \left.\lim_{\eta\to 1}\eta^2(\eta^2-1)^{-1}z^2\right), \ \kappa \text{ even} \\ z\ {}_2F_1\left(\tfrac{1}{4}+\dfrac{\rho}{2}, \tfrac{1}{4}-\dfrac{\rho}{2}; \tfrac{3}{2};\right. \\ \qquad\qquad \left.\lim_{\eta\to 1}\eta^2(\eta^2-1)^{-1}z^2\right), \ \kappa \text{ odd.} \end{cases} \quad \text{(I.5)}$$

Thus Wick's approximate inside solution is only equal to the exact one in the limit $\eta=1$, where it has a zero radius of convergence. Since Wick's inside solution is regular and absolutely convergent near $\eta^2z^2=(1-\eta^2)$ and has a well-behaved analytic continuation past this point while the actual solution around $z^2=0$ is irregular in this neighborhood [the Heun's function converges only at $\eta^2z^2=-(1-\eta^2)$], we conclude the following: Wick's inside solution may be considered as a reasonable approximation to the exact one for $\eta^2z^2<(1-\eta^2)$. However, we may not use the analytic continuation of this approximation at $\eta^2z^2=\eta^2z_0^2\gg(1-\eta^2)$ in order to obtain the eigenvalue spectrum.

APPENDIX II

In (52), (53) we make the following transformation:

$$\begin{aligned} \Lambda_\kappa^2 &= k_\kappa^2+A^2K^2(\eta), \\ Q(x) &= R(x)+A^2K^2(\eta). \end{aligned} \quad \text{(II.1)}$$

We then have

$$y_\kappa''+[k_\kappa^2-R(x)]y_\kappa=0, \quad \text{(II.2)}$$

with $R(0)=R(\pi)=\infty$, $R(\pi/2)=A^2K^2(\eta)$. A corresponding Schrödinger equation in which all important properties of (II.2) are present is

$$\psi''+[m^2-\mu^2\sin^{-2}x]\psi=0. \quad \text{(II.3)}$$

Here $V(0)=V(\pi)=\infty$, $V(\pi/2)=\mu^2$. Also, the "steepness" of $V(x)$ is proportional to μ^2 while that of $R(x)$ is proportional to $K^2(\eta)$. We make a rough correspondence by setting $AK(\eta)=B\mu$. The eigenvalues of (II.3) are known to be $m_\kappa^2=(\kappa+S)^2$ where $\mu^2=s(s-1)$.[21] Thus, if $K(\eta)\gg 1[1\gg(1-\eta^2)^{\frac{1}{2}}]$, we have for the original eigenvalues of the B.S. equation

$$\lambda_{L,\kappa}(\eta)\simeq K^{-2}(\eta)(\kappa+AK(\eta)/B+\tfrac{1}{2}+O(K^{-2}(\eta))^2 + A^2-(2\eta^2-1)/2.$$

If we choose A and B so that $\lim\lambda_{L,0}\to(1-\eta^2)^{\frac{1}{2}}$, $\eta\to 1$, we obtain the first part of (54). For $\kappa>0$, we then have

$$\lambda_{L,\kappa}(\eta)\simeq A\kappa/BK(\eta), \quad \kappa>0.$$

Using the series expansion for $K(\eta)$ in the region $\eta\simeq 1$, the second part of Eq. (54) follows.

[21] S. Flügge and H. Marschall, *Rechenmethoden der Quantentheorie* (Springer-Verlag, Berlin, 1952), p. 65.

Internal Structure of Spinning Particles

DAVID FINKELSTEIN
Physics Department, Stevens Institute of Technology, Hoboken, New Jersey, and Institute of Mathematical Sciences, New York University, New York

(Received May 25, 1955)

Elementary particle models with internal degrees of freedom have been investigated within the framework of special relativity and orthodox quantum mechanics. Classical arguments indicate that systems whose extensions are $\lesssim$ their Compton wavelength have spin excitation energies $\gtrsim$ their rest mass. The principal aim of this paper is enumeration and classification of particles with rigid internal structure and a useful classification of particle models is by their symmetry groups. In nonrelativistic mechanics this classification shows that there are only the three well-known types of rigid systems that might be labeled by number of degrees of freedom as [0], [2], and [3] and are exemplified by an ideal point, diatomic molecule and rotator, respectively; while of the three types, but one, [3], possesses a spin-$\frac{1}{2}$ state of the Pauli-election type. The corresponding analysis for relativistic mechanics shows there are nine types labeled here [0], [2], [3], [3′], [4], [4′], [4″], [5], and [6], and in addition two one-parameter infinities of types [3$_f$] and [5$_f$] ($0\leq f\leq\pi$). An algorithm exists for obtaining the spin-spectra of rigid structures from their symmetry groups. Of the $9+2\infty$ types, just three ([4], [5], and [6]) possess spin-$\frac{1}{2}$ states of the Dirac-electron type. The apparent rest mass depends upon the internal rotational state of the particle, as is shown by an unrealistic example of a Lagrangian which is an extension of that of the Klein-Gordon particle.

I. INTRODUCTION

THERE have been many attempts to bring order to the array of observed particles by calling some of them excited states of others. To do this is to attribute to the basic particles certain internal degrees of freedom[1] which, being capable of excitation, can account for the existence of various states with different properties. In many cases, this additional degree of freedom has described a motion outside of customary space-time—a rotation in isotopic spin-space, or a motion in six-dimensional relativity, etc. If only for the sake of completeness, we shall investigate here the possibilities within the present frameworks of quantum theory and special relativity.

Particles with spin present an interesting problem in this respect. First, of course, they cannot be completely structureless point masses whose states are represented in the original Schroedinger way by scalar wave functions $\psi=\psi(x,y,z,t)$ of position in space-time alone. Second, it is well known that even a composite system of such ideal point masses possesses no half-odd-integer spin states, so that an electron or a μ meson or any other particle of spin $\frac{1}{2}$ cannot be a tightly bound rotating aggregate of point masses with

$$\psi=\psi(x_1,\cdots,x_n). \tag{1}$$

Thus, it might appear that no mechanical model can possess spin $\frac{1}{2}$. Yet, ignoring for the moment the requirements that relativity places upon such theories, it is well known that a simple mechanical system is at hand which will exhibit spin $\frac{1}{2}$ as a result of ordinary rotation: the ideal rigid rotator, whose state is given by a wave function depending on the spatial coordinates x,y,z and three Euler angles θ,ϕ,χ:[2]

$$\psi=\psi(x,y,z;\theta,\phi,\chi). \tag{2}$$

The existence of such a mechanical model is not a contradiction: in quantum mechanics a system of ideal point masses, no matter how strongly bound, differs essentially from an *ideal* rigid rotator by the greater stringency of the regularity requirements on its wave functions.[1] It is easy to see that the simpler system of an ideal diatomic molecule—or ideal dipole, as it will be called—whose states have the form

$$\psi=\psi(x,y,z,\theta,\phi) \tag{3}$$

does not possess states of half-integer angular momentum; and thus the natural conclusion is that if a nonrelativistic mechanical model of a half-spin particle is to be sought, the simplest possible is the ideal rigid rotator.[2]

This conclusion is not at odds with the Pauli representation of half-spin particles; just as any atom in a p-state is necessarily represented by a vector wave function

$$\psi=\psi_m(x,y,z), \quad m=0,\pm1, \quad \text{or} \quad 1,2,3 \tag{4}$$

any structure whatever in a state of spin $\frac{1}{2}$ must be represented by a Pauli spinor $\psi=\psi_\alpha(x,y,z)$ ($\alpha=\pm\frac{1}{2}$, or 1,2). However, it will be extremely artificial to introduce, say, Euler angles into the wave function of a spinning particle to "explain" its spin, if its spin actually has but the single value $\frac{1}{2}$. In such a procedure the angles could have little physical significance, and it would be impossible to define any one of them with a precision better than

$$\Delta\theta>\hbar/2\Delta J\hbar\sim1 \text{ radian}. \tag{5}$$

[1] F. Bopp, Z. Naturforsch. **3a**, 568 (1948); H. Honl, Z. Naturforsch. **3a**, 573 (1948); F. Bopp and R. Haag, Z. Naturforsch. **52**, 644 (1950); H. Yukawa, Phys. Rev. **77**, 219 (1950); R. L. Ingraham, Nuovo cimento **12**, 825 (1954); Hara, Marumori, Ohnuki, and Shimodaira, Progr. Theoret. Phys. (Japan) **12**, 177 (1954) and others.

[2] F. Bopp and R. Haag, Z. Naturforsch. **5a**, 644 (1950) discuss nonrelativistic spin models of this type.

The question raised here is whether, therefore, these particles truly exhibit but one spin, or whether it is possible for them to change their spin under the influence of external torques.

It is not permissible to answer this question within the theoretical framework of the Pauli spin formalism, which is constructed to permit the formulation only of interactions that commute with the magnitude of the spin; and it is not possible to answer it experimentally from the behavior of the particles at low energy. Such a hypothetical change in spin would not appear as a mere fine structure in spectral lines; it would be a catastrophic change in the nature of the particle. The magnitudes of the energies involved may be judged from relations familiar in the theory of rotational spectra of molecules. If E is the energy of rotation of a system and the "spin" J is on the order of unity,

$$E\sim\hbar^2/2I, \tag{6}$$

where I is a moment of inertia. To compare this energy with the rest mass M, we observe that $I\sim MR^2$ where R is a measure of the extension of the system, and that $\hbar/Mc=\lambda$ is the Compton wavelength. Then

$$E\sim(\lambda/R)^2Mc^2. \tag{6'}$$

Thus if $\lambda\ll R$, $E\ll Mc^2$. For molecular systems, of course R may be taken as an atomic size, say the Bohr radius, and λ as a proton Compton wavelength, so that $\lambda/R\sim(m/M)(1/137)\ll 1$ and $E\ll Mc^2$ ordinarily. However, for the "radius of gyration" R of an elementary particle it would be implausible to use a length much greater than its Compton wavelength λ or much less than its classical Coulomb radius $r_0=e^2/Mc^2=\lambda/137$ and in these opposite extremes the energy absorbed in a spin transition is, by (6'),

$$\begin{aligned} &E\sim Mc^2, \quad \text{if} \quad R\sim\lambda, \\ &\sim(137)^2Mc^2, \quad \text{if} \quad R\sim r_0. \end{aligned} \tag{7}$$

Thus in any case the process is relativistic, and it is conceivable for large mass ratios to result in this manner.

Since the above estimates of E are large, it becomes necessary to put these considerations upon a relativistically invariant footing. This is the purpose of the present paper: to parallel the above heuristic discussion in a consistent relativistic theory, and to lay the groundwork for more detailed calculations.

It should be observed that to do this there are three points to be treated in order:

First, we shall enumerate all possible rigid structures (Parts II, III, IV). The only possibilities in nonrelativistic mechanics were the ideal point, the ideal dipole, and the ideal rotator; the enumeration in the covariant theory is not self-evident, and algebraic methods must be used. It turns out that there are not three but eleven possibilities, not all of which have been exploited in the literature.

Second, we shall investigate the spin spectrum of each model, to find whether it possesses states of spin $\frac{1}{2}$ (Part V). In nonrelativistic mechanics the answer was yes for but one of the three models, the rotator. In relativistic mechanics the answer is yes for three of the eleven models.

Third, we shall investigate the energy spectrum associated with the spin spectrum (Part VI). While the previous two points were questions of kinematics, requiring no knowledge of the Lagrangian, this is a question of dynamics, requiring a choice of Lagrangian, and the results must be strongly affected by interactions. Only a preliminary treatment of this question is presented in this paper, and the problem of interactions is not treated. Clearly a closer study of this question is necessary before a comparison of the theory with reality is permissible. The present paper is devoted rather to the determination of the systems under consideration and of their most permanent properties.

We shall, therefore, discuss covariant theories of localized systems with internal degrees of freedom, first from the point of view of classical mechanics and then from the point of view of quantum theory. To specify a point in the classical configuration space of such a system there must be given a point $x=(x^i)$ in space-time, and in addition, some kind of additional coordinates,

$$q=(q_1,\cdots,q_n), \tag{8}$$

specifying the internal configuration. We introduce a simple classification of all possible kinds of internal degrees of freedom q based on the symmetry properties of the quantity q. Unfortunately, the procedure may be summarized most concisely in the terminology of continuous groups of transformations, of which no knowledge will be assumed after the following summary. The central idea is mathematically elementary[3]: if a group (the Lorentz group now) acts transitively on a set, the set is in a 1-1 correspondence with a quotient space of the group. Now, if Q is the manifold over which q varies, it may be assumed—perhaps after sufficient subdivision of Q—that the Lorentz group G acts transitively upon Q. It follows that Q may be realized as a coset space G/G_0 of G modulo some subgroup G_0. G_0 determines the kinematics of the system. Indeed, if A_0 is the Lie algebra of G_0 and A of G, then any velocity $\dot{q}$ (thought of as determining an infinitesimal motion $q\to q+\dot{q}du$) may be represented by an element of the quotient space A/A_0, so classically the phase space is the direct sum

$$(G/G_0)\oplus(A/A_0); \tag{9}$$

while quantum mechanically, if $\Psi(Q)$ is the space of wave functions of the system (internal coordinates only), then $\Psi(Q)$ may be identified with the subspace of $\Psi(G)$ (complex functions on the Lorentz group)

[3] C. Chevalley, *The Theory of Lie Groups* (Princeton University Press, Princeton, 1946), p. 30.

consisting of those functions $\psi(g)$ invariant under G_0. Thus the first of the three points above, the enumeration of all kinematics, amounts to the enumeration-up-to-equivalence of all subgroups G_0 of the Lorentz group. The second point, the determination of the spin spectra, requires the decomposition of the subspace $\Psi(Q)$ into subspaces invariant under G. $\Psi(Q)$ is an invariant subspace of $\Psi(G)$ and its decomposition is accomplished, therefore, by the decomposition of $\Psi(G)$, i.e., by the well-known reduction of the regular representation, and can readily be computed. The particle can possess no states which are absent in this decomposition, and the dynamics may also exclude some of the terms actually present in this decomposition. The third point, the energy determination, requires at very least the choice of a Lagrangian for the free field. This can be done as follows. There is a unique (up to a constant factor) left-invariant quadratic form on G regarded as a differentiable manifold. Hence there is also one on $Q=G/G_0$, to be written $\|\dot{q}\|^2$. Thus, there is only one invariant quadratic Lagrangian function of $(q,\dot{q})$, again except for an arbitrary factor,

$$L=\tfrac{1}{2}\kappa^2\|\dot{q}\|^2. \tag{10}$$

Thus if the classical equations of motion are required to be completely invariant and linear in the second derivatives, their solutions are completely determined as geodesics on G/G_0. Similar requirements imposed upon the wave equation serve to determine the quantum field equations, for the metric on G/G_0 fixes a Laplacian operator Δ_g, the "Casimir operator" on Q.

We now carry out the procedure outlined above.

II. CLASSIFICATION OF INTERNAL STRUCTURES

Consider the effect of Lorentz transformations upon the internal coordinates q. (Terminology: the *Lorentz transformations* L are those $x\to bx+h$ preserving interval $|\Delta x|$. These include the *homogeneous Lorentz transformations*, where $h=0$, which in turn include the (space-time) rotations G where also $\det b>0$ and $b_0^0>0$.) The intent of the epithet "internal" is that a space-time translation is to leave the numbers q unaltered:

$$x\to x+h, \quad q\to q. \tag{11}$$

On the other hand, a space-time rotation $x\to bx$ may (or may not) have some effect on q; and in general q undergoes an arbitrary point transformation

$$x\to bx, \quad q\to boq \tag{12}$$

where boq will be written for the effect of b operating on q. The property of a group of transformations

$$(bb')oq=bo(b'oq) \tag{13}$$

must be required of the operation boq, where b and b' are arbitrary Lorentz transformations.

For any q, consider the collection $G(q)$ of all Lorentz rotations leaving q fixed: $G(q)oq=q$. From (13) it is evident that $G(q)$ is a subgroup of the Lorentz rotations G; it will be called the symmetry group (in G) of the point q. Referring again to the examples of a point particle and a dipole particle in Part I, $G(q)$ should be thought of as the group of space-time rotations "about" q. We observe that if q and q' are connected by a Lorentz transformation then their symmetry groups are equivalent: if

$$q'=boq,$$

then

$$G(q')=bG(q)b^{-1}. \tag{14}$$

The infinitesimal elements of G [or of $G(q)$] correspond to skew tensors $a_{ij}=-a_{ji}$ and form a collection which will be designated by A [or $A(q)$ respectively]. We will always assume that $G(q)$ is connected, so that it is generated by $A(q)$. $A(q)$ is closed under the operations of addition, multiplication by a real number, and commutation: the quantities

$$a+a',\ ca,\ [a,a'] \tag{15}$$

belong to $A(q)$ whenever a,a' do; and similarly for A. The classification of internal structures which we shall employ amounts to specifying $A(q)$ up to equivalence for each point q.

Special interest attaches to those cases where $A(q)$ is the same (up to equivalence) for all q, because of their simplicity and because all other possibilities can be built up out of such simple cases. In the following Part III, it will be shown that this type of structure may be regarded as rigid.

III. COVARIANT CONCEPT OF RIGIDITY

It is customary to call a body rigid in classical mechanics if it is made of particles whose mutual separations are fixed. This is not a satisfactory starting point for us, since such a system has only integer spins. It is especially unsatisfactory as a description of a supposedly primitive particle. However, such a system of points has several properties which can be expressed without reference to internal structure and which will not be incongruous in an elementary particle. We shall exhibit two such properties here:

First, such a system has only translational and rotational degrees of freedom. From any one configuration of the system it is possible to obtain any other by applying the purely geometric operations of translation and rotation to the system as a whole (or to the reference frame). This is usually expressed by saying that the Euclidean group acts *transitively* on the configuration space or that the configuration space is homogeneous (with respect to the Euclidean group).

Alternatively, for such a system there is no scalar invariant function of the coordinates except the trivial $f=\text{const}$. This expresses the fact that the interparticle separations and angles are constants, and it is not difficult to see that it is equivalent to transitivity.

Second, such a system possesses a weak sort of localizability in that its coordinates can be split into one part, "center-of-mass," which transforms as a position vector under the Euclidean group and another part, orientation, which is invariant under translation. This too can be expressed purely as a relation between the Euclidean group and the configuration space; it is equivalent to the assertion that no translation leaves any configuration fixed.

Thus there is a natural way to generalize the essential properties of the rotators of classical mechanics to a relativistic mechanics: (a) the configuration space in which the particle wanders in the course of proper time is homogeneous with respect to the group of space-time translations and rotations, and (b) no point of it is fixed under any space-time translation. It follows that a point of this configuration space has the form (x,q), where $x=(x^i)$ is a point in space-time we shall call the position of the particle and $q=(q_1,\cdots,q_n)$ is a collection of additional coordinates we shall call the orientation of the particle. It is clear that $0\leq n\leq 6$ and that q, which is invariant under translation, is transformed transitively by the space-time rotations alone. We shall call a system possessing these two properties (a) and (b) rigid for want of a better term.

Any two points of the configuration space of a rigid system have equivalent symmetry groups, by (14).

It is highly doubtful that forces exist capable of binding several particles into a system which will remain rigid under processes as energetic as the spin transitions considered here, so that it is of interest to investigate nonrigid systems. However, an elementary particle can be rigid in the above sense, and it is therefore fitting to survey all possibilities of this type.

IV. ENUMERATION OF RIGID STRUCTURES

By the kinematics of a particle we will understand the specification not only of its configuration space as a manifold but also of the manner goq in which a space-time rotation g transforms a point q of this space. It will now be shown that the kinematics of a rigid structure is completely defined by the symmetry algebra $A(q_0)$ for one point q_0. First, we have assumed that $G(q_0)$ is generated by its infinitesimals so $G(q_0)$ is determined. Now designate by $G(q,q_0)$ the set of space-time rotations transforming q_0 into q; $G(q,q_0)$ is a left coset of $G(q_0,q_0)=G(q_0)$, and it may be taken that the one-to-one correspondence

$$q\leftrightarrow G(q,q_0) \tag{16}$$

is an isomorphism. Thus we can identify the points q with the cosets of $G(q_0)$, $Q\sim G/G(q_0)$, and the law of transformation of Q is

$$goq\leftrightarrow gG(q,q_0) \tag{17}$$

where $gG(q,q_0)$ represents the result of multiplying each element of $G(q,q_0)$ in turn by g. This provides the entire kinematics.

To enumerate all possible rigid covariant kinematics it remains only to enumerate all the possibilities for $A(q_0)$ up to equivalence, since equivalent groups determine isomorphic configuration spaces by the above procedure. We shall separately consider the possible dimensions $0,1,\cdots,6$ for $A(q_0)$. The algebra of dimension $6-m$ leads to a particle of m internal degrees of freedom which will be designated by $[m]$ with further symbols where necessary.

[6]. The zero-dimensional algebra is the trivial one containing only 0, the group it generates is the identity 1 and the configuration space is $G/1$ or G itself. The particle may be thought of as a small *vierbein* or as four points not all in the same two-space. The nonquantum theory of this four-dimensional rotator was put forward by Klein[4] in a remarkable anticipation of the formalism of special relativity; his parametrization of this configuration space by Cayley-Klein parameters is the most convenient for may purposes, essentially associating with each point of the configuration space a Dirac spinor ξ subject to the conditions

$$\xi^+\xi=1,\quad \xi^+\gamma_5\xi=0. \tag{18}$$

(4 complex numbers$=$8 real numbers, less 2 constrainst, leaving 6 degrees of freedom.)

[5]. The infinitesimal Lorentz transformations (units: $\hbar=c=1$; metric: $+---$),

$$x^i\hookrightarrow x^i+w^ix^jd\tau,\quad (i,j=0,1,2,3)$$

correspond to skew-tensors $w_{ij}=-w_{ji}$, or equivalently to the spin operators

$$\omega=\tfrac{1}{4}iw^{ij}\sigma_{ij}=i\mathbf{w}\cdot\boldsymbol{\sigma}, \tag{19}$$

where $\sigma_{ij}=\sigma_k$, $\sigma_{i0}=i\sigma^i$ ($i,j,k=1,2,3$ cyclically) and the complex 3-vector

$$\mathbf{w}=\tfrac{1}{2}(w_{23}+iw_{10},\ w_{31}+iw_{20},\ w_{12}+iw_{30}) \tag{20}$$

is constructed from the tensor w_{ij} in much the same way that the Hertzian vector $\mathcal{D}+i\mathcal{H}$ is constructed from the electromagnetic field tensor F_{ij}. The correspondence (19) will be written

$$\omega=\Sigma(w_{ij})=\Sigma(w). \tag{21}$$

Any skew tensor a defines a one-dimensional algebra consisting of its real multiples, the closure requirements (15) being trivially satisfied. If $\mathbf{a}$ is the 3-vector associated with a by (20) then the only independent scalars which can be constructed from a_{ij} are $\mathrm{Re}\mathbf{a}\cdot\mathbf{a}$ and $|\mathrm{Im}\mathbf{a}\cdot\mathbf{a}|$, and so the algebras can be separated into equivalence classes according to the values of the invariant ratio

$$\mathrm{Re}\mathbf{a}\cdot\mathbf{a}:|\mathrm{Im}\mathbf{a}\cdot\mathbf{a}|.$$

Either this ratio is $0:0$, or it can be put in the form

$$\cos f:\sin f,\quad 0\leq f\leq\pi.$$

[4] F. Klein, *The Mathematical Theory of the Top* (Princeton University Press, Princeton, 1896); H. Goldstein, *Classical Mechanics* (Addison-Wesley Press, Cambridge, 1951), p. 180.

In the former case, the algebra can be transformed into

$$[5]=\{\sigma_+\}, \tag{22}$$

where the spin operator associated with a generator of [5] by (19) is used to define [5], and

$$\sigma_+=\frac{\sigma_1+i\sigma_2}{2}=\begin{pmatrix}0&1\\0&0\end{pmatrix}. \tag{23}$$

In the latter case, the algebra is equivalent to

$$[5_f]=\{e^{if/\pi}\sigma_3\},\ 0\leq f\leq\pi. \tag{24}$$

There are no others. There are thus "$1+\infty$" distinct kinematics of five degrees of freedom. This in sharp distinction to the situation in classical mechanics, where there are only three distinct rigid kinematics in all. Of all the structures exhibited in (22) and (24) it can be shown that only [5], [5_0], and [5_π] are exemplified by rigid sets of distinct points, as in Fig. 1. (This is shown by a study of the fixed points of the infinitesimal Lorentz transformations belonging to the associated algebra.)

[4]. Beyond this point the case analysis becomes quite tedious and only the results will be listed. The only rigid systems of four degrees of freedom are

$$\begin{aligned}[4]&=\{\sigma_3,\ i\sigma_3\},\\ [4']&=\{\sigma_+,\ i\sigma_3\},\\ [4'']&=\{\sigma_+,\ i\sigma_+\}.\end{aligned} \tag{25}$$

None of these possess point models, it can be shown. [4] will be of further interest due to its spin spectrum, and a parametrization is helpful: the points of the configuration space of [4] may be put in correspondence with skew tensors w_{ij} (or with 3-vectors $\mathbf{w}$ according to (20)) which obey the condition

$$\mathbf{w}\cdot\mathbf{w}=0. \tag{26}$$

A skew tensor and its associated three-vector obeying (26) will be called null; both its invariants vanish. The best known example of a null tensor, of course, is the field of a plane light wave $\mathbf{w}=\mathbf{H}+i\mathbf{E}$; $\mathbf{E}\cdot\mathbf{H}=0=E^2-H^2$. A suggestive description of the particle [4] other than a null six-vector is the associated two-spinor or Pauli spinor ξ_a: just as the particle [6] can be regarded as a point to which is attached a Dirac spinor, the particle [4] can be regarded as a point to which is attached a Pauli spinor.[5] This Pauli spinor, advantageously, is subject to no constraints.

A realization of the particle [4''] is a point to which is attached a skew tensor w_{ij} subject to the constraints

$$\mathbf{w}\cdot\mathbf{w}=1 \tag{27}$$

instead of (26). A particle of this structure was introduced by Frenkel[6] as a classical model for the electron. However, it will be shown that its canonically quantized theory cannot describe a spin-$\frac{1}{2}$ particle.

[3]. The rigid systems of three degrees of freedom are associated with the symmetry algebras

$$\begin{aligned}[3]&=\{\sigma_1,\sigma_2,\sigma_3\},\\ [3']&=\{\sigma_+,\sigma_-,i\sigma_3\},\\ [3_f]&=\{\sigma_+,i\sigma_+,e^{if/\pi}\sigma_3\}.\end{aligned} \tag{28}$$

There are no others. A convenient parametrization for the configuration spaces of some of these particles is by a four-vector r^i. (See Fig. 1.) This four-vector is subject to the constraints:

$$\begin{aligned}r^2&=\ 1\ \text{ for }\ [3],\\ &=\ 0\ \text{ for }\ [3_0],\\ &=-1\ \text{ for }\ [3'].\end{aligned} \tag{29}$$

A model for an elementary particle of this kinematic structure was proposed by Yukawa in his nonlocal meson theory, where the cases [3] and [3'] appear as particles of space-like and time-like extension respectively.[7] The remaining systems of three internal rigid degrees of freedom, namely the [3_f] with $0<f\leq\pi$, cannot be realized by models consisting of points in real space-time.

[2]. There is one structure of two degrees of freedom:

$$[2]=\{\sigma_+,i\sigma_+,\sigma_3,i\sigma_3\}.$$

[1]. There is none of one degree of freedom. This is also the case in nonrelativistic mechanics.

[0]. The structure [0] is, of course, the ideal point and its symmetry algebra is the entire algebra A.

Having enumerated all rigid structures, our next goal is the examination of their spin spectra.

V. SPIN SPECTRA

We shall obtain only partial information about the particle spectra without specifying a Lagrangian. Under the infinitesimal transformation,

$$x'^i=\epsilon^i+\epsilon_j{}^i x^j, \tag{30}$$

the wave function $\psi(x,q)$ transforms according to

$$\delta\psi=-i(\epsilon^i p_i+\tfrac{1}{2}\epsilon^{ij}J_{ji}). \tag{31}$$

Here

$$p_i=-i\partial/\partial x^i$$

and

$$\begin{aligned}J_{ik}&=L_{ik}+S_{ik},\\ L_{ik}&=x_i p_k-x_k p_i,\end{aligned}$$

where S_{ik} is a differential operator with respect to the q alone and represents the contribution of the internal rotation to the angular momentum J_{ik} of the particle.

[5] The correspondence between null tensors and Pauli spinors is discussed by H. A. Kramers, *Quantentheorie des Elektrons und der Strahlung* (Akademische Verlagsgesellschaft, Leipzig, 1938), p. 260; E. T. Whittaker, Proc. Roy. Soc. (London) **A158**, 38 (1937); and E. M. Corson, *Introduction to Tensors, Spinors, and Relativistic Wave-Equations* (Hafner, New York, 1953), p. 31.

[6] J. Frenkel, Z. Physik **37**, 243 (1926); H. A. Kramers, reference 5, p. 229.

[7] H. Yukawa, Phys. Rev. **77**, 219 (1950).

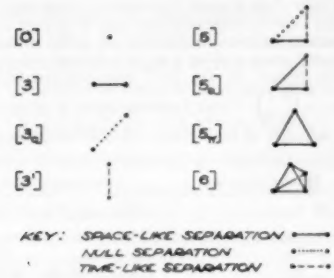

FIG. 1. Realizable rigid structures. These figures posses the same symmetry group as the indicated rigid structure. They may be regarded only as particular group-theoretic realizations of the corresponding internal structure. (In the diagram for [5], the dashed line should be solid.)

Let $\mathbf{S}$ be the 3-vector associated with S_{ik}, in the manner of (20), and let $\mathbf{S}^*$ be the similar quantity obtained by replacing the explicit i by $-i$ in (20). Then it is well known that the commutation rules for the infinitesimal Lorentz transformation may be written simply

$$\begin{aligned} \mathbf{S}\times\mathbf{S}&=i\mathbf{S},\\ \mathbf{S}^*\times\mathbf{S}^*&=i\mathbf{S}^*,\\ [\mathbf{S},\mathbf{S}^*]&=0. \end{aligned} \tag{32}$$

Thus, the vector $\mathbf{S}$ has the same commutation rule as a three-dimensional angular momentum vector, although it is not formally Hermitian. $\mathbf{S}^*$ commutes with $\mathbf{S}$ and possesses the same commutation rules and so a maximal commuting set of operators formed from the S_{ik} is

$$S^2,S_3;\ S^{*2},S_3^*. \tag{33}$$

Any function of q can be expanded in terms of simultaneous eigenfunctions of the set (33). We shall now discuss these eigenfunctions.

The $\psi(q)$ are subject to a regularity condition employed by Bopp and Haag[1]: $G\psi$ shall be finite-dimensional. Here $G\psi$ represents the collection of all functions of q obtained by applying all the members of G to ψ, and taking linear combinations. As has been pointed out,[1] this condition contains the customary continuity requirements and implies for the systems of nonrelativistic mechanics the statements of Part I concerning spin-spectra from which the present discussion stems. This condition excludes two-valued functions of q in many cases but not all. In the relativistic case this condition has the additional consequence that the functions of q associated with the infinite-dimensional irreducible representations of G, unitary or otherwise,[8] are excluded. Given that $G\psi$ contains only a finite number of linearly independent functions, the commutation rules (32) imply by well-known methods[9] that the eigenvalues of the set (33) have the form

$$s(s+1),m;\ s^*(s^*+1),m^*$$

where

$$\begin{aligned} &s=0,\tfrac{1}{2},1,\cdots,\\ &m=-s,-s+1,\cdots,s-1,s;\\ &s^*=0,\tfrac{1}{2},1,\cdots,\\ &m^*=-s^*,-s^*+1,\cdots,s^*-1,s^*, \end{aligned} \tag{34}$$

respectively. A corresponding eigenfunction will be written

$$\psi(q)=\psi_{sms^*m^*}(q), \tag{35}$$

with additional labels in cases of degeneracy. S^2 and S^{*2} are scalars under G but are interchanged by time-reflection. Thus the invariant subspaces of the space $\Psi(Q)$ of internal states under the (extended) Lorentz group are of the form

$$\Psi(s,s^*)=\Psi_{ss^*}\oplus\Psi_{s^*s}\quad\text{if}\quad s\neq s^* \tag{36}$$

(direct sum), and

$$\Psi(s,s)=\Psi_{ss},$$

where Ψ_{ss^*} represents an irreducible invariant subspace under G associated with the specified values of S^2 and S^{*2}. The intrinsic three-dimensional angular momentum is $\mathbf{S}+\mathbf{S}^*$ and its magnitude has the quantum numbers

$$|s-s^*|,\ |s-s^*|+1,\cdots,s+s^*$$

in the space $\Psi(s,s^*)$, by the usual rules for composition of two commuting angular momentum vectors. The wave function of a Dirac particle has the same transformation properties as a vector in the four-dimensional subspaces $\Psi(0,\frac{1}{2})$. We must inquire whether such a subspace appears in the decomposition of the function space $\Psi(Q)$ associated with each of the $9+2\infty$ possibilities enumerated in Part IV; and if so, how often. This can be answered by the most cursory inspection of the associated symmetry algebras $A(q_0)$:

[6]. The decomposition of $\Psi(Q)=\Psi(G)$ into irreducible invariant subspaces is well known[10] to contain $(2s+1)(2s^*+1)$ isomorphs of Ψ_{ss^*}, so that the Dirac spinor subspace $\Psi(0,\frac{1}{2})$ appears twice. For the further work a review of this decomposition is necessary.

With each Lorentz rotation $b=b^i{}_j$ is associated a 2×2 spin matrix $\beta=\Sigma(b)=\beta_a{}^\gamma$ such that

$$\det\beta=1,\ \beta^H\sigma_i\beta=\sigma_k b^k{}_i(\sigma_0\equiv1). \tag{37}$$

(The sign of β is not determined.) For $Q=G$, each wave-function $\psi(q)$ is thus a function $\psi[\beta]$ of a 2×2 spin matrix β (and its complex conjugate β^*). We put

$$\begin{aligned} \beta_a{}^1&=\xi_a,\\ \beta_a{}^2&=\eta_a, \end{aligned} \tag{38}$$

so that

$$\psi[\beta]=\psi(\xi,\eta,\xi^*,\eta^*),$$

[8] V. Bargmann, Ann. Math. **48**, 568 (1947); P. A. M. Dirac, Proc. Roy. Soc. (London) **A183**, 284 (1945); I. M. Gelfand and M. Neumark, J. Phys. (U.S.S.R.) **10**, 93 (1946) and *Unitarnie Predstavleniia Klassicheskih Grupp*, Acad. Sci. U.S.S.R. (1950); Harish Chandra, Proc. Roy. Soc. (London) **A189**, 372 (1947).

[9] P. A. M. Dirac, *Principles of Quantum Mechanics* (Oxford University Press, Oxford, 1947), p. 140.

[10] H. Weyl, *Theory of Groups and Quantum Mechanics* (Dover Publications, New York, 1931), p. 316.

for it is more convenient to regard ψ as a function of the two spinors ξ and η. Because $\psi(q)$ is a scalar, for any Lorentz rotation g

$$g\psi(b)=\psi(g^{-1}b)=\psi[\gamma^{-1}\beta]=\psi(\gamma^{-1}\xi,\gamma^{-1}\eta,(\gamma^{-1}\xi)^*,(\gamma^{-1}\eta)^*)$$

$[\gamma=\sum(g)]$, so ξ and η transform separately. The functions ψ which are homogeneous of fixed degrees in ξ,η,ξ^*, and η^* clearly form an invariant subspace of $\Psi(G)$ and this subspace is irreducible. Designating this subspace by $\Psi_{sm's^*m^{*\prime}}$, the relation between the spin eigenvalues s, s^* and the degrees is indicated by

$$\Psi_{sm's^*m^{*\prime}}\sim\xi^{s+m'}\eta^{s-m'}(\xi^*)^{s^*+m^{*\prime}}(\eta^*)^{s^*+m^{*\prime}}, \quad (39)$$

where m' and $m^{*\prime}$ are auxiliary invariant quantum numbers. In the nonrelativistic rotator the quantum number corresponding to m' is the component of angular momentum along the body z-axis.[1] The range of the quantum number m' is from $-s$ to $+s$ in steps of unity, $2s+1$ values in all, and there are $2s^*+1$ values for $m^{*\prime}$. Therefore, there are in all $(2s+1)(2s^*+1)$ distinct subspaces belonging to the same values of s and s^*.

Thus the particle [6] is highly composite from the point of view of group representations.

[5]–[0]. The wave functions of [5]—or any of the other particles to be discussed—can be regarded in two distinct ways in their dependence on q. Up to now they have been regarded as assigning a complex value $\psi(q)$ to each coset q of a fixed subgroup of G, namely the symmetry group of the particle. Such a function $\psi(q)$ naturally defines a function on G itself, to be designated $\psi(g)$, where

$$\psi(g)=\psi(q), \quad \text{if} \quad gq_0=q. \quad (40)$$

Thus, the value of $\psi(g)$ is simply that associated with the coset to which g belongs. The resulting set of functions will be identified with $\Psi(Q)$ henceforth. Its characteristic property, of being constant on cosets of $G(q_0)$, is equivalent to invariance under right multiplication by $G(q_0)$:

$$\psi(g)=\psi(gg_0) \text{ for } \psi \text{ in } \Psi(Q),\ g_0 \text{ in } G(q_0). \quad (41)$$

It is enough to assert (41) for the infinitesimal g_0, which form the symmetry algebra $A(q_0)$:

$$\delta\psi(g)=0 \text{ for } \delta g=iga,\ \psi \text{ in } \Psi(Q),\ a \text{ in } A(q_0). \quad (42)$$

Now the criterion (42) can be used to see whether a given Ψ_{ss^*} is represented in $\Psi(Q)$ by ascertaining whether any $\Psi_{sm's^*m^{*\prime}}$ is included in $\Psi(Q)$. From the invariance of the subspace $\Psi_{sm's^*m^{*\prime}}$ under Lorentz transformation it is sufficient to verify (42) for $g=1$. Thus, $\Psi_{sm's^*m^{*\prime}}$ is in $\Psi(Q)$, if, and only if

$$\psi(1+ia)=\psi(1) \text{ for all } \psi \text{ in } \Psi_{sm's^*m^{*\prime}},\ a \text{ in } A(Q). \quad (43)$$

Together with (39) and the list of all $A(Q)$ in Table I, (43) provides an algorithm for getting the spin spectrum of each rigid structure. Again, terms present in this spin spectrum may be excluded subsequently by the dynamical equations of the system.

TABLE I. Under *Type* is given the number of degrees of internal freedom. When there is more than one type of a given number of degrees of freedom, primes or subscripts are added to distinguish. Under *Symmetry group* is given a set of infinitesimals generating the symmetry group, in the 2×2 spin-representation. Here $\sigma_+=\frac{1}{2}(\sigma_1+i\sigma_2)=\begin{pmatrix}0&1\\0&0\end{pmatrix}$. Under *Parametrization* is given a coordinate system for some of the types, with the constraints if any.

Type	Symmetry group	Parametrization
[6]	0	4-spinor ξ; $\xi^+\xi=1$, $\xi^+\gamma_5\xi=0$
[5]	σ_+	
[5′]	$e^{il/2}\sigma_3$	
[4]	$\sigma_+,i\sigma_+$	6-vector $(\mathbf{E},\mathbf{H})$; $(\mathbf{E}+i\mathbf{H})^2=0$
[4′]	$\sigma_+,i\sigma_3$	
[4″]	$\sigma_3,i\sigma_3$	6-vector $(\mathbf{E},\mathbf{H})$; $(\mathbf{E}+i\mathbf{H})^2=1$
[3]	$\sigma_1,\sigma_2,\sigma_3$	4-vector r^i; $r_ir^i=1$
[3′]	$i\sigma_1,i\sigma_2,\sigma_3$	4-vector r^i; $r_ir^i=-1$
[3′]	$\sigma_+,i\sigma_+,e^{il/2}\sigma_3$	
[2]	$\sigma_+,i\sigma_+,\sigma_3,i\sigma_3$	
[0]	$\sigma_1,\sigma_2,\sigma_3,i\sigma_1,i\sigma_2,i\sigma_3$	

We will discuss only a particularly easy question: which structures possess Dirac states $\Psi(0,\frac{1}{2})$? The subspaces in point are by (39)

$$\Psi_{\frac{1}{2}\frac{1}{2}00}\sim\xi,\ \Psi_{\frac{1}{2}-\frac{1}{2}00}\sim\eta,\ \Psi_{00\frac{1}{2}\frac{1}{2}}\sim\xi^*,\ \Psi_{00\frac{1}{2}-\frac{1}{2}}\sim\eta^*.$$

It is readily seen now that $\Psi_{\frac{1}{2}\frac{1}{2}00}$ and $\Psi_{00\frac{1}{2}\frac{1}{2}}$ belong to $\Psi(Q)$ only if the first column $a_a{}^1$ of each matrix in the 2×2 spin representation of $A(Q)$ given in Table I vanishes, while $\Psi_{\frac{1}{2}-\frac{1}{2}00}$ and $\Psi_{00\frac{1}{2}-\frac{1}{2}}$ are present only if the second column $a_a{}^2$ vanishes. Inspection of Table I shows that only the structures [4], [5], and [6] possess either of these properties. We thus conclude: *only the structures [4], [5] and [6] can have Dirac-like states.*

Of these three structures, two can be realized by rigid systems of space-time points, [5] and [6]. (See Fig. 1.) If anything, this makes these two less appealing as models for an elementary particle. The simplest case [4] does not have this property and has some intriguing characteristics of its own. It can be described as a point in space-time to which is attached as internal coordinate a six-vector $(\mathbf{E},\mathbf{H})$ subject to

$$\mathbf{E}^2-\mathbf{H}^2=0,\ \mathbf{E}\cdot\mathbf{H}=0, \quad (44)$$

according to (25), where $\mathbf{w}=\mathbf{H}+i\mathbf{E}$. Such a six-vector, usually associated with a spin-one particle, can by its rotation *give rise to spin-$\frac{1}{2}$ states*, while a four-vector, or a six-vector not obeying (44), cannot. Of course, the wave-functions of these states are double-valued, and devoid of singularities. It seems that the structure [4] might be worthy of further study.

VI. ENERGY SPECTRA

In the present section, a covariant Lagrangian is selected for mathematical simplicity to show how the rotational energy of the structures considered can contribute to their rest mass. Since the Lagrangian chosen is very unrealistic only the briefest exposition is appropriate.

The form chosen for the Lagrangian density L is analogous to that of the Klein-Gordon particle, and is the sum of a scalar which is quadratic in ψ and a scalar which is quadratic in the first derivatives of ψ.

$$L=\tfrac{1}{2}[\partial_i\psi^*\partial^i\psi-\eta^2\partial_\alpha\psi^*\partial^\alpha\psi-m^2\psi^*\psi]. \tag{45}$$

Here $\partial_i\equiv\partial/\partial x^i$. Likewise, ∂_α represents differentiation with respect to the internal coordinates q^α, and the metric form $\gamma_{\alpha\beta}dq^\alpha dq^\beta=dq_\alpha dq^\alpha$ assumed for the internal coordinates q is discussed in a footnote.[11]

The action principle is then

$$\delta\int_V L(dx)(dq)=0,$$

where

$$(dx)=dx^0\cdots dx^3$$

and

$$(dq)=\gamma^{\frac{1}{2}}dq^1\cdots dq^N,\ (\gamma=\det\gamma_{\alpha\beta})$$

are invariant volume elements and V is a volume in $4+N$-dimensional configuration space. This leads to the wave equation

$$(\Box-\eta^2\Delta_q+m^2)\psi=0, \tag{46}$$

where $\Box=\partial_t{}^2-\nabla^2$ and $\Delta_q=\gamma^{-\frac{1}{2}}\partial_\alpha\gamma^{\frac{1}{2}}\partial^\alpha$ are the Laplacians with respect to the external and internal coordinates. Inasmuch as this is a second-order differential equation it is not of the Schrödinger form. Only for certain models is it possible to write an invariant equation of the first order in time differentiation. We present the above wave-equation only for its simplicity and generality. The second-order scalar differential operator Δ_q can be expressed, of course, in terms of the first-order differential operators $\mathbf{S}$ and $\mathbf{S}^*$ introduced in Part V:

$$\Delta_q=-\tfrac{1}{2}(S^2+S^{*2}).$$

Thus, the eigenfunctions and the eigenvalues of Δ_q have the form

$$\Delta_q Y_{ss^*}(q)=-\tfrac{1}{2}(s(s+1)+s^*(s^*+1))Y_{ss^*}(q),$$

and if ψ is expanded in terms of these "internal spherical harmonics", the coefficient $\psi_{ss^*}(x)$ of $Y_{ss^*}(q)$ in this expansion obeys the wave equation

$$[\Box+m^2+\tfrac{1}{2}\eta^2(s(s+1)+s^*(s^*+1))]\psi_{ss^*}(x)=0.$$

Defining the rest mass M by the relation $p_ip^i=M^2$, it is seen that the state ψ_{ss^*} has the rest mass

$$M_{ss^*}=m\left[1+\tfrac{1}{2}\left(\frac{\eta}{m}\right)^2[s(s+1)+s^*(s^*+1)]\right]^{\frac{1}{2}}. \tag{47}$$

If one puts $\lambda=m^{-1}$ for the Compton wavelength of the unrotating particle and $R=\eta^{-1}$, then by (47) the spin energy E when $\lambda\ll R$ is

$$E\sim(\lambda/R)^2mc^2.$$

Thus η^{-1} is like a radius of gyration. For $\lambda\sim R$ or $\lambda>R$, the result (7) of Part I is modified considerably: from (47) it follows that the rest mass M of an excited state of this particle is ~137 [instead of $(137)^2$] times the rest mass m of the state of spin zero, if the classical Coulomb radius of the particle is taken for its radius of gyration. In nature the situation appears reversed: $m_\pi\sim2\times137m_e$, the particle of spin zero is heavier than one of spin $\frac{1}{2}$.

This Lagrangian (45) is quite unsatisfactory, but shows the possibility of a covariant quantum theory for one particle. The many-particle or second-quantized theory will not be treated in this paper.

ACKNOWLEDGMENTS

It is a pleasure to acknowldege the aid of J. Percus, R. Schiller, and G. Yevick in this work.

[11] This form is completely determined throughout q-space up to a constant scale factor when its value is given for a single differential dq at any one point q, if it is assumed—as we do—that the form is invariant under Lorentz transformations. Because Q is realized as a quotient space of G, to fix scale factor it suffices to define a metric on the Lorentz group itself, as is required for the case [6] where $Q=G$. In that case, we take for the index α the couple $\alpha=(i,j)$ with $i<j=0,1,2,3$. Setting $dq^\alpha=\epsilon^{ij}$, where ϵ^{ij} is the skew-symmetric tensor associated with an infinitesimal Lorentz transformation in (29), we then define $dq_\alpha dq^\alpha=\frac{1}{2}\epsilon_{ij}\epsilon^{ij}$.

Letters to the Editor

PUBLICATION of brief reports of important discoveries in physics may be secured by addressing them to this department. The closing date for this department is five weeks prior to the date of issue. No proof will be sent to the authors. The Board of Editors does not hold itself responsible for the opinions expressed by the correspondents. Communications should not exceed 600 words in length and should be submitted in duplicate.

Lifetimes of the τ^+ and $K_L{}^+$-Mesons*

G. HARRIS, J. OREAR, AND S. TAYLOR

Department of Physics, Columbia University, New York, New York

(Received August 22, 1955)

PRELIMINARY lifetime values have been obtained for τ^+ amd $K_L{}^+$-mesons by measuring the Bevatron K-beam[1] attenuation relative to the beam pions and protons of the same momentum over a distance of 70 inches (proper time of 0.82×10^{-8} sec). Two identical stacks of 39 Ilford G5 pellicles, 6 inches by 7 inches by 600μ, were exposed separately 70 inches apart using the same copper target and Bevatron energy of 6.2 Bev. Regions of the same momentum, 356 Mev/c, in both stacks were area scanned for τ's and track scanned for heavy mesons. Track scanning, which involves following all gray tracks starting at a distance corresponding to a 2-cm residual range for K-mesons, gives values for the K- and τ-meson fluxes along with a check on the area scanning efficiency; *viz.*, no new τ's were found by track scanning in the region area scanned. Area scanning gives an improved τ-meson flux particularly in the near stack, but must be corrected for the fraction of heavy mesons lying outside the scanned area. This fraction is known from the track scanning data.

A total of 35 τ's and 77 K's in the near stack, and 17 τ's and 156 K's in the far stack were used to give the data in Table I. These data yield the following lifetimes: $\tau_K=(7_{-1}{}^{+1.5})\times10^{-9}$ sec, $\tau_\tau=(8_{-2}{}^{+5})\times10^{-9}$ sec. All errors shown are purely statistical. Alternate decays are not included in the τ data. The K_L-figures include all heavy mesons with single secondaries near minimum ionization. The ratio of beam pions to protons is the same over the regions scanned in both stacks[2] indicating that the K to p or π ratios over the regions of emulsion used are independent of solid angle and focusing conditions.

TABLE I. Flux determinations.

Stack	Target distance in inches	Proton exposure	Light beam tracks per cm²	Proton beam tracks per cm²	K_L-flux per cm²	τ flux per cm²
A	108	4.2×10^{13}	$(7.5\pm0.5)\times10^{4}$	$(47\pm2)\times10^{8}$	1310 ± 150	63.5 ± 11.5
B	178	6.0×10^{13}	$(1.6\pm0.15)\times10^{5}$	$(8.25\pm0.6)\times10^{8}$	87 ± 9	5.0 ± 1.3

The ratio of K- to τ mesons is (20.8 ± 4.5) in stack A and (17.5 ± 4.8) in stack B. Since the two K/τ ratios are the same within statistics, there is no indication of a difference in lifetime. The $K_{\tau 2}$ lifetime could be significantly different from the above lifetime since at the distance of the near stack only about 25% of the K_L-mesons are $K_{\tau 2}$.[3] The above lifetimes are consistent with other values obtained from Berkeley.[4]

We are indebted to many members of the University of California Radiation Laboratory for their generous hospitality and assistance in making the exposures.

* Supported in part by a National Science Foundation research grant and the joint program of the Office of Naval Research and the U. S. Atomic Energy Commission.

[1] Kerth, Stork, Birge, Haddock, and Whitehead, Phys. Rev. 99, 641(A) (1955).

[2] Pion decay corrections to the flux of light beam tracks are less than 3%.

[3] Ritson, Pevsner, Fung, Widgoff, Zorn, Goldhaber, and Goldhaber, Pisa Conference on Elementary Particles, June, 1955 (unpublished).

[4] L. Alvarez and S. Goldhaber, Nuovo cimento (to be published); and Chupp, Goldhaber, Goldhaber, Iloff, Lannutti, Pevsner, and Ritson, University of California Radiation Laboratory Report UCRL-3021 (unpublished).

Speculations on Heavy Mesons*

T. D. LEE AND J. OREAR

Department of Physics, Columbia University, New York, New York

(Received August 22, 1955)

FROM the analysis of Dalitz[1] it is becoming necessary to assume that the $K_{\tau 2}{}^\pm$ and $K_{\tau 2}{}^\pm$ are due to at least two different charged particles. Recent experimental evidence[2] encourages the hypothesis that the observable lifetimes are exactly the same (at least after travel times $>10^{-9}$ sec). As a solution to this possible dilemma we propose that there exist two heavy mesons, the $\theta^\pm$ and the $\tau^\pm$, where $\theta^\pm\to\pi^\pm+\pi^0$ and $\tau^\pm\to\pi^\pm+2\pi$. We propose further that the heavier of these two has a lifetime of 10^{-8} sec with a significant branching ratio for gamma decay to the lighter one. Finally, if we assign a lifetime of order 10^{-9} sec or less to the lighter one, we achieve a situation where both particles can have different lifetimes but in most experiments appear to have exactly the same lifetime. Because of Dalitz's results[1] we require the τ to be a particle which cannot decay into two pions because of spin and parity conservation. However, both τ and θ may contribute to the $K_{\mu 2}$, $K_{\mu 3}$, $K_{\tau 2}$, and $K_{\tau 3}$ while the θ may also contribute to a part of the $K_{\tau 3}$ (unless the spin and parity of the θ are 0+). We now discuss all the cascade possibilities.

Case I. θ and τ both have zero spin (single-gamma decay forbidden).—

$$\theta^\pm\to\tau^\pm+2\gamma, \tag{1}$$

or

$$\tau^\pm\to\theta^\pm+2\gamma. \tag{2}$$

With our present knowledge it is not possible to calculate accurately how large a mass difference is needed to give a two-gamma decay time of 10^{-8} sec. Our estimates show that a mass difference as small as 10 Mev is reasonable if one assumes that the θ and τ are strongly coupled through nucleon-hyperon intermediate states.

Case II. θ and τ do not both have zero spin.—

(a) $M_\theta > M_\tau$.

$$\theta^\pm \rightarrow \tau^\pm + \gamma. \tag{3}$$

For magnetic dipole radiation, a mass difference $\lesssim 100$ kev is required. Electric dipole requires just a few kev. A larger (and intuitively more reasonable) mass difference is permissible if we can manufacture a selection rule forbidding the strong coupling between θ and τ. The most convenient selection rule in the framework of the Gell-Mann scheme[3] is conservation of strangeness, S.[4] Because of the existence of the θ^0, the θ must have its usual assignment

$$(S)_{\theta^\pm} = \pm 1 \quad \text{or} \quad I_\theta = \tfrac{1}{2}. \tag{4}$$

The only possibility left for the τ is

$$(S)_{\tau^\pm} = \pm 2 \quad \text{or} \quad I_\tau = 0. \tag{5}$$

Two important consequences of this assignment are that the τ^0 should not exist, in contrast to the existence of θ^0 and $\bar{\theta}^0$, and that a τ^+ cannot be produced in association with a single Λ^0 or Σ. However, it may be produced by the following reactions:

$$\pi^- + p \rightarrow \Xi^- + \tau^+, \tag{6}$$

$$p + n \rightarrow \Lambda^0 + \Lambda^0 + \tau^+. \tag{7}$$

(b) $M_\tau > M_\theta$. From the production experiments, the K-mesons must be produced abundantly together with Λ^0 and Σ. Since in this case the $\tau^\pm$ is to be the longer-lived particle, its strangeness must be ± 1. Consequently in this case the conservation-of-strangeness selection rule is not possible and the mass difference must not be greater than ~ 100 kev unless the gamma radiation is of higher order than dipole.

The possible existence of a $\tau^\pm$ with a strangeness different from the $\theta^\pm$ permits the $\tau^\pm$ to have a lifetime very much shorter than the $\theta^\pm$, since they would then not be strongly coupled through intermediate nucleon-hyperon states. One is now tempted to speculate further whether the decay of the $\tau^\pm$ may be connected in some way with the universal Fermi interaction. We have explored the possibility of regarding the universal Fermi interaction as a secondary process via a virtual emission of $\tau^\pm$. In order to give the desired scalar and tensor coupling for the Fermi interaction, the $\tau^\pm$ has to be described by a pseudovector field,[5] ϕ_ρ ($\rho = 1,2,3,4$), coupled to the fermions by

$$H = g_{AB} \bar{\psi}_A \gamma_\mu \gamma_\nu \psi_B \frac{\partial \phi_\rho}{\partial x_\lambda} \epsilon_{\mu\nu\rho\lambda} + g_{AB}' \bar{\psi}_A \psi_B \phi_\rho^2, \tag{8}$$

where (A,B) represents the (p,n), (μ,ν), and (e,ν) groups, and $\epsilon_{\mu\nu\rho\lambda}$ is the isotopic antisymmetric tensor. The interaction (8) would give the decay of $\tau^\pm$ into 3π, $\mu+\nu$, and $e+\nu$ with comparable rates. If one sets $g_{p\pi} \sim g_{\mu\nu} \sim g_{e\nu}$, then from the strength of the Fermi interactions one obtains for the $\tau^\pm$ lifetime $\sim 10^{-16}$ sec.

We wish to thank the theoretical group at the Radiation Laboratory, University of California for several communications which have contributed to the above discussion.

* Supported by the joint program of the U. S. Atomic Energy Commission and the Office of Naval Research.

[1] R. Dalitz, Proceedings of the Fifth Annual Rochester Conference on High-Energy Physics (Interscience Publishers, Inc., New York, 1955), and private communication.

[2] Harris, Orear, and Taylor, preceding Letter [Phys. Rev. **100**, 932 (1955)].

[3] M. Gell-Mann, Phys. Rev. **92**, 833 (1953).

[4] Conservation of strangeness is mathematically equivalent to conservation of the z component of isotopic spin, I_z. For mesons, $S = 2(Q - I_z)$ where Q is the charge.

[5] According to the latest analysis of Dalitz, the $K_{\pi 2}$ data cannot exclude a $(1+)$ particle, although $(0-)$ gives a better fit. All spin and parity configurations where two-pion decay is also possible are strongly excluded for spins less than six.

Angular Correlation in the Beta Decay of the Neutron

J. M. Robson

Chalk River Laboratory, Atomic Energy of Canada Limited, Chalk River, Ontario, Canada

(Received August 22, 1955)

THE electron-neutrino angular correlation coefficient has been determined for the beta decay of the neutron by measuring the momentum spectrum of those electrons which are emitted in a restricted angular range of approximately 145° to 175° from the proton recoil direction.

Figure 1 shows a plan view of the apparatus mounted at the face of the *NRX* reactor. A collimated neutron beam traverses an aluminum vacuum tank, passing through an aluminum center-electrode assembly which is held at +7000 volts and is equipped with guard rings to maintain a uniform potential around the beam.

The apparatus on the left-hand side of the figure is a lens-type beta spectrometer using ring focusing to set the momentum resolution at seven percent full width at half-maximum, and a scintillation counter as detector. It is equipped with two entrance apertures, one of which is in the center-electrode assembly, and the second is 12 inches away from the neutron beam. Tests with a Cs^{137} source showed that these apertures in combination with two baffles on the center-electrode assembly restricted the beta spectrometer to accepting only those electrons which originated at points in the neutron beam within ± 1.5 cm from its intercept with

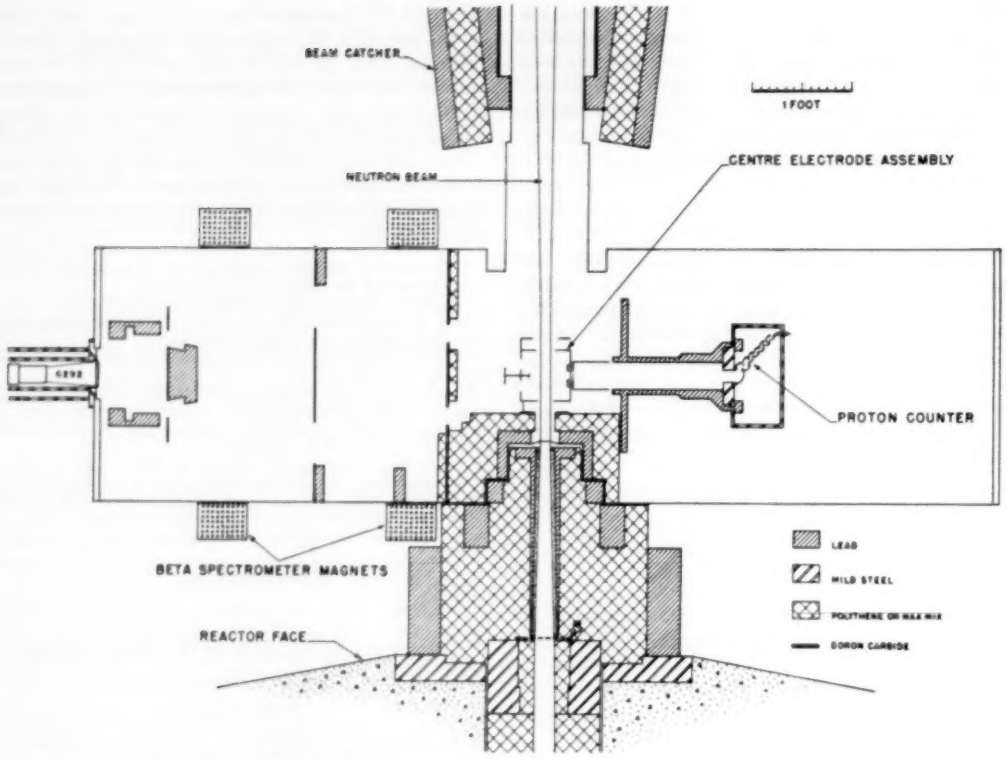

FIG. 1. Plan view of the apparatus mounted at the face of the *NRX* reactor.

the spectrometer axis. Thus the beta spectrometer defines the size of the neutron source and defines the angular range from which electrons can be accepted.

Those protons, resulting from neutron decay events in the defined region of the beam, which recoiled within $\pm 10°$ from an extension of the beta-spectrometer axis, can leave the center-electrode assembly through a gridded aperture. They are then accelerated and electrostatically focused onto the first dynode of an electron multiplier. Thus if, in a neutron decay event, the proton reaches the electron multiplier and the electron reaches the scintillation counter, then the angle between these two particles is in the restricted range of approximately 145° to 175°. The efficiency of the apparatus for detecting an event with a given angle between the proton and electron was obtained in detail by a Monte Carlo calculation using the FERUT computer by the University of Toronto.

Coincidences were sought between the scintillation counter and the electron multiplier, a time sorter being used to measure the transit time of the protons. Figure 2 shows the results of one run with the random coincidences subtracted. The peak occurs at the correct delay and is of the correct width for protons resulting from neutron decays in the particular geometry used. Furthermore, runs with a boron shutter placed in the neutron beam at *S*, Fig. 1, gave similar individual counting rates but gave no genuine coincidences above the random background, confirming that the genuine coincidences are due to neutron decay events.

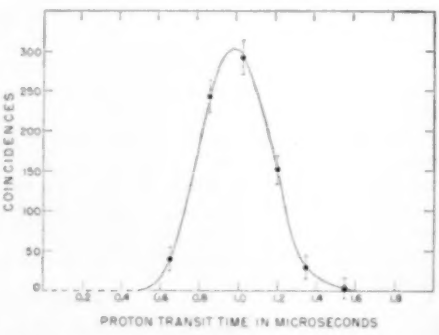

FIG. 2. Coincidences plotted against proton transit time. The beta spectrometer was set at 400 kev for this 24-hour run.

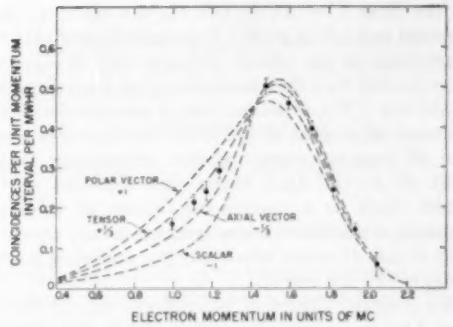

FIG. 3. The momentum spectrum of the electrons. The points represent the experimental data with standard deviations, and the dashed curves are the theoretical spectrum shapes for the pure interactions normalized by least squares.

The momentum spectrum of the electrons was obtained by taking a series of such runs. At each spectrometer setting runs were taken with different electron multiplier bias voltages so that an extrapolation to zero bias gave the number of coincidences per unit neutron intensity independent of slight variations in the gain of the electron multiplier. All runs were normalized by a neutron beam monitor. The result of all runs taken from September, 1954 to June, 1955 is shown in Fig. 3. In this figure the dashed curves are the calculated spectrum shapes for the pure beta-decay interactions using the Monte Carlo results for the detection efficiency of the geometry used in the experiment. They have been normalized by least-squares fitting to the experimental points. The best least-squares fit is obtained with the electron-neutrino angular correlation coefficient equal to $+0.089$ with a standard deviation of ± 0.108. This result is consistent with a beta-decay interaction of the form ST with $g_T^2/g_S^2 = 1.49_{-0.86}^{+1.44}$.

I wish to thank Dr. J. M. Kennedy and the computing staff of the Theoretical Physics Branch for arranging the Monte Carlo calculations and for calculating the theoretical spectrum shapes.

Cross Sections and the Complex Potential*

C. E. PORTER

Brookhaven National Laboratory, Upton, Long Island, New York

(Received August 30, 1955)

A NUMBER of calculations[1-4] have shown the importance of the edge-diffuseness of a complex potential in scattering problems. In the course of studying the characterization, especially at low energies, of such a potential in more detail a rather simple relation has been obtained between cross-section *ratios* and the imaginary part of the potential. For brevity we restrict our discussion to S-waves.

If we write the radial wave function as u/r, the differential equation for u is

$$\frac{d^2u}{dr^2}+\left[k^2+\frac{2M}{\hbar^2}(V+iW)\right]u=0, \tag{1}$$

with u subject to the boundary and normalization conditions:

$$u(0)=0, \quad u(r)\underset{r\to\infty}{\longrightarrow}v(r). \tag{2}$$

One can show that the wave number times the ratio of the reaction cross section to the elastic cross section is given by

$$k\sigma_r/\sigma_{el}=-\mathrm{Im}(k\cot\delta), \tag{3}$$

where δ is the complex phase shift. By exploring the consequences of Eqs. (1) to (3) it is possible to obtain the *exact* result

$$|v(0)|^2\left(\frac{k\sigma_r}{\sigma_{el}}\right)=\frac{2M}{\hbar^2}\int_0^\infty dr\, u^*(r)W(r)u(r). \tag{4}$$

A similarly simple result involving the ratio of the total cross section to the elastic cross section follows from Eq. (4) if $|v(0)|^2k$ is added to both sides. It is also possible to relate the real part of $k\cot\delta$ to the real part of the potential as is done in formulating variational principles with real potentials,[5] but the connection with the cross sections is not as direct. Expressions related to Eq. (4) have been given in a paper[6] on barrier penetration effects in light nuclei; however, the natural appearance of partial cross-section ratios and the application to low-energy neutron measurements do not seem to have been emphasized.

The form for $v(r)$ that is commonly used in discussions of effective range theory[7] is

$$v(r)=\sin(kr+\delta)/\sin\delta, \quad |v(0)|^2=1. \tag{5}$$

If $v(r)$ is so chosen that $u(r)$ is the S-wave solution for an incident plane wave of unit amplitude, then

$$v(r)=\frac{(4\pi)^{\frac{1}{2}}}{k}e^{i\delta}\sin(kr+\delta), \quad |v(0)|^2=\sigma_{el}. \tag{6}$$

In the case of low-energy neutron measurements,[8-10] the reaction cross section in Eq. (4) should be replaced by the cross section for compound nucleus formation, and the elastic cross section should be replaced by the shape-elastic cross section.[11] Using the normalization of Eq. (6), the known connection between the cross section for compound nucleus formation and the ratio $\Gamma_n^{(0)}/D$ of the average reduced neutron width to the average level spacing, and the usual expression for

complex scattering length,[12] one obtains from Eq. (4) that the strength function[12] $s(E)=\langle\gamma^2\rangle/D$ can be expressed at zero energy as

$$s(0)=-\frac{1}{\pi}\,\mathrm{Im}\frac{a}{R}=\frac{1}{2}\frac{\lambda^{(0)}}{R}\frac{\Gamma_n^{(0)}}{D},$$
$$=\frac{M}{2\pi^2\hbar^2R}\int_0^\infty dr\,|u_0(r)|^2W(r), \tag{7}$$

where R is the nuclear radius, a is the complex scattering length, $\lambda^{(0)}$ is the wavelength divided by 2π to which the neutron width is reduced, and $u_0(r)$ is the gross neutron wave function at zero energy.

Equations (4) and (7) may be of use in numerical calculations since, once $u(r)$ is known either by integrating Eq. (1) or by approximating its solution [by a square well solution, for example, if one is interested in the effect of rounding the edge of the well which leads to complicated exact forms for $u(r)$], the integral can be evaluated for a given choice of $W(r)$.

* Work performed under contract with the U. S. Atomic Energy Commission.

[1] Melkanoff, Nodvik, Saxon, and Woods (private communiaction). The writer is grateful for a prepublication copy of their work.

[2] Z. Janković, Phil. Mag. **46**, 376 (1955).

[3] P. E. Nemirovski, International Conference on the Peaceful Uses of Atomic Energy, No. 654, 1955 (unpublished).

[4] Morrison, Muirhead, and Murdoch, Phil. Mag. **46**, 795 (1955).

[5] P. M. Morse and H. Feshbach, *Methods of Theoretical Physics* (McGraw-Hill Book Company, Inc., New York, 1953), p. 1125.

[6] B. E. Freeman and J. L. McHale, Phys. Rev. **89**, 223 (1953).

[7] See, for example, H. A. Bethe, Phys. Rev. **76**, 38 (1949).

[8] Harvey, Hughes, Carter, and Pilcher, Phys. Rev. **99**, 10 (1955).

[9] Bollinger, Coté, and Le Blanc (private communication). The writer wishes to express his thanks for the privilege of seeing the data of these authors prior to publication.

[10] S. E. Darden, Phys. Rev. **99**, 748 (1955).

[11] Feshbach, Porter, and Weisskopf, Phys. Rev. **96**, 448 (1954); see also paper No. 830, International Conference on the Peaceful Uses of Atomic Energy, 1955.

[12] M. L. Goldberger and F. Seitz, Phys. Rev. **71**, 294 (1947), Eq. (14).

[13] R. G. Thomas, Phys. Rev. **97**, 224 (1955). The writer would like to thank Dr. Thomas for calling his attention to the connection between the strength function and the imaginary part of the complex scattering length.

Systematics of Fission Asymmetry

W. J. Swiatecki

Institute for Mechanics and Mathematical Physics and The Gustaf Werner Institute for Nuclear Chemistry, Uppsala, Sweden

(Received July 11, 1955)

ACCORDING to the liquid drop model the threshold energy for fission tends to[1]

$$E_{\text{threshold}}=c_1[(Z^2/A)_0-(Z^2/A)]^3, \tag{1}$$

in the limit $[1-(Z^2/A)/(Z^2/A)_0]\ll 1$. Here c_1 is a constant and $(Z^2/A)_0\sim 50$.[2] It is easily shown[3] that the dependence on the *cube* of $[(Z^2/A)_0-(Z^2/A)]$ is much more general than the assumption of an incompressible liquid drop. [The exponent three is associated with the existence of a point of inflection—a triple zero—in a plot of potential energy against deformation in the limit $Z^2/A\to(Z^2/A)_0$.] Many generalizations of the model (such as a nonuniform density or even the inclusion of additional forces assumed to vary smoothly with Z and A) would affect only the numerical magnitudes of $(Z^2/A)_0$ and c_1.

To a similar degree of generality it can be shown[3] that if below a certain value of Z^2/A $[Z^2/A<(Z^2/A)_c]$ the symmetrical saddle-point shape[1] becomes unstable against asymmetric distortions[4] [in the liquid drop model $(Z^2/A)_c/(Z^2/A)_0$ is somewhere around 0.5–0.7 [3]], there appear two asymmetric saddle-point shapes, whose degree of asymmetry is proportional to $[(Z^2/A)_c-(Z^2/A)]^{\frac{1}{2}}$, i.e.,

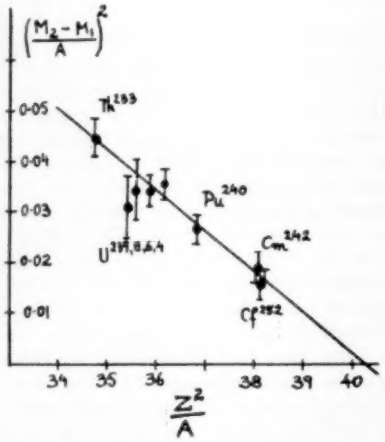

FIG. 1. The square of the relative degree of asymmetry, $(M_2-M_1)/A$, as a function of Z^2/A.

$$\text{Asymmetry}=\pm c_2[(Z^2/A)_c-(Z^2/A)]^{\frac{1}{2}}, \tag{2}$$

and whose threshold energy lies below the threshold of the symmetric saddle point shape by an amount

$$\Delta E=c_3[(Z^2/A)_c-(Z^2/A)]^2. \tag{3}$$

Equation (2) suggests that the degree of asymmetry in nuclear fission should decrease in a characteristic manner with increasing Z^2/A. As a measure of the degree of asymmetry we have taken the distance M_2-M_1 between the peaks in the double-humped fission yield curve, and in Fig. 1 we have plotted $(M_2-M_1)^2/A^2$ against Z^2/A of the target nucleus. The asymmetry is seen to decrease with Z^2/A and the

trend is consistent with a straight line, defining $(Z^2/A)_c = 40.2 \pm 0.7$. The equation of the line leads to the semiempirical formula,

$$M_2 - M_1 = 0.090(40.2 \pm 0.7 - Z^2/A)^{\frac{1}{2}}A. \quad (4)$$

One may combine Eq. (4) with the relation:

$$M_2 + M_1 = A - \nu$$

(ν = number of neutrons emitted in fission),

to predict the positions of the peaks in the yield curves of elements that have not yet been investigated. If an average value $\bar{\nu} = 2.8$ is used, one finds

$$M_2 = \tfrac{1}{2}A - 1.4 + 0.045(40.2 \pm 0.7 - Z^2/A)^{\frac{1}{2}}A, \quad (5)$$

$$M_1 = \tfrac{1}{2}A - 1.4 - 0.045(40.2 \pm 0.7 - Z^2/A)^{\frac{1}{2}}A. \quad (6)$$

The present analysis provides a reason for the empirical observation that in the fission of different elements the position of the heavy peak remains approximately constant. If the degree of asymmetry remained unchanged from nucleus to nucleus, both peaks would move towards higher masses with increasing A. In fact, there is superimposed on this shift a coming together of the peaks with increasing Z^2/A. Since the over-all trend of Z^2/A is to increase with A, the result is that for the light peak the two shifts add up whereas for the heavy peak they partly cancel. This is illustrated in Table I, where M_2 and M_1, calculated according to (5) and (6), are compared with the observed values.

TABLE I. Positions of the peaks in the fission yield curves.

Compound nucleus	Position of peaks: Observed[a] M_2	Observed[a] M_1	Formulas (5), (6) M_2	Formulas (5), (6) M_1	Remarks	Reference
Th^{232}	140	91	139.1	91.1	Low-energy neutron fission	b
U^{239}	140	98	141.1	95.1		c
U^{236}	138.5	95	138.2	95.0		d
U^{234}	137	93	136.2	95.0		b, e
Pu^{240}	138	99	137.9	99.3		c
U^{238}	140	96	140.2	95.0	Spontaneous fission	f, g
Cm^{242}	136	103	134.7	104.5		g
Cf^{252}	139	108	140.2	109.0		h

[a] The uncertainty in the observed values of M_2 and M_1 is of the order of ± 1 or ± 2 mass units. (It is more in the cases of U^{239} and U^{234}.) No systematic attempt has been made to adjust $A - M_2 - M_1$ to agree with available information on the number of emitted neutrons.
[b] A. Turkevich and J. B. Niday, Phys. Rev. **84**, 52 (1951).
[c] E. B. Steinberg and M. S. Freedman, *Radiochemical Studies: The Fission Products* (McGraw-Hill Book Company, Inc., New York, 1951). Paper No. 219, National Nuclear Energy Series, Plutonium Project Record, Vol. 9, Div. IV, Part V.
[d] Glendenin, Steinberg, Inghram, and Hess, Phys. Rev. **84**, 860 (1951).
[e] Steinberg, Glendenin, Inghram, and Hayden, Phys. Rev. **95**, 867 (1954).
[f] G. W. Wetherill, Phys. Rev. **92**, 907 (1953).
[g] E. P. Steinberg and L. E. Glendenin, Phys. Rev. **95**, 431 (1954).
[h] E. P. Steinberg and L. E. Glendenin, J. Inorg. Nuc. Chem. **1**, 45 (1955).

Further measurements of fission asymmetries would be interesting, especially in the region of Z^2/A close to the critical value, where the present considerations suggest a rapid decrease of $M_2 - M_1$.

It is a pleasure to acknowledge stimulating discussions with Professor S. G. Thompson, Dr. A. C. Pappas, and Dr. T. Maris.

[1] N. Bohr and J. A. Wheeler, Phys. Rev. **56**, 426 (1939).
[2] A. E. S. Green, Phys. Rev. **95**, 1006 (1954).
[3] W. J. Swiatecki (to be published).
[4] D. L. Hill and J. A. Wheeler, Phys. Rev. **89**, 1102 (1953).

Systematics of Spontaneous Fission Half-Lives

W. J. SWIATECKI

Institute for Mechanics and Mathematical Physics and The Gustaf Werner Institute for Nuclear Chemistry, Uppsala, Sweden

(Received July 18, 1955)

SEVERAL authors have noted the over-all trend of spontaneous fission half-lives to decrease with increasing Z^2/A as well as the considerable deviations (by several powers of 10) from any smooth dependence on this parameter.[1] We should like to discuss the close correlation which seems to exist between the half-lives and the finer details in the systematics of the ground-state masses of nuclei.[2]

A simple way of exhibiting this correlation is to plot the deviation $\delta\tau$ from a straight line in a plot of $\tau[\tau = \log_{10}(\text{half-life})]$ *vs* Z^2/A, against deviations (δM) of the masses M of the nuclei from a smooth reference surface $M_{ref}(A,Z)$. We made such a plot, with M_{ref} taken to be the semiempirical mass surface of Green[3] (based on the liquid drop model):

$$\delta M = M - M_{ref},$$

$$M_{ref} = 1000A - 8.3557A + 19.120A^{\frac{1}{3}} + 0.76278Z^2/A^{\frac{1}{3}} + 25.444(N-Z)^2/A + 0.420(N-Z) \text{ millimass units.} \quad (1)$$

The experimental masses M were taken from Glass *et al.*[4]

In the case of even-even nuclei the plot of $\delta\tau$ *vs* δM suggested a series of straight lines, one for each Z, indicating that for the isotopes of one element special stability of a nucleus (small δM) is invariably associated with a longer lifetime (large $\delta\tau$). The lines had approximately the same slope, thus defining a spontaneous-fission hindrance factor which corresponds to about 10^5 times longer lifetime for each millimass unit of extra stability. This suggested that if the observed lifetimes were corrected for the variations in stability of the ground states, a more regular dependence of τ on Z^2/A might be discernible.

Figure 1 shows the effect on the plot of τ *vs* Z^2/A of adding to the observed τ_{exp} an empirical correction $k\delta M$ ($k \sim 5$ if δM in mMU). For even-even nuclei the values of $\tau_{exp} + k\delta M$ define a fairly smooth curve, with indications of a similar curve for odd-A nuclei. [In a

preliminary plot the hindrance factor k was taken to be 5. A small but significant further smoothing of the points resulted from making k vary with Z^2/A according to $k=5-(Z^2/A-37.5)$. This is the case shown in Fig. 1.]

The result can be stated in the form of an empirical formula for half-lives; e.g., for even-even nuclei,

$$\tau_{ee}=f(Z^2/A)-k\delta M, \qquad (2)$$

where f is the curve defined by the even-even points in Fig. 1. The relation of the points for odd-A nuclei to the curve obtained from (2) by a shift upwards of 6.6 units is also shown in Fig. 1. The lifetime of the odd-odd nucleus E^{254} (einsteinium, $Z=99$) is consistent with a further shift of 4.9 units. The curve $f(Z^2/A)$ can be

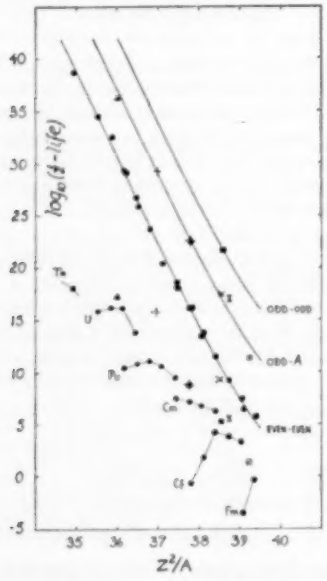

FIG. 1. Plot of spontaneous fission half-lives against Z^2/A. The observed lifetimes τ_{exp} occupy the bottom left-hand part of the figure; the "corrected" values $\tau_{exp}+k\delta M$ group themselves around the three curves. Experimental points for even-even nuclei are joined by straight lines. Odd-A nuclei are designated by special symbols which, reading from left to right along the odd-A curve, refer to U^{235}, Pu^{239}, Bk^{249}, Cf^{249}, E^{253} (einsteinium, $Z=99$), and Fm^{255} (fermium, $Z=100$). The odd-odd nucleus E^{254} is marked by a square.

represented for example by a cubic, which leads to the following formulas for the lifetimes:

$$\left.\begin{aligned}\tau_{ee}&=18.2\\ \tau_{\text{odd }A}&=24.8\\ \tau_{oo}&=29.7\end{aligned}\right\}-7.8\theta+0.35\theta^2+0.07\theta^3-(5-\theta)\delta M, \qquad (3)$$

where $\theta=(Z^2/A)-37.5$, and δM is the deviation in mMU of the experimental mass from the surface (1). Table I compares the observed half-lives with the values calculated by means of (3). The remarkable

TABLE I. Values of $\log_{10}$(half-life).

Nucleus	Experimental[a]	Formula (3)	Nucleus	Experimental[a]	Formula (3)
Even-even nuclei			Even-even nuclei		
Th 230	≥7.18	19.39	Cf 246	3.32	3.27
232	18.15	18.84	248	3.85	3.92
U 232	13.90	13.56	250	4.18	4.24
234	16.30	15.98	252	1.82	1.60
236	16.30	15.21	254	−0.70	−1.02
238	15.90	15.52	Fm 254	−0.30	−0.85
Pu 236	9.54	9.66	256	−3.52	−3.02
238	10.69	11.57	Odd-A nuclei		
240	11.08	11.09			
242	10.86	11.22	U 235	17.26?	18.02
244	10.40	10.13	Pu 239	15.74	15.42
Cm 240	6.28	6.27	Bk 249	8.78	8.67
242	6.86	7.27	Cf 249	9.18	8.65
244	7.15	7.09	E 253	5.48	4.38
246	7.48	7.88	Fm 255	1.30	2.79
			Odd-odd nuclei		
			E 254	5.18	5.17

[a] The experimental values are from a summary by A. Ghiorso, kindly lent to me by Professor S. G. Thompson.

degree of smoothing achieved by means of the unsophisticated correction $k\delta M$ is illustrated by the fact that the deviations from (3) rarely exceed 0.5. (Note that a shift in τ of this amount would be produced by an error of 0.1 mMU in δM.)

The importance of shell structure in the fission process is suggested by the fact that, according to the present considerations, the oscillations of the masses (associated with individual particle structure) in the range $\delta M=1-3$ mMU shorten the lifetimes by factors of 10^5 to 10^{15}. On the other hand the irregularities in the original plot of τ_{exp} against Z^2/A are seen to be largely due to irregularities in the ground-state masses, associated with *shell structure in the ground-state configuration*. The smoothness of the points $\tau_{exp}+k\delta M$ suggests that, after correcting for shell structure in the ground-state configuration, the description of the fission process in terms of a model in which single-particle features are treated in an average way may be useful. Qualitative reasons for the greater validity of such an averaged description for the more strongly deformed nuclear shapes occurring in fission may be found in the disappearance for such shapes of degeneracies in the energy spectrum associated with the proximity to a spherically symmetric configuration.

It is a pleasure to acknowledge discussions with Professor S. G. Thompson and Dr. A. C. Pappas and stimulating contacts with Dr. Aage Bohr and Dr. B. R. Mottelson and members of the C.E.R.N. Theoretical Study Group in Copenhagen.

[1] See for example J. R. Huizenga, Phys. Rev. **94**, 158 (1954).
[2] The existence of correlations between nuclear masses, fission thresholds, and half-lives has been considered by Professor D. Frisch, to whom I am greatly indebted for stimulating discussions.
[3] A. E. S. Green, Phys. Rev. **95**, 1006 (1954).
[4] Glass, Thompson, and Seaborg, J. Inorg. Nuc. Chem. **1**, 3 (1955).

Nuclear Interaction in Flight of a Σ Hyperon*

W. F. Fry, J. Schneps, G. A. Snow,† and M. S. Swami

Department of Physics, University of Wisconsin, Madison, Wisconsin

(Received September 6, 1955)

In the course of a systematic study of K^--mesons produced by the Berkeley Bevatron,[1] an interaction in flight of a charged hyperon was found. A projection drawing of the event is shown in Fig. 1. The K-meson

Fig. 1. A star produced by a stopped K^--meson is shown at point A. The hyperon from the K^--star caused a second star B after traveling a distance of 1.2 cm. The Σ^+ hyperon from star B decays from rest into a minimum-ionizing particle, presumably a π^+ meson.

star (point A in Fig. 1) has only one gray track, and a low-energy electron track. After 1.2 cm the particle which produced the gray track caused a star (point B in Fig. 1) with two outgoing tracks. One of these particles stopped after 22.5 microns and gave rise to a minimum-ionizing particle. The multiple scattering along the minimum track gives a $p\beta$ of 175±35 Mev/c which corresponds to a kinetic energy of 115±20 Mev for a π meson. This value for the energy identifies the short track from the interaction as a Σ hyperon. Since the hyperon decayed from rest we assume that it was positively charged. The gray track from the K^--meson star which caused star B did not have enough kinetic energy to produce a hyperon in the interaction B; therefore it was undoubtedly a Σ hyperon. From the grain density we estimate the kinetic energy of the hyperon to be about 80 Mev at the point of origin and about 40 Mev at the point of interaction. The kinetic energy of the Σ hyperon after the interaction was 1.5 Mev and the kinetic energy of particle 1 was 18.8 Mev, assuming that it was a proton. The residual momentum indicates that one or more neutral particles were involved.

Most probably this event is an example of an inelastic scattering of a positively charged Σ hyperon, although the possibility cannot be excluded that the hyperon from the K^--meson star was negatively charged and underwent two successive charge exchange scatterings in the nucleus.

This was the only interaction of a Σ hyperon that was found from a total hyperon track length of 9.8 cm. This length was observed in following 35 charged hyperons from 207 K^--stars.[1] It is obviously not possible to obtain an interaction cross section from one event; however, the event would suggest that Σ hyperons interact strongly with nuclear matter.[2] One other hyperon interaction event which is known to us is a disappearance in flight of a charged hyperon reported by Hill *et al.*[3]

We are grateful to Professor E. J. Lofgren for making the facilities of the Bevatron available to us and to Mr. Ray Kerth for his help in obtaining the exposures.

* Supported in part by the U. S. Atomic Energy Commission and by the Graduate School from funds supplied by the Wisconsin Alumni Research Foundation.

† On leave of absence from Brookhaven National Laboratory.

[1] Fry, Schneps, Snow, and Swami, Phys. Rev. **100**, 950 (1955).

[2] It is interesting to note that not only can the Σ hyperon interact strongly with nuclear matter via the K-meson field, but also via the π-meson field because the isotopic spin is different from zero.

[3] Hill, Gardner, and Crew (private communication).

Nuclear Moments in *jj*-Coupling

S. Sengupta

Government College, Darjeeling, West Bengal, India

(Received August 23, 1955)

Recently Lawson[1] has shown that nuclear electric quadrupole moments of any I-state arising out of any equivalent proton configuration $(lj)^n$ can be calculated without explicitly setting up the wave functions in question. His method can, however, be easily extended to equivalent configurations containing both neutrons and protons.

Magnetic and electric moments for a configuration $(lj)^n$, where n includes both neutrons and protons, can be written in the form

$$\mu=\tfrac{1}{2}(g_N+g_P)I_z+(g_N-g_P)\textstyle\sum_i j_{iz}\tau_{i3},$$
$$Q=\tfrac{1}{2}\textstyle\sum_i(3z_i^2-r_i^2)-\sum_i(3z_i^2-r_i^2)\tau_{i3}, \quad (1)$$

where g_N and g_P are the Landé factors for the single neutron and proton in the lj-state; j_{iz}, τ_{i3} refer to the total angular momentum and isotopic spin of the ith

nucleon. The summation i evidently extends over all the equivalent nucleons n. Assuming that the total isotopic spin T and its third component $T_3=(N-Z)/2$ are good quantum numbers, we shall determine the matrix of μ and Q in any nucleon state $(ITMM_\tau)$, where the M_τ's are the eigenvalues of T_3.

For the first term in μ we get the matrix elements simply by writing M in place of I_z. The second term contains the summation $S=\sum_i j_{iz}\tau_{i3}$. From the commutation property of j_i and τ_i with I and T, we get

$$S_{IT}{}^{MM_\tau}=(ITMM_\tau|S|ITMM_\tau)$$
$$=f(ITM_\tau)M=g(ITM)M_\tau.$$

From this we can easily prove that

$$S_{IT}{}^{MM_\tau}=(S_{IT}{}^{IT}/IT)MM_\tau=S(I,T)MM_\tau. \quad (2)$$

The eigenfunctions $\psi(ITMM_\tau)$ can be expressed in terms of the normalized antisymmetric single nucleonic functions $\chi_k(MM_\tau)$, where k indicates one of the possible sets of quantum numbers $(m_1m_{\tau 1},m_2m_{\tau 2}\cdots)$ such that $\sum_i m_i=M$ and $\sum_i m_{\tau i}=M_\tau$. Thus,

$$\psi(ITMM_\tau)=\sum_k \alpha_k(ITMM_\tau)\chi_k(MM_\tau),$$

and

$$\chi_k(MM_\tau)=\frac{1}{n!}\sum_P(-1)^pP\phi_1(m_1m_{\tau 1})\phi_2(m_2m_{\tau 2})\cdots \times\phi_n(m_nm_{\tau n}), \quad (3)$$

where P is the permutation operator and p its parity. The α's in (3) satisfy the equations:

$$\sum_k \alpha_k{}^*(I'T'MM_\tau)\alpha_k(ITMM_\tau)=\delta_{IT,I'T'},$$
$$\sum_{IT}\alpha_{k'}{}^*(ITMM_\tau)\alpha_k(ITMM_\tau)=\delta_{kk'}. \quad (4.1)$$

From these equations, a straightforward calculation gives

$$\sum_{IT}S_{IT}{}^{MM_\tau}=\sum_k\int\chi_k{}^*(MM_\tau)S\chi_k(MM_\tau)d\tau_1\cdots d\tau_n$$
$$=\sum_k\sum_i m_i{}^k m_{\tau i}{}^k=R(M,M_\tau). \quad (4)$$

$R(M,M_\tau)$ can easily be calculated from all possible sets of $(m_1m_{\tau 1},m_2m_{\tau 2}\cdots)$ corresponding to any MM_τ. Utilizing Eq. (4), we at once get

$$S(I,T)=\frac{1}{I}\left\{\frac{R(I,T)}{T}-\frac{R(I,T+1)}{T+1}\right\}$$
$$=\frac{1}{I+1}\left\{\frac{R(I+1,T)}{T}-\frac{R(I+1,T+1)}{T+1}\right\}. \quad (5)$$

The value of μ for any IT-state can thus be calculated from (1) with the help of (2) and (5).

For calculating the quadrupole moments we write

$$Q_1=\sum_i(3z_i{}^2-r_i{}^2) \quad \text{and} \quad Q_2=\sum_i(3z_i{}^2-r_i{}^2)\tau_{i3}.$$

It is well known that[2]

$$(ITMM_\tau|Q_1|ITMM_\tau)$$
$$=Q_1{}^{ITMM_\tau}=\frac{3M^2-I(I+1)}{I(2I-1)}Q_1{}^{IT}, \quad (6)$$

and arguments similar to that given in (2) will give

$$(ITMM_\tau|Q_2|ITMM_\tau)=Q_2{}^{ITMM_\tau}$$
$$=\frac{3M^2-I(I+1)}{I(2I-1)}\frac{M_\tau}{T}Q_2{}^{IT}. \quad (6.1)$$

Calculation of the matrices with the wave functions (3) will now lead to the equations[1]

$$\sum_{IT}Q_1{}^{ITMM_\tau}=\sum_k\int\chi_k{}^*(MM_\tau)\sum_i(3z_i{}^2-r_i{}^2)$$
$$\times\chi_k(MM_\tau)d\tau_1\cdots d\tau_n=\sum_k\sum_i q_j{}^{m_i{}^k}=AM_\tau, \quad (7)$$

where $q_j{}^m$ is the matrix of $(3z^2-r^2)$ for a single nucleon in the state j, $j_z=m$; and it is easily proved that[3]

$$q_j{}^j=q_j=-\frac{(2j-1)}{(2j+2)}\langle r^2\rangle.$$

Similarly, for Q_2 we get

$$\sum_{IT}Q_2{}^{ITMM_\tau}=\sum_k\sum_i m_{\tau i}{}^k q_j{}^{m_i{}^k}=BM_\tau. \quad (7.1)$$

Equations (7), (7.1) combined with (6), (6.1) can now be utilized to find $Q_1{}^{IT}$ and $Q_2{}^{IT}$ for any state, and the quadrupole moment of the state will be given by

$$Q^{IT}=\tfrac{1}{2}Q_1{}^{IT}-Q_2{}^{IT}.$$

The method has the defect that for more than one IT-state arising out of any configuration we can get only the average μ and Q for the states.

The author is grateful to the Government of West Bengal for a research grant which made the work possible.

[1] R. D. Lawson, this issue [Phys. Rev. **100**, 845 (1955)].
[2] E. Feenberg and G. E. Page, *Quantum Theory of Angular Momentum* (Addison-Wesley Press, Cambridge, 1953).
[3] S. Sengupta, Indian J. Theoret. Phys. **2**, 121 (1954).

p-p Interactions at 3 Bev*

R. Cester, T. F. Hoang, and A. Kernan†
Physics Department, University of Rochester, Rochester, New York
(Received July 25, 1955)

ILFORD G-5 emulsions were exposed to the 3-Bev internal beam of the Brookhaven proton synchroton in order to study p-p interactions in emulsion: the

incident beam energy was determined to be 2.95±0.15 Bev by the relative scattering technique.[1] The plates were scanned under high magnification using the "on-track" scanning technique. Only those events were accepted for analysis which obeyed criteria necessary to insure their compatibility with a two-body nucleon interaction, i.e., an interaction with a hydrogen atom of the emulsion or a bound proton of an emulsion nucleus. The criteria are: (1) an even number of tracks emerging from the interaction of which at most two are protons; (2) no evidence of nuclear recoil; (3) a proton emerging at an angle θ cannot have an energy greater than an elastically scattered proton at that angle.

Of 102 events analyzed at present which satisfy these criteria, 81 can be interpreted as p-p interactions, giving a mean free path of 340 cm for p-p interactions at 3 Bev. By extrapolating to 3 Bev the results of Shapiro, Chen, and Leavitt[2] for total p-p cross sections by counter measurements, and using the known composition of the emulsion, a mean free path of 704 cm is expected. This indicates that approximately one-half of the p-p interactions are with bound protons; the detailed analysis of the data supports this conclusion.

TABLE I. Comparison of experimental data with Fermi statistical theory and the Peaslee excited-state model.

	Elastic events	Single π production	Double π production	Triple π production	$\frac{\sigma_1}{\sigma_2}$ [a]	$\frac{\sigma_1(\pi^+)}{\sigma_1(\pi^0)}$ [b]
Experimental results	17_{-4}^{+5}	39_{-13}^{+10}	19_{-6}^{+11}	6_{-4}^{+2}	$2.0_{-1.5}^{+2}$	$2.5_{-1.5}^{+3.5}$
% values	$21_{-7}^{+6}\%$	$48_{-16}^{+10}\%$	$23_{-10}^{+17}\%$	$7_{-4}^{+4}\%$		
Predictions of Fermi model	3%	67%	29%	1%	2.3	3
Predictions of Peaslee model					2.5[c]	5

[a] σ_1/σ_2 is the ratio of the cross sections for single and double production.
[b] $\sigma_1(\pi^+)/\sigma_1(\pi^0)$ is the ratio of the number of π^+ and π^0 mesons produced in the single production process.
[c] $\frac{\sigma_1}{\sigma_2}=\frac{6}{25}\left(\frac{\sigma_1(\pi^+)+\sigma_2(\pi^+)}{\sigma_2(\pi^-)}-\frac{26}{6}\right)$ for the Peaslee model, where $\sigma_1(\pi^+)$ is the number of π^+ mesons produced in the single-π events and $\sigma_2(\pi^+)$ and $\sigma_2(\pi^-)$ are the number of π^+ and π^- produced in the two-π events.

Energy and mass determinations were carried out by grain counting, scattering, and range measurements and in each case an attempt was made to reconstruct the event completely. The cases of elastic scattering could be positively identified by energy and angle measurements and the test of coplanarity. For most of the events, calculation of the missing mass permitted a decisive differentiation between single and multiple π meson production. in 84% of the cases of single π production, the energy and direction of emission of the neutral particle could be accurately determined. The events in which a π^+ and π^- were produced could also be accurately reconstructed.

Table I presents the results of the analysis with upper and lower limits of error. The errors in the elastic events are due to the fact that in collisions with bound protons the motion of the target nucleon tends to destroy the unique relationship between energy and angle and prevents a positive identification. The limits of error in the single and double π events arise from

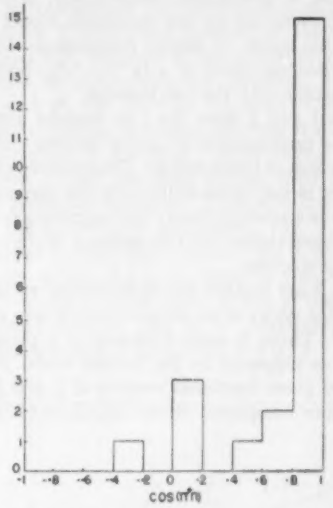

FIG. 1. Angular distribution in c.m. system of π^+ mesons with respect to nucleon of lower energy in the c.m. system, for single π^+ production.

those two-pronged events in which insufficient data and/or the Fermi energy of the bound proton gives rise to some uncertainty. Three of the events ascribed to triple production are rather uncertain; they are four-pronged events for which the process $(pp\pi^+\pi^-)$

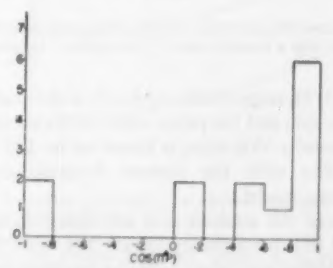

FIG. 2. Angular distribution in c.m. system of π^0 mesons with respect to the proton of lower energy in the c.m. system, for single π^0 production.

can be ruled out, but which can be interpreted as $(pn\pi^+\pi^+\pi^-)$. The upper limit for triple production is set by including in this category the two-pronged events with a calculated missing mass much larger than that expected for one neutral particle.

The experimental results are compared with the values predicted by the Fermi statistical theory[3] and the Peaslee excited-state model.[4] The percentages for

the various processes are compared with those calculated on the basis of the statistical model from the formula of Lepore and Stuart.[5] The experimental value of σ_1/σ_2, where σ_1 and σ_2 are the cross sections for single and double π production, respectively, is compared with that predicted by the statistical model and the excited-state model. A similar comparison is made for the experimental value of $\sigma_1(\pi^+)/\sigma_1(\pi^0)$; both results are compatible with the two theories.

Figures 1 and 2 show the c.m. angular distribution for single π production of π^+ and π^0 mesons with respect to the nucleon of lower energy. The evidence of angular correlation is not reconcilable with the present formulation of the statistical theory and suggests a production process characterized by the emission of the π meson by a single nucleon.

In Fig. 3 are plotted the experimental values calculated for the decay of an excited nucleon into a nucleon and a π^+. There is some evidence of a peak around 150 Mev as suggested by the Peaslee model. However, this model gives fractional weights of $\frac{3}{4}$ and $\frac{1}{4}$ for the intermediate compound states $(T_z', T_z) = (3/2, -1/2)$

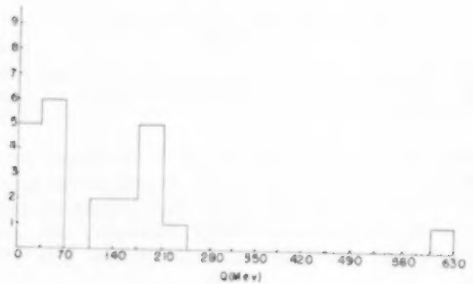

FIG. 3. Q values calculated for the decay of an excited intermediate state into a nucleon and π^+, for single π^+ emission.

and $(1/2, 1/2)$, respectively, where T_z is the z component of isotopic spin and the prime refers to the excited state. Experimentally this ratio is found to be 1/6 which is incompatible with the present formulation of the excited-state model.

Details of the analysis and additional data will be presented in a forthcoming paper. We wish to thank Mrs. V. Miller and Mrs. J. Milks for their assistance in scanning and to express our appreciation to the Brookhaven Cosmotron staff for their assistance in obtaining the exposure.

* This work was assisted by the U. S. Atomic Energy Commission.

† American Association of University Women Fellow.

[1] M. Koshiba and M. F. Kaplon, Phys. Rev. **97**, 193 (1955).

[2] C. P. Leavitt, Proceedings of the Fifth Annual Rochester Conference on High-Energy Nuclear Physics (Interscience Publishers, Inc., New York, 1955), p. 41.

[3] E. Fermi, Progr. Theoret. Phys. (Japan) **5**, 570 (1950); E. Fermi, Phys. Rev. **92**, 452 (1953); Phys. Rev. **93**, 1434 (1954).

[4] D. Peaslee, Phys. Rev. **94**, 1085 (1954); **95**, 1580 (1954).

[5] J. V. Lepore and R. N. Stuart, Phys. Rev. **94**, 1724 (1954).

Effects of Finite Amplitude in Coulomb Excitation*

G. BREIT AND J. P. LAZARUS

Yale University, New Haven, Connecticut

(Received July 15, 1955; revised manuscript received August 29, 1955)

THE standard theory of Coulomb excitation[1,2] makes use exclusively of first-order effects of the field of the incident particle. Estimates described below show, however, that the probability amplitudes in close collisions are large enough to be considered, especially in connection with angular distribution effects.[2] On the semiclassical theory the excitation of sublevels of $J=2$ with magnetic quantum numbers μ from an initial level $J=0$ has the probability

$$\sum_\mu |c_\mu|^2 = \frac{49\pi}{100\hbar^2}(Z_1 e^2 Q)^2 \sum_\mu \left| \int_{-\infty}^{t} e^{i\omega t} Y_{2\mu} \frac{dt}{r^3} \right|^2,$$

where $Y_{2\mu}$ is the spherical harmonic normalized to unity for integration over solid angles, r the interparticle separation, Z_1 the projectile's charge, and Q the nuclear quadrupole moment. At the perihelion ($t=0$) of close collisions,

$$(\textstyle\sum_\mu |c_\mu|^2)_{t=0} = 0.068 (Z_1 e^2/\hbar v)^2 (Q/a'^2)^2,$$

where $2a'$ is the distance of closest approach and v is the relative velocity. Taking nominally the nuclear charge $Z_2=78$, $Z_1=1$, $Q=7\times10^{-24}$ cm^2, one obtains $|c_\mu| = (0.065, 0.053, 0.065)$ for $\mu=(2, 0, -2)$ and $\sum_\mu |c_\mu|^2 = 0.011$. On its way out, the projectile causes transitions from sublevels μ' of the excited state or from other states. There is, in addition, the effect of the first order c_μ giving an effect on c_μ itself. The change in a c_μ is thus of the order of 6 percent of a c_μ, corresponding to 12 percent in gamma intensity from μ, provided phase relations are disregarded. For $J=2\to J=2$ transitions, one finds a factor $(2\sqrt{5})/7 = 0.64$ relative to $J=0\to J=2$ but the $\mu=2$ to $\mu=0$, $\mu=-2$ to $\mu=0$ transitions double the effect on $|c_0|$. While the estimate of 12 percent does not apply to gamma angular correlation coefficients directly, a literal application of first-order theory is seen to be questionable.

The finite-amplitude effects need consideration in connection with gamma angular distribution measurements[3] and inelastic scattering studies. In principle they are capable of supplying information on *static quadrupole moments* of excited states as well as transition moments between excited states. The effects would stand out better in coincidence experiments giving the final projectile direction and the associated gamma distribution. The essential amplitude parameter is

$$Z_1 e^2 Q/\hbar v a'^2 \propto m^{\frac{1}{2}} E^{\frac{1}{2}}/Z_1 Z_2^2,$$

where m is the reduced mass. For fixed a', conditions for compound nucleus formation are roughly similar;

the effect is proportional to $Z_1^{\frac{1}{3}}m^{\frac{1}{3}}$ and has an enhanced importance for *heavy ion bombardment*. A change from protons to N^{14} in the bombardment of heavy nuclei increases the redistribution effects by a factor ~ 10, while a change from protons to alpha particles gives a factor $2\sqrt{2}=2.8$.

* This research was supported by the Office of Ordnance Research, U. S. Army, and by the U. S. Atomic Energy Commission.

[1] K. A. Ter Martirosyan, J. Exptl. Theoret. Phys. (U.S.S.R.) **22**, 284 (1952); K. Alder and A. Winther, Phys. Rev. **96**, 237 (1954); G. Breit and P. B. Daitch, Phys. Rev. **96**, 1447 (1954).

[2] K. Alder and A. Winther, Phys. Rev. **91**, 1578 (1953); L. C. Biedenharn and M. E. Rose, Oak Ridge National Laboratory Report ORNL-1789, 1954 (unpublished); L. C. Biedenharn and C. M. Class, Phys. Rev. **98**, 691 (1955); Biedenharn, McHale, and Thaler, Phys. Rev. **100**, 376 (1955).

[3] P. H. Stelson and F. K. McGowan, Phys. Rev. **98**, 249(A) (1955).

Electric-Monopole Transitions in Atomic Nuclei*

E. L. Church† and J. Weneser‡

Brookhaven National Laboratory, Upton, Long Island, New York

(Received September 14, 1955)

LOW-ENERGY electric-monopole, or $E0$ transitions, ($\Delta I=0$, no), proceed solely by internal conversion, with zero units of angular momentum transferred to the ejected electron. Gamma-ray emission of this multipole order is strictly forbidden, although $E0$ pair production is possible for transition energies $>2mc^2$. It has not been previously emphasized that (1) the electric-monopole mode of de-excitation is available between any two equal-parity states of the same spin, zero or otherwise, (2) that in such cases, $E0$ internal conversion may compete favorably with the paralleling $M1$ and $E2$ radiative transitions in heavy nuclei, and (3) that monopole matrix elements, $\langle i|\sum r_p^2|f\rangle$, may be particularly useful in the study of nuclear structure.

Figure 1 presents the transition probability for monopole conversion in the K shell for various atomic numbers.[1,2] The "strength parameter," ρ, is defined by

$$\langle i|\sum r_p^2|f\rangle=\rho R_0^2, \qquad (1)$$

where $R_0=1.20\times10^{-13}A^{\frac{1}{3}}$ cm. In the naive approximation of complete overlap of the initial and final nuclear wave functions (the "Weisskopf" approximation for higher multipoles[3]), ρ would be of the order of unity. Conversion in the L shell occurs almost entirely in the L_I subshell, with K/L conversion ratios falling between 6 and 4 for $Z=70-100$. The results in Fig. 1 have been computed in the "point-nucleus" approximation for the electron wave functions.[4] Calculations of the effects of the finite nuclear size and atomic screening indicate that these results should be increased by 10 to 20% for $Z=85$. The data in Fig. 1, therefore, correspond to conservative lower limits for the total $E0$ conversion probability.

Transitions between two equal-parity states of the same spin are usually thought of as proceeding only by $M1$ and $E2$ transitions. $E0$ conversion is also possible in such cases. A convenient measure of the monopole contribution is ϵ^2, the ratio of the rate of $E0$ *conversion* to the rate of $E2$ *gamma-ray* emission, defined in analogy with δ^2, the ratio of the rates of $M1$ to $E2$ gamma-ray emission. Empirical lifetimes of $E2$ ground-state transitions in even-even nuclei with $Z=60-80$ are between 10 and 100 times shorter than the corresponding Weisskopf estimates.[5] Even with this enhancement of the quadrupole component, Fig. 1 indicates that values of ϵ^2 of the order of unity are to be expected for energies $\sim 1mc^2$, if ρ is set equal to one. Since δ^2 is frequently of the order of unity or less in these nuclei, the $E0$ mode of decay may be of considerable importance. This situation is illustrated in Fig. 2.

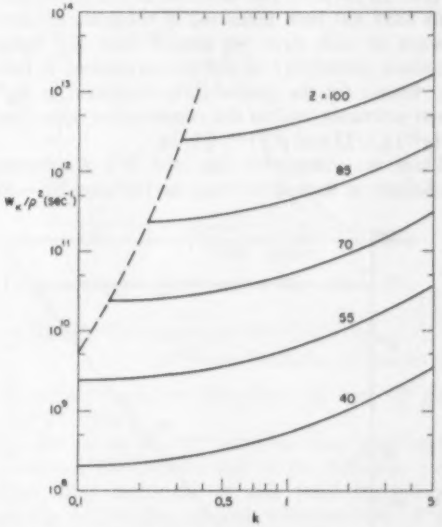

FIG. 1. Transition probability for electric-monopole conversion in the K shell divided by ρ^2, as computed in the "point-nucleus" approximation. Results are given for various atomic numbers as functions of the nuclear transition energy, k, in units of mc^2. The strength parameter, ρ, defined by Eq. (1), is of the order of unity in the "Weisskopf" approximation.

As pointed out by Scharff-Goldhaber and Weneser,[6] there exists a large and regular class of moderately heavy even-even nuclei having 2+ first- and second-excited states. Such nuclei provide a fertile field for the search for data on monopole transitions, which until now have been available only from a study of a few isolated $E0$ transitions of the $0+\rightarrow 0+$ type. Sufficient experimental data are already available for the determination of upper limits for the monopole contributions in two transitions of the $2+\rightarrow 2+$ type:

the 677-kev transition in Hg^{198}, and the 331-kev transition in Pt^{196}. Experimental values of the K-conversion coefficients,[7,8] α_K, and the $M1/E2$ mixing ratios,[9,10] δ^2 are available for these transitions. The latter were determined by measurement of the gamma-gamma directional correlation between the mixed transition and the subsequent $2+\rightarrow 0+$ pure $E2$ ground-state transition. The relationship between these quantities is

$$\epsilon_K^2=(\alpha_{\text{exp}}-\alpha_{E2})-\delta^2(\alpha_{M1}-\alpha_K), \qquad (2)$$

where α_{E2} and α_{M1} are the K-conversion coefficients of the pure $E2$ and $M1$ transitions, respectively. Substitution of the experimental values of α_K and δ^2, and the theoretical values of α_{E2} and α_{M1} from Rose *et al.*,[11] indicates that ϵ_K^2 is zero to within the limits of experimental error. If one uses the quoted limits of experimental error and assumes a 2% interpolation uncertainty in the values of α_{E2} and α_{M1}, one obtains the upper limits $\epsilon_K^2(Hg^{198})\leq 2\times 10^{-3}$ and $\epsilon_K^2(Pt^{196})\leq 5\times 10^{-3}$. The lifetimes of the mixed transitions have not been measured in these nuclei. In the absence of such data we assume that the reduced transition probability of the $E2$ component is twice[12] that known for the ground-state transition in Hg^{198}.[5] These estimates lead to the conservative upper limits $\rho(Hg^{198})\leq 1/13$ and $\rho(Pt^{196})\leq 1/34$.

There is evidence[13,14] that the $M1$ K-conversion coefficients of Rose *et al.*[11] may be too large by ~35% for $Z\sim 80$. If the values of α_{M1} are lowered by this amount, the upper limits of the strength parameters become $\rho(Hg^{198})\leq 1/6$ and $\rho(Pt^{196})\leq 1/21$. Thus, at least in the case of Pt^{196}, experiment seems to indicate that the monopole matrix element is strongly attenuated. In comparison, monopole transitions of the $0+\rightarrow 0+$ type in C^{12}, O^{16}, and Ge^{72} exhibit strength parameters lying between 1/2 and 1/9.[2,15,16]

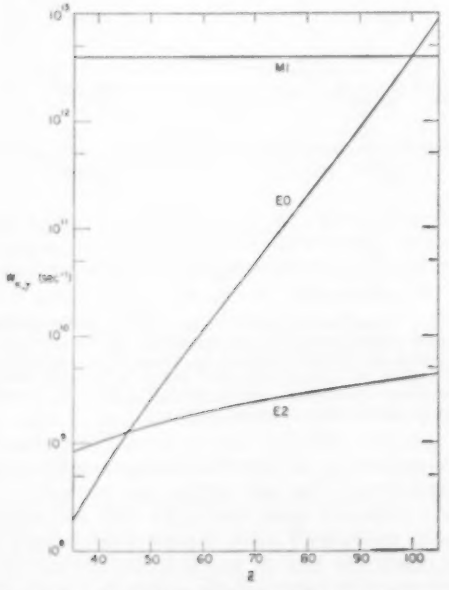

FIG. 2. Transition probability for electric-monopole conversion in the K shell as a function of atomic number for a transition energy of one mc^2. These results have been derived from Fig. 1 by assuming $\rho=1$. The analogous "Weisskopf" estimates of the $M1$ and $E2$ gamma-ray transition probabilities are included for comparison

Monopole matrix elements computed for reasonable interpretations of the pure shell model and of the various collective models are found to vanish to lowest order. The experimental determination of the magnitudes of such matrix elements, therefore, would provide a sensitive probe into the finer details of nuclear models. Definite measurements of ρ in heavy nuclei might be conveniently obtained from directional-correlation experiments involving the K-conversion electrons of the mixed $E0+M1+E2$ transition since the $E0-E2$ interference term appearing in the coefficient of $P_2(\cos\theta)$ is then proportional to ϵ instead of its square.

An extensive analysis of the effects of the finite nuclear size and atomic screening on the absolute and relative conversion properties of $E0$ transitions is being carried out, in addition to the evaluation, with M. E. Rose, of the expected conversion-electron correlation functions. These results, as well as a detailed discussion of the significance of $E0$ matrix elements, are being prepared for submittal to *The Physical Review*.

We thank Dr. M. Goldhaber and Dr. J. E. Monahan for helpful discussions.

* Work performed under the auspices of the U. S. Atomic Energy Commission.

† On leave from Frankford Arsenal, Philadelphia, Pennsylvania.

‡ Now on leave at the University of Illinois, Urbana, Illinois.

[1] H. Yukawa and S. Sakata, Proc. Phys.-Math. Soc. Japan **17**, 397 (1935); R. Thomas, Phys. Rev. **58**, 714 (1940).

[2] S. D. Drell, Oak Ridge National Laboratory Report ORNL-792, 1950 (unpublished); S. D. Drell and M. E. Rose, Progr. Theoret. Phys. Japan **7**, 125 (1952).

[3] V. F. Weisskopf, Phys. Rev. **83**, 1073 (1951).

[4] The large components of the electron wave functions are set equal to the point Coulomb values at the nuclear radius. The corresponding dependence on the small components is eliminated since only the lowest order nuclear matrix element is considered.

[5] See, for example, A. W. Sunyar, Phys. Rev. **98**, 653 (1955).

[6] G. Scharff-Goldhaber and J. Weneser, Phys. Rev. **98**, 212 (1955).

[7] Elliott, Preston, and Wolfson, Can. J. Phys. **32**, 153 (1954).

[8] M. T. Thieme and E. Bleuler, Phys. Rev. **99**, 1646 (1955); private communication (July, 1955).

[9] D. Schiff and F. R. Metzger, Phys. Rev. **90**, 849 (1953); C. D. Schrader, Phys. Rev. **92**, 928 (1953).

[10] R. M. Steffen, Phys. Rev. **89**, 665 (1953); private communication (August, 1955).

[11] Rose, Goertzel, and Perry, Oak Ridge National Laboratory Report ORNL-1023, 1951 (unpublished).

[12] Based on the "free-vibration" model of reference 6. There is no experimental evidence for or against this factor, which, if neglected, would lower ρ by ~30%.

[13] L. A. Sliv, Zhur. Eksptl'. i Teort. Fiz. **21**, 770 (1951).

[14] A. H. Wapstra and G. J. Nijgh (private communication to M. Goldhaber, September, 1955).

[15] L. I. Schiff, Phys. Rev. **98**, 1281 (1955).

[16] The lifetime of the 1.41-Mev $E0$ transition in Po^{214}(RaC') is not known well enough to justify an estimate of its strength parameter.

Decay Rates of C^{14}, N^{14*}, and O^{14}†

R. Sherr, J. B. Gerhart, H. Horie,* and W. F. Hornyak

Palmer Physical Laboratory, Princeton University, Princeton, New Jersey

(Received August 3, 1955)

THE very long lifetime of the C^{14} β decay has been variously explained[1] (1) by the assumption of a parity change; (2) by assuming C^{14} to be pure $^1S_0$ and N^{14} almost pure $^3D_1$ (ΔL-forbidden); or (3) by chance cancellation in the matrix element for the decay. The first of these has been eliminated on experimental grounds, while the second is theoretically objectionable.[1] Jancovici and Talmi[2] have shown that cancellation can occur if large tensor forces are considered. An improvement in their calculations has been made by Visscher and Ferrell[3] and by Lane[4] in reducing the magnitude of the tensor force required.

C^{14}, O^{14}, and the first excited state of N^{14} at 2.31 Mev are three states belonging to the same ($T=1$) multiplet and to a good approximation their wave functions should be identical. Jancovici and Talmi calculated the matrix element for the β^+ transition of O^{14} to the ground state of N^{14}; they showed that Coulomb forces would modify the wave function of O^{14} slightly but sufficiently to reduce the cancellation somewhat and thus produce an appreciably larger matrix element than that for the C^{14} decay. In the present Letter, we wish to report measurements on the decay of O^{14} to the ground state of N^{14}, and on the lifetime of the $M1$ γ transition from the analog state in N^{14} at 2.31 Mev. Both measurements support the "cancellation" hypothesis.

Following the notation of Jancovici and Talmi,[2] the wave function for C^{14} is taken as $x\psi(^1S_0)+y\psi(^3P_0)$ and that for N^{14} as $\alpha\psi(^3S_1)+\beta\psi(^1P_1)+\gamma\psi(^3D_1)$. The C^{14} β-decay matrix element is given by[2]

$$\left|\int\boldsymbol{\sigma}\right|^2=6(x\alpha-y\beta/\sqrt{3})^2=4.4\times10^{-6}; \qquad (1)$$

and for O^{14}, approximately,

$$\left|\int\boldsymbol{\sigma}\right|^2=6[(1-My^2)x\alpha-(1+Mx^2)y\beta/\sqrt{3}]^2, \qquad (2)$$

where

$$M=[\langle{}^1S_0|e^2/r|{}^1S_0\rangle-\langle{}^3P_0|e^2/r|{}^3P_0\rangle](E'-E)^{-1}$$

and E' and E are the excitation energies of the two p^{-2}, $(J,T)=(0,1)$ states of C^{14}. The effect of the Coulomb perturbation is a reduction of x for O^{14} by the factor $1-My^2$ and an increase of y by about the same amount (M is positive). The experimental value of $|\int\boldsymbol{\sigma}|^2$ is given by[5] $|\int\boldsymbol{\sigma}|^2=6550/1.37ft$.

It is clear that if the C^{14} is pure $^1S_0$ ($y=0$), the O^{14} decay is equally forbidden. The same result follows for the $M1$ transition of N^{14*} under explanation (2). The half-life of N^{14*} is

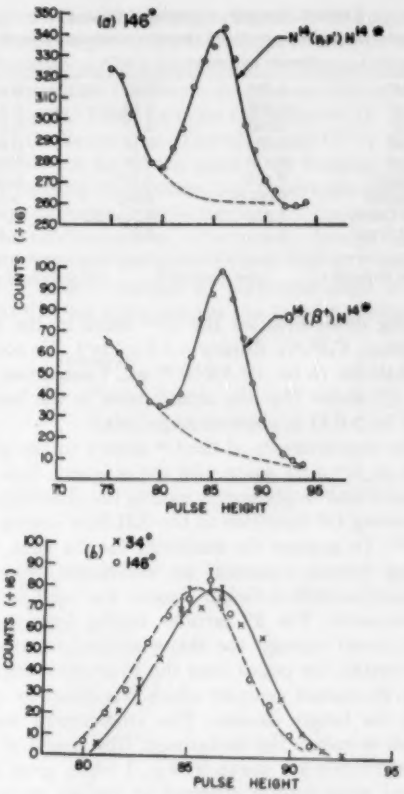

FIG. 1. Doppler shift of the 2.31-Mev γ ray in N^{14}.

$$T_{\frac{1}{2}}=4.50\times10^{-15}\{4.71(x\alpha-y\beta/\sqrt{3})+[(2/3)^{\frac{1}{2}}x\beta-(2/9)^{\frac{1}{2}}y\alpha+(5/18)^{\frac{1}{2}}y\gamma]\}^{-2}(\text{sec}). \qquad (3)$$

If the second term vanishes, Eqs. (1) and (3) yield $T_{\frac{1}{2}}=2.8\times10^{-10}$ sec.

The lifetime of the N^{14*} state has been investigated by observing the Doppler shift in the 2.31-Mev γ ray emitted after excitation of this state by inelastic scattering of 19-Mev protons. Observations of the energy of the γ ray were made at 34° and 146° with respect to the incident proton beam, with a scintillation spectrometer. In order to determine the Doppler shift, we measured the unshifted energy of the γ ray in the decay of O^{14}. The latter is produced by the (p,n) reaction on N^{14} in the same target. Typical photopeak spectra are shown in Fig. 1(a); the dotted lines indicate the backgrounds subtracted in analyzing these spectra. Two runs at 34° gave a Doppler shift of $(+0.70\pm0.17)\%$, while the three at 146° gave $(-0.86\pm0.13)\%$. Figure 1(b) shows the shift between 34° and 146° for the inelastically excited γ ray in one set of measurements. This Doppler shift is approximately the maximum one would expect from the kinematics of the reaction, indicating that the lifetime is less than the

TABLE I. Nuclear properties of C^{14} and N^{14}.

	Present calculation	J-T[a]	V-F[b]
x^2	0.592	0.42	0.59
y^2	0.408	0.58	0.41
α^2	0.066	0.07	0.016
β^2	0.296	0.14	0.066
γ^2	0.638	0.79	0.92
μ(nm)	0.404[c]	0.377	0.332
Q(barns)	0.0071[c]	0.011	0.011
$E'-E$(Mev)	5.6 or 7.3	4.7 or 6.2	2.7 or 3.5
$T_{\frac{1}{2}}(10^{-14}$ sec)	1.6	2.2	2.3

[a] See reference 2. [b] See reference 3. [c] Experimental values.

slowing down time for the N^{14*} recoil in the target (Melmac, $C_8H_7N_6$, density $\sim$1.5 g/cm^3). We estimate the half-life to be $<3.5\times10^{-13}$ sec. Comparison with Eq. (3) shows that the second term in the brackets must be >0.11 in absolute magnitude.[6]

The measurements of the O^{14} branch to the ground state of N^{14} were made with the magnetic lens spectrometer and target system used in the observation[5] of the strong O^{14} transition to the 2.31-Mev analog state in N^{14}. To increase the sensitivity for the weak, high-energy branch expected, an anthracene crystal in conjunction with a Geiger counter was used with the spectrometer. The β^+ particles issuing from the exit port passed through the thin-windowed counter into the crystal; the pulses from the latter were displayed on a 20-channel analyzer which was gated by pulses from the Geiger counter. This arrangement was desirable to reduce the background. The results of these measurements are shown in Fig. 2 which gives a few typical pulse spectra observed at various settings of the spectrometer. The inset figure is a Kurie plot of the high-energy transition data; the line was drawn to pass through the known end point of the spectrum. From these measurements, we conclude that the branching ratio is $(0.60\pm0.10)\%$ leading to an ft value of $(2.0\pm0.3)\times10^7$ sec. The corresponding value of $|\int\boldsymbol{\sigma}|^2$ is 2.4×10^{-4}, about 50 times larger than the C^{14} matrix element. From Eq. (2) it is evident that y cannot be zero or negligibly small. Consistency with the results

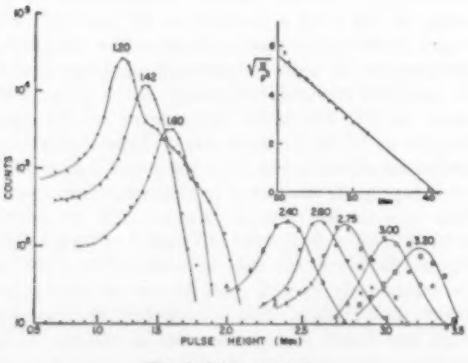

FIG. 2. O^{14} β spectrum.

of these measurements required finite values for all the coefficients in the wave functions.

These results can in principle be combined with the magnetic moment of N^{14} to yield a specific set of coefficients for the wave functions. Unfortunately, $(E'-E)$ in Eq. (2) is unknown experimentally. Alternatively we can use $|\int\boldsymbol{\sigma}|^2$ for C^{14} and the magnetic and the quadrupole moments of N^{14} to compute the coefficients. (Normalization requires $x^2+y^2=1$ and $\alpha^2+\beta^2+\gamma^2=1$.) The moments of N^{14} are given by

$$\mu=0.88\alpha^2+0.5\beta^2+0.31\gamma^2=0.404\,(\text{nm}), \tag{4}$$

$$Q=[-\beta^2/5+7\gamma^2/50+4(5)^{\frac{1}{2}}\alpha\gamma/25]\langle r^2\rangle = 0.0071\,(\text{barn}).^7 \tag{5}$$

Combining these with (1) one obtains the values listed in Table I. The signs of all coefficients are the same, and $\langle r^2\rangle$ was assumed to be 6.64×10^{-26} cm^2. Inserting these values in Eq. (2), using the experimental result for $|\int\boldsymbol{\sigma}|^2$ for O^{14}, one finds $M=0.036$; the Coulomb perturbation decreases x for O^{14} by $\sim2\%$. From the calculations of Jancovici and Talmi we can infer $E'-E$ for the present parameters. The computed values of $E'-E$ and of $T_{\frac{1}{2}}$ are also listed in Table I. Two possible values of $E'-E$ occur because the sign of $\int\boldsymbol{\sigma}$ for C^{14} is unknown. For comparison, the last two columns give the coefficients of Jancovici and Talmi[2] and of Visscher and Ferrell[3] and the corresponding values of μ, Q, $(E'-E)$, and $T_{\frac{1}{2}}$ computed with the above equations.

The value of $(E'-E)$ is particularly interesting; it should correspond to the energy of the first excited 0+ state in C^{14} arising from the p^{-2} configuration. Experimentally, there are a number of states in C^{14} starting at 6.09 Mev.[8] In particular the mode of decay[9] and the parity[8] of the level at 6.89 Mev are consistent with an assignment 0+. Furthermore, the 0+ level in N^{14} at 8.62 Mev can have $T=1$ and if so, one would expect this state in C^{14} at about 6.3 Mev. Further experimental and theoretical work on the levels of C^{14} is required to definitely locate the state in question.

We are greatly indebted to Professor E. Feenberg and to Dr. A. M. Lane for stimulating discussions and suggestions, and to W. W. Stone and D. C. Sutton for assistance in taking data.

† This work was supported by the U. S. Atomic Energy Commission and the Higgins Scientific Trust Fund.

* On leave from Department of Physics, University of Tokyo, Tokyo, Japan.

[1] D. R. Inglis, Revs. Modern Phys. **25**, 390 (1953); E. Feenberg, *Shell Theory of the Nucleus* (Princeton University Press, Princeton, 1955), p. 105.

[2] B. Jancovici and I. Talmi, Phys. Rev. **95**, 289 (1954).

[3] W. M. Visscher and R. A. Ferrell, Phys. Rev. **99**, 649(A) (1955); also private communication.

[4] A. M. Lane (private communication).

[5] J. B. Gerhart, Phys. Rev. **95**, 288 (1954).

[6] Essentially the same result and conclusion have recently been reported by J. Thirion and R. Barloutaud, Compt. rend. **240**, 2136 (1955).

[7] A. Bassompierre, Compt. rend. **240**, 285 (1955).

[8] McGruer, Warburton, and Bender, Phys. Rev. **99**, 632(A) (1955); also private communication. See also F. Ajzenberg and T. Lauritsen, Revs. Modern Phys. **27**, 77 (1955).

[9] Mackin, Mims, and Mills, Phys. Rev. **98**, 43 (1955).

Observation of Antiprotons*

OWEN CHAMBERLAIN, EMILIO SEGRÈ, CLYDE WIEGAND, AND THOMAS YPSILANTIS

Radiation Laboratory, Department of Physics, University of California, Berkeley, California

(Received October 24, 1955)

ONE of the striking features of Dirac's theory of the electron was the appearance of solutions to his equations which required the existence of an antiparticle, later identified as the positron.

The extension of the Dirac theory to the proton requires the existence of an antiproton, a particle which bears to the proton the same relationship as the positron to the electron. However, until experimental proof of the existence of the antiproton was obtained, it might be questioned whether a proton is a Dirac particle in the same sense as is the electron. For instance, the anomalous magnetic moment of the proton indicates that the simple Dirac equation does not give a complete description of the proton.

The experimental demonstration of the existence of antiprotons was thus one of the objects considered in the planning of the Bevatron. The minimum laboratory kinetic energy for the formation of an antiproton in a nucleon-nucleon collision is 5.6 Bev. If the target nucleon is in a nucleus and has some momentum, the threshold is lowered. Assuming a Fermi energy of 25 Mev, one may calculate that the threshold for formation of a proton-antiproton pair is approximately 4.3 Bev. Another, two-step process that has been considered by Feldman[1] has an even lower threshold.

TABLE I. Characteristics of components of the apparatus.

S1, *S2*	Plastic scintillator counters 2.25 in. diameter by 0.62 in. thick.
C1	Čerenkov counter of fluorochemical 0-75, ($C_8F_{16}O$); $\mu_D=1.276$; $\rho=1.76$ g cm^{-3}. Diameter 3 in.; thickness 2 in.
C2	Čerenkov counter of fused quartz: $\mu_D=1.458$; $\rho=2.2$ g cm^{-3}. Diameter 2.38 in.; length 2.5 in.
Q1, *Q2*	Quadrupole focusing magnets: Focal length 119 in.; aperture 4 in.
M1, *M2*	Deflecting magnets 60 in. long. Aperture 12 in. by 4 in. $B\cong 13\,700$ gauss.

There have been several experimental events[2-4] recorded in cosmic-ray investigations which might be due to antiprotons, although no sure conclusion can be drawn from them at present.

With this background of information we have performed an experiment directed to the production and detection of the antiproton. It is based upon the determination of the mass of negative particles originating at the Bevatron target. This determination depends on the simultaneous measurement of their momentum and velocity. Since the antiprotons must be selected from a heavy background of pions it has been necessary to measure the velocity by more than one method. To date, sixty antiprotons have been detected.

Figure 1 shows a schematic diagram of the apparatus. The Bevatron proton beam impinges on a copper target and negative particles scattered in the forward direction with momentum 1.19 Bev/c describe an orbit as shown in the figure. These particles are deflected 21° by the field of the Bevatron, and an additional 32° by magnet $M1$. With the aid of the quadrupole focusing magnet $Q1$ (consisting of 3 consecutive quadrupole magnets) these particles are brought to a focus at counter $S1$, the first scintillation counter. After passing through counter $S1$, the particles are again focused (by $Q2$), and deflected (by $M2$) through an additional angle of 34°, so that they are again brought to a focus at counter $S2$.

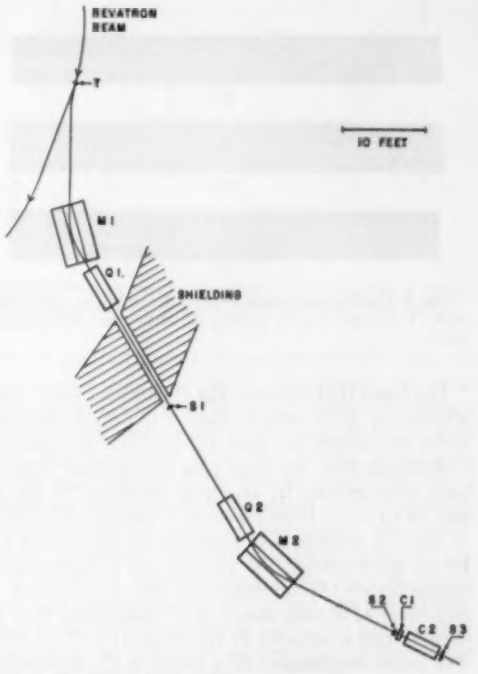

FIG. 1. Diagram of experimental arrangement. For details see Table I.

The particles focused at $S2$ all have the same momentum within 2 percent.

Counters $S1$, $S2$, and $S3$ are ordinary scintillation counters. Counters $C1$ and $C2$ are Čerenkov counters. Proton-mass particles of momentum 1.19 Bev/c incident on counter $S2$ have $v/c=\beta=0.78$. Ionization energy loss in traversing counters $S2$, $C1$, and $C2$ reduces the average velocity of such particles to $\beta=0.765$. Counter $C1$ detects all charged particles for which $\beta>0.79$. $C2$ is a Čerenkov counter of special design that counts only particles in a narrow velocity interval, $0.75<\beta<0.78$. This counter will be described in a separate publication. In principle, it is similar to

some of the counters described by Marshall.[5] The requirement that a particle be counted in this counter represents one of the determinations of velocity of the particle.

The velocity of the particles counted has also been determined by another method, namely by observing the time of flight between counters $S1$ and $S2$, separated by 40 ft. On the basis of time-of-flight measurement the separation of π mesons from proton-mass particles is quite feasible. Mesons of momentum 1.19 Bev/c have $\beta=0.99$, while for proton-mass particles of the same momentum $\beta=0.78$. Their respective flight times over the 40-ft distance between $S1$ and $S2$ are 40 and 51 millimicroseconds.

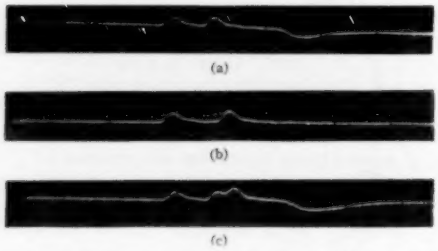

FIG. 2. Oscilloscope traces showing from left to right pulses from $S1$, $S2$, and $C1$. (a) meson, (b) antiproton, (c) accidental event.

The beam that traverses the apparatus consists overwhelmingly of π^- mesons. One of the main difficulties of the experiment has been the selection of a very few antiprotons from the huge pion background. This has been accomplished by requiring counters $S1$, $S2$, $C2$, and $S3$ to count in coincidence. Coincidence counts in $S1$ and $S2$ indicate that a particle of momentum 1.19 Bev/c has traversed the system with a flight time of approximately 51 millimicroseconds. The further requirement of a coincidence in $C2$ establishes that the particle had a velocity in the interval $0.75<\beta<0.78$. The latter requirement of a count in $C2$ represents a measure of the velocity of the particle which is essentially independent of the cruder electronic time-of-flight measurement. Finally, a coincident count in counter $S3$ was required in order to insure that the particle traversed the quartz radiator in $C2$ along the axis and suffered no large-angle scattering.

As outlined thus far, the apparatus has some shortcomings in the determination of velocity. In the first place, accidental coincidences of $S1$ and $S2$ cause some mesons to count, even though a single meson would be completely excluded because its flight time would be too short. Secondly, the Čerenkov counter $C2$ could be actuated by a meson (for which $\beta=0.99$) if the meson suffered a nuclear scattering in the radiator of the counter. About 3 percent of the mesons, which ideally should not be detected in $C2$, are counted in this manner. Both of these deficiencies have been eliminated by the insertion of the guard counter $C1$, which records all particles of $\beta>0.79$. A pulse from $C1$ indicates a particle (meson) moving too fast to be an antiproton of the selected momentum and indicates that this event should be rejected. In Table I, the characteristics of the components of the apparatus are summarized.

The pulses from counters $S1$, $S2$, and $C1$ were displayed on an oscilloscope trace and photographically recorded. From the separation of pulses from $S1$ and $S2$ the flight time of the particle could be measured with an accuracy of 1 millimicrosecond, and the pulse in the guard counter $C1$ could be measured. Figure 2 shows three oscilloscope traces, with the pulses from $S1$, $S2$, and $C1$ appearing in that order. The first trace (a) shows the pulses due to a meson passing through the system. It was recorded while the electronic circuits were adjusted for meson time of flight for calibration purposes. The second trace, Fig. 2(b), shows the pulses resulting from an antiproton. The separation of pulses from $S1$ and $S2$ indicates the correct antiproton time of flight, and the absence of the $C1$ pulse shows that no meson passed through $C1$. The third trace, Fig. 2(c), shows the accidental coincidence of two mesons with a difference of time such as to register in the electronic circuits. Either the presence of a pulse from $C2$ or the presence of multiple pulses from $S1$ or $S2$ would be

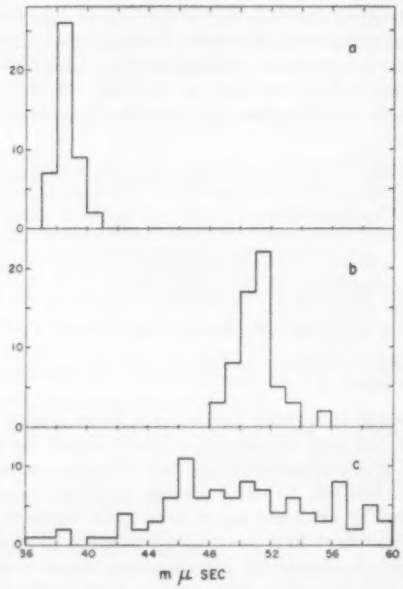

FIG. 3. (a) Histogram of meson flight times used for calibration. (b) Histogram of antiproton flight times. (c) Apparent flight times of a representative group of accidental coincidences. Times of flight are in units of 10^{-9} sec. The ordinates show the number of events in each 10^{-10}-sec intervals.

sufficient to identify the trace as due to one or more mesons.

An over-all test of the apparatus was obtained by changing the position of the target in the Bevatron, inverting the magnetic fields in $M1$, $M2$, $Q1$, and $Q2$, and detecting positive protons.

Each oscilloscope sweep of the type shown in Fig. 2 can be used to make an approximate mass measurement for *each* particle, since the magnetic fields determine the momentum of the particle and the separation of pulses $S1$ and $S2$ determine the time of flight. For protons of our selected momentum the mass is measured to about 10 percent, using this method only.

The observed times of flight for antiprotons are made more meaningful by the fact that the electronic gate time is considerably longer than the spread of observed antiproton flight times. The electronic equipment accepts events that are within ± 6 millimicroseconds of the right flight time for antiprotons, while the actual antiproton traces recorded show a grouping of flight times to ± 1 or 2 millimicroseconds. Figure 3(a) shows a histogram of meson flight times; Fig. 3(b) shows a similar histogram of antiproton flight times. Accidental coincidences account for many of the sweeps (about $\frac{2}{3}$ of the sweeps) during the runs designed to detect antiprotons. A histogram of the apparent flight times of accidental coincidences is shown in Fig. 3(c). It will be noticed that the accidental coincidences do not show the close grouping of flight times characteristic of the antiproton or meson flight times.

Mass measurement.—A further test of the equipment has been made by adjusting the system for particles of

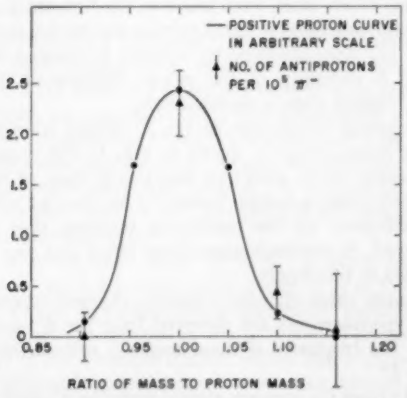

FIG. 4. The solid curve represents the mass resolution of the apparatus as obtained with protons. Also shown are the experimental points obtained with antiprotons.

different mass, in the region of the proton mass. A test for the reality of the newly detected negative particles is that there should be a peak of intensity at the proton mass, with small background at adjacent mass settings. By changing only the magnetic field values of $M1$, $M2$, $Q1$, and $Q2$, particles of different momentum may be chosen. Providing the velocity selection is left completely unchanged, the apparatus is then set for particles of a different mass. These tests have been made for both positive and negative particles in the vicinity of the proton mass. Figure 4 shows the curve obtained using positive protons, which is the mass resolution

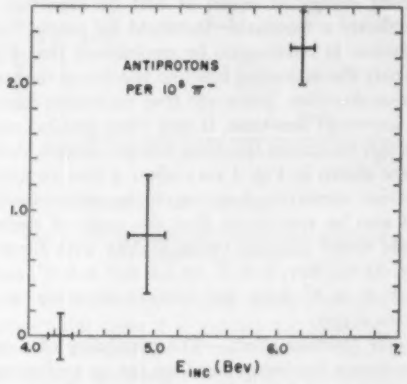

FIG. 5. Excitation curve for the production of antiprotons relative to meson production as a function of Bevatron beam energy.

curve of the instrument. Also shown in Fig. 4 are the experimental points obtained with antiprotons. The observations show the existence of a peak of intensity at the proton mass, with no evidence of background when the instrument is set for masses appreciably greater or smaller than the proton mass. This test is considered one of the most important for the establishment of the reality of these observations, since background, if present, could be expected to appear at any mass setting of the instrument. The peak at proton mass may further be used to say that the new particle has a mass within 5 percent of that of the proton mass. It is mainly on this basis that the new particles have been identified as antiprotons.

Excitation function.—A very rough determination has been made of the dependence of antiproton production cross section on the energy of the Bevatron proton beam. A more exact determination will be attempted in the future, but up to the present it has not been possible to monitor reliably the amount of beam actually striking the target. Furthermore, the solid angle of acceptance of the detection apparatus may not be independent of Bevatron energy since the shape of the orbit on which the antiprotons emerge depends somewhat on the magnetic field strength within the Bevatron magnet. It has, however, been possible to measure the ratio of antiprotons to mesons (both at momentum 1.19 Bev/c) emitted in the forward direction from the target as a function of Bevatron energy. The resulting approximate excitation function is shown in the form of three experimental points in Fig. 5.

Even at 6.2 Bev, the antiprotons appear only to the extent of one in 44 000 pions. Because of the decay of pions along the trajectory through the detecting apparatus, this number corresponds to one antiproton in 62 000 mesons generated at the target. It will be seen from Fig. 5 that there is no observed antiproton production at the lowest energy. Although the production of antiprotons does not seem to rise as sharply with increasing energy as might at first be expected, the data indicate a reasonable threshold for production of antiprotons. It must again be emphasized that Fig. 5 shows only the excitation function relative to the meson excitation function, hence the true excitation function is not known at this time. If and when detailed meson production excitation functions become known, data of the type shown in Fig. 5 may allow a true antiproton production excitation function to be determined. It should also be mentioned that the angle of emission from the target actually varies slightly with Bevatron energy. At 6.2 Bev, it is 3°, at 5.1 Bev it is 6°, and at 4.2 Bev it is 8° from the forward direction at the Bevatron target.

Possible spurious effects.—The possibility of a negative hydrogen ion being mistaken for an antiproton is ruled out by the following argument: It is extremely improbable that such an ion should pass through all the counters without the stripping of its electrons. It may be added that except for a few feet near the target the whole trajectory through the apparatus is though gas at atmospheric pressure, either in air or, near the magnetic lenses, in helium gas introduced to reduce multiple scattering.

None of the known heavy mesons or hyperons have the proper mass to explain the present observations. Moreover, no such particles are known that have a mean life sufficiently long to pass through the apparatus without a prohibitive amount of decay since the flight time through the apparatus of a particle of proton mass is 10.2×10^{-8} sec. However, this possibility cannot be strictly ruled out. In the description of the new particles as antiprotons, a reservation must be made for the possible existence of previously unknown negative particles of mass very close to 1840 electron masses.

The observation of pulse heights in counters $S1$ and $S2$ indicates that the new particles must be singly charged. No multiply charged particle could explain the experimental results.

Photographic experiments directed toward the detection of the terminal event of an antiproton are in progress in this laboratory and in Rome, Italy, using emulsions irradiated at the Bevatron, but to this date no positive results can be given. An experiment in conjunction with several other physicists to observe the energy release upon the stopping of an antiproton in a large lead-glass Čerenkov counter is in progress and its results will be reported shortly. It is also planned to try to observe the annihilation process of the antiproton in a cloud chamber, using the present apparatus for counter control.

The whole-hearted cooperation of Dr. E. J. Lofgren, under whose direction the Bevatron has been operated, has been of vital importance to this experiment. Mr. Herbert Steiner and Mr. Donald Keller have been very helpful throughout the work. Dr. O. Piccioni has made very useful suggestions in connection with the design of the experiment. Finally, we are indebted to the operating crew of the Bevatron and to our colleagues, who have cheerfully accepted many weeks' postponement of their own work.

* This work was done under the auspices of the U. S. Atomic Energy Commission.

[1] G. Feldman, Phys. Rev. **95**, 1967 (1954).
[2] Evans Hayward, Phys. Rev. **72**, 937 (1947).
[3] Amaldi, Castagnoli, Cortini, Franzinetti, and Manfredini, Nuovo cimento **1**, 492 (1955).
[4] Bridge, Courant, DeStaebler, and Rossi, Phys. Rev. **95**, 1101 (1954).
[5] J. Marshall, Ann. Rev. Nuc. Sci. **4**, 141 (1954).

Observations of Negative *K*-Mesons and Charged Hyperons*

W. F. Fry, J. Schneps, G. A. Snow,† and M. S. Swami

Department of Physics, University of Wisconsin, Madison, Wisconsin

(Received August 31, 1955)

TWO pellicle stacks were exposed, in a negative K-meson channel of the Bevatron, to particles from a target bombarded by 6.2-Bev protons. The pellicles were area scanned for stars produced by stopped K^--mesons. Thirty stars were found in the first stack and have been described in detail previously.[1] In the second stack, 177 stars produced by stopped K^--mesons were found. A summary of the salient features of these 207 K^--meson stars is reported here.

The prong distribution of the K^--meson stars with one or more prongs is shown in Fig. 1. The stopped K^--mesons which produced zero-prong stars or stars with only a fast π meson, would not be detected with a high efficiency by the method of scanning that was employed. A few such cases were found but are not included in this report.

In many cases, charged π mesons, charged hyperons, and hyperfragments are observed from the K^--meson stars. The frequency of these events is summarized in Table I.[2]

In 15 cases the hyperon ejected from the K^- star was clearly positively charged because it decayed from rest or decayed in flight into a proton. In 12 cases the hyperon was clearly negatively charged because it produced a star from rest. In addition there were 3 events where a particle of nucleonic mass, from a K-meson star, came to rest in the emulsion with an associated low-energy electron at the ending. Although it is possible that some of these electrons may be

accidental coincidences, it seems more probable that these electrons resulted from the atomic capture of stopped negative hyperons. It is to be expected that an appreciable fraction of the stopped negative hyperons would not produce stars in emulsion.[1] We estimate that the probability of electron ejection by a negative hyperon and a μ^- meson is of the same order of magnitude, i.e., about 25%.[2] The number of zero-prong hyperon stars is thus estimated to be $3/0.25=12$. The ratio Σ^-/Σ^+ is estimated to be 1.5. If one uses the hypothesis of charge independence for the reactions

TABLE I. Frequency of various types of events.

Class	Number of stars	Remarks
Stars with charged π mesons	64	
Stars with hyperfragments	12	4 hyperfragments decayed mesonically.
Σ^+ decays into a π meson[a] from rest	5	
Σ^+ decays into a proton from rest	6	
Σ^+ decays in flight into a proton	4	In 3 of these 4 cases $v_p<v_\Sigma$. Therefore the possibility of inelastic proton scattering cannot be excluded. In all 4 cases the Q is consistent with a Σ^+ decay.
$\Sigma^\pm$ decays in flight into a $\pi^\pm$ meson[a]	5	
Σ^- stars produced from rest	12	11 of these stars have one prong, 1 has two prongs.
Tracks end with associated electrons	3	These particles are probably Σ^- hyperons which produced zero-prong stars.

[a] Minimum-ionizing particles from hyperon decays are assumed to be π mesons. None of these particles stopped in the emulsion.

that involve the Σ hyperons[1,4] the number of Σ^0 hyperons that were produced is estimated to be 23 [i.e., $\frac{1}{2}(\Sigma^++\Sigma^-)$]. All of the K^--meson stars without charged hyperons are consistent with the assumption that a neutral hyperon was produced in each case. The ratio of Σ hyperons to Λ^0 hyperons is found to be $66/141\cong 0.5$. The probability that a Λ^0 hyperon will be come trapped in a nuclear fragment and produce a hyperfragment is found to be $12/141\cong 9\%$.

It is found that about 70% of the stars with Σ hyperons have π mesons while about 37% of the K^--stars with Λ^0 hyperons have π mesons (π^0 mesons and Σ^0 hyperons are included in this estimate). The average energy of the π mesons from K^--stars with Λ^0 hyperons is considerably greater than the π-meson energy from stars with Σ hyperons. Because of this difference in energy, it is expected that more of the π mesons from stars with Λ^0 hyperons will be absorbed than from stars with Σ hyperons. This effect may partially explain the difference in the percentages (70 *vs* 37%).

Several facts suggest that the basic capture process for negative K-mesons is

$$K^-+\mathfrak{N}\rightarrow Y+\pi,$$

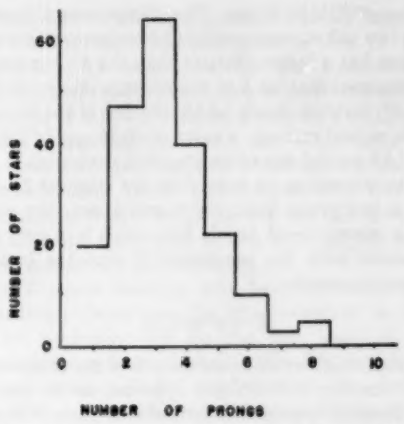

FIG. 1. The prong distribution of stars produced by stopped K^--mesons.

namely: (1) the relatively large number of stars with π mesons (~100 cases if π^0 mesons are included),[1,4] (2) the energy distribution of the charged hyperons, as shown in Fig. 2, strongly supports this reaction when the Fermi momentum of the nucleons is considered, and (3) in all cases the visible kinetic energy plus the π-meson rest mass is considerably less than the rest energy of the K^--meson.

A few of the energetic charged hyperons may be due to the absorption of the K-meson by two nucleons, although the possibility that they are due to capture by a single nucleon of high Fermi momentum cannot be excluded.

Since the detection efficiency for charged hyperon decays from K^--meson stars is very high, an unbiased estimate of the lifetime can be obtained. The combined lifetime of the Σ^+ and Σ^- hyperons is obtained from the 9 decays in flight by using the maximum-likehood method[5] and is found to be $(0.34_{-0.08}{}^{+0.14})\times 10^{-10}$ sec. A second method[6] of estimating the lifetime is to utilize both positive and negative hyperons which stop as well as those that decay in flight. This yields a lifetime of

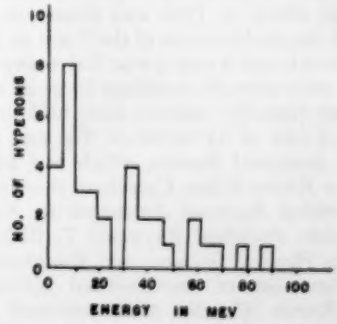

FIG. 2. The energy distribution of the charged hyperons.

$(1.41_{-0.27}^{+0.19})\times10^{-10}$ sec. The disagreement between these two values may possibly be understood if the Σ^- hyperon has a longer lifetime than the Σ^+ hyperon. If it is assumed that all 5 of the mesonic decays in flight were Σ^+, we then obtain for the lifetime of the Σ^+ alone, by the second method, a value of $(0.76_{-0.15}^{+0.19})\times10^{-10}$ sec.[7] (All quoted errors are standard deviations.)

It is interesting to note that the stopped Σ^- stars have a low prong multiplicity and a very low visible kinetic energy (~10 Mev). This result is in very good agreement with the prediction[8-11] that the basic Σ^- capture process is

$$\Sigma^-+p\rightarrow n+\Lambda^0.$$

In conclusion we reiterate that all of our observations on K^- mesons and charged hyperons are in excellent agreement with the predictions of Gell-Mann,[8] Nakano and Nishijima,[9] Pais,[10] and Sachs.[11]

The authors are indebted to Professor E. J. Lofgren for making the facilities of the Bevatron accelerator available to us. We are grateful to Mr. Roy Kerth for setting up the K-meson channel and assisting in the exposures. Mr. Donald Wold assisted in the scanning and analysis. Discussions with Professor R. G. Sachs and Professor G. Takeda were stimulating and helpful.

* Supported in part by the U. S. Atomic Energy Commission, and by the Graduate School from funds supplied by the Wisconsin Alumni Research Foundation.

† On leave of absence from Brookhaven National Laboratory.

[1] Fry, Schneps, Snow, and Swami, Phys. Rev. **100**, 939 (1955). Also, references to the work of others on K^--stars are given in this paper.

[2] Of approximately 600 tracks of nuclear particles from the K^--stars, only 20 left the emulsion stack.

[3] W. F. Fry, Nuovo cimento **10**, 490 (1953).

[4] K. M. Watson, Phys. Rev. **85**, 852 (1952).

[5] M. S. Bartlett, Phil. Mag. **44**, 249 (1953).

[6] Castagnoli, Cortini, and Franginetti, Nuovo cimento **12**, Suppl. **2**, 448 (1954).

[7] Dahanayake, Francois, Fujimoto, Iredale, Waddington, and Yasin, Nuovo cimento **1**, 888 (1955).

[8] M. Gell-Mann, Phys. Rev. **92**, 833 (1953).

[9] T. Nakano and K. Nishijima, Progr. Theoret. Phys. (Japan) **10**, 581 (1953).

[10] A. Pais, Physica **19**, 869 (1953); Nuovo cimento (to be published).

[11] R. G. Sachs, Phys. Rev. **99**, 1576 (1955), and private communications.

PHYSICAL REVIEW VOLUME 100, NUMBER 3 NOVEMBER 1, 1955

Proceedings of the American Physical Society

MINUTES OF THE MEETING HELD AT MEXICO CITY, MEXICO, AUGUST 29–31, 1955

(Corresponding to *Bulletin of the American Physical Society*, Vol. 30, No. 5)

THE second Mexico meeting of the American Physical Society was held on the last three days of August, 1955. Those who had for five years been looking forward to a repetition of the 1950 Mexico meeting were amply gratified, and those who came for the first time experienced pleasures beyond what they could have foreseen. This was our first joint meeting with the Sociedad Mexicana de Física, which in 1950 was still in a nascent state. This was also our first meeting in the Ciudad Universitaria, which in 1950 was mostly an empty field with the steel skeleton of the Torre de Ciencias rising above it and is now a vast University campus adorned with splendid buildings in great number. All of our scientific sessions were held in one or another of four of its buildings. The first of them was the Inaugural Session, which was addressed in turn by Rector Nabor Carrillo of the University —Universidad Nacional Autónoma de Mexico is its full title; President Raymond T. Birge of the American Physical Society; and President Carlos Graef Fernandez of the Sociedad Mexicana de Física. Rector Carrillo then returned to the rostrum and formally opened our convention in the name of the President of the Republic, Adolfo Ruiz Cortines.

No distinction was made between the two Societies in arranging the programme: that is to say, papers both invited and contributed were distributed according to their topics, regardless of the affiliation of the speakers. Nearly all of the papers were given in English, a somewhat humiliating testimonial to the lesser competence of "norteamericanos" in mastering a foreign tongue. Professor S. A. Korff, however, gave an invited paper in Spanish, "El orígen de los rayos cosmicos," and also a few contributed papers were given in the language of the host country. All abstracts were rendered into Spanish and published in that language in a special issue of the *Revista Mexicana de Física*, by courtesy of the Sociedad and of Dr. Marcos Moshinsky, its editor. Nearly all of the invited papers pertaining to cosmic rays were chosen from the elementary-particle side of that fascinating field, for the remainder was the theme of the International Cosmic-Ray Congress held in the following week at Guanajuato. To this Congress our members were graciously invited.

The registration at the meeting amounted to 287, of which 66 were from Mexico and all but a few of the others from the United States. The gain over 1950 was about 40%; the Secretary is convinced that it would have been much greater but for the competition of several important congresses in Europe.

The banquet of the Society was held in the Jockey Club on Wednesday evening with an attendance of 120. The after-dinner speakers were Rector Nabor Carrillo and Dr. Manuel Sandoval Vallarta. This banquet will be happily remembered for the quality of the speeches and the quality of the food, the cocktails, and the wines, and the sumptuous décor.

It was perfectly obvious that a considerable expense had been incurred by those who arranged this fine meeting. Despite our solicitations, no part of this expense was met by the American Physical Society. We are informed that contributions, in amounts unrevealed to us, were made by the Universidad Nacional Autónoma de Mexico, the Instituto de Geofísica, Ingenieros Civiles Asociados, and Philips Set. Our gratitude is due to all. A cocktail party was given by the University on Tuesday afternoon. The ladies enjoyed the privilege of a tour of the University, a tour of distinguished homes in the neighborhood, and other excursions. For these they are indebted to Señora Carlos Graef Fernandez and those who helped her. Words of appreciation must also be spoken for the secretarial staff and for the many others who helped us and whose names we do not know.

No Council meeting was held at Mexico, and accordingly there is no list of elections to be given.

This probably will be the last issue of these Proceedings to be published in *The Physical Review*. Future issues will be published in the *Bulletin*. The abstracts of the remaining meetings of 1955 will be published in the *Review*.

KARL K. DARROW, *Secretary*
American Physical Society
Columbia University
New York 27, New York

Errata Pertaining to Abstracts F6 and Y12

F6, by W. E. Dreger, L. D. McIsaac, J. L. Mackin and J. R. Lai. In line 9 instead of "gamma rays of low intensity have been found at energies of 570 kev and 77 kev," read "gamma rays of low intensity have been found at energies of 570 kev and 770 kev."

Y12, by Richard A. Ferrell. In line 4 instead of "several times larger" read "many times larger." In line 15 instead of "5.2×10^{-10} sec" read "5.2×10^{-9} sec." In line 16 instead of "2.3×10^{-10} sec" read "1.3×10^{-9} sec."

PROGRAMME

MONDAY MORNING AT 10:30

Auditorio de Humanidades

(R. T. BIRGE AND CARLOS GRAEF FERNANDEZ presiding)

Inaugural Session

Addresses of Welcome and Response

A1. El Origen de los Rayos Cosmicos. S. A. KORFF, *New York University.* (50 min.)

MONDAY AFTERNOON AT 15:00

Auditorio de Humanidades

(CARLOS GRAEF FERNÁNDEZ presiding)

Invited Papers

E1. The Teaching of Physics in Mexico. SALVADOR MOSQUEIRA R., *Centro de Documentacion Cientifica y Tecnica, S. E. P. Unesco.* (30 min.)

E2. Experimental Nuclear Physics in the University of Mexico. FERNANDO ALBA ANDRADE, *Universidad de Mexico.* (30 min.)

E3. Nuclear Energy Levels Observed from Inelastic Proton Scattering Experiments. W. W. BUECHNER, *M.I.T.* (30 min.)

E4. Neutron Experiments with a Van de Graaff Generator. E. L. HUDSPETH, *University of Texas.* (20 min.)

E5. Dynamic Compressions for Some Twenty-Five Solids and Liquids at Explosively Attainable Pressures. J. M. WALSH, *Los Alamos Scientific Laboratory.* (30 min.)

MONDAY AFTERNOON AT 15:00

Auditorio de Ciencias

(R. F. BACHER presiding)

Invited Paper

F1. Relative Stability of Even Mass-Number Isobars. J. D. KURBATOV, *Ohio State University.* (20 min.)

Radioactive Nuclei

F2. Decay of Ne^{23}.† J. R. PENNING AND F. H. SCHMIDT, *University of Washington.*—We have studied the beta- and gamma-ray spectra of 40-sec[1] Ne^{23} with stilbene and NaI scintillation spectrometers using a fast-slow coincidence arrangement and a 20-channel analyzer. The active neon was produced by the $Na^{23}(d,2p)$ reaction on a NaCl target in the University of Washington 60-inch cyclotron. The gas was swept through a liquid nitrogen charcoal trap to a remote source chamber by means of a continuous flow system. Two gamma rays with energies of 436 kev and 1647 kev and relative intensities of 1.0 and 0.04, respectively, are in coincidence. These transitions can be identified with known energy levels in Na^{23}. Several higher-energy gamma rays may be present with a total intensity less than 0.4% of the 436-kev gamma. Approximately 70% of the beta transitions (end point = 4.40±0.05 Mev) lead to the ground state. Another 29% (end point = 3.95±0.05 Mev) are in coincidence with the 436-kev gamma. Lower-energy beta rays (end point ~2.4 Mev) are in coincidence with the 1647-kev gamma. Work on this isotope is still in progress.

† Work supported in part by the U. S. Atomic Energy Commission.

[1] H. Brown and V. Perez-Mendez, Phys. Rev. **78**, 812 (1950).

F3. Decay of $Neon^{24}$.† B. J. DROPESKY AND A. W. SCHARDT, *Los Alamos Scientific Laboratory.*—The new nuclide Ne^{24} has been produced by bombarding neon gas with 1.83-Mev tritons, the reaction being $Ne^{22}(t,p)Ne^{24}$. The β- and γ-scintillation spectrometers with coincidence circuits were used to study this activity. The Ne^{24} half-life is 3.4±0.1 min. The daughter activity, Na^{24}, was identified. The γ rays of 471±5 and 875±10 kev were observed (relative intensity 10:1). The former corresponds to the first excited state (472±8 kev)[1] of Na^{24}; their sum corresponds to the third excited state (1341 ±8 kev).[1] Fermi analysis of the β spectrum resolved a strong group of 1.95 Mev and a very weak group of ~4.3 Mev. The 875-kev γ ray was observed to be coincident with β radiation

but the 471-kev γ ray was found coincident with neither β nor γ radiation. These data can be interpreted as follows: about 90% of the Ne^{24} disintegrations proceed by the 1.95-Mev β transition to the 471-kev level in Na^{24}. The remaining 10% reach this level via the 875-kev transition. The absence of coincidences with the 471-kev γ ray indicates that this level is isomeric. The high-energy β group is probably a β transition from the 471-kev level to the 1.38-Mev level of Mg^{24} (energy difference 4.61 Mev).

† This work performed under the auspices of the U. S. Atomic Energy Commission.
[1] A. Sperduto and W. W. Buechner, Phys. Rev. **88**, 574 (1952).

F4. Gamma Energies in Tc^{97} following K Capture in Ru^{97}. J. M. Cork, M. K. Brice, L. C. Schmid, and R. G. Helmer, *University of Michigan.*—Ruthenium enriched in mass 96 from its normal 5.7% up to 95.5% was placed in the maximum flux of the Argonne pile for both short and long irradiations. Studies were made with both magnetic photographic and scintillation spectrometers. Strong conversion electron lines were observed from which several gamma rays not previously reported were evaluated. Gamma rays with energies of 109.1, 216.1, 325.1, and 570 kev decay with the half-life of Ru^{97} which appears to be 2.44 days. Other highly converted gamma rays with energies of 90.2 and 99.2 kev decay with a longer life, presumably associated with Tc^{97m}. The multipolarities of most transitions are determined and a reasonable nuclear level scheme proposed.

F5. Investigation of I^{128}. N. Benczer, B. Farrelly, L. Koerts, and C. S. Wu, *Columbia University.*—The β and γ radiations of I^{128} have been investigated and its decay scheme proposed. Three β groups were found with energies 2.120, 1.665, and 1.140 Mev and relative abundance 82.2%, 15.8%, and 2.03%, respectively. The γ radiation was investigated with a single channel and a selective coincidence scintillation spectrometer. Four γ radiations were found with energies 0.455, 0.540, 0.750, and 0.980 Mev and relative intensities 100:9.7:1.7:1.8, respectively. The 0.455-Mev and 0.540-Mev γ rays are in coincidence and in the β branch. The 0.980-Mev line is the crossover radiation. The 0.750-Mev line is in coincidence with the Te X-rays, hence in the electron capture branch of the decay. The relative intensities of these γ radiations obtained from coincidence measurements agree with those obtained from the single spectrum analysis. It was also determined that the branch of $(K+L)$-capture is only 6.4% of the total decay. Furthermore the ratio of K-capture to the first excited state to that to the ground state of Te is about 1:20. From the calculated ft values one can assign spin and parity 1^+ to the ground state of I^{128}. These results are in very good agreement with the predictions based on the regularity of nuclear energy levels of even-even nuclei in the region $66<A<150$.[1]

[1] G. S. Goldhaber and J. Weneser, Phys. Rev. **98**, 1186 (1955).

F6. Radioactive Decay of W^{181} and W^{185}. W. E. Kreger, L. D. McIsaac, J. L. Mackin, and J. R. Lai, *U. S. Naval Radiological Defense Laboratory.*—The decay of W^{181} and W^{185} has been studied using beta- and gamma-ray scintillation spectrometers and ion chamber detectors. A W source from Oak Ridge was used in which both activities were present. The beta decay of W^{185} was followed and found to have a half-life of 74.5 days in agreement with values mentioned in the literature. Gamma rays of low intensity have been found at energies of 570 kev and 77 kev using a large crystal NaI spectrometer. The half-life for decay of these gammas appear to agree with the half-life for the beta dacay. There is a strong x-ray of 59.5 kev which has a half-life of around 110 days. This x-ray most probably follows the K-capture decay of W^{181} to Ta^{181}. A decay scheme will be proposed for these isotopes.

F7. Decay of Pt^{191}.† E. P. Tomlinson and R. A. Naumann, *Princeton University.*—Further spectrometer data are reported from Pt fractions separated from Ir after bombardment by deuterons in the Brookhaven cyclotron. These confirm the γ rays reported earlier[1] of 42, 82, 97, 129, 172, 179, 221, 268, 352, 361, 410, 458, 540, and 626 kev, and support the Pt^{191} decay scheme proposed earlier by us and independently, but in large part identically, by Cork *et al.*[2] The 42-kev transition is clearly present, with the 2.7-day Pt^{191} half-life, in Pt separated from deuteron bombarded Ir. Also fitting the proposed decay scheme we now find evidence for γ rays of 47, 188, 447, 496, and 543 kev. In addition, we find conversion lines assignable to γ rays of 219, 223, 267, 271, 571, 585, and 590 kev which do not fit the proposed decay scheme, but which all follow the characteristic half-life of Pt^{191}. Work is continuing in an attempt to find the positions for these latter transitions. Some graphic examples of effects of source and backing thickness will be presented.

† This work was supported by the U. S. Atomic Energy Commission and the Higgins Scientific Trust Fund.
[1] Tomlinson, Naumann, and Mihelich, Phys. Rev. **94**, 794 (1954).
[2] Cork, Brice, Schmid, Hickman, and Nine, Phys. Rev. **94**, 1218 (1954).

F8. Gamma-Gamma Directional Correlations in Cs^{134}.† A. E. Everett and M. J. Glaubman, *Princeton University.*—We have found the directional correlations of the 1.37–0.605, 1.17–0.801, and 0.796–0.605-Mev cascades in the decay of Cs^{134} to be given by: $A_2=0.107$, 0.095, and 0.111, ± 0.015, $A_4=0.015$, 0.006, and 0.016, ± 0.02, respectively. All of these values are consistent with 4-2-0 cascades, and agree with the decay scheme suggested by Cork *et al.*[1] In this case the five observed gamma rays are $E2$, the excited states of Ba^{134} are at 0.605 (2+), 1.17 (2+), 1.40 (4+), and 1.97 (4+) Mev, and the 0.563-Mev $E2$ transition[2] is between the second and first excited states and is speeded up by a factor of 15 compared to the crossover. All this is very typical to even-even nuclei in this region. However, the decay scheme of the Washington group[3] cannot be completely excluded, since a 4-2-0 directional correlation can also be interpreted as due to a 3-2-0, 3-1-0, or 2-2-0 cascade in which the first transition is mixed.

† This work was supported by the U. S. Atomic Energy Commission and the Higgins Scientific Trust Fund.
[1] Cork, Le Blanc, Nester, Martin, and Price, Phys. Rev. **90**, 444 (1953).
[2] Keister, Lee, and Schmidt, Phys. Rev. **97**, 451 (1955).

F9. Directional Correlation of the Cd^{111} Gamma-Gamma Correlation with Gaseous In^{111} Sources.* L. M. Noble and R. M. Steffen, *Purdue University.*—Using differential pulse-height selection to eliminate scattering effects, the Cd^{111} gamma-gamma directional correlation as displayed by gaseous sources of $InCl_3$ and InI_3 has been measured. Gaseous $InCl_3$ exhibits a directional correlation, $W(\theta)=1-(0.105\pm 0.005)\times P_2(\cos\theta)$, whose anisotropy is between the one of the correlation displayed by dilute aqueous solutions of $InCl_3$, $W(\theta)=1-(0.172\pm 0.003)P_2(\cos\theta)$, and the one displayed by polycrystalline $InCl_3$, $W(\theta)=1-(0.033\pm 0.003)P_2(\cos\theta)$. Gaseous InI_3 shows a considerably smaller anisotropy of the directional correlation than gaseous $InCl_3$. Measurements at different pressure and temperature values indicate that in both cases the correlation is independent of the collision rate of the molecules in the gas within the range of about 100 to 1000 collisions per lifetime of the intermediate nuclear state. Preliminary results of delayed correlation measurements indicate a time-dependent interaction mechanism in the gaseous sources.

* Supported by the U. S. Atomic Energy Commission.

MONDAY AFTERNOON AT 15:00

Auditorio de Comercio

(MARCOS MOSHINSKY presiding)

Theoretical Physics, I

G1. Nucleon Distribution in Ca^{40}. J. CALLAWAY AND R. D. WOODS, *University of Miami.*—The independent particle model has been applied to a calculation of the distribution of nucleons in Ca^{40}. A square-well potential was chosen of 40-Mev depth and radius $1.4\times10^{-13}A^{\frac{1}{3}}$ cm, which yields approximately correct binding energy for the last neutron. Spin orbit coupling was included by a term proportional to the radial derivative of the potential. This gives a delta function which produces a discontinuity in the radial derivative of the wave functions at the boundary. The inclusion of this term produces significant though small changes in the calculated nucleon distribution. Coulomb effects have been studied by perturbation theory. For this nucleus (and generally for $N=Z$ nuclei), the percentage of protons outside the well is greater than the percentage of neutrons. From this nucleon distribution a new potential well is constructed. This can be used to calculate a more self-consistent distribution.

G2. Model for the Potential between Nucleon and Nucleus. C. L. CRITCHFIELD AND ROBERT LOWEN, *University of Minnesota.**—Interaction between a neutron and a nuclear core (mass A) is assumed to vanish at mutual separation $>R$ and to vary as $-V_n+a_nr^2$ when $r\leq R$. Given R, values of V_n and a_n are found such as: (1) give the observed separation energy and (2) permit continuation of ordinary oscillator wave functions inside onto Hankel functions outside $r=R$. For a proton interacting with the core, the same radius R is assumed but different constants V_p and a_p are found to get the proper separation energy and so as to continue oscillator functions onto Coulomb wave functions outside. To estimate R the model was applied to the "mirror" nuclei where the difference in harmonic potentials is mainly that of a uniformly charged sphere acting only on the proton. The results fit well with the accepted radii but the average potentials vary markedly. Magic (core) numbers 16 and 40 show very deep potentials, but there is a steady weakening between 16 and 28. The purpose of the model is to facilitate isolation of the spin-orbit, symmetry, and other effects through the use of well-known wave functions.

* Present address: CONVAIR, San Diego, California.

G3. Poles of the *S*-Matrix for the Cloudy Crystal Ball Model. JUAN MANUEL LOZANO, *Instituto de Física, México.*—Feshbach, Porter, and Weisskopf[1] have proposed a model for nuclear reactions with neutrons, in which the interaction is given by a complex potential $V=-V_0(Hi\xi)$. Using this potential, we obtained the R- and S-functions associated with this model, and we have discussed the analytic properties of these functions. Because of the imaginary part in the potential, the R-function has the analytic properties discussed by Wigner[2] only in certain regions of the energy complex plane. Therefore, the allowed regions for poles of the S-function are modified, but in such a way that a dynamical description[3] of the scattering is still possible.

[1] Feshbach, Porter, and Weisskopf, Phys. Rev. 96, 448 (1954).
[2] E. P. Wigner, Ann. Math. 53, 36 (1951).
[3] J. M. Lozano, Rev. fis. Méx. 2, 155 (1953).

G4. Electric Quadrupole Moment and Corrections to the Magnetic Moment of the Deuteron for Velocity Dependent Tensor Forces. L. ESTRADA, *Instituto de Física, México.*—Recently, Moshinsky[1] has introduced in the equations of motion for two nucleons, velocity dependent central and tensor forces, and for certain cases these equations are soluble in terms of known functions. Following this formalism, the electric quadrupole moment and the correction to the magnetic moment of the deuteron are calculated in an explicit fashion due to the simple form of the wave function. In particular, the effect of changes in the velocity dependent tensor force on these moments are analyzed. With the results obtained here, and those for neutron-proton scattering mentioned in the following abstracts, we expect to determine the values of the parameters that appear in the velocity dependent central and tensor forces.

[1] M. Moshinsky, J. phys. et radium 15, 264 (1954).

G5. Scattering Length and Effective Range for Velocity Dependent Tensor Forces. A. MONDRAGÓN, *Instituto de Física, México.*—The interactions between two nucleons for position dependent central and tensor forces have been discussed by Chew and Goldberg[1] and by Christian.[2] In the present paper, we apply their formalism to the case when the interaction between the two nucleons is given by the velocity dependent central and tensor forces, recently proposed by Moshinsky.[3] We obtain a development of $k\cot\delta$ in a power series of the energy, whose coefficients depend only on the wave functions at zero energy. In particular, we obtain the scattering length and effective range, in terms of the parameters that appear in the velocity dependent potentials.

[1] G. F. Chew and L. Goldberg, Phys. Rev. 75, 1637 (1949).
[2] R. S. Christian, Phys. Rev. 75, 1675 (1949).
[3] M. Moshinsky, J. phys. et radium 15, 264 (1954).

G6. Scattering by a Velocity-Dependent Potential. IGNACIO RENERO, *Instituto de Física, México.*—In a recent paper, Moshinsky[1] has considered the problem of the velocity-dependent tensor force, obtaining the form of the potential as well as the solutions to the wave equations and the boundary conditions on the spherical surface defined by the range of the tensor force. Taking into account these results, the scattering of a nucleon by a velocity dependent tensor force is analyzed in the present paper, following the general outline of Wigner and Eisenbud.[2] Since the wave function, but not its derivative, is continuous over the spherical surface, it proves to be advantageous to define an R-matrix for the interior region which, in turn, makes it possible to obtain the usual R-matrix, taking into account the boundary conditions. Making use of the well-known relations between the R- and S-matrices, the S-matrix is calculated. In addition, some of the analytic properties of these matrices are studied. Finally, the R-matrix is expanded in terms of the energy in order to identify the coefficients of the expansion with those effective range and scattering length obtained by Mondragón in the preceding abstract.

[1] M. Moshinsky, J. phys. et radium. 15, 264 (1954).
[2] E. Wigner and L. Eisenbud, Phys. Rev. 72, 29 (1947).

G7. Polarization in the Theory of the Giant Resonances of Neutron Scattering. A. M. LANE AND L. VERLET, *M.I.T.*—If the neutron-nucleus interaction is represented as an average potential well, the neutrons cannot lose energy so there is no absorption. The total wave function is simply a product of the target and single-particle wave functions. The effect of the neglected interactions is to cause the absorption of this

initial state into the compound nucleus states. A measure of this process, related to the absorption potential, can be defined as the root of the expectation value of the square of the neglected interactions taken in the initial state. This turns out to be ~20 Mev and energy independent.[1] Professor Wigner suggested that this large value results from not including polarization effects in the initial state. We have tried to express such effects by multiplying the previous initial state with a two-body correlation function which should represent those previously neglected interactions that, in the language of Brueckner, give rise to coherent scattering processes. The foregoing value has been reduced by this device to 12 Mev (10 Mev with exchange).

[1] Lane, Thomas, and Wigner, Phys. Rev. **98**, 693 (1955).

G8. Nucleon-Nucleus Interaction with Polarization. ERICH VOGT, *Princeton University.*—The giant resonances of the average total neutron cross sections have been interpreted by Lane, Thomas, and Wigner[1] in terms of maxima in the nucleon-nucleus interaction. In their model, the second moment of the reduced width distribution, about these maxima, is given by the expectation value, for the ground state, of the square of the nucleon-nucleus potential V, which mixes the single-particle states into the other states of the shell model. The square root of this second moment may be roughly equal to the half-width of the reduced width distribution. If so, the value of (20 Mev)[2] obtained for the second moment by Lane, Thomas, and Wigner is much too large. As suggested by Professor Wigner, the calculation of the second moment was modified by introducing a part of V into the definition of the target nucleus wave functions. This introduces nucleon-target correlations into these wave functions. The value of the second moment is reduced to (12 Mev)[2]. This result agrees with that of Lane and Verlet[2] who used a somewhat different approach to the same problem.

[1] Lane, Thomas, and Wigner, Phys. Rev. **98**, 693 (1955).
[2] A. M. Lane and L. Verlet (preceding abstract).

G9. Low-Energy Neutron Scattering and the Bound State Problem.* R. D. LAWSON, *University of California, Berkeley.* The hyperbolic potential, $V(r) = -V_0/\cosh^2\alpha r$, has been used to examine the position of the zero-energy S-wave resonances as a function of A. For $V_0 = 125$ Mev, $\alpha_0 = \alpha A^{\frac{1}{3}} = 1.71 \times 10^{-13}$ cm^{-1}, the zero-energy S-wave resonances occur at $A \sim 15$, 58, 148, in good agreement with experiment. Furthermore, the $2S$-state at $A = 32$ is bound by 6.4 Mev and the $3S$-state at $A = 140$ is bound by 8 Mev. The rms radius from this potential is $\sim 0.78 \times 10^{-13}$ cm, which is about 15% smaller than indicated by the electron scattering measurements. However, this potential drops off too rapidly and will not bind the high angular-momentum states in heavy nuclei. We have also examined potentials of the form $V(r) = -V_0[1-(1-e^{-\alpha r})^n]$ where n is integer ≥ 2. For $n = 4$, $V_0 = 116$ Mev, and $\alpha_0 = 3.34 \times 10^{13}$ cm^{-1}, we can fit the S-wave resonances and S-state binding energies; however, again the higher angular-momentum states are not bound. We estimate that in order to bind the high angular-momentum states with such a potential, the exponent n must be ~10, indicating an extremely flat nuclear potential.

* Supported by the Office of Ordnance Research, U. S. Army.

G10. (Abstract withdrawn.)

MONDAY AFTERNOON AT 15:00

Auditorio de Ingeniería

(NABOR CARRILLO presiding)

Symposium of the Division of Fluid Dynamics

Fluid-Dynamics Problems in Geophysics

H1. Fluid Dynamics Problems in Geophysical Sciences (Los Problemas de la Dinámica Fluída en las Ciencias Geofísicas). FRANÇOIS N. FRENKIEL, *Applied Physics Laboratory, Johns Hopkins University.* (30 min.)

H2. Earthquake Surface Waves in the Period Range 1–500 Seconds. MAURICE EWING, *Columbia University.* (30 min.)

H3. The Dynamics of Equatorial Waves in the Ocean (La Dinámica de las Ondas Ecuatorialas en el Océano). GORDON W. GROVES, *Scripps Institution of Oceanography.* (30 min.)

H4. Progress in Hydromagnetism. W. M. ELSASSER, *University of Utah.* (30 min.)

H5. Fluid Motions in the Terrestrial Atmosphere. N. C. GERSON, *Geophysics Research Directorate.* (30 min.)

TUESDAY MORNING AT 9:00

Auditorio de Ingeniería

(F. E. GODDARD, JR. presiding)

Symposium of the Division of Fluid Dynamics

J1. Transient Surface Temperatures in the Shock Tube. WALKER BLEAKNEY, *Princeton University.* (30 min.)

J2. Stochastic Aspects of Classical Dynamics. HAROLD GRAD, *New York University.* (30 min.)

J3. New Light on the Boundary Layer Transition Problem. G. B. SCHUBAUER, *National Bureau of Standards.* (30 min.)

J4. A Dynamic Model for the Viscous Sublayer of a Turbulent Flow along a Smooth Boundary. H. A. EINSTEIN, *University of California, Berkeley.* (30 min.)

J5. Similarity Laws for the Nonequilibrium Turbulent Boundary Layer. DONALD COLES, *California Institute of Technology.* (30 min.)

TUESDAY MORNING AT 9:30

Auditorio de Humanidades

(R. PEPINSKY presiding)

Invited Papers in Solid-State Physics

K1. Cyclotron Resonance in Semiconductor Crystals. CHARLES KITTEL, *University of California, Berkeley.* (30 min.)

K2. The Silicon Solar Battery. G. L. PEARSON, *Bell Telephone Laboratories.* (30 min.)

K3. Perdida de energia por electrones en cuerpos solidos. L. MARTON, *National Bureau of Standards.* (30 min.)

K4. Recent Progress in Energy-Band Theory. J. C. SLATER, *M.I.T.* (30 min.)

K5. X-Ray Absorption Edges and Chemical Binding. H. P. HANSON, *University of Texas.* (30 min.)

TUESDAY MORNING AT 9:30

Auditorio de Ciencias

(H. S. BRIDGE presiding)

Cosmic Rays; "Elementary" Particles

L1. Interplanetary Magnetic Fields and Cosmic Rays. LEVERETT DAVIS, JR., *California Institute of Technology.*—The often postulated magnetic field of 10^{-4} gauss along a spiral arm of the galaxy seems not to penetrate the solar system, since low-energy cosmic rays occasionally reach the earth from the sun. A field free cavity extending to roughly 10^{2} to 10^{3} times the radius of the earth's orbit would be expected by magneto-hydrodynamics if the sun emits corpuscular radiation at the rate given by Biermann.[1] Such a cavity would trap cosmic rays with energy less than 10^{11} ev for many sunspot cycles. Expected variations over a cycle in cavity radius could explain the 4% variation in cosmic-ray intensity found by Forbush.[2] A solar origin of all cosmic rays seems inconsistent with the energy spectrum and the presence of very high-energy particles. With a galactic origin the cavity would explain the absence of primary electrons and perhaps part but not all of the cutoff at low energies. A solar magnetic field introduces some complications but seems likely to be confined to polar regions by the corpuscular radiation.

[1] Z. Astrophys. **29**, 274 (1951).
[2] J. Geophys. Research **59**, 525 (1954).

L2. On the Absence of Meteorological Effects on the World-Wide Sunspot Variation in Cosmic-Ray Ionization. SCOTT E. FORBUSH, *Carnegie Institution of Washington.*—The world-wide sunspot variation in annual means of cosmic-ray ionization has been reported,[1] and it was shown that this variation did not arise from transient decreases in cosmic-ray intensity which sometimes accompany magnetic storms. The question arises whether variations with solar cycle in the height of the 100-millibar pressure level could explain, through μ-meson decay effects, the sunspot variation in cosmic-ray ionization. The average seasonal wave in cosmic-ray intensity at Cheltenham has an amplitude of 1.45% and is opposite in phase to the average seasonal wave, amplitude 260 m, in the height of the 100-millibar pressure level derived from U. S. Weather Bureau radiosonde data for the period 1944–53. The ratio of these amplitudes gives 5.6% decrease in cosmic-ray intensity per kilometer increase in height of the 100-millibar level. The range in annual mean heights of the 100-millibar level (1944–53) was only 75 m and these exhibited no variation with solar cycle. Thus the sunspot variation in cosmic-ray intensity does not arise from this cause.

[1] S. E. Forbush, Phys. Rev. **98**, 1163 (1953).

L3. High-Altitude Cosmic-Ray Neutron Intensity Variations.* R. K. SOBERMAN AND S. A. KORFF, *New York University.*—Three groups of balloon flights carrying boron trifluoride counters were made from geomagnetic latitudes 10.1°N, 55.1°N, and 88.6°N.[1] From the data obtained, curves of neutron intensity *versus* atmospheric depth for depths less than 700 mb are plotted. The mean absorption lengths for neutrons in the equilibrium portion of the atmosphere were found to be $L(10.1°)=212$ g/cm², $L(55.1°)=164$ g/cm², and $L(88.6°)=164$ g/cm². The depths of the neutron intensity maxima were found to be $\theta_{max}(10.1°)=120\pm5$ mb, $\theta_{max}(55.1°)=100\pm5$ mb, and $\theta_{max}(88.6°)=75\pm5$ mb. From these results and those of other investigators, a family of curves of neutron intensity *versus* atmospheric depth is drawn for geomagnetic latitudes at 10-degree intervals between 0° and 90°N. From this the low-energy neutron capture per square centimeter per second by the $N^{14}(n,p)$ reaction in the atmosphere is calculated and plotted as a function of geomagnetic latitude. It is found that the observed neutron intensity varies by about 420% from 0° to 90°N. A value of 5.8×10^{18} sec^{-1} is obtained for the total number of low-energy neutrons captured in the atmosphere.

* Supported by a joint program of the U. S. Atomic Energy Commission and the Office of Naval Research.
[1] Neuburg, Soberman, Swetnick, and Korff, Phys. Rev. 97, 1276 (1955).

L4. Charge with Time of the Low-Energy Part of the Cosmic-Ray Spectrum.* H. V. NEHER, *California Institute of Technology.*—By comparing results of balloon flights carrying ionization chambers to high altitudes at different phases of the solar cycle, it is possible to arrive at an estimate of the energy distribution of that part of the primary cosmic-ray spectrum that varies. It is concluded that all of the major types of cosmic-ray changes are similar and are probably caused by the same mechanism. The action of this mechanism is such that low-energy particles are primarily affected. The evidence is that during the summer of 1954, when the sun was very inactive, this modulating mechanism was so ineffective that not only were very low-energy cosmic-ray particles allowed to come into the earth but that the fluctuations near the geomagnetic pole were also very low. Both of these experimental facts are consistent with Forbush's finding of a 180° phase shift between solar activity and cosmic-ray intensity.

* Assisted by the joint program of the Office of Naval Research and the U. S. Atomic Energy Commission.

L5. Observations on Pion Tracks in a Liquid Hydrogen Bubble Chamber.* D. E. NAGLE AND R. H. HILDEBRAND, *University of Chicago.*—A liquid hydrogen bubble chamber has been successfully operated in an external pion beam of the Chicago cyclotron. Photographs of good quality showing tracks due to 100-Mev negative pions will be presented. The use of this equipment to study pion-nucleon interactions will be discussed.

* Research supported by a joint program of the Office of Naval Research and the U. S. Atomic Energy Commission.

L6. Nonmesonic Decay of a Helium Hyperfragment. B. STILLER, N. SEEMAN, AND M. M. SHAPIRO, *Naval Research Laboratory.*—In a G.5 emulsion stack exposed to the cosmic rays in an equatorial balloon flight, we have observed an event which is most simply interpreted as the disintegration of a ^{4}He* hyperfragment according to the scheme $^4\text{He}^*\rightarrow p+d+n+Q$, where $Q=167.7\pm2.9$ Mev. From the Q-value and the relevant masses, the binding energy of the Λ^0 in the fragment is 1.7 ± 2.9 Mev, in agreement with values previously obtained from mesonic disintegrations of ^{4}He*. This low binding energy may be compared to the much larger value, 20.6 Mev, with which the "last neutron" is bound in normal He^4. The energy of the proton was 114.7 ± 2.7 Mev, that of the deuteron, 36.3 ± 0.2 Mev, and that of the neutron (from conservation of momentum) 16.7 ± 0.8 Mev. The fragment, emerging from a star of type $11+7_a$ (in the Bristol notation), traveled 633 μ before coming to rest. All the measurements, including those on the fragment track, are consistent with the foregoing decay scheme. Other interpretations are considered and are shown to be very unlikely.

L7. Interactions of Negative *K*-Particles at Rest.* WARREN W. CHUPP, GERSON GOLDHABER, SULAMITH GOLDHABER, AND FRANCIS H. WEBB, *University of California, Berkeley.*—The 6.1-Bev proton beam of the Berkeley bevatron incident on a 0.9-in.-thick copper target produces a K-particle beam which enters a magnetic strong-focusing and analyzing system placed at 90° to the proton mean.[1] Stacks of Ilford G.5, 600 μ stripped pellicles have been exposed to the K^--particles of momenta 350 Mev/c and 410 Mev/c. The proper time of flight is approximately 10^{-8} sec for these particles. The K^--endings in the emulsion were found by the method of following along the track from the incident edge all particles of $2\times$minimum ionization. Twenty-two cases of K^--stoppings have been recorded to date. They may be described as follows: (1) six capture stars which definitely emit π mesons and three possible additional cases; (2) one definite case of Σ^+ emission associated with π emission; (3) one possible Σ^+ with no π associated; (4) two possible cases of Σ^- emission (one of these is associated with π emission); (5) one $K^-\rho$; (6) ten cases where no π or Σ is observed. All these events will be discussed in further detail.

*This work was performed under the auspices of the U. S. Atomic Energy Commission.
[1] Kerth, Stork, Birge, Haddock, and Whitehead, Bull. Am. Phys. Soc. 30, No. 3, 41(A) (1955).

L8. Decay of an Anomalous Charged *K*-Meson.* E. M. HARTH† AND M. M. BLOCK,‡ *Duke University.*—The decay of a positively charged particle was observed in the gas of a 20-atmosphere hydrogen-filled diffusion cloud chamber operated in an external 2.7-Bev proton beam of the Cosmotron.[1] The particle came from the wall, traveled 15 cm, and decayed through an angle of $111.5\pm1.0°$. Both primary and secondary were estimated to have specific ionization $I=2\pm\frac{1}{2}$. A unique feature of this event is that, both from visual estimates and microphotometer measurements, both fragments appeared to have *equal* ionizations (independent of absolute values). The primary and secondary momenta were 500 ± 25 and 87 ± 5 Mev/c. The secondary is identifiable as an L-meson, while from absolute ionization and momentum the primary has an estimated mass between 1150 and 1650 m_e. Taking the ionizations of primary and secondary as *equal*, from momentum ratios we deduce primary masses of 1575 ± 95 and 1210 ± 75 m_e, if the secondary is a pion or muon, respectively. Assuming the two-body decay scheme $K^+\rightarrow\theta^0+\pi^+$, the computed K-meson mass is 1462 ± 15 m_e.

* Work supported by a joint contract with the U. S. Atomic Energy Commission and the Office of Naval Research.
† On leave of absence from Naval Research Laboratory.
‡ A portion of this work performed while stationed at the Naval Research Laboratory.
[1] We would like to thank Dr. R. P. Shutt and his group at Brookhaven National Laboratory for kindly making available these exposures.

L9. Evidence for the β Decay of Neutral *V*-Particles.* M. M. BLOCK, E. M. HARTH,† AND M. E. BLEVINS, *Duke University.*—Two V^0's, each having one of its decay products identifiable as an electron, were observed to decay in the gas of a 20-atmosphere hydrogen-filled diffusion cloud chamber exposed to an external 1.9-Bev π^- beam of the Cosmotron.[1] In event 1, the two minimum ionizing tracks have an included angle of $43.5\pm1°$; the positive and negative particles have momenta $p+=1240+200$, $p-=8.1\pm0.1$ Mev/c. In event 2, $p+=43\pm4$, $p-=228\pm20$ Mev/c, with an included angle of $68\pm1°$; both particles appear to have minimum ionization. The upper mass limits of the negative particle of event 1 and

the positive of event 2 are 16 and 93 m_e, respectively; thus these particles are assumed to be electrons. In event 2, the momentum and ionization of the negative particle are compatible with its being a light meson. Assuming that both events represent decays of the *same* neutral particle into a pion and electron, the Q-values are 18 and 48 Mev, indicating that it is probably necessary to invoke a three-body decay scheme involving an additional neutral particle.

* Work supported by a joint contract with the U. S. Atomic Energy Commission and the Office of Naval Research.
† On leave of absence from Naval Research Laboratory.
‡ We would like to thank Dr. R. P. Shutt and his group at Brookhaven National Laboratory for kindly making available these exposures.

Post-Deadline Papers, If Any

TUESDAY MORNING AT 9:30

Auditorio de Comercio

(FERNANDO ALBA ANDRADE presiding)

Reactions of Transmutation; Scattering

M1. Study of $Li^7(p,p'\gamma)$ and $Li^7(p,\gamma)$ Reactions.* R. M. WILLIAMSON, *Duke University*, AND K. W. JONES, *University of North Carolina*.—The yield of hard and soft gammas from Li^7+p has been studied in the region of 2-Mev proton energy. Theoretical analysis of Wilkinson[1] makes a study of the behavior of the hard gammas over a wide proton energy interval of interest. The yield of 478-kev gammas taken at 135° shows a steady rise from 1.5 to 2.6 Mev with a 10% dip at 1.88 Mev,[2] apparently corresponding to a Wigner cusp. A 2-in.×2-in. NaI scintillator allowed a partial separation of the 16- and 19-Mev capture gammas. Capture gamma data taken at 0° shows a 20% rise at 2.05 Mev with a width of 300 kev in agreement with Price.[3] The 90° data shows a peak twice as high, of similar width and position, which is asymmetric with respect to proton energy. This data indicates that only the 16-Mev gamma is resonant. The intensity ratio of 16- to 19-Mev gammas is 3/2 to within 30% between 1 and 3.5 Mev. The intensity of both gammas at 0° divided by the intensity at 90° is 1.5 ± 0.4 at 2.7-Mev and 3.5-Mev proton energy.

* This work was supported in part by the U. S. Atomic Energy Commission.
[1] D. H. Wilkinson, Phil. Mag. **45**, 259 (1954).
[2] R. C. Hanna, Phil. Mag. **46**, 381 (1955).
[3] P. C. Price, Proc. Phys. Soc. (London) **A67**, 849 (1954).

M2. $Li(p,n)$ Reaction near Threshold.* H. W. NEWSON, *Duke University*.—The shape of the total neutron yield curve for this reaction has been measured in detail from threshold to 2.5 Mev. Between 1.89 and 1.94 Mev the cross section follows the equation, $\sigma=(5/2)\pi\lambda^2 x/(1+x)^2$, where $x=\Gamma_n/\Gamma_p=1$ at 50 kev above threshold. Small deviations occur above 1.93 Mev, apparently due to the effect of the resonance at 2.25 Mev. Large deviations occur up to 4 kev above threshold; this is apparently the region where protons drop below threshold energy while traversing the target. The neutron yield near threshold appears to be almost entirely due to a single resonance several hundred kev wide which peaks so near the threshold energy that the term $(E-E_0)^2/\Gamma^2$, which usually appears in the Breit-Wigner formula, may be neglected in the above equation. The absolute value for the cross section as calculated here is in excellent agreement with the determination of Taschek and Hemmindinger. The thermal cross section for the $Be^7(n,p)$ reaction is calculated to be 45 000 b, in good agreement with Hanna. An attempt has been made to fit the experimental points with the 2^- level and the 3^+ level proposed by Adair for the peak at 2.25 Mev; the calculated values fall decidedly below the experimental at 2.4–2.6 Mev. Evidently, at least one more resonance must contribute to the reaction in the energy region studied.

* This work was supported in part by the U. S. Atomic Energy Commission.

M3. Scattering of Alpha Particles from Helium and the 3-Mev State in Be^5. G. C. PHILLIPS, J. L. RUSSELL, AND C. W. REICH, *The Rice Institute*.—The singly charged alpha particle beam from The Rice Institute electrostatic generator has been used to study the scattering in helium gas in the energy interval 3 to 6 Mev using a large volume, differentially pumped, gas scattering chamber. Excitation curves were obtained at c.m. angles of 30°33.5′, 40°, 54°44′, and 70°7.5′. All curves except the 54° curve show an anomaly at 6-Mev bombarding energy. All of the excitation curves are consistent with a level in Be^5 at 2.9 Mev of width 0.8 Mev and of spin 2^+. Phase-shift analyses have been carried out to fit the excitation curves and angular distributions at 4.2, 4.75, and 5.4-Mev bombarding energies. The s-wave phase shift monotonically decreases from about 115° to 90° between 3.8 and 5.8 Mev. The d-wave phase shift increases from zero near 3 Mev and attains a value of 90° at about 6 Mev.

M4. Excitation Curve for $Be^9(n,\alpha)He^6$.* ABDUL R. SATTAR, IRA L. MORGAN, AND EMMETT L. HUDSPETH, *University of Texas*.—Neutrons in the energy interval 3.3 to 6.1 Mev have been produced by bombarding thin deuterium targets with deuterons accelerated by the University of Texas Van de Graaff machine. Neutrons emerging at 10° fell on a beryllium ring, and the He^6 activity induced in the ring was measured with an anthracene counter. Counts were recorded for 5 sec (about six half-lives) following a controlled neutron bombardment. The excitation function rises to a maximum at $E_n=3.73$ Mev, then declines to approximately 0.6 of this value at $E_n=6.1$ Mev; weak resonances for $E_n=3.73$ and 4.27 Mev are indicated, but more data will be required to establish these definitely. Absolute values of the cross section are now being obtained, so that our data may be compared quantitatively to other measurements[1] which were obtained with neutrons of lower energy (1.9 to 4.0 Mev).

* Assisted by the U. S. Atomic Energy Commission.
[1] Allen, Burcham, and Wilkinson, Proc. Roy. Soc. (London) **192**, 114 (1947).

M5. Neutrons from the Proton Bombardment of B^{11}.† F. AJZENBERG,‡ A. RUBIN, AND G. D. JOHNSON, *Boston University*, AND M. MAZARI,§ *M.I.T.*—A thin target of isotopic boron has been bombarded with 7.03-Mev protons from the M.I.T.—O.N.R. Van de Graaff generator. Ilford C-2 emulsions, 400 μ thick, placed at five angles to the incident beam, have been used to measure the neutron spectra. Preliminary results at four angles (1600 tracks) show groups corresponding to the ground state ($Q=-2.80\pm0.06$ Mev) and to an excited state of C^{11} at 2.04 ± 0.08 Mev. At each of the four angles, the ground state group is several times more intense than the

group corresponding to the first excited state. A weak neutron group of lower energy is also observed: it may be due to the reaction $Si^{30}(p,n)P^{30}$. Further scanning is in progress.

† This work has been supported in part by the U. S. Air Force, through the Office of Scientific Research, and in part by the Office of Naval Research.
‡ On leave of absence at Department of Physics, Columbia University, New York.
§ Permanent address: Institute of Physics, National University of Mexico, Mexico City.

M6. Energy Levels in F^{19}.† H. A. Hill and J. M. Blair, *University of Minnesota.*—Using a proportional counter, α particles from the reaction $O^{18}(p,\alpha)N^{15}$ were observed at 90° for incident protons ranging in energy from 0.7 and 3.5 Mev (laboratory coordinate system). Above the threshold for the reaction $O^{18}(p,n)F^{18}$ (2.58 Mev) neutrons were observed at 0°, using a "long counter" as a detector. The target, an NiO foil made using oxygen enriched in O^{18}, was measured to be 18 kev thick for protons of 1.890 Mev. The α particle and neutron yields were measured simultaneously in order that a comparison could be made of the energies at which resonances appear in the yields from the two reactions. Prominent resonances for the (p,α) reaction were observed at proton energies of 0.838, 1.688, 1.761, 2.007, 2.378, 2.637, 2.770, 2.929, 3.071, 3.165, and 3.475 Mev, with weaker resonances at intermediate energies. The most prominent resonances in the (p,n) reaction were observed at 2.649, 2.772, 3.040, 3.163, 3.264, 3.388, and 3.484 Mev.

† This work supported in part by the Office of Naval Research and the U. S. Atomic Energy Commission.

M7. (p,p') and (p,α) Reactions of Potassium.* A. Sperduto and W. W. Buechner, *M.I.T.*—Potassium-iodide targets were bombarded with protons at energies of 6.0, 7.0, and 7.5 Mev and the reaction products analyzed with the broad-range magnetic spectrograph at several angles up to 130 degrees to the incident beam. Proton and alpha-particle groups, ranging in energy from about 2 to 7.5 Mev, were recorded on nuclear track emulsions. In addition to the elastically scattered proton groups identified with the target and contaminant nuclei, seventeen proton groups have been observed which result from inelastic collisions. One of these has been identified with the 4.431 level in C^{12}. On the basis of intensity considerations and the energy shift observed with changes in incident energy and angle, the remaining sixteen groups have been assigned to the $K^{39}(p,p')K^{39}$ reaction. Preliminary measurements indicate levels in K^{39} at the following energies: 2.53, 2.82, 3.03, 3.61, 3.89, 3.95, 4.10, 4.11, 4.14, 4.48, 4.52, 4.69, 4.77, 4.94, 5.02, and 5.18 Mev. Several alpha-particle groups are also observed which are from the $K^{39}(p,\alpha)A^{36}$ reaction, the ground-state Q-value for which is 1.28 Mev.

* This work has been supported in part by the joint program of the Office of Naval Research and the U. S. Atomic Energy Commission.

M8. Energy Levels of Si^{28}.* A. Rubin and F. Ajzenberg,† *Boston University*, and Hans Mark, *M.I.T.*—The $Al^{27}(d,n)Si^{28}$ reaction has been observed with 2.17-Mev deuterons from the M.I.T.–Rockefeller Van de Graaff generator. The resultant neutrons have been studied by means of Ilford C-2 emulsions, 400 μ thick, placed at nine angles to the incident deutron beam. Preliminary results at 0° and 90° (3000 tracks) indicate 12 groups corresponding to excited states of Si^{28}. Assuming the first state of Si^{28} to be at 1.78 Mev[1] (in this experiment, 1.76 ±0.10 Mev), the other groups correspond to states at 4.37± 0.15, 4.79±0.15, 6.26±0.06, 6.83±0.06, 7.32±0.10, 7.89± 0.08, 8.49±0.06, 9.25±0.12, 9.86±0.08, 10.09±0.12 (?), and 10.65±0.08 Mev. The ground state of Si^{28} was not observed: the upper limit to the intensity of the corresponding neutron group is 0.1 (0°) and 0.2 (90°) of the intensity of the group corresponding to the first excited state.

* This work has been supported in part by the U. S. Air Force, through the Office of Scientific Research, and in part by the Office of Naval Research.
‡ On leave of absence at Department of Physics, Columbia University, New York.
[1] P. M. Endt and J. C. Kluyver, Revs. Modern Phys. **26**, 95 (1954).

M9. Coulomb Excitation of Cu, Zn, As, Se, and Ru. G. M. Temmer and N. P. Heydenburg, *Carnegie Institution of Washington.*—Continuing our studies of excited states in medium-heavy nuclei with alphas up to 7 Mev,[1] we have investigated gamma rays from natural Cu, Zn, and As^{75}, as well as enriched isotopes of Se, Ru^{99}, and Ru^{101}.[2] As expected, the even-even nuclei yield only one gamma ray from their first-excited 2^+ states; the odd nuclei show up to four gamma rays. We have made use of angular distribution measurements, excitation functions, and coincidence counting to establish decay schemes in As^{74}, Se^{77}, and Ru^{101}. In Se^{77} we observe the 17.5-sec 160-kev isomeric transition; it is excited indirectly via an 86-kev cascade from a 244-kev state. A state at 457 kev (not seen following beta decay) is deexcited by both direct ground-state transition and a 21-kev cascade to the 244-kev level. In Ru^{101}, we see levels at 127 kev and 307 kev and the 180-kev cascade between them; only an 89.5-kev state is found in Ru^{99}. We merely list the other transitions observed (in kev): $Cu^{(63)}$, 690 and 990; $Zn^{(64)}$, 1040; As^{75}, 200, 283, 574, 814; Se^{74}, 635; Se^{76}, 567; Se^{78}, 615; Se^{80}, 654; Se^{82}, 880. The reduced transition probabilities $B(E2)$ (in 10^{-48} Cm^4) for Se^{74} through Se^{82} are 0.32, 0.60, 0.54, 0.37, and 0.124. All other B-values will be presented.

[1] N. P. Heydenburg and G. M. Temmer, Bull. Am. Phys. Soc. **30**, No. 3, 17 (1955); G. M. Temmer and N. P. Heydenburg, Phys. Rev. **98**, 1308 (1955).
[2] Isotopes courtesy of G. Scharff-Goldhaber (Se) and Oak Ridge National Laboratory (Ru).

M10. Inelastic Scattering of Photons from Au^{197}. L. Meyer-Schützmeister and V. L. Telegdi, *University of Chicago.*—A lower limit of the total inelastic nuclear photon scattering cross section of Au was determined as a function of energy by measuring the yield of the reaction $Au^{197}(\gamma,\gamma')Au^{197m}$(7.5 sec) as a function of betatron energy. The use of pneumatic transfer and of Na J-counters in good geometry with samples of metal disks of 16 g enabled one to obtain good statistics and detailed decay curves down to 5 Mev. The result shows that the cross section falls off steeply as soon as the competition from (γ,n) becomes possible. The maximum cross section of about 2.5 mb is reached at 7.8±0.2 Mev. This disagrees with earlier work of Cameron and Katz but shows qualitatively the same behavior as Rh. The results indicate a second peak of the cross section at about 15 Mev, where the "giant resonance" has its maximum, in agreement with recent work of Hayward and Fuller on elastic scattering of Au. The cross section of the reaction $Au^{197}(\gamma,2n)Au^{195m}$(30 sec) was also determined with the same equipment.

M11. Protons from the Bombardment of Several Elements with 40-Mev Alpha Particles. R. M. Eisberg, G. Igo, and H. E. Wegner, *Brookhaven National Laboratory.**—Thin targets of Au, Ag, and Cu were bombarded with 40-Mev alpha particles and the energy spectra of protons emitted at 150° were measured. According to the compound nucleus model, the level density of the residual nucleus is proportional to $N/E\sigma$, where N is the probability that the compound nucleus emits a proton of energy E and σ is the cross section for the inverse reaction. For each element, log $(N/E\sigma)$ plotted as a function of the excitation energy of the residual nucleus E_r is concave downward. This is in qualitative agreement with the Fermi gas level density formula: $K\exp(AE_r)^{\frac{1}{2}}$. For Au, $N/E\sigma$ fits this formula with $A=5.8$ Mev^{-1} when $E_r>2$ Mev; when

$E_\gamma < 2$ Mev, $N/E\sigma$ increases less rapidly with increasing E_γ than the formula. For Ag, $N/E\sigma$ fits with $A = 4.7$ Mev^{-1} for all E_γ. For Cu, $N/E\sigma$ fits with $A = 5.4$ Mev^{-1} when $E_\gamma > 4.5$ Mev; when $E_\gamma < 4.5$ Mev, $N/E\sigma$ increases more rapidly than the formula. In the region of 150°, the cross section for the emission of lower-energy protons is isotropic, but the cross section for high-energy protons decreases slightly with increasing angle. Thus the spectra, in the region of small E_γ, are probably contaminated with protons from noncompound nucleus processes.

* Research carried out under the auspices of the U. S. Atomic Energy Commission.

M12. Scattering of 30–90 Mev Gamma-Rays by Protons.* C. L. OXLEY AND V. L. TELEGDI, *The University of Chicago.*—We have measured the (elastic) scattering of photons by protons using the bremsstrahlung beam from 98-Mev betatron electrons, a liquid hydrogen target, and a converter-telescope detector. The counter efficiency was found from the response to monoenergetic electrons incident upon a series of partial thicknesses of the regular lead converter. The product of counter efficiency and incident gamma spectrum rises from zero near 20 Mev to a nearly constant value from 35–90 Mev. By measuring the scattering from 1/20 and 1/40 radiation length carbon targets, we have satisfied ourselves that, at the angles measured, we are free from shower effects which would go quadratically with target thickness. A simultaneous measurement of scattered electrons convinces us that false gamma counts from converted electrons or electrons not rejected by the anticoincidence are negligible. The cross sections have been measured to 8% statistical accuracy at 60, 90, 120, and 150 degrees. The cross section shows little deviation from the Thomson value except for a rise at 60 degrees. Further data on the forward scattering will be presented.

* Research supported by a joint program of the Office of Naval Research and the U. S. Atomic Energy Commission.

M13. Elastic Proton-Proton Scattering in the Bev Range.* BRUCE CORK, AND W. A. WENZEL, *University of California, Berkeley.*—Measurement of the differential cross section for elastic proton-proton scattering as a function of angle at Bevatron energies is in progress. The internal beam monitored by an electrostatic induction electrode strikes a polyethylene target in the upstream end of a straight section. Protons scattered at angles from 10° to 45° in the laboratory emerge through a thin (0.090-in.) aluminum window on the outside radius of the bevatron. These are detected by a two-counter telescope in coincidence with a similar telescope on the inside radius of the bevatron, which detects the larger angle recoil. Fourfold coincidences with a time resolution of 6×10^{-9} sec and good geometrical resolution (10^{-4} steradian) permit separation of the elastic peak from a rather large inelastic background. Preliminary center-of-mass angular distributions are as follows:

2.24 Bev: 43°, 3.0; 56.5°, 1.2; 69°, 0.70; 92.5°, 0.40,
3.49 Bev: 46.5°, 0.45; 63°, 0.15; 77°, 0.13,
4.40 Bev: 52°, 0.20; 67.5°, 0.11.

Absolute values indicate millibarns per steradian with order-of-magnitude accuracy only. Experiments are under way to increase the accuracy of the absolute measurements and to extend the measurements to smaller angles and higher energies.

* This work was performed under the auspices of the U. S. Atomic Energy Commission.

M14. Total-Absorption Spectrometer Measurements of the Gamma Rays Emitted from Targets Bombarded with 6.2-Bev Protons.* ROGER W. WALLACE, MALVERN H. L. JESTER,† AND JOHN M. BRABANT, *University of California, Berkeley.*—A Čerenkov spectrometer has been constructed that consists of a piece of glass, containing 52% of PbO, 12 in. in diameter and 14 in. long, viewed by four 5-in.-diameter photomultipliers. The Čerenkov radiation emitted by electron showers initiated by incident gamma rays is nearly proportional to the incident gamma-ray energy from 50 Mev to 1.4 Bev. The spectrometer has been calibrated up to 1.4 Bev by the pulses produced by electrons deflected in a magnetic field. This calibration allows cosmic-ray μ mesons to be used to check the energy scale. Above 200 Mev, the measured energy resolution of the spectrometer is 30% and is approximately independent of energy. To eliminate incident charged particles, the spectrometer is operated behind a 13-in.-diameter anticoincidence plastic scintillator counter. Only those showers are analyzed that start in a lead converter 4 in. in diameter by 3/8 in. thick placed behind the anticoincidence counter and in front of a thin coincidence counter. The sum of the four photomultiplier pulses is fed into a fast 10-channel pulse-height analyzer. The spectrum of gamma rays observed from circulating protons up to 6.2 Bev will be presented.

* This work was performed under the auspices of the U. S. Atomic Energy Commission.
† Present address: Lt. M. H. L. Jester, 485283, USN, VR 31, NAS, Norfolk, Virginia.

TUESDAY AFTERNOON AT 15:00

Auditorio de Humanidades

(R. T. BIRGE presiding)

Invited Papers

N1. Hundimienta de Ciudades (The Sinking of Cities). NABOR CARRILLO, *Universidad de Mexico.* (40 min.)

N2. Recent Experiments with the Bevatron. E. O. LAWRENCE, *University of California, Berkeley.* (30 min.)

N3. Initial Performance of the Cornell Strong-Focusing Synchrotron. R. R. WILSON, *Cornell University.* (30 min.)

N4. The Present Status of Radio-Carbon Dating. J. L. KULP, *Columbia University.* (40 min.)

TUESDAY AFTERNOON AT 15:00

Auditorio de Ciencias

(L. MARTON presiding)

Optical Physics; Electron Physics

Q1. Flame Zone Spectroscopy of Solid Propellants. II. R. G. REKERS AND D. S. VILLARS, *U. S. Naval Ordnance Test Station.*—With the aid of the automatic-feed strand bomb previously described,[1] spectra of *JPN* burning in nitrogen have been investigated over the visible and ultraviolet. Throughout the pressure range, 300 to 500 psi nitrogen, emission from the flame zone exhibits a continuous background which extends into the ultraviolet to approximately 3200 A. Accompanying this continuum are some of the more prominent lines of spectra due to sodium, potassium, calcium, copper, and iron. Calcium oxide bands in the 6260 region (orange system) and in the 5500 region (green system) have been identified. Furthermore, a multitude of weak lines is observed in the wavelength region 4600 to 5800 A. Both the Swan and the high-pressure bands attributed to C_2 are present in this flame. The dividing line between flame and fizz zones does not appear to be sharp. No absorption in the visible region has been found in the fizz zone over the pressure range 25 to 150 psi nitrogen. Nitric-oxide absorption originally noted has been shown to originate from the external atmosphere surrounding the flame. This indicates that formation of NO_2 is a secondary reaction.

[1] R. G. Rekers and D. S. Villars, Rev. Sci. Instr. **25**, 424–429 (1954).

Q2. Precision of Microwave Spectrographs.* M. W. P. STRANDBERG AND M. PETER, *M.I.T.*—Microwave molecular beam spectroscopes using either absorption or emission of radiation, or particle counting techniques, operate within the same realm of techniques. The ultimate frequency precision of each of these forms of beam spectroscopy is thus simply expressible in terms of common parameters. Then based on only the most general considerations the particle counting system has the highest probability of defining a point on the atomic or molecular resonance curve by the square root of ratio of the photon energy to the thermal noise energy kT. Practical considerations can shift this ratio many orders of magnitude either way. The microwave absorption spectroscope is unique in being able to operate without state selection and without beam flow. In this form of operation the resolution is less because of Doppler broadening. However, the over-all precision of an absorption spectrograph can be greatly increased over beam operation since the amount of active material, and hence power handling capability, can be greatly increased without the need of absurd flow handling capacity.

* This work was supported in part by the Signal Corps; the Office of Scientific Research, Air Research and Development Command; and the Office of Naval Research.

Q3. Intensity of Vibronic Bands in 3000–5000 A Absorption System of Chlorine Dioxide.* J. K. WARD, *Boeing Airplane Company*, AND C. M. LOYD, *A & M College of Texas* (introduced by J. B. Coon).—The Franck-Condon principle relates the relative intensities of the vibronic bands of an absorption system to the change in geometry of the molecule during the associated electronic transition. The vibrational frequencies[1] and the geometry of both ground and excited state[2] of the chlorine dioxide molecule are known. On the basis of this information, the Condon overlap integrals were evaluated to the harmonic approximation, giving theoretical relative intensities for the bands of progressions (a) $(v_1'00)\rightarrow(000)$ and (b) $(v_1'10)\rightarrow(000)$. Measurements of the relative intensities of the bands of these progressions were made photographically at several different concentrations and path lengths. A rotating sector was used for plate calibration. About twenty determinations with optical densities of 0.1 to 0.6 were made for each band, avoiding extreme densitometer readings. Background intensities were subtracted. The close agreement between theory and experiment for the (b) progression suggests that the harmonic approximation permits reasonably accurate calculated intensities. For the (a) progression, the experimental intensities are considerably larger, after $v_1'=8$, than those theoretically predicted. This indicates some additional intensity effect.

* Supported by Air Research and Development Command.
[1] J. B. Coon and E. Ortiz, Phys. Rev. **82**, 766(A) (1951).
[2] J. K. Ward, Phys. Rev. **82**, 845(A) (1954).

Q4. Excited States of Oxygen from Energy Transfer and Light Absorption. DAVID H. VOLMAN, *University of California, Davis.*—Recent results[1] on the deactivation of the excited state of oxygen reached by energy transfer from Hg $^3P_1$ as determined by rate of ozone formation show that the added gases in order of efficiency as deactivators are He, A, N_2, and CO_2. Helium is by far the poorest whereas A and N_2 are about equal in efficiency. Deactivation of the excited triplet O_2 $^3\Sigma_u^+$ to lower electronic states is not a probable process for either A or He, since energy resonance is not possible with the rare gases in this energy region. The results may be explained, however, if one assumes that the excited state is vibrationally excited O_2 in the ground electronic state $^3\Sigma_g^-$. The order of the effects of added gases on the formation of ozone from oxygen absorbing light of 1849 A are opposite to the foregoing. These results are explained by attributing the effects of the added gases to a reaction involving O atoms. Since absorption at 1849 A is in the Schumann-Range bond system, the $^3\Sigma_u^-$ state of O_2 must give O atoms by predissociation as first postulated by Flory.[2]

[1] D. H. Volman, J. Am. Chem. Soc. **76**, 6034 (1954).
[2] P. J. Flory, J. Chem. Phys. **4**, 23 (1936).

Q5. Faraday Effect in Gases—Experiment and Theory.* L. R. INGERSOLL AND D. H. LIEBENBERG, *University of Wisconsin.*—Measurements made in this Laboratory on the Faraday effect in gases over the spectral range from 3635 A to 9875 A[1] now give sufficient material for theoretical application. Methane and nitrogen provide a check for diamagnetic molecules, and the recent Verdet values for oxygen at low pressures, which were unavailable to Serber,[2] should provide an adequate check for paramagnetic molecules in the Van Vleck—Serber theory. The anomalous behavior of hydrogen and deuterium—that is, their Verdet values differ by 2%—presents some difficulties for the theory. Reviewing the work of Okazaki[3] and using more recent data, the index of refraction is determined for several normal gases. New experimental results have been obtained for xenon and krypton and the departures from the normal theory in the series of noble gases are noted.

* This work has been supported by the U. S. Office of Naval Research.
[1] L. R. Ingersoll and W. L. James, Rev. Sci. Instr. **24**, 23 (1953); L. R. Ingersoll and D. H. Liebenberg, J. Opt. Soc. Am. **44**, 566 (1954). Also recent unpublished material.
[2] R. Serber, Phys. Rev. **41**, 495 (1932).
A. Okazaki, Mem. Ryojun Coll. Eng. **10**, 19 (1937).

Q6. γ-Ray Absorption Measurements of Density of the Upper Atmosphere. E. T. BYRAM, T. A. CHUBB, AND H. FRIEDMAN, *U. S. Naval Research Laboratory.*—NRL Aerobee

16, flown at White Sands Proving Ground, December 1, 1953, was equipped with photon counters to measure solar x-ray emission between 10 and 100 A. A helium filled tube equipped with a thin window of Mylar polyester film responded almost exclusively to wavelengths from 44 to 50 A. Using laboratory data on x-ray absorption in air and the rocket measurements of x-ray intensity *versus* altitude, the air density was found to be approximately one third the value published by the Rocket Panel[1] between 110 and 130 km. Similar results were obtained from an aluminum window photon counter sensitive to wavelengths from 10 to 18 A. At lower altitudes, 70 to 90 km, densities computed from absorption of Lyman α(λ1216 A), measured in several flights in 1952, agreed well with Rocket Panel data.

[1] Rocket Panel, Phys. Rev. **88**, 1027 (1952).

Q7. Application of Space-Charge Theory to the Determination of Electron Emitter Properties.* W. B. NOTTINGHAM, *M.I.T.*—Basic space-charge theory depends on the simultaneous solution of three equations. These equations are: (1) Poisson's, (2) Boltzmann's density relation, and (3) the equation of current continuity. The solution of these equations applicable to parallel plane electrodes leads to methods that serve also for coaxial cylinders. Tubes have been constructed with oxide cathodes and a ratio of radii collector to emitter of 2.5. The emitter specifications to be evaluated and reported on include the a constant in amp/m^2 and the work factor Φ in ev. These constants are useful in the simplified current density expression which is $a\exp(-\Phi/V_T)$. The temperature expressed as V_T is $T/11\,600$. Also the Richardson constants A_R and ϕ_R and the temperature coefficient of the true work function are determined. The analysis yields a value for the true work function of the collector.

* This work was supported in part by the Signal Corps; the Office of Scientific Research, Air Research and Development Command; and the Office of Naval Research.

Q8. Criterion for the Occurrence of Luminescence. C. C. KLICK AND G. A. RUSSELL, *U. S. Naval Research Laboratory*, AND D. L. DEXTER, *University of Rochester** *and N.R.L.*—A mechanism will be suggested for the nonradiative quenching of excited states of simple impurity centers, namely a crossover to the ground electronic state of the center immediately after excitation and before thermal equilibrium has had time to come about. It is proposed that this mechanism is responsible for the absence of strong luminescence in some impurity and color centers, e.g., the F-center in alkali halide crystals. The quenching process proposed here is applicable only for certain geometries of the configuration coordinate diagram, which will be discussed with a view to a criterion for strong luminescence. The quenching mechanism is consistent with known configuration coordinate curves and leads to a prediction which is experimentally verified, to the effect that the wavelength of emitted radiation is not more than twice that of the light absorbed by the center. The same mechanism shows the possibility of photoconductivity arising from absorption in discrete lines even at low temperatures.

* Research supported in part by the U. S. Air Force through the Office of Scientific Research of the Air Research and Development Command.

Q9. Absorption Cross Section for Light in Perfect Solids.* D. L. DEXTER, *University of Rochester.*—The interactions of an atom with its neighbors in an idealized solid are taken into account explicitly in treating the absorption of light, as contrasted with the usual introduction of an "effective" field and mass. It will be shown that in simple cases the total cross section of an atom in a given absorption line j is uninfluenced by the dipole coupling with the same transition in neighboring atoms of density n, although the transition probability per atom is increased by the factor $[1+(\pi n/3)2e^2|\mathbf{r}_j|^2/\epsilon_j]^2$. Thus the "effective fields" for polarization, for absorption cross section, and for transition probability are all different. Additional correction terms arise from transitions $l\neq j$ in the neighbors, from exchange and overlap effects, and from higher multipole effects. These additional effects are in general important.

* Research supported in part by the U. S. Air Force through the Office of Scientific Research of the Air Research and Development Command.

Q10. Electron Impact Studies with Trimethylamine.* HERMAN BRANSON AND L. B. GARNER II, *Howard University.*—In a study of the ions produced from $(CH_3)_3N$ in a 60° mass spectrometer by varying the energy of the electrons, we have used the relation $A(x)\geq D(M-X)-I(x)$ to compute $I(x)$, the ionization potential, with $D(x)$, the dissociation energy, determined from a thermochemical cycle. Our results are

Mass	Reaction	Ion	$A(x)$	$D(x)$	$I(x)$
59		$(CH_3)_3N$	9.36		9.36
44	$CH_3+(CH_3)_2N$	$(CH_3)_2N$	12.02	3.58	8.44
29	$2CH_3+CH_2N$	CH_2N	15.24	6.68	8.56
15	$CH_3+(CH_3)_2N$	CH_3	13.11	3.58	9.53
14	$(CH_3)_2N+CH_3+H$	CH_3	18.17	7.38	10.79
13	$(CH_3)_2N+CH+2H$	CH	21.79	10.91	10.88
12	$(CH_3)_2N+C+3H$	C	25.10	14.41	10.69

All values are in electron volts and the probable error is ±0.2. The $I(x)$ values are to be read less than or equal to. The thermochemical cycles gave 3.58 as the energy of the first C−N bond, 3.10 for the second, and 2.85 for the third in trimethylamine with $D(N-N)=9.76$ ev.

* This work is being supported by the U. S. Atomic Energy Commission and the Office of Naval Research.

Q11. Post-Bombardment Conductivity of MgO Crystals.* M. A. POMERANTZ, J. F. MARSHALL, AND R. A. SHATAS, *Bartol Research Foundation.*—In the course of investigations of the currents induced by the passage of 1.3-Mev electrons from the linear accelerator through thin single crystals of MgO at elevated temperatures, it has been observed that conductivity persists after the termination of bombardment by the high-energy beam. Oscillographic measurements with provision for eliminating the effects of buildup of space charge[1] in the temperature range 620°–695°K reveal an exponential decay with time constants τ, between 150 μsec and 9.5 μsec, respectively. The measured temperature-dependence, $\tau=\tau_0\exp(E/kT)$, agrees with that predicted on the basis of a simple theoretical model and yields an activation energy $E=1.4$ ev. Corresponding time constants as long as 10^6 sec at 343°K are measued at lower temperatures with a micromicroammeter. This procedure provides a new method for determining the numbers and depths of trapping centers in insulating crystals.

* Assisted by the Office of Ordnance Research, U. S. Army.
[1] Pomerantz, Shatas, and Marshall, Phys. Rev. (to be published).

Q12. Pulse Characteristics of CdSe Crystals. T. FIELDS, E. J. SCHILLINGER, AND J. KENSKI, *V. A. H., Hines, and DePaul University.*—Cadmium selenide crystals were exposed to beta particles from P^{32} and the resultant pulse characteristics determined. Counting efficiency *versus* field strength was measured, giving approximately linear relationship. A technique of determining the effective ionization potential of this semi-conductor is described, yielding values from 4.0 to 7.5 ev per ion pair for three tested crystals.

Q13. Irradiation Effects in Some Organic Compounds. T. H. ANDERSON, R. D. JORDAN, AND R. S. ALGER, *U. S. Naval Radiological Defense Laboratory.*—Simple organic compounds excited at 90°K by bombardment with electrons or x-rays develop color centers and exhibit thermoluminescence

similar to that found in inorganic systems. In the glassy alcohols, the color centers are stable in the dark at low temperatures but can be bleached either by white light or by thermal excitation. The absorption bands have a simple broad bell shape with the peak occurring for methanol at 5200 A; ethanol, 55 A; ethylene glycol, 5200 A; and glycerol, 5000 A. The bands widths and maxima are greater than that produced in KBr under the same exposure conditions, indicating a greater sensitivity. Crystalline ketonic compounds also colored, but, additionally, showed thermoluminescence spectrally similar to the known ultraviolet excited fluorescence of carbonyl compounds.[1] Acetone, diethyl ketone, and phenyl acetone had single glow peaks indicating a trap depth of 0.15 ev. Heptanone, undecanone, and tridecanone showed additional broad peaks at 0.22 ev. Optical bleaching removed both color and luminescence. The order of increasing dosage necessary to produce a given degree of coloring is ethanol, acetone, ether, chloroform, acetic acid, and benezene. This series follows the trend of the G-values for radiation decomposition.

[1] W. E. Kaskaw and A. B. F. Duncan, J. Chem. Phys. 16, 223 (1948).

TUESDAY AFTERNOON AT 15:00

Auditorio de Comercio

(SALVADOR MOSQUEIRA presiding)

General Physics

R1. Spin Resonance in Metals as Altered by the Overhauser Effect. J. I. KAPLAN, *U. S. Naval Research Laboratory.*—It is shown that the electron spin resonance absorption line shape in metal particles, small compared to thin skin depth, can be appreciably altered by the Overhauser effect. In a special limiting case the line shape will depend upon the direction of sweep of the applied constant field H_0. In general the absorption will be nonsymmetrical.

R2. Electron Spin Resonance in Cu-Mn and Ag-Mn Alloys. J. OWEN,* M. E. BROWNE, AND A. F. KIP, *University of California, Berkeley.*—We have observed resonance absoprtion in alloys containing 0.05 to 2.0 atomic percent Mn, using wavelengths of 1.25 and 3.0 cm, a temperature range of 2°–290°K, and a magnetic field range of 0–10 kgauss. The specimens have been in the form of 0.005-in. thick sheets. We find that for a given concentration of Mn, both Ag and Cu alloys give a similar absorption line. The position, width, and shape of the line depend on Mn concentration and temperature. With 0.05% Mn, the g-value is close to 2.0 at all temperatures, but, as the Mn concentration is increased, the line shifts to lower fields and the apparent g-value is greater than 2 by an amount which varies very roughly as concentration/temperature. No hfs from the Mn nuclei has been observed even in the most dilute alloys used so far, where the line width (~100 gauss at 2°K and increasing with T) is considerably less than the expected hyperfine splitting. The results are not inconsistent with the assumption that the resonance is due to Mn^{2+} ions which are coupled together by fairly strong exchange interaction. A theory of the exchange which arises via the conduction electrons is being developed by Professor C. Kittel, and this shows some agreement with the experimental results.

* F.O.A. Fellow.

R3. Zeeman Effects and Magnetic Properties of Neodymium Salts.* G. H. DIEKE AND L. HEROUX, *The Johns Hopkins University.*—The Zeeman effect of the absorption lines of rare earth salts can give a quantitative evaluation of the crystal field as well as the magnetic properties of the salts and the classification of the electronic levels. Data at liquid helium temperature were obtained on five neodymium salts. The effects are highly anisotropic and quite different for the various salts. They can be interpreted from the Stark splitting in crystal fields of appropriate symmetry which produce in first approximation a mixing of Stark levels with different M. The composition of normal states of the following trigonal neodymium compounds are: magnesium double nitrate, 0.84 $(M=1/2)0.12(5/2)0.24(7/2)$; bromate, $0.63(1/2)0.37(7/2)$; ethyl sulfate, $0.35(1/2)0.03(5/2)0.62(7/2)$. The second Stark level of the double nitrate is $0.73(3/2)0.27(9/2)$. The order of the sublevels of the excited states appears to be different for different salts. The magnetic susceptibilities derived from the data are strongly anisotropic at low temperatures and bear no relation to those of the free ions.

* Work done with the support of the U. S. Atomic Energy Commission.

R4. Critical Phenomena in the Triethylamine-Water System. F. KOHLER* AND O. K. RICE, *University of North Carolina.*—The system triethylamine-water, which has a lower critical point at 18.29°C, is the only one for which the details of the critical behavior have been reported to be in agreement with the production of a "derby hat" region, according to Mayer's theory of condensation.[1] Therefore the consolute curve should have a horizontal section of at least the width of the "derby hat" region, which was reported to extend from $x=0.65$ to $x=0.10$ (x being the molefraction of triethylamine). In contradiction to this, our experimental findings show no horizontal section in this concentration range. There is, however, pretty good evidence for a horizontal portion of the consolute curve from $x=0.0935$ to $x=0.0636$ (which corresponds to $\varphi=0.442$ and $\varphi=0.343$, φ being the volume fraction). Over a greater concentration range $(T-T_c)^{1/3}$ or, better $(T-T_c+0.007)^{1/3}$, is proportional to $\varphi'-\varphi''$ (φ' and φ'' refer to the consolute curve at temperature T, T_c being the critical temperature). This is the same relation as is found for systems with upper critical points, but the cubic curve in this case is somewhat flatter than for the other systems.

* Participant in the F.O.A. Scientist's Research Project.
[1] J. E. Mayer, Changements des phases, Compt. rend., 2e Reunion chim. Phys. (Paris, 1952), p. 35.

R5. Systematic Application of Physical and Mathematical Methods to the Exploitation of Mexican Oil Fields. A. ROMERO-JUÁREZ AND J. HEFFERAN V, *Petróleos Mexicanos, México.*—This paper reports the way in which physical principles have been applied to increase the recoverable reserves in Mexican oil fields. By use of the methods developed by M. Muskat, W. Hurst, R. J. Schilthuis, and M. C. Leverett, among others, it is possible to solve a number of problems related to the prediction of oil reservoir behavior, to calculate the effect of water or gas injection, optimum rate of production, or the effect of a fracture or acid treatment, for instance. Special consideration is given to the problem of describing the variation in time of the buildup pressure of a

partially penetrating well; this is a nonsteady state flow problem which has been encountered frequently and which is not treated in the available literature. Solution of the type of problems described and its systematic application has effectively contributed, and will do even more so in the near future, to improve the methods of exploitation of our natural oil resources, a necessary condition to meet the impressive rate of increasing consumption (12 to 15% per annum) of fuels in this country.

R6. Some Observations of Geomagnetic Micropulsations. H. J. DUFFUS, *Pacific Naval Laboratory, British Columbia,* (introduced by W. N. English).—The diurnal variation and the spatial and frequency distributions of the components of geomagnetic micropulsations are found to disagree qualitatively with all theories as to their origin. Being narrow band trains of sinusoidal waves with amplitudes of 0.01 to 10×10^{-4} gauss and periods of 1 to 500 sec they occupy the frequency range of electromagnetic background below that caused by thunderstorm activity and above that associated with sudden commencements and diurnal variations. Observations have been made simultaneously in Canada at Esquimalt, B.C., and Halifax, N.S. Three mutually perpendicular induction coils 15 ft in diameter are used with simple filters and dc amplifiers. The dirunal variation of activity during the daylight hours shows two maxima which are approximately equally spaced about local noon. The frequency distribution during the daylight hours shows frequencies between 0.5 and 1.0 cycle per minute to have maximum probability. This single maximum is at variance with the double maximum found by observers at Eskdalemuir in the U.K.

R7. Some New Linear-System Integral Transform Relations. MALCOLM K. BRACHMAN, *Independents' Geophysical Surveys Corporation,* AND J. ROSS MACDONALD, *Texas Instruments Inc.*—Earlier work[1-3] has shown that the Mellin transform is a powerful tool for treating lumped- or distributed-constant electrical or mechanical linear systems exhibiting dispersion. A useful new relation between the Mellin transforms of $G(\tau)$, the relaxation-time distribution function, and $\alpha(t)$, the indicial admittance or decay function, will be discussed. In addition, a new integral transform connecting $G(\tau)$ and $\alpha(t)$ will be treated together with direct relations between $G(\tau)$ and the real and imaginary parts of the system response function $Q(\omega)$. Laplace, Fourier, Mellin, and Hilbert transforms connecting the quantities characterizing a linear dispersive system will be summarized and their use illustrated. The utility of complex Dirac delta functions in such work also will be discussed.

[1] M. K. Brachman and J. R. Macdonald, Physica **XX**, 1266 (1954).
[2] M. K. Brachman, J. Appl. Phys. **26**, 497 (1955).
[3] M. K. Brachman and J. R. Macdonald (submitted to J. Franklin Inst.).

R8. Phase Centers of Microwave Antennas. DAVIDCARTER, *Convair.*—This paper is concerned with the location of the phase centers of microwave antennas. The inadequacy of conventional aperture theory for the accurate description of phase centers is discussed. Formulas are developed, and for numerical indications, calculations are made for paraboloidal reflectors of different f/D ratios and a class of primary patterns which provide an approximate representation of a great many common feeds. The results are presented in graphical form to provide useful design information and show the dependence of principal E- and H-plane phase center location on feed and dish parameters. Contrary to the prediction of aperture theory, it is shown that the phase centers of axially symmetric antennas are not in the aperture plane, but that they are dispersed about it.

R9. Apparatus for a New Magnetism Laboratory. CHARLES F. SQUIRE, *The Rice Institute.*—A 300-kw direct current generator, which is Diesel engine driven, has been installed by us for special research purposes. A small building just for the generator was designed to reduce vibration, and an exhaust to minimize noise and fumes was constructed. The electric control features are of interest to research physicists because they permit a wide range of very steady current in the magnet laboratory. The 4-ton flywheel on the Diesel engine assures steady speed and makes possible a great flexibility of output current and voltage. Our first big magnet was built by us at modest cost and is similar to the iron yoke type[1] now in wide use. Performance figures are given for the 2-in. pole gap, 5½-in. pole diameter (Armco magnet iron), for power up to 75 kw. The special equipment for cryogenic studies are items fitted to our research needs. Finally, we discuss the design of our proposed 300-kw magnet. We acknowledge a grant from the Robert A. Welch Foundation. The Office of Naval Research has kindly made the big generator available for our use and we are indebted to several groups for technical advice.

[1] F. Bitter and F. E. Reed, Rev. Sci. Instr. **22**, 171 (1951).

R10. Nuclear Paramagnetism of Liquid Helium-3.* H. E. RORSCHACH, JR., AND W. V. HOUSTON, *The Rice Institute.*—A new method of treating the nuclear excitations in a liquid has been developed to treat the problem of the Curie law deviation of liquid helium-3.[1] The excitation spectrum of the liquid is estimated from a treatment of the nuclear motion in a periodic potential. A band structure results which suggests that the single-particle spectrum consists of a single narrow band of Bloch-type states below a continuum. The susceptibility ratio χ/χ_c (where χ_c is the Curie value) can be calculated for this spectrum; the agreement with experiment is good below 0.4°K. Above 0.4°K, the theoretical curve falls below the experimental values. This deviation above 0.4°K can be understood in terms of the nuclear correlations, and a simple way of estimating the correlations will be described.

* Supported in part by the National Science Foundation.
[1] Fairbank, Ard, and Walters, Phys. Rev. **95**, 566 (1954).

R11. On the Origin of the Lambda Transition in Liquid Helium. LOUIS GOLDSTEIN, *Los Alamos Scientific Laboratory.*—In recent work an indirect and qualitative proof has been presented on the kinetic energy origin of the lambda transition.[1] The proof is based on the temperature variation of the mean potential energy, per atom, exchange energy included, across the lambda point. Combining these calculated potential energies with the empirical liquid helium binding energies, we have obtained the approximate mean kinetic energies per liquid atom over a temperature interval containing the lambda point. The mean kinetic energy was found to exhibit a highly nonsymmetric cusp at the lambda point, with a sharply increasing branch, in the He II range, at the approach of transition temperature. This provides a quantitative sharpening of the proof for the kinetic energy origin of the lambda transition. In addition, the calculated mean kinetic energies directly demonstrate the existence of the very large zero-point kinetic energy of liquid helium over the explored liquid temperature range.

[1] L. Goldstein and J. Reekie, Phys. Rev. **98**, 857 (1955).

R12. Experimental Thermal Conductivities of Gases and Gaseous Mixtures. J. M. DAVIDSON, *General Electric Company, Richland.*—The thermal conductivities of nitrogen, helium, carbon dioxide, neon, and their binary mixtures were determined at zero degrees centigrade relative to the best estimated value for air. The thermal conductivities of mixtures of helium–carbon dioxide at 100°C were also determined. The method used was an unsteady state determination using large concentric cylinders similar to that used by Winkleman. Empirical relationships between mole fraction and conductivity were determined where applicable and they agree with the experimental curves within 5%. The results of this

work are in agreement with known data of other investigators, where available, and are believed accurate to within 2 to 5% of the absolute value of the thermal conductivity.

R13. Semi-Absolute Electrostatic Voltmeter. José Mireles Malpica, *Instituto Politécnico Nacional, Mexico.*—Invariance of force-voltage characteristics between two conductors with respect to a linear expansion or contraction of the system, and its simple relationship when distance of separation between conductors is maintained constant, permit a one-point calibration carried out in a standarizing laboratory with the aid of an absolute instrument to be extended to all the members of a family of instruments. One number represents the root-mean-square voltage, the other dynes. It is possible to build a semi-absolute voltmeter suitable to any range of voltages chosen; other datum needed is the value of "g" of the locality. The force voltage relationship is practically unaffected by atmospheric pressure and humidity. For high voltages, spherical electrodes one radius apart have been chosen, with the lower half of the upper electrode as the voltage sensitive element. A special balance and counter-weight support the sensitive electrode. A spiral spring calibrated in dynes moved by a graduated dial balances the force of attraction, maintaining the separation between the electrodes fixed. The balance, spring, and an index are located inside the upper sphere. For low voltages, multiple flat parallel electrodes close together are used. Insulating supports maintain in position the elements of the instrument.

Wednesday Morning at 9:30

Auditorio de Humanidades

(Manuel Sandoval Vallarta presiding)

Invited Papers on "Elementary" Particles

S1. Charged *K* Mesons. H. S. Bridge, *M.I.T.* (30 min.)
S2. Photoplate Studies on the *K*-Meson Family. A. Pevsner, *M.I.T.* (30 min.)
S3. Recent Studies of V Particle Production. G. H. Trilling, *California Institute of Technology.* (30 min.)
S4. Heavy Mesons and Hyperons: A Progress Report. W. B. Fretter, *University of California.* (30 min.)

Wednesday Morning at 9:00

Auditorio de Ciencias

(E. S. Akeley presiding)

Invited Papers in Theoretical Physics

T1. Divergences in Field Theory. Alejandro Medina, *Universidad de Mexico.* (30 min.)
T2. Collective Motions and Nuclear Reactions. Marcos Moshinsky, *Universidad de Mexico.* (30 min.)
T3. Theory of Gravitation. Carlos Graef Fernandez, *Universidad de Mexico.* (30 min.)
T4. Some Attempts at Quantization of the Gravitational Field. F. J. Belinfante, *Purdue University.* (30 min.)

Wednesday Morning at 9:30

Auditorio de Comercio

(R. J. Seeger presiding)

Fluid Dynamics and Allied Topics

U1. Linearized Flow Theory and Shock Waves in Metals. G. E. Duvall, *Stanford Research Institute.*—The steady, irrotational, supersonic flow of a compressible fluid in a plane is approximately described by a wave equation if the Mach number of the flow is but slightly greater than unity.[1] The shock waves induced in solids by detonation of high explosives are in many cases adequately treated by a hydrodynamic theory, and, since the Mach number is only slightly greater than unity, the linearized theory can be applied. Two problems are considered. The collision of two metal plates traveling at high velocity results in a stable flow if the angle between the colliding plates does not exceed a value B_0. B_0 as calculated by the linearized theory turns out to be in good agreement with more exact calculations. A more complicated experiment is analyzed in which a layer of explosive is placed on each side of an iron plate, and the two layers are detonated simultaneously at the same end. The pressure behind the detonation front is assumed to be given by a Prandtl-Busseman calculation and the plate is found to be split into two, three, or more pieces, depending on the ratio of explosive to thick thickness. This is in qualitative agreement with the experiments.

[1] G. N. Ward, *Linearized Theory of High Speed Flow* (Cambridge University Press, Cambridge, England, 1955).

U2. A Proposed Change in Scaling Laws for Explosive Phenomena. Everett F. Cox, *Sandia Corporation.*—Over-

pressure measurements from chemical and nuclear explosions prove that, without explicitly stated qualifications for meteorological conditions, presently accepted primary scaling laws[1] for blast pressures in air are erroneous. A modification of the scaling laws is therefore proposed: "*Under similar weather conditions*, vector distances to equal overpressures, and time values at radii of equal overpressures, are proportional to the cube roots of charge weights." From this proposition, and considering blast energy dissipation and acoustic refraction for any weather situation, an equation for peak overpressure *versus* distance is derived involving only two empirically determined quantities: signal duration and the effective energy reflection factor over real terrain. For overpressures of less than 30 millibars, this equation has been reasonably well confirmed experimentally over wide ranges of weather conditions and explosion energies.

[1] R. H. Cole, *Underwater Explosions* (Princeton University Press, Princeton, New Jersey, 1948), Chaps. 4 and 7; Los Alamos Scientific Laboratory, *The Effects of Atomic Weapons* (McGraw-Hill Book Company, Inc., New York, 1950), Eqs. 3.16.1 and 3.16.2.

U3. Observations of Ionospheric Drifts over Puerto Rico. MIGUEL WIEWALL, JR., *Universidad de Puerto Rico.*—Three receivers with antennas at the corners of a right-angled triangle with sides 129 m in length receive the ionospheric echoes of the pulses sent by a nearby transmitter at 2.33 Mc. The interference pattern at ground level produced by echoes returned from various points in the ionosphere possesses motion which is a function of the component motions of the ionized matter in the ionosphere. This appears at the receiver antennas as fading of the returned echoes with time lags between the fades. Analysis of the data thus obtained may yield (a) the drift component and (b) the turbulence component of the motions in the ionosphere. Fading records have been obtained for a transmitting frequency of 2.33 Mc, during daylight hours several days each week, since February, 1954. Similar records for 4.57 Mc have been obtained since June, 1954. The data have been analyzed for direction of drift by the method of similar fades. Data for selected months have been subjected to analysis by the six-point correlation method. The results are summarized and compared.

U4. Application of Light-Scattering Theory to the Measurement of Density Fluctuations in Turbulent Fluids. HOWARD A. STINE AND WARREN WINOVICH, *NACA.*—It is shown that photometric measurements in the scattered field produced by passing a plane light wave through a nonabsorbing turbulent fluid can be used to define the integral scale and average intensity of density fluctuations. The analysis is based upon the scattering cross section deduced by Booker and Gordon and thus assumes isotropic fluctuations having an exponentially decaying autocorrelation. It is also predicated on the hypothesis that the scattering centers are large as compared to the radiation wavelength. Photometric data taken through turbulent boundary layers in air are compared with theory to show that, even though the density fluctuations are thought to be anisotropic, the functional agreement is good. Thus, the technique promises to be a powerful tool for the detection and measurement of density fluctuations in compressible boundary layers, wakes, and jets.

U5. Use of Electric Arc Heating in Ultra-High Temperature Aerodynamics. R. W. PERRY AND D. E. BLOXSOM, *ARO, Inc.*—Since the composition of air heated directly by electrical discharge apparently cannot be appreciably "frozen" by any practical quenching rate,[1] it is possible that arc-heated air may be simply expanded in a nozzle to produce useful flows with very high stagnation temperatures. Such flows have previously been achieved only indirectly and inefficiently by passing a strong shock wave through still air and then further expanding the shock-heated and compressed air to the desired velocity. A description is given of small-scale experimental studies on the composition of arc-heated air after expansion, and of the generation and maintenance of strong shock waves at high densities, using the sustained-discharge type of electrically driven shock tube.

[1] Steinmetz, Chem. Met. Eng. **22**, 353 (1920).

U6. Hydrodynamic Impact of Curved Surfaces. M. D. BLEDSOE, *David Taylor Model Basin, U. S. Navy,* AND V. G. SZEBEHELY, *David Taylor Model Basin, U. S. Navy, George Washington University, and University of Maryland* (introduced by E. H. KENNARD).—The effect of form parameters on the impact pressure are studied for the case of an elongated body striking the still water surface. The body rotates around a fixed axis parallel to the undisturbed water surface and normal to the longitudinal axis of the body. Its transverse sections (intersections of the contour of the body with planes normal to the longitudinal axis) are expressed as polynomials. The body is assumed to be rigid and the water incompressible. For the foregoing model, the pressure developed on the body is computed as a function of time and position. Several bodies are generated by changing systematically the transverse sections, and the effect of the shape on the pressure distribution, on the location of the maximum pressure, etc., is presented. The method presented is based on the basic equations for unsteady, incompressible potential flow.

U7. Slow Motions. K. M. SIEGEL AND A. L. MAFFETT, *University of Michigan.*—A generalization of the separation-of-variables technique[1] previously employed to obtain a stream function for the flow of a viscous fluid about a sphere and a prolate spheroid is presented. Hobson[2] used a method due to Basset[3] to transform an electrostatic potential into an ideal stream function for an ogive (minor segment of a circle rotated about its chord). A generalization of Basset's method[4] is applied to a Payne[5] ideal stream function to obtain a slow motion (or viscous) stream function for an ogive.

[1] K. M. Siegel, Phys. Rev. **82**, 311 (1951).
[2] E. W. Hobson, Cambridge Phil. Trans. **XIV**, 211 (1889).
[3] A. B. Basset, *Hydrodynamics* (Cambridge University Press, Cambridge England, 1888).
[4] Siegel, Halpin, and Maffett, Phys. Rev. **95**, 658 (1954).
[5] L. E. Payne, Quart. Appl. Math. **X**, No. 3 (October, 1952).

U8. Drag in a Rotating Cylinder Apparatus near Conditions of Free Molecule Flow. J. M. BOWYER, *Convair Aircraft Corporation,* AND L. TALBOT, *University of California, Berkeley.*—An experimental study was made of the drag on a rotating cylinder near conditions of free molecule flow. The results of this study are compared with a solution to the Boltzmann equation obtained by Wang Chang and Uhlenbeck for a similar flow between parallel flat plates in relative motion, their result having been modified so as to agree to zeroth approximation with the free molecule flow solution for a rotating cylinder. The agreement between experiment and theory was found to be good with argon and air, provided the rotor Mach number was less than 0.15 and the Knudsen number based on gap width was greater than 2. The agreement between theory and experiment was less good for helium and krypton. The discrepancies may have been the result of large differences in properties between these gases and the contaminating residual gases (chiefly air). Irrespective of the medium, agreement was also poorer at rotor Mach numbers above 0.2 or at Knudsen numbers less than 2. These disagreements are to be expected, since the theory is valid only for small Mach number and large Knudsen number.

U9. Magnetohydrodynamic Waves in an Ionized Plasma. W. A. NEWCOMB, *University of California, Livermore.*—Magnetohydrodynamic waves are studied by the method used by Landau[1] for plasma oscillations. We linearize the Boltzmann equation for small perturbations from equilibrium, and then solve it for arbitrary initial conditions, neglecting collisions. For large times the solution approaches a plane

wave with complex frequency, and a dispersion formula is obtained, relating frequency to wave number. Our results differ somewhat from those of the conventional hydrodynamic treatment. The waves are damped, even without collisions, by a mechanism similar to the Landau damping of plasma oscillations. At zero temperature the two circularly polarized components have slightly different velocities, giving rise to a Faraday effect. The magnitude of the Faraday effect increases with temperature because of shear stresses produced by thermal motions of the particles. Beyond a certain critical temperature, the thermal stresses begin to increase more rapidly, and one circularly polarized component has a much larger velocity than is given by the hydrodynamic treatment, while the other has a much lower velocity. At still higher temperatures the waves cannot exist because of heavy damping.

[1] L. Landau, J. Phys. **10**, 25 (1946).

U10. Fluctuation of Sound Transmitted in the Ocean. R. W. STEWART AND W. N. ENGLISH, *Pacific Naval Laboratory.*—Further analysis and sea experiments over a ½-mile path at frequencies near 18 kc have confirmed and extended the results previously reported.[1] The standard deviation of the fluctuation calculated over samples of 100 pulses typically lies between 1 and 4 db with maximum about 10 db. The auto correlation calculated over a few minutes is near unity for intervals less than 0.1 second, then falls sharply to a mean of 0.5 at 0.3 second, and is close to zero at 2 to 10 seconds. As the sample size is increased, longer fluctuation periods are continually revealed. The average cross correlation with horizontal hydrophone separation is high for spacings of a few feet and is still 0.5 at 24 feet. In contrast, with vertical separation it is low until the spacing has been reduced to a few inches. Typically, the spread of cross correlations is much wider than if drawn from a single population of normal distribution. The cross correlation between simultaneous pulses at two frequencies over the same path has a zero median, but again a wider distribution than expected.

[1] H. L. Grant and R. W. Stewart, Phys. Rev. **92**, 1087(A) (1953).

WEDNESDAY MORNING AT 9:30

Auditorio de Ingeniería

(C. KITTEL presiding)

Solid-State Physics

V1. Intermolecular Force Fields in High Polymers Composed of Alternating Dipole Chains. WERNER BRANDT, *E. I. du Pont de Nemours and Co., Inc.*—Our semi-empirical potential energy function of interaction between polymeric chain molecules has been extended from the nondipolar case of polyethylene[1] to molecular chains composed of alternating atomic dipoles. From this function, the lattice energy per chain recurrent unit at 0°K has been calculated for polytetrafluoroethylene $(-CF_2-CF_2-)_n$ and polytrifluoromonochloroethylene $(-CF_2-CFCl-)_n$. The contributions from dispersion, induction, and orientation forces have been estimated. The force-constants of the Lennard-Jones (12-6) potential of the $(-CF_2-)$ group are $\sigma=5.45$ A and $\epsilon/k=18.2°$ K, of the $(-CFCl-)$ group $\sigma=6.11$ A and $\epsilon/k=25.1°$K. The compressibilities and their pressure dependence of both polymers, calculated from the energy of chain interaction, are in agreement with experimental data.[2,3]

[1] W. Brandt, Phys. Rev. **98**, 243 (1955).
[2] P. W. Bridgman, Proc. Am. Acad. Arts Sci. **76**, 71 (1948).
[3] C. F. Weir, J. Research Natl. Bur. Standards **46**, 207 (1951); *ibid.* **53**, 245 (1954).

V2. A Computation of the Vacancies Created by Heavy Corpuscular Radiation. W. S. SNYDER AND J. NEUFELD, *Oak Ridge National Laboratory.*—In a monoatomic substance, it is considered that a moving atom of energy E displaces an atom of the medium if upon collision the energy loss y exceeds a threshold $\alpha\sim25$ ev, but that the striking atom replaces it if $E-y<\alpha$. Thus the number of vacancies is not equal to the number of atoms displaced or "knocked out" from their original sites. The number of displaced atoms has been calculated by the authors,[1] and the methods used there have been applied to calculate the number of vacancies. It is found that, in general, the number of vacancies is about ½ the number of displaced atoms and is, for velocities of the initial atom $<c^2/\hbar$, given by $E/3\alpha$.

[1] W. S. Snyder and J. Neufeld, Phys. Rev. **97**, 1637–1646 (1955).

V3. The Effect of Impurities on Lattice Vibrations.* ELLIOTT W. MONTROLL AND R. B. POTTS, *University of Maryland.*—An impurity, such as an isotope, hole, or interstitial in an otherwise perfect lattice, can give rise to a localized vibrational mode with a normal frequency above the band. These localized modes and frequencies can be calculated either by direct solution of the difference equations for the normal frequencies or by use of Green's functions.[1] A determination of zero point energies enables the force law between two impurities (e.g., two isotopes, or an interstitial and a hole) to be computed. Results have been obtained for the one-dimensional and the simple cubic lattices.

* This research was supported by the Office of Scientific Research of the Air Research and Development Command.
[1] A similar procedure has been used in the theory of electrons in solids: G. F. Koster and J. C. Slater, Phys. Rev. **95**, 1167 (1954).

V4. On the Variation with Temperature of the Thermal Conductivity of Seven Alkali Halides. KATHRYN A. MCCARTHY AND STANLEY S. BALLARD,* *Tufts University.*—The thermal conductivity of crystalline barium fluoride, calcium fluoride, cesium bromide, cesium iodide, potassium bromide, potassium chloride, and sodium chloride have been measured over the temperature range from 230°K to 370°K, using the comparison method previously reported.[1] Thermal conductivity was found to decrease with increasing temperature within this temperature range, for all seven crystals. For potassium bromide, potassium chloride, and sodium chloride, thermal conductivity varies approximately as T^{-1}; for calcium fluoride the function is more nearly $T^{-1}\exp(-\Theta/2T)$, where Θ is the Debye temperature. These results seem to be reasonably consistent with the theoretical predictions of Klemens,[2] namely that for $T\cong\Theta$, thermal conductivity should vary inversely with T, whereas when $T\cong\Theta/6$, the $T^{-1}\exp(-\Theta/2T)$ relationship is applicable. The temperatures at which we made the measurements approximate the Debye temperatures for potassium bromide, potassium chloride, and sodium chloride but are intermediate between Θ and $\Theta/6$ for calcium fluoride, for which $\Theta=474°$K. It would be interesting to extend these thermal conductivity measurements to somewhat lower temperatures, to be compared with those of Eucken and Kuhn, and de Haas and Biermasz at very low temperatures.

* Present address: Scripps Institution of Oceanography.
[1] Ballard, McCarthy, and Davis, Rev. Sci. Instr. **21**, 905–907 (1950).
[2] P. G. Klemens, Proc. Roy. Soc. (London) **A208**, 108 (1951).

V5. Surface Trapping in Germanium. H. A. GEBBIE, *M.I.T.*, AND K. BLODGETT III, *Polaroid Corp.*—Measurements of the steady-state photoconductance *versus* light intensity have been used to investigate surface states. The response for *N*-type specimens in the temperature range 200°K–240°K could generally be represented by a linear component and a component showing saturation with increasing intensity. The latter is attributed to trapping of minority carriers in localized states. It is now found that the number of these states available is dependent on the history of the etched surfaces and can be changed by ion bombardment. This suggests surface traps. Concentrations of 10^{12} per cm^2 have been measured, and a decrease with time after etching is observed when the surfaces are in contact with oxygen. The rate of hole-electron recombination was dominated by the surface term and could be found from the linear component of photoconductance. No correlation has so far been found between the trap concentration and the surface recombination rate. This suggests that more than one type of center is present on these surfaces. The excess noise spectra in these crystals is influenced by trapping, and changes in noise with surface history have also been observed.

V6. Interaction of Elementary Particles. JOSEPH G. BARREDO,* *Rocasolano Institute.*—Considering the time derivative of the number of dipoles in line with carriers, trions, as the characteristic variable of a system of particles, the equation $I=EqF(4qzd/m)^{-\frac{1}{2}}t^{-\frac{1}{2}}\exp(2EF/RT)$ was deduced which gives the current I produced by the recombination of elementary particles as a function of the mass m, the charges q and z of the particles, the length of the dipole d, the Faraday F, the energy of activation of the trion E, and the time t. This equation unifies the description of electrical phenomena not explained by equilibrium statistics in which neither the recombination phenomena nor the time were taken into account.[1] The value 2 of the exponent was proved experimentally to be 2 ± 0.001 for the recombination of electrons, holes, and protons in semiconductors and in matter in other states of aggregation.

* Now at the University of Chicago.
[1] J. G. Barredo, Phys. Rev. **83**, 243 (1951); *ibid.* **98**, 229 (1955); J. Chem. Phys. **19**, 1065 (1951); Bull. Am. Phys. Soc. **30**, No. 2, 19(A) (1955).

V7. The Arrangement of Atoms in Wollastonite-Type Crystals. M. J. BUERGER, *M.I.T.*—Pectolite, $NaHCa_2Si_3O_9$, has space group $P\bar{1}$, $a=7.99$ $b=7.04$ $c=7.02$ A, $\alpha=90°\,03'$, $\beta=95°\,17'$, $\gamma=102°\,28'$. In the Patterson map, $P(xz)$, two sets of rotation peaks and their unsymmetrical conjugates were found. With the aid of these, two minimum function maps, $M_2(xz)$, were readily prepared. These were scaled to the weights of their respective rotation peaks and combined to form $M_4(xz)$. This revealed the general nature of the structure. Next, the Patterson function $P(xy)$ was decomposed into a symmetrical (monoclinic) component and a less symmetrical superstructure component. The Patterson map corresponding to the superstructure $\partial P(xy)$ was readily solved by minimum function $\partial M_2(xy)$ for the locations of the unsymmetrical atoms. When this was combined with the full minimum function $M_2(xy)$, the entire structure was evident. In this way the locations of the 15 atoms of the assymetrical unit were found by direct methods. The same methods were also applied to Wollastonite, $CaSiO_3$. Details of these structures are given elsewhere. They are definitely based upon SiO_3^{-2} chains, whose shape is responsible for the triclinic symmetry.

V8. Concerning Present Limitations of X-Ray Analyses of Organic Natural Products.* O. CANO-CORONA, *Universidad Nacional Autónoma de Mexico*, AND R. PEPINSKY, *The Pennsylvania State University.*—The usefulness of x-ray structure analysis in biochemistry can be enhanced if both diffractionists and chemists understand the conditions under which an x-ray determination is feasible. Factors which enter into criteria for amenability of crystals to complete analysis are outlined. Consider an optically active molecule with perhaps fifteen or more nonhydrogen atoms, no heavy atom, and of unknown configuration. Unless the cell symmetry is extremely favorable, a successful analysis is at present unlikely. Successful application of (correct!) statistical methods depends upon favorable symmetry and chemically recognizable features. Introduction of heavy atoms, and particularly anomalous scatterers, vastly improves the situation. With optically active molecules of twice this size, analyses should be attempted only if favorable heavy atoms are present, some chemical information concerning configuration is available, and the cell symmetry is advantageous. Success with still larger molecules may be possible only if major structural principles have been established through examination of molecular fragments and recognition—on chemical or physical grounds—of severe limitations upon the manner in which these fragments can combine. Accuracy of atomic coordinates decreases, and computational costs climb rapidly, with molecular size.

* Assisted by Rockefeller Foundation and National Institutes of Health.

V9. Developments in the Statistical Approach to X-Ray Crystal Analysis.* V. VAND AND R. PEPINSKY, *The Pennsylvania State University.*—Earlier claims for the statistical approach to phase determination in x-ray analysis foundered on incorrect statistics. The approach aimed at extracting a single "most probable" solution. When correct statistics are employed, it can be shown that the "most probable" solution need not correspond to the *correct* solution, even when homometric solutions are excluded. The probability for this correspondence is likely to be quite low for equal-atom structures of even moderate complexity. Cochran and Douglas have placed the statistical approach on a sounder basis by selecting sets of solutions of comparatively high probability, derived by a matrix method utilizing Sayre's relations. Their procedure involved between minutes and hours of time on the high-speed electronic computer EDSAC. We have modified the procedure by introducing constraint matrices and more efficient methods for searching for the more probable phase permutations. Therewith we can perform *by hand* computations on structures similar to those examined by Cochran and Douglas, and in times comparable to those required on EDSAC. Use of our procedures with a high-speed digital computer will permit application to more complex structures in reasonable periods of time. Utilizing X-RAC, we have also introduced strong criteria of boundedness and chemical reasonability which permit selection between the solutions.

* Development supported by the Office of Naval Research and National Institutes of Health.

V10. Direct X-Ray Determination of Absolute Configurations of Optically Active Molecules.* Y. SAITO, Y. OKAYA, AND R. PEPINSKY, *The Pennsylvania State University.*—We have shown that when anomalous scattering atoms are present in a crystal, the convolution of the imaginary part of scattering material is represented by

$$P_s(u,v,w)=\Sigma_{hkl}|F_{hkl}|^2\sin 2\pi(hu+kv+lw).^1$$

$P_s(u,v,w)$ shows peaks of height $f_j'\cdot f_i''-f_j''\cdot f_i'$ at (u,v,w) and $f_j''\cdot f_i'-f_j'\cdot f_i''$ at $(-u,-v,-w)$, where $f_j=f_j'+if_j''$, etc. This permits identification of vectors *from* the anomalous scatterer *to* normal scatterers, and hence directly gives the absolute configuration of noncentric distributions about the anomalous scatterer. The method has been applied to hexagonal 2-*d*-$[Co(en)_3]Cl_3\cdot NaCl\cdot 6H_2O$ (en = ethylene diamine), via a generalized projection using intensities $I(hki2)$ and $I(hk\bar{i}2)$ $[=I(\bar{h}\bar{k}i2)$, by symmetry], with CuKα radiation scattered anomalously by the cobalt atoms. X-RAC computation of

$$P_s^{c2}=\tfrac{1}{2}\Sigma_{hk}(F_{hki2}^2-F_{hk\bar{i}\langle 2\rangle}^2)\cos 2\pi(hu+kv)$$

revealed the structure and absolute configuration straightforwardly. The results are in agreement with a previous analysis[2] according to the technique described by Bijvoet.[3]

* Development supported by Office of Naval Research and National Institutes of Health.
[1] Okaya, Saito, and Pepinsky, Phys. Rev. (to be published).
[2] Saito, Nakatsu, Shiro, and Kuroya, Acta Cryst. 7, 636 (1954); *ibid.* (to be published).
[3] J. M. Bijvoet, Nature 173, 888 (1954).

V11. Crystal Engineering: A New Concept in Crystallography.* R. PEPINSKY, *The Pennsylvania State University.*—Crystallization of organic ions with metal-containing complex ions of suitable sizes, charges, and solubilities results in structures with cells and symmetries determined chiefly by packing of the complex ions. These cells and symmetries are to a good extent controllable; hence crystals with advantageous properties can be "engineered." X-ray examination of a large number of such structures show the complex ions ideally placed for structure factor phase determination, both by the direct contribution of the ions to the structure factors and through image seeking in interatomic vector maps. Locations of the complex ions are readily established from such maps. Use of optically active complex ions of known hand permits direct establishment of the absolute configuration of optically active organic ions included in the lattice. Use of complex ion salts also facilitates introduction of anomalous scatterers into optically active crystals, to permit application of the direct method for structure determination recently developed by Okaya, Saito, and Pepinsky.[1] Examples of structures of a number of complex ion salts with organic ions are presented to illustrate these concepts.

* Assisted by the Rockefeller Foundation and the National Institutes of Health.
[1] Okaya, Saito, and Pepinsky, Phys. Rev. (to be published).

WEDNESDAY AFTERNOON AT 14:30

Auditorio de Humanidades

(W. B. FRETTER presiding)

Invited Papers

W1. Origin of the Knee of the Latitude Effect of Cosmic Rays. MANUEL SANDOVAL VALLARTA, *Universidad de Mexico.* (30 min.)

W2. The Low-Energy End of the Primary Cosmic-Ray Spectrum. E. P. NEY, *University of Minnesota.* (30 min.)

W3. Studies of Extra-Terrestrial Phenomena during the International Geophysical Year. J. A. SIMPSON, *University of Chicago.* (40 min.)

W4. Design Considerations for Research Reactors. L. B. BORST, *New York University.* (30 min.)

WEDNESDAY AFTERNOON AT 14:30

Auditorio de Ingeniría

(J. C. SLATER presiding)

Invited Papers

X1. Neutron Crystallography. RAY PEPINSKY, *Pennsylvania State University.* (30 min.)

X2. Neutron Diffraction Studies of Metal-Hydrogen Systems. S. S. SIDHU, *Argonne National Laboratory.* (30 min.)

X3. The Magnetic Properties of Superconductors. C. F. SQUIRE, *The Rice Institute.* (30 min.)

WEDNESDAY AFTERNOON AT 15:00

Auditorio de Ciencias

(JOSÉ MIRELES MALPICA presiding)

General Nuclear Physics

Y1. Report on a Liquid Helium Bubble Chamber.* W. M. FAIRBANK, E. M. HARTH,† M. E. BLEVINS, AND G. G. SLAUGHTER, *Duke University.*—Liquid helium at the normal boiling point and one atmosphere pressure was superheated by expanding the helium vapor above the liquid, and good tracks of Compton electrons from a ½ mc Na^{22} source were obtained. The bubble chamber consisted of a Pyrex cylinder 5.5 cm in diameter and about 10 cm long, which was immersed in a bath of liquid helium. The tracks were photographed in a dark field. Good contrast was achieved in spite of the very similar indexes of refraction of helium in its liquid and vapor phase by placing the camera almost in line with the source of

light. The sensitive time of the chamber both before and after expansion, as well as the dependence of bubble density on specific ionization and track age, are being investigated.

* Work supported by the Office of Naval Research and the Office of Ordnance Research.
† On leave of absence from Naval Research Laboratory.

Y2. Efficiency of Zinc Sulfide—Plastic Counters for Fast Neutrons.* W. J. RHEIN, *Spring Hill College.*—Scintillators which respond to fast neutrons were prepared by molding activated zinc sulfide and transparent hydrocarbon plastics (1.5 parts to 10) into cylinders 5 cm in diameter and 1.6 cm high. They were fitted to a photomultiplier and used for counting fast neutrons. These counters are insensitive to gamma rays. The absolute efficiencies of these counters were determined for monoenergetic neutrons between zero and six Mev, and for several values of the discriminator bias in the scaler. Typical efficiencies for counting 4-Mev neutrons are 0.003 with 20 v bias, 0.0003 with 30 v bias. The efficiencies increased linearly with the energy of the neutrons. Three types of clear plastics were tried in the scintillators, and they all gave nearly equal results. Graphs of efficiencies and of pulse height analyses of the scintillators will be shown.

* Work done at the University of Texas and supported by the U. S. Atomic Energy Commission.

Y3. Determination of the Magnetic Field Strength H and Its Vector Potential A in Terms of the Magnetic Field Strength H_0 on a Plane Surface, with Application to the Spiral Ridged FFAG Accelerator.* EDWARD S. AKELEY, *Purdue University and the Midwestern Universities Research Association.*—If $\nabla \mathbf{x} \mathbf{H} = \nabla \cdot \mathbf{H} = \nabla \cdot \mathbf{A} = 0$, then $\mathbf{H}$ and $\mathbf{A}$ are expressible as operators operating on $\mathbf{H}_0$ and $\mathbf{A}_0$, for instance

$$\mathbf{A}_t = C_\Delta \mathbf{A}_{t0} + S_\Delta [\Delta_t A_{z0} + \mathbf{k} \mathbf{x} \mathbf{H}_{t0}],$$

where $\mathbf{k}$ is a unit vector perpendicular to the plane, z the corresponding coordinate. The subscript t denotes the component of a vector in the plane. Δ_t and ∇_t are, respectively, the Laplacian and nabla operators in the plane. $C_\Delta = \cos z\sqrt{\Delta_t}$ and $S_\Delta = \sin z\sqrt{\Delta_t}/\sqrt{\Delta_t}$ are operators. Furthermore, given $\mathbf{H}_0$, $\mathbf{A}_0$ must satisfy a single coordinate equation, but otherwise may be chosen arbitrarily. These relations were particularly useful in studying the magnetic field of the spiral ridged FFAG accelerator

* Assisted by the National Science Foundation.

Y4. A Čerenkov Counter for High-Energy Cosmic Rays. D. C. MOORE AND R. J. HANSON, *University of Nebraska.*—The fact that charged particles moving with a velocity less than c/n do not produce Čerenkov radiation makes it possible to construct a counter containing a dielectric which will count all particles with a velocity greater than c/n (where c is the velocity of light in a vacuum and n is the optical index of refraction of the dielectric). If a gas is used as dielectric, the counter will be sensitive to only extremely energetic particles. A counter, using Freon 13 B-1 as a dielectric, has been designed and is under construction. It will operate at pressures up to 15 atmospheres with an index of up to 1.015. By operating at different pressures, it is expected that particles can be detected with lower velocity limits from 0.985 c to 0.9999 c. Design details and such performance measurements as have been made will be discussed

Y5. Properties of Halogen-Quenched Geiger Counters.* H. SHERMAN, *New York University.*—Time lags in chlorine and iodine-quenched Geiger counters have been investigated as a function of various parameters. Pulsed soft x-rays of quarter microsecond duration were used as the source of ionization. Van Zoonen and Prast[1] and Shinohara and Akutsu[2] have measured the efficiencies of bromine-quenched counters as a function of radial distance of the ionizing event from the central wire, and the latter have given a relationship for the efficiency of these counters which depends upon the concentration and the negative ion attachment probability of the halogen constituent. In our experiments, using a pencil of soft x-rays, similar measurements of efficiency have been made for chlorine and iodine. Experimental values of time lags and efficiency will be presented and compared with the foregoing work.

* Supported by the Office of Naval Research and the Air Research and Development Command.
[1] D. Van Zoonen and G. Prast, Jr., Appl. Sci. Research **B3**, 1 (1952); **B4**, 196 (1954).
[2] K. Shinohara and I. Akutsu, J. Sci. Research Inst. (Tokyo) **47**, 80 (1953).

Y6. Effects of Operating Proportional Counters in High Gamma Fields.* J. T. BRACKEN,† E. A. ROLLOR,† AND J. A. MOHRBACHER, *Convair Aircraft Corporation.*—The effect of positive ion space charge in an argon-filled proportional counter was studied by observing the change in amplitude of Po alpha pulses when the counter was operated in high gamma fields. A decrease in pulse height of approximately 40% was observed when the counter was operated at 1000 v in a gamma field of 11 r/hr. The change in gas amplification was measured as a function of both the gamma field intensity and applied voltage. An empirical relationship was obtained which describes the new gas amplification as a function of the initial gas amplification and gamma field intensity.

* Work was performed under contract with Wright Air Development Center of the Air Force.
† Now at Lockheed Aircraft Corporation, Marietta, Georgia.

Y7. Ionization of Cloud-Chamber Tracks.* E. K. BJÖRNERUD,† *California Institute of Technology.*—A photoelectric method for measuring the specific ionization of tracks on cloud-chamber photographs is described. An important feature of the method is the use of a comparison track of known ionization in the same part of the chamber. A microphotometer slit is made to scan the track perpendicular to its direction, and a tracing of the transmission of the track relative to the background transmission is obtained. A parameter relating the transmission of the track in question to the transmission of the comparison track is obtained directly from the tracings. Identified π-μ decays are used to establish a calibration curve, and the method is applied to various unknown tracks. The error of measurement is of the order of 10%. A theoretical treatment of the problem is carried out to show the effects of various physical parameters not easily ascertained experimentally.

* Assisted in part by the joint program of the Office of Naval Research and the U. S. Atomic Energy Commission.
† Now at The RAND Corporation, Santa Monica, California.

Y8. Apparent Length of Tracks in Nuclear Emulsions. T. A. BRODY, *National University of Mexico.*—In a previous publication, a two-dimensional model of a nuclear emulsion was used to determine an empirical formula giving the variation of length ΔL of a nuclear track as a function of the background grain density d and the linear grain density D in the track as

$$\Delta L = 19.54 + 6.02d - 0.283D - 0.087dD.$$

In the present paper, this formula is verified by measurements on nuclear emulsions containing uranium α particle and proton tracks whose linear grain density is varied by differing development, and a background of varying density obtained by controlled exposure to γ rays.

Y9. Neutron Total Cross Section Measurements between 13.0 and 16.2 Mev. M. MAZARI, F. ALBA, AND V. SERMENT, *National University of Mexico.*—As a continuation of earlier work,[1] neutron total cross-section measurements in Al, Fe, Ni, Cu, Zn, Ag, Sn, Hg, Pb, and Bi were obtained with monoenergetic neutrons from a $H^3(d,n)He^4$ reaction. The experiments were done in order to extend the available information

obtained from 0 to 3 Mev by the Wisconsin Group,[2] from 3 to 13 Mev by Nereson and Darden,[3] and at 14.12 Mev by Coon, Graves, and Barschall.[4] Preliminary results in the studied region are as follows: Al increases its total cross section, probably approaching a maximum, while in Fe, Cu, Ni, and Zn, the cross section decreases smoothly with increasing neutron energy; Ag has a maximum cross section σ_t of 4.40 barns at about 12.5 Mev, and Sn a σ_t of 4.70 barns at 13.5 Mev; in Hg, Pb, and Bi, the maximum cross sections seem to be at 16.0, 15.4, and 15.8 Mev with a σ_t of 5.49, 5.58, and 5.75 barns, respectively.

[1] Bonner, Alba, Fernandez, and Mazari, Phys. Rev. **94**, 651 (1954).
[2] Miller, Adair, Bockelman, and Darden, Phys. Rev. **88**, 83 (1952).
[3] N. Nereson and S. Darden, Phys. Rev. **89**, 775 (1953); **94**, 1678 (1954).
[4] Coon, Graves, and Barschall, Phys. Rev. **88**, 562 (1952).

Y10. Neutron Detection with BaF_2 Scintillator.* NORMAN A. BOSTROM, EMMETT L. HUDSPETH, AND IRA L. MORGAN, *University of Texas.*—In extending earlier work in this laboratory on the reaction $F^{19}(n,\alpha)N^{16}$, we have sought to measure the absolute cross section by use of a BaF_2 scintillator. Such crystals used with a Dumont 6292 photomultiplier and a Cs^{137} source yielded pulses of approximately one-fifth the height of those obtained from NaI(Tl). The delayed activity from N^{16} is readily detectable in such a crystal and has been measured as a function of discriminator biasing. Large numbers of low-energy pulses, which cannot be explained on the basis of the presently known decay scheme of N^{16}, are observed; these may originate from β rays of very low energy. An estimated *lower limit* to the cross section for the reaction at $E_n = 4.3$ Mev (near the first resonance) is tentatively set as 30 millibarns; this figure may be revised upward considerably, pending further study of the decay spectrum. Direct determination of the cross section through observation of the α particles formed in very small crystals is now being attempted. The possibility of general use of BaF_2 crystals as fast neutron detectors is also under investigation.

* Assisted by the U. S. Atomic Energy Commission.

Y11. Nuclear Moments of Gadolinium from Optical Hyperfine Structure.* F. A. JENKINS AND D. R. SPECK, *University of California.*—Separated isotopes are used for the first time to investigate the structures due to Gd^{155} and Gd^{157}. The superior resolution afforded by multilayer-coated etalons shows that contrary to previous assumptions[1] the spins must be small. All resolved patterns show only three to five components. It is possible to interpret these by assigning $I = 3/2$ to both odd isotopes. In the wide structure of the unclassified line λ4436.1, the fifth component is ascribed to the most abundant even isotope present, and the others do not obey the interval rule. Four-component lines like 5856.2, and the many three-component ones like 5015.0, are explainable as due to the superposition in different relative positions of this even isotope component on a four-line pattern. With the revised value of the spin, which is at present incomprehensible on the shell model, a recalculation of the magnetic moments yields $\mu(155) = -0.31$ and $\mu(157) = -0.38$ nm. An attempt will be made to confirm these values by studying the Gd II lines, using a new type of ultraviolet-transmitting multilayers. Work on the isotope shifts is also in progress.

* Supported by the National Science Foundation.
[1] K. Murakawa, Phys. Rev. **96**, 1544 (1954).

Y12. Coulomb Enhancement of Positron Annihilation in Metals.* RICHARD A. FERRELL, *University of Maryland.*—Free electron theory lifetimes for positrons annihilating in metals are several times larger than observed.[1] Coulomb attraction causes the discrepancy by increasing the electron density at the positron. On the other hand, positronium formation does not take place in a metal, as seen from the absence of both a slow decay[1] and a narrow 2-photon angular correlation.[2] Taking Landsberg's screened coulomb potential,[3] which yields the sodium soft x-ray emission tail, we have made a perturbation calculation of the enhancement of the annihilation rate in sodium. Landsberg's range is sufficiently short not to give binding and lead to positronium formation. Free electron theory predicts a mean annihilation lifetime of positrons in sodium of 5.2×10^{-10} sec, while we find about 2.3×10^{-10} sec, in better agreement with the experimental value[1] of $(1.5\pm0.5)\times10^{-10}$ sec. The relation to Bohm-Pines theory will be discussed.

* Research supported by the Office of Naval Research.
[1] S. DeBenedetti and H. J. Richings, Phys. Rev. **85**, 377 (1952); R. E. Bell and R. L. Graham, Phys. Rev. **90**, 644 (1953).
[2] R. E. Green and A. T. Stewart, Phys. Rev. **98**, 486 (1955).
[3] P. T. Landsberg, Proc. Phys. Soc. (London) **A63**, 806 (1949).

Y13. Thick Target Bremsstrahlung Spectra for 1.00-, 1.50-, and 2.00-Mev Electrons. E. A. EDELSACK AND W. E. KREGER, *U. S. Naval Radiological Defense Laboratory.*—A study of thick target spectra of the bremsstrahlung radiation for electrons was undertaken. The NRDL 2-Mev positive ion electrostatic generator was used as the source of monoenergetic electrons calibrated relative to the $Be^9(\gamma,n)$ threshold taken as 1630 kev and the $Li^7(p,n)$ threshold taken as 1881.4 kev. The long-time energy stability of the accelerator was approximately ±2%. The present measurements are concerned only with the radiation from gold, silver, copper, and aluminum targets at electron energies of 1.00, 1.50, and 2.00 Mev. The target thickness for each element at each energy was 10% greater than the calculated maximum range of electrons in the target material at the particular energy involved. Also a 0.125-in. thick gold target was used for some spectral measurements to determine the effect of the additional target thickness on the shape of the spectra. The photon distribution was measured with a 4-in. by 4-in. single crystal gamma-ray scintillation spectrometer. The angle ψ between the collimator-spectrometer axis and the direction of the incident electrons was adjusted so that $\psi = 0°$. Some measurements were also made for a value of $\psi = 90°$. The angle θ between the plane of the target and the incident electron beam was 45° for all measurements. Preliminary experimental results will be presented and these results will be compared with computed spectra using existing theory.

WEDNESDAY AFTERNOON AT 14:30

Auditorio de Comercio

(ALEJANDRO MEDINA presiding)

Theoretical Physics, II

Z1. The *T-T* Interaction. R. M. FRANK AND J. F. GAMMEL, *Los Alamos Scientific Laboratory.*—We have made a phase shift analysis of some data[1] on the elastic scattering of tritons by tritons. The data can be fit with a ^1S phase shift (δ) which is about that resulting from scattering by a hard sphere of radius $a = 2.35\times10^{-13}$ cm. If a $^3P-\delta$ is also used

in the analysis, the data requires it to be zero.[2] Since the ^1S state of He^4 is bound by 12.25 Mev relative to two free tritons, the $^1S-\delta$'s must result from a strongly attractive interaction. Such an interaction can give rise to scattering which looks like that resulting from a hard sphere. An example of this occurs in the ^3S state in n-d scattering. Although it is probably absurd to do so, one wonders if there is any connection between the absence of P-wave scattering in T-T and p-p scattering. A possible explanation of the smallness of the $^3P-\delta$ is that the radius of the T-T system is small and the energy is low. It would be interesting to know if the $^3P-\delta$ remains small at higher energies (10 Mev).

[1] Dale Hollaway, Los Alamos Scientific Laboratory, unpublished data at 1.799 and 2.613 Mev.
[2] A confusion of solutions (probably a continuum of them) results if spin orbit splitting is allowed. Since the data can be interpreted in a simple manner, it seems unreasonable to allow spin orbit splitting anyhow.

Z2. Single-Meson Production in Nucleon-Nuclei Collisions.* ALBERT D. WHEALON, *The Ramo-Wooldridge Corporation.*—Total cross sections for the production of charged π mesons during elastic scattering of protons and neutrons by heavy nuclei are computed as functions of beam energy. The nucleus is represented by a static external field and the meson-nucleon coupling taken to be pseudoscalar (γ^5). The closure theorem (i.e., unitarity of the S-matrix) is exploited to express the total cross section in terms of the imaginary part of the forward scattering amplitudes of higher order processes. Feynman-Dyson relativistic perturbation rules are then applied to calculate the single meson emission probability in first Born approximation. The relation $\lim_{\epsilon\to 0}(x-i\epsilon)^{-1}=P(1/x)+i\pi\delta(x)$ is used to separate the imaginary contributions from the parametric integrals. It is found that renormalization effects do not contribute to these imaginary terms and therefore need not be explicitly separated. Graphs of the cross section *versus* nucleon energy will be presented, as well as critical comments on the approximations employed.

* Based on portions of a doctoral thesis submitted to M.I.T. in June, 1952.

Z3. Pion-Pair Production. JUAN DE OYARZABAL, *Universidad de México e Instituto Nacional de la Investigación Científica.*—The present paper analyzes the process of the decay of a neutral tau meson into a neutral and two charged pions. This process seems to be in agreement with the experiment recently reported by Mr. H. Yagoda,[1] who observed in a nuclear emulsion a production of a positive and a negative pion pair without any other associated ionizing particles.

[1] Herman Yagoda, Phys. Rev. **98**, 103 (1955).

Z4. Production of Pairs in the Capture of Slow Neutrons by Protons. A. T. PEASLEE, JR.,* *Harvard University.*—The capture of slow neutrons by protons may be regarded as an isomeric decay. A possible electrodynamic decay process is the emission of an electron-positron pair. Combining the Born approximation total $M1$ internal pair production coefficient[1] for an energy equal to the deuteron's binding energy with the radiative capture cross section,[2] one finds that the total pair production cross section for the capture of unpolarized thermal neutrons by protons is 0.11 millibarn. Since the ^1S to ^3S transition produces a purely transverse current, the pair production is a measure of the same nuclear currents as the more probable radiative capture. Since the latter process is well understood and since the Born approximation is clearly valid in this case, the predicted pair production cross section should agree with experiment. Other electrodynamic modes of decay of the same order in α, such as the conversion of the target's electrons, are much less probable.

* Now at the Los Alamos Scientific Laboratory, Los Alamos, New Mexico.
[1] M. E. Rose, Phys. Rev. **76**, 678 (1949).
[2] H. Feshbach and J. Schwinger, Phys. Rev. **84**, 194 (1951).

Z5. Matrix Element Relations in Beta Decay Theory and Nuclear Forces. T. AHRENS, *Lockheed Aircraft Corporation.*—Relative magnitudes of beta decay matrix elements constitute a potential source of information about the nature of nuclear forces. As one relates different matrix elements to one another, commutators of the Hamiltonian with beta decay operators appear. These seem to be analyzable on the basis of fairly general assumptions regarding the character of of nuclear forces.[1] Relations for the analysis of antidiagonal matrix elements of mixed signature, such as, e.g., $\int\beta\alpha L$ (L=lepton covariant), are set up. Each of them involves, generally among other commutators, a Hamiltonian commutator whose beta decay operator is also antidiagonal but of uniform signature, in the mentioned example αL. Analogous relations for antidiagonal matrix elements of uniform signature, like $\int\alpha L$, do not contain such terms. In general, these terms can have a noticeable effect only if they are at least two orders of magnitude larger than their diagonal counterparts. Certain types of forces might accomplish this.[2] Careful analysis of nonunique beta spectra of nonallowed shape should lend itself to the determination of whether or not a sufficiently large "antidiagonal effect" exists.

[1] D. L. Pursey, Phil. Mag. **42**, 1193 (1951); T. Ahrens and E. Feenberg, Phys. Rev. **86**, 64 (1952).
[2] D. C. Peaslee, Phys. Rev. **91**, 1447 (1953).

Z6. The Possibility of Interpreting Beta Decay Spectra in Terms of Nuclear Forces. M. M. MILLER AND T. AHRENS, *Lockheed Aircraft Corporation.*—Beta decay correction factors contain nuclear matrix elements whose coefficients differ in general from one another in energy dependence. Unless leading terms of at least two coefficients differ from each other in energy dependence, little reliable knowledge about matrix element ratios can be gained from experimental spectral shapes. An exception is provided if the leading terms of equal energy dependence cancel out. Thus, ones attention is confined to nonunique spectra. Consideration of first forbidden spectra should furthermore be restricted to nonallowed shapes, unless statistical interpretations are employed.[1] Limiting the beta interaction to the form S,T,P permits one to draw the following conclusions: first forbidden evidence, strongly suggesting $S+T$,[2] can be explained by both the presence and absence of special nuclear forces (these forces have commutators with uniformly signed diagonal and antidiagonal operators that differ markedly from one another)[3]; second forbidden evidence, favoring $S+T$, is better explained by the presence of such special forces. More data are needed, however, to make a definite decision.

[1] R. W. King and D. C. Peaslee, Phys. Rev. **94**, 1284 (1954).
[2] G. E. Lee-Whiting, Phys. Rev. **97**, 463 (1955).
[3] Preceding abstract.

Z7. On the Field of Bhabha Equation. FERNANDO E. PRIETO C., *Universidad de México e Instituto Nacional de la Investigación Científica.*—The purpose of this paper is to present some properties of the field of Bhabha equation for a particle with two different states of mass and spin, properties which are very useful in the treatment of problems by the usual techniques of field theory. Charge conjugation of the field is considered, and vacuum state is defined. Vacuum expectation values of second-order terms in the field variables are given, and an explicit form of the Feynman propagation function is obtained. It is shown that the interaction of Bhabha field with a scalar meson field with scalar and vector coupling leads to a second-order potential which presents the same formal aspect of a Bethe potential. The field formalism of Bhabha equation is completely similar to that of Dirac equation, and, as long as the commutation rules for the matrices of the field are not explicitly used, corresponding expressions look identical. It is to be expected that the difference between both formalisms will appear only if higher order calculations are performed.

Z8. Some Neglected Mathematics in the Solution of Vibration Problems. DAN MCLACHLAN, JR., *Stanford Research Institute.*—In dealing with a vibrating mass having nonlinear restoring forces, without damping, one needs solutions of equations of the type,

$$m\frac{d^2\psi}{dt^2} = \pm K\psi|\psi|^{(p-1)},$$

where p is any positive real number. It is suggested that the solutions could be had in a closed form by doing the same thing that has been done for the linear systems, namely supplying tables similar to the trigonometric tables. These new tables are not based on the circle as are the sine and cosine values, but upon other closed figures that are equally interesting. It is shown that when the force function is a power series in ψ, the solutions in special cases reduce to well-known elliptic functions and the less known hyperelliptic functions as well as others that have received almost no attention. It is also shown that the solutions to the problems of vibrating strings, membranes, and wave boxes are products of the corresponding functions for the vibrating mass.

Z9. Theory of Multiple Quantum Transitions.* M. N. HACK, *Princeton University.*—Multiple quantum transitions, first discussed by M. Goeppert-Mayer,[1] are currently being observed in atomic and molecular beam experiments.[2] The theory of these transitions can be developed on the basis of the integral equation for the transition matrix $U(t)$. Since spontaneous emission is a negligible process in these experiments, it is unnecessary to quantize the electromagnetic field. As a consequence of the selection rules, the leading term for an n-quantum transition occurs in the nth order of the Liouville-Neumann solution and accounts for the principal observed characteristics of the multiple quantum transitions, namely: (1) generalized Bohr condition for resonance, $\omega = |E_b - E_a|/n\hbar$; (2) narrow uncertainty width, $\Delta\omega \cong 2\pi/nt$; (3) preferential suppression with decreasing rf field; (4) dependence on the location of intermediate states. For $n=2$, the theory reduces to that of Mayer[1] and Hughes and Grabner.[3] Higher order corrections can be treated and are in agreement with the theory of Salwen.[4]

* This work was supported in part by the U. S. Atomic Energy Commission and the Higgins Scientific Trust Fund.

[1] M. Goeppert-Mayer, Ann. phys. **9**, 273 (1931).

[2] V. W. Hughes and L. Grabner, Phys. Rev. **79**, 314 (1950); **79**, 829 (1950); **82**, 561 (1951); P. Kusch, Phys. Rev. **93**, 1022 (1954); Reynolds, Christensen, Hamilton, Lemonick, Pipkin, and Stroke, Bull. Am. Phys. Soc. **30**, No. 3, 13(A) (1955); V. W. Hughes and J. S. Geiger, Bull. Am. Phys. Soc. **30**, No. 3, 66(A) (1955).

[3] H. Salwen (to be published).

Z10. Quantum-Statistical Derivation of the Transport Equation for Mixtures of Dilute Gases with Molecules of Arbitrary Spins. A. W. SAENZ, *Laboratorio Naval de Investigación.*—In a previous study[1] we derived a transport equation for a gas composed of particles of spin zero. In the present investigation we extend this work to mixtures of dilute gases $\alpha = 1, \ldots, l$ having spins S_α. We employ the properties of suitable time-averaged Wigner distribution functions ($d.f.$'s), time-dependent scattering theory, and assume: (1) that binary collisions are predominant; (2) that the degree of degeneration of the components is slight; (3) molecular chaos hypotheses which take into account the S_α's; (4) that the time-smoothed $d.f.f^{(1,\alpha)}$ for the αth component is only macroscopically dependent on space and time; and (5) that the state of the gas mixture differs but slightly from thermodynamic equilibrium. The collision integrals in the equation for $f^{(1,\alpha)}$ are expressed in terms of *exact* cross sections for binary collisions between the various types of molecules.

[1] To be published. A summary is given in Bull. Am. Phys. Soc. **30**, No. 3, 38(A) (1955).

WEDNESDAY EVENING

(Hour and place to be designated.)

Banquet of the Sociedad Mexicana de Fisica and the American Physical Society

SUPPLEMENTARY PROGRAMME

SP1. Semi-Absolute Measurements of Voltage and Current.* JOSÉ MIRELES MALPICA, *Instituto Politécnico Nacional, Mexico.*—The electrical force-voltage relationship between the surface of conductors and also the magnetic force-current relationship between filamentary conductors remain unchanged when the dimensions of the system undergoes a linear expansion or contraction. This invariance allows the calibration of one instrument to extend to a whole family of instruments with only one-point calibration. This possibility has been subjected to laboratory tests with very satisfactory results, utilizing, in the case of voltages, metallic hollow spheres and double flat spirals with noninductive leads in the case of currents. Since the measurement of high voltages is of scientific and technical importance and this method is considered a definite improvement, effort was focused in this direction. A satisfactory mechanical arrangement has been found which permits voltage measurements with great ease and precision by semi-absolute methods. The fundamental importance of the method resides in the possibility for any researcher of improvising an accurate voltage measuring devise without the need of calibrating it. All he has to know is that the geometry of his system is correct within experimental tolerances, the intensity of gravity in his locality, and the standard force-voltage relationship given in the paper.

* To be given at the end of Session R if time permits.

Author Index to Papers Presented at the 1955 Mexico Meeting

Ahrens, T.—Z5
Ajzenberg, F., A. Rubin, G. D. Johnson, and M. Mazari—M5
Akeley, Edward S.—Y3
Alba Andrade, Fernando—E2
Anderson, T. H., R. D. Jordan, and R. S. Alger—Q13
Barredo, Joseph G.—V6
Belinfante, F. J.—T4
Benczer, N., B. Farrelly, L. Koerts, and C. S. Wu—F5
Bjornerud, E. K.—Y7
Bleakney, Walker—J1
Biedsoe, M. D. and V. G. Szebehely—U6
Block, M. M., E. M. Harth, and M. E. Blevins—L9

Borst, L. B.—W4
Bostrom, Norman A., Emmett L. Hudspeth, and Ira L. Morgan—Y10
Bowyer, J. M. and L. Talbot—U8
Brachman, Malcolm K., and J. Ross Macdonald—R7
Bracken, J. T., E. A. Rollor, and J. A. Mohrbacher—Y6
Brandt, Werner—V1
Branson, Herman and L. B. Garner II—Q10
Bridge, H. S.—S1
Brody, T. A.—Y8
Buechner, W. W.—E3
Buerger, M. J.—V7
Byram, E. T., T. A. Chubb, and H. Friedman—Q6
Callaway, J. and R. D. Woods—G1
Cano-Corona, O. and R. Pepinsky—V8
Carrillo, Nabor—N1
Carter, David—R8
Chupp, Warren W., Gerson Goldhaber, Sulamith Goldhaber, and Francis H. Webb—L7
Coles, Donald—J5
Cork, Bruce and W. A. Wenzel—M13
Cork, J. M., M. K. Brice, L. C. Schmid, and R. G. Helmer—F4
Cox, Everett F.—U2
Critchfield, C. L. and Robert Lowen—G2
Davidson, J. M.—R12
Davis, Leverett, Jr.—L1
De Oyarzabal, Juan—Z3
Dexter, D. L.—Q9
Dieke, G. H. and L. Heroux—R3
Dropesky, B. J. and A. W. Schardt—F3
Duffus, H. J.—R6
Duvall, G. E.—U1
Edelsack, E. A. and W. E. Kreger—Y13
Einstein, H. A.—J4
Eisberg, R. M., G. Igo, and H. E. Wegner—M11
Elsasser, W. M.—H4
Estrada, L.—G4
Everett, A. E. and M. J. Glaubman—F8
Ewing, Maurice—H2
Fairbank, W. M., E. M. Harth, M. E. Blevins, and G. G. Slaughter—Y1
Fernandez, Carlos Graef—T3
Ferrell, Richard A.—Y12
Fields, T., E. J. Schillinger, and J. Kenski—Q12
Forbush, Scott E.—L2
Frank, R. M. and J. F. Gammel—Z1
Frenkiel, François N.—H1
Fretter, W. B.—S4
Gebbie, H. A. and K. Blodgett III—V5
Gerson, N. C.—H5
Goldstein, Louis—R11
Grad, Harold—J2
Groves, Gordon W.—H3
Hack, M. N.—Z9
Hanson, H. P.—K5
Harth, E. M. and M. M. Block—L8
Hill, H. A. and J. M. Blair—M6
Hudspeth, E. L.—E4
Ingersoll, L. R. and D. H. Liebenberg—Q5
Jenkins, F. A. and D. R. Speck—Y11
Kaplan, J. L.—R1
Kittel, Charles—K1
Klick, C. C., G. A. Russell, and D. L. Dexter—Q8
Kohler, F. and O. K. Rice—R4
Korff, S. A.—A1
Kreger, W. E., L. D. McIsaac, J. L. Mackin, and J. R. Lai—F6
Kulp, J. L.—N4
Kurbatov, J. D.—F1
Lane, A. M. and L. Verlet—G7
Lawrence, E. O.—N2
Lawson, R. D.—G9
Lozano, Juan Manuel—G3
Malpica, José Mireles—R13, SP1
Marton, L.—K3
Mazari, M., F. Alba, and V. Serment—Y9
McCarthy, Kathryn A. and Stanley S. Ballard—V4
McLachlan, Dan, Jr.—Z8
Medina, Alejandro—T1
Meyer-Schützmeister, L. and V. L. Telegdi—M10
Miller, M. M. and T. Ahrens—Z6
Mondragón, A.—G5
Montroll, Eliott W. and R. B. Potts—V3
Moore, D. C. and R. J. Hanson—Y4
Moshinsky, Marcos—T2
Mosqueira, R., Salvador—E1
Nagle, D. E. and R. H. Hildebrand—L5
Neher, H. V.—L4
Newcomb, W. A.—U9
Newson, H. W.—M2
Ney, E. P.—W2
Noble, L. M. and R. M. Steffen—F9
Nottingham, W. B.—Q7
Owen, J., M. E. Browne, and A. F. Kip—R2
Oxley, C. L. and V. L. Telegdi—M12
Pealsee, A. T., Jr.—Z4
Pearson, G. L.—K2
Penning, J. R. and F. H. Schmidt—F2
Pepinsky, R.—V11, X1
Perry, R. W. and D. E. Bloxsom—U5
Pevsner, A.—S2
Phillips, G. C., J. L. Russell, and C. W. Reich—M3
Pomerantz, M. A., J. F. Marshall, and R. A. Shatas—Q11
Prieto, C., Fernando, E.—Z7
Rekers, B. G. and D. S. Villars—Q1
Renero, Ignacio—G6
Rhein, W. J.—Y2
Romero-Juárez, A. and J. Hefferan V.—R5
Rorschach, H. E. Jr., and W. V. Houston—R10
Rubin, A., F. Ajzenberg, and Hans Mark—M8
Saenz, A. W.—Z10
Saito, Y., Y. Okaya, and R. Pepinsky—V10
Sattar, Abdul R., Ira L. Morgan, and Emmett L. Hudspeth—M4
Schubauer, G. B.—J3
Sherman, H.—Y5
Sidhu, S. S.—X2
Siegel, K. M. and A. L. Maffett—U7
Simpson, J. A.—W3
Slater, J. C.—K4
Snyder, W. S. and J. Neufeld—V2
Soberman, R. K. and S. A. Korff—L3
Sperduto, A. and W. W. Buechner—M7
Squire, Charles F.—R9, X3
Stewart, R. W. and W. N. English—U10
Stiller, B., N. Seeman, and M. M. Shapiro—L6
Stine, Howard A., and Warren Winovich—U4
Strandberg, M. W. P. and M. Peter—Q2
Temmer, G. M. and N. P. Heydenburg—M9
Tomlinson, E. P. and R. A. Naumann—F7
Trilling, G. H.—S3
Vallarta, Manuel Sandoval—W1
Vand, V. and R. Pepinsky—V9
Vogt, Erich—G8
Volman, David H.—Q4
Wallace, Roger W., Malvern H. L. Jester, and John M. Brabant—M14
Walsh, J. M.—E5
Ward, J. K. and C. M. Loyd—Q3
Whealon, Albert D.—Z2
Wiewall, Miguel, Jr.—U3
Williamson, R. M. and K. W. Jones—M1
Wilson, R. R.—N3

Minutes of the 1955 Fall Meeting of the New York State Section Held at Clarkson College of Technology, Potsdam, New York, October 7 and 8, 1955

THE thirty-fourth meeting of the New York State Section was held at Potsdam, New York with Clarkson College of Technology acting as host to about 60 registrants. On Friday afternoon members enjoyed a tour of the St. Lawrence River Power Development and Seaway Projects, and were entertained at a tea given by President and Mrs. W. G. Van Note of Clarkson College. The after-dinner lecture was sponsored jointly by the Section and the Clarkson College-St. Lawrence University Sigma Xi Club. The speaker was Dr. C. W. Gartlein of Cornell University who gave an illustrated lecture on "The Study of the Aurora and the International Geophysical Year."

The Saturday morning and afternoon sessions were devoted to eight invited papers, the titles of which are listed below.

D. H. Tomboulian, *Secretary*
New York State Section
Cornell University
Ithaca, New York

Invited Papers

Recent Cathode-Ray Developmental Work. W. F. Westendorp, *General Electric Company.*

Refractive Index of Colloidal Solutions. M. Kerker and A. Chou, *Clarkson College of Technology.*

Light Scattering by Optical Glasses. R. D. Maurer, *Corning Glass Works.*

Vapor Pressure of the Solution of He^3 in Liquid He^4. T. P. Tseng, *Clarkson College of Technology.*

Electromechanical Behavior of Single Crystals of Barium Titanate. E. J. Huibregtse, *International Business Machines Corporation.*

Ultrasonic Investigation of the Vibrational Energy Transitions in N_2O Induced by Molecular Collisions with H_2O and D_2O. H. M. Wight, *Corning Glass Works.*

Standards of Length and Wavelength. R. W. Stanley, *Clarkson College of Technology.*

Experimental Study of the Electromagnetic Spectrum Emitted by High-Energy Electrons Accelerated in a Synchrotron. D. H. Tomboulian, *Cornell University.*

Minutes of the Fall Meeting of the Ohio Section of the American Physical Society Held at Wright-Patterson Air Force Base, Ohio, October 14 and 15, 1955

THE fall meeting of the Ohio Section of the American Physical Society was held at Wright-Patterson Air Force Base, Ohio, on October 14 and 15, 1955. To the staff of the U. S. Air Force Technological Institute, especially, Major General Ralph P. Swofford, Dr. William J. Price, Dr. William Lehmann, and Dr. Paul B. Taylor of the Aeronautical Research Laboratory, we owe our sincere thanks for the opportunity to visit Wright-Patterson Air Force Base and the several laboratories, for the program of tours, overnight accommodation, and the thoughtful care of our smallest needs. It was a large meeting, 72 registered not including men at the Base itself, 21 colleges were represented, 9 corporations having research facilities, and three government research agencies besides the organizations at the Base.

On Friday, October 14, Major General Swofford, the Commandant, USAFIT began the program with an over-all picture of military research organizations. Mr. Wendell Koch, Director of Research, Wright Air Development Center explained in some detail the several laboratories, their organization and responsibilities. Dr. N. F. Beardsley, Aerial Reconnaissance Laboratory, spoke of "Physics of the Infrared"; Dr. Walter Wessel, U. S. Air Force Institute of Technology, spoke on "Particle Masses as an Eigenvalue Problem." Friday afternoon was used to visit the several laboratories at the Base and also see the end result, a fighter squadron. At the Friday evening dinner Dr. Elmer Hutchisson, Case Institute of Technology, spoke on "The Role of Physics in Today's Education."

Saturday morning, October 15, was devoted to the contributed papers, two of which provided no abstracts; **Applied Physics Research at the Detroit Arsenal,** by R. A. Pulk, *Detroit Arsenal*; and **Current Misconceptions of the Coefficient of Sliding**

Friction, by CHARLES A. MANEY, *Defiance College.*

The abstracts of the other ten papers follow.

LEON E. SMITH, *Secretary*
The Ohio Section of
The American Physical Society
Denison University,
Granville, Ohio

1. Gated Phototube for Fast Pulse Operation. D. V. BREITENBECHER, *Physics Research Branch, Aeronautical Research Laboratory, Wright Air Development Center.*—In the neutron time-of-flight spectrometer a method of gating the phototube used with the neutron detector was needed. A gamma pulse 100 to 1000 times larger than the neutron pulses had to be removed. Because of circuit considerations, it was impractical to gate the tubes "off" during the gamma pulse. It was, therefore, decided to gate the tubes "on" during the time neutrons were to be counted. It was required that the phototubes reach maximum sensitivity within 1 microsecond. Pulsing the photocathode would not produce the desired effect. The time constant of the photocathode was too large, being 3 microseconds for Dumont 6292 and 8 microseconds for the 5819. It was decided then to pulse special dynodes of the phototube. This was accomplished by grounding the fourth dynode and applying a positive supply voltage between this dynode, through the voltage divider, to the anode. A negative voltage was applied between the fourth dynode and the photocathode. The first dynode was clamped at the correct potential by a divider network. A positive voltage was applied across a divider network to the second and third dynodes. This voltage essentially cut off the phototubes. In order to "turn on" the phototubes, a negative pulse was applied to dynodes two and three.

In this type of gate the time required for a 6292 or 5819 to reach full sensitivity was less than 1 microsecond. The cathode remains on at all times, but in the case of the 6292 the maximum average or maximum peak current is never reached.

2. Quantum Yield of a Cadmium Sulfide Photovoltaic Cell.[*] R. E. MARBURGER, D. C. REYNOLDS, L. L. ANTES, AND R. S. HOGAN, *Physics Research Branch, Aeronautical Research Laboratory, Wright Air Development Center.*—In his article on the photovoltaic effect, Lehovec derives the equation

$$E=\rho_0(Je/h\nu)\cdot\alpha\cdot A-\rho_0 I \qquad (1)$$

where E is photovoltage, J is transmitted light, α is quantum yield, A is absorption coefficient, ρ_0 is dark barrier layer resistance, and I is photocurrent. For the cadmium sulfide cell all quantities except α are experimentally measurable, and the equation may be solved for α, the quantum yield. When I is the short-circuit current, $E=0$, and Eq. (1) becomes

$$\alpha=Ih\nu/JeA,$$

which is the number of electrons per second appearing in the external circuit divided by the number of absorbed, contributing quanta. If A is assumed to be 1.00, i.e., all quanta transmitted into the crystal are contributing to the effect, then α assumes its lower limit. The diffusion length in CdS was measured, using a photovoltaic cell. It was found to be approximately 1 mm. Under this condition, it is evident that the assumption of $A=1.00$ in the region near the absorption cutoff will lead to a loss in quantum yield for thick crystals. The light is mostly absorbed near the surface, and recombination occurs before the electrons can reach the barrier. A curve of α *vs* wavelength based on experimental data, without varying the value of A will thus be particularly depressed in the region of wavelengths just above 5200 A.

[*] Marburger, Reynolds, Antes, and Hogan, J. Chem. Phys. (to be published).

3. Cadmium Sulfide Photorectifier. LAWRENCE C. GREENE, *Physics Branch, Aeronautical Research Laboratory, Wright Air Development Center, Wright-Patterson Air Force Base.*—The preparation and properties of a CdS photorectifier are discussed and it is shown that the effect is a barrier region effect and not a volume effect. The cells made from low-resistance CdS crystals show high resistance in both directions in the dark, but become conducting in the forward direction when illuminated. Light to dark current ratios of 10^6 have been observed. With an applied field of 1 to 1.5 volts ac or dc, an output of as much as several hundred milliamperes has been obtained. Both static and dynamic characteristics are given for varying intensities of illumination. The spectral response of the cell is given and it is shown that there are two peaks, one at the absorption cutoff and another at 5600 A, the sensitivity tailing off toward the red. The gain of the cell is measured as a function of radiation intensity and is found to be expressed approximately by a double exponential. It is also found that the response decreases exponentially as the exciting radiation is moved away from the barrier region. The effect of gamma radiation is discussed. A model is proposed involving the formation of a quasi-intrinsic region by diffusion of the barrier into the crystal.

4. State of Order of Cd-poor $MgCd_3$. B. WELBER AND B. M. ROSENBAUM, *Lewis Laboratory, NACA.*—Previous investigations[1,2] have yielded conflicting results as to whether the system Mg–Cd has an ordered state on the Cd-poor side of $MgCd_3$. To resolve this question, a sample of the alloy containing 72.14 atomic percent Cd was prepared, homogenized, and given an appropriate heat treatment to bring it to equilibrium at toom temperature. Its specific heat as a function of temperature was then measured with an adiabatic vacuum calorimeter and was found to display a maximum of finite height at 99.2°C. It follows that in equilibrium the alloy is ordered at room temperature and undergoes a second-order transition to the disordered state at the indicated temperature. The associated heat of transformation as estimated from the curve amounts to 2.53 cal/gram.

[1] Nagasaki, Hirabayashi, and Nagasu, Nippon Kinzoku Gakkai-Shi **13**, 1 (1949); Hirabayashi, Nagasaki, Maniwa, and Nagasu, Nippon Kinzoku Gakkai-Shi **13**, 6 (1949).
[2] Homiakov, Holler, and Troshkina, Moscow University Reports **6**, 55 (1950).

5. Longitudinal Photomagnetoelectric Effect in Germanium. GERHART GROETZINGER AND JACK ARON, *Lewis Laboratory, NACA.*—It was found earlier by one of us[1] that the photo-emf developed along the direction parallel to the gradient of light absorption in an illuminated cuprous oxide crystal is reduced by the application of a transverse magnetic field. In the present work it was shown that this effect also occurs in high-purity n-type germanium (resistivity 50 ohm cm). The size of the effect is approximately quadratic in the field up to about 2000 gauss, is then linear up to 4000 gauss and, subsequently saturates. The diminution of the photo-emf is about 10% for a field of 500 gauss while in cuprous oxide a field of 36 000 gauss produces a decrease of only 0.6%.[1]

[1] G. Groetzinger, Phys. Z. **36**, 169 (1935); **36**, 216 (1935).

6. Thermoelectric Power of AuCu in Nonequilibrium States. P. SCHWED, H. COOPER, AND R. W. WEBELER, *Lewis Laboratory, NACA.*—The states through which mechanically or thermally disordered AuCu anneals at various temperatures were previously investigated[1] by joint measurement of the coefficient of magnetoresistivity and the resistivity. This study has been extended by measurement of the resistivity ρ and of the thermoelectric power Q (*vs Pt*) of samples of AuCu in various nonequilibrium states. One set of samples was disordered by quenching from 750°C; annealing curves were obtained at 100°, 149°, 198°, and 258°C. A second set was

first ordered and then cold worked to essentially complete disorder, and annealing curves taken at 149°C and 258°C. Of the former set, the $Q-\rho$ curves for 100° and 149°C showed a maximum at $\rho=11.5$ μ-ohm cm while none was observed in the curves for any of the other cases. It follows from the detailed results that to specify the state of the alloy it is necessary to give, in addition to ρ and Q, at least one other quantity such as the coefficient of magnetoresistivity.

[1] Wiener, Schwed, and Groetzinger, J. Appl. Phys. **26**, 609 (1955); Wiener, Groetzinger, and McCollum, J. Appl. Phys. **26**, 857 (1955).

7. Instrument for Measurement of Information Stored on Photographic Film.* A. A. Silvidi, G. K. Schoepfle, K. L. Warren, and F. L. Brooks, *Kent State University, Kent, Ohio* and M. Horowitz, *Aerophysics Department, Goodyear Aircraft Corporation.*—An instrument has been constructed in order to measure the approximate information content of a message stored on film. The device has been given the name "photoquantizer" because it measures the average densities of small rectangular areas of the original film and then exposes corresponding areas of new film to produce a quantized copy of the original. Automatic electrical counters tally the number of areas N_i whose average densities lie in the ith density interval. The information is computed according to the formula used by Kretzmer[1]

$$H=-\sum_{i=1}^{L} p_i \log p_i,$$

where H is maximum possible information content per sample, L is number of density intervals, and

$$p_i=N_i/\sum_{i=1}^{L} N_i.$$

As an example of how the instrument is utilized, pictures of radar ppi presentations were studied and results of the information measurements will be presented. If the small rectangular area is the size of the cathode-ray tube spot and if the separation of density levels represents the original noise power, then H will closely measure the maximum original information content.

* Supported by U. S. Air Force, Wright Air Development Center, Dayton, Ohio.

[1] E. R. Kretzmer, Bell System Tech. J. **31**, 751 (1952).

8. Sargent Diagram and Comparative Half-Lives for Allowed K-Capture Transitions of Nuclides with $Z\leqslant 60$. L. S. Cheng, *Capital University and Ohio State University.*—Modified Sargent diagram of K-capture transitions of both odd and even nuclides with $Z\leqslant 60$ shows an allowed transition band having a width about 1.4 in. logarithm scale and a slope 2 in. log-log plot, with superallowed transitions above and first-forbidden transitions below it.[1] This provides further support for the Fermi theory of beta decay for allowed transitions. After the exclusion of the nuclides which show particularly low-transition probabilities such as Zn^{65},[2] Co^{59},[3] and those which have the magic number configurations in parent nuclides such as Co^{53}, Ni^{57}, and Sn^{111}; investigation of regularities in comparative half-lives of the allowed K-capture transitions has been attempted. (1) The K-capture for odd nuclides can be classified as either unlike-core or like-core transitions.[4] In general the former class has a slightly higher $\log ft$ value ($\sim$0.35 higher) than the latter class for fixed $N-Z$.[5] A trend of increase in $\log ft$ value with increasing neutron excess may be discerned. (2) The K-capture for even nuclides can be classified according to the odd proton and the odd neutron having either $(l\pm\frac{1}{2}, l\pm\frac{1}{2})$ or $(l\pm\frac{1}{2}, l\mp\frac{1}{2})$ configuration.[4] The former class has high $\log ft$ values ($\geqslant 5.5$) while the latter class has a low $\log ft$ value (<5.5).[4] They all show a trend of decrease in $\log ft$ value with increasing mass number.

[1] Part of this Sargent diagram has been submitted to The Physical Review for publication.
[2] J. F. Perkins and S. K. Haynes, Phys. Rev. **92**, 687 (1953).
[3] Cork, Price, and Schmid, Phys. Rev. **99**, 703 (1955).
[4] L. W. Nordheim, Report of Indiana Conference on Nuclear Spectroscopy and Shell Model, pp. 18–21 (1953).
[5] M. C. Redlich and E. P. Wigner, Phys. Rev. **95**, 122 (1954).

9. On a Certain Blindness in Physicists. W. M. Pierce, *Ohio University.*—Two theses are presented: first, that the shortages in people interested in science begin at the elementary level, and continue at the secondary level, for two fundamental reasons, inadequate teacher preparation and inadequate organization of curricular materials. The second thesis will be that solutions to the problem of shortages are being sought by physicists in the same tradition which has prevailed for the past fifty years, ignoring completely the changed conditions in high school particularly with which they have to deal. Suggestion as to the lines of a possible solution other than the traditional will be indicated.

10. Quantum Theory from Nonquantal Principles. Alfred Landé, *The Ohio State University.*—Instead of accepting the rules of quantum theory as axioms, or because they yield experimentally confirmed results, it is possible to see them as manifestations of two simple physical principles, namely, (1) that of *continuity* of cause and effect applied to the entropy of diffusion, in contrast to the Gibbs paradox of classical statistical thermodynamics, and (2) that of *conjugacy* which defines observables q and p as conjugates when they possess a constant probability density in qp-space. From (1) follows the necessity of admitting a continuity of equality values between equality and total inequality, i.e., between inseparability and total separability, manifested as a fractional separability, typified by the Stern-Gerlach effect, and leading to a schema of transition probabilities in general. The superposition of complex probability amplitudes is not a new independent law of nature but is implicit in the general metric of real probabilities. From (2) it follows that the probability amplitude $\psi(q,p)$ must necessarily have the form $\exp(iqp/\text{const})$. The principles (1) and (2) thus explain why there is a *periodic* relation between conjugates, i.e., they solve the oldest "enigma" of the quantum theory.

Letters:

. . . . . G. Harris, J. Horne, and S. Taylor 935

. . . . . Lee and T. Cotter 937

. . . . . F. M. Rinaldi 939

. . . . . C. E. Penny 939

. . . . . W. J. Sobkowiak 944

. . . . . W. J. Sobkowiak 947

. . . . . Schnepp, G. A. [illegible], and M. S. Sweat 950

. . . . . S. Sunggyun 955

. . . . . R. Cotter, T. S. Hsiang, and A. Kovacs 960

. . . . . G. Smith and J. P. Lasaga 963

. . . . . E. L. Church and J. Wenzel 967

. . . . . B. Gerbarg, H. Hollis, and W. P. Harvych 968

. . . . . , Clyde Wiegand, and Shannon Vyshnavis 977

. . . . . Schnepp, G. A. [illegible], and M. S. Sweat 980

. . . . . on, August 29–31, 1955 (Corresponding to *Bulletin of the American Physical* . . . . . 20, No. 8) 982

. . . . . Young Section Held at Clarkson College of Technology, Potsdam, New York, [illegible] and 8, 1955 977

. . . . . of the American Physical Society Held at Wright-Patterson Air Force Base, [illegible] ember 14 and 15, 1955 977